UNIVERSITAT POLITÈCNICA DE VALÈNCIA

DOCTORADO EN INGENIERÍA Y PRODUCCIÓN INDUSTRIAL

TESIS DOCTORAL

"Hacia una economía circular: revalorización de productos de la semilla de *Salvia hispanica L.* en el sector de los biopolímeros"

Autor:

Iván Domínguez Candela

Dirigida por:

Dr. Jaime Lora García

Dr. Vicent Fombuena Borrás

Mayo de 2023

UNIVERSITAT POLITÈCNICA DE VALÉNCIA

DOCTORADO EN INGENIERÍA Y PRODUCCIÓN INDUSTRIAL

TESIS DOCTORAL

"Hacia una economía circular: revalorización de productos de la semilla de *Salvia hispanica L.* en el sector de los biopolímeros"

Iván Domínguez Candela

El Dr. Jaime Lora García, Catedrático de Universidad y el Dr. Vicent Fombuena Borrás, Titular de Universidad, ambos pertenecientes al Departamento de Ingeniería Química y Nuclear de la Universitat Politècnica de València en calidad de directores de la Tesis Doctoral (modalidad Doctorado Internacional) presentada por D. Iván Domínguez Candela, con el título "**Hacia una economía circular: revalorización de productos de la semilla de *Salvia hispanica L.* en el sector de los biopolímeros**"

CERTIFICAN

Que la presente memoria, "**Hacia una economía circular: revalorización de productos de la semilla de *Salvia hispanica L.* en el sector de los biopolímeros"**, para aspirar al grado de Doctor por la Universitat Politècnica de València reúne las condiciones adecuadas para constituir la tesis doctoral de D. Iván Domínguez Candela (modalidad Doctorado Internacional).

Asimismo, certifican que la citada tesis doctoral se ha realizado en el Instituto de Seguridad Industrial, Radiofísica y Medioambiental (YSYRIM) y Tecnología de materiales (ITM) de la Universitat Politècnica de València y en el departamento de Ingeniería Química de University of Aberdeen (Escocia).

Y para que conste a los efectos oportunos, firman la presente en Alcoy a 20 de marzo de 2023.

Fdo. Dr. Jaime Lora García

Fdo. Dr. Vicent Fombuena Borrás

AGRADECIMIENTOS

Antes de comenzar, me gustaría agradecer a todas las personas que han hecho posible la presentación de mi tesis doctoral.

Primero, a mis directores de tesis por haberme dado la oportunidad de crecer como investigador y por aportarme tantísimo durante estos años. Vicent y Jaime, muchas gracias por vuestros consejos y por la libertad que me habéis ofrecido, estoy seguro de que no habría podido encontrar mejores directores de tesis. Gracias por guiarme y apoyarme cuando las cosas no pintaban bien. Sois un referente. Muchas gracias por permitirme descubrir el mundo de la docencia, ¡sobre todo con mucha variedad!

Al departamento de Ingeniería Química y Nuclear (DIQN) del Campus de Alcoy, muchas gracias a Fernanda, Salva, Antonia y Carlos.

A todos mis compañeros de laboratorio que han hecho más ameno estos años. Nunca me olvidaré de los buenos momentos, consejos y risas. Gracias Lerma, Alexis, Aina y, casi se me olvida, ¡Aarón! También agradecer a los doctorandos del ITM Jaume, Juan, Ramón, Diego y Sandra, por su ayuda y colaboración.

A los profesores del Instituto de Tecnología de Materiales (ITM), gracias, Dani y Pelayo.

A la gran hospitalidad que recibí en mi estancia predoctoral en Aberdeen. Gracias Alf por todo, me has ayudado a ser más independiente, aprender nuevas formas de investigar y permitir que existan nuevas colaboraciones. ¡No olvidaré las cenas entre semana que nos llevaban a países asiáticos, y a veces no tan asiáticos! Gracias también a mis compañeros de laboratorio que me ayudaron a integrarme y disfrutar de la gran Escocia, un abrazo a Iman, Noor, Jonathan, Rebecca y Fadhilah. También a Jaime, José y a todas las personas increíbles que conocí.

A mis padres, por creer en mi y apoyarme durante toda mi carrera universitaria. Sin vosotros no habría sido posible nada. Mencionar también a mis yayos, Maruja, tata, José, Sara y Kevin. Siempre os tendré ahí.

A Leo, Javi e Irene por hacerme sentir siempre como en casa. Gracias por todo.

A mi compañera de vida, Ro. Gracias por aguantarme en mis momentos más complicados, por acompañarme en mis estancias, y hacerme ver las cosas de otra manera. Sin tu apoyo no hubiera podido conseguir esto. También a mi trupe, gracias a mi Hera, Maya, Charlie y Frida, cada cual más pesado.

A todos mis amigos que han estado ahí durante estos años, Irene, Cristina, Alex, Dani, Poli, JD, y muchos más. También a los "Alcoyanos", Jorge, Germán, Penades, Nicole, Isa, Youssef y Josep. Espero que una vez al año no haga daño.

Por último, y no menos importante, agradecer a los financiadores de mi ayuda.

A la Universitat Politècnica de València por el soporte financiero de este proyecto (PAID-2019-SP20190013)

A la Conselleria d'Educació, Cultura i Esport de la Generalitat Valenciana por la ayuda otorgada (ACIF/2020/233) y por el soporte financiero de mi estancia (CIBEFP/2021/53).

RESUMEN

La producción masiva de plásticos ha generado graves problemas medioambientales, ya que su lenta degradación y alta persistencia en el medio ambiente causa la acumulación de residuos plásticos en los océanos y tierras. Como respuesta, se está llevando a cabo una búsqueda activa de alternativas más sostenibles, incluyendo biopolímeros, materiales compostables y biodegradables, polímeros reciclados y materiales biológicos. Se están desarrollando nuevas tecnologías para la producción de envases y productos que sean más sostenibles y reciclables, y se están promoviendo iniciativas de educación y concienciación para reducir el consumo y fomentar el reciclaje. La búsqueda de alternativas sostenibles es una prioridad urgente para abordar los impactos ambientales de los plásticos.

La semilla de chía tiene un gran potencial en el campo de los biopolímeros debido a su alto contenido de ácidos grasos poliinsaturados (alrededor de un 30% en peso de la semilla) y cuya harina de chía está formada por proteínas, mucílago, carbohidratos y residuos lignocelulósicos principalmente. Estos componentes pueden ser utilizados para producir biopolímeros naturales y biodegradables, que pueden ser una alternativa más sostenible a los polímeros sintéticos tradicionales.

La presente tesis doctoral evalúa la capacidad de emplear la semilla de chía como recurso renovable funcional en el campo de los biopolímeros. Tras un proceso de extracción se evalúa la posibilidad de modificar químicamente los ácidos grasos poliisaturados presentes en los ácidos grasos del aceite de chía. Por tanto, uno de los primeros objetivos marcados es la optimización de un proceso como la epoxidación del aceite de chía, no realizada en la comunidad científica hasta el momento.

El desarrollo de este aceite de chía epoxidado (ECO) permite su posterior testado como plastificante de origen bio en biopolímeros intrínsecamente rígidos y frágiles como el PLA. Además, este mismo aceite epoxidado puede emplearse como compatibilizante entre moléculas apolares, como son las matrices poliméricas, y las cargas lignocelulósicas, como la propia harina de chía, introducidas para mitigar el impacto ambiental y aumentar la revalorización de subproductos de la semilla de chía. El empleo de ECO como compatibilizante se ha llevado a cabo con matrices basadas

en PLA y biopolietileno (Bio-HDPE), desarrollando biopolímeros biodegradables y no biodegradables para diferentes sectores.

También se ha desarrollado un aceite de chía maleinizado (MCO). La introducción de esta molécula de anhídrido maleico en el triglicérido le permite tener una elevada reactividad apta para el desarrollo de un nuevo bioplastificante, como se ha demostrado mediante la introducción en matrices de PLA, e incluso para su empleo como endurecedores de resinas de tipo epoxi. Se lleva a cabo por primera vez el desarrollo de una resina termoestable basada al 100 % en ECO como base de la resina epoxy y MCO como endurecedor bio.

Finalmente, el aceite de chía también puede emplearse como materia prima para la obtención de glicolípidos con comportamiento de cristal líquido. Estos glicolípidos serán estudiados para conocer su potencial como surfactante en aplicaciones cosméticas o en aplicaciones energéticas para la conversión y almacenamiento de energía en presencia de compuestos que interaccionan con la luz solar.

Por tanto, las investigaciones desarrolladas en la presente tesis doctoral han permitido explorar por primera vez el empleo de la semilla de chía como fuente de materia prima renovable para la obtención de compuestos activos aplicables al sector de los biopolímeros. Para ello se han desarrollado nuevos compatibilizantes y plastificantes mediante el desarrollo del ECO y del MCO, la revalorización de la harina de chía mediante su adición en matrices poliméricas desarrollando nuevos WPC y desarrollando, por primera vez, una resina termoestable originaria al 100% de la semilla de la chía.

RESUM

La producció massiva de plàstics ha generat greus problemes mediambientals, ja que la seua lenta degradació i alta persistència en el medi ambient causa l'acumulació de residus plàstics en els oceans i terres. Com a resposta, s'està duent a terme una cerca activa d'alternatives més sostenibles, incloent-hi biopolímers, materials compostables i biodegradables, polímers reciclats i materials biològics. S'estan desenvolupant noves tecnologies per a la producció d'envasos i productes que siguen més sostenibles i reciclables, i s'estan promovent iniciatives d'educació i conscienciació per a reduir el consum i fomentar el reciclatge. La cerca d'alternatives sostenibles és una prioritat urgent per a abordar els impactes ambientals dels plàstics.

La llavor de xia té un gran potencial en el camp dels biopolímers a causa del seu alt contingut d'àcids grassos poliinsaturats (al voltant d'un 30% en pes de la llavor) i la farina de xia de la qual està formada per proteïnes, mucílag, carbohidrats i residus lignocelulósics principalment. Aquests components poden ser utilitzats per a produir biopolímers naturals i biodegradables, que poden ser una alternativa més sostenible als polímers sintètics tradicionals.

La present tesi doctoral avalua la capacitat d'emprar la llavor de xia com a recurs renovable funcional en el camp dels biopolímers. Després d'un procés d'extracció s'avalua la possibilitat de modificar químicament els àcids grassos poliisaturats presents en els àcids grassos de l'oli de xia. Per tant, un dels primers objectius marcats és l'optimització d'un procés com l'epoxidació de l'oli de xia, no realitzada en la comunitat científica fins al moment.

El desenvolupament d'aquest oli de xia epoxidado (ECO) permet el seu posterior testat com a plastificant d'origen bio en biopolímers intrínsecament rígids i fràgils com el PLA. A més, aquest mateix oli epoxidado pot emprar-se com compatibilizant entre molècules apolares, com són les matrius polimèriques, i les càrregues lignocelulósiques, com la pròpia farina de xia, introduïdes per a mitigar l'impacte ambiental i augmentar la revaloració de subproductes de la llavor de xia. L'ocupació d'ECO com compatibilizant s'ha dut a terme amb matrius basades en PLA

i biopolietileno (Bio-HDPE), desenvolupant biopolímers biodegradables i no biodegradables per a diferents sectors.

També s'ha desenvolupat un oli de xia maleinizado (MCO). La introducció d'aquesta molècula d'anhídrid maleic en el triglicèrid li permet tindre una elevada reactivitat apta per al desenvolupament d'un nou bioplastificant, com s'ha demostrat mitjançant la introducció en matrius de PLA, i fins i tot per al seu ús com a enduridors de resines de tipus epoxi. Es duu a terme per primera vegada el desenvolupament d'una resina termoestable basada al 100% en ECO com a base de la resina epoxi i MCO com a enduridor bio.

Finalment, l'oli de xia també pot emprar-se com a matèria primera per a l'obtenció de glicolípids amb comportament de cristall líquid. Aquests glicolípids seran estudiats per a conéixer el seu potencial com a surfactant en aplicacions cosmètiques o en aplicacions energètiques per a la conversió i emmagatzematge d'energia en presència de compostos que interaccionen amb la llum solar.

Per tant, les investigacions desenvolupades en la present tesi doctoral han permés explorar per primera vegada l'ús de la llavor de xia com a font de matèria primera renovable per a l'obtenció de compostos actius aplicables al sector dels biopolímers. Per a això s'han desenvolupat nous compatibilizants i plastificants mitjançant el desenvolupament del ECO i del MCO, la revaloració de la farina de xia mitjançant la seua addició en matrius polimèriques desenvolupant nous WPC i desenvolupant, per primera vegada, una resina termoestable originària al 100% de la llavor de la xia.

Abstract

The mass production of plastics has led to serious environmental problems, as their slow degradation and high persistence in the environment causes the accumulation of plastic waste in oceans and land. In response, there is an active search for more sustainable alternatives, including biopolymers, compostable and biodegradable materials, recycled polymers and bio-based materials. New technologies are being developed for the production of packaging and products that are more sustainable and recyclable, and education and awareness initiatives are being promoted to reduce consumption and encourage recycling. The search for sustainable alternatives is an urgent priority to address the environmental impacts of plastics.

Chia seed has great potential in the field of biopolymers due to its high content of polyunsaturated fatty acids (around 30% by weight of the seed) and chia flour is mainly composed of proteins, mucilage, carbohydrates and lignocellulosic residues. These components can be used to produce natural and biodegradable biopolymers, which can be a more sustainable alternative to traditional synthetic polymers.

This doctoral thesis evaluates the capacity of using chia seed as a functional renewable resource in the field of biopolymers. After an extraction process, the possibility of chemically modifying the polyunsaturated fatty acids present in the fatty acids of chia oil is evaluated. Therefore, one of the first objectives is the optimisation of a process such as the epoxidation of chia oil, which has not been carried out in the scientific community until now.

The development of this epoxidised chia oil (ECO) allows its subsequent testing as a bio-based plasticiser in intrinsically rigid and fragile biopolymers such as PLA. Furthermore, this same epoxidised oil can be used as a compatibiliser between apolar molecules, such as polymeric matrices, and lignocellulosic fillers, such as chia flour itself, introduced to mitigate the environmental impact and increase the revaluation of chia seed by-products. The use of ECO as a compatibiliser has been carried out with

PLA and biopolyethylene (Bio-HDPE) based matrices, developing biodegradable and non-biodegradable biopolymers for different sectors.

A maleinised chia oil (MCO) has also been developed. The introduction of this maleic anhydride molecule in the triglyceride allows it to have a high reactivity suitable for the development of a new bioplasticiser, as has been demonstrated by introducing it into PLA matrices, and even for use as hardeners in epoxy-type resis. For the first time, the development of a thermosetting resin based 100% on ECO as the base of the epoxy resin and MCO as the bio hardener is carried out.

Finally, chia oil can also be used as a raw material to obtain glycolipids with liquid crystal behaviour. These glycolipids will be studied for their potential as surfactants in cosmetic applications or in energy applications for energy conversion and storage in the presence of compounds that interact with sunlight.

Therefore, the research carried out in this doctoral thesis has made it possible to explore for the first time the use of chia seeds as a source of renewable raw material for obtaining active compounds applicable to the biopolymer sector. To this end, new compatibilisers and plasticisers have been developed through the development of ECO and MCO, the revaluation of chia flour by adding it to polymeric matrices, developing new WPCs and developing, for the first time, a thermosetting resin made from 100% chia seed.

Tabla de contenidos

LISTADO DE ARTÍCULOS *19*

ECUACIONES *21*

ABREVIATURAS Y TÉRMINOS *25*

LISTADO DE FIGURAS *31*

LISTADO DE TABLAS *41*

I. INTRODUCCIÓN *45*

I.1. Problemática medioambiental **47**

I.2. Polímeros en ingeniería **54**

I.2.1. Polímeros termoplásticos 54

I.2.2. Polímeros termoestables 69

I.2.3. Aditivos en formulaciones de polímeros 71

I.3. Aceites vegetales en ingeniería **76**

I.3.1. Principales propiedades y producción de aceites vegetales 78

I.3.2. Métodos de extracción de aceites 83

I.3.3. Modificaciones aplicadas a aceites vegetales 85

I.3.4. Aplicaciones de los aceites vegetales modificados 91

I.3.5. Responsabilidad de uso 93

I.4. Semilla de chía **95**

I.4.1. Producción mundial 95

I.4.2. Composición del aceite de chía 96

I.4.3. Composición del residuo seco 97

REFERENCIAS **99**

II. ESTUDIOS PREVIOS *119*

II.1 "Development and characterization of Polyester and Acrilated-Based Composite with Hydroxyapatite and Halloysite Nanotubes for Medical Applications" **123**

Abstract 125

Keywords 125

Introduction 126

Experimental 129

Results and discussion 133

Conclusions ... 140
Acknowledgments ... 141
References ... 141

III. OBJETIVOS Y PLANIFICACIÓN ... *149*

III.1. OBJETIVOS GENERAL ... **151**

III.2. OBJETIVOS ESPECÍFICOS ... **151**

IV. RESULTADOS Y DISCUSIÓN ... *155*

IV.1 "Physicochemical Characterization of Novel Epoxidized Vegetable oil from Chia Seed Oil" ... **163**
Abstract ... 165
Keywords ... 165
Introduction ... 166
Experimental ... 169
Results and discussion ... 175
Conclusions ... 189
Acknowledgments ... 190
References ... 190

IV.2 "Dual Plasticizer/Thermal Stabilizer Effect of Epoxidized Chia Seed Oil (*Salvia hispanica L.*) to Improve Ductility and Thermal Properties of Poly(Lactic Acid)" ... **203**
Abstract ... 205
Keywords ... 205
Introduction ... 206
Experimental ... 209
Results and discussion ... 213
Conclusions ... 225
Acknowledgements ... 226
References ... 226

IV.3 "Contribution to a Circular Economy Model: From Lignocellulosic Wastes from the Extraction of Vegetable Oils to the Development of a New Composite" ... **237**
Abstract ... 239
Keywords ... 239
Introduction ... 240
Experimental ... 243
Results and discussion ... 249
Conclusions ... 270

Acknowledgements ... 271
References ... 271

IV.4 "Novel compatibilizers and plasticizers developed from epoxidized and maleinized chia oil in composites based on PLA and chia seed flour" ... 285
Abstract ... 287
Keywords ... 287
Introduction ... 288
Experimental ... 290
Results and discussion ... 296
Conclusions ... 317
Acknowledgements ... 318
References ... 319

IV.5 "Development of a novel epoxy resin based on epoxidized chia oil as matrix and maleinized chia oil as bio-renewable crosslinker" ... 335
Abstract ... 337
Keywords ... 337
Introduction ... 338
Experimental ... 340
Results and discussion ... 345
Conclusions ... 359
Acknowledgements ... 361
References ... 361

IV.6 "Light-responsive bent-core liquid crystals as candidates for energy conversion and storage" ... 377
Abstract ... 379
Introduction ... 380
Experimental ... 381
Results and discussion ... 383
Conclusions ... 400
Acknowledgements ... 401
Supplementary information ... 401
References ... 410

V. CONCLUSIONES ... *423*

V.1. CONCLUSIONES PARCIALES ... **425**

V.2. CONCLUSIÓN GENERAL ... **429**

LISTADO DE ARTÍCULOS

La presente tesis doctoral se ha realizado a parir de un compendio de los siguientes artículos y manuscritos:

I. Physicochemical Characterization of Novel Epoxidized Vegetable Oil from Chia Seed Oil
II. Dual Plasticizer/Thermal Stabilizer Effect of Epoxidized Chia Seed Oil (*Salvia hispanica L.*) to Improve Ductility and Thermal Properties of Poly(Lactic Acid)
III. Contribution to a Circular Economy Model: From Lignocellulosic Wastes from the Extraction of Vegetable Oils to the Development of a New Composite
IV. Novel compatibilizers and plasticizers developed from epoxidized and maleinized chia oil in composites based on PLA and chia seed flour
V. Development of a novel epoxy resin based on epoxidized chia oil as matrix and maleinized chia oil as bio-renewable crosslinker.

El artículo relacionado como estudio previo para un futuro articulo aplicado al aceite de chía como cristal líquido:

VI. Light-responsive bent-core liquid crystals as candidates for energy conversion and storage

El artículo relacionado con el estudio previo a la presente tesis ha sido:

I. Development and Characterization of Polyester and Acrylate-Based Composites with Hydroxyapatite and Halloysite Nanotubes for Medical Applications

ECUACIONES

$$\% \, Mass \; loss = \frac{Mi - Mf}{Mi} \times 100$$

Mi= masa inicial de la masa seca

Mf= masa final de la masa seca

$$IV = \frac{12.69 \times c \times (V_1 - V_2)}{m}$$

IV= índice de yodo de la muestra

c= concentración de disolución de tiosulfato sódico

V_1= Volumen de $Na_2S_2O_3$ para valorar el blanco

V_2= Volumen de $Na_2S_2O_3$ para valorar la muestra

m= masa de la muestra

$$X_{IV}(\%) = \left(\frac{IV_0 - IV_f}{IV_0}\right) \times 100$$

X_{IV}= conversión dobles enlaces

IV_0= índice de yodo inicial

IV_f= índice de yodo final

$$O_o(wt.\%) = 1.6 \times N_i \times \frac{(V - B)}{W}$$

O_o= contenido de oxígeno oxiránico

N_i= Normalidad de HBr en CH_3COOH

V= Volumen de HBr en CH_3COOH para valorar la muestra

B= Volumen de HBr en CH_3COOH para valorar el blanco

W= masa de la muestra

$Y_{OO}(\%) = \left(\frac{O_o}{O_{the}}\right) \times 100$	Y_{OO}= conversión de oxígeno oxiránico O_o= contenido en oxígeno oxiránico experimental O_{the}= contenido en oxígeno oxiránico teórico
$O_{the}(\text{wt.}\%) = \left(\frac{\frac{IV_o}{2AM_i}}{\left[100 + \left(\frac{IV_o}{2AM_i}\right) \times AM_o\right]}\right) \times AM_o \times 100$	O_{the}= contenido en oxígeno oxiránico teórico IV_0= índice de yodo inicial AM_i= peso molecular del Iodo AM_o= peso molecular del oxígeno
$S = \left(\frac{O_o}{O_{the}}\right) \times \left(\frac{IV_o}{IV_o - IV_f}\right)$	S= selectividad al oxígeno oxiránico O_o= contenido en oxígeno oxiránico experimental O_{the}= contenido en oxígeno oxiránico teórico IV_0= índice de yodo inicial IV_f= índice de yodo final
$EEW\ (g \cdot eq^{-1}) = \left(\frac{1000 \times\ W}{(V - B) \times\ N_i}\right)$	EEW= peso equivalente epoxi W= masa de la muestra V= Volumen de HBr en CH_3COOH para valorar la muestra B= Volumen de HBr en CH_3COOH para valorar el blanco N_i =Normalidad de HBr en CH_3COOH

$\rho_r = \frac{W_s - W_e}{W_w - W_e}$	ρ_r= densidad relativa W_s= masa de la muestra con picnómetro W_e= masa del picnómetro vacío W_w= masa de agua con picnómetro
$\Delta E = \sqrt{\Delta L^2 + \Delta a^2 + \Delta b^2}$	ΔE = variación de color ΔL= variación de luminancia Δa= variación de verde a rojo Δb= variación de azul a amarillo
$X_c\ (\%) = \left[\frac{\Delta H_m - \Delta H_{cc}}{\Delta H_{m(100\%)}}\right] \cdot \frac{1}{w_{sample}} \times 100$	X_c = grado de cristalinidad ΔH_m= entalpía de fusión ΔH_{cc}= entalpía de cristalización en frío $\Delta H_{m(100\%)}$= entalpía de fusión del polímero 100% cristalino w_{sample}= peso de la muestra
$W_l\ (\%) = \frac{w_0 - w}{w_0} \cdot 100$	W_l= porcentaje de pérdida de masa w_0= masa inicial de la muestra w = masa final de la muestra
$W_{abs}\ (\%) = \frac{w - w_0}{w_0} \cdot 100$	W_{abs}= porcentaje de masa a w_0= masa inicial de la muestra w = masa final de la muestra

$\text{Gel content (\%)} = \frac{w_f}{w_0} \cdot 100$	w_f= masa final de la muestra w_0 = masa inicial de la muestra
$\mathrm{C}_O = \frac{\varepsilon_O A}{h} = 1.11 \times 10^{-10}\mathrm{F}$	C_O= capacitancia en el vacío ε_O = permitividad en el vacío A = área activa de la celda h = grosor de la celda
$\eta = \frac{E_S}{(E_S + E_L)}$	η= eficiencia de almacenamiento de energía E_S = energía almacenada E_L= energía disipada

ABREVIATURAS Y TÉRMINOS

AGs o FA	ácidos grasos
AGSO	aceite de semilla de huevo aminado
APS	3-(2-aminoethilamina) propil trimethoxisilano
BCLCs	cristales líquidos de núcleo doblado
Bio-HDPE	polietileno de ultra alta densidad renovable
Bio-LDPE	polietileno de baja densidad renovable
Bio-PE	polietileno renovable
Bio-PET	Polietileno tereftalato renovable
Bio-PP	polipropileno renovable
Bio-PS	poliestireno renovable
Bio-PVC	policloruro de vinilo renovable
C14-C18	cadenas de 14 y 22 carbonos
C16:0	ácido palmítico
C18:0	ácido esteárico
C18:1	ácido oléico
C18:1 OH	ácido ricinoleico
C18:2	ácido linoleico
C18:3	ácido linolénico
CH_4	metano
CO_2	dióxido de carbono
CO_2eq	dióxido de carbono equivalente
Col	fase columnar
Col_{ob}	columnar oblicua
CSF	harina de chía
CSO o CO	aceite de chía
DC	conglomerado oscuro con límite de grano torcido
dc	corriente continua
DEHP	dietilhexil ftalato
DGEBA	diglicidil éter de bisfenol A

DIBP	diisobutil ftalato
DMEM	medio eagle modificado
DMTA	análisis térmico mecánico dinámico
DTMA	
DSC	calorimetría diferencial de barrido
DTG	primera derivada de la curva termogravimétrica.
ECO o ECSO	aceite de chía epoxidado
EDS	espectroscopia de rayos X de energía dispersiva
EDTA	ácido eildiaminotetraacético
EEW	peso equivalente epoxi
EGDMA	dimetilacrilato de etilenglicol
ELO	aceite epoxidado de linaza
EMA	etil metacrialto
E_s	energía almacenada
ESBO o ESO	aceite epoxidado de soja
EVO	aceite vegetal epoxidado
F-gas	gases fluorados
FAME	metil esteres
FRA	analizador de respuesta frecuencia
G′ o E′	módulo de almacenamiento
GC	cromatografía de gases
GEI	gases del efecto invernadero
GPS	3-glycidyloxypropyl) trimethoxysilane
H_2O_2:DB	ratio molar de peróxido de hidrógeno respecto dobles
MR	enlaces
HA	hidroxipatita
HBr	ácido bromhídrico
HDT	temperatura de deflexión térmica
HEMA	2-hidroxietilo metacrilato
HFC	hidrofluorocarbonos
HHPA	hexahidroftalatico anhídrido
HNTs	nanotubos de halloisita

ITO	óxido de índio y estaño
IY o IV	índice de yodo
MA	anhídrido maleico
LC	Cristal líquido
MCO	aceite maleinizado de chía
MFI	índice de fluidez
MLO	aceite maleinizado de linaza
MNA	anhídrico metil nádico
MPS	trimethoxi propilsilano
MTHPA	metil tetrahidroftalatico anhídrido
MUFA	ácidos grasos monoinsaturados
N_2O	óxido nitroso
O_o	contenido de oxigeno oxiránico
O_{the}	oxígeno oxiránico teórico
P-E	polarización frente campo eléctrico
PA y A	poliamida y Acrílica
PA-11	poliamida-11
PBAT	poli(butilén adipato-co-tereftalato)
PBS	poli(butilén succinato)
PBS	solución salina tamponada con fosfato
PBSA	poli(butilén succinato-co-adipato)
PC	policarbonato
PCF	perfluorocarbonos
PCL	poli(caprolaptona)
PDLA	poli D-láctico
PDLLA	poli D-,L-láctico
PE	poliéster
PE	polietileno
PE-g-MA	copolimero de injerto de etileno injertado y anhídrido maleico
PEEK	polieteretercetona
PEG	polietilen glicol

PEO	
PEMA	poli(etil metacrilato)
PES	poliéter sulfona
PET	tereftalato de polietileno
PHAs	polihidroxialcanoatos
PHB	poli(3-hidroxibutirato)
PHBH	poli(3-hidroxibutirato-co-3-hidroxihexanoato)
PHBV	poli(3-hidroxibutirato-co-3- hidroxivalerato)
PHEMA	poli(2-hidroxietilo metacrilato)
(P(HEMA-co-EMA))	poli(etil metacrilato) copolimerizado con etil metacrialto
phr	partes por cada cien de resina
PKA	cardamol derivado de fenalcamina
PLA	ácido Poliláctico
PLLA	poli L-Láctico
POM	microscopio óptico polarizado
POM	polioximetileno
PP	polipropileno
P_r	polarización remanente
P_s	polarización de saturación
PS	poliestireno
PSN	harina de cáscara de almendras
PTs	ftalatos
PUFA	ácido graso poliinsaturado
PVC	policloruro de vinilo
RMN	resonancia magnética nuclear
S	selectividad
SBF	fluido humano simulado
SEM	microscopia electrónica de barrido
SF_6	hexafluoruro de azufre
SFA	ácidos grasos saturados
SmC_AP_A	esméctic C antiferroelectrico polar (anticlinico)

SmCP	fase polar esméctica C
$T_{5\%}$	temperatura a la pérdida de 5% en peso
tan δ	factor de amortiguamiento
T_{cc}	temperatura de cristalización en frío
TCSF	harina de chía tratada con silano
T_g	temperatura transición vítrea
TGA	análisis termogravimétrico
THF	tetrahidrofurano
THPA	tetrahidroftalatico anhídrido
T_m	temperatura de fusión
T_{max}	temperatura de máxima degración
TPU	poliuretano termoplastico
UP	poliéster insaturado
VFT	vogel-Fulcher-Tamman
VST	temperatura de reblandecimiento Vicat
WPC	wood plastic composite
X_c	cristalinidad
Y_{oo}	rendimiento oxigeno oxiránico
^{1}H NMR	resonancia magnética nuclear de protones
α-C18:3	ácido α-linolénico
ΔH_{cc}	entalpía de la cristalización en frío
ΔH_m	entalpía de la fusión
α-C18:3(9,11,13)	ácido alfa-eleoestearico
γ	proceso baja temperatura movimiento molecular
γ-C18:3	ácido γ -linolénico
ε'	constante elástica dieléctrica
ε''	factor de pérdida dieléctrico
η	eficiencia de energía almacenada
θ	ángulo de inclinación
σ'	conductividad compleja

LISTADO DE FIGURAS

Figura I.1. Emisiones antropogénicas de GEI a la atmósfera. Adaptado de [3]. 47
Figura I.2. Producción mundial de plásticos y su previsión hasta 2050. Adaptado de [8]. 49
Figura I.3. Clasificación de polímero según el origen y capacidad de biodegradarse. Adaptado de [23]. 55
Figura I.4. Unidad monomérica de algunos de los polímeros de origen petroquímico no biodegradables: (a) comunes, (b) técnicos y (c) de altas prestaciones. 57
Figura I.5. Monómeros de algunos de los polímeros de origen petroquímico biodegradables: (a) alifáticos y (b) aromáticos. 59
Figura I.6. Esquema general de obtención de polímeros biobasados mediante materia primera de 1ra generación. Adaptado de [52]. 62
Figura I.7. Clasificación de polímeros de origen renovable biodegradables. 63
Figura I.8. Polímeros de la familia polihidroxialcanoatos (PHA). 65
Figura I.9. Obtención de los monómeros de ácido láctico a partir de fuentes renovables disponibles. Adaptado de [63]. 66
Figura I.10. Métodos para la polimerización de monómeros del ácido láctico para formar PLA. Adaptado de [67]. 67
Figura I.11. Esquema del proceso de compostaje del PLA. 68
Figura I.12. Representación esquemática del entrecruzamiento obteniendo una red tridimensional. Adaptado de [74]. 69
Figura I.13. Representación esquemática de las teorías de plastificación. Adaptado de [84]. 73
Figura I.14. Ejemplo de estructura química del triglicérido. 76
Figura I.15. Ejemplo de estructura química de triglicéridos con enlaces en posición *cis* y *trans*. 81
Figura I.16. Producción de aceites vegetales a nivel mundial. Adaptado de [113]. 82
Figura I.17. Esquema de prensado de aceite mediante el método por husillo. 83
Figura I.18. Esquema de la reacción de epoxidación. Adaptado de [126]. 87
Figura I.19. Esquema de reacciones secundarias durante la reacción de epoxidación. Adaptado de [130]. 88

Figura I.20. Mecanismos de adición del anhídrido maleico en la reacción de maleinización del aceite vegetal. Adaptado de [141]. 90
Figure II.1. Variation of contact angle in compounds based on (a) PCL/PLA and (b) PHEMA/EMA. 134
Figure II.2. SEM images (5000x) taken for hydroxyapatite nucleation analysis on samples based on PCL/PLA. 135
Figure II.3. SEM images (5000x) taken for hydroxyapatite nucleation analysis on samples based on PHEMA/EMA. 136
Figura II.4. Ca/P ratio after 7 and 14 days of incubation in SBF obtained by EDS on nanocomposites based on: a) PCL and PCL/PLA, b) PHEMA and P(HEMA-co-EMA). 137
Figure II.5. SEM images (400×) taken for cell proliferation at 1 and 14 days on samples based on PCL/PLA and PHEMA/EMA. 138
Figure II.6. Results of degradation: mass loss (%) after 4, 8 and 12 weeks for PCL-based materials 139
Figure II.7. Results of Young Modulus following 4, 8 and 12 weeks of degradation for PCL/PLA based materials. 140
Figura III.1. Representación esquemática del trabajo realizado durante la tesis doctoral. 153
Figure IV.1.1. Schematic representation of epoxidation by means of in situ formed peroxyacids. 169
Figure IV.1.2. Effect on Iodine value (IV) of the MR 0.75 and 1.50 during the epoxidation process. 178
Figure IV.1.3. Effect on oxirane oxygen (O_o) of the MR 0.75 and 1.50 at 60°C during the epoxidation process. 179
Figure IV.1.4. Effect on Iodine value (IV) of the temperature (60 °C, 70 °C, and 75 °C) with MR 1.50 during the epoxidation process. 180
Figure IV.1.5. Effect on oxirane oxygen (O_o) of the temperature (60 °C, 70 °C, and 75 °C) using MR 1.50 during the epoxidation process. 182
Figure IV.1.6. FTIR spectrum of CSO. 183

Figure IV.1.7 .FTIR spectra of ECSO obtained with different epoxidation conditions by the analysis of characteristic peaks of the double bonds (a) 3010 cm^{-1} ($=CH_{(v)}$), (b) 1652 cm^{-1} ($C=C_{(v)}$) and (c) 723 cm^{-1} ($C=C_{(cis\text{-}\delta)}$).....184
Figure IV.1.8. FTIR spectra of ECSO obtained with different epoxidation conditions by the analysis of characteristics peaks of (a) oxirane oxygen, and (b) hydroxyl groups.....185
Figure IV.1.9. Comparison of CSO and ECSO by ^{1}H NMR spectra.....186
Figure IV.1.10. Influence of the MR and temperature on the color during the epoxidation process of the chia seed oil (CSO). (a) Untreated chia seed oil (CSO), (b) ECSO MR 0.75 at 60 °C, (c) ECSO MR 1.50 at 60 °C, (d) ECSO MR 1.50:1 at 70 °C and (e) ECSO MR 1.50 at 75 °C.....189
Figure IV.2.1. Schematic representation of chemical interactions between PLA and ECO.....209
Figure IV.2.2. Plot evolution of characteristic stress-strain curves of PLA with different epoxidized chia seed oil (ECO) contents.....215
Figure IV.2.3. Plot evolution of tensile mechanical properties of PLA with different epoxidized chia seed oil (ECO) contents.....215
Figure IV.2.4. Plot evolution of Shore D hardness and impact absorbed energy of PLA with different epoxidized chia seed oil (ECO) content.....216
Figure IV.2.5. Fracture surface morphology of Charpy test at 1000x by field emission scanning electron microscopy (FESEM): (a) neat PLA; (b) PLA_2.5%ECO; (c) PLA_5%ECO; (d) PLA_7.5%ECO; (e) PLA_10%ECO; and (f) PLA_10%ECO at 2500×.
.....217
Figure IV.2.6. Plot evolution of dynamic mechanical thermal analysis (DMTA) of PLA with different ECO contents: (a) storage modulus (G'); (b) damping factor (tan δ).....218
Figure IV.2.7. Thermal parameters of degradation of PLA with different epoxidized chia seed oil (ECO) contents. (a) Weight loss; (b) derivative thermogravimetry. $T_5\%$ is temperature at 5% weight loss; T_{max} is temperature at maximum degradation....222
Figure IV.2.8. Visual appearance of disintegration under composting conditions..223
Figure IV.2.9. Weight loss recorded during disintegration test.....224

Figure IV.2.10. Migration of epoxidized chia seed oil (ECO) plasticizer in PLA matrix by n-hexane solvent extraction. 225
Figure IV.3.1. Fracture surface morphology of Charpy test by FESEM at 1000x: (a) Bio-based high-density polyethylene; (b) 20 wt.% untreated chia seed flour; (c) 20 wt.% treated chia seed flour. 253
Figure IV.3.2. Evolution of storage modulus (G') of bio-based high-density polyethylene (Bio-HDPE) with 20 wt.% of untreated (20UT) and treated (20T) chia seed flour. 254
Figure IV.3.3. Thermal parameters of degradation of bio-based high-density polyethylene (Bio-HDPE) with 20 wt.% of untreated (20UT) and treated (20T) chia seed flour (CSF). (a) Weight loss; (b) Derivative thermogravimetry 256
Figure IV.3.4. Water uptake of bio-based high-density polyethylene (Bio-HDPE) with 20 wt.% of untreated (20UT) and treated (20T) chia seed flour. 257
Figure IV.3.5. Weight loss of bio-based high-density polyethylene (Bio-HDPE) with 20 wt.% of untreated (20UT) and treated (20T) chia seed flour. 258
Figure IV.3.6. Effect of weight percentage of treated chia seed flour with APS on tensile properties in bio-based high-density polyethylene (Bio-HDPE): (a) Tensile strength; (b) Tensile modulus; (c) Elongation at break. 260
Figure IV.3.7. Effect of weight percentage of treated chia seed flour with APS on flexural properties in bio-based high-density polyethylene (Bio-HDPE). 261
Figure IV.3.8. Fracture surface morphology of Charpy test by FESEM at 250 × with different percentage of treated chia seed flour: (a) Bio-based high-density polyethylene; (b) 10 wt.%; (c) 20 wt.% (d) 30 wt.%; (e) 40 wt.%. 263
Figure IV.3.9. Evolution of storage modulus (G') in bio-based high-density polyethylene (Bio-HDPE) with different weight percentage of treated chia seed flour with APS. 264
Figure IV.3.10. Thermal parameters of degradation of bio-based high-density polyethylene (Bio-HDPE) with different weight percentage of treated chia seed flour with APS. (a) Weight loss; (b) Derivative thermogravimetry. $T_{5\%}$ is temperature at 5% weight loss; T_{max1} and T_{max2} is maximum degradation temperature for first and second stage. 266

Figure IV.3.11.. Water uptake of bio-based high-density polyethylene (Bio-HDPE) with different weight percentage of treated chia seed flour with APS. 267
Figure IV.3.12. Visual appearance of bio-based high-density polyethylene (Bio-HDPE) with different weight percentage of treated chia seed flour with APS. 268
Figure IV.3.13. Weight loss of bio-based high-density polyethylene (Bio-HDPE) with different weight percentage of treated chia seed flour with APS. 270
Figure IV.3.14. Visual appearance of disintegration of bio-based high-density polyethylene (Bio-HDPE) with different weight percentage of treated chia seed flour with APS under compost conditions. 270
Figure IV.4.1. Scheme of the chemical structure of different compatibilizers used. 291
Figure IV.4.2. FTIR spectra of poly(lactic acid) (PLA) and 15 wt.% chia seed flour (CSF) composites with different compatibilizers. 297
Figure IV.4.3. Mechanical properties of poly(lactic acid) (PLA) and 15 wt.% chia seed flour (CSF) composites with different compatibilizers; (a) tensile strength and modulus, (b) elongation at break. 300
Figure IV.4.4. (a) Surface morphology of chia seed flour (CSF) by field emission electron microscopy (FESEM) at 500x; (b) Histogram of CSF particles. 303
Figure IV.4.5. Surface morphology of fractured samples by field emission electron microscopy (FESEM) of poly(lactic acid) (PLA) and 15 wt.% chia seed flour (CSF) composites at 500x: (a) PLA; (b) PLA/CSF; (c) PLA/CSF_S; (d) PLA/CSI; (e) PLA/CSF_ECO; (f) PLA/CSF_MCO. 305
Figure IV.4.6. Differential scanning calorimetry (DSC) of poly(lactic acid) (PLA) and 15 wt.% chia seed flour (CSF) composites with different compatibilizers at 10 $^{o}C \cdot min^{-1}$. 308
Figure IV.4.7. (a) Thermogravimetric analysis (TGA) and (b) first derivate thermogravimetric (DTG) curves of poly(lactic acid) (PLA) and 15 wt.% chia seed flour (CSF) composites with different compatibilizers. 310
Figure IV.4.8. Dynamic mechanical thermal analysis (DMTA) of poly(lactic acid) (PLA) and 15 wt.% chia seed flour (CSF) composites with different compatibilizers; (a) storage modulus (G') and (b) damping factor (tan δ). 312
Figure IV.4.9. Water uptake of poly(lactic acid) (PLA) and 15 wt.% chia seed flour (CSF) composites with different compatibilizers. 314

Figure IV.4.10. Weight loss during the disintegration process in controlled compost oil of poly(lactic acid) (PLA) and 15 wt.% chia seed flour (CSF) composites with different compatibilizers. 316
Figure IV.4.11. Visual appearance of the disintegration process in controlled compost oil of poly(lactic acid) (PLA) and 15 wt.% chia seed flour (CSF) composites with different compatibilizers. 317
Figure IV.5.1. Monomer preparation and chemical structure of bio-based epoxy resin, crosslinkers and initiator. Note that only generic addition of maleic anhydride in MCO is shown, but various modes can take place. 341
Figure IV.5.2. Fourier transform infrared (FT-IR) spectrum of raw materials: (a) CO, (b) ECO, (c) MCO and (d) MNA. 347
Figure IV.5.3. ^{1}H NMR spectra of novel bio-based crosslinker (MCO) with possible types of MA incorporation. 348
Figure IV.5.4. Differential scanning calorimetry (DSC) of ECO crosslinked with different MNA:MCO mixtures at 10 $^{o}C\ min^{-1}$. 351
Figure IV.5.5. Visual appearance of ECO crosslinked with different MNA:MCO mixtures after Soxhlet extraction. 353
Figure IV.5.6. Fourier transform infrared **(**FT-IR) spectra of cured samples of ECO crosslinked with different MNA:MCO mixtures. 354
Figure IV.5.7. Flexural properties of ECO crosslinked with different MNA:MCO mixtures. 355
Figure IV.5.8. Schematic proposal of polymerization effect of different MNA:MCO mixtures on crosslinked ECO structures. 356
Figure IV.5.9. Dynamic mechanical thermal analysis (DMTA) of ECO crosslinked with different MNA:MCO mixtures; (a) storage modulus (E') and (b) damping factor. 358
Figure IV.5.10. SEM images of fractured samples of crosslinked ECO with different MNA:MCO mixtures at 500×: (a) MNA100, (b) MNA70:MCO30, (c) MNA50:MCO50 and (d) MNA70:MCO30. 359
Figure IV.6.1. Chemical structure and notation used to refer to the pristine bent-core compounds (NG75, IP33 and IP33) and mixtures containing 5% molar % of azobenzene molecules (5%-IP33 and 5%-IP31). 382

Figure IV.6.2. Selected polarised optical microphotographs showing the mesophases displayed by the pristine bent-core compounds (a, b, c) and the mixtures containing 5% of IP33 (d) and IP31 (e). Scale bar corresponds to 40 μm. SmC_AP_A: smectic C antiferroelectric polar (anticlinic); Col_{ob}: oblique columnar.....385
Figure IV.6.3. 3D-plots showing the dielectric loss factor, ε'', as a function of frequency and temperature, corresponding to: (a) NG75; (b) IP33; (c) IP31; (d) 5%-IP33; and (e) 5%-IP31, obtained in isothermal steps, on cooling from their isotropic phases. 387
Figure IV.6.4. Effect of direct current electrical fields of various amplitudes on the dielectric loss factor, ε'', measured in the smectic phase of NG75 (T=90 ^{o}C), and assignation of the α and β relaxations to molecular modes. 388
Figure IV.6.5. Arrhenius plots obtained for the maxima ($fmax$) of the dielectric loss factor curves, ε'', and apparent activation energies, E_a, estimated for the α and β relaxations (see white points as selected linear regions).....388
Figure IV.6.6. Hysteresis loops and associated polarised optical micrographs showing the ferroelectric response of IP33 at: (a) 50Hz and (b) 1 Hz (T=130 ^{o}C, SmCP phase).....391
Figure IV.6.7. UV-visible spectra of the light-responsive bent-core based samples: (a) IP33, IP31, 5%-IP33 and 5%-IP31 measured in ~10^{-5} M THF solutions at room temperature (IP31 and IP33: 1.2 x 10^{-5} M; 5%-IP31: 11.3 x 10^{-5} M; 5%-IP33: 37.8 x 10^{-5} M). IP31 spectra measured before and at different times after light irradiation (260 mW $\cdot$ cm^{-2}; 365 nm): (b) in THF solution at room temperature; and (c) on a film cast on quartz at its mesophase (145 °C). Arrows in (b) and (c) indicate signal recovery after UV irradiation (t = 0 min) while samples were kept in the dark.....392
Figure IV.6.8. Frequency dependence of the real component, σ', of the complex conductivity, σ *, measured at the mesophases of the light-responsive bent-core based materials before (blue), during (orange) and after (grey) UV illumination (200 mW $\cdot$ cm^{-2}; 365 nm).....394
Figure IV.6.9. Time-dependence of the dielectric elastic constant, ε', measured at 1 Hz and 160 ^{o}C (mesophases range) for the four light-responsive bent-cores under study, when submitted to UV off-on-off cycles (200 mW $\cdot$ cm^{-2}; 365 nm). Arrows and steps correspond to 5%-IP31. 395

Figure IV.6.10. Hysteresis loops showing the effect of light on the ferroelectric response for the samples containing azo-bent core molecules (values taken at 1 Hz in their mesophases).....397
Figure IV.6.11. Polarised optical micrographs obtained for IP31 at T=166 ^{o}C: (a) application of UV irradiation (1200 mW · cm^{-2}; 365 nm), followed by (b) strong electrical fields (75 kV · cm^{-1}), resulting in a granular smectic phase. 399
Figure IV.6.12. Polarised optical micrograph obtained for a IP31 sample following the UV and electrical fields cycle described in Figure IV.6.11, resulting in coexisting regions of columnar and smectic phases. 399
Figure IV.S6.1. Picture of the experimental setting including the polarised optical microscope, the Linkam heating stages holding the ITO measuring cells, the Dymax Bluewave QX4 TM LED probe, and connexions to the dielectric and ferroelectric analysers. 401
Figure IV.S6.2. Differential scanning calorimetry (DSC) thermograms obtained for the five samples under study, in their cooling (above), and second heating (below) scans at ±10 ^{o}C · min^{-1}. The small peak appearing at around 100 ^{o}C on the reheating curves of NG75-containing compounds did not correspond to any phase transition reported earlier (see **Table IV.S6.1** below), nor was visible under our current microscope experiments. 402
Figure IV.S6.3. Double logarithmic plots of the dielectric elastic constant, ε', as a function of frequency and temperature, corresponding to the five bent-core based materials, obtained in isothermal steps on cooling from their isotropic phases. 402
Figure IV.S6.4. Double logarithmic plots of the dielectric loss factor, ε'', as a function of frequency and temperature, corresponding to the five bent-core based materials, obtained in isothermal steps on cooling from their isotropic phases.....403
Figure IV.S6.5. Double logarithmic plots of the real component of the complex conductivity, σ', as a function of frequency and temperature, corresponding to the five bent-core based materials, obtained in isothermal steps on cooling from their isotropic phases. 403
Figure IV.S6.6. Effect of direct current electrical fields of various amplitudes on the dielectric loss factor, ε'', measured in the columnar phase of IP31 (T=145 °C), and assignation of the α and β relaxations. 404

Figure IV.S6.7. Polarised optical micrographs obtained for IP31 at 145 °C, showing the banana leaves textures typical of columnar phases, before (left), during (middle) and after (right) application of electrical fields at 50 Hz (up) and 1 Hz (down). 404
Figure IV.S6.8. Hysteresis loops showing the ferroelectric response of the five samples; frequency dependence. 405
Figure IV.S6.9. Hysteresis loops showing the ferroelectric response of: (a) NG75 and its mixtures with IP33 and IP31 (130 °C, 50 Hz); (b) temperature effect on 5%-IP33 in its smectic phase (50 Hz). 405
Figure IV.S6.10. UV-visible spectra of the light-responsive bent-core based materials measured before and at different times after light irradiation (260 mW · cm^{-2}; 365 nm): (a) IP33; (b) 5%-IP33; (c) IP31; (d) 5%-IP31. Insets show the π* ← n transition in the *cis*-azobenzene at peak ~440 nm. Measurements were taken for THF solutions at room temperature (IP31 and IP33: 1.2 x 10^{-5} M; 5%-IP31: 11.3 x 10^{-5} M; 5%-IP33: 37.8 x 10^{-5} M). 406
Figure IV.S6.11. Graphs showing the kinetics of *cis*-to-*trans* (thermal) back-isomerisation for the pristine samples in solution, using the maximum absorbance values (~440 nm) of their UV-visible spectra at different times while kept in the dark (A_t) after light irradiation (A_0) (260 mW · cm^{-2}; 365 nm), until the curves recover their initial values prior to irradiation (A_∞). Estimation of the half-life times, $t_{1/2}$.....406
Figure IV.S6.12. Frequency dependence of the real component, σ', of the complex conductivity, σ*, measured at the mesophase of NG75 before (blue), during (orange) and after (grey) UV illumination (200 mW · cm^{-2}; 365 nm). 407
Figure IV.S6.13. Selected double logarithmic plots of the dielectric loss factor, ε'', as a function of frequency and temperature, for IP33 and 5%-IP33, measured before (No UV), during (UV on), and after (UV off), light irradiation (200 mW · cm^{-2}; 365 nm).407
Figure IV.S6.14. Selected double logarithmic plots of the dielectric loss factor, ε'', as a function of frequency and temperature, for IP31 and 5%-IP31, measured before (No UV), during (UV on), and after (UV off), light irradiation (200 mW · cm^{-2}; 365 nm).408

LISTADO DE TABLAS

Tabla I.1. Fuente de emisión de GEI a nivel mundial por sectores [6]. 48
Tabla I.2. Estructura química de ácidos grasos comunes con diferente grado de saturación y longitud de cadenas. Adaptado de [101]. 78
Tabla I.3. Clasificación de los principales aceites vegetales. 79
Tabla I.4. Comparativa de los métodos de extracción de aceites a partir de plantas oleaginosas. 85
Tabla I.5. Principales AGs de los aceites más empleados en el sector polimérico..... 97
Tabla I.6. Estimación de la composición de la semilla de chía tras la extracción de aceite en base a bibliografía. Adaptado de [165-166]. 98
Table II.1. Composition and coding of PCL, PCL/PLA, PHEMA, and P(HEMA-co-EMA) composites. 130
Table IV.1.1. Iodine value and theoretical oxirane oxygen content of different vegetable oils. 167
Table IV.1.2. Content of fatty acids presents in chia seeds (expressed as g of fatty acid/100 g of oil) and comparison with other studies. 177
Table IV.1.3. Main parameters used to characterize the epoxidation process of the chia seed oil (CSO) at different molar ratios and temperatures. 179
Table IV.1.4. Comparative of physico-chemical properties of chia seed oil (CSO) and epoxidized chia seed oil (ECSO). 188
Table IV.2.1. Composition of ECO plasticized PLA materials and labelling. 210
Table IV.2.2. Vicat softening temperature (VST) and heat deflection temperature (HDT) of PLA with different epoxidized chia seed oil (ECO) content. 219
Table IV.2.3. Main thermal parameters of PLA plasticized with different ECO contents obtained using DSC. 220
Table IV.3.1. Weight composition of Bio-HDPE with chia seed flour (CSF) materials and labelling. 246
Table IV.3.2. Mechanical properties for Bio-HDPE with untreated and treated chia seed flour. 252
Table IV.3.3. Main thermal parameters of Bio-HDPE with untreated and treated chia seed flour obtained using DSC. 255

Table IV.3.4. Effect of weight percentage of treated chia seed flour with APS on Shore D Hardness and impact absorbed energy. 262
Table IV.3.5. Main thermal parameters of Bio-HDPE with different weight percentage of treated chia seed flour with APS obtained using DSC. 265
Table IV.3.6. Colour coordinates (L*, a*, b*) for different weight percentage of treated chia seed flour with APS. 268
Table IV.3.1. Summary of compositions and codes of samples manufactured. 292
Table IV.4.2. Impact-absorbed energy and Shore D hardness of poly(lactic acid) (PLA) and 15 wt.% chia seed flour (CSF) composites with different compatibilizers. 302
Table IV.4.3. Main thermal properties of poly(lactic acid) (PLA) and 15 wt.% chia seed flour (CSF) composites with different compatibilizers in terms of glass transition temperature (T_g), cold crystallization temperature (T_{cc}), cold crystallization enthalpy (ΔH_{cc}), melting Temperature (T_m), melting enthalpy (ΔH_m) and crystallinity (X_c). 308
Table IV.5.1. Mixture percentages of ECO crosslinked with different proportions of MNA and MCO. 343
Table IV.5.2. Phase angle (δ) as a function of curing time of ECO crosslinked with different MNA:MCO mixtures obtained by plate-plate oscillatory rheometry. 352
Table IV.5.3. Gel content of ECO crosslinked with different MNA:MCO mixtures. 353
Table IV.5.4. Influence of cured samples based on ECO crosslinked with different MNA:MCO mixtures in terms of impact-absorbed energy and shore D hardness. 357
Table IV.6.1. Thermal parameters obtained for the bent-cores by differential scanning calorimetry (DSC), measured on second heating (10 $^{o}C \cdot min^{-1}$) scans, and by polarised optical microscopy (POM) measured on cooling (1 $^{o}C \cdot min^{-1}$). 384
Table IV.6.2. Values for saturated polarisation values, P_s, remanent polarisation, P_r, energy storage (E_s) and efficiency (η), as a function of UV light irradiation during 1 Hz ferroelectric loops, estimated at their respective mesophases: 130 ^{o}C (a); 145 ^{o}C (b); 90 ^{o}C (c, d). 397
Table IV.S6.1. Phase transition temperatures (obtained by polarised optical microscopy, POM, on heating and cooling ranges, 10 $^{o}C \cdot min^{-1}$); and phase structure

parameters obtained by Small Angle X-ray diffraction, SAXS, for the three pristine samples. 409
Table IV.S6.2. Values for saturated polarisation values, P_s, remanent polarisation, P_r, and energy storage, estimated for NG75 and its mixtures with IP33 and IP31, at 130 ^oC, and 50 Hz. 409
Table IV.S6.3. Half-live ($t_{1/2}$) values estimated for the *cis*-isomers, obtained from the maxima of the UV-vis curves as a function of time, **Figure IV.S6.10**. 409
Table IV.S6.4. Times required to yield 95% of the steady state ε' during isothermal experiments upon irradiation (correlate to **Figure IV.S6.9.**) 410

I. INTRODUCCIÓN

I.1. Problemática medioambiental

En la actualidad se está observando una clara problemática medioambiental que viene precedida desde los inicios de la revolución industrial (siglo XVIII-XIV), y que se acentuó con la producción masiva de plástico y combustión de productos fósiles a partir de la década de los 70 [1]. Esta problemática, conocida como "cambio climático" o "global warming" en inglés, se debe al aumento en la concentración de los "gases del efecto invernadero" (GEI) emitidos a la atmósfera. Entre los diferentes GEI, destacan el dióxido de carbono (CO_2), metano (CH_4), oxido nitroso (N_2O), y los gases fluorados (F-gas): hidrofluorocarbonos (HFC), hexafluoruro de azufre (SF_6) y perfluorocarbonos (PCF), entre otros. A pesar de que algunos gases presentan mayor efectividad como GEI, por ejemplo, el CH_4 con 28 veces más respecto al CO_2 [2], este último es el que mayor concentración en la atmósfera representa, con aproximadamente dos tercios del total de los GEI [3]. Por esta razón, toda la emisión de GEI emitidas a la atmósfera se miden en CO_2eq, teniendo en cuenta el potencial de calentamiento de cada gas diferente del CO_2. En la Figura I.1 se muestra la contribución de cada gas en las emisiones antropogénicas netas mundiales.

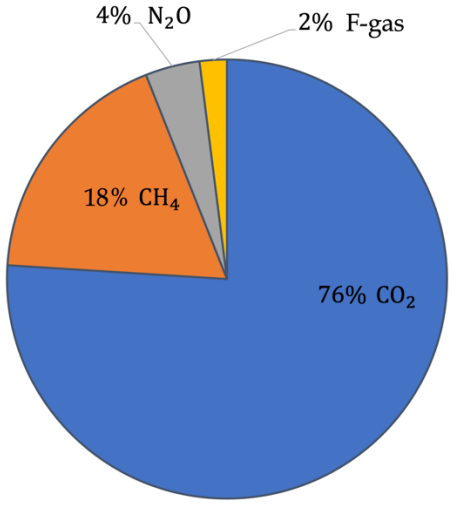

Figura I.1. Emisiones antropogénicas de GEI a la atmósfera. Adaptado de [3].

La generación de GEI está estrictamente relacionada con la quema de combustibles fósiles para la generación de energía eléctrica, transporte y diferentes procesos de

fabricación y producción de servicios, y se espera un crecimiento de la demanda de casi un 30% para 2035. Este aumento se debe a la creciente natalidad mundial, donde hay una previsión de aumento del 26% en 2050 con una población que podría alcanzar una cifra de 9.7 billones [4]. De esta energía, solo el 40% es de origen renovable, y para el año 2035 se espera que esta alcance el 55% de la energía producida [5]. En la Tabla I.1, se observa la contribución de GEI emitidos por diferentes sectores derivados de la actividad humana.

Tabla I.1. Fuente de emisión de GEI a nivel mundial por sectores [6].

	Contribución GEI (%)
Energía en industria	24,2
Agricultura	18,4
Energía Residencial	17,5
Transporte	16,2
Otros derivados de la energía	15,3
Industria	5,2
Residuos	3,2

A pesar de que la gran mayoría de contribución de GEI es por parte de la producción energética, agrícola y transporte (73,2% del total), una de las industrias que suele pasar por alto debido a su baja contribución es la del plástico. En la actualidad, la producción del plástico supone el equivalente a más del 3% de las emisiones mundiales provenientes de combustibles fósiles [7]. La emisión que conlleva la generación del plástico no solo es durante el proceso de producción, si no que también se libera durante su fin de ciclo de vida, por ejemplo, durante la gestión final de estos residuos. La previsión anual global de producción de plástico ha aumentado rápidamente de 100 millones de toneladas en 2002 a 367 millones de toneladas en 2020 [8] tal y como se puede observar en la Figura I.2. Cabe destacar que la producción mencionada no incluye la producción de plásticos reciclados, por lo que la producción real sería aún mayor. La tendencia es alcista, a pesar de que en 2020 se observe una producción ligeramente inferior al año anterior (2019) debido a la crisis mundial provocada por la crisis sanitaria del COVID-19. Para el año 2050 se espera que aumente la producción hasta las 590 millones de toneladas, significando un aumento del 60% respecto al 2020 [9].

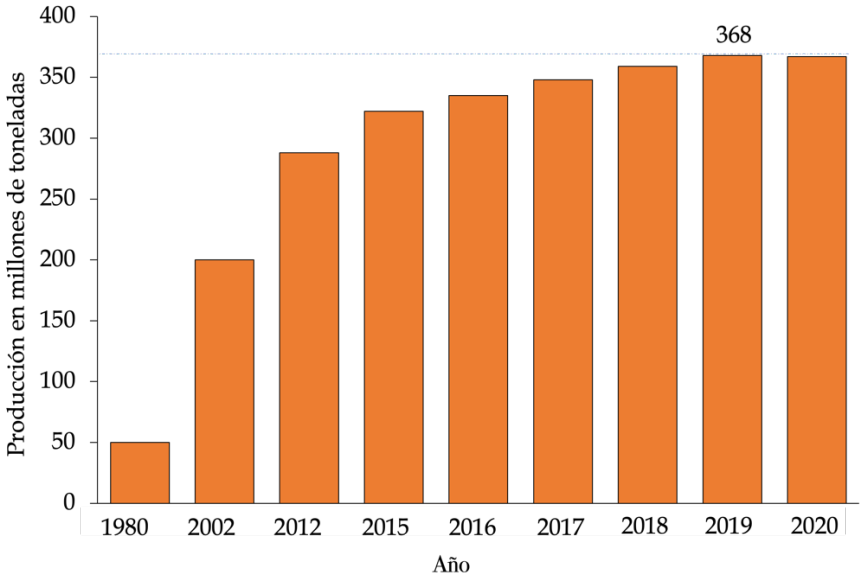

Figura I.2. Producción mundial de plásticos y su previsión hasta 2050. Adaptado de [8].

El crecimiento de producción de la industria del plástico contribuirá a aumentar del 3% al 15% las emisiones de GEI debido al aumento de la demanda de productos plásticos, siendo entonces una de las fuentes de emisión con mayor contribución [10]. De acuerdo con datos de la agencia internacional de energía, la gran mayoría de GEI provenientes de la industria del plástico es debido al empleo del petróleo como materia prima precursora de los polímeros y al uso de energía fósil para su producción [11]. Además, más del 90% de los diferentes tipos de plásticos comerciales producidos (aproximadamente 1000) provienen de materia prima de origen fósil, con un consumo del 6% del combustibles fósiles a nivel global [12]. En la evaluación cuantitativa de la emisiones de GEI de los plásticos a lo largo de su ciclo de vida, se pueden destacar tres etapas [13].

Etapa de extracción y producción de materia prima

Abarca todo lo necesario desde que se extrae la materia prima hasta que llega a la industria para la conversión en polímeros. Es la etapa donde se produce la mayor emisión de GEI, con un 61% del total del ciclo de vida. Entre los polímeros con mayor emisión destacan por un lado la familia de las poliolefinas entre las que se encuentran el polipropileno (PP) y el polietileno (PE), debido a que su consumo global representa un 50% del mercado de plásticos. Por otro destacan polímeros como el poliéster (PE), la poliamida (PA) y las resinas acrílicas (AA).

Etapa de procesado

Se produce la transformación que convierte los polímeros en productos finales. En esta etapa destacan las principales formas de procesado de polímeros como pueden ser el moldeo, el roto moldeo, la extrusión o la inyección. Estas contribuyen en un 30% en la emisión de GEI debido principalmente al consumo energético necesario para la transformación de la materia prima en productos de consumo.

Etapa del fin de ciclo de vida

Esta etapa es la que mayor controversia genera, haciendo referencia a la gestión final de los productos de origen petroquímico con una contribución aproximada del 9% en la emisión de GEI. Existen diferentes gestiones finales de los productos pláticos: (1) vertederos, donde los productos son almacenados durante largos peridodos de tiempo; (2) reciclaje con el fin de disminuir el empleo de materia prima virgen y, por último, (3) la incineración con el objetivo de generar energía debido al alto poder calorífico de los polímeros. La incineración es la gestión con mayor emisión de GEI con una contribución del 60% respecto a los diferentes tipos de gestión de productos plásticos tras su ciclo de vida, y representando el 5,4% respecto al ciclo de vida total.

A pesar de estos datos, se debe recalcar que la responsabilidad medioambiental no es solo disminuir las emisiones de GEI y con ello contribuir a mitigar el cambio climático, si no que es importante también preservar el hábitat y el medioambiente en buenas condiciones. Es por lo que la gestión de los residuos es una de las partes más importantes. De acuerdo con el informe generado por Plastics Europe [14], más de 29

millones de toneladas de residuos plásticos fueron recogidos en 2020 en Europa. De esa cantidad, el 76,6% fue gestionada correctamente, principalmente mediante una etapa de reciclaje (34.6%) o de recuperación energética (42%). En el caso de la incineración, es un proceso donde se emite gran cantidad de gases contaminantes no solo de GEI, si no de metales pesados y compuestos orgánicos que afectan al medioambiente, y como consecuencia, también a los seres humanos [15]. Por otro lado, el 23,4% fue destinado a vertederos, generando un considerable impacto visual además de problemas medioambientales. Sin embargo, existen residuos plásticos no gestionados mediante los medios correctos, depositándose en el medioambiente como en océanos, ríos y medios terrestres, donde acaban afectando a los diferentes ecosistemas. Además, en la gran mayoría de productos plásticos, estos residuos no tienen la capacidad de ser biodegradados por el medioambiente, con lo cual se trata de residuos de muy larga estabilidad y por tanto difícil eliminación por medios naturales. Se estima que en todo el mundo se vierte entre 4,6 y 12,7 millones toneladas de plástico a los océanos cada año, lo que equivale a 50 kg de plástico por cada metro de costa mundial [16].

Durante los últimos años, varias estrategias han sido propuestas para reducir la emisión de GEI y el impacto medioambiental de los plásticos. Entre las propuestas, se debate tanto el origen de la energía empleada para su producción como de la materia prima de origen del plástico, las cuales serán descritas continuación.

Sustitución de plásticos de origen petroquímico

La sustitución de plásticos de origen petroquímico por plásticos derivados de fuentes de origen renovable como del azúcar de caña o maíz, es una de las propuestas que mayor peso tiene en la actualidad. De acuerdo con el estudio realizado por Spierling *et al.* [17] y teniendo en cuenta las limitaciones de disponibilidad de información, se estima que, si se sustituyeran 2/3 de todos los plásticos por los de origen renovable, se emitirían entre 241 y 316 millones de toneladas menos de CO_2eq a la atmósfera por año. En la actualidad, nos encontramos con una baja cuota de mercado de plásticos de origen renovable con menos del 1% [18]. Por ello, tanto la unión europea (UE) como los países más concienciados con el medioambiente, han

propuesto diferentes estrategias para incentivar la producción y uso de plásticos de origen renovable [19].

Producción de plásticos mediante energía renovable

Este es uno de los escenarios más interesantes, donde la producción de plásticos se lleva a cabo con energía obtenida a partir de fuentes renovables. Aunque es cierto que esta estrategia requiere de una modificación sustancial del actual escenario energético, se ha estimado que es posible disminuir entre un 50 y 75% las emisiones de CO_2eq mediante el empleo de energía renovable [20]. Debido a que los procesos de transformación de polímeros requieren de elevada cantidad de energía, la sustitución del actual sistema energético por un modelo basado en las energías renovables, requiere de un elevado esfuerzo sostenido en el tiempo por parte de todos los actores energéticos.

Reciclaje

El reciclaje es una de las propuestas más afianzadas por parte de la población y la industria. A pesar de que en el proceso de reciclaje pueden existir pérdidas de materia prima y calidad de la misma, este método es una de las gestiones de fin de vida más interesante. Estudios recientes estimaron que un escenario donde la totalidad de los productos poliméricos de origen petroquímico fueran reciclados, las emisiones de GEI serían similares o incluso menores que, comparándolo con la sustitución total por polímeros de origen renovable [13].

Otras de las propuestas que es independiente de lo comentado con anterioridad, es disminuir la tasa de producción. Esto podría permitir una disminución de GEI, pero debido a la falta de regulación en ciertos países, es un objetivo complicado de alcanzar. En el caso de la UE, la producción se ha visto controlada, e incluso ha disminuido respecto a años anteriores. Por ejemplo, desde 2009 hasta 2017 la producción anual aumentó de 55 a 64,5 millones de toneladas. Sin embargo, en el año 2020 la producción de plásticos se ha reducido de nuevo hasta valores de 2009 con 55 millones de toneladas [21]. Por tanto, para disminuir progresivamente las emisiones de GEI no bastaría con las estrategias mencionadas de

forma independiente, siendo un escenario conjunto y complicado de realizar, al menos, a corto-medio plazo. Por ello, una combinación de todas ellas es la que permitiría obtener unos resultados óptimos con el fin de disminuir la emisión lo antes posible. Es tal la importancia que según la comisión de la UE [22], las emisiones de GEI deben reducirse al menos un 55% para el 2030 comparado con los valores en 1990.

I.2. Polímeros en ingeniería

Como se ha comentado en el anterior apartado, tanto el origen como la gestión final del ciclo de vida de los polímeros, tienen una clara influencia en la capacidad contaminante de éstos. Todos los problemas ocasionados por la incorrecta gestión de los residuos por parte de la población y producción descontrolada en la industria de los plásticos, ha ocasionado una concienciación por parte de la sociedad. En la actualidad, la comunidad científica está continuamente buscando nuevas formulaciones para obtener materiales poliméricos más sostenibles y respetuosos con el medioambiente.

I.2.1. Polímeros termoplásticos

Los polímeros termoplásticos son ampliamente utilizados tanto a nivel cotidiano como a nivel industrial. Presentan una alta contribución en el cambio climático, ya que la producción de termoplásticos solo en Europa fue de 50 millones de toneladas en 2021. Los polímeros termoplásticos se pueden dividir en función de su origen y su capacidad de biodegradación tal y como se muestra en la Figura I.3, cuya contribución en las emisiones de GEI varían según esta clasificación.

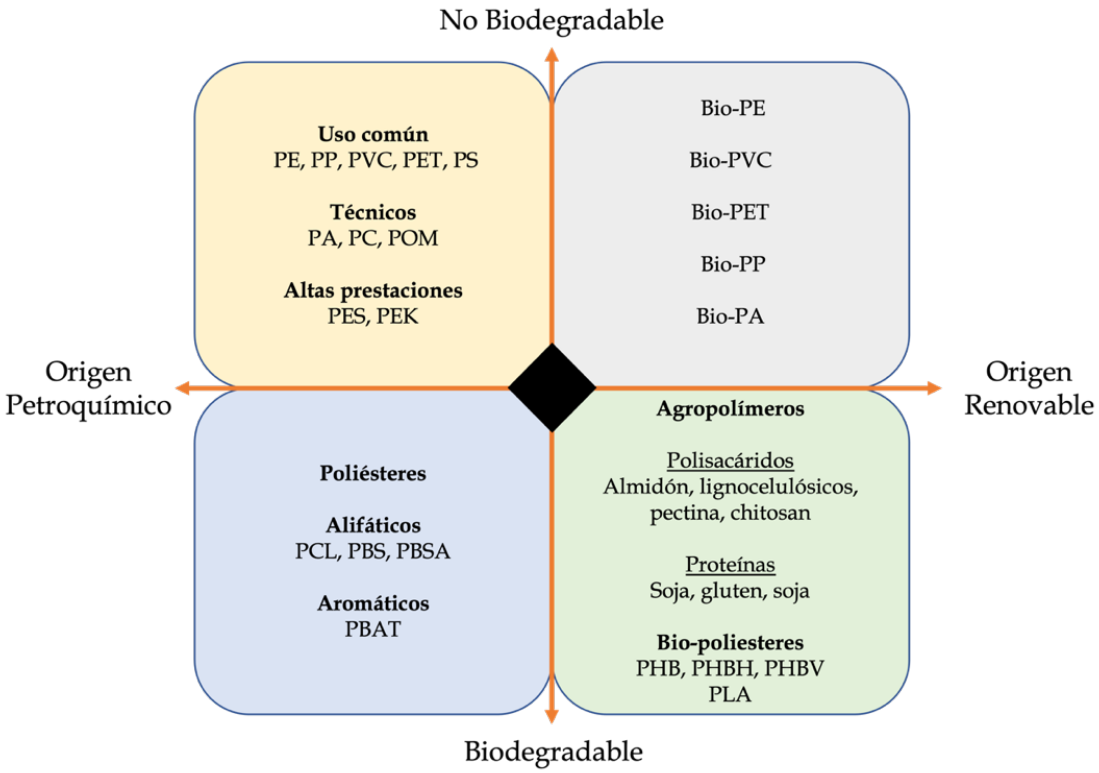

Figura I.3. Clasificación de polímero según el origen y capacidad de biodegradarse. Adaptado de [23].

I.2.1.1. Polímeros de origen fósil no biodegradables

En general, este tipo de polímeros son los de mayor empleo y conocimiento desde que se comenzaron a comercializar a principios del siglo XX. En ellos se emplea el petróleo como fuente de materia prima, lo que los convierte en polímeros de elevada producitividad en los procesos de transformación y bajo coste. En la actualidad, la gran mayoría de información que se procesa, tanto de emisiones de GEI como sobre consecuencias de la producción y gestión de residuos, es por parte de este grupo de polímeros. En este grupo se puede encontrar desde los plásticos de uso común ("commodities"), los cuales no requieren una gran exigencia mecánica, hasta plásticos más técnicos.

Los plásticos comunes más empleados en orden decreciente de demanda son: el PE en toda su gama de alta, media y baja densidad, PP, policloruro de vinilo (PVC), polietileno tereftalato (PET) y poliestireno (PS). Este grupo es utilizado sobre todo para uso cotidiano donde sus propiedades no se ven comprometidas por elevados esfuerzos mecánicos. En nuestro día a día es posible encontrarlos en sectores como el

de automoción [24], juguete [25], embalaje [26] o la construcción [27], con una cuota de mercado del 74% de todos los plásticos [28]. Estos son ampliamente utilizados por su bajo coste, buena procesabilidad y en general buenas propiedades para los requerimientos exigidos en el día cotidiano [29]. Se trata del grupo de polímeros que más GEI emiten a la atmósfera debido a su gran producción y demanda. La problemática de este grupo radica en que la materia prima de obtención es de origen fósil y son productos no biodegradables. Los problemas ambientales que conllevan estos productos pueden reducirse con una gestión correcta de reciclaje, tal y como se ha comentado con anterioridad.

Por otro lado, también existen otro tipo de polímeros con aplicaciones más específicas en ingeniería. En primer lugar, los llamados plásticos técnicos están comprendidos por las PA, policarbonato (PC) o el polioximetileno (POM) entre otros. Al ser plásticos destinados a aplicaciones concretas, el coste de producción se incrementa en comparación a los plásticos comunes. A pesar de ello, están pensados para que presenten un mayor ciclo de vida con una producción mucho menor, no generando un alto impacto medioambiental. Entre las aplicaciones más frecuentes, la PA es utilizada para aplicaciones automovilistas con altas temperaturas y especialmente sometidas al desgaste, como la poliamida 6,6 (PA6,6) [30], el PC como sustitución progresiva al vidrio en los parabrisas de los automóviles [31], y el POM en asientos de válvula en automoción [32].

Por último, entre los plásticos de altas prestaciones destacarían por un lado, la poliéter sulfona (PES) ampliamente utilizado en la fabricación de membranas para varias aplicaciones [33] y por otro lado, la polieter éter cetona (PEEK) en aplicaciones médicas como implantes craneales [34] o para aplicaciones aeroespaciales [35]. En la Figura I.4 se muestra la estructura de los polímeros mencionados con anterioridad.

Sin embargo, teniendo en cuenta el masivo uso de productos de un solo uso, la poca cuota de reciclaje y la no biodegradación [36], nuevas alternativas se están buscando para disminuir el impacto medioambiental.

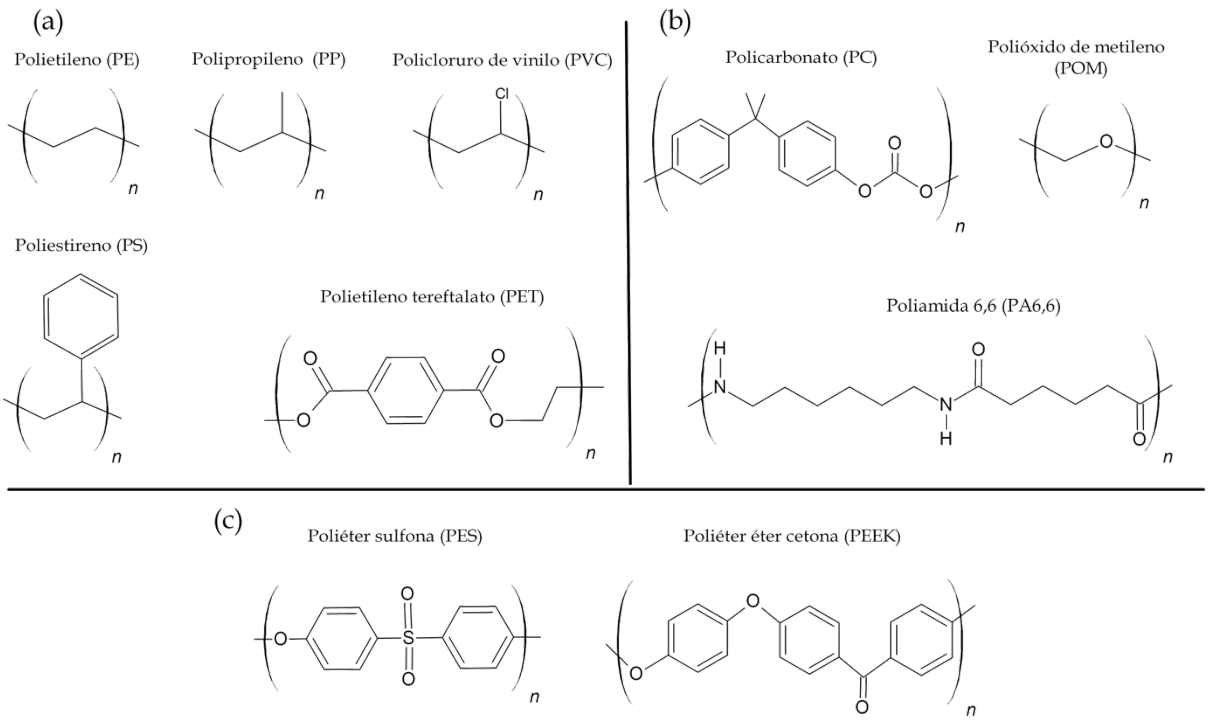

Figura I.4. Unidad monomérica de algunos de los polímeros de origen petroquímico no biodegradables: (a) comunes, (b) técnicos y (c) de altas prestaciones.

I.2.1.2. Polímeros de alto rendimiento medioambiental

Una de las propuestas para el reemplazo de los plásticos convencionales es el uso de polímeros con alto rendimiento medioambiental. Se debe indicar que dentro de este grupo, existe una diferencia bien definida entre biopolímeros y polímeros biobasados. Mientras que todos los biobasados son biopolimeros, no todos los biopolimeros pueden considerarse biobasados. Atendiendo a la definición de la Asociación Europea de los Bioplásticos, los biopolimeros deben ser o biodegradables, o proceder de una fuente renovable, o presentar ambas características [37]. Por otro lado, la ASTM define como material biobasado aquellos que provienen totalmente o de forma significativa a partir de fuentes renovables como productos de la agricultura, materiales de base biológica o de fuentes alternativas como residuos de comida [38]. De esta forma, existen polímeros biobasados pero que no necesariamente deben ser biodegradables. Respecto a la sostenibilidad de un polímero biobasado, esta dependerá de varios factores como la fuente de origen, el proceso de producción, y la gestión el ciclo final de vida del producto. Además, se considera una materia prima

renovable siempre y cuando la tasa de reposición de fuente es comparable o incluso mayor que el ratio de consumición [23].

Una de las características más importantes de algunos biopolímeros es la capacidad de biodegradación. La estructura química del polímero puede conferir más susceptibilidad para que la descomposición química ocurra a través de la acción de microorganismos, hongos, algas o bacterias, dando lugar a productos como dióxido de carbono, sales y agua [39]. Los factores que pueden afectar en este proceso son las cadenas largas de carbono, como por ejemplo la del PP que lo hace resistente a la biodegradación; la presencia de heteroatomos como puede ser la presencia de átomos de oxígenos en las cadenas; la hidrofilidad favoreciendo la actividad de los microorganismos encargados de llevar a cabo la biodegradación e incluso la cristalinidad y peso molecular, que dificulta el proceso de degradación [40]. Por otro lado, no todos los polímeros que pueden biodegradarse son compostables, ya que la compostabilidad es un método específico de biodegradación. Siguiendo la definición de compostabilidad, el polímero debe reunir tres requisitos para ser considerado como tal: (1) capacidad de biodegradarse, (2) presentar facilidad desintegrándose y, (3) no debe presentar afectos adversos o ecotoxidad tras la composición. Se debe indicar que un polímero compostable debe alcanzar una degradación superior al 90% en un periodo menor de 180 días (6 meses) en condiciones de compost [41].

Todos estos biopolímeros son propuestas más sostenibles para el medioambiente, por lo que a continuación se mostrarán los aspectos más importantes de los tres diferentes grupos existentes.

Polímeros de origen fósil y biodegradables

Estos polímeros se sintetizan a partir de materia prima de origen fósil (petróleo) pero, sin embargo, su determinada estructura química les confiere la capacidad de biodegradarse. Los principales polímeros de origen fosil y con capacidad de biodegradación son poliéster alifáticos y/o aromáticos.

Uno de los poliésteres alifáticos más destacado es la poli(caprolaptona) (PCL), que se obtiene de la apertura del anillo de la caprolactona haciendo uso de catalizadores orgánicos complejos como el octoato de estaño ($Sn(Oct)_2$) [42]. Es un

material flexible, biocompatible, y su degradación es mas lenta que otros poliésteres, por lo que se utiliza en aplicaciones médicas de larga duración con procesos de biodegradación de 2 a 4 años [43]. Por otro lado, el poli(butilén succinato) (PBS) también es un poliéster alifático obtenido de la policondensación del 1,4-butanodiol y del acido succínico o también de su anhídrido mediante la acción de un catalizador de carácter metálico [44]. Es considerado uno de los polímeros de origen fósil y biodegradables más prometedores en su grupo debido a su buena resistencia química, procesabilidad y biodegradación, con propiedades mecánicas incluso comparables con el PE y PP. Sin embargo, su alta cristalinidad le proporciona una velocidad de degradación menor que la del PCL [45]. Una forma de favorecer la biodegradación del polímero es mediante la incorporación del ácido adípico durante la síntesis química del PBS con el 1,4-butanodiol, obteniendo así el poli(butilén succinato-co-adipato) (PBSA) [46].

Respecto a los aromáticos, el poli(butilén adipato-co-tereftalato) (PBAT) es unos de los polímeros biodegradables más empleados. Este presenta una alta flexibilidad, con unas buenas propiedades de procesado e hidrofilidad. Presenta incluso mayor elongación a la rotura que otros poliéster biodegradables como el ácido poliláctico (PLA) o PBS, siendo adecuado para aplicaciones como films de uso agrícola y envasado de alimentos [47].

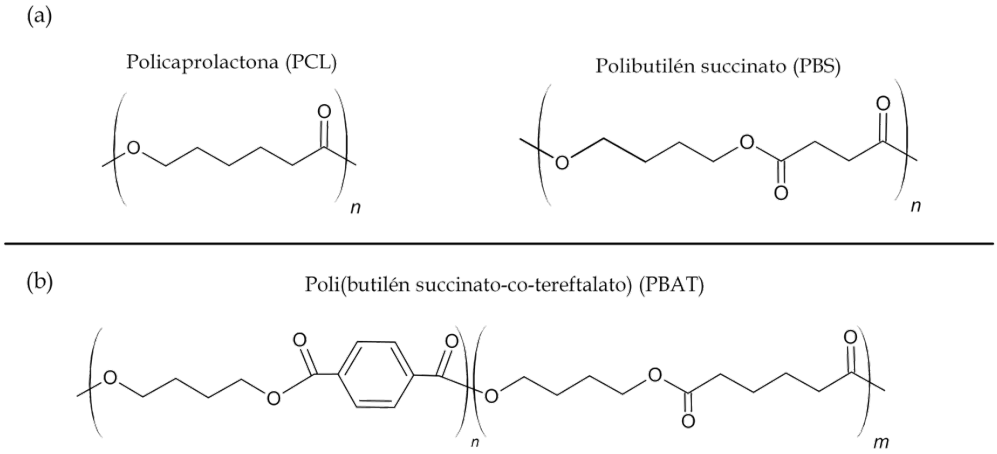

Figura I.5. Monómeros de algunos de los polímeros de origen petroquímico biodegradables: (a) alifáticos y (b) aromáticos.

Polímeros de origen renovable no biodegradables

Este grupo de polímeros presentan estructuras químicas similares a las de origen petroquímico, con la salvedad de que la materia prima de origen es obtenida a partir de fuentes renovables. A pesar de que la procedencia de la materia prima sea diferente, los polímeros obtenidos presentan similares o idénticas propiedades que las de origen petroquímico. Dentro de este grupo de biopolímeros se pueden encontrar el polipropileno (Bio-PP), polietileno (Bio-PE), polietileno tereftalato (Bio-PET), poliestireno (Bio-PS) o policloruro de vinilo (Bio-PVC). Estos representan el 35.8% de la cuota de biopolímeros fabricados [18]. Algunos de estos polímeros como el Bio-PE, Bio-PET, Bio-PVC o Bio-PS, son sintetizados mediante del monómero del etileno a partir del bioetanol. En este caso, el Bio-PE es el polímero biobasado más utilizado dentro de este grupo. Respecto al proceso de obtención del Bio-PE, se debe indicar que permite disminuir de forma significativa las emisiones de GEI. Por ejemplo, una tonelada métrica de PE obtenido de forma tradicional mediante materia prima de origen petroquímico, genera unas emisiones en torno a 3,5 toneladas métricas de CO_2eq, mientras que de origen renovable permite capturar y eliminar hasta 2,5 toneladas de GEI de la atmósfera [48]. Esta es una propuesta atractiva que permite disminuir en gran medida las emisiones de GEI durante el proceso de producción de estos polímeros, ya que sus prestaciones son similares o idénticas a los polímeros de origen petroquímico.

Una de los principales precursores de origen bio para el desarrollo de biopolímeros de origen bio y no biodegradables es el bioetanol. Este se puede obtener a partir de tres tipos diferentes de materias primas.

- **Primera generación:** son los que provienen de materia prima apta para el consumo humano como el azúcar, el almidón o el maíz, etc. Es una de las fuentes más empleadas, sobre todo con la producción de biocombustibles que se obtiene a partir del bioetanol. Este tipo de producción ha generado preocupación tanto a nivel social como económico por el empleo de un recurso apto para el consumo de alimentos como fuente de obtención de polímeros, debido a que los precios de ciertos cultivos se incrementaron como consecuencia de la generación de los biocombustibles [49].

- **Segunda generación:** Sse emplean los residuos agrícolas como fuente de partida, como el bagazo de la caña de azúcar o la paja del arroz, los cuales están compuestos por hemicelulosa y celulosa principalmente. Son propuestas mas respetuosas con el medioambiente que las anteriores ya que reaprovechan residuos agrícolas, son abundantes y no compiten con las materias primas comestibles. La elevada presencia de polisacáridos en este tipo de residuo agrícola, en torno a 75%, son una propuesta atractiva para fermentar estos azúcares para la obtención de bioetanol.

- **Tercera generación:** la materia prima proviene de las algas, siendo una de las técnicas más atractivas debido a su alto conteniendo en carbohidratos y lípidos. Entre las ventajas destaca su alta capacidad de crecer en diferentes hábitats y su rapidez en el crecimiento. Sin embargo, la falta de tecnología eficiente y su alto coste, dificulta la comercialización del bioetanol a partir de esta fuente [50].

A pesar de las diferentes propuestas, actualmente la mayor producción de bioetanol es empleando materia prima de primera generación [51]. La obtención de bioetanol a través de residuos agrícolas (segunda generación) es menos atractiva industrialmente, sin embargo, ya existen empresas como VYNOVA que comercializan productos de Bio-PVC a través de esta vía. La figura I.6 muestra un esquema general de obtención de polímeros biobasados a partir de la caña de azúcar, siendo actualmente una de las materias primas más empleadas en este propósito.

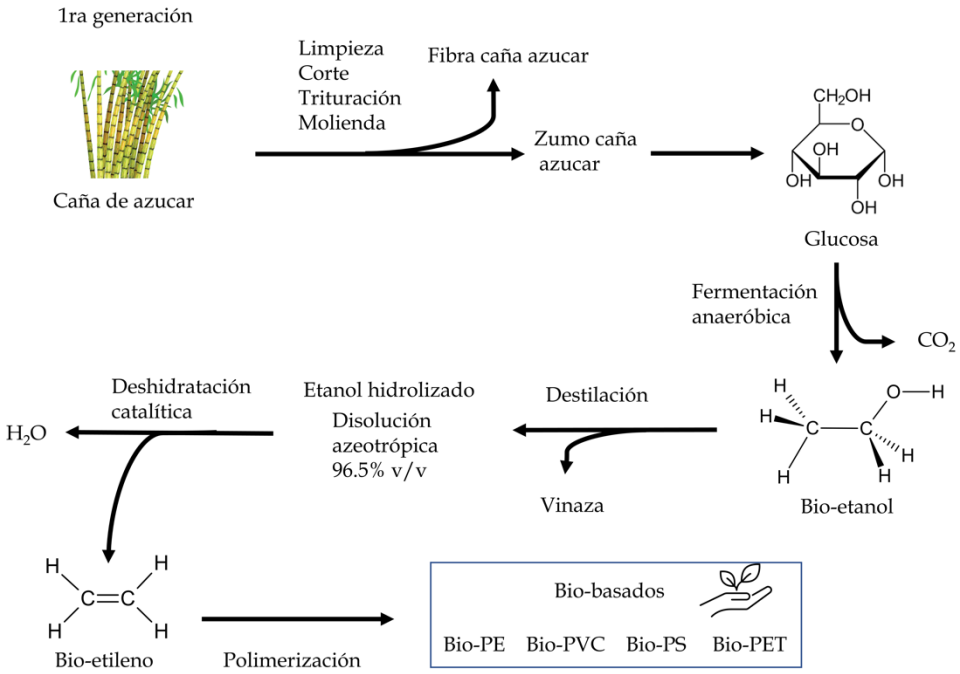

Figura I.6. Esquema general de obtención de polímeros biobasados mediante materia primera de 1ra generación. Adaptado de [52].

Polímeros de origen renovable biodegradables

Los biopolímeros ya comentados con anterioridad tienen un gran interés tanto industrial como científico debido a que son capaces de disminuir el impacto medioambiental en comparación con los petroquímicos no biodegradables. Sin embargo, siguen presentando algunas carencias como la fuente de origen, siendo algunos petroquímicos y otros renovables, o incluso algunos de ellos sin la posibilidad de biodegradarse. El siguiente grupo presenta un gran interés ya que, por un lado, la materia prima proviene de fuentes renovables, y, por otro lado, este tipo de materiales pueden ser degradados bajo condiciones de compost al final del ciclo de vida. El compost obtenido tras la descomposición puede servir para utilizarlo como fuente de abono para cultivos que puedan abastecer las nuevas materias primas renovables, cerrando así un ciclo con una baja huella de carbono. Sin embargo, se tratan de polímeros que presentan limitaciones tanto a nivel técnico como económico. Esto limita su uso a nivel industrial, y es por ello que los científicos buscan nuevas maneras de obtener materiales con mejores propiedades técnicas y a un precio menor con el fin, de que puedan comercializarse de forma común y sustituir a los polímeros que más impacto medioambiental generan. Diferentes fuentes de materia prima han sido

estudiadas para la obtención de estos polímeros. Se pueden dividir en dos grandes grupos, esquematizado en la Figura 1.7.

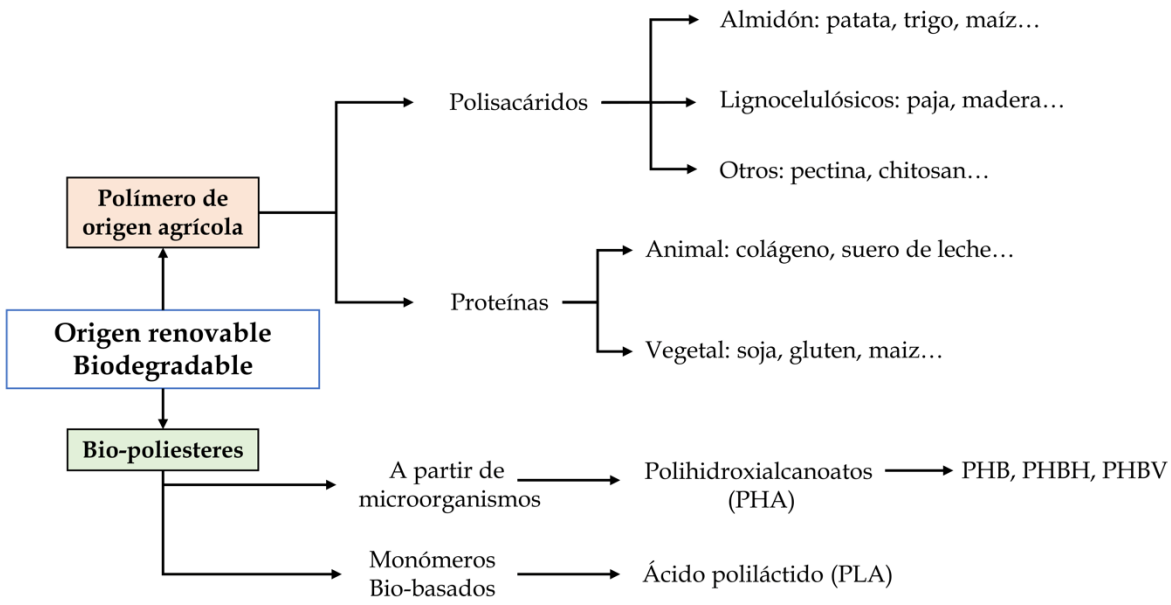

Figura I.7. Clasificación de polímeros de origen renovable biodegradables.

Polímero de origen agrícola

Se dividen en (1) polisacáridos y (2) proteínas, los cuales son materias primas de gran abundancia. Los polisacáridos con mayor importancia son el almidón, pectina, quitosano, lignina y celulosa. A excepción del almidón, las demás fuentes necesitan de una modificación química para ser empleados como termoplásticos. Por otro lado, dentro de las proteínas puede haber tanto de origen animal como el colágeno y suero de leche, mientras que de origen vegetal destaca la proteína de soja, gluten o maíz. Algunas características de estos grupos son: la rápida degradación, hidrofilidad, y en algunos casos en ambiente húmedos presentan propiedades mecánicas poco deseables [53]. En la actualidad, se está investigando sobre la mejora de algunas deficiencias como las propiedades mecánicas y la sensibilidad al agua. Una de las aplicaciones más comunes es la formación de recubrimientos para productos comestibles [54].

Biopoliésteres

Este grupo se puede dividir en dos, (1) los que provienen de la extracción de materia de los microorganismos y (2) los que emplean técnicas de biotecnología para su producción. Los polihidroxialcanoatos (PHAs) son una familia de polímeros que son sintetizados intracelularmente por bacterias (en torno a 300 pueden sintetizarlo), acumulando entre el 30-80% de su peso [55]. Teniendo en cuenta que uno de los inconvenientes es el precio, algunas de las soluciones es implementar nuevas estrategias para mejorar el rendimiento del proceso y modificar genéticamente las bacterias. Otra alternativa para la disminución del coste es emplear residuos industriales de la agricultura como fuente de carbono para el proceso [56]. El polímero más destacado de la familia de PHA es el poli(3-hidroxibutirato) (PHB), pero existen otros como el poli(3-hidroxibutirato-co-3-hidroxihexanoato) (PHBH) o poli(3-hidroxibutirato-co-3- hidroxivalerato) (PHBV), cuyas estructuras se observan en la Figura I.8. La biodegradación de los PHA dependerá de factores como la cristalinidad [57], la presencia de copolimeros u homopolimeros [58], pero generalmente presenta una mayor ratio de degradación que el PLA. Zhang y Thomas [59] observaron que el PHB se degradaba primero de forma superficial mediante el ataque de las enzimas segregadas por los microorganismos en condiciones de compostaje a temperatura ambiente, y que luego se va extendiendo hacia el interior. Además, la biodegradación era con una velocidad mayor que la del PLA. Por ello, las aplicaciones en las que destaca son las referidas a productos con poca vida útil como el envase y embalaje, o en el campo de la biomedicina dado su biocompatibilidad [60].

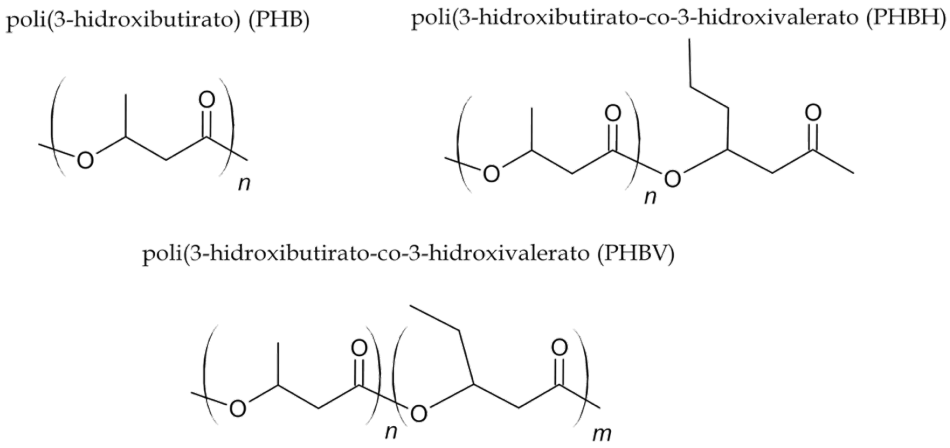

Figura I.8. Polímeros de la familia polihidroxialcanoatos (PHA).

Por otro lado, uno de los polímeros biobasados biodegradables con mayor producción a nivel industrial es el ácido poliláctico (PLA). Se obtiene a partir de monómeros biobasados como el ácido láctico tras la fermentación de carbohidratos (azúcares) principalmente con la bacteria *Lactobacillus* [61]. En función de la cepa empleada, se puede obtener dos isómeros diferentes del monómero del ácido láctico, el D-ácido láctico y el L-ácido láctico. Generalmente durante la fermentación, el isómero natural con mayor abundancia es el L-ácido láctico mediante la bacteria *Lactobacillus* [62]. En la Figura 1.9. se muestra el esquema para la obtención de los monómeros de ácido láctico a partir de diferentes fuentes de materia prima renovable. A medida que la obtención de sacarosa es más compleja, es necesario realizar mayor tratamiento a la materia de partida. Por ejemplo, el pretratamiento necesario para el bagazo de caña de azúcar es más sencillo y menos costoso que a partir de almidón. En el caso de los procedentes de materiales lignocelulósicos, también es posible, pero uno de los principales obstáculos es la eficiencia de la hidrólisis de carbohidratos a azúcares, la cual sigue en continua investigación [63].

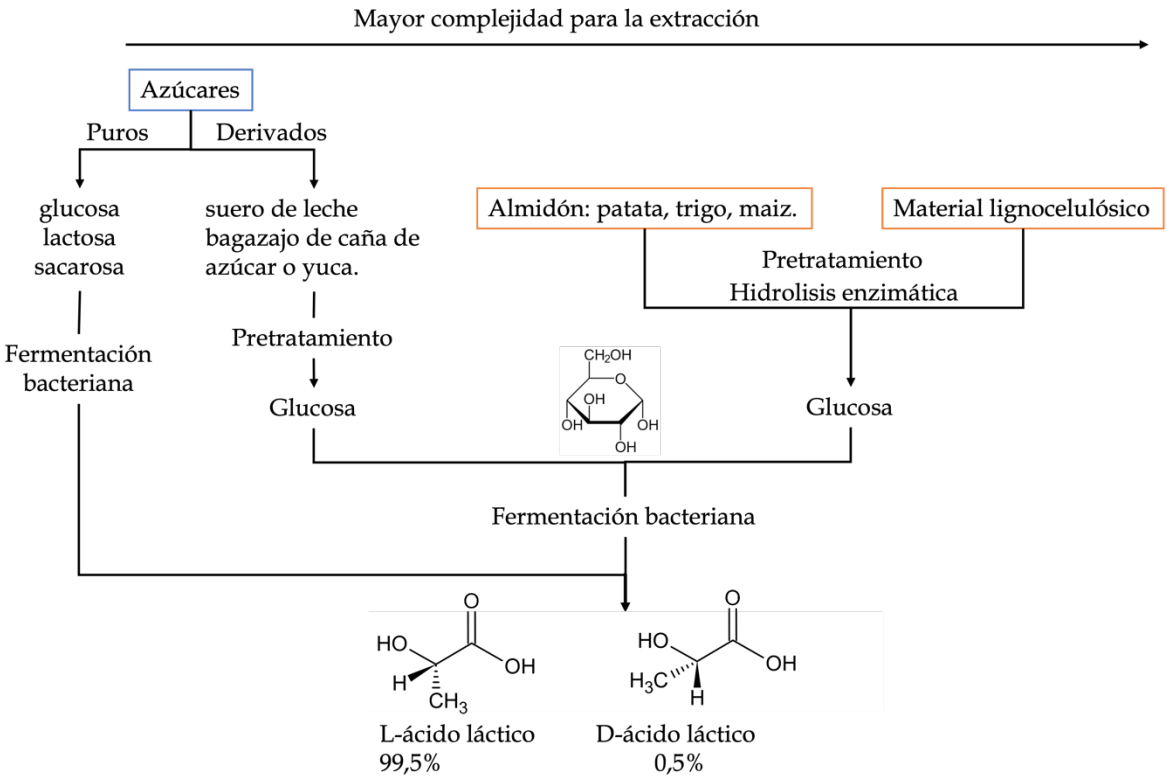

Figura I.9. Obtención de los monómeros de ácido láctico a partir de fuentes renovables disponibles. Adaptado de [63].

A partir de los monómeros se produce la polimerización para la obtención del PLA. Diversos métodos para la obtención de este polímero han sido reportados en literatura, los cuales se muestran de forma esquematizada en la Figura 1.10. Tanto el primero como el segundo método parten de la condensación o deshidratación de los monómeros para la obtención del prepolímero de bajo peso molecular. Sin embargo, el método con disolvente requiere altas temperaturas y vacío para la eliminación del agua y producir el prepolímero de bajo peso molecular, y seguidamente necesita extensores de cadena como epóxidos o isocianatos para aumentar el peso molecular [64]. El caso de la condensación libre de disolvente se produce y purifica mediante destilación de un dímero cíclico llamado láctida, que seguidamente produce la polimerización mediante la apertura de los anillos mediante catalizadores ("*ring opening polymerization*") (ROP). Es posible controlar el peso molecular obtenido controlando la temperatura, tipo de catalizador y tiempos de residencia [65]. Por último, existe un método que mediante la deshidratación azeotrópica mediante

catalizadores como el $Sn(Oct)_2$ permite obtener el PLA de alto peso molecular tal y como en los métodos expuestos anteriormente [66].

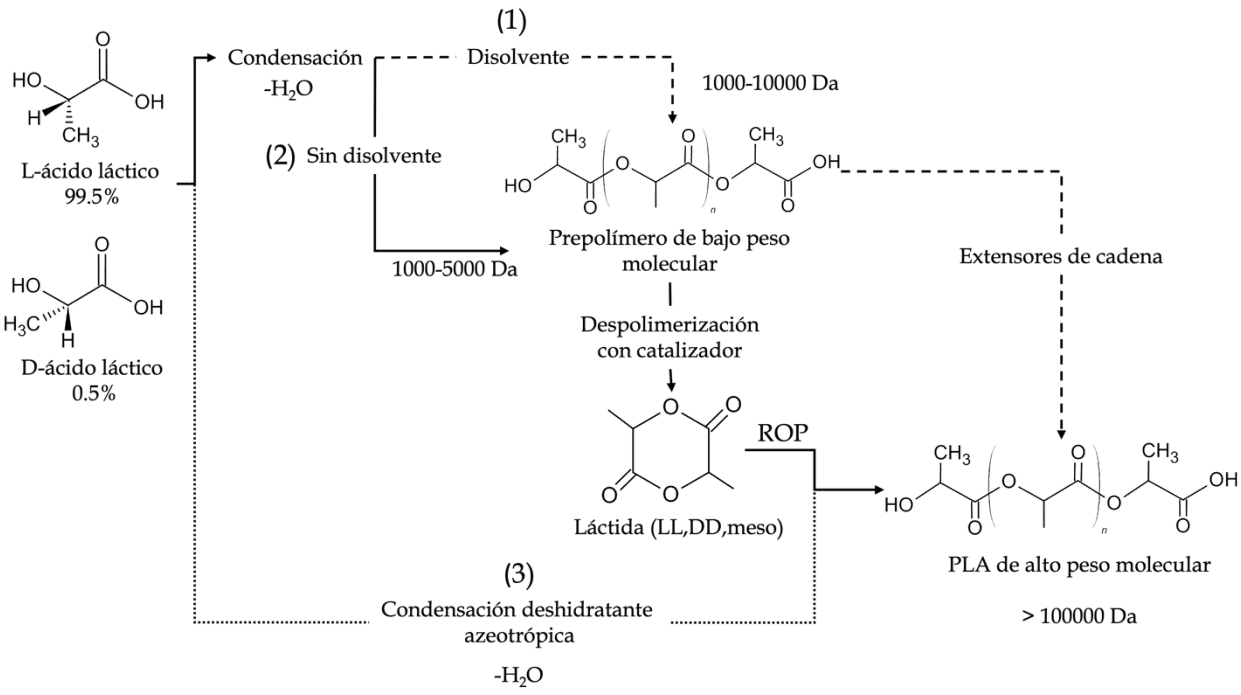

Figura I.10. Métodos para la polimerización de monómeros del ácido láctico para formar PLA. Adaptado de [67].

El PLA presenta un fácil procesado, transparencia, biodegradación, no toxicidad y su producción es económicamente viable, permitiéndole ser ampliamente utilizado como films transparente, vasos, bandejas, etc [68]. Presenta mayor resistencia a la biodegradación tanto bajo compost como en condiciones normales en comparación con el PHB, lo que puede conferirle una mayor estabilidad para aplicaciones de mayor vida útil y en condiciones normales. La biodegradación del PLA se produce primero mediante la hidrólisis no enzimática de forma superficial, dando lugar oligómeros con un menor peso molecular. Como consecuencia, éstos si que pueden ser metabolizados por los microorganismos generando agua y dióxido de carbono en condiciones aeróbicas. En la Figura I.11. se muestra un esquema de la posible biodegradación del PLA en un proceso de compostaje.

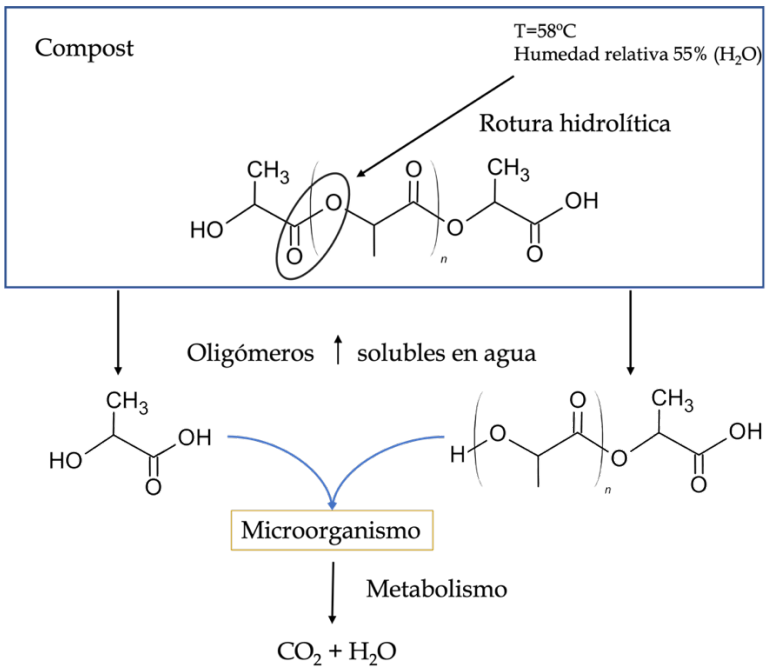

Figura I.11. Esquema del proceso de compostaje del PLA.

Las propiedades del PLA pueden modificarse en función de la estereoquímica, es decir, de la presencia de cada isómero, obteniéndose así el poli D-láctico (PDLA), poli L-láctico (PLLA) o una mezcla de ambos, el poli D-L-láctico (PDLLA). Esto le confiere diferente cristalinidad al polímero, y con ello, diferentes propiedades mecánicas y de biodegradación. Un ejemplo sería el PLLA, que presenta una estructura semicristalina con unas mejores propiedades mecánicas, pero bajas propiedades dúctiles y una menor capacidad de biodegradación. Los autores Tsuji y Ikada [69] descubrieron que una mezcla de ambos isómeros PDLLA le confieren unas mayores propiedades térmicas que los homopolímeros por separado, y una mayor ductilidad y biodegradabilidad que el homopolímero PLLA. En la actualidad, se está realizando numerosos estudios para poder mejorar algunos inconvenientes que presenta el PLA como su alta fragilidad, caracterizada por baja resistencia al impacto y poca ductilidad. Entre las propuestas más innovadoras destacan la obtención de mezclas o "blends" con otros biopolímeros como el PBS [70] o la PCL [71], o la adicción de plastificantes biobasados. Dentro de esta línea de introducción de plastificantes biobasados, destaca el empleo de aceites vegetales modificados químicamente, ya que, en líneas generales, pueden aportar mejoras en la ductilidad sin ver mermadas las propiedades biodegradativas. [72].

I.2.2. Polímeros termoestables

Los termoestables, a pesar de representar una cuota total de mercado de menos del 20%, son ampliamente utilizados a nivel industrial [73]. Forma parte de la familia de los plásticos, y se caracterizan por partir de disoluciones líquidas que, tras desencadenarse un proceso de entrecruzamiento de las cadenas, se obtiene materiales sólidos de forma irreversible. Generalmente, el proceso de entrecruzamiento comienza con la adición de un iniciador, que permite la primera generación de radicales disponibles para comenzar a producirse la reacción. La reticulación se obtiene cuando la funcionalidad de uno o más monómeros involucrados es superior a 2, es decir, que presente mas de dos grupos reactivos para que se produzca la unión de monómeros hasta alcanzar redes tridimensionales. La formación de una red tridimensional se muestra de forma esquemática en la Figura I.12.

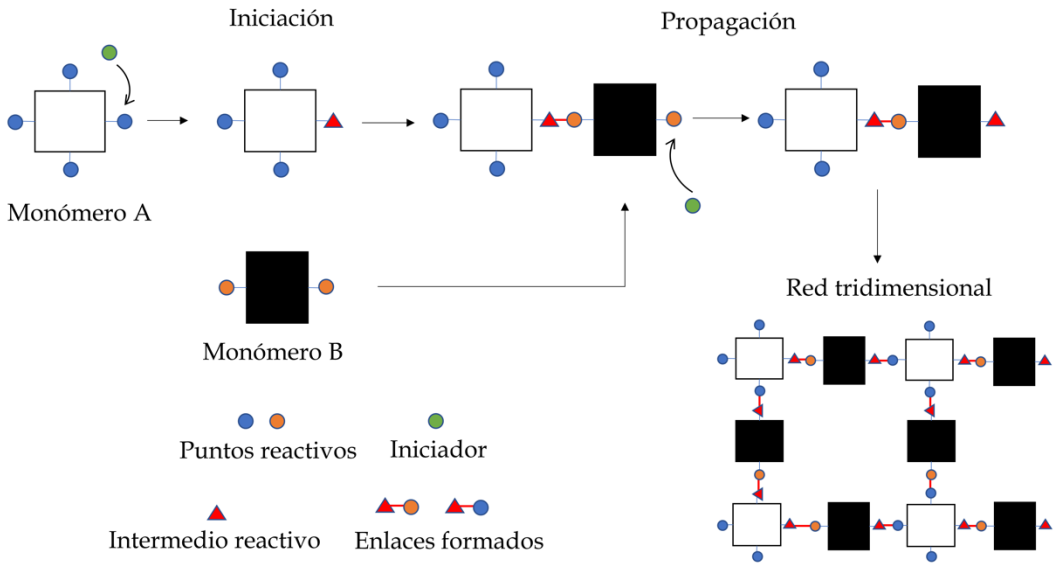

Figura I.12. Representación esquemática del entrecruzamiento obteniendo una red tridimensional. Adaptado de [74].

Los materiales termoestables se pueden diferenciar en función del tipo de resina base empleada. Entre los tipos disponibles destacan las fenólicas, poliéster insaturado (PU), urea de formaldehido y resina epoxi. Estas resinas se utilizan comúnmente como barnices, recubrimientos, adhesivos y en los materiales

compuestos con diferentes refuerzos como fibras de vidrio, donde se destacaría el empleo de poliéster insaturado o resinas epoxi.

Las resinas de PU son las más empleadas en aplicaciones donde existe un equilibrio entre coste y buenas propiedades termomecánicas. Las resinas de PU se obtienen a partir de una reacción de esterificación entre ácidos o anhídridos con un grupo de alcoholes denominados polioles. Posteriormente, se produce una poliadición de estos poliésteres con monómeros de estireno para que se produzca el entrecruzamiento, mejorando las propiedades finales y disminuyendo el coste de producción. Uno de los objetivos actuales es disminuir el uso de este reactivo debido a su origen petroquímico y efectos nocivos para la salud [75]. Una de las iniciativas que se han empleado es la sustitución de compuestos de origen petroquímico por origen renovable. Por ejemplo, diversas resinas se han obtenido sustituyendo el poliol por otros de origen renovable como el 1,3 propanodiol. También se ha empleado ácido adípico, acidos saturados y ácido fumárico como ácidos carboxílicos de origen renovable [76]. Respecto al estireno, algunos autores han estudiado alternativas de origen renovable mediante el empleo de derivados del metacrilato como metacrilato de metilo, metacrilato de laurilo o dimetacrilato de butanodiol. A pesar de la elevada rigidez, los compuestos empleados seguían presentando cierta volatilidad y no todos disolvían completamente la resina de PU [77].

Por otro lado, las resinas epoxi es la más empleada con una cuota de mercado de aproximadamente del 70%. Estas ofrecen mejor calidad en lo que a propiedades técnicas se refiere, y es por ello que su coste es superior a las de poliéster insaturado [78]. Las resinas epoxi, caracterizadas por su bajo peso molecular, se obtienen casi en su totalidad a partir de fuentes no renovables, y las más empleada es el diglicidil éter de Bisfenol A (DGEBA). Se obtiene a partir de la epiclorhidrina y Bisfenol A en presencia de hidróxido de sodio (NaOH), dando como resultado un monómero con grupos epoxi en cada extremo de la estructura. Sin embargo, el Bisfenol A se obtiene de origen petroquímico y constituye más de la mitad de DGEBA, fabricando resinas con un impacto medioambiental alto. El empleo de esta resina también presenta otro inconveniente, debido a que el Bisfenol A genera un efecto nocivo para la salud [79]. Actualmente se está buscando alternativas de origen renovable para la sustitución de

las resinas de Bisfenol A. Algunos autores han obtenido resinas a partir de modificaciones química de la lignina, donde se sustituye gradualmente el empleo de DGEBA por éter glicidil de lignina [80]. Otra de las líneas de investigación más interesantes para incrementar el contenido ecológico es el empleo de epóxidos derivados de aceites vegetales. Esta materia prima es modificada químicamente con el objetivo de introducir grupos epoxi en los dobles enlaces disponibles en la estructura del triglicerido. Algunas investigaciones se centran en obtener resinas epoxis parcialmente ecológicas sustituyendo progresivamente las de origen petroquímico [81]. Por otro lado, las resinas epoxi se pueden obtener en presencia de otros co-reactivos con grupos funcionales como alcoholes, aminas, anhídridos, etc. Estos co-reactivos son denominanos endurecedores, los cuales se introducen en una resina base para reducir costes u obtención de propiedades finales deseadas. Al igual que ocurre con las resinas epoxi, los endurecedores empleados presentan también un impacto medioambiental alto como consecuencia de su obtención a partir de recursos fósiles, destacando el empleo de anhídridos, aminas o ácidos carboxílicos [82]. En este sentido, los aceites vegetales modificados también son objetivos de investigación.

I.2.3. Aditivos en formulaciones de polímeros

En la actualidad, la gran mayoría de los plásticos requiere de aditivos para optimizar las propiedades finales de los productos. Estos aditivos pueden destinarse a mejorar algunas propiedades como pueden ser las mecánicas, la protección frente agentes externos, la modificación de propiedades intrínsecas del polímero o la reducción de costes.

Para la mejora de las prestaciones mecánicas se utilizan refuerzos cuya naturaleza y precio pueden ser muy variados. Además, estos son claves en la fabricación de materiales compuestos. Por otro lado, los aditivos se emplean ampliamente con una doble función: la protección frente agentes externos, como la luz UV o ignifugantes, o la modificación de propiedades como plastificantes, colorantes, o compuestos antiestáticos. Finalmente, la reducción de costes se lleva principalmente mediante el empleo de cargas, las cuales se emplean en grandes cantidades.

De estos aditivos empleados en la industria plástica, a continuación, se detallarán los plastificantes y las cargas, haciendo hincapié en el empleo de estos aditivos de origen bio.

I.2.3.1. Plastificantes

Uno de los aditivos más habituales son los plastificantes, los cuales permiten mejorar la procesabilidad y flexibilidad del material polimérico fabricado. Al aumentar la flexibilidad de las cadenas poliméricas, se aumenta la fluidez del material y disminuye las temperaturas de fusión y transición vítrea, lo que favorece una mejor procesabilidad y una reducción del coste energético. Por otro lado, las propiedades mecánicas resistentes como la resistencia a tracción, el módulo de tracción o la dureza disminuyen [83]. De forma genérica, en bibliografía se ha reportado diferentes teorías que explican el efecto del plastificante en los materiales poliméricos. En la Figura I.13. Se muestras la representación de las principales teorías [84].

- **Teoría de gel:** el polímero plastificado estaría formado por una red tridimensional donde las moléculas del plastificante están unidas mediante fuerzas secundarias a las cadenas poliméricas, reduciendo así los puntos de anclaje del polímero con otras cadenas colindantes.
- **Teoría de lubricación:** el plastificante actúa como lubricante que facilita el deslizamiento de unas cadenas con otras cuando se produce un esfuerzo mecánico.
- **Teoría del volumen libre:** es la teoría más aceptada en la comunidad científica, donde la incorporación del plastificante permite aumentar el espacio libre entre cadenas, favoreciendo un mayor movimiento interno, aumentando la ductilidad.

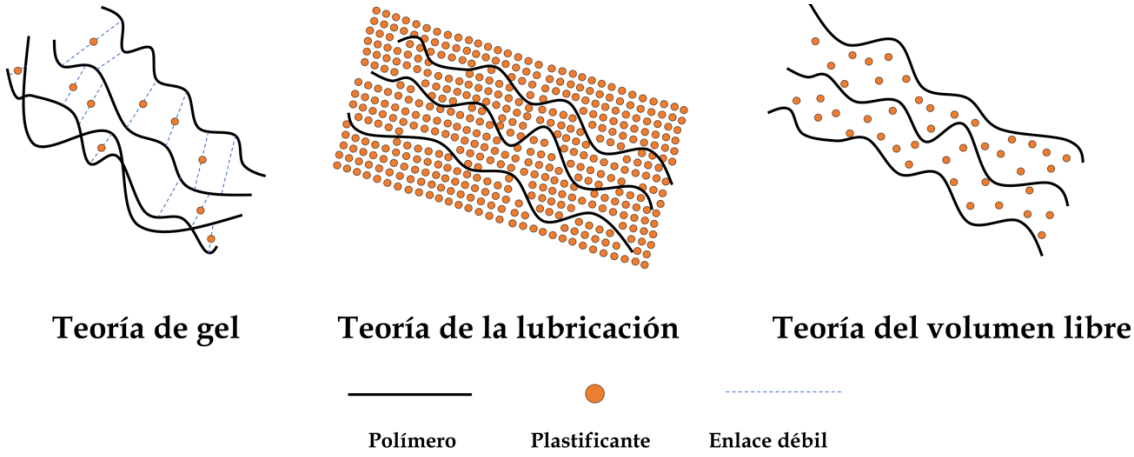

Figura I.13. Representación esquemática de las teorías de plastificación. Adaptado de [84].

Los plastificantes que se emplean se pueden clasificar según el peso molecular y la compatibilidad con el polímero [85].

En función del peso molecular se puede encontrar los monoméricos y poliméricos. Por un lado, los que presenta una estructura molecular única y simple son los monoméricos, cuyo peso molecular varía entre 300 y 600 $g \cdot mol^{-1}$. Sin embargo, presentan alta volatilidad y migración en el polímero. Son plastificantes cuya permanencia en el polímero es más reducida, pero a pesar de ello es ampliamente empleado a nivel industrial por su bajo coste. Por otro lado, los plastificantes poliméricos presentan mayor peso molecular entre 1000 y 10.000 $g \cdot mol^{-1}$, y como consecuencia, su volatilidad y migración es menor. Es por ello que, en sectores donde la permanencia del plastificante es un factor clave, como en el sector del envasado de productos alimentarios, este tipo de plastificantes son muy empleados a pesar de tener un precio más elevado.

En función de la capacidad de compatibilizar con el polímero existen plastificantes de tipo primarios y secundarios. Los plastificantes primarios presentan alta compatibilidad con el polímero, incluso cuando hay concentraciones altas. Sin embargo, los plastificantes secundarios presentan una compatibilidad más limitada con el polímero. Un exceso de plastificante puede dar lugar a un polímero con problemas de migración debido a la exudación. Son empleados juntamente con los plastificantes primarios para la reducción de costes u optimización de propiedades.

La gran mayoría de los plastificantes empleados a nivel industrial son de origen petroquímico, y presentan baja resistencia a la migración. Los plastificantes más empleados provienen de la familia de los ftalatos, cuya producción anual es aproximadamente el 80% del total de plastificantes [86]. En la actualidad, la preocupación medioambiental y el conocimiento de los aspectos adversos para la salud de esta familia de plastificantes, está generando la búsqueda de nuevas alternativas para solucionar estos inconvenientes. En este sentido, los aceites vegetales modificados químicamente presentan un alto interés por los siguientes motivos: son de origen renovable y presentan alta disponibilidad, se caracterizan por un mayor peso molecular reduciendo la migración del plastificante respecto a los ftalatos, las cadenas del aceite vegetal pueden incorporarse entre las cadenas poliméricas aumentando el volumen libre y, los grupos reactivos del aceite modificado puede interactuar con las cadenas poliméricas mejorando la compatibilidad.

I.2.3.2. Cargas

Las cargas empleadas en el sector de los polímeros se introducen principalmente con el fin de abaratar el producto final y otorgar al polímero de unas propiedades determinadas. Entre las posibles cargas, destacan el empleo de los denominados "fillers" de origen inorgánico, como el $CaCO_3$ o el TiO_2 y cargas de origen orgánico, como restos lignocelulósicos.

Estos últimos permiten aumentar el contenido ecológico de los polímeros obteniendo así lo que se denomina *wood plastic composites* (WPC). A pesar de que inicialmente los WPC empleaban madera como carga, en la actualidad también se emplean subproductos de industrias alimentarias. Una de las que mayor residuo genera anualmente es la industria del aceite. En general, el rendimiento de extracción en industria no excede del 20-25%, siendo el resto material lignocelulósico, proteínas, almidones y minerales en términos generales. Teniendo en cuenta que la extracción de los aceites se produce en lugares geográficos específicos y la gran cantidad producida de subproductos, la gestión de estos ocasiona un problema tanto económico como medioambiental [87]. Una parte de estos residuos son empleados

como producto alimentario en la industria ganadera [88], pero en la actualidad se están buscando más alternativas para mejorar la gestión de estos subproductos.

Alguna de las ventajas que presenta la fabricación de WPC es el empleo de un tipo de cargas muy numerosas y con elevada disponibilidad, de bajo coste y que además pueden ser procesadas con las mismas técnicas que los polímeros: extrusión e inyección principalmente [89]. Uno de los problemas que presenta es la falta de compatibilidad entre las cargas lignocelulósicas (con pocos puntos reactivos) y las matrices poliméricas orgánicas. Como solución a este problema, se añaden compatibilizantes que mejoran la interacción entre las partículas lignocelulósicas y la matriz polimérica. Los compatibilizantes son compuestos que contienen grupos reactivos cuya finalidad es formar un puente de unión entre la carga y la matriz polimérica. Generalmente, las cargas orgánicas empleadas presentan alta cantidad de grupos -OH en su estructura, y necesitan de un grupo intermedio como el compatibilizante para mejorar la compatibilidad con la matriz.

Algunos ejemplos del empleo de residuos alimentarios como cargas en matrices son mostrados a continuación. En el trabajo llevado a cabo por Amar *et al.* [90] se estudia el empleo de la harina del hueso de la oliva con y sin tratamiento superficial empleando viniltriacetoxy silano como compatibilizante en una matriz de PP donde previamente se ha reaccionado con MA. En dicho estudio se observó que los dos tratamientos mejoraron la compatibilidad, mejorando propiedades como la estabilidad térmica y el módulo de Young, entre otros. También en otra investigación realizada por Mysiukiewicz *et al.* [91] se emplea la harina de la semilla de linaza con diferentes contenidos de aceite residual en una matriz de PLA. En todos los casos se observó que la adición de la harina de linaza permite fabricar productos de consumo biodegradables.

I.3. Aceites vegetales en ingeniería

Los aceites vegetales poseen una serie de características intrínsecas que los hace tener gran interés en su aplicación en el sector de los polímeros. Como se ha descrito previamente en el apartado I.2.3.1, los aceites vegetales destacan por su su elevada disponibilidad con un coste relativamente bajo, provienen de materias primas renovables y pueden ser modificados químicamente para aumentar su funcionalidad [92].

Los aceites vegetales son compuestos no volátiles presentes en la naturaleza que están compuestos por triglicéridos, los cuales son tres moléculas de ácidos grasos (AGs) unidos por una molécula de glicerol. Los AGs son cadenas alifáticas que puede contener entre 14 y 22 carbonos (C14-C22) con un grupo carboxilo en el extremo [93]. De forma general, los aceites vegetales están compuestos por un 95% de triglicéridos mientras que el 5% restante son AG libres [94]. Estos triglicéridos contienen dobles enlaces que pueden situarse en diferente número y posición en la cadena de triglicéridos. En la Figura I.14. se representa un triglicérido compuesto por 3 AG con diferente grado de insaturación.

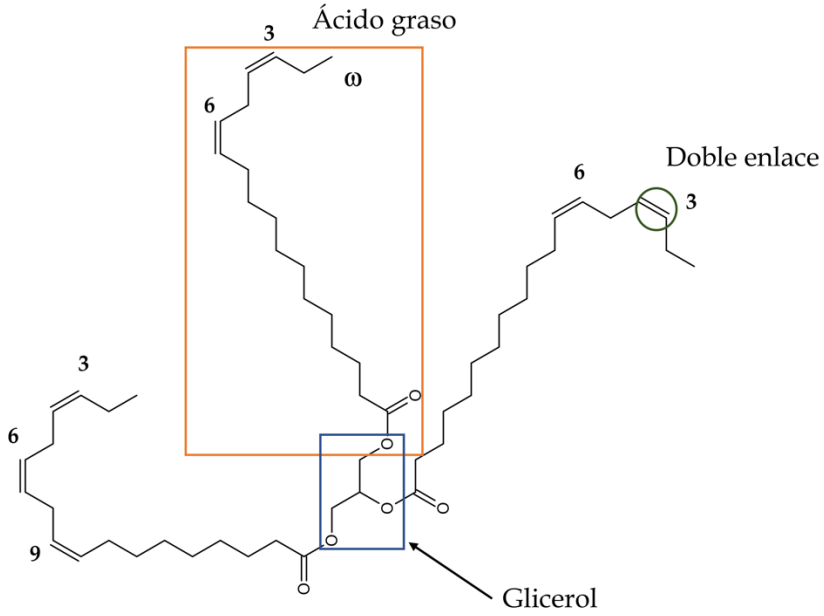

Figura I.14. Ejemplo de estructura química del triglicérido.

Los AGs presentan cierta reactividad debido a las insaturaciones, es decir, los dobles enlaces (C=C) existentes en su cadena alifática. Su creciente uso como materia prima en industrias como la polimérica [95], desarrollo de combustibles [96] o en automoción [97], es debido a la posibilidad de modificarlos químicamente a través de sus puntos reactivos con el fin de aumentar su reactividad y modificar la interacción respecto a otras moléculas . Una forma de clasificar los aceites vegetales es en función del grado de insaturación que presenta en su estructura química:

- **Saturados:** son aquellos que no presentan dobles enlaces en su estructura. Suelen estar presentes en grasas animales las cuales son sólidas a temperatura ambiente, debido a que la ausencia de dobles enlaces disminuye el punto de fusión [98]. Los AGs pertenecientes a esta categoría son el mirístico, palmítico o esteárico, entre otros.
- **Monoinsaturados:** hace referencia a los AGs que presentan únicamente un doble enlace en su estructura, como es el caso del palmitoleico, margaloreleico y oleico.
- **Poliinsaturados:** presentan más de un doble enlace en la molécula de ácido graso, es decir, 2, 3 e incluso 4 insaturaciones (C=C) en algunos casos. Los AGs más conocidos son el linoleico y linolénico.

Los triglicéridos de los aceites vegetales presentan una mezcla de AGs con diferente grado de insaturación, siendo la única excepción el aceite de Jojoba, el cual únicamente presenta AGs con 1 insaturación. Normalmente, el grado de insaturación se expresa con el índice de yodo (IY) siguiendo la normativa correspondiente [99]. Éste indica la cantidad de gramos de I_2 que han sido absorbidos por el aceite como consecuencia de la disponibilidad de dobles enlaces en la estructura por cada 100 g de aceite. A pesar de que los aceites sean estables, la presencia de estas insaturaciones les confiere la posibilidad de oxidarse e hidrolizarse, disminuyendo la presencia de las insaturaciones. Por tanto, en la naturaleza se puede encontrar diversos AGs en función de la longitud de la cadena de carbono y de las insaturaciones. Respecto al tipo de AGs disponibles en la naturaleza, en la Tabla I.2 se muestra los más comunes desde C14 a C22. Se debe indicar que los AGs más predominantes son las moléculas con 18 átomos de carbono (C18) con diferentes grados de saturación como el oleico, linoleico

y linolenico. En el caso del linolénico, existe una variante en función de la posición de los dobles enlaces en la cadena alifática. El γ-linolénico presenta los dobles enlaces en los C6, C9 y C12, mientras que el α-linolénico en C3, C6 y C9 partiendo del extremo alifático (ω). Esta diferencia en el posicionamiento le confiere mayor reactividad inicial al triglicérido, donde las insaturaciones más cercanas al extremo ω están mas accesibles para su modificación [100]. Por otro lado, los AGs con longitudes de C14, C20 o C22 son los menos abundantes en los aceites vegetales.

Tabla I.2. Estructura química de ácidos grasos comunes con diferente grado de saturación y longitud de cadenas. Adaptado de [101].

Ácidos grasos	Estructura química	Carbonos: Dobles Enlaces
Mirístico	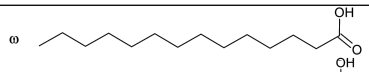	C14:0
Palmítico	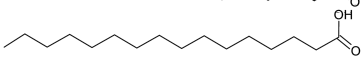	C16:0
Palmitoleico	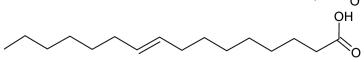	C16:1
Margárico	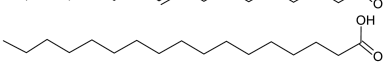	C17:0
Margaloreleico	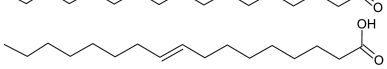	C17:1
Esteárico	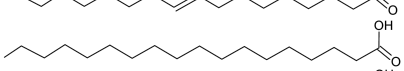	C18:0
Oleico	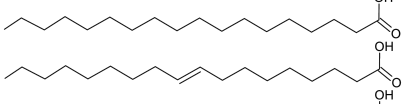	C18:1
Linoleico	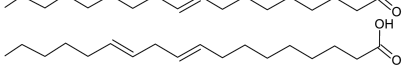	C18:2
α-Linolénico	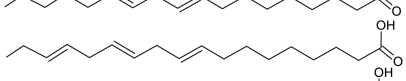	C18:3
γ-Linolénico	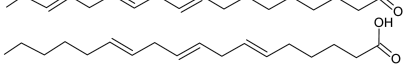	C18:3
Araquídico	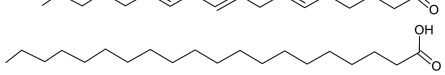	C20:0
Behénico	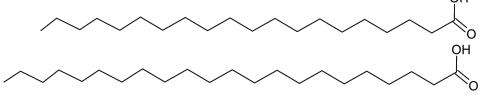	C22:0

C:DE: longitud de cadena de carbono (C) y número de dobles enlaces (DE).

I.3.1. Principales propiedades y producción de aceites vegetales

Existe una gran variedad de aceites vegetales de los cuales se pueden dividir en comestibles y no comestibles (Tabla I.3.). Algunos de los AGs comestibles son considerados beneficiosos para la salud humana, ya que ayudan entre otros aspectos a la regulación del nivel de azúcar en sangre, poseen efecto antiinflamatorio o incluso pueden actuar como antioxidantes [102]. El empleo como alimento por parte del ser humano no está estrictamente relacionado con el número de insaturaciones del aceite.

Por ejemplo el aceite de ricino no es comestible presentando un IY de 161 I_2 g/100 g aceite [103]. Por otro lado, el aceite de coco, se encuentra en estado sólido a temperatura de 25 ºC con un valor nulo de IY, siendo apto para el consumo humano [104].

Tabla I.3. Clasificación de los principales aceites vegetales.

	Comestibles [105]						**No comestibles**	
Ácidos grasos (AG)[a]	**Linaza**	**Soja**	**Girasol**	**Colza**	**Oliva**	**Palma**	**Ricino [106]**	**Tung [107]**
Palmítico (C16:0)	5,5	11	6	4,1	13,7	39	1,25	2,3
Esteárico (C18:0)	3,5	4	4	1,8	2,5	5	1,31	2,4
Oleico (C18:1)	19,1	23,4	42	60,9	71,1	45	3,81	5,6
Linoleico (C18:2)	15,3	53,3	47	21,0	10	9	5,21	6,3
Linolénico (C18:3)	56,6	7,8	1	8.8	0,6	-	0,81	0,1
Otros	-	-	-	12,6	2,1	2	87,61[b]	83,3[c]
Media D:E[d]	6,59	4,60	4,17	3,9	3,29	1,89	3,00	7,95
Índice de yodo[e] [108]	170-204	120-139	110-145	110-126	75-94	49-55	80-90	160-175 [109]

% en peso; (b) Ácido ricinoleico (C18:1 OH) en un 99.5%; (c) Ácido α-eleoesteárico (α-C18:3 (9,11,13)) en un 98,7%; (d) Media dobles enlaces por triglicérido; (e) unidades g I_2 /100 g de aceite.

Desde el punto de vista ingenieril, los aceites vegetales más interesantes son los que presentan mayor cantidad de insaturaciones. Debido a que están formados por triglicéridos, se suele expresar la media de dobles enlaces por cada triglicérido en función del porcentaje másico que presenta cada uno de los AGs. En la Tabla I.3 también se observa el porcentaje de AGs que presentan, además de la media de dobles enlaces por triglicérido. Se debe indicar que el porcentaje de AGs depende del tipo de variante y de las condiciones de crecimiento [110], por ello el IY mostrado representa solamente una estimación promedio. Se debe mencionar que la reactividad de los aceites no depende únicamente de la cantidad de estos, si no que también de la posición que presenten en la cadena alifática y de su isomería. De forma natural, los AGs de lo aceites vegetales suelen presentar los dobles enlaces en posición *cis*. Estos enlaces son menos estables y por tanto más reactivos que los presentes en la posición

trans, la cual es más estable químicamente. Además, los enlaces *cis* le confieren una estructura química con mayor grado de plegamiento de las moléculas, mientras que los enlaces *trans* o las no insaturaciones permiten que el triglicérido sea más lineal favoreciendo el empaquetamiento [111]. Por ejemplo, el aceite de tung contiene un valor elevado de media de dobles enlaces por triglicérido (7,95) debido a la presencia del ácido α-eleoestearico (α-C18:3 (9,11,13)), cuya distribución de dobles enlaces es diferente al ácido α y γ- linolénico (α-C18:3 y γ-C18:3, respectivamente). En la Figura I.15. se observa la diferencia entre ambos, destacando el isómero y la posición de los dobles enlaces. Comparando dichos AGs, en primer lugar, los α-C18:3 y γ-C18:3 presentan todos sus dobles enlaces en *cis* y en posiciones más cercanas al extremo alifático que el ácido α-eleoestearico, el cual presenta los enlaces en *cis*-9, *trans*-11, *trans*-13 siendo además conjugados. Esto le proporciona al aceite de tung menor reactividad que el ácido α y γ-linolénico si se observa la Tabla I.3. Comparando el aceite de linaza (6,59 dobles enlaces por triglicérido) con el de tung (7,95 dobles enlaces por triglicérido), se observa que a pesar de la mayor cantidad de insaturaciones, el índice de yodo de del aceite de tung es menor. El aceite de linaza presenta un valor de 170-204 g I_2/100 g de aceite y el tung un valor menor de 160-175 g I_2/100 g de aceite, a pesar de que este último presente mayor cantidad de dobles enlaces por triglicérido. Esta diferencia es debido a la menor accesibilidad de los dobles enlaces a la hora de cuantificar el IY, empleándose el método de bromación con el reactivo de Wijs siguiendo la normativa correspondiente ISO 3961. Este método de medición no es apto para los aceites que presentan dobles enlaces conjugados (más estables que los no conjugados), como es el de tung, donde no hay suficiente espacio para la incoporación del compuesto halogenado que permite el cálculo [109]. La reactividad de estos enlaces para su funcionalización mediante reacciones químicas como la epoxidación o maleinización se mostrará en el apartado I.3.3.

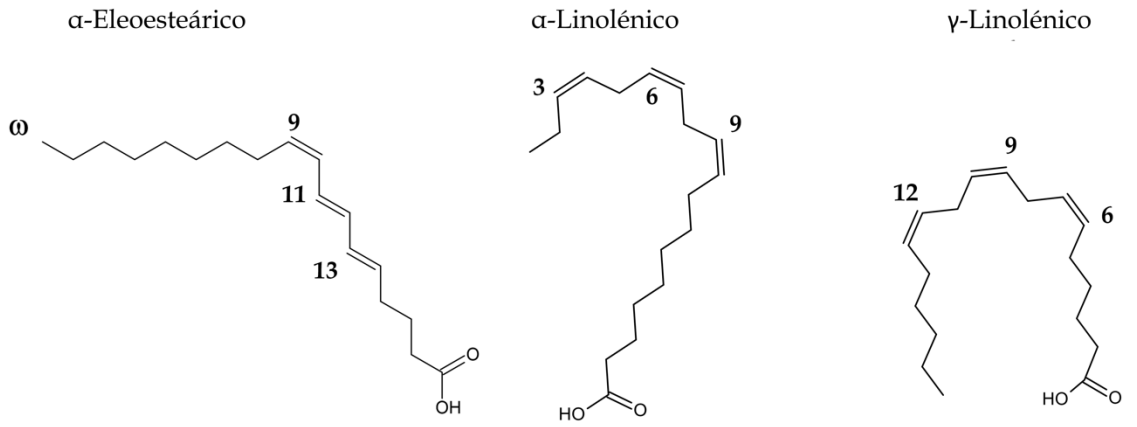

cis-9, *trans*-11, *trans*-13 *cis*-3, *cis*-6, *cis*-9 *cis*-6, *cis*-9, *cis*-12

Figura I.15. Ejemplo de estructura química de triglicéridos con enlaces en posición *cis* y *trans*.

Una vez descrita la estructura química de los triglicéridos presentes en los aceites vegetales, en la Figura I.16. se muestran los aceites con mayor producción mundial entre los años 2015 y 2021. La tendencia de la producción es alcista con un incremento del 26,5% entre los años 2015 y 2021, siendo una materia prima importante tanto para la industria alimentaria como para usos industriales. El aceite que encabeza el ranking de producción es el aceite de palma. Este representa casi el 40% de los aceites más consumidos y ha sido uno de los que mayor crecimiento ha presentado, sobretodo debido a su uso en alimentación. Uno de los inconvenientes de la masiva producción de este aceite es la gran deforestación que está produciendo en lugares asiáticos, generando un gran impacto medioambiental [112]. Seguidamente, el aceite de soja es el segundo más producido a nivel mundial precedido del aceite de colza, girasol, coco y oliva. El destino mayoritario de estos aceites es el alimentario, pero también algunos son empleados en aplicaciones industriales.

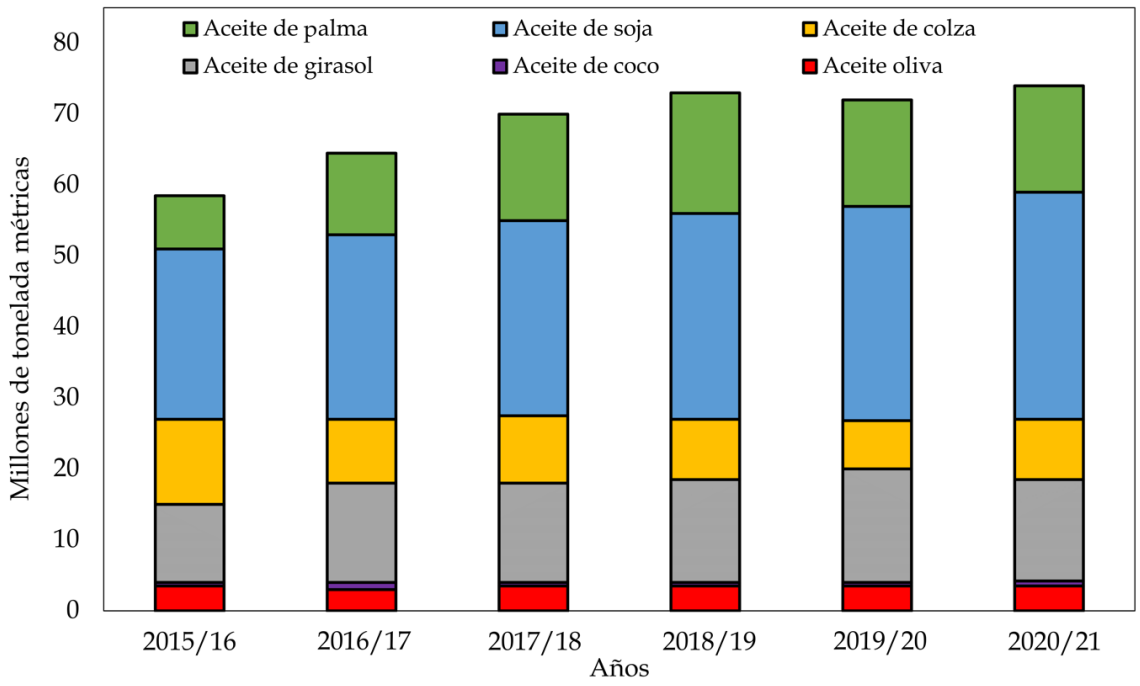

Figura I.16. Producción de aceites vegetales a nivel mundial. Adaptado de [113].

En el caso del aceite de soja, es también empleado en aplicaciones como la fabricación de jabones, en la industria farmacéutica, como aditivo en combustibles biodiesel, aceites hidráulicos o como materia prima para fabricación de resinas debido a su alta disponibilidad de insaturaciones [114]. Otro aceite con aplicaciones parecidas es el de colza o palma, que incluso a pesar de ser comestibles y tener altos consumos a nivel mundial, también fueron empleados para la producción de biodiesel [115]. Por otro lado, un aceite que no incluido en los más producidos a nivel mundial es el aceite de linaza. Como se ha comentado con anterioridad, es comestible pero no tiene un gran uso en esta industria, por lo que su producción se limita a fines industriales. Es empleado como barniz para la madera o como endurecedor de masillas, también empleándose en la obtención de resinas sintéticas [116]. La elevada cantidad de dobles enlaces le proporciona una gran variedad de aplicaciones mediante modificaciones previas, tal y como ocurre con el aceite de soja. La producción del aceite de linaza es cercana a 600.000 toneladas métricas anuales [117], siendo incluso inferior al aceite de oliva con 4.5 millones de toneladas métricas anuales. La gran diferencia de las producciones de linaza en comparación a las demás es debido a su uso exclusivamente industrial, mientras que los restantes presentan un gran peso en la industria alimentaria.

I.3.2. Métodos de extracción de aceites

La extracción del aceite vegetal a partir de diferentes semillas oleaginosas se puede llevar a cabo mediante diferentes aproximaciones, entre las que destacan el prensado mecánico, mediante el empleo de disolventes, empleo de CO_2 y la extracción enzimática [118].

I.3.2.1. Prensado mecánico

Este tipo de extracción es el método más antiguo empleado y se puede realizar mediante el prensado hidráulico o prensado mediante husillos o tornillos sinfín. Una de las ventajas respecto a otros procesos es el bajo coste de la extracción y el bajo impacto medioambiental generado, ya que no emplea ningún tipo de disolvente. Aunque el método hidráulico es ampliamente empleado, la extracción por husillo es un proceso continuo más moderno y eficaz, donde el paso de un husillo va comprimiendo las semillas conforme se va acercando al extremo [119]. En la Figura I.17. se muestra un esquema del prensado mediante husillo. Un factor que influye en el rendimiento es la temperatura, trabajando a temperatura ambiente o elevadas temperaturas. El prensado en temperatura ambiente tiene menor rendimiento que el caliente, pero a pesar de ello logra preservar una mayor calidad del aceite.

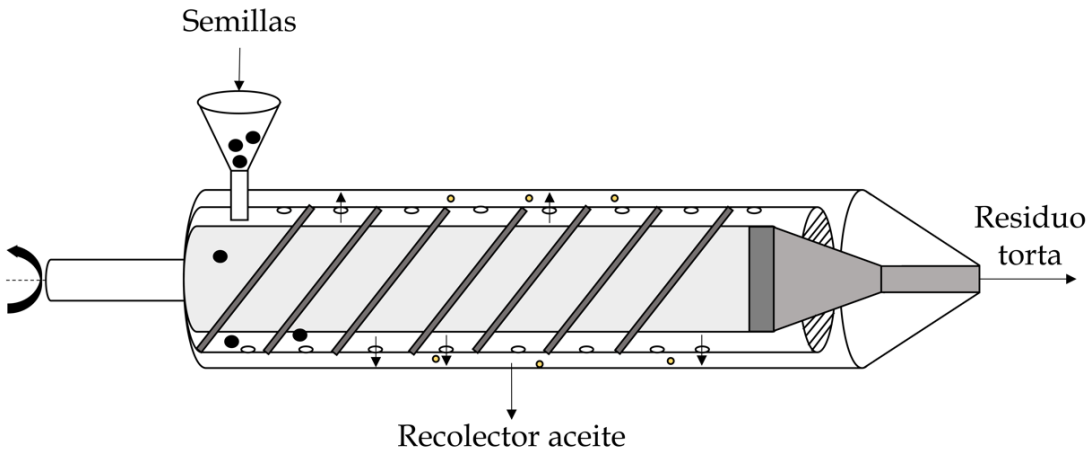

Figura I.17. Esquema de prensado de aceite mediante el método por husillo.

I.3.2.2. Extracción mediante disolventes

Es el método más eficaz desde el punto de vista del rendimiento de extracción de aceites a partir de semillas. El rendimiento dependerá de factores como del tipo de superficie o grosor de la semilla triturada. Este tipo de procesos de extracción utilizan disolventes orgánicos como pueden ser el hexano o el éter debido a su gran afinidad para disolver el aceite a temperaturas elevadas (hasta el punto de ebullición 50-70 ^{o}C en función del disolvente empleado) con consumos de disolvente entre los 15 mL y los 500 mL por cada kg de aceite. A pesar de que se trabaje en condiciones atmosféricas y el coste energético sea bajo, el proceso requiere del empleo de un disolvente orgánico que debe ser tratado posteriormente para evitar su vertido. [120].

I.3.2.3. Extracción mediante dióxido de carbono

Este método requiere de dióxido de carbono (CO_2) a altas presiones para poder realizar la extracción del aceite. El principio de este método radica en que las semillas tratadas y molidas entran en contacto con el CO_2 a alta presión (estado líquido), permitiendo disolver el aceite a temperaturas siempre menores al punto crítico, es decir, 31 ^{o}C para el CO_2. Seguidamente, se produce una reducción de presión hasta alcanzar la atmosférica generando un cambio de fase de CO_2 a estado gaseoso y, por tanto, liberando el aceite en estado líquido. Las ventajas de este método son el no uso de compuestos orgánicos, empleado el CO_2 como disolvente no tóxico, altamente disponible, barato y no inflamable. Sin embargo, requiere de altas presiones (hasta 200 bares) para su obtención con el riesgo que conlleva a nivel operacional [121].

I.3.2.4. Extracción enzimática

Es una de las alternativas más interesantes para la extracción de aceites debido al empleo de un disolvente acuoso como medio para la extracción. Este proceso emplea enzimas, donde previamente las semillas son molidas para favorecer la extracción. Después, se añade la enzima específica en concentraciones cercanas al 1% en peso respecto a la semilla para que digiera la materia sólida de la semilla. Las enzimas específicas digieren las paredes celulares, permitiendo que el aceite quede en forma de emulsión. Por último, se produce la separación del aceite mediante

centrifugación, y se procede al secado del aceite. Uno de los inconvenientes presentes en este proceso es el alto coste de las enzimas y el largo proceso de incubación. Entre las ventajas que presenta este método destaca el empleo de agua como disolvente, evitando grandes flujos de disolvente orgánicos, y que incluso es posible utilizar este método conjuntamente con otras técnicas de extracción [122].

En la Tabla I.4. se muestra las características más importantes de cada proceso de extracción. Desde el punto de vista medioambiental, el método mediante prensado mecánico es el más apropiado por su bajo coste operacional, facilidad en el proceso y el no empleo de disolvente.

Tabla I.4. Comparativa de los métodos de extracción de aceites a partir de plantas oleaginosas.

Método extracción	Disolvente	Presión	Rendimiento	Complejidad[(b)]	Coste operación
Mecánico	-	0-70 MPa[(a)]	Bajo-Medio	Bajo	Bajo
Solvente	Hexano/éter	-	Medio-Alto	Bajo-medio	Bajo-medio
CO_2 supercrítico	CO_2+co-disolvente	>200 bar	Medio-Alto	Bajo-medio	Medio-alto
Enzimático	Agua	-	Medio-Alto	Alto	Alto

[(a)] presión mediante fuerza mecánica de prensado, [(b)] complejidad en el proceso de producción.

I.3.3. Modificaciones aplicadas a aceites vegetales

Una vez extraído el aceite y conocido el potencial que presenta su empleo a nivel industrial debido a sus insaturaciones, se mostrarán las dos modificaciones químicas más empleadas: la epoxidación y la maleinización. Ambos procesos son ampliamente usados en la industria de los polímeros para el desarrollo de plastificantes, compatibilizantes, barnices, etc. Además, existen otros procesos como hidroxilación, acrilación o incluso acrilación/epoxidación, siendo menos empleados actualmente en la industria polimérica.

I.3.3.1. Epoxidación

La reacción de epoxidación es una de las modificaciones químicas más empleadas en los aceites vegetales. Los aceites epoxidados que más se emplean en la industria son el aceite de linaza con IY entre 170 y 204 I_2 g/100 g aceite, y el aceite de

soja con IY entre 120 y 130 I_2 g/100 g aceite. Los motivos de su empleo son por su alto IY y bajo coste. Esta modificación consiste en la adición de un grupo epoxi (C-O-C) sustituyendo el doble enlace (C=C) presente en el triglicérido. De tal forma que conforme mayor cantidad de insaturaciones presente dicho aceite, mayor podrá ser la cantidad de grupos epoxi que puedan introducirse. Esto conlleva mayor interacción entre el aceite modificado y su posterior aplicación. Existen diferentes métodos para que se produzca la epoxidación del aceite en función del portador del grupo epoxi. Las posibilidades existentes son:

- Epoxidación con ácidos percarboxílicos o método Prilezhaev.
- Epoxidación con oxígeno molecular.
- Epoxidacion con halohidrinas.

De estas posibilidades, el método llamado Prilezhaev es la que más se emplea en la actualidad. Esta reacción consiste en emplear los ácidos percarboxílicos como principal método de transporte de oxígeno hasta los dobles enlaces, formando el grupo epoxi. Sin embargo, dado que esta reacción puede generar mezclas explosivas, es recomendable que la formación de los ácidos percarboxílicos sean *in situ* con la presencia de un ácido mineral como puede ser el ácido sulfúrico [123]. Respecto a los dos restantes métodos de epoxidación, diferentes estudios muestran que no son tan eficientes. En el caso de la epoxidación mediante oxígeno molecular, la reacción se genera a partir de un mecanismo de radicales poco estables. Esto da lugar a grandes cantidades de subproductos, además de generar una mezcla de grupos epoxi *cis* y *trans,* presentando poca selectividad [124]. Por otro lado, el empleo de halohidrinas es una ruta que es poco respetuosa con el medioambiente, debido a que este método emplea reactivos que dan lugar a subproductos como halógenos, éteres, dihaluros y sales [125].

Método Prilezhaev

Es el método más conocido y empleado a nivel industrial para epoxidar aceites vegetales. Por un lado, se emplean perácidos como oxidantes (ácidos carboxílicos + H_2O_2) permitiendo la transferencia de la molécula de oxígeno desde la fase acuosa hasta la fase orgánica. Una vez que se produce la conversión de dobles enlaces a

grupos epoxis, se vuelve a obtener un ácido carboxílico para volver a reaccionar con el H_2O_2 presente en la fase acuosa. Este método permite obtener los grupos epoxi en posición *cis* siempre y cuando los dobles enlaces se encuentren en dicha posición. Por otro lado, es necesario emplear catalizadores para que se produzca la reacción, donde en este método se emplean catalizadores homogéneos. En la Figura I.18. se muestra el esquema de reacción de epoxidación mediante el método Prilezhaev.

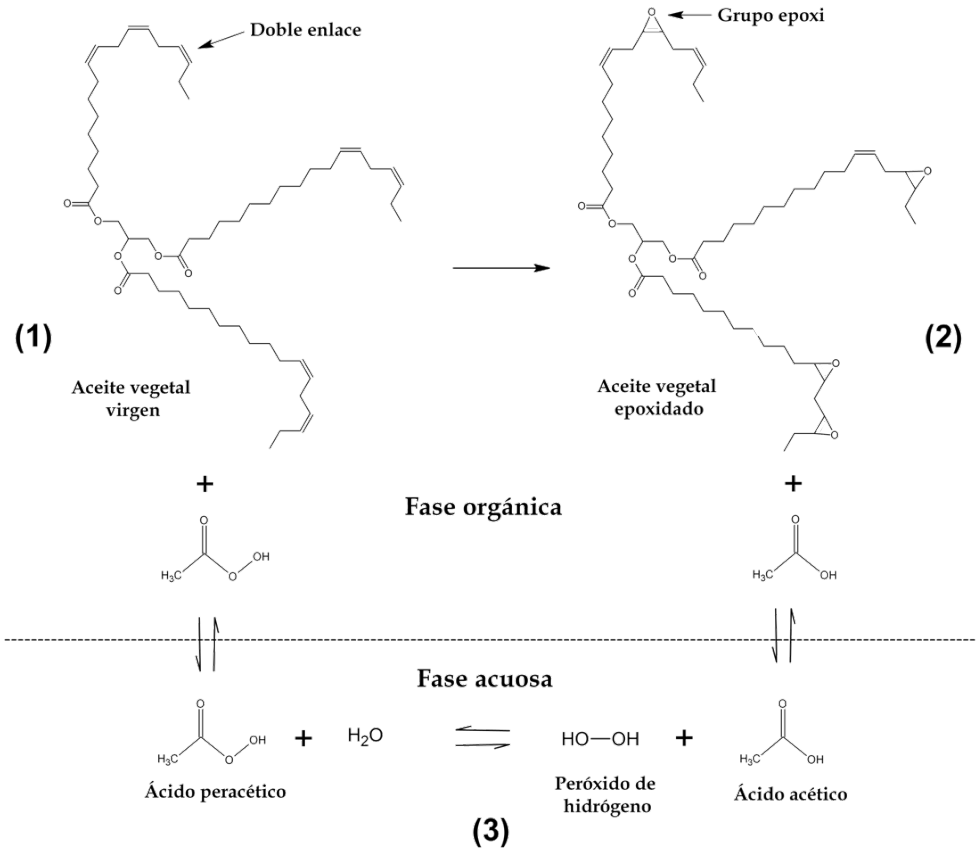

Figura I.18. Esquema de la reacción de epoxidación. Adaptado de [126].

Respecto a los ácidos carboxílicos empleados en presencia del oxidante (H_2O_2) para dar lugar al perácido, varios estudios han sido realizados para estudiar la reactividad de estos en la reacción de epoxidación. La reactividad de los ácidos carboxílicos de menor a mayor es: ácido acético, ácido benzoico, ácido fórmico y ácido *m*-clorobenzoico. Sin embargo, los provenientes del benzoico presentan alto coste y mayor dificultad a la hora de la separación con la parte oleosa [127]. Por ese motivo, los más empleados son el ácido acético y fórmico, cuya efectividad varía en función del rango de temperaturas empleado. En el caso del ácido acético, se ha observado

que actúa con mayor efectividad en rangos mayores de 60 ºC, mientras que el ácido fórmico es utilizado entre 40 ºC y 60 ºC [128].

Por otro lado, los catalizadores homogéneos empleados en este método convencional son los ácidos inorgánicos, como el ácido sulfúrico, ácido clorhídrico, ácido nítrico o ácidos fosfórico. La efectividad de estos también ha sido estudiada, destacando que la conversión de dobles enlaces al grupo epoxi fue mayor mediante el empleo del ácido sulfúrico y fosfórico [129]. Sin embargo, la cantidad de catalizador influye consideradamente en el rendimiento de la reacción de epoxidación. Por ejemplo, una baja concentración de catalizador no permitirá que se produzca una correcta conversión, mientras que una alta concentración generará reacciones secundarias con su consecuente apertura del grupo epoxi.

Las posibles reacciones segundarias pueden aparecer debido a las cantidades no optimizadas de ácidos fuertes inorgánicos, peróxido de hidrógeno, agua y ácidos carboxílicos. La reacción de estos compuestos con el grupo epoxi ya generado durante la misma reacción, produce una apertura del grupo epoxi disminuyendo el rendimiento. En la Figura I.19. se muestras las posibles reacciones segundarias que se pueden obtener. Una de las propuestas para la disminución de estas reacciones secundarias, es estudiar los parámetros que influyen en la reacción de cada aceite vegetal, como las cantidades de reactivos a emplear, temperatura, agitación y tiempo de reacción.

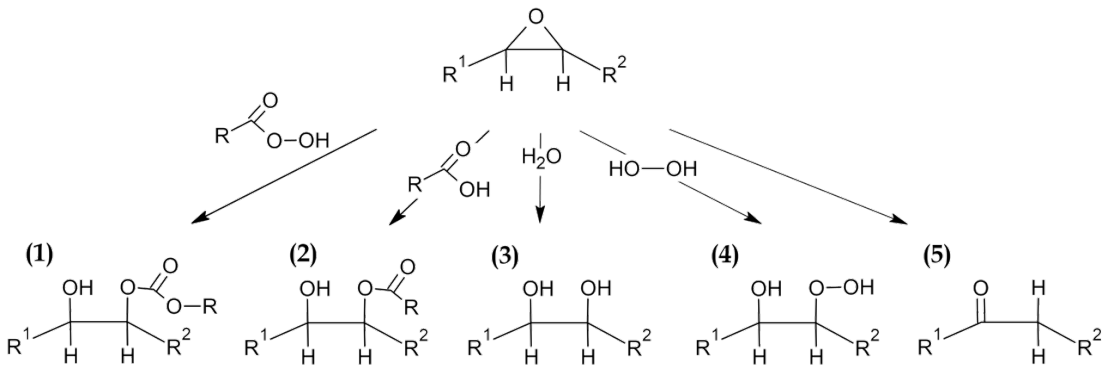

Figura I.19. Esquema de reacciones secundarias durante la reacción de epoxidación. Adaptado de [130]

En la actualidad también se está empleando el mismo método de epoxidación mediante perácidos empleando catalizadores diferentes a los ácidos inorgánicos. Entre los catalizadores homogéneos, destacan los organo-metálicos como óxido de molibdeno o metil trióxido de renio. Sin embargo, presentan dificultad a la hora de la separación y recuperación del catalizador además de que su sostenibilidad a escala industrial es baja [131]. También se emplean otros catalizadores basados en titanio o vanadio en presencia de otros peróxidos orgánico como tert butilo de hidroperóxido, empleando tolueno [132]. Estos catalizadores homogéneos alternativos no pueden reemplazar los convencionales ácidos fuertes, ya que o emplean disolventes tóxicos como tolueno o no muestran el rendimiento adecuado. La epoxidación enzimática es otra alternativa ya estudiada en literatura. Se trata de una reacción donde intervienen 3 fases:la acuosa, la oleosa y la sólida que contiene en este caso las enzimas inmovilizadas. A pesar de que presenten alta selectividad y suprime en gran medida las reacciones secundarias, sigue presentando limitaciones a escala industrial como el alto coste de las enzimas, la gran cantidad de disolventes y la rápida desactivación bajo determinadas condiciones [130]. Por otro lado, los catalizadores heterogéneos basados en titanio y resinas ácidas de intercambio iónico como la Amberlite IR-120 son las más comunes. El uso de estos permite solucionar los inconvenientes de los ácidos inorgánicos con cantidades no optimizadas, pero su empleo a nivel industrial es también limitado por la gran cantidad de catalizadores necesarias (entorno al 20% en peso del sustrato) para obtener un producto con alto porcentaje epoxi.

Por tanto, actualmente a nivel industrial el catalizador más empleado es el ácido sulfúrico debido a su alto rendimiento, bajo coste y baja cantidad empleada, lográndose rendimientos catalíticos muy aceptables [133].

I.3.3.2. Maleinización

La reacción de maleinización es una de las modificaciones más conocidas junto a la epoxidación. Es tal la importancia que incluso es posible encontrar estos productos a nivel comercial como es el caso del aceite maleinizado de linaza o de soja [134]. A nivel de investigación, también se encuentras diferentes estudios de maleinización del aceite de algodón [135], cáñamo [136] o ricino, entre otros [137].

La reacción se lleva a cabo mediante una única etapa añadiendo el anhídrido maleico (MA) como reactivo con la finalidad de incorporarlo en la estructura del aceite vegetal. Generalmente, las temperaturas empleadas en la reacción están en torno 180-230 ºC. En bibliografía, la metodología más común es la adicción del reactivo en tres etapas escalonadas de 1 hora a 180, 200 y 220 ºC. Sin embargo, otros autores emplearon diferentes temperaturas, e incluso una búsqueda de mayor eficiencia mediante el empleo de disolventes [138-139]. Como resultado general de la reacción, se obtiene un grupo maleato unido a la estructura del aceite, cuya posición en el triglicérido puede variar en función de la posición de los dobles enlaces. En la reacción de maleinización pueden darse lugar dos tipos de adición del MA. El primer tipo de adición es mediante la reacción -ene, donde el doble enlace no conjugado del aceite actúa como punto de unión (-ene) con el doble enlace presente en el MA. Como consecuencia, un nuevo enlace se forma tras la migración del doble enlace del ácidoraso para formar el enlace químico con el MA. El segundo mecanismo que puede darse lugar es mediante la reacción de Diels-Alder. Este mecanismo ocurre siempre y cuando haya presencia de un doble enlace conjugado, como los presentes en los ácidos grasos [140]. Los mecanismos de reacción que dan lugar al grupo maleato en la reacción de maleinización se muestra en la Figura I.20.

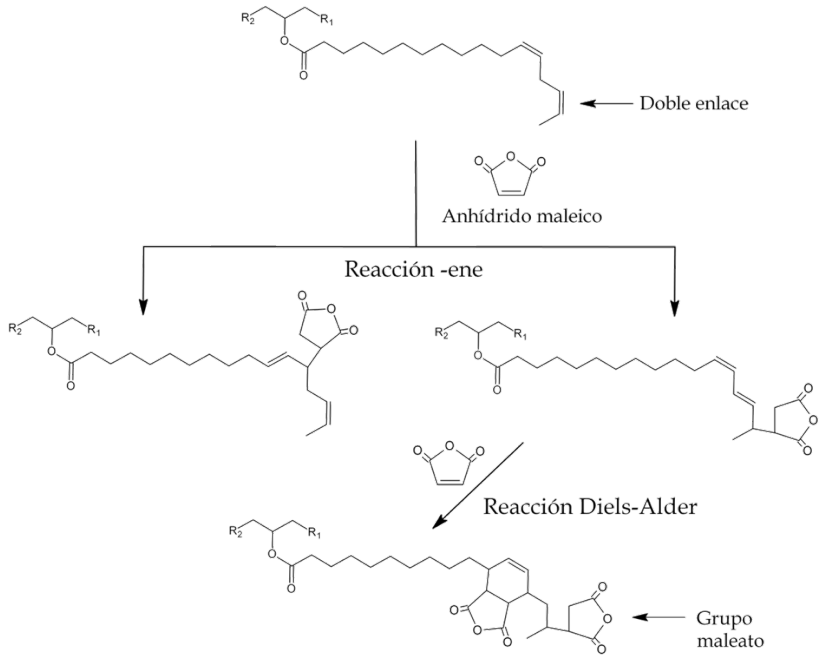

Figura I.20. Mecanismos de adición del anhídrido maleico en la reacción de maleinización del aceite vegetal. Adaptado de [141].

La técnica para poder conocer la cantidad de grupos maleatos insertados en la estructura del aceite vegetal es mediante el cálculo del índice de acidez. De acuerdo con la norma ISO 660, es posible conocer los miligramos de hidróxido potásico (KOH) necesarios para neutralizar los AGs libres del aceite. Además, teniendo en cuenta que el KOH es también capaz de neutralizar el MA, es posible conocer como transcurre dicha reacción. Tal y como se ha comentado anteriormente, a pesar de que esta reacción no consume la totalidad de las insaturaciones del aceite, el IY inicial del aceite es un valor que se tiene que tomar en consideración. Los AGs que presenten mayor reactividad, es decir, los que mayores insaturaciones presentan, serán los que previsiblemente presenten mayor interés en este tipo de reacciones. Sin embargo, las condiciones de la reacción como la temperatura, tiempo y cantidad de reactivo empleado, son parámetros que afectan al rendimiento. El estudio realizado por Zlatanic *et al.* [142], indica que el exceso de MA no implica una mayor sustitución, si no que además requiere un mayor consumo de tiempo para la separación del reactivo no reaccionado. Por otro lado, una temperatura excesiva y/o tiempo, también implica que la cantidad Adherida a la molécula disminuya como consecuencia de la competición de la reacción ene y Diels-Alder con la degradación de MA [143].

I.3.4. Aplicaciones de los aceites vegetales modificados

Los aceites vegetales modificados presentan una gran aplicabilidad a nivel industrial, donde se puede encontrar numerosos estudios en bibliografía tanto aplicado en materiales termoplásticos como en termoestables.

Aplicaciones en termoplásticos

Una de las alternativas que más interés presenta es el empleo de aceites vegetales como plastificantes de origen renovable. Estos presentan bajo coste, no toxicidad y debido a su alto peso molecular cercano a los 900 $g \cdot mol^{-1}$ permiten solucionar el inconveniente de la migración que presentan los plastificantes comunes, como los ftalatos. Es por ello que diferentes propuestas han sido empleadas con aceites vegetales modificados químicamente para aumentar la compatibilidad con los polímeros. Qinghe *et al*. [144] estudió la plastificación del PVC con aceite epoxidado de ricino con un 25 partes por cada cien de resina (phr), donde se obtuvieron valores

de migración bajos. otro ejemplo sería la investigación realizada por Ferri *et al*. [145], donde se emplea el aceite maleinizado de linaza (5-20 phr) como plastificante en una matriz de PLA. En dicho estudio se observó un incremento del 1020% de alargamiento a la rotura respecto al PLA virgen, con una disminución del 5-6 ºC de la temperatura de transición vítrea y un aumento de la energía absorbida tras impacto de casi el doble. En referido a compatibilizantes, los aceites vegetales pueden también juegar un papel importante. Tal y como se ha comentado, los compatibilizantes deben presentar grupos reactivos, y los aceites vegetales funcionalizados son una alternativa. En bibliografía se puede encontrar estudios realizados con aceites epoxidados y maleinizados. Un ejemplo sería el realizado por Maria *et al.* [146] donde estudió el efecto de la cáscara de argán en una matriz de bio polietileno de ultra alta densidad (Bio-HDPE) empleando diferentes compatibilizantes como el copolimero de injerto de etileno injertado y anhídrido maleico (PE-g-MA) y aceite maleinizado de linaza. En dicho estudio se observó una mejora de compatibilidad de la cáscara de argán junto a una mejor estabilidad térmica.

Aplicaciones en termoestables

Los compuestos derivados de aceites vegetales modifiados químicamente se pueden emplear como resina de tipo epoxi e incluso como endurecedor de tipo anhídrido. Los más empleado como base para el desarrollo de una resina epoxi son el aceite epoxidado de linaza y soja los cuales están disponibles a nivel comercial. La obtención de resinas a partir de estos aceites epoxidados con endurecedores tipo anhídridos de origen petroquímico le confiere al material final propiedades interesantes, como es la mayor ductilidad. Sin embargo, la T_g es inferior a las comerciales encontrándose éstas en torno a los 100 ºC. Estas propiedades finales de la resina entrecruzada están totalmente relacionadas con la estructura interna del material, donde se sustituye la resina epoxi tradicional con bajo peso molecular, por la molécula de triglicérido que presenta mayor peso molecular y tamaño. En los casos donde se requieren mayores prestaciones, es necesario mitigar las desventajas de mayor ductilidad y menor T_g aportada por los aceites vegetales. Algunos autores se han centrado en la mezcla de resinas de origen petroquímico con epoxi obtenidas de origen renovable, para obtener unas mejores propiedades. Un ejemplo es Gupta *et al.*

[147], que realizó un estudio añadiendo desde 0 a 30 phr de DGEBA al aceite epoxidado de soja, empleando el anhídrido ftalaico como endurecedor. En dicho estudio se observo una mejora de 68.3 a 107.3 ^{o}C en la T_g con la incorporación de 30 phr de DGEBA.

En lo referido a los aceites maleinizados, generalmente son empleados como agente de entrecruzamiento en presencia de una resina epoxi. Su incorporación también le confiere mayor flexibilidad al material, tal y como ocurre con las resinas epoxi de origen vegetal. En este sentido, Rosu *et al.* [148] empleó aceite de ricino maleinizado como endurecedor en una matriz de DGEBA para ser destinado como material aislante para posibles aplicaciones de recubrimiento.

I.3.5. Responsabilidad de uso

En los capítulos anteriores se ha comentado el potencial que presentan los aceites vegetales y su importancia como aditivo o base para la obtención de materiales ecológicos. No obstante, el empleo de aceites vegetales despierta dos dilemas: (1) la producción tras el cultivo de plantas empleando terreno que puede ser destinado a cultivar alimentos; (2) algunos aceites vegetales son comestibles, con lo que aumenta la demanda y, por tanto, aumenta el precio de estos alimentos. Este último hecho ya ocurrió en la producción de biodiesel a partir de aceites vegetales, donde el 80% del precio final del biodiesel era debido al coste de los aceites [149].

A pesar de ello, el empleo de los aceites vegetales para la obtención de bioplásticos no compromete la disponibilidad de terreno para uso agrícola. De acuerdo con European Bioplastics [18], la tierra empleada para el cultivo de materia prima de origen renovable en la producción de bioplásticos es entorno a 0.8 millones de hectáreas en 2022. En representación a toda la superficie agrícola mundial (5000 millones de hectáreas), únicamente representa el 0,015% de la superficie. En el caso de seguir la previsión de crecimiento de bioplasticos, se prevé que para 2027 represente tan solo un 0,06% de la superficie agrícola. Estos valores muestran que no existe una competencia entre las materias primas para producción de plástico y obtención de alimentos. Para una mayor referencia y comparación, los biocombustibles hacen uso del 4% de la superficie cultivable, valores muy lejanos al de los bioplásticos.

En lo referido a los precios, en la actualidad existen aceites con fines industriales que siguen empleándose ampliamente para usos comestibles sin gran repercusión en el coste. Un ejemplo es el aceite de soja, que es empleado para obtención de biocombustibles y en la industria del plástico como aceite epoxidado, sin comprometer su uso para el consumo humano. Su precio desde el 2010, ha ido disminuyendo hasta alcanzar una estabilidad desde 2015 hasta 2020, donde a partir de la pandemia mundial COVID-19, su precio se encareció hasta la actualidad [150].

I.4. Semilla de chía

Salvia hispanica L., comúnmente conocida como chía, es una planta herbácea nativa de América central. Durante su crecimiento requiere suelos no muy húmedos y abundante sol, donde las flores dan lugar al fruto que contiene las semillas de chía. Se trata de una semilla comestible y fuente de nutrientes. La primera referencia de su empleo se traslada al 3500 A.C en América central [151] pero durante los últimos años se ha expandido su empleo debido a los beneficios que aporta su consumo.

I.4.1. Producción mundial

La plantación de la semilla de chía se produce principalmente en Bolivia, Ecuador, Colombia, Guatemala, México, Perú y China. El mayor productor es México, el cual exporta a países como Estados Unidos, Japón o paises europeos, entre otros. Tras el aumento de popularidad, países africanos como Uganda han comenzado la plantación de este cultivo. El rendimiento del cultivo de las semillas depende de las condiciones climatológicas, pero su rendimiento puede rondar desde 200 hasta 2000 kg por ha [152-153]. Estos valores son muy similares a los obtenidos por las semillas de linaza (1200-1500 kg por ha) [154] pero inferiores comparados con la semilla de soja con 5000 kg por ha [155].

En lo referido a la producción mundial de semillas de chía, en el 2019 se registró la venta de 66 mil toneladas métricas. La previsión para el 2027 es de 100 mil toneladas métricas, suponiendo un 34% más de ventas. Respecto al aceite de chía, no se encuentra entre lo más producidos basándonos en la Figura I.16. debido a su relativa novedad. Este aceite no es ampliamente utilizado como ocurre con otros aceites vegetales, empleándose en cantidades pequeñas como suplemento alimenticio. En líneas generales el cultivo de la chía se destina mayoritariamente al propio consumo de la semilla (50% de la producción total). Un 20% restante se destina a la producción de harina de chía para productos alimentarios y otro 20% se destina a la obtención de aceite. El 10% se destina a la utilización de la chía como espesante, tras su hidratación. [156].

I.4.2. Composición del aceite de chía

La semilla de chía está compuesta por aceite con altos niveles de AGs, mientras que el resto de la semilla contiene mayoritariamente proteínas y fibras. Varios estudios han reportado que la variación de la composición depende de los parámetros climatológicos durante su crecimiento [157].

Por un lado, el aceite de chía se puede extraer mediante diversos métodos como se comentó en el apartado I.3.2. Su contenido en aceite puede variar desde el 25 al 40 % en peso de la semilla de chía. Los AGs que contiene son de elevada calidad, con un contenido del 80% de AGs poliinsaturados PUFAs. De hecho, es el aceite vegetal con mayor contenido de alfa-linolénico (omega-3) disponible, en torno al 55-67% [158]. Algunos autores han sugerido el empleo de este aceite como complemento alimentario debido a sus beneficios, pero a pesar de ello no es tan empleado como otros aceites vegetales. El aceite obtenido de la semilla de chía es uno de los que mayor grado de instauración presenta entre los aceites disponibles, con índices de yodo en el rango de 180-205 g I_2/100 g de aceite [159-160]. De forma más detallada, y con la finalidad de comparar los AGs del aceite de chía con los aceites empleados en mayor proporción en la industria de polímeros, en la Tabla I.5 se resume los principales AGs presentes en cada uno.

En dicha tabla se indica que el aceite de chía contiene la menor cantidad de AGs saturados y monoinsaturados. En lo referido a la reactividad, la Tabla I.5. también especifica la cantidad de dobles enlaces por cada triglicérido, siendo un indicativo de la reactividad para posibles modificaciones químicas. En este sentido, el aceite de chía presenta una media de dobles enlace de 7,1 mientras que el de linaza es 6,56. Teniendo en cuenta que estos valores pueden variar en función de las condiciones de cultivo y de la semilla, en general el aceite de chía presenta la misma o incluso mayor cantidad de dobles enlaces por triglicérido que el aceite de linaza. Por tanto, la mayor reactividad del aceite de chía abre la posibilidad de ser utilizado como alternativa a los actuales aceites empleados en la industria polimérica. Otra característica interesante del aceite de chía es la alta capacidad antioxidante. La presencia de flavonoles, ácido cafeico o clorogénico, los cuales poseen elevadas propiedades

antioxidantes, abre las puertas a procesos de extracción para su empleo como antioxidantes en aplicaciones poliméricas, como por ejemplo en films para el envasado de productos alimentarios. [161].

Tabla I.5. Principales AGs de los aceites más empleados en el sector polimérico.

Ácidos grasos (AGs)[a]	**Soja [162]**	**Linaza [163]**	**Chia [164]**
Palmítico (C16:0)	16,9	5,1	6,8
Esteárico (C18:0)	5,15	4,3	2,71
Oleico (C18:1)	16,04	15,8	6,17
Linoleico (C18:2)	47,57	16,5	18,6
α-Linolénico (C18:3)	12,11	56,6	64,4
Araquídico (C20:0)	1,40	0,17	0,28
Eicosenoico (C20:1)	0,45	0,17	0,020
AG saturados[b]	23,43	9,57	9,79
AG monoinsaturados[b]	16,49	15,97	6,45
AG poliinsaturados[b]	59,68	73,1	83,0
Media D:E[c]	4,43	6,56	7,1

[a] % en peso; [b] Cálculos realizados tras la suma de sus correspondientes ácidos grasos (AGs); [c] Media dobles enlaces por triglicérido. Nota: la diferencia de ácidos grasos respecto a la Tabla I.3 es debido a la diferente procedencia de las semillas, cuyos valores de ácidos grasos pueden variar.

I.4.3. Composición del residuo seco

Por otro lado, tras el proceso de extracción del aceite de chía, se genera un residuo sólido denominado torta. La torta obtenida, que tras el proceso de molienda da lugar a una harina, estará compuesta mayoritariamente por carbohidratos, proteínas, vitaminas y minerales. En la Tabla I.6. se resume la composición aproximada de la semilla de chía.

Tabla I.6. Estimación de la composición de la semilla de chía tras la extracción de aceite en base a bibliografía. Adaptado de [165-166].

Componentes			**% respecto a la semilla**
Lípidos			25-35
Carbohidratos			50,3-56,7
	Fibras Soluble	Mucílago	3,0-3,60
	Fibra Insoluble	Celulosa	17,6-19,1
		Hemicelulosa	24,2-28,0
		Lignina	5,49-6
Proteínas			18-24
			µg/g de semilla
Minerales	Fósforo		8,60-9,19
	Calcio		4,56-6,31
	Potasio		4,07-7,26
	Magnesio		3,35-4,49
Antioxidantes	Ácido gálico		0,05-11
	Ácido caféico		27-30,89
	Ácido clorogenico		4,68

Nota: la suma de los valores porcentuales se excede del 100% al deberse de aproximaciones en la composición química. Además, los datos reflejados son para una determinada procedencia de semilla por lo que la composición podría variar entre diferentes fuentes.

Tal y como se observa en la Tabla I.6., los carbohidratos representan más de la mitad de la semilla de chía y aproximadamente el 73% de la harina obtenida tras el proceso de extracción de aceite. Las fibras solubles representan solo el 6% de los carbohidratos, siendo el componente mayoritario el mucílago, es decir, elementos de alto peso molecular con gran capacidad de retención de agua [161]. En lo referido a las proteínas, su contenido representa aproximadamente entre el 18 y 24%, siendo valores similares a los porcentajes reportados en otros alimentos como lentejas, guisantes o garbanzos [167]. Por último, la semilla también presenta minerales y antioxidantes con contenidos inferiores al 1%.

REFERENCIAS

[1] T. M. Letcher. 1 - Global warming—a complex situation. In Climate Change (Third Edition), Letcher, T.M., Ed.; Elsevier: 2021; pp. 3-17.

[2] S. A. Montzka, Dlugokencky, E. J., Butler, J. H. Non-CO2 greenhouse gases and climate change. Nature 2011, 476, 43-50, doi:10.1038/nature10322.

[3] J. S. P.R. Shukla, R. Slade, A. Al Khourdajie, R. van Diemen, D. McCollum, M. Pathak, S. Some, P. Vyas, R. Fradera, M. Belkacemi, A. Hasija, G. Lisboa, S. Luz, J. Malley, (eds.). Summary for Policymakers. In: Climate Change 2022: Mitigation of Climate Change. Contribution of Working Group III to the Sixth Assessment Report of the Intergovernmental Panel on Climate Change; 2022. doi:10.1017/9781009157926.001.

[4] Growing population estimation. Available online: https://www.un.org/en/global-issues/population (accessed on 27 julio).

[5] Global outlook on electricity generation 2020-2050, by energy source. Available online: https://www.statista.com/statistics/238610/projected-world-electricity-generation-by-energy-source/]. (accessed on 9 de septiembre).

[6] Emissions CO2 by sector. Available online: https://ourworldindata.org/emissions-by-sector (accessed on 8 de septiembre).

[7] H. V. Ford, Jones, N. H., Davies, A. J., Godley, B. J., Jambeck, J. R., Napper, I. E., Suckling, C. C., Williams, G. J., Woodall, L. C., Koldewey, H. J. The fundamental links between climate change and marine plastic pollution. Science of the Total Environment 2022, 806, doi:10.1016/j.scitotenv.2021.150392.

[8] Annual production of plastics worldwide from 1950 to 2020. Available online: https://www.statista.com/statistics/282732/global-production-of-plastics-since-1950/ (accessed on 8 de septiembre).

[9] Plastic production forecast worldwide 2025-2050. Available online: https://www.statista.com/statistics/664906/plastics-production-volume-forecast-worldwide/ (accessed on 8 de septiembre).

[10] A. Olhoff, Christensen, J. M. Emissions gap report 2018. UNEP DTU Partnership: Copenhagen, Denmark 2018.

[11] T. C. E. Progress. International Energy Agency. Paris, France 2017.

[12] D. Bourguignon. Plastics in a circular economy: Opportunities and challenges. European Parliamentary Research Service: Brussels, Belgium 2017.

[13] J. Zheng, Suh, S. Strategies to reduce the global carbon footprint of plastics. Nature Climate Change 2019, 9, 374-+, doi:10.1038/s41558-019-0459-z.

[14] PlasticsEurope. Plastics- the Facts 2021: An analysis of European plastics production, demand and waste data Available online: https://www.plasticseurope.org (accessed on 8 de septiembre).

[15] R. Sharma, Sharma, M., Sharma, R., Sharma, V. The impact of incinerators on human health and environment. Reviews on environmental health 2013, 28, 67-72, doi:10.1515/reveh-2012-0035.

[16] J. R. Jambeck, Geyer, R., Wilcox, C., Siegler, T. R., Perryman, M., Andrady, A., Narayan, R., Law, K. L. Plastic waste inputs from land into the ocean. Science 2015, 347, 768-771, doi:10.1126/science.1260352.

[17] S. Spierling, Knuepffer, E., Behnsen, H., Mudersbach, M., Krieg, H., Springer, S., Albrecht, S., Herrmann, C., Endres, H.-J. Bio-based plastics - A review of environmental, social and economic impact assessments. Journal of Cleaner Production 2018, 185, 476-491, doi:10.1016/j.jclepro.2018.03.014.

[18] European Bioplastics. Bioplastics market data Available online: https://www.european-bioplastics.org/market/ (accessed on 8 de septiembre).

[19] European Comission. A European strategy for plastics in a circular economy Available online: https://www.europarc.org/wp-content/uploads/2018/01/Eu-plastics-strategy-brochure.pdf (accessed on 12 de septiembre).

[20] I. D. Posen, Jaramillo, P., Landis, A. E., Griffin, W. M. Greenhouse gas mitigation for US plastics production: energy first, feedstocks later. Environmental Research Letters 2017, 12, doi:10.1088/1748-9326/aa60a7.

[21] Annual production of plastics in Europe from 1950 to 2020. Available online: https://www.statista.com/statistics/987838/plastics-production-volume-in-the-eu-28/ (accessed on 12 de septiembre).

[22] Regulation (EU) 2021/1119 of the European Parliament and of the Councing establishing the framework for achieving climate neutrality and amending Regulations (EC) No 401/2009 and (EU) 2018/1999 ('European Climate Law'). 2021, 1-17.

[23] M. Niaounakis, Niaounakis, M. Biopolymers: Processing and Products Introduction; 2015; pp. 1-77.

[24] F. M. Al-Oqla, Sapuan, S. M., Ishak, M. R., Nuraini, A. A. A decision-making model for selecting the most appropriate natural fiber - Polypropylene-based composites for automotive applications. Journal of Composite Materials 2016, 50, 543-556, doi:10.1177/0021998315577233.

[25] M. A. Babich, Bevington, C., Dreyfus, M. A. Plasticizer migration from children's toys, child care articles, art materials, and school supplies. Regulatory Toxicology and Pharmacology 2020, 111, doi:10.1016/j.yrtph.2019.104574.

[26] C. Sanchez, Hortal, M., Aliaga, C., Devis, A., Cloquell-Ballester, V. A. Recyclability assessment of nano-reinforced plastic packaging. Waste Management 2014, 34, 2647-2655, doi:10.1016/j.wasman.2014.08.006.

[27] H. Stichnothe, Azapagic, A. Life cycle assessment of recycling PVC window frames. Resources Conservation and Recycling 2013, 71, 40-47, doi:10.1016/j.resconrec.2012.12.005.

[28] G.-X. Wang, Huang, D., Ji, J.-H., Voelker, C., Wurm, F. R. Seawater-Degradable Polymers-Fighting the Marine Plastic Pollution. Advanced Science 2021, 8, doi:10.1002/advs.202001121.

[29] M. Arslan, Acik, G., Tasdelen, M. A. The emerging applications of click chemistry reactions in the modification of industrial polymers. Polymer Chemistry 2019, 10, 3806-3821, doi:10.1039/c9py00510b.

[30] D. L. Francisco, Paiva, L. B., Aldeia, W. Advances in polyamide nanocomposites: A review. Polymer Composites 2019, 40, 851-870, doi:10.1002/pc.24837.

[31] N. De Vietro, Belforte, L., Lambertini, V. G., Fracassi, F. Low pressure plasma modified polycarbonate: A transparent, low reflective and scratch resistant material for automotive applications. Applied Surface Science 2014, 307, 698-703, doi:10.1016/j.apsusc.2014.04.105.

[32] C. C. Ibeh. Thermoplastic materials: properties, manufacturing methods, and applications; CRC Press: 2011.

[33] T. A. Otitoju, Ahmad, A. L., Ooi, B. S. Recent advances in hydrophilic modification and performance of polyethersulfone (PES) membrane via additive blending. Rsc Advances 2018, 8, 22710-22728, doi:10.1039/c8ra03296c.

[34] I. V. Panayotov, Orti, V., Cuisinier, F., Yachouh, J. Polyetheretherketone (PEEK) for medical applications. Journal of Materials Science-Materials in Medicine 2016, 27, doi:10.1007/s10856-016-5731-4.

[35] R. I. Shekar, Kotresh, T. M., Rao, P. M. D., Kumar, K. Properties of High Modulus PEEK Yarns for Aerospace Applications. Journal of Applied Polymer Science 2009, 112, 2497-2510, doi:10.1002/app.29765.

[36] A. Dey, Dhumal, C. V., Sengupta, P., Kumar, A., Pramanik, N. K., Alam, T. Challenges and possible solutions to mitigate the problems of single-use plastics used for packaging food items: a review. Journal of Food Science and Technology-Mysore 2021, 58, 3251-3269, doi:10.1007/s13197-020-04885-6.

[37] European Bioplastics. What are bioplastics? Available online: https://www.european-bioplastics.org/bioplastics/ (accessed on 13 de septiembre).

[38] A. S. f. T. a. M. (ASTM). Bio-based products testing. 2022, D6866-22.

[39] N. E. (UNE). Envases y embalajes. Requisitos de los envases y embalajes valorizables mediante compostaje y biodegradación. Programa de ensayo y criterios de evaluación para la aceptación final del envase o embalaje. 2005, UNE-EN 13432:2001/AC:2005.

[40] S. S. Ali, Elsamahy, T., Koutra, E., Kornaros, M., El-Sheekh, M., Abdelkarim, E. A., Zhu, D., Sun, J. Degradation of conventional plastic wastes in the environment: A review on current status of knowledge and future perspectives of disposal. Science of the Total Environment 2021, 771, doi:10.1016/j.scitotenv.2020.144719.

[41] A. S. f. T. a. M. (ASTM). Standard Specification for Labeling of Plastics Designed to be Aerobically Composted in Municipal or Industrial Facilities. 2021, D6400-21.

[42] R. F. Storey, Sherman, J. W. Kinetics and mechanism of the stannous octoate-catalyzed bulk polymerization of epsilon-caprolactone. Macromolecules 2002, 35, 1504-1512, doi:10.1021/ma010986c.

[43] M. A. Woodruff, Hutmacher, D. W. The return of a forgotten polymer-Polycaprolactone in the 21st century. Progress in Polymer Science 2010, 35, 1217-1256, doi:10.1016/j.progpolymsci.2010.04.002.

[44] E. Takiyama, Fujimaki, T. Bionolle biodegradable plastic through chemical synthesis In Proceedings of the 3rd International Scientific Workshop on Biodegradable Plastics and Polymers, Osaka, Japan, 1993; pp. 150-174.

[45] M. Barletta, Aversa, C., Ayyoob, M., Gisario, A., Hamad, K., Mehrpouya, M., Vahabi, H. Poly(butylene succinate) (PBS): Materials, processing, and industrial applications. Progress in Polymer Science 2022, 132, doi:10.1016/j.progpolymsci.2022.101579.

[46] M. Puchalski, Szparaga, G., Biela, T., Gutowska, A., Sztajnowski, S., Krucinska, I. Molecular and Supramolecular Changes in Polybutylene Succinate (PBS) and Polybutylene Succinate Adipate (PBSA) Copolymer during Degradation in Various Environmental Conditions. Polymers 2018, 10, doi:10.3390/polym10030251.

[47] P. Bordes, Pollet, E., Averous, L. Nano-biocomposites: Biodegradable polyester/nanoclay systems. Progress in Polymer Science 2009, 34, 125-155, doi:10.1016/j.progpolymsci.2008.10.002.

[48] S. A. Ashter. Types of Biodegradable Polumers. Introduction to bioplastics engineering; William Andrew: 2016; Volume 5.

[49] R. W. Harrison. The Food versus Fuel Debate: Implications for Consumers. Journal of Agricultural and Applied Economics 2009, 41, 493-500, doi:10.1017/S1074070800002947.

[50] S. A. Jambo, Abdulla, R., Azhar, S. H. M., Marbawi, H., Gansau, J. A., Ravindra, P. A review on third generation bioethanol feedstock. Renewable & Sustainable Energy Reviews 2016, 65, 756-769, doi:10.1016/j.rser.2016.07.064.

[51] C. Monica Mendieta, Elizabet Cardozo, R., Esteban Felissia, F., Martin Clauser, N., Evangelina Vallejos, M., Cristina Area, M. Bioconversion of Wood Waste to Bio-ethylene: A Review. Bioresources 2021, 16, 4411-4437, doi:10.15376/biores.16.2.Mendieta.

[52] V. Siracusa, Blanco, I. Bio-Polyethylene (Bio-PE), Bio-Polypropylene (Bio-PP) and Bio-Poly(ethylene terephthalate) (Bio-PET): Recent Developments in Bio-Based Polymers Analogous to Petroleum-Derived Ones for Packaging and Engineering Applications. Polymers 2020, 12, doi:10.3390/polym12081641.

[53] L. Averous, Halley, P. J. Biocomposites based on plasticized starch. Biofuels Bioproducts & Biorefining-Biofpr 2009, 3, 329-343, doi:10.1002/bbb.135.

[54] H. J. Park, Byun, Y. J., Kim, Y. T., Whiteside, W. S., Bae, H. J. Processes and Applications for Edible Coating and Film Materials from Agropolymers; 2014; pp. 257-275.

[55] M. V. Cruz, Paiva, A., Lisboa, P., Freitas, F., Alves, V. D., Simoes, P., Barreiros, S., Reis, M. A. M. Production of polyhydroxyalkanoates from spent coffee grounds oil obtained by supercritical fluid extraction technology. Bioresource Technology 2014, 157, 360-363, doi:10.1016/j.biortech.2014.02.013.

[56] S. Rodriguez-Perez, Serrano, A., Pantion, A. A., Alonso-Farinas, B. Challenges of scaling-up PHA production from waste streams. A review. Journal of Environmental Management 2018, 205, 215-230, doi:10.1016/j.jenvman.2017.09.083.

[57] N. Koyama, Doi, Y. Effects of solid-state structures on the enzymatic degradability of bacterial poly(hydroxyalkanoic acids). Macromolecules 1997, 30, 826-832, doi:10.1021/ma961195r.

[58] D. D. Rosa, Calil, M. R., Guedes, C. D. F., Rodrigues, T. C. Biodegradability of thermally aged PHB, PHB-V, and PCL in soil compostage. Journal of Polymers and the Environment 2004, 12, 239-245.

[59] M. Zhang, Thomas, N. L. Blending Polylactic Acid with Polyhydroxybutyrate: The Effect on Thermal, Mechanical, and Biodegradation Properties. Advances in Polymer Technology 2011, 30, 67-79, doi:10.1002/adv.20235.

[60] K. W. Meereboer, Misra, M., Mohanty, A. K. Review of recent advances in the biodegradability of polyhydroxyalkanoate (PHA) bioplastics and their composites. Green Chemistry 2020, 22, 5519-5558, doi:10.1039/d0gc01647k.

[61] Y.-J. Wee, Kim, J.-N., Ryu, H.-W. Biotechnological production of lactic acid and its recent applications. Food Technology and Biotechnology 2006, 44, 163-172.

[62] P. Van Wouwe, Dusselier, M., Vanleeuw, E., Sels, B. Lactide Synthesis and Chirality Control for Polylactic acid Production. Chemsuschem 2016, 9, 907-921, doi:10.1002/cssc.201501695.

[63] A. Djukic-Vukovic, Mladenovic, D., Ivanovic, J., Pejin, J., Mojovic, L. Towards sustainability of lactic acid and poly-lactic acid polymers production. Renewable & Sustainable Energy Reviews 2019, 108, 238-252, doi:10.1016/j.rser.2019.03.050.

[64] J. Lunt, Shafer, A. L. Polylactic Acid Polymers from Com. Applications in the Textiles Industry. Journal of Industrial Textiles 2000, 29, 191-205, doi:10.1177/152808370002900304.

[65] K. Masutani, Kimura, Y. PLA Synthesis. From the Monomer to the Polymer. In Poly(Lactic Acid) Science and Technology: Processing, Properties, Additives and Applications, Jimenez, A., Peltzer, M., Ruseckaite, R., Eds.; RSC Catalysis Series; 2015; pp. 3-36.

[66] K. Berger, Gregorova, A. Thermal Stability of Modified End-Capped Poly(lactic acid). Journal of Applied Polymer Science 2014, 131, doi:10.1002/app.41105.

[67] S. Corneillie, Smet, M. PLA architectures: the role of branching. Polymer Chemistry 2015, 6, 850-867, doi:10.1039/c4py01572j.

[68] L. T. Sin, Rahmat, A. R., Rahman, W. Polylactic Acid: PLA Biopolymer Technology and Applications; 2013; pp. 1-341.

[69] H. Tsuji, Ikada, Y. Crystallization from the melt of poly(lactide)s with different optical purities and their blends. Macromolecular Chemistry and Physics 1996, 197, 3483-3499, doi:10.1002/macp.1996.021971033.

[70] S. Su, Kopitzky, R., Tolga, S., Kabasci, S. Polylactide (PLA) and Its Blends with Poly(butylene succinate) (PBS): A Brief Review. Polymers 2019, 11, doi:10.3390/polym11071193.

[71] T. Takayama, Todo, M., Tsuji, H. Effect of annealing on the mechanical properties of PLA/PCL and PLA/PCL/LTI polymer blends. Journal of the Mechanical Behavior of Biomedical Materials 2011, 4, 255-260, doi:10.1016/j.jmbbm.2010.10.003.

[72] A. Orue, Eceiza, A., Arbelaiz, A. Preparation and characterization of poly(lactic acid) plasticized with vegetable oils and reinforced with sisal fibers. Industrial Crops and Products 2018, 112, 170-180, doi:10.1016/j.indcrop.2017.11.011.

[73] Plastics Europe. Plastics-The Facts 2021. An analysis of European Plastics Production, Demand and Wasta Data 2022.

[74] A. Marotta, Faggio, N., Ambrogi, V., Cerruti, P., Gentile, G., Mija, A. Curing Behavior and Properties of Sustainable Furan-Based Epoxy/Anhydride Resins. Biomacromolecules 2019, 20, 3831-3841, doi:10.1021/acs.biomac.9b00919.

[75] K. Puangsansuk, Opaprakasit, M., Udomkichdecha, W., Potiyaraj, P. Effects of Saturated Acids on Physical Properties of UPE Resins Prepared from Recycled PET Products. Journal of Polymers and the Environment 2009, 17, 65-70, doi:10.1007/s10924-009-0122-2.

[76] T. J. Farmer, Castle, R. L., Clark, J. H., Macquarrie, D. J. Synthesis of Unsaturated Polyester Resins from Various Bio-Derived Platform Molecules. International Journal of Molecular Sciences 2015, 16, 14912-14932, doi:10.3390/ijms160714912.

[77] S. Cousinet, Ghadban, A., Fleury, E., Lortie, F., Pascault, J.-P., Portinha, D. Toward replacement of styrene by bio-based methacrylates in unsaturated

polyester resins. European Polymer Journal 2015, 67, 539-550, doi:10.1016/j.eurpolymj.2015.02.016.

[78] R. Auvergne, Caillol, S., David, G., Boutevin, B., Pascault, J. P. Biobased Thermosetting Epoxy: Present and Future. Chemical Reviews 2014, 114, 1082-1115, doi:10.1021/cr3001274.

[79] F. S. vom Saal, Myers, J. P. Bisphenol A and risk of metabolic disorders. Jama 2008, 300, 1353-1355.

[80] B. Xue, Tang, R., Xue, D., Guan, Y., Sun, Y., Zhao, W., Tan, J., Li, X. Sustainable alternative for bisphenol A epoxy resin high-performance and recyclable lignin-based epoxy vitrimers. Industrial Crops and Products 2021, 168, doi:10.1016/j.indcrop.2021.113583.

[81] F. I. Altuna, Esposito, L. H., Ruseckaite, R. A., Stefani, P. M. Thermal and Mechanical Properties of Anhydride-Cured Epoxy Resins with Different Contents of Biobased Epoxidized Soybean Oil. Journal of Applied Polymer Science 2011, 120, 789-798, doi:10.1002/app.33097.

[82] C. Ding, Matharu, A. S. Recent Developments on Biobased Curing Agents: A Review of Their Preparation and Use. Acs Sustainable Chemistry & Engineering 2014, 2, 2217-2236, doi:10.1021/sc500478f.

[83] M. A. da Silva, Adeodato Vieira, M. G., Gomes Macumoto, A. C., Beppu, M. M. Polyvinylchloride (PVC) and natural rubber films plasticized with a natural polymeric plasticizer obtained through polyesterification of rice fatty acid. Polymer Testing 2011, 30, 478-484, doi:10.1016/j.polymertesting.2011.03.008.

[84] M. Bocque, Voirin, C., Lapinte, V., Caillol, S., Robin, J.-J. Petro-Based and Bio-Based Plasticizers: Chemical Structures to Plasticizing Properties. Journal of Polymer Science Part a-Polymer Chemistry 2016, 54, 11-33, doi:10.1002/pola.27917.

[85] A. D. Godwin, Krauskopf, L. G. Monomeric plasticizers. Handbook of vinyl formulating. John Wiley & Sons Inc, Hoboken 2008, 173-238.

[86] J. Yang, Li, Y., Wang, Y., Ruan, J., Zhang, J., Sun, C. Recent advances in analysis of phthalate esters in foods. Trac-Trends in Analytical Chemistry 2015, 72, 10-26, doi:10.1016/j.trac.2015.03.018.

[87] E. Puertolas, Koubaa, M., Barba, F. J. An overview of the impact of electrotechnologies for the recovery of oil and high-value compounds from vegetable oil industry: Energy and economic cost implications. Food Research International 2016, 80, 19-26, doi:10.1016/j.foodres.2015.12.009.

[88] C. M. Ajila, Brar, S. K., Verma, M., Tyagi, R. D., Godbout, S., Valero, J. R. Bio-processing of agro-byproducts to animal feed. Critical Reviews in Biotechnology 2012, 32, 382-400, doi:10.3109/07388551.2012.659172.

[89] A. Wechsler, Hiziroglu, S. Some of the properties of wood-plastic composites. Building and Environment 2007, 42, 2637-2644, doi:10.1016/j.buildenv.2006.06.018.

[90] B. Amar, Salem, K., Hocine, D., Chadia, I., Juan, M. J. Study and Characterization of Composites Materials Based on Polypropylene Loaded with Olive Husk Flour. Journal of Applied Polymer Science 2011, 122, 1382-1394, doi:10.1002/app.34084.

[91] O. Mysiukiewicz, Barczewski, M., Skorczewska, K., Szulc, J., Klozinski, A. Accelerated Weathering of Polylactide-Based Composites Filled with Linseed Cake: The Influence of Time and Oil Content within the Filler. Polymers 2019, 11, doi:10.3390/polym11091495.

[92] J. Carlos Ronda, Lligadas, G., Galia, M., Cadiz, V. Vegetable oils as platform chemicals for polymer synthesis. European Journal of Lipid Science and Technology 2011, 113, 46-58, doi:10.1002/ejlt.201000103.

[93] M. R. Ghosi Mobaraki, Abedian Kenari, A., Bahrami Gorji, S., Esmaeili, M. Effect of dietary fish and vegetable oil on the growth performance, body composition, fatty acids profile, reproductive performance and larval

resistance in pearl gourami (Trichogaster leeri). Aquaculture Nutrition 2020, 26, 894-907, doi:10.1111/anu.13048.

[94] G. Gultekin, Atalay-Oral, C., Erkal, S., Sahin, F., Karastova, D., Tantekin-Ersolmaz, S. B., Guner, F. S. Fatty acid-based polyurethane films for wound dressing applications. Journal of Materials Science-Materials in Medicine 2009, 20, 421-431, doi:10.1007/s10856-008-3572-5.

[95] D. P. Pfister, Xia, Y., Larock, R. C. Recent Advances in Vegetable Oil-Based Polyurethanes. Chemsuschem 2011, 4, 703-717, doi:10.1002/cssc.201000378.

[96] J. A. Melero, Milagrosa Clavero, M., Calleja, G., Garcia, A., Miravalles, R., Galindo, T. Production of Biofuels via the Catalytic Cracking of Mixtures of Crude Vegetable Oils and Nonedible Animal Fats with Vacuum Gas Oil. Energy & Fuels 2010, 24, 707-717, doi:10.1021/ef900914e.

[97] G. Karmakar, Ghosh, P., Sharma, B. K. Chemically Modifying Vegetable Oils to Prepare Green Lubricants. Lubricants 2017, 5, doi:10.3390/lubricants5040044.

[98] K. J. Harrington. Chemical and physical properties of vegetable oils esters and their effect on diesel fuel performance. Biomass 1986, 9, 1-17, doi:10.1016/0144-4565(86)90008-9.

[99] Aceites y grasas de origen animal y vegetal. Determinación del índice de yodo 2018, ISO 3961:2018.

[100] J. La Scala, Wool, R. P. Effect of FA composition on epoxidation kinetics of TAG. Journal of the American Oil Chemists Society 2002, 79, 373-378, doi:10.1007/s11746-002-0491-9.

[101] N. J. Fox, Stachowiak, G. W. Vegetable oil-based lubricants - A review of oxidation. Tribology International 2007, 40, 1035-1046, doi:10.1016/j.triboint.2006.10.001.

[102] E. R. Sherwin. Antioxidants for vegetable-oils. Journal of the American Oil Chemists Society 1976, 53, 430-436, doi:10.1007/bf02605739.

[103] C. S. Osorio-Gonzalez, Gomez-Falcon, N., Sandoval-Salas, F., Saini, R., Brar, S. K., Ramirez, A. A. Production of Biodiesel from Castor Oil: A Review. Energies 2020, 13, doi:10.3390/en13102467.

[104] Y. J. Ng, Tham, P. E., Khoo, K. S., Cheng, C. K., Chew, K. W., Show, P. L. A comprehensive review on the techniques for coconut oil extraction and its application. Bioprocess and Biosystems Engineering 2021, 44, 1807-1818, doi:10.1007/s00449-021-02577-9.

[105] A. Gandini. Polymers from plant oils; Smithers Rapra: 2015.

[106] L. Canoira, Galean, J. G., Alcantara, R., Lapuerta, M., Garcia-Contreras, R. Fatty acid methyl esters (FAMEs) from castor oil: Production process assessment and synergistic effects in its properties. Renewable Energy 2010, 35, 208-217, doi:10.1016/j.renene.2009.05.006.

[107] Y. H. Chen, Chen, J. H., Chang, C. Y., Chang, C. C. Biodiesel production from tung (Vernicia montana) oil and its blending properties in different fatty acid compositions. Bioresource Technology 2010, 101, 9521-9526, doi:10.1016/j.biortech.2010.06.117.

[108] F. D. Gunstone, Harwood, J. L. The lipid handbook with CD-ROM; CRC press: 2007.

[109] T. Suzuki, Sumimoto, K., Fukada, K., Katayama, T. Iodine value of tung biodiesel fuel using Wijs method is significantly lower than calculated value. Journal of Wood Science 2021, 67, doi:10.1186/s10086-021-01987-3.

[110] P. J. White. Fatty acids in oilseeds (vegetable oils). In Fatty acids in foods and their health implications; CRC Press: 2007; pp. 241-276.

[111] M. J. Sadler. Fatty acids | Trans Fatty Acids*. In Encyclopedia of Human Nutrition (Second Edition), Caballero, B., Ed.; Elsevier: Oxford, 1998; pp. 230-237.

[112] D. S. Wilcove, Koh, L. P. Addressing the threats to biodiversity from oil-palm agriculture. Biodiversity and Conservation 2010, 19, 999-1007, doi:10.1007/s10531-009-9760-x.

[113] Oil Crops Yearbook. U.S Department of Agriculture-Economic Research Service 2022.

[114] Á. M. Villar Del Fresno. Soja. Aplicaciones múltiples. Farmacia Profesional 2002, 16, 78-83.

[115] S. P. Singh, Singh, D. Biodiesel production through the use of different sources and characterization of oils and their esters as the substitute of diesel: A review. Renewable & Sustainable Energy Reviews 2010, 14, 200-216, doi:10.1016/j.rser.2009.07.017.

[116] F. N. Jones. Alkyd resins. Ullmann's Encyclopedia of Industrial Chemistry 2000.

[117] Linseed Oil Production. Nation Master 2019.

[118] N. Karak, Karak, N. Vegetable oils and their derivatives; 2012; pp. 57-60.

[119] A. V. Yate, Narvaez, P. C., Orjuela, A., Hernandez, A., Acevedo, H. A systematic evaluation of the mechanical extraction of Jatropha curcas L. oil for biofuels production. Food and Bioproducts Processing 2020, 122, 72-81, doi:10.1016/j.fbp.2020.04.001.

[120] C. H. Fornasari, Secco, D., Santos, R. F., Benetoli da Silva, T. R., Galant Lenz, N. B., Tokura, L. K., Lenz, M. L., Melegari de Souza, S. N., Zanao Junior, L. A., Gurgacz, F. Efficiency of the use of solvents in vegetable oil extraction at oleaginous crops. Renewable & Sustainable Energy Reviews 2017, 80, 121-124, doi:10.1016/j.rser.2017.05.123.

[121] J. M. Ferreira De Almeida-Couto, Barbosa Abrantes, K. K., Barao, C. E., Wisniewski, A., da Silva, C., Cabral, V. F., Cardozo-Filho, L. Pressurized mixture of CO2 and propane for enhanced extraction of non-edible vegetable oil. Journal of Supercritical Fluids 2021, 171, doi:10.1016/j.supflu.2021.105171.

[122] P. W. Mwaurah, Kumar, S., Kumar, N., Attkan, A. K., Panghal, A., Singh, V. K., Garg, M. K. Novel oil extraction technologies: Process conditions, quality parameters, and optimization. Comprehensive Reviews in Food Science and Food Safety 2020, 19, 3-20, doi:10.1111/1541-4337.12507.

[123] A. Campanella, Fontanini, C., Baltanas, M. A. High yield epoxidation of fatty acid methyl esters with performic acid generated in situ. Chemical Engineering Journal 2008, 144, 466-475, doi:10.1016/j.cej.2008.07.016.

[124] B. B. Wentzel, Alsters, P. L., Feiters, M. C., Nolte, R. J. M. Mechanistic studies on the Mukaiyama epoxidation. Journal of Organic Chemistry 2004, 69, 3453-3464, doi:10.1021/jo030345a.

[125] G. Sienel, Rieth, R., Rowbottom, K. T. Epoxides. In Ullmann's Encyclopedia of Industrial Chemistry, 6th ed.; 2003; Volume 12, pp. 269-284.

[126] Y. Meng, Taddeo, F., Aguilera, A. F., Cai, X., Russo, V., Tolvanen, P., Leveneur, S. The Lord of the Chemical Rings: Catalytic Synthesis of Important Industrial Epoxide Compounds. Catalysts 2021, 11, doi:10.3390/catal11070765.

[127] P. T. Wai, Jiang, P., Shen, Y., Zhang, P., Gu, Q., Leng, Y. Catalytic developments in the epoxidation of vegetable oils and the analysis methods of epoxidized products. Rsc Advances 2019, 9, 38119-38136, doi:10.1039/c9ra05943a.

[128] Z. S. Petrovic, Zlatanic, A., Lava, C. C., Sinadinovic-Fiser, S. Epoxidation of soybean oil in toluene with peroxoacetic and peroxoformic acids - kinetics and side reactions. European Journal of Lipid Science and Technology 2002, 104, 293-299, doi:10.1002/1438-9312(200205)104:5<293::Aid-ejlt293>3.0.Co;2-w.

[129] S. Dinda, Patwardhan, A. V., Goud, V. V., Pradhan, N. C. Epoxidation of cottonseed oil by catalysed by liquid aqueous hydrogen peroxide inorganic acids. Bioresource Technology 2008, 99, 3737-3744, doi:10.1016/j.biortech.2007.07.015.

[130] S. M. Danov, Kazantsev, O. A., Esipovich, A. L., Belousov, A. S., Rogozhin, A. E., Kanakov, E. A. Recent advances in the field of selective epoxidation of

vegetable oils and their derivatives: a review and perspective. Catalysis Science & Technology 2017, 7, 3659-3675, doi:10.1039/c7cy00988g.

[131] J. Birtill, Centi, G., Van Santen, R. A. "Catalysis for Renewables: From Feedstock to Energy Production". Platinum Metals Review 2008, 52, 229-230, doi:10.1595/147106708x364922.

[132] M. Farias, Martinelli, M., Bottega, D. P. Epoxidation of soybean oil using a homogeneous catalytic system based on a molybdenum (VI) complex. Applied Catalysis a-General 2010, 384, 213-219, doi:10.1016/j.apcata.2010.06.038.

[133] K. Saremi, Tabarsa, T., SHakeri, A., Babanalbandi, A. Epoxidation of soybean oil. Annals of biological research 2012, 3, 4254-4258.

[134] Commercial maleinized linseed and soybean oil. Available online: https://www.vandeputte.com/en/malenised-LO--SO__239__257.aspx (accessed on 15/12/2022).

[135] A. Carbonell-Verdu, Boronat, T., Quiles-Carrillo, L., Fenollar, O., Dominici, F., Torre, L. Valorization of Cotton Industry Byproducts in Green Composites with Polylactide. Journal of Polymers and the Environment 2020, 28, 2039-2053, doi:10.1007/s10924-020-01751-6.

[136] A. Lerma-Canto, Gomez-Caturla, J., Herrero-Herrero, M., Garcia-Garcia, D., Fombuena, V. Development of Polylactic Acid Thermoplastic Starch Formulations Using Maleinized Hemp Oil as Biobased Plasticizer. Polymers 2021, 13, doi:10.3390/polym13091392.

[137] E. Mistri, Routh, S., Ray, D., Sahoo, S., Misra, M. Green composites from maleated castor oil and jute fibres. Industrial Crops and Products 2011, 34, 900-906, doi:10.1016/j.indcrop.2011.02.008.

[138] D. Rosu, Mustata, F., Tudorachi, N., Musteata, V. E., Rosu, L., Varganici, C. D. Novel bio-based flexible epoxy resin from diglycidyl ether of bisphenol A cured

with castor oil maleate. Rsc Advances 2015, 5, 45679-45687, doi:10.1039/c5ra05610a.

[139] T. Eren, Kusefoglu, S. H. Hydroxymethylation and polymerization of plant oil triglycerides. Journal of Applied Polymer Science 2004, 91, 4037-4046, doi:10.1002/app.13608.

[140] B. Pellegrene, Hammer, T. J., Pugh, C., Soucek, M. D. Maleated soybean oil derivatives as versatile reactive diluents: Synthesis, characterization, and evaluation. Journal of Applied Polymer Science 2022, 139, doi:10.1002/app.51814.

[141] C. Gaglieri, Alarcon, R. T., de Moura, A., Magri, R., da Silva-Filho, L. C., Bannach, G. Green and Efficient Modification of Grape Seed Oil to Synthesize Renewable Monomers. Journal of the Brazilian Chemical Society 2021, 32, 2120-2131, doi:10.21577/0103-5053.20210104.

[142] A. Zlatanic, Lava, C., Zhang, W., Petrovic, Z. S. Effect of structure on properties of polyols and polyurethanes based on different vegetable oils. Journal of Polymer Science Part B-Polymer Physics 2004, 42, 809-819, doi:10.1002/polb.10737.

[143] R. C. Amos, Kuska, M., Mesnager, J., Gauthier, M. Thermally induced maleation of soybean and linseed oils: From benchtop to pilot plant. Industrial Crops and Products 2021, 166, doi:10.1016/j.indcrop.2021.113504.

[144] Q. Fu, Long, Y., Gao, Y., Ling, Y., Qian, H., Wang, F., Zhu, X. Synthesis and properties of castor oil based plasticizers. Rsc Advances 2019, 9, 10049-10057, doi:10.1039/c8ra10288k.

[145] J. M. Ferri, Garcia-Garcia, D., Montanes, N., Fenollar, O., Balart, R. The effect of maleinized linseed oil as biobased plasticizer in poly (lactic acid)-based formulations. Polymer International 2017, 66, 882-891, doi:10.1002/pi.5329.

[146] M. Jorda-Reolid, Gomez-Caturla, J., Ivorra-Martinez, J., Stefani, P. M., Rojas-Lema, S., Quiles-Carrillo, L. Upgrading Argan Shell Wastes in Wood Plastic

Composites with Biobased Polyethylene Matrix and Different Compatibilizers. Polymers 2021, 13, doi:10.3390/polym13060922.

[147] A. P. Gupta, Ahmad, S., Dev, A. Modification of Novel Bio-Based Resin-Epoxidized Soybean Oil by Conventional Epoxy Resin. Polymer Engineering and Science 2011, 51, 1087-1091, doi:10.1002/pen.21791.

[148] D. Rosu, Mustata, F., Tudorachi, N., Varganici, C. D., Rosu, L., Musteata, V. E. A study on coating properties of an epoxy system hardened with maleinized castor oil. Progress in Organic Coatings 2016, 99, 480-489, doi:10.1016/j.porgcoat.2016.07.009.

[149] G. Santori, Di Nicola, G., Moglie, M., Polonara, F. A review analyzing the industrial biodiesel production practice starting from vegetable oil refining. Applied Energy 2012, 92, 109-132, doi:10.1016/j.apenergy.2011.10.031.

[150] Precio aceite de soja-dólares americanos por tonelada métrica. index mundi 2022.

[151] A. Sosa-Baldivia, Ruiz-Ibarra, G., de la Torre, R. R. R., Lopez, R. R., López, A. M. The chia (Salvia hispanica): past, present and future of an ancient Mexican crop. Australian Journal of Crop Science 2018, 12, 1626-1632.

[152] W. Coates. Whole and Ground Chia (Salvia hispanica L.) Seeds, Chia Oil - Effects on Plasma Lipids and Fatty Acids; 2011; pp. 309-315.

[153] C. Baginsky, Arenas, J., Escobar, H., Garrido, M., Valero, N., Tello, D., Pizarro, L., Valenzuela, A., Morales, L., Silva, H. Growth and yield of chia (Salvia hispanica L.) in the Mediterranean and desert climates of Chile. Chilean Journal of Agricultural Research 2016, 76, 255-264, doi:10.4067/s0718-58392016000300001.

[154] S. Dixit, Kanakraj, S., Rehman, A. Linseed oil as a potential resource for bio-diesel: A review. Renewable & Sustainable Energy Reviews 2012, 16, 4415-4421, doi:10.1016/j.rser.2012.04.042.

[155] A. P. De Souza, Burgess, S. J., Doran, L., Hansen, J., Manukyan, L., Maryn, N., Gotarkar, D., Leonelli, L., Niyogi, K. K., Long, S. P. Soybean photosynthesis and crop yield are improved by accelerating recovery from photoprotection. Science 2022, 377, 851-+, doi:10.1126/science.adc9831.

[156] Chia Seeds Market Size Worth $4.7 Billion By 2025. Grand View Research. 2019. Available online: https://www.grandviewresearch.com/press-release/global-chia-seeds-market (accessed on 14 October 2021). Available online: https://www.grandviewresearch.com/press-release/global-chia-seeds-market (accessed on

[157] R. Ayerza. Seed's protein and oil content, fatty acid composition, and growing cycle length of a single genotype of chia (Salvia hispanica L.) as affected by environmental factors. Abstracts of Papers of the American Chemical Society 2010, 240.

[158] N. M. Ali, Yeap, S. K., Ho, W. Y., Beh, B. K., Tan, S. W., Tan, S. G. The Promising Future of Chia, Salvia hispanica L. Journal of Biomedicine and Biotechnology 2012, doi:10.1155/2012/171956.

[159] Y. P. Timilsena, Vongsvivut, J., Adhikari, R., Adhikari, B. Physicochemical and thermal characteristics of Australian chia seed oil. Food Chemistry 2017, 228, 394-402, doi:10.1016/j.foodchem.2017.02.021.

[160] S. S. Fernandes, Tonato, D., Mazutti, M. A., de Abreu, B. R., Cabrera, D. d. C., Montes D'Oca, C. d. R., Prentice-Hernandez, C., de las Mercedes Salas-Mellado, M. Yield and quality of chia oil extracted via different methods. Journal of Food Engineering 2019, 262, 200-208, doi:10.1016/j.jfoodeng.2019.06.019.

[161] M. Rubi Segura-Campos, Antonio Chel-Guerrero, L., Abram Betancur-Ancona, D. Salvia hispanica: Nutritional and Functional Potential. In Functional Properties of Traditional Foods, Kristbergsson, K., Otles, S., Eds.; Integrating Food Science and Engineering Knowledge Into the Food Chain; 2016; Volume 12, pp. 115-118.

[162] D. S. Ivanov, Lević, J. D., Sredanović, S. A. Fatty acid composition of various soybean products. Food and Feed Research 2010, 37, 65-70-65-70.

[163] A. Bayrak, Kiralan, M., Ipek, A., Arslan, N., Cosge, B., Khawar, K. M. FATTY ACID COMPOSITIONS OF LINSEED (LINUM USITATISSIMUM L.) GENOTYPES OF DIFFERENT ORIGIN CULTIVATED IN TURKEY. Biotechnology & Biotechnological Equipment 2010, 24, 1836-1842, doi:10.2478/v10133-010-0034-2.

[164] M. Demin, Rabrenovic, B., Pezo, L., Lalicic-Petronijevic, J. Influence of chia seeds (Salvia hispanica L.) and extra virgin olive oil addition on nutritional properties of salty crackers. Journal of Food Measurement and Characterization 2020, 14, 378-387, doi:10.1007/s11694-019-00300-7.

[165] M. I. Capitani, Spotorno, V., Nolasco, S. M., Tomas, M. C. Physicochemical and functional characterization of by-products from chia (Salvia hispanica L.) seeds of Argentina. Lwt-Food Science and Technology 2012, 45, 94-102, doi:10.1016/j.lwt.2011.07.012.

[166] B. Kulczynski, Kobus-Cisowska, J., Taczanowski, M., Kmiecik, D., Gramza-Michalowska, A. The Chemical Composition and Nutritional Value of Chia Seeds-Current State of Knowledge. Nutrients 2019, 11, doi:10.3390/nu11061242.

[167] B. L. Olivos-Lugo, Valdivia-Lopez, M. A., Tecante, A. Thermal and Physicochemical Properties and Nutritional Value of the Protein Fraction of Mexican Chia Seed (Salvia hispanica L.). Food Science and Technology International 2010, 16, 89-96, doi:10.1177/1082013209353087.

II. ESTUDIOS PREVIOS

Previamente a la investigación de biopolímeros con alto rendimiento ecológico empleando la semilla de chía, se realizó una investigación centrada en compuestos ecológicos derivados del poliéster con cargas inorgánicas de bajo coste para su revalorización. El estudio preliminar permitió determinar el potencial que presentan los poliésteres, como el PLA, tras la incorporación de cargas y la estabilidad en condiciones de degradación. A partir de este estudio, se ha permitido abordar e identificar los retos parciales que se plantean en la presente tesis doctoral. Por un lado, el empleo de formulaciones de poliéster, concretamente con el PLA, como matriz potencial en sectores como el envase y embalaje, donde la biodegradación del material es un factor importante. Por otro lado, la incorporación de cargas de bajo coste y alta disponibilidad, con su optimización en las formulaciones para la obtención de compuestos con bajo impacto medioambiental y propiedades mecánicas deseables. A partir de esto, se decidió abordar el empleo de carga lignocelulósica derivada de la semilla de chía, debido a su alta disponibilidad, biodegradabilidad y bajo coste para su aprovechamiento en el sector de los biopolimeros.

El estudio previo se centra en el desarrollo de compuestos biodegradables derivados del poliéster como es la PCL y el PLA para ser empleados en el campo de la biomedicina. Está enfocado en la sustitución de materiales convencionales para la remodelación de fracturas óseas, donde el empleo de poliésteres bioabsorbibles son una alternativa en este campo. Las formulaciones realizadas contienen cargas biocerámicas, aportando nuevas funcionalidades como la mayor actividad biológica, que permite acelerar el crecimiento óseo y la mejora en las propiedades mecánicas. Las cargas empleadas son la hidroxiapatita, ampliamente empleada como relleno tisular y los nanotubos de haloisita, con el fin de emplearse en futuros estudios como elementos de difusión controlada de fármacos como antioxidantes. En estudios anteriores se optimizó las cantidades añadidas de cada carga, además de estudiar la capacidad de proliferación y viabilidad celular empleando ambas cargas en diferentes matrices derivadas de poliéster, pero con diferente hidrofobicidad. La novedad del presente trabajo se centra en el estudio de la tasa de degradación hidrolítica de los compuestos obtenidos derivados del poliéster y su efecto en las propiedades mecánicas. Esto es uno de los requisitos más importantes a la hora de introducir dicho

compuesto como prótesis, donde el 75% del cuerpo humano es agua y los materiales empleados se verán afectados por este medio.

II.1 "Development and characterization of Polyester and Acrilated-Based Composite with Hydroxyapatite and Halloysite Nanotubes for Medical Applications"

Elena torres[1], **Ivan Dominguez-Candela[2]**, Sergio Castello-Palacios[3], Anna Vallés-Llunch[3], Vicent Fombuena[2]

[1] Textile Industry Research Association (AITEX), Plaza Emilio Sala 1, 03801, Alcoy, Spain

[2] Technological Institute of Materiales (ITM), Universitat Politècnica de Valéncia (UPV), Plaza Ferrándiz y Carbonell 1, 03801 Alcoy, Spain

[3] Centre of Biomaterials and Tissue Engineering, Universitat Politècnica de València (UPV), Camí de Vera s/n, 46022 Valencia, Spain

Polymers

2020, 12(8), p.1703-1716.

"Development and characterization of Polyester and Acrilate-Based Composite with Hydroxyapatite and Halloysite Nanotubes for Medial Applications"

Abstract

We aimed to study the distribution of hydroxyapatite (HA) and halloysite nanotubes (HNTs) as fillers and their influence on the hydrophobic character of conventional polymers used in the biomedical field. The hydrophobic polyester (PCL) was blended with its more hydrophilic counterpart PLA and the hydrophilic acrylate poly (2-hydroxyethyl methacrylate) (PHEMA) was analogously compared to poly (ethyl methacrylate) (PEMA) and its copolymer. The addition of HA and HNTs clearly improve surface wettability in neat samples (PCL and PHEMA), but not that of the corresponding binary blends. Energy-dispersive X-ray spectroscopy mapping analyses show a homogenous distribution of HA with appropriate Ca/P ratios between 1.3 and 2, even on samples that were incubated for seven days in simulated body fluid, with the exception of PHEMA, which is excessively hydrophilic to promote the deposition of salts on its surface. HNTs promote large aggregates on more hydrophilic polymers. The degradation process of the biodegradable polyester PCL blended with PLA, and the addition of HA and HNTs, provide hydrophilic units and decrease the overall crystallinity of PCL. Consequently, after 12 weeks of incubation in phosphate buffered saline the mass loss increases up to 48% and mechanical properties decrease above 60% compared with the PCL/PLA blend.

Keywords

Biomedical polymers; hydroxyapatite; halloysite; mechanical properties

Introduction

Tissue engineering has been exploring new methods to replace missing human tissues through biomaterials-based scaffolds, usually engineered to drive cell growth and provide shape to the creation of the new tissue. However, we should consider alternatives when selecting materials for bone fracture remodeling since conventional materials used for these applications include metallic prostheses, bone grafts, or polymers. Currently, biopolymers are being intensively studied to replace both metal prostheses and autologous bone grafts because metal prostheses induce poor bone regeneration with formation of fragile porous bone [1] and, although autologous bone grafts induce the growth of strong bone, donor bone is needed, requiring additional chirurgical interventions, eventually causing infections [2]. Thus, polymers having easy processability to obtain desired geometries and special functionalities to accelerate bone growth will be the best option to treat bone fracture remodeling. Accordingly, biopolymers used as scaffolds for tissue engineering applications need to overcome two significant challenges. First, the biodegradation process should be controlled with non-toxic degradation by-products eliminated through natural pathways. Secondly, the material should maintain its structural and mechanical properties to avoid malformation of the new regenerated bone while healing [3].

Among all the biopolymers used for tissue engineering, bioabsorbable aliphatic polyesters are the dominant scaffolding materials because of their biodegradability properties. Biodegradable aliphatic polyesters, containing the ester functional group in their main chain, undergo hydrolytic cleavage generating oligomers, which will be subsequently assimilated into the surrounding environment. PCL, PLA and PHB, approved by the U.S. Food and Drug Administration, are the most studied polyesters due to their easy processability and their tunability regarding crystallinity, thermal transition and mechanical strength properties [4,5]. The degradation rate and mechanical properties of biopolymers will be affected by the hydrophobicity, crystallinity and acidity of the selected polymer.

The hydrophobic biopolymer PCL is extensively used in drug delivery devices showing excellent biological activity. Accordingly, studies focused on its use as a scaffold and internal fixation system, although its low mechanical properties cannot meet the structural requirements of the host tissue. Consequently, an appropriate addition of fillers or blends could provide an adequate mechanical stiffness to resist in vivo stresses, preventing new tissue deformation [6,7,8]. As examples, Lowry *et al*. [9] tested PCL composites as internal fixation devices, observing a higher strength when using a PCL/bone complex compared with bony humerus healed with a stainless-steel implant. These observations are in concordance with the studies developed in the last decade by Rudd and co-workers [10,11,12,13,14].

Introduction of specific bioceramics can also confer new functions, such as higher biological activity. Thereupon, HA is broadly use as an inexpensive filler in tissue engineering [15,16,17] because of its osteoconductive properties, low inflammatory response and low toxicity in humans [18,19], based on the mineral phase of the human bone being mainly composed (around 60 wt. %) of HA [20]. Therefore, introduction of HA into a polymer induces the formation of an apatite layer with similar characteristics to those of the bone mineral phase [21], in as much as HA improves cell attachment [22,23], inducing the differentiation of mesenchymal cells into osteoblasts, which accelerates bone formation [8]. Different authors observed both mechanical and biological improvement of biopolymer matrices with the addition of HA [24,25].

The PCL low stiffness can also be attributed to using halloysite nanotubes (HNTs) [26,27] which are an inexpensive biocompatible clay extensively used in biomedicine for drug delivery due to their tubular shape. HNTs also support cell adhesion, ascribed to HNTs surface nano-roughness, which acts as an anchor frame [28], and the interaction between silanol groups present on the HNTs surface [29] with hydroxyl and amino groups present on proteins.

In a previous study [30], mechanical and thermal properties of PCL were studied by modifying the additive percentage of the bioactive fillers HA and HNTs. Accordingly, the additive threshold was stablished in 7.5 wt. % of HNTs and 20 wt. %

of HA achieving a noticeable improvement in mechanical properties with the simultaneous addition of the two fillers. As a result, the flexural modulus improved up to 112.3% reaching values of 886.8 Mpa (standard deviation = 42.1), and Young's modulus increased to 109.3% with its greatest value at 449.6 Mpa (standard deviation = 17.12). Knowing that HA promotes the formation of a layer of new bone, and that HA and HNTs alter hydrophobicity behavior, in a second study, [23], biological properties such as cell viability, proliferation and morphology supplied by both fillers were studied and compared on different pairs of polymers with similar chemical nature but different hydrophobicity. Accordingly, the hydrophobic polyester PCL was modified when it blended with PLA and combined with HA nanoparticles and HNTs. However, the hydrophilic PHEMA was copolymerized as monomer with ethyl methacrylate (EMA) and also combined with HA and HNTs. These polymers, although dissimilar to PCL and PLA in terms of chemical nature and biodegradability, were chosen for comparison purposes because they are used for hard tissue applications. Initially, the in vitro biological development of polymers with different hydrophobicity showed that cells preferably proliferate on moderately hydrophobic surfaces (PCL/PLA). However, over longer culture periods, cell proliferation increased on more hydrophilic materials (P(HEMA-co-EMA)). Inorganic nanoparticles (HA and HNTs) improve cell viability and proliferation compared to the raw materials. We assumed that reduced cell spreading on hydrophobic surfaces at long culture times might occur as a consequence of two effects: protein absorption competition and the steric hindrance effect (solvation).

We acknowledge that the contributions of the previous studies [23,30] need to be accomplished by monitoring the degradation rate of biodegradable polyesters modified with HA and HNT. Biomedical polymers, after implantation, undergo significant changes regarding mechanical properties influenced by their degradation process. Considering that 75% of the human body is composed of water, hydrolytic degradation of aliphatic polyesters is an interesting feature for tissue engineering materials. Bone remodeling implies time-limited applications, which requires the elimination or degradation of the biopolymer after use to restore the surrounding living medium.

For all the above-mentioned reasons, we studied the bioactivity of polyester (PCL, PCL/PLA and PLA) and acrylates (PHEMA, P(HEMA-co-EMA) sets and their HA- and HNT-based nanocomposites, as well as the degradability of the polyester-based set. To determine the correct distribution of the fillers, a study was conducted using SEM-EDS and an evaluation of their wettability by measuring the contact angle. Finally, to demonstrate if the loads introduced in the nanocomposites diffuse to the environment, we evaluated the mechanical properties of the nanocomposites using tensile and flexion tests.

Experimental

Materials

PCL, with trade name CAPA 6500, was provided by Solvay Interox (Solvay Interox, Warrington, UK). CAPA 6500 is a high-molecular-weight thermoplastic linear polyester derived from its own lactone monomer. PLA Ingeo™ biopolymer 6201D is a thermoplastic available in pellet form with a glass transition temperature of 55–60°C and a melting point of 155–170°C. NatureWorks LLC (Nature Works LLC, Minnetonka, MN, USA). HA with chemical formula (Hca5O13P3), halloysite nanotubes ($Al_2Si_2O_5$ $(OH)_4$ $2H_2O$), EMA with 99% purity, and HEMA, with a minimum of purity of 96%, were supplied by Sigma-Aldrich (Madrid, Spain). Benzoin and ethylene glycol dimethacrylate 98% (EGDMA) were used as ultraviolet initiator and crosslinking agent during the preparation of HEMA/EMA compounds. Both were also supplied by Sigma Aldrich.

Preparation of the Polymer-Based Hybrids

The first set of materials based on PCL and PLA were received in pellet form and dried prior to their preparation in an air oven at 50 and 60 °C, respectively, to remove humidity. In parallel, HA and HNTs were dried separately in a vacuum oven for 48 h at 200 and 80 °C. The proportions detailed in Table II.1 were weighed and pre-mixed in a zipper bag. By a twin screw co-rotating extruder with different temperature profiles, the mixtures were mechanically homogenized. Specifically, for PCL-based compounds, the temperature profile was 65/75/85/90 °C, and for PLA based-

compounds, we used temperatures of 170/173/176/18°C. After the extrusion process, the samples were cooled to room temperature and pelletized. Again, prior to the injection process, the different compounds were dried under the same conditions as mentioned above. The injection was carried out in a Meteor 270/75 injection molding machine (Mateu and Solé, Barcelona, Spain) using as temperature profiles of the extruder: 80/80/85/85/90°C for PCL compounds and 170/173/175/180°C for PLA compounds. Next, 13 mm diameter samples were punched out.

Table II.1. Composition and coding of PCL, PCL/PLA, PHEMA, and P(HEMA-co-EMA) composites.

Code	Composition (wt.%)			
	PCL	PLA	HA	HNTs
PCL	100	-	-	-
PCL_20HA	80	-	20	-
PCL_20HA_7.5HNTs	72.5	-	20	7.5
PCL/PLA	50	50	-	-
PCL/PLA_20HA	40	40	20	-
PCL/PLA_20HA_7.5HNTs	36.25	36.25	20	7.5
Code	Composition (wt.%)			
	HEMA	EMA	HA	HNTs
PHEMA	100	-	-	-
PHEMA_20HA	80	-	20	-
PHEMA_20HA_7.5HNTs	72.5	-	20	7.5
P(HEMA-co-EMA)	50	50	-	-
P(HEMA-co-EMA)_20HA	40	40	20	-
P(HEMA-co EMA)_20HA_7.5HNTs	36.25	36.25	20	7.5

The second set of compounds, based on ethyl methacrylate (EMA) and hydroxyl-2-ethyl methacrylate (HEMA), was obtained by simultaneous polymerization of the monomers, as summarized in Table II.1. Using a 1:1 monomer ratio between HEMA and EMA to obtain the copolymer, the mixtures were stirred with 1 wt. % benzoin and 0.5 wt. % EGDMA. The corresponding ratios of HA and HNTs were added and stirred for 15 min. Each mixture was injected into a glass template for polymerization in an ultraviolet oven for 24 h and subsequently a 24 h post-polymerization process in an oven at 90 ^{o}C was required. The samples were immersed in boiling ethanol and cut into 13 mm diameter samples.

Contact Angle Measurements

The water contact angles (WCAs) of the nanocomposites were measured on the surface of the dry samples in the sessile drop mode. An Easy Drop Standard goniometer model FM140 (110/220 V, 50/60 Hz) supplied by Krüss GmbH (Hamburg, Germany) was used for this purpose. To determine the water contact angle, we used the Drop Shape Analysis SW21 (DSA1) software. A minimum of five replicates of each sample were analyzed, yielding a standard deviation of less than 5%.

Mechanical Properties

Tensile properties of PCL/PLA blends loaded with HA and HNTs were obtained using a universal test machine (Ibertest ELIB 30, SAE Ibertest, Madrid, Spain) according to ISO 527. Assays were carried out with a 5 kN load cell and a crosshead speed of 10 mm·min^{-1}. Moreover, to determine the Young's modulus more accurately, an axial extensometer IB/MFQ-R2 from Ibertest (Madrid, Spain) coupled to the universal test machine was used. The Young's modulus was calculated in each case from the stress–strain initial slope and averaged from five replicates.

Hydroxyapatite Nucleation

Hydroxyapatite nucleation was followed on three replicates per sample and time point. First, a simulated body fluid (SBF) solution with an ion concentration close to that of human blood plasma was prepared by the method proposed by Kokubo and coworkers [31,32]. To obtain the SBF, we prepared two solutions. Solution 1 consisted of 1.599 g of NaCl (Scharlau, 99% pure), 0.045 g of KCl (Scharlau 99% pure, Barcelona, Spain), 0.110 g of $CaCl_2 \cdot 6H_2O$ (Fluka 99% pure, Madrid, Spain) and 0.061 g of $MgCl_2 \cdot 6H_2O$ (Fluka) in deionized ultrapure water (Scharlau) up to 100 mL. Solution 2 was prepared by dissolving 0.032 g of $Na_2SO_4 \cdot 10H_2O$ (Fluka), 0.071 g of $NaHCO_3$ (Fluka) and 0.046 g of $K_2HPO_4 \cdot 3H_2O$ (Aldrich, 99% pure) in water up to 100 mL. Both solutions were buffered at pH 7.4 by adding the necessary amounts of aqueous 1 Mtris-hydroxymethyl aminomethane, $(CH_2OH)_3CNH_2$ (Aldrich), and 1 M hydrochloric acid (HCl, Aldrich, 37% pure). Next, both solutions were mixed to obtain

SBF with the following molar ion concentrations: 142 Na^+, 5.0 K^+, 1.5 Mg^{2+}, 2.5 Ca^{2+}, 148.8 Cl^-, 4.2 HCO^-, 1.0 HPO^{2-} and 0.5 SO^{2-} mM. Samples were immersed in individual vials containing 10 mL of SBF solution with hydrazine (NaH_2) to prevent bacterial proliferation. The vials were placed in an incubator at 37 ^oC and 5% CO_2. A set of samples were withdrawn after 7 and 14 days.

Cell Seeding

NIH 3T3 fibroblast cells were expanded in the presence of 4.5 g L^{-1} glucose supplemented with 10% fetal bovine serum (Thermo Fisher, Gibco, Waltham, MS, USA) and 1% penicillin/streptomycin (P/S; Thermo Fisher, Gibco) in Dulbecco's modified Eagle medium (DMEM; Thermo Fisher, Gibco) at 37 ^oC in a 5% CO_2 incubator until confluence. After reaching confluence (3 days), cells were withdrawn from the culture flask. To proceed, 5 mL of versene solution (0.48 mM) formulated in 0.2 g ethyldiaminotetraacetic acid (EDTA) per liter of phosphate buffered saline (PBS) supplied by ThermoFisher (Gibco), were added for 5 min at 37 ◦C, and then removed. After, to neutralize the versene solution, 10 mL of DMEM was added, and the suspensions were centrifugated at 1000 rpm for 5 min. Then, the cells were resuspended in 1 mL medium, counted, diluted and seeded on the samples at a density of 2 × 104 cells cm^{-2}.

Morphological Analysis

A ZEISS FESEM ULTRATM 55 scanning electron microscopy (SEM) device was used to analyze the morphology of the HA coatings and the NIH 3T3 fibroblast cells and their layout on the surfaces. The morphology of the HA coatings was studied by SEM and energy-dispersive X-ray spectroscopy (EDS) images obtained to validate the formation of a hydroxyapatite layer and the Ca/P ratio. To this end, the samples were sputter-coated with carbon under vacuum through a BALL-TEC/SCD 005 sputter coater. The mapping spectra were taken at 15 kV of acceleration voltage and 5 mm working distance; a secondary electron detector was used. Silicon was used as optimization standard. The mappings were taken at a magnification of 5000×.

In the study of NIH 3T3 fibroblast cells, arrangements were analyzed after 1 and 14 days of incubation. After each period, the culture medium was removed to rinse the samples in phosphate buffer (PB; Affymetrix, Santa Clara, CF, USA) and samples fixed with 4% paraformaldehyde solution during 30 h at 37 ºC. A vacuum system was used to remove the water and to avoid any deformations on cell morphology. For this purpose, samples were rinsed in PBS twice and carefully frozen in liquid nitrogen and transferred to a freezer-dryer for drying.

Degradation of PCL and PCL/PLA Based Hybrids

Degradation of PCL and PCL/PLA loaded with HA and HNTs was followed in vitro at 37 ◦C using PBS (0.01 M (NaCl 0.138 M; KCl 0.0027 M) with a pH 7.4, at 25 ºC was supplied by Sigma Aldrich). Due to the stability of thermostable compounds based on PHEMA, this study was only carried out on compounds based on PCL. With the aim of accelerating the process, samples were previously immersed in a 2M NaOH solution for 24 h. Three replicates of each composition were immersed in individual tubes with 10 mL of Dulbecco's Phosphate Buffered Saline (DPBS, Sigma Aldrich) (pH 7.4) with screw caps and maintained at 37 ºC in an incubator. Each sample was removed after 4, 8 and 12 weeks, rinsed thoroughly with deionized water, and dried in an oven at 35 ºC for 12 h.

The weight loss and the mechanical Integrity of the materials were evaluated. An electronic balance with a resolution of 0.1 mg was used to determine the mass loss as follows:

$$\%\, Mass\ loss = \frac{Mi - Mf}{Mi} \times 100 \qquad \textbf{Equation II.1}$$

where *Mi* is the initial mass and *Mf* is the final mass of the dry sample.

Results and discussion

The water contact angle formed in the range of 40°–70° on a polymeric surface is known to influence cell attachment, since chemical surface interactions are a key

factor during the bio-adhesion process [33]. Polymers with contact angles in this range, with a different chemical nature, were thus selected for this analysis, and their hydrophilicity was slightly modified by blending or copolymerizing with others of the same family. Therefore, polymer chemical surfaces were modified by blending hydrophilic/hydrophobic polymers and/or filling the polymer matrix with HA or HNT to analyze their role in wettability.

From the results in Figure II.1., we can discern that the most hydrophobic sample was PCL with a contact angle of 105°. Blending PCL with the more hydrophilic PLA, the surface wettability improved 25.3%, with a value of 83.7°. Conversely, PHEMA was at the hydrophilic end, with a contact angle of 59.7°, and the copolymerization with the more hydrophobic EMA decreased surface wettability up to 73.7°. The addition of HA and HNTs clearly improved surface wettability on neat samples (PCL and PHEMA), but this effect was scarcely observed in mixed samples (PCL/PLA and P(HEMA-co-EMA)), considering the standard deviation. This effect could be attributed to the intermediate wettability of these samples, with contact angles in the vicinities of 80°, together with their heterogeneous composition at the nanoscale.

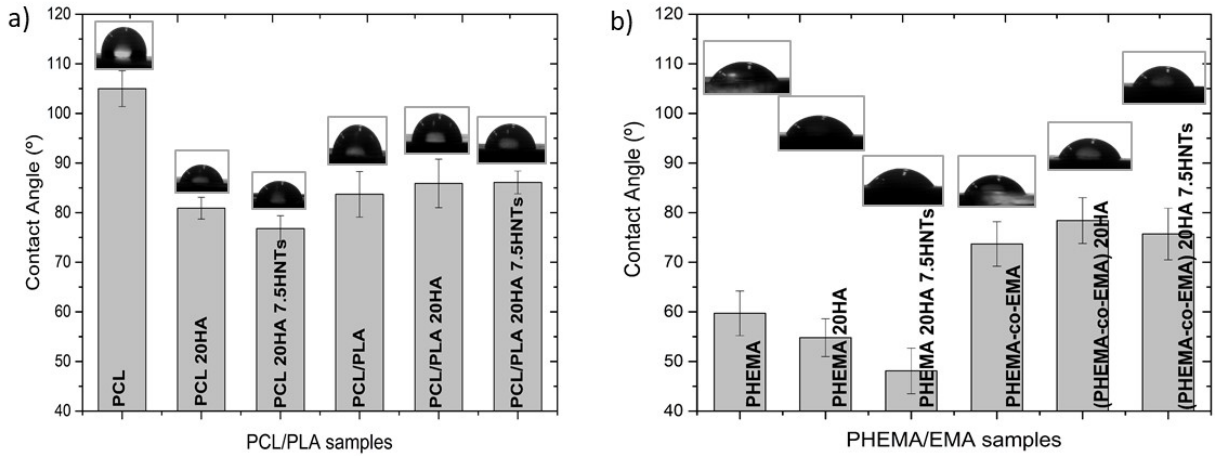

Figure II.1. Variation of contact angle in compounds based on (a) PCL/PLA and (b) PHEMA/EMA.

After determining the wettability of the samples and the influence of the addition of HA and HNTs fillers, a SEM-EDS analysis was conducted to firstly determine if the loads were homogeneously dispersed and, secondly, to assess the

formation of a hydroxyapatite layer resulting from the incubation in SBF at 37 °C. In addition, the EDS analysis (EDS spectra not shown) allowed the quantification of the Ca/P ratio and the comparison with that of the stoichiometric HA ($Ca_{10}(PO_4)_6(OH)_2$), Ca/P = 1.67 [34].

Figure II.2. shows the images obtained after 7 and 14 days in SBF on the samples based on PCL/PLA. After seven days, the PCL-based hybrids did not efficiently induce apatite growth. Precipitation on PCL and PCL/PLA compounds without needle conformation corresponded to the salt dissolved in SBF medium, usually NaCl. The samples with HA filler provided nucleation sites, and the silanol groups (Si–OH) present in HNTs provide favorable locations for apatite nucleation. We speculated that the electrostatic interaction drives the formation of calcium silicate [35], since comparing pure polymers (especially PCL and PCL/PLA blends) with HA- and HNTs-modified materials, the nucleation efficiency increases with the filler. We already showed that both polar carboxyl groups and hydroxyl groups induce apatite nucleation [36].

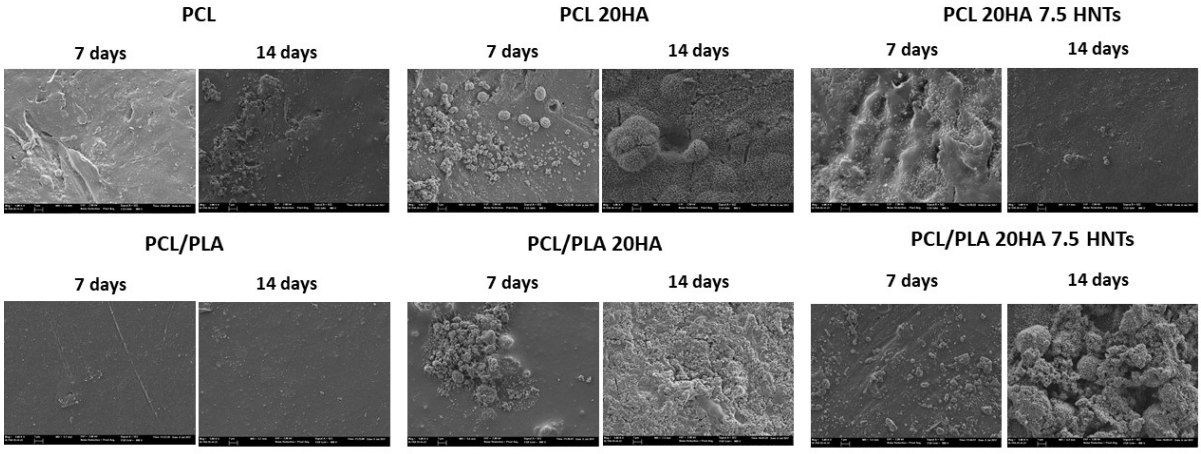

Figure II.2. SEM images (5000x) taken for hydroxyapatite nucleation analysis on samples based on PCL/PLA.

However, Figure II.3. summarizes SEM images of samples based on PHEMA/EMA. The polymethacrylate-based hybrids induced efficient apatite growth, with the exception of pure PHEMA, on which only scattered precipitated salts were observed on the surface. On the contrary, the P(HEMA-co-EMA) surface showed plenty of precipitates forming large and clear cauliflowers with intricate needle-

shaped crystals [36]. As observed, once apatite nucleates on a location, it grows radially outward [37], creating cauliflower or hemispherical structures combined to form a continuous layer. Due to the weak hydrophilicity of P(HEMA-co-EMA), the biological activity is higher than PHEMA, where the number of apolar groups available for nucleation per unit volume on the surface is greater. Therefore, the P(HEMA-co-EMA) surface adsorbs Ca^{2+} ions from the SBF solution more efficiently, thereby increasing the concentration of Ca^{2+} ions on the surface, and also forming Ca–P nucleation sites [38]. The first layer of apatite molecules generates the cauliflower aggregates from the secondary nucleation, observed especially in P(HEMA-co-EMA). This process induces a spherical growth perpendicular to the surface structure, which leads to the formation of clusters or grape-like structures [21].

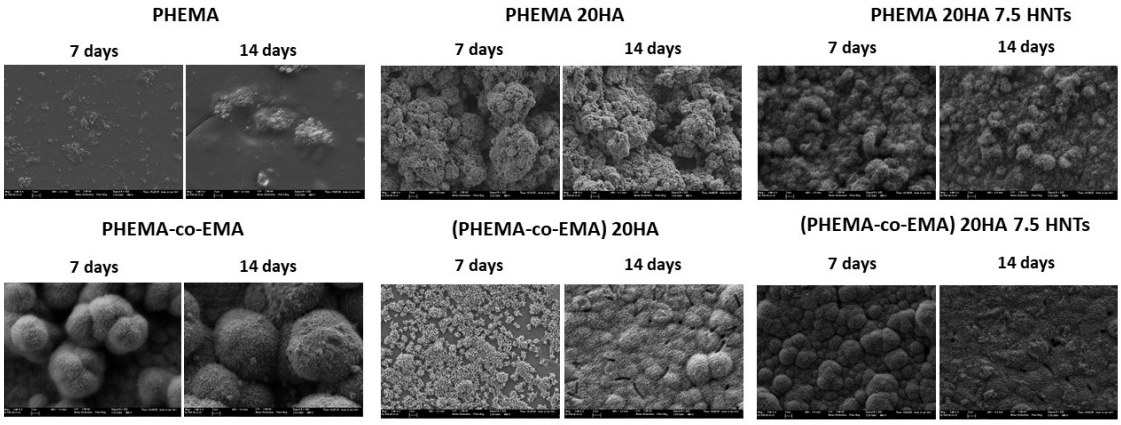

Figure II.3. SEM images (5000x) taken for hydroxyapatite nucleation analysis on samples based on PHEMA/EMA.

Figure II.4. reveals the assessment of the Ca/P ratio to verify the formation of hydroxyapatite layers. In most determinations, the Ca/P atomic ratio remained in acceptable values between 1.3 and 2, which pointed to the formation of calcium and phosphate deposits resembling physiological apatite structures [34]. Particularly, the highest Ca/P ratios were obtained in the PCL, PHEMA and PHEMA 20HA samples after an incubation period of seven days, all with values higher than 1.8. After 14 days of incubation, the Ca/P ratio tended to the physiological ratio of 1.67 in most samples. However, PHEMA did not show calcium on the surface after 14 days of incubation. The hydrophilic character of this polymer probably hinders the deposition of salts on its surface and their evolution toward HA. This observation coincides with that of [36],

where its closely-related poly (hydroxyethyl acrylate) (PHEA) did not induce an efficient apatite growth, whereas its copolymer with EMA did.

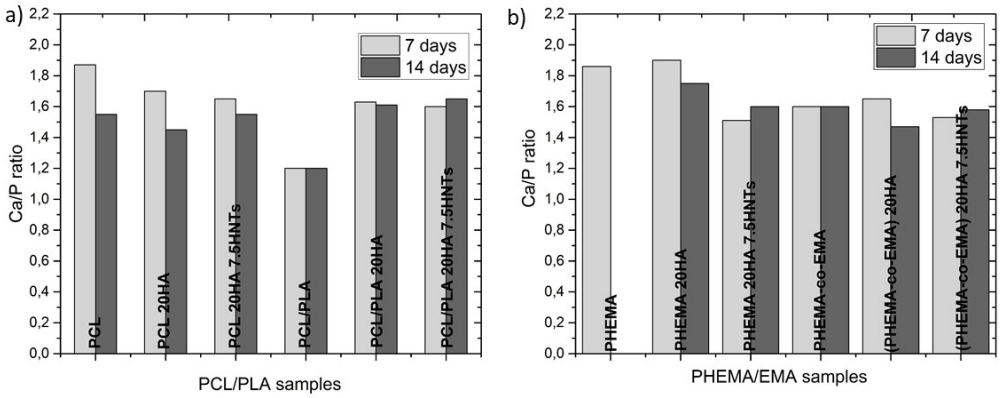

Figura II.4. Ca/P ratio after 7 and 14 days of incubation in SBF obtained by EDS on nanocomposites based on: a) PCL and PCL/PLA, b) PHEMA and P(HEMA-co-EMA).

In the SEM morphological images (Figure II.5.), we see the in vitro biological development of polymers with different hydrophobicity. At initial stages (day 1), cells preferably proliferated and colonized moderately on the hydrophobic surface (PCL/PLA, with contact angle of 83.7°, as summarized in Figure 1). Thus, cells appear round, where interactions occur primarily between them or with the extracellular matrix, thus resulting in a monolayer of cells with few bonding sites with the polymer surface. When longer incubation periods were analyzed (14 days), cell proliferation was favored in more hydrophilic polymers, as is the case of P(HEMA-co-EMA), with a contact angle of 73.7°. In these samples, cells exhibited a flatter morphology, establishing contact with the polymer surface. With the addition of HA and HNTs inorganic fillers, in general terms, we observed an increase in proliferation compared with the raw materials. As different authors have concluded, this improvement can be attributed to the generation of new reactive sites with Ca^{2+} and PO_4^{3-} groups present in HA that bind with negative carboxylate and positive amino groups in proteins, respectively [39,40,41,42]. However, due to the presence of silanol groups (Si–OH) located at the surface of HNTs, the formation of hydrogen bonds between HNTs and proteins is allowed [29]. The results showed a greater proliferation at initial stages on moderately hydrophobic polymers (PCL/PLA), whereas over longer culture periods, more hydrophilic polymers P(HEMA-co-EMA) seem to improve cell

proliferation, in concordance with the results by Zhou *et al.* [42]. Using polyvinyl alcohol (PVA), a highly hydrophilic polymer, the authors concluded that highly polar OH groups on neat PVA films might account for the delayed attachment of bone cells. Thus, we can possibly assume that reduced cell spreading on hydrophobic surfaces at long culture times might occur as a consequence of the protein absorption competition and the steric hindrance effect (solvation).

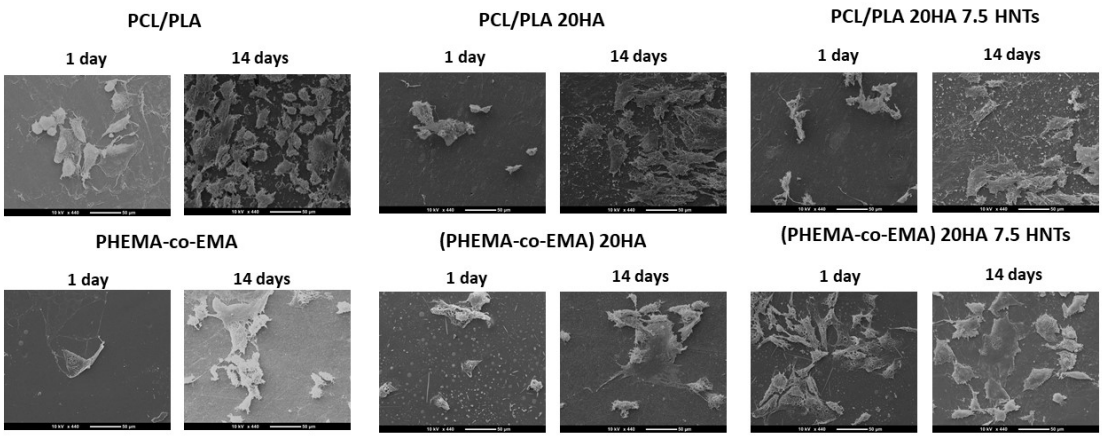

Figure II.5. SEM images (400×) taken for cell proliferation at 1 and 14 days on samples based on PCL/PLA and PHEMA/EMA.

Regarding the mechanical properties, PLA is a hard polymer with good mechanical properties, its brittleness being its main disadvantage. However, PCL is a very soft polymer with a slow degradation rate. After mixing PLA and PCL, the synergy results in retaining the advantages of each polymer. Compared to pure PLA, the mixture has greater flexibility, hydrophobicity and crystallinity, which translate into a slower degradation rate (several months to years) [43]. To study if the PCL crosslinking factor (crystallinity) limits the mobility of the chains and, therefore, the degradation rate, an analysis of the mass loss and mechanical properties after 4, 8 and 12-weeks of incubation in PBS was conducted. The PCL crystallinity tends to reduce the chain mobility and thus its hydrolysis by means of the hindered access of enzymes to the polymer matrix [23].

From the results shown in Figure II.6, the PCL-based material did not show significant mass loss after degradation in PBS at 37 °C for 12 weeks. Although the mass loss of all PCL-based samples gradually increased, compared with samples containing

inorganic fillers, the mass loss of pure PCL increased rapidly during the 12-week degradation process. The lower mass loss was observed in samples with HA because HA contains hydroxyl groups, which can neutralize the medium by reacting with degraded acid by-products, thereby reducing the effect of acid catalysis on PCL hydrolysis [44]. Conversely, PCL/PLA blends showed a maximum mass loss rate of the samples when using the two fillers, 41% after 12 weeks. Blending PCL with PLA provides hydrophilic units and reduces the overall crystallinity of PCL, thereby improving the accessibility of water molecules and ester bonds, and increasing the hydrolysis rate [45]. The addition of fillers provides hydrophobicity, and the nano-roughness of the surface promotes interaction with water molecules and thus causes hydrolytic cracking. Therefore, the evolution of mass loss is related to the mechanical properties, which were followed through the analysis of their Young's moduli, gathered in Figure II.7.

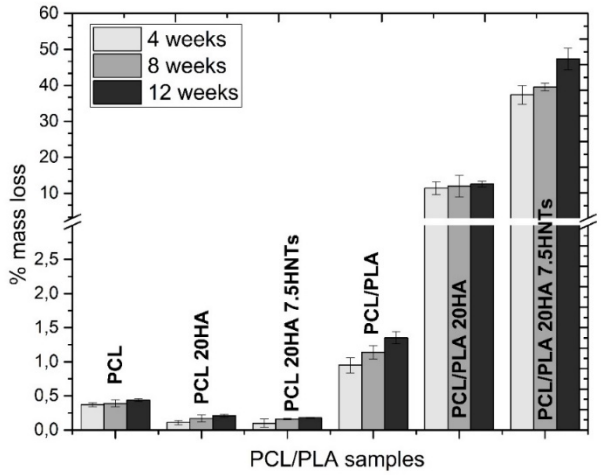

Figure II.6. Results of degradation: mass loss (%) after 4, 8 and 12 weeks for PCL-based materials

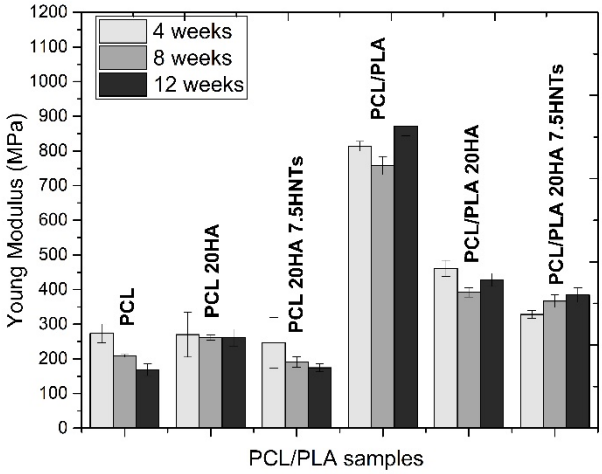

Figure II.7. Results of Young Modulus following 4, 8 and 12 weeks of degradation for PCL/PLA based materials.

The Young's modulus of the PCL samples was about 275 Mpa. We observed that as the incubation time and the percentage of mass loss increased, the mechanical properties gradually decreased. The neat PCL samples showed a sharp decrease in Young's modulus, but those with HA retained their Young's modulus due to the filler reinforcement. However, the samples with HA and HNT showed a gradual decrease in mechanical properties over time, since the additional threshold of the nanoloads could be exceeded as the polymer degraded, and the agglomerates could act as weak points and failure initiation points. Blending PCL with PLA resulted in the Young's modulus increasing to 800 Mpa. In PCL/PLA blends with the presence of inorganic fillers, the faster degradation rate, associated with more hydrophilic properties and more amorphous phases, led to a faster decline in mechanical properties. More precisely, the PCL/PLA 20HA 7.5 HNTs blend provided a Young's modulus 60% lower than that of the PCL/PLA blend.

Conclusions

Studying the influence of the HA and HNTs fillers on the wettability of the selected polyesters and acrylates, we measured water contact angles, which corroborated that PCL is the most hydrophobic sample, whereas PHEMA is

hydrophilic. The addition of HA and HNTs clearly improved the surface wettability of neat samples, but not of the binary samples (PCL/PLA and P(HEMA-co-EMA)).

Secondly, distribution of the fillers into the polymer matrices was studied through EDS mapping. A homogeneous distribution of HA was observed on all polymers, with the exception of PHEMA. Nonetheless, the presence of HNTs yields large aggregates on more hydrophilic polymers, derived from the hydrophobic character of the nanotubes, resulting in a good dispersion in non-polar polymers and creating agglomerations in hydrophilic polymers due to the lower interfacial adhesion. Considering HA nucleation on polymer surfaces, hydrophobic polymers did not show an efficient induction of apatite growth. Conversely, large hydroxyapatite cauliflower-shaped crystals formed on moderately hydrophilic surfaces. We discovered that PHEMA is excessively hydrophilic, so promotes HA nucleation on its surface.

Finally, the evaluation of the degradation rate of the biodegradable PCL-based samples demonstrated that both the blending PCL with PLA and the addition of HA and HNTs provide hydrophilic units, as well as decrease the overall crystallinity of PCL, thereby improving the accessibility of water molecules to ester linkages and thus the hydrolytic cleavage. Consequently, the faster degradation rate and reduced mass lead to a faster drop of mechanical properties.

Acknowledgments

I. Dominguez-Candela thanks the Universitat Politècnica de València for the financial support through an FPI-UPV grant (PAID-01-19).

References

[1] Noyama, Y.; Miura, T.; Ishimoto, T.; Itaya, T.; Niinomi, M.; Nakano, T. Bone Loss and Reduced Bone Quality of the Human Femur after Total Hip Arthroplasty under Stress-Shielding Effects by Titanium-Based Implant. Mater. Trans. 2012, 53, 565–570.

[2] Temple, J.P.; Hutton, D.L.; Hung, B.P.; Huri, P.Y.; Cook, C.A.; Kondragunta, R.; Jia, X.; Grayson, W.L. Engineering anatomically shaped vascularized bone

grafts with hASCs and 3D-printed PCL scaffolds. J. Biomed. Mater. Res. 2014, 102, 4317–4325.

[3] Lee, K.H.; Kim, H.Y.; Khil, M.S.; Ra, Y.M.; Lee, D.R. Characterization of nano-structured poly (epsilon-caprolactone) nonwoven mats via electrospinning. Polymer 2003, 44, 1287–1294.

[4] Li, X.; Cui, R.; Sun, L.; Aifantis, K.E.; Fan, Y.; Feng, Q.; Cui, F.; Watari, F. 3D-Printed biopolymers for tissue engineering application. Int. J. Polym. Sci. 2014.

[5] Washington, K.E.; Kularatne, R.N.; Karmegam, V.; Biewer, M.C.; Stefan, M.C. Recent advances in aliphatic polyesters for drug delivery applications. Wiley Interdiscip. Rev. Nanomed. Nanobiotechnol. 2017, 9.

[6] Venkatesan, J.; Kim, S.K. Nano-Hydroxyapatite composite biomaterials for bone tissue engineering-a review. J. Biomed. Nanotechnol. 2014, 10, 3124–3140.

[7] Chen, G.Q.; Wu, Q. The application of polyhydroxyalkanoates as tissue engineering materials. Biomaterials 2005, 26, 6565–6578.

[8] Rezwan, K.; Chen, Q.Z.; Blaker, J.J.; Boccaccini, A.R. Biodegradable and bioactive porous polymer/inorganic composite scaffolds for bone tissue engineering. Biomaterials 2006, 27, 3413–3431.

[9] Lowry, K.J.; Hamson, K.R.; Bear, L.; Peng, Y.B.; Calaluce, R.; Evans, M.L.; Anglen, J.O.; Allen, W.C. Polycaprolactone/glass bioabsorbable implant in a rabbit humerus fracture model. J. Biomed. Mater. Res. 1997, 36, 536–541.

[10] Corden, T.J.; Jones, I.A.; Rudd, C.D.; Christian, P.; Downes, S.; McDougall, K.E. Physical and biocompatibility properties of poly-epsilon-caprolactone produced using in situ polymerization: A novel manufacturing technique for long-fibre composite materials. Biomaterials 2000, 21, 713–724.

[11] Onal, L.; Cozien-Cazuc, S.; Jones, I.A.; Rudd, C.D. Water absorption properties of phosphate glass fiber-reinforced poly-epsilon-caprolactone composites for craniofacial bone repair. J. Appl. Polym. Sci. 2008, 107, 3750–3755.

[12] Ahmed, I.; Parsons, A.J.; Palmer, G.; Knowles, J.C.; Walkers, G.S.; Rudd, C.D. Weight loss, ion release and initial mechanical properties of a binary calcium phosphate glass fibre/PCL composite. Acta Biomater. 2008, 4, 1307–1314.

[13] Gough, J.E.; Christian, P.; Scotchford, C.A.; Rudd, C.D.; Jones, I.A. Synthesis, degradation, and in vitro cell responses of sodium phosphate glasses for craniofacial bone repair. J. Biomed. Mater. Res. 2002, 59, 481–489.

[14] Gough, J.E.; Christian, P.; Unsworth, J.; Evans, M.P.; Scotchford, C.A.; Jones, I.A. Controlled degradation and macrophage responses of a fluoride-treated polycaprolactone. J. Biomed. Mater. Res. 2004, 69, 17–25.

[15] Choi, W.-Y.; Kim, H.-E.; Koh, Y.-H. Production, mechanical properties and in vitro biocompatibility of highly aligned porous poly (epsilon-caprolactone) (PCL)/hydroxyapatite (HA) scaffolds. J. Porous Mater. 2013, 20, 701–708.

[16] Yeo, M.G.; Kim, G.H. Preparation and characterization of 3D composite scaffolds based on rapid-prototyped PCL/beta-TCP struts and electrospun pcl coated with collagen and ha for bone regeneration. Chem. Mater. 2012, 24, 903–913.

[17] Salerno, A.; Zeppetelli, S.; Di Maio, E.; Iannace, S.; Netti, P.A. Design of bimodal pcl and pcl-ha nanocomposite scaffolds by two step depressurization during solid-state supercritical CO2 foaming. Macromol. Rapid Commun. 2011, 32, 1150–1156.

[18] Jackson, I.T.; Yavuzer, R. Hydroxyapatite cement: An alternative for craniofacial skeletal contour refinements. Br. J. Plast. Surg. 2000, 53, 24–29.

[19] Miller, L.; Guerra, A.B.; Bidros, R.S.; Trahan, C.; Baratta, R.; Metzinger, S.E. A comparison of resistance to fracture among four commercially available forms of hydroxyapatite cement. Ann. Plast. Surg. 2005, 55, 87–92.

[20] Lawson, E.E.; Barry, B.W.; Williams, A.C.; Edwards, H.G.M. Biomedical applications of Raman spectroscopy. J. Raman Spectrosc. 1997, 28, 111–117.

[21] Loty, C.; Sautier, J.M.; Boulekbache, H.; Kokubo, T.; Kim, H.M.; Forest, N. In vitro bone formation on a bone-like apatite layer prepared by a biomimetic process on a bioactive glass-ceramic. J. Biomed. Mater. Res. 2000, 49, 423–434.

[22] Roach, P.; Eglin, D.; Rohde, K.; Perry, C.C. Modern biomaterials: A review-bulk properties and implications of surface modifications. J. Mater. Sci. Mater. Med. 2007, 18, 1263–1277.

[23] Torres, E.; Valles-Lluch, A.; Fombuena, V.; Napiwocki, B.; Lih-Sheng, T. Influence of the hydrophobic-hydrophilic nature of biomedical polymers and nanocomposites on in vitro biological development. Macromol. Mater. Eng. 2017, 302.

[24] Chen, B.Q.; Sun, K. Mechanical and dynamic viscoelastic properties of hydroxyapatite reinforced poly (epsilon-caprolactone). Polym. Test. 2005, 24, 978–982.

[25] Heo, S.J.; Kim, S.E.; Wei, J.; Hyun, Y.T.; Yun, H.S.; Kim, D.H.; Shin, J.W. Fabrication and characterization of novel nano- and micro-HA/PCL composite scaffolds using a modified rapid prototyping process. J. Biomed. Mater. Res. 2009, 89, 108–116.

[26] Lee, K.-S.; Chang, Y.-W. Thermal, mechanical, and rheological properties of poly (epsilon-caprolactone)/halloysite nanotube nanocomposites. J. Appl. Polym. Sci. 2013, 128, 2807–2816.

[27] Liu, M.; Guo, B.; Du, M.; Lei, Y.; Jia, D. Natural inorganic nanotubes reinforced epoxy resin nanocomposites. J. Polym. Res. 2008, 15, 205–212.

[28] Zhou, W.Y.; Guo, B.; Liu, M.; Liao, R.; Rabie, A.B.M.; Jia, D. Poly (vinyl alcohol)/Halloysite nanotubes bionanocomposite films: Properties and in vitro osteoblasts and fibroblasts response. J. Biomed. Mater. Res. 2010, 93, 1574–1587.

[29] Xue, W.; Bandyopadhyay, A.; Bose, S. Mesoporous calcium silicate for controlled release of bovine serum albumin protein. Acta Biomater. 2009, 5, 1686–1696.

[30] Torres, E.; Fombuena, V.; Valles-Lluch, A.; Ellingham, T. Improvement of mechanical and biological properties of Polycaprolactone loaded with Hydroxyapatite and Halloysite nanotubes. Mater. Sci. Eng. C-Mater. Biol. Appl. 2017, 75, 418–424.

[31] Abe, Y.; Kokubo, T.; Yamamuro, T. Apatite coating on ceramics, metals and polymers utilizing a biological process. J. Mater. Sci. Mater. Med. 1990, 1, 233–238.

[32] Kokubo, T.; Takadama, H. How useful is SBF in predicting in vivo bone bioactivity? Biomaterials 2006, 27, 2907–2915.

[33] Xue, L.; Greisler, H.P. Biomaterials in the development and future of vascular grafts. J. Vasc. Surg. 2003, 37, 472–480.

[34] Kim, H.M.; Kishimoto, K.; Miyaji, F.; Kokubo, T.; Yao, T.; Suetsugu, Y.; Tanaka, J.; Nakamura, T. Composition and structure of the apatite formed on PET substrates in SBF modified with various ionic activity products. J. Biomed. Mater. Res. 1999, 46, 228–235.

[35] Takadama, H.; Kim, H.M.; Miyaji, F.; Kokubo, T.; Nakamura, T. Mechanism of apatite formation induced by silanol groups – TEM observation. J. Ceram. Soc. Jpn. 2000, 108, 118–121.

[36] Lluch, A.V.; Ferrer, G.G.; Pradas, M.M. Biomimetic apatite coating on P(EMA-co-HEA)/SiO2 hybrid nanocomposites. Polymer 2009, 50, 2874–2884.

[37] Hutchens, S.A.; Benson, R.S.; Evans, B.R.; O'Neill, H.M.; Rawn, C.J. Biomimetic synthesis of calcium-deficient hydroxyapatite in a natural hydrogel. Biomaterials 2006, 27, 4661–4670. [Google Scholar] [CrossRef]

[38] Kim, H.M.; Himeno, T.; Kawashita, M.; Kokubo, T.; Nakamura, T. The mechanism of biomineralization of bone-like apatite on synthetic hydroxyapatite: An in vitro assessment. J. R. Soc. Interface 2004, 1, 17–22.

[39] Azzopardi, P.V.; O'Young, J.; Lajoie, G.; Karttunen, M.; Goldberg, H.A.; Hunter, G.K. Roles of electrostatics and conformation in protein-crystal interactions. PloS ONE 2010, 5.

[40] Hynes, R.O. Iintegrins-versatility, modulation, and signaling in cell-adhesion. Cell 1992, 69, 11–25.

[41] Wassell, D.T.H.; Hall, R.C.; Embery, G. Adsorption of bovine serum-albumin onto hydroxyapatite. Biomaterials 1995, 16, 697–702.

[42] Zhou, H.; Wu, T.; Dong, X.; Wang, Q.; Shen, J. Adsorption mechanism of BMP-7 on hydroxyapatite (001) surfaces. Biochem. Biophys. Res. Commun. 2007, 361, 91–96.

[43] Middleton, J.C.; Tipton, A.J. Synthetic biodegradable polymers as orthopedic devices. Biomaterials 2000, 21, 2335–2346.

[44] Li, H.Y.; Chen, Y.F.; Xie, Y.S. Photo-crosslinking polymerization to prepare polyanhydride/needle-like hydroxyapatite biodegradable nanocomposite for orthopedic application. Mater. Lett. 2003, 57, 2848–2854.

[45] Albertsson, A.C.; Varma, I.K. Aliphatic polyesters: Synthesis, properties and applications. Degrad. Aliphatic Polyest. 2002, 157, 1–40.

polymers

MDPI

Article

Development and Characterization of Polyester and Acrylate-Based Composites with Hydroxyapatite and Halloysite Nanotubes for Medical Applications

Elena Torres [1], Ivan Dominguez-Candela [2], Sergio Castello-Palacios [3], Anna Vallés-Lluch [3] and Vicent Fombuena [2,*]

[1] Textile Industry Research Association (AITEX), Plaza Emilio Sala 1, 03801 Alcoy, Spain; etorres@aitex.es
[2] Technological Institute of Materials (ITM), Universitat Politècnica de València (UPV), Plaza Ferrándiz y Carbonell 1, 03801 Alcoy, Spain; ivdocan@epsa.upv.es
[3] Centre for Biomaterials and Tissue Engineering, Universitat Politècnica de València (UPV), Camí de Vera s/n, 46022 Valencia, Spain; sercaspa@iteam.upv.es (S.C.-P.); avalles@ter.upv.es (A.V.-L.)
* Correspondence: vifombor@upv.es

Received: 14 July 2020; Accepted: 28 July 2020; Published: 29 July 2020

Abstract: We aimed to study the distribution of hydroxyapatite (HA) and halloysite nanotubes (HNTs) as fillers and their influence on the hydrophobic character of conventional polymers used in the biomedical field. The hydrophobic polyester poly (ε-caprolactone) (PCL) was blended with its more hydrophilic counterpart poly (lactic acid) (PLA) and the hydrophilic acrylate poly (2-hydroxyethyl methacrylate) (PHEMA) was analogously compared to poly (ethyl methacrylate) (PEMA) and its copolymer. The addition of HA and HNTs clearly improve surface wettability in neat samples (PCL and PHEMA), but not that of the corresponding binary blends. Energy-dispersive X-ray spectroscopy mapping analyses show a homogenous distribution of HA with appropriate Ca/P ratios between 1.3 and 2, even on samples that were incubated for seven days in simulated body fluid, with the exception of PHEMA, which is excessively hydrophilic to promote the deposition of salts on its surface. HNTs promote large aggregates on more hydrophilic polymers. The degradation process of the biodegradable polyester PCL blended with PLA, and the addition of HA and HNTs, provide hydrophilic units and decrease the overall crystallinity of PCL. Consequently, after 12 weeks of incubation in phosphate buffered saline the mass loss increases up to 48% and mechanical properties decrease above 60% compared with the PCL/PLA blend.

Keywords: biomedical polymers; hydroxyapatite; halloysite; mechanical properties

1. Introduction

Tissue engineering has been exploring new methods to replace missing human tissues through biomaterials-based scaffolds, usually engineered to drive cell growth and provide shape to the creation of the new tissue. However, we should consider alternatives when selecting materials for bone fracture remodeling since conventional materials used for these applications include metallic prosthesis, bone grafts, or polymers. Currently, biopolymers are being intensively studied to replace both metal prostheses and autologous bone grafts because metal prostheses induce poor bone regeneration with formation of fragile porous bone [1] and, although autologous bone grafts induce the growth of strong bone, donor bone is needed, requiring additional chirurgical interventions, eventually causing infections [2]. Thus, polymers having easy processability to obtain desired geometries and special functionalities to accelerate bone growth will be the best option to treat bone fracture remodeling. Accordingly, biopolymers used as scaffolds for tissue engineering applications need to overcome two significant challenges. First, the biodegradation process should be controlled with non-toxic

III. OBJETIVOS Y PLANIFICACIÓN

III.1. OBJETIVOS GENERAL

El objetivo general de este trabajo es el desarrollo de nuevas formulaciones con alto rendimiento ecológico empleando la semilla de chía como recursos renovables con alto potencial. Por un lado, el aceite es modificado químicamente mediante procesos de epoxidación y maleinización con la finalidad de ser empleados como agente plastificante, compatibilizante o como resinas. Además, como trabajo futuro se realizará su modificación química para ser empleado como surfactante con alto contenido ecológico. Por otro lado, el residuo obtenido del proceso de extracción del aceite es empleado como cargas lignocelulósicas para la obtención de materiales con alto rendimiento ecológico empleando la economía circular.

III.2. OBJETIVOS ESPECÍFICOS

Con la finalidad de alcanzar los objetivos generales, se han planteado una serie de objetivos específicos que han sido desarrollados a lo largo de la tesis doctoral. Los objetivos específicos son clasificados en función de la aplicación de la semilla de chía como recurso funcional. Los objetivos específicos son los siguientes:

Estudio de los parámetros de la reacción de epoxidación

1. Estudio del efecto de los parámetros de la reacción de la epoxidación del aceite de chía en el contenido de grupos epoxi y propiedades físicoquímicas.

Plastificación

2. Evaluación de la incorporación de diferentes cantidades de aceite de chía epoxidado como plastificante en formulaciones de PLA.

Incorporación de cargas lignocelulósicas

3. Estudio del efecto de la incorporación de diferentes cantidades de harina de chía tratada con silanos como carga lignocelulósica en formulaciones de Bio-HDPE.
4. Estudio del efecto de la incorporación de diferentes compatiblizantes como potenciales sustitutos a los de origen petroquímico para la mejora de compatibilidad de la harina de chía en formulaciones de PLA.

Termoestables

5. Evaluación del efecto de la incorporación de derivados del aceite de chía como resina base y endurecedor de origen bio como sustituyente del endurecedor anhídrido maleico para la obtención de materiales termoestables con alto rendimiento medioambiental.

Por otro lado, como estudio previo a la obtención de glicolípidos derivados del aceite de chía y su caracterización como cristal líquido, se realizó la siguiente investigación relacionada con la caracterización de las propiedades de los cristales líquidos en aplicaciones energéticas.

Cristales líquidos

6. Desarrollo y evaluación de las propiedades de mezclas de cristales líquidos sensibles a la luz como candidatos en la conversión y almacenamiento de energía en condensadores.

En la Figura III.1. se muestra la planificación de forma esquemática de la fase de investigación para la consecución de los objetivos particulares planteados.

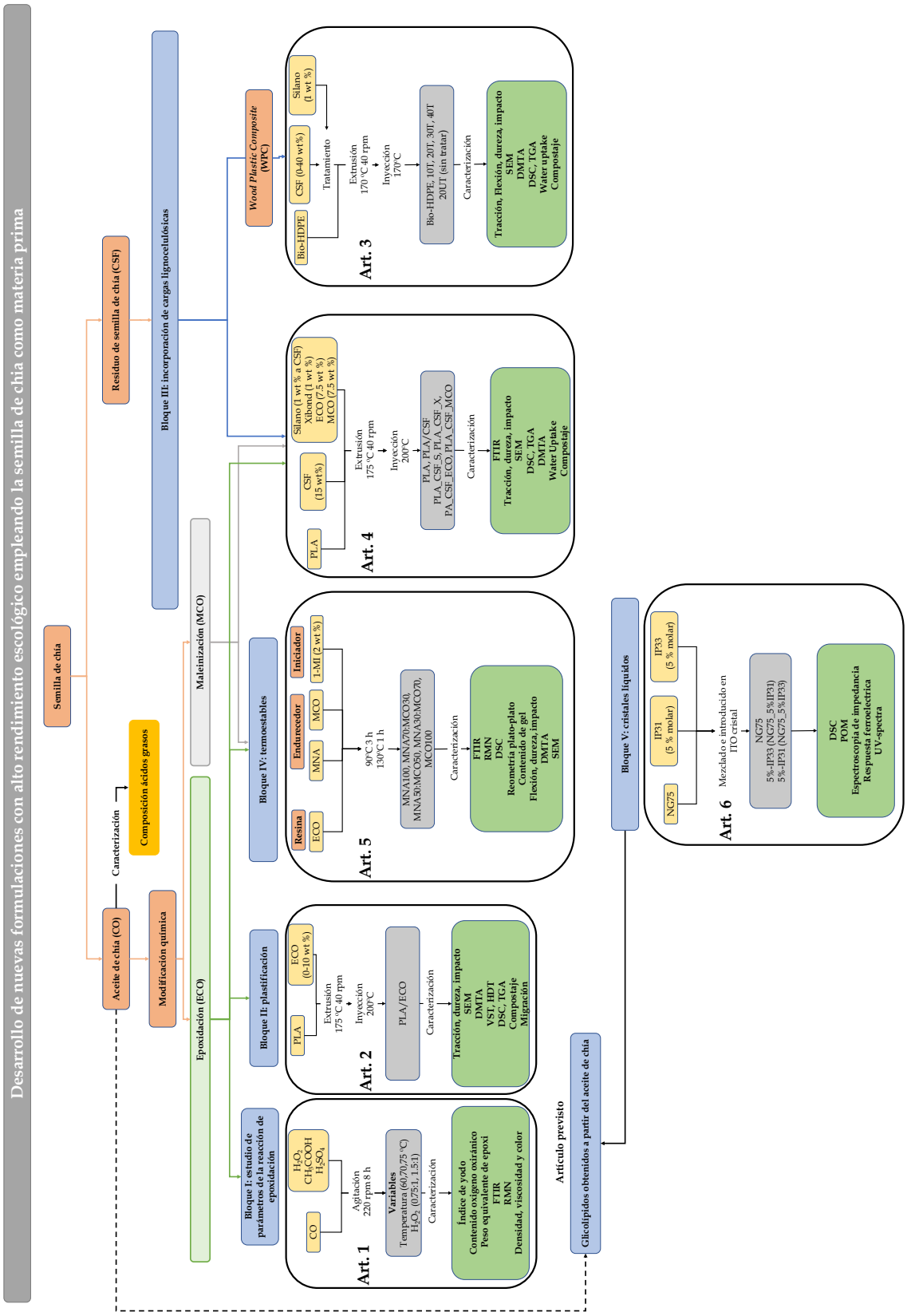

Figura III.1. Representación esquemática del trabajo realizado durante la tesis doctoral.

IV. RESULTADOS Y DISCUSIÓN

En el presente trabajo de investigación se ha centrado en la revalorización y aplicación de los productos de la semilla de chía (*Salvia Hispanica L.*) en el campo de los biopolímeros. Las siguientes secciones muestran los resultados más relevantes obtenidos durante la investigación. Los resultados se han clasificado en 5 bloques dependiendo de la aplicación de los productos obtenidos de la semilla de chía.

En lo referido al quinto bloque, se trata de un estudio previo para la caracterización de cristales líquidos para un futuro estudio de la aplicación del aceite de chía como nuevo surfactante. En dicho bloque se realizará una introducción particular con la finalidad de explicar los conceptos básicos y la relación con la semilla de chía.

Bloque I: estudio de los parámetros de la reacción de epoxidación

Este bloque se centra en el estudio de los parámetros que intervienen en la reacción de epoxidación del aceite de chía. El objetivo es conocer que efecto tiene la temperatura y la cantidad de peróxido empleado en el rendimiento de epoxidación. El seguimiento de la reacción se realiza mediante el análisis de valoración química para conocer los dobles enlaces disponibles y el porcentaje de grupos epoxi añadidos al aceite de chía. La comprobación de los grupos epoxi se realiza empleando FTIR y H-NMR, midiendo también las propiedades fisicoquímicas más importantes de los aceites epoxidados obtenidos. De acuerdo con los resultados, este nuevo aceite epoxidado puede ser empleado como alternativa a los ya existentes a nivel comercial. Los aspectos más relevantes se exponen en el Capítulo IV.1.

Capítulo IV.1. "Physicochemical Characterization of Novel Epoxidized Vegetable oil from Chia Seed Oil"

Bloque II: plastificación

Este bloque evalúa la capacidad plastificante del aceite epoxidado de chía como nuevo aditivo en el PLA. Se realiza un completo estudio del efecto del plastificante, donde se varía el porcentaje de plastificante añadido para mejorar la baja plasticidad del PLA. Se trabaja tanto con piezas inyectadas como en forma de film para la evaluación de propiedades mecánicas y térmicas, además de estudiar su compostabilidad o migración, entre otras. Este estudio se enfoca en mejorar los inconvenientes que muestra el PLA, siendo uno de los biopolímeros referentes más empleados a nivel industrial. Los aspectos más relevantes se exponen en el Capítulo IV.2.

Capítulo IV.2. "Dual Plasticizer/Thermal Stabilizer Effect of Epoxidized Chia Seed Oil (*Salvia hispanica L.*) to Improve Ductility and Thermal Properties of Poly (Lactic Acid)"

Bloque III: incorporación de cargas lignocelulósicas

Este bloque se centra en la incorporación del residuo resultante tras la extracción del aceite de chía, en forma de harina, en polímeros con alto rendimiento medioambiental. En un primer caso, se emplea el Bio-HDPE derivado de la caña de azúcar como matriz, donde se realiza un estudio para mejorar la compatibilidad de la harina de chía empleando silanos. En este caso se obtiene un *wood plastic composites* (WPC), con la idea de contribuir a un modelo económico basado en una la economía circular.

En un segundo estudio, se incorporan los residuos de chía en una matriz de PLA pero, con el objetivo de mejorar las propiedades mecánicas y su compatibilidad con la carga, se emplean compatibilizantes alternativos. En este sentido, se emplean dos modificaciones del aceite de chía: el aceite epoxidado y el aceite maleinizado actuando como plastificantes y/o compatibilizantes alternativos de origen renovable. Los aspectos más relevantes se exponen en el Capítulo IV.3. y Capítulo IV.4.

Capítulo IV.3. "Contribution to a Circular Economy Model: From Lignocellulosic Wastes from the Extraction of Vegetable Oils to the Development of a New Composite"

Capítulo IV.4. "Novel compatibilizers and plasticizers developed from epoxidized and maleinized chia oil in composites based on PLA and chia seed flour"

Bloque IV: termoestables

Continuando con la aplicación de derivados de la semilla de chía en el campo de los biopolímeros, en este capítulo se emplean aceites de chía modificados químicamente para obtener materiales termoestables de origen bio. Por un lado, el aceite epoxidado de chía es empleado como resina base. Por otro lado, se realiza una mezcla de endurecedores empleando anhídrico metil nádico (MNA) de origen petroquímico y el aceite maleinizado de origen renovable. En este caso, se evalúa el efecto del aceite maleinizado en las propiedades finales del material termoestable. Primero se realiza el estudio de los grupos reactivos presentes en las materias primas. Posteriormente, se optimizan las condiciones de entrecruzado de la resina y finalmente se evalúan las propiedades termo-mecánicas de las muestras. El empleo de los aceites modificados obtenidos permite modelar las propiedades de las resinas curadas en función de la mezcla de endurecedores utilizada. Los aspectos más relevantes se exponen en el Capítulo IV.5.

Capítulo IV.5. "Development of a novel epoxy resin based on epoxidized chia oil as matrix and maleinized chia oil as bio-renewable crosslinker"

Bloque V: cristales líquidos

Este bloque se enfoca como un estudio previo para afianzar el conocimiento sobre una futura obtención de glicolípidos derivados del aceite de chía, presentando un comportamiento de cristal líquido. Las muestras utilizadas en el actual bloque son cristales líquidos compuestos de núcleo curvados, siendo uno de ellos no cromóforo (NG75), y otros dos cromóforos (IP-33 y IP-31). Se evalúa la capacidad de converión y almacenamiento de energía realizando mezclas del 5 % molar de cada compuesto cromóforo con NG75, para promover efectos foto inducidos. Se estudia el comportamiento molecular en función de la temperatura, frecuencia y voltaje, además de evaluar la capacidad de almacenar energía cuando se aplica luz ultravioleta. Tras el estudio se confirma el potencial de emplear este tipo de cristales líquidos como conversor y almacenamiento de energía y la posibilidad de aplicarlo poseteriormente en el aceite de chía modificado químicamente. Los aspectos más relevantes se exponen en el Capítulo V.6.

Capítulo V.6. "Light-responsive bent-core liquid crystals as candidates for energy conversion and storage"

Bloque I: estudio de los parámetros de la reacción de epoxidación

IV.1 "Physicochemical Characterization of Novel Epoxidized Vegetable oil from Chia Seed Oil"

Ivan Dominguez-Candela[1], Alejandro Lerma-Canto[2], Salvador Cayetano Cardona[1], Jaime Lora[1], Vicent Fombuena[2]

[1] Instituto de Seguridad Industrial, Radiofísica y Medioambiental (ISIRYM), Universitat Politècnica de València (UPV), Plaza Ferrándiz y Carbonell, s/n, 03801 Alcoy, Spain

[2] Technological Institute of Materiales (ITM), Universitat Politècnica de València (UPV), Plaza Ferrándiz y Carbonell 1, 03801 Alcoy, Spain

Materials

2022, 15(9), p.3250-3269.

"Physicochemical Characterization of Novel Epoxidized Vegetable Oil from Chia Seed Oil"

Abstract

In this study, a novel epoxidized vegetable oil (EVO) from chia seed oil (CSO) has been obtained, with the aim to be employed in a great variety of green products related to the polymeric industry, as plasticizers and compatibilizers. Previous to the epoxidation process characterization, the fatty acid (FA) composition of CSO was analyzed using gas chromatography (GC). Epoxidation of CSO has been performed using peracetic acid formed in situ with hydrogen peroxide and acetic acid, applying sulfuric acid as catalyst. The effects of key parameters as temperature (60, 70, and 75 °C), the molar ratio of hydrogen peroxide:double bond (H_2O_2:DB) (0.75:1.0 and 1.50:1.0), and reaction time (0–8 h) were evaluated to obtain the highest relative oxirane oxygen yield (Y_{oo}). The evaluation of the epoxidation process was carried out through iodine value (IV), oxirane oxygen content (O_o), epoxy equivalent weight (EEW), and selectivity (S). The main functional groups were identified by means of FTIR and ^{1}H NMR spectroscopy. Physical properties were compared in the different assays. The study of different parameters showed that the best epoxidation conditions were carried out at 75 °C and H_2O_2:DB (1.50:1), obtaining an O_o value of 8.26% and an EEW of 193 ($g \cdot eq^{-1}$). These high values, even higher than those obtained for commercial epoxidized oils such as soybean or linseed oil, show the potential of the chemical modification of chia seed oil to be used in the development of biopolymers.

Keywords

Chia seed oil; fatty acids composition; epoxidized vegetable oil; epoxy equivalent weight

Introduction

Nowadays, fossil-based materials use is increasing greenhouse gas emissions, wastes in landfills, and the exhaustion of non-renewable resources [1]. This situation leads to the need to find new alternatives in order to decrease the elevated production of fossil-based materials. One of the most promising renewables resources is vegetable oils (VO) because of their availability, relatively low cost, and non-toxicity [2]. According to the latest data of European Bioplastics Association, the land used to produce the renewable feedstock is approximately 0.0013% in 2021 and is estimated to increase up to 0.058% in 2026 [3]. This increase continues to be a very low value compared with food and feed land used (25% in 2021), indicating that there is not competition between the renewable feedstock for feed, food, and the production of bioplastics. In case of VO production, it increases each year where approximately 20% is used for industrial applications due to the concern of environmental problems [4]. VO is mainly formed by triglycerides, which are composed of three fatty acids (FAs) connected to glycerol molecules. In their structure, carbon-carbon double bonds enable VO to be easily transformed, increasing their reactivity. One of the several ways to take advantage of these double bonds in VO is through the epoxidation reaction, which introduces oxirane oxygen in double bonds [5]. Epoxidized vegetable oils (EVOs) are used as reagents and intermediates in the manufacture of polymers and are commonly used as plasticizers, compatibilizers, stabilizers, reactive diluents, or epoxy matrices for composites [6,7,8,9]. Several EVOs have been reported in the literature, highlighting studies of linseed [10], cottonseed [11], soybean [12], karanja [13] or castor oil [14], among others [15,16,17,18].

Notwithstanding, one of the VO with the most significant potential, due to its high amount of double bonds present in the FA chains, is the chia seed oil (CSO) (*Salvia hispanica, L.*). As it is possible to observe in Table IV.1.1., the iodine value (IV) of CSO, which is a parameter used to determine the number of unsaturation in fats, oils, and waxes, is above 190 g I_2/100 g. For this reason, CSO is one of the VO with the greatest potential for use in different sectors. Nowadays, CSO presents a market share of 20% of chia market with an expected increase of 23.4% from 2019 to 2025 in order to use it for food and non-food applications [19]. Regarding food applications,

although is not widely used as others edible VOs, it is employed as food complements and cooking oil [20]. Some authors have also suggested the addition of CSO in food applications due to its high benefits [21,22]. On the other hand, as non-food applications, CSO has been epoxidized and employed as environmentally friendly plasticizer in one of the most promising industrial applications [23]. However, this study showed a lack of assessed parameters such as temperature and reagents concentration that can enhanced the epoxidation yield and no physico-chemical characterizations were carried out. Therefore, CSO could be one of the best VO candidates to be epoxidized, due to its high availability of double bonds, which can lead to obtain one of the highest theoretical oxirane oxygen content (Oo) even higher than EVOs of greater industrial use (linseed and soybean). CSO has the potential to obtain more O_o using fewer amounts of reagents (sulphuric and acetic acid or hydrogen peroxide e.g.), resulting in a low-cost process and a more environmentally friendly EVO [24,25,26].

Table IV.1.1. Iodine value and theoretical oxirane oxygen content of different vegetable oils.

Vegetable Oil	Initial Iodine Value (IV_0, g I_2/100 g)	Theoretical Oxirane Oxygen Content (O_o, %)	References
Castor	84	5.03	[14]
Soybean	126	7.36	[27]
Rubber	156	8.95	[28]
Cottonseed	107	6.32	[11]
Linseed	188	10.6	[29]
Canola	112	6.60	[5]
Sunflower	130	7.57	[30]
Palm	62	3.76	[12]
Olive	127	7.41	[31]
Corn	115	6.76	[32]
Chia seed	197	11.05	Present study

Regarding the epoxidation process, selectivity (S) and O_o vary depending on the catalyst used to obtain epoxides. Different methods have been studied, each with its advantages and disadvantages. For example, Guenter *et al.* employed molecular oxygen to carry out the epoxidation process [33]. This method could be low-cost and ecological using silver as the catalyst, but it is restricted to precursors like ethylene or

butadiene and is not very efficient. The same authors studied the possibility of using halohydrins through hypohalous acids and their respective salts, but this route was not environmentally friendly [33]. The most employed route to synthesize EVOs is the use of hydrogen peroxide with in situ formed peroxyacid, as can be observed in Figure IV.1.1. This route presents some benefits compared to preformed peroxyacids, such as safer processing and handling, as well as requiring a minimum quantity of reagents to produce EVOs [34]. However, this route can lead to thermal runaway due to the exothermic reaction [35]. In order to reduce this risk, several actions can be considered such as comprehensive temperature control with adequate cooling capacity or dosing rate [36]. In this regard, this issue is taking into account industrially due to this route is the most employed [37]. Moreover, it is commonly known that, in many epoxidation processes, the excess of molar ratio reagents and/or higher temperatures can lead to side-reactions, being the most common the oxirane ring cleavage. The ring-opening has been studied for the purpose of comprehending the influence of factors in these side-reactions. For instance, Cai *et al.* [38] have studied the ring-opening for the epoxidation of cottonseed oil, where evaluated the effect of reagents taking into account the kinetic model. Furthermore, in the recent literature, the use of different epoxidation methods such as chemoenzymatic, polyoxometalates or heterogeneous catalytic systems in the presence of titanium silicate or ion exchange resin has been reported to overcome this drawback [4]. However, homogeneous catalysts have been proved to be more effective for industrial-scale plants to produce EVOs in batch reaction over 8 h [39,40]. In this regard, the use of strong mineral acid with acetic acid leads to a higher reaction rate [41].

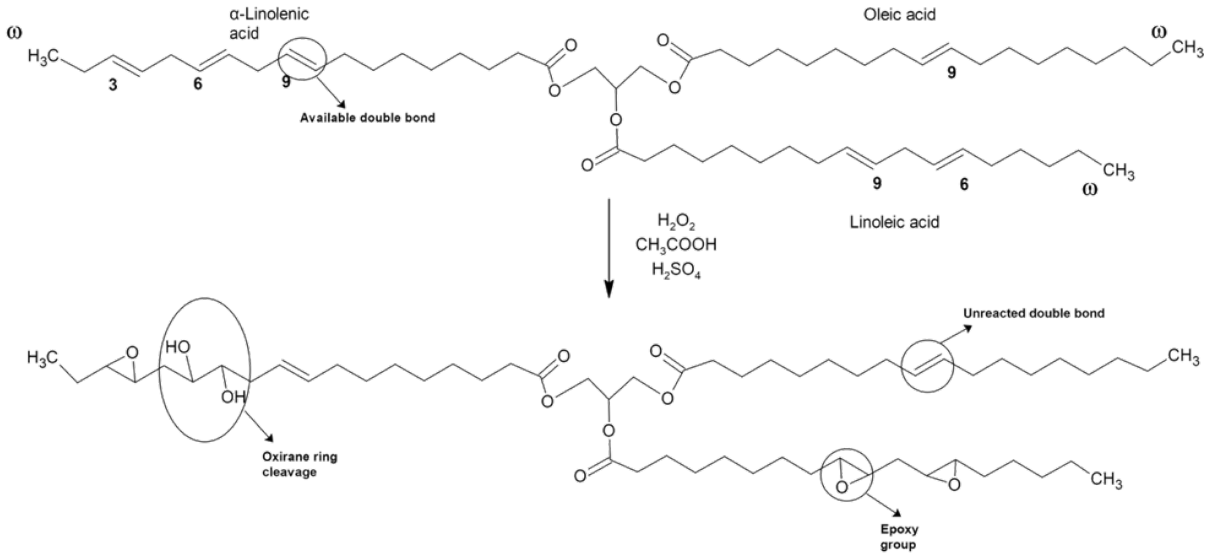

Figure IV.1.1. Schematic representation of epoxidation by means of in situ formed peroxyacids.

The main purpose of this study was to develop a new EVO from chia seed oil (ECSO) as a raw material due to its great potential, determined by the high IV. This new EVO was carried out by in situ epoxidation process with acetic acid and hydrogen peroxide. In this way, a new reagent for use in the polymeric industry can be obtained through a naturally renewable resource as an alternative to the current petrochemical compounds or commercially available EVOs. After the analysis by GC of the composition of the fatty acids of chia oil obtained by cold mechanical extrusion, the epoxidation process was carried out, optimizing key parameters such as temperature, the molar ratio of H_2O_2:DB, and reaction time. The oxirane oxygen content (O_o) was analyzed by titration method and the functional groups were confirmed using FTIR as well as ^{1}H NMR spectroscopy. Further characterization was performed to evaluate the changes in physical-chemical parameters such as specific gravity, dynamic viscosity, and colorimetric coordinates.

Experimental

Materials

Chia seed (*Salvia hispanica, L.*) was supplied by Frutoseco (Bigastro, Alicante, Spain) and CSO was obtained by cold extraction using a CZR-309 press machine (Changyouxin Trading Co., Zhucheng, China). Aqueous hydrogen peroxide (30

wt.%), glacial acetic acid (99.7 wt.%), and sulphuric acid (96 wt.%) were purchased from Sigma Aldrich (Sigma Aldrich, Madrid, Spain). Reagents required for IV characterization such as Wijs solution (Icl), 0.1 N sodium thiosulphate solution ($Na_2S_2O_3$), potassium iodide (KI), and cyclohexane (C_6H_{12}), were supplied from Sigma Aldrich (Sigma Aldrich, Madrid, Spain). To determine oxirane oxygen content, chlorobenzene (C_6H_5Cl), crystal violet indicator, potassium acid phthalate ($KHC_8H_4O_4$), and 0.1 N HBr solution in glacial acetic acid were supplied from Panreac Química S.L.U. (Castellar del Vallés, Barcelona, Spain).

Epoxidation Process

Epoxidation reaction was performed in a three-necked round-bottom flask (1000 mL capacity). The flask, equipped with a two-bladed stirrer, was immersed in a thermostatic water bath where the temperature could be controlled to ± 0.1 °C of the desired temperature. A propeller mechanical stirrer was connected to the central neck, a drop-wise device was introduced in one of the side necks, and a thermometer was connected to the third neck.

Epoxidation of CSO was carried out using a peroxyacid generated in situ from an organic acid. The most widely used in this process are formic (HCOOH) and acetic (CH_3COOH) acids due to their high reactivity. The efficiency of these oxidants depends on the operating temperature, taking into account that according to literature, acetic acid is the most effective above 60 °C [42]. Furthermore, acting as the catalyst, sulphuric (H_2SO_4) and nitric acid (HNO3) are the most employed. In this regard, sulphuric acid with an optimal value of 3 wt.% with respect to the sum of the masses of hydrogen peroxide and acetic acid, was the most effective inorganic acid in order to obtain the highest conversion to oxirane oxygen, as was reported [43]. Therefore, the procedure is summarized as follows: firstly, 232 g of CSO (0.776 mol double bond for each 100 g of oil) and 25.3 g of glacial acetic acid were maintained at a constant temperature (60 °C) and stirring rate (220 rpm), which allowed a sufficient agitation to ensure proper mass transfer. After 10 min, sulphuric acid and hydrogen peroxide were mixed and added dropwise. The addition was completed within half an hour, at a constant rate following the method reported by Dinda *et al.* [44]. Two

different H_2O_2:DB molar ratios (MR) mentioned previously (MR 0.75 and MR 1.50) at 60 °C were studied. MR 1.50 has been selected as the optimal amount of peroxide, which means 1.50 moles of H_2O_2 for one mole of double blonds [45]. It should be noted that CSO contains a higher iodine value compared to other VOs and, thus, a higher Oo can be obtained. Therefore, MR 0.75 (half of the MR 1.50) has also been tested in this epoxidation process in order to study the effect of hydrogen peroxide and the possibility to achieve a reduction of the chemical compounds used. With respect to the temperature, different tests have been carried out at 60, 70, and 75°C ± 1°C, studying the reaction from 0 to 8 h considering the ranges reported in previous literature [46]. Samples were extracted at 0.5, 1.0, 1.5, 2.0, 4.0, 6.0 and 8.0 h, after adding the peroxide and sulphuric acid to monitor the reaction process. The collected samples were cooled at room temperature and then washed with water until they were acid-free up to pH neutral. To purify and remove the excess of water, samples were centrifuged 10 min at 7000 rpm.

Characterization

Fatty Acid Composition

Prior to quantitative determination, Fas of oils have been transformed into methyl esters (FAMEs) following the standard method ISO 12966. The Fas profile was determined using HP/Agilent 6890 N gas chromatograph (Palo Alto, CA, USA) with Agilent 5973 N mass spectrometer detector (GC-MS). Equipment is provided with a splitless injector, ionization detector mode (70 eV), and integrator. The GC-MS method applied was according to ISO 12966. A DB-5MS capillary column (30 m length, 0.25 mm inner diameter, and 0.25 mm film thickness) from Teknokroma (Barcelona, Spain) was used using a temperature program from 140 to 300°C at 20°C/min. The injector and detector temperatures used were 280 and 300°C, respectively. The sample injection volume was 1 µL using a splitless injector. Helium was used as carrier gas at a flow rate of 1 µL/min. Each FA was identified through the retention time comparison between pure commercial standard and the studied sample. FA results were expressed as percentages of the total regarding FAMEs.

Iodine Value (IV)

The iodine value is referred to the mass of Iodine (I_2 in grams) absorbed by 100 g of oil. It is an index used to determine the amount of unsaturation (double bonds) in Fas. This value was determined using Wijs solution (Icl) that reacted with double bonds and it was possible to detect the evolution by using sodium thiosulfate solution. IV was determined according to ISO 3961 using Equation IV.1.1:

$$IV = \frac{12.69 \times c \times (V_1 - V_2)}{m} \qquad \textbf{Equation IV.1.1}$$

where IV refers to the mass of Iodine per 100 g of oil (g I_2/100 g oil), c to the normality of sodium thiosulfate solution 0.1 N ($Na_2S_2O_3$), V_1 to the volume of $Na_2S_2O_3$ needed for titration of the blank (mL), V_2 to the volume of $Na_2S_2O_3$ needed for titration of the sample (CSO) (mL), and m refers to the amount of sample used (g). Moreover, it is possible to determine the conversion of double bond (X_{IV}) using Equation IV.1.2 [10]:

$$X_{IV}(\%) = \left(\frac{IV_0 - IV_f}{IV_0}\right) \times 100 \qquad \textbf{Equation IV.1.2}$$

where IV_0 is the initial iodine value of the VO sample and IV_f is the final iodine value of the EVO after the epoxidation process. At least five measurements were made for each sample and the average values were reported.

Oxirane Oxygen Content (O_o)

The number of epoxy groups was determined using the direct method of titration with hydrobromic acid (HBr) solution in glacial acetic acid, using ASTM D1652. The sample was dissolved in chlorobenzene, followed by the addition of drops of crystal violet and titration using 0.1 N HBr in glacial acetic acid. The oxirane oxygen content (O_o) was calculated with Equation IV.1.3:

$$O_o(wt.\%) = 1.6 \times N_i \times \frac{(V - B)}{W} \qquad \textbf{Equation IV.1.3}$$

where N_i refers to the normality of HBr in glacial acetic acid, V to the volume of HBr solution for titration of the sample (mL), B to the volume of HBr solution for titration of the blank (mL), and W refers to the amount of sample used (g). At least five measurements were made for each sample and the average values were reported.

To determine the percentage conversion to oxirane (Y_{OO}) Equation IV.1.4 has been employed:

$$Y_{OO}(\%) = \left(\frac{O_o}{O_{the}}\right) \times 100 \qquad \textbf{Equation IV.1.4}$$

where, O_o is the oxirane oxygen content experimentally obtained and O_{the} is the theoretical maximum oxirane oxygen content that was calculated using Equation IV.1.5 [43]:

$$O_{the}(\text{wt.}\%) = \left(\frac{\frac{IV_o}{2AM_i}}{\left[100 + \left(\frac{IV_o}{2AM_i}\right) \times AM_o\right]}\right) \times AM_o \times 100 \qquad \textbf{Equation IV.1.5}$$

Regarding Equation IV.1.5, IV_o is the initial iodine value of the sample, AM_i is the atomic mass of Iodine (126.9 g/mol), and AM_o is the atomic mass of oxygen (16 g/mol). Moreover, the selectivity for oxirane oxygen (S) can be determined using Equation IV.1.6 [47].

$$S = \left(\frac{O_o}{O_{the}}\right) \times \left(\frac{IV_o}{IV_o - IV_f}\right) \qquad \textbf{Equation IV.1.6}$$

Epoxy Equivalent Weight (EEW)

The epoxy equivalent weight (*EEW*) is defined as the mass, expressed in grams, of the epoxy resin which contains one equivalent of the epoxy group (g·eq^{-1}). It is one of the most important features of epoxy resins, which is related to the crosslinking density and allows the calculation of the required amount of crosslinking agent for

the curing process [49]. The *EEW* of ECSO was obtained following ASTM D1652 via titration using Equation IV.1.7:

$$EEW\ (\mathrm{g}\cdot\mathrm{eq}^{-1}) = \left(\frac{1000\times\ W}{(V-B)\times\ N_i}\right) \qquad \textbf{Equation IV.1.7}$$

Fourier Transform InfraRed (FTIR) Spectroscopy

The substitution of double bonds and changes in functional groups was identified by Fourier Transform Infrared (FTIR) spectroscopy equipped with a horizontal attenuated total reflection modulus (ATR). Both CSO and ECSO were analyzed using a Bruker Vector 22 (Bruker Española, S. A, Madrid, España), averaging 20 scans at 4000–400 cm^{-1} and 4 cm^{-1} of resolution. It must be remarked that this method is immediate and straightforward to evaluate the possible change of the main functional groups, allowing to correlate the progress of epoxidations from infrared studies. However, the titration method obtains a better accuracy than the FTIR spectroscopy method, as has been reported by [15,49]. Thus, the FTIR method was used to verify the evolution of the main functional groups.

Nuclear Magnetic Resonance (NMR) Spectroscopy

^{1}H NMR spectroscopy was employed to compare and confirm the chemical structure of CSO and ECSO. Samples were analyzed using a Bruker AMX 500 unit (Bruker BioSpin GmbH, Rheinstetten, Germany) at 25 °C. Samples of 40 mg were dissolved in 0.6 mL of deuterated chloroform ($CDCl_3$), mixed for 10 s and transferred to 5 mm NMR tubes for data acquisition.

Physico-Chemical Properties

The method used to determine changes in specific gravity was a pycnometer, according to ASTM D1963. This method uses a 25 mL pycnometer maintaining a constant temperature of 25 °C. All densities of liquids were obtained against water. The specific gravities of untreated CSO and epoxidized were measured using Equation IV.1.8:

$$\rho_r = \frac{W_s - W_e}{W_w - W_e}$$ **Equation IV.1.8**

where W_s is the weight (g) of the sample in the pycnometer, W_e is the weight (g) of the empty pycnometer, and W_w is the weight (g) of water in the pycnometer. At least five measurements were obtained with a maximum deviation of 3×10^{-3}.

Dynamic viscosities were obtained using two Cannon-Fenske viscosimeters of 300 and 450 mm with flow ranges from 5×10^{-5} to 2.5×10^{-4} $m^2 \cdot s^{-1}$ and from 5×10^{-4} to 2.5×10^{-2} $m^2 \cdot s^{-1}$, respectively, at 20 °C. The assay has been carried out following the guidelines of the ASTM D-445. Viscosimeter was introduced in a water bath monitoring the temperature with a precision of ± 0.1 °C. At least five measurements were measured with a maximum dynamic viscosity deviation of 1.02 mPa·s.

The colorimetric coordinates of CSO and ECSO were measured using a Hunter Lab Colorimeter (Colour Flex, Hunter Associates Inc., Reston, VA, USA). The instrument (45°/0° geometry, D45 optical sensor, 10° observer) was calibrated before the experiments with Black and White reference tiles, and Green tiles were used to verify the correct operation. The values of luminance (L*) (0–100) represent lightness, parameters a* and b* indicate the approach from green (negative) to red (positive), and from blue (negative) to yellow (positive), respectively. At least five measurements were made for each sample and the average values were reported. Color variation was evaluated by using Equation IV.1.9:

$$\Delta E = \sqrt{\Delta L^2 + \Delta a^2 + \Delta b^2}$$ **Equation IV.1.9**

Results and discussion

CSO Extraction and Fatty Acid Composition

CSO was extracted by double cold extraction in a press machine to avoid chemical changes in the FA composition caused by high temperatures and the use of chemical solvents. Firstly, whole seeds were pressed to obtain oil and cake. Then, the residual cake was pressed again in order to obtain a higher yield of oil extraction. At

the end of the pressing process, oil was filtered and centrifuged at 4000 rpm to be cleaned, and then it was stored in a cold dark room. The yield of extracted CSO was increased from 20.4% for the first process to 24.5% adding up the oil obtained from the second press of the chia cake. This slow increase of extraction yield with the second press shows that no longer than two presses are considered economically feasible, as reported by Kasote *et al.* [50]. This total yield is in the same range that was reported by Ixtaina *et al.* [51], in which the production yield of CSO was 24.8%.

The FA composition obtained by GC and the comparison with results published by other authors are shown in Table 2. As it can be observed, CSO presents a low proportion of saturated fatty acids (SFAs), with a value of 10.7%, integrated by myristic (0.06%), palmitic (7.2%), stearic (2.88%), and arachidic (0.55%) acids. With respect to monounsaturated fatty acids (MUFAs), it is observed even a lower proportion (4.41%), with palmitoleic (0.09%) and oleic (4.32%) acids. The higher content is found in polyunsaturated fatty acids (PUFAs) with 84.9%, which provides the most CSO double bonds: Linoleic (15.8%), γ-Linolenic (0.41%), and α-Linolenic (68.6%). The main difference between γ-Linolenic and α- Linolenic is the position of the double bond, where α-Linolenic contains the double bond in the 3rd, 6th, and 9th carbon position with respect to methyl terminus, whereas γ-Linolenic in 6th, 9th and 12th position. The high amount of α-Linolenic acid in the Fas profile provides better reactivity due to the position of double bonds in the carbon chain. The double bonds closer to the methyl terminus in the 3rd position present more reactivity than the 6th and 9th as has been reported by Scala and Wool [140], where the kinetics of the epoxidation process of vegetable oil was studied. Furthermore, CSO is the seed oil with the highest α-Linolenic content known compared to other studies of vegetable oils [53]. The results of the Fas of CSO are in concordance with the results reported by other authors, as is gathered in Table IV.1.2. The slight difference is probably due to the seed origin that has influenced FA composition. Some authors have reported that the FA profile and its quantity depend on several environmental factors such as temperature, light, or soil type [54].

Table IV.1.2. Content of fatty acids presents in chia seeds (expressed as g of fatty acid/100 g of oil) and comparison with other studies.

	Fatty Acids (Fas)	In This STUDY	Demin *et al.* [53]	Kulczyński *et al.* [55]
SFAs	Myristic (C14:0)	0.06	0.04	0.06
	Palmitic (C16:0)	7.20	6.84	7.04
	Stearic (C18:0)	2.88	2.71	2.84
	Arachidic (C20:0)	0.55	0.28	0.02
	Total SFAs	10.7	9.87	9.96
MUFAs	Palmitoleic (C16:1)	0.09	0.24	0.03
	Oleic (C18:1)	4.32	6.17	7.3
	Total MUFAs	4.41	6.41	7.33
PUFAs	Linoleic (C18:2)	15.8	18.6	18.9
	γ-Linolenic (C18:3)	0.41	n.m[1]	n.m[1]
	α-Linolenic (C18:3)	68.6	64.4	63.8
	Total PUFAs	84.9	83	82.7

[1] Where n.m means not mentioned.

Effect of Molar Ratio H_2O_2:Double Bond in the Epoxidation Process

To investigate the effect of molar ratio H_2O_2:DB, two experiments were made at MR 0.75 and 1.50 applying a constant temperature of 60 °C. In these conditions, both *IV* and O_o analyses were obtained to monitor the epoxidation reaction. As it is possible to observe in Figure IV.1.2., IV_0 was 197 g I_2/100 g of oil for CSO, which is in accordance with Imran *et al.* [56] and Timilsena *et al.* [57], where both obtained values of 193 and 204 g I_2/100 g of oil, respectively. The plot representation shows that once the epoxidation process takes place, the *IV* decreases due to the reaction of double bonds, as reported by Campanella *et al.* [58] with soybean oil. In the assay carried out at MR 1.50, the *IV* decreases more sharply, showing a greater rate yield in the process of double bonds substitution. However, although the results using MR 1.5 have been better than those with MR 0.75, the authors do not consider it appropriate to increase the MR above 1.5, due to an excess of reagents can cause side-reactions as the oxirane ring cleavage. In addition, the slope of the *IV* curve changes at the first 4 h, being less pronounced with MR 0.75 due to less initial oxygen active donor in the reaction for the lower hydrogen peroxide ratio, which is strongly related to the reduction of IV.

Therefore, using MR 1.50 at 60 °C, *IV* is reduced up to 80.1 g I_2/100 g of oil after 8 h of reaction, reaching almost a value of 60% for X_{IV}. However, lower values were obtained using MR 0.75, with 42.2% for X_{IV} and 114 g I_2/100 g of oil for *IV*.

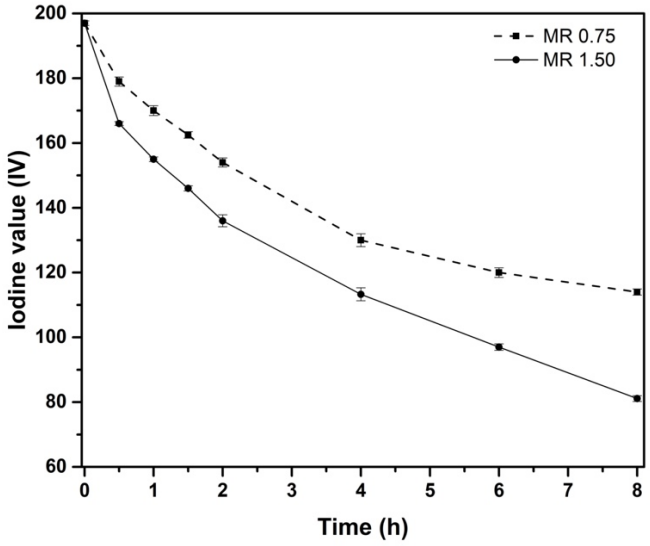

Figure IV.1.2. Effect on Iodine value (IV) of the MR 0.75 and 1.50 during the epoxidation process.

Figure IV.1.3. shows the plot evolution of O_o and *EEW*. Inversely proportional to *IV*, when MR increases, the presence of O_o increases as well. As reaction time proceeds, significant differences were observed comparing both MR. It is known that hydrogen peroxide is an active oxygen donor in the reaction [27]. Thus, when MR is increased from 0.75 to 1.50, an increase of O_o can be noticed. The reason for this result is the increase In peracetic acid formation due to a higher amount of hydrogen peroxide [10]. Peracetic acid acts as a vector of oxygen, causing a conversion improvement. Then, doubling the amount of hydrogen peroxide, an increase of 36.8% in O_o from 4.48 wt.% to 6.13 wt.% was obtained at the end of the reaction. Taking Equation (5) into account, a theoretical maximum oxirane oxygen content (O_{the}) of 11.05% was obtained, thus achieving a Y_{oo} value of 55.6% for MR 1.50. This epoxidation yield value can be ascribed to the lower efficiency of acetic acid at 60 °C, when the most effective temperature is observed above 60 °C [42]. Results are gathered in Table 3.

Related to selectivity (*S*) (values also summarized in Table IV.1.3.), it is possible to appreciate that this value slightly decreases at MR 1.50 compared to MR 0.75. These

results demonstrate that there are double bonds that were not replaced by epoxy groups. Although X_{IV} and Y_{oo} for MR 1.50 are higher than for MR 0.75, the opposite occurs with S. It is known that higher MR leads to an increment of Y_{oo} and the presence of hydrolysis reactions, i.e., epoxy ring cleavage [28]. For that reason, S for MR 1.50 is slightly lesser than for MR 0.75 due to more presence of side-reactions caused by a higher amount of hydrogen peroxide. This is another reason why the use of higher reagent ratios is not technically feasible, as the high reactivity of the fatty acids present in chia oil causes unwanted side reactions. Therefore, the highest O_o and lowest EEW values were obtained for MR 1.50 with values of 6.13 wt.% and 260 g·eq^{-1}, respectively.

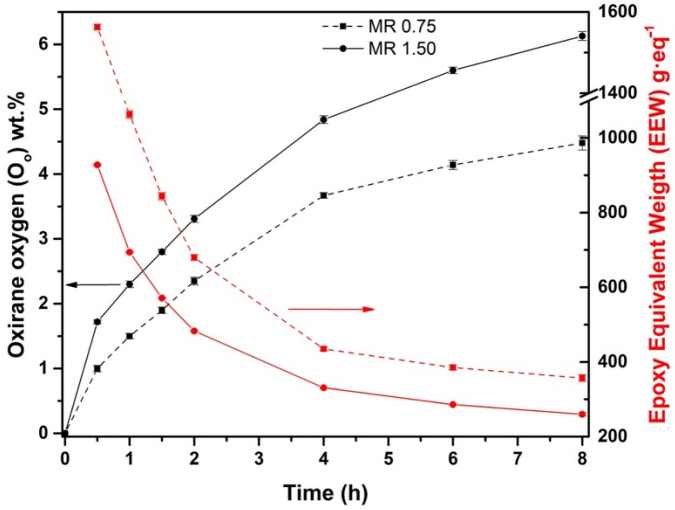

Figure IV.1.3. Effect on oxirane oxygen (O_o) of the MR 0.75 and 1.50 at 60°C during the epoxidation process.

Table IV.1.3. Main parameters used to characterize the epoxidation process of the chia seed oil (CSO) at different molar ratios and temperatures.

Epoxi	Temperature (°C)	MR [1]	Ivf [2]	XIV [3]	O_o [4]	EEW [5] (g·eq^{-1})	Y_{OO} [6]	S [7]
1	60	0.75	114 ± 0.94	42.2 ± 0.48	4.48 ± 0.11	357 ± 8.9	39.9 ± 1.02	0.946 ± 0.0188
2	60	1.50	80.1 ± 0.87	59.4 ± 0.41	6.13 ± 0.12	260 ± 4.94	55.6 ± 1.07	0.935 ± 0.0192
3	70	1.50	37.9 ± 0.62	80.8 ± 0.32	7.61 ± 0.10	210 ± 3.10	68.9 ± 0.98	0.853 ± 0.0170
4	75	1.50	13.1 ± 1.52	93.4 ± 0.75	8.26 ± 0.11	193 ± 2.39	74.8 ± 0.78	0.801 ± 0.0179

[1] Hydrogen peroxide to double bond; [2] Final iodine value; [3] Conversion iodine value; [4] Oxirane oxygen content; [5] Epoxy equivalent weight; [6] Conversion to oxirane; [7] Selectivity.

Effect of the Temperature in the Epoxidation Process

The influence of temperature on the epoxidation process was studied at 60 °C, 70 °C, and 75 °C with the best MR (1.50) previously detailed. In Figure IV.1.4, it is possible to observe an increase in *IV* conversion at higher temperatures. As happened previously, the slope of *IV* showed a sharper change at the first 4 h. This behavior can be ascribed to the higher reactivity of double bonds present in the 3rd position of methyl terminus of fatty acid in α-Linolenic acid [52], which react faster at the initial time of the experiments. In contrast, the less reactive double bonds (6th and 9th) present in α-Linolenic acid, Linoleic, and Oleic acid take a longer time to react. Then, increasing the temperature from 60 °C to 75 °C, an *IV* of 13.1 g I_2/100 g of oil was obtained with regard to 80.1 g I_2/100 g of oil at 60 °C. Therefore, the temperature is shown as the key factor to increase the conversion of *IV*.

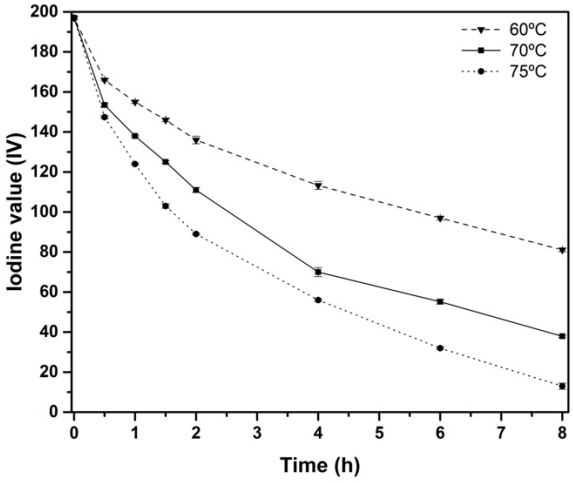

Figure IV.1.4. Effect on Iodine value (IV) of the temperature (60 °C, 70 °C, and 75 °C) with MR 1.50 during the epoxidation process.

Regarding the formation of epoxy groups plotted in Figure IV.1.5, it increases as temperature increases, accelerating the kinetic of epoxidation to form oxirane oxygen [46]. In the same way as with *IV*, the O_o slope is higher at the first 4 h of reaction whereas, after that time, this trend decreases. This reduction in reaction rate can be related to the decomposition of peracetic acid, acetic acid, and hydrogen peroxide along the time [59]. With the higher temperature (75 °C) studied, it is possible to obtain the highest value of O_o, 8.26 wt.%, or lowest *EEW*, 193 g·eq^{-1}, obtaining a Y_{oo} of 74.8%.

An increase of 15°C from 60 °C to 75 °C contributes to an improvement of 25.7% for O_o. It should be noted that higher temperatures and extended time, increase the O_o but can also cause a greater oxirane cleavage rate [44]. As Campanella *et al.* [60] and Gan *et al.* [61] studied for temperatures higher than 75 °C in soybean and palm oil, respectively, the oxirane ring was destabilized, which slowed the growth of the conversion to epoxy groups, even reducing the oxirane oxygen formed. In this sense, all temperatures studied showed almost no conversion to epoxy groups from 6 h onwards, being more pronounced with the temperature of 75 °C. For this reason, the authors did not consider it appropriate to carry out the epoxidation process at higher temperatures.

Regarding the selectivity, *S*, gathered in Table IV.1.3., it is possible to compare that it decreases substantially as temperature increases. At 70 °C and 75 °C the best O_o have been obtained, as well as the lowest *S*. Thus, *S* decreases as higher is the temperature, which indicates an increase in oxirane cleavage. Although Y_{oo} was 74.8% with these conditions, an interesting wt.% of O_o or *EEW* have obtained if they are compared to other reports. Dinda *et al.* [44] used the same epoxidation method with cottonseed oil, reaching 4.96 wt.% for O_o with 80% for Y_{oo}. Furthermore, Mungroo *et al.* [5] studied the epoxidation of Canola oil using ion exchange resin as the catalyst, where 6.13 wt.% for O_o and 90% for Y_{oo} could be obtained. With the current values obtained with ECSO (8.26 wt.% for O_o or *EEW* 193 g·eq^{-1}), it is possible to forecast that it could be an excellent EVO as an alternative to the commercially available VO. A comparative example is found in the study carried out by Samper *et al.* [62], where epoxidized soybean oil with *EWW* of 238 g·eq^{-1}, is used to manufacture a composite laminate with engineering applications. In addition, another example is reported by Fombuena *et al.* [63], where green composites are manufactured using commercial epoxidized linseed oil with 8 wt.% as epoxy matrix. Therefore, the present ECSO contains equal or even higher wt.% of O_o or lower *EEW* than the most commercially available EVOs.

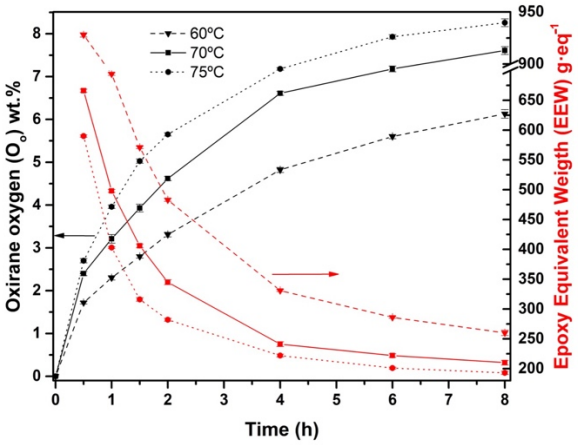

Figure IV.1.5. Effect on oxirane oxygen (O_o) of the temperature (60 °C, 70 °C, and 75 °C) using MR 1.50 during the epoxidation process.

FTIR Analysis

As an alternative to evaluating the characterization of the epoxidation reaction through titration, FTIR spectroscopy is shown as an efficient tool for determining the representative peaks. Figure IV.1.6. shows the spectrum of untreated CSO, taken as reference. The characteristic peaks of double bonds are associated with 3010 cm^{-1} (=$CH_{(v)}$) due to stretching of cis-olefinic bonds, 1652 cm^{-1} (C=$C_{(v)}$) caused by stretching of disubstituted cis-olefins, and 723 cm^{-1} (C=$C_{(cis\text{-}\delta)}$) due to the combination of out-of-plane deformation and rocking vibration in cis-disubstituted olefins. Other characteristics peaks associated to methyl and methylene groups are obtained from 2961 to 2851 cm^{-1} (-$CH_{3(asym\text{-}v)}$ and -$CH_{2(sym\ and\ asym\text{-}v)}$) and from 1462 to 1375 cm^{-1} (-$CH_{2(asym\text{-}\ \delta)}$ and –$CH_{3(sym\text{-}\ \delta)}$). Finally, the peak at 1743 cm^{-1} represents a carbonyl stretching (C=$O_{(v)}$) of ester groups, and also the peak obtained at 821 cm^{-1} (C-O-$C_{(v)}$) should be noted, barely visible in the untreated CSO but indicative of oxirane oxygen. Compared to the characteristic peaks of untreated CSO described in the literature, such as Timilsena *et al.* [64], a slight difference is shown due to the origin of seed and climate conditions, which can influence the fatty acid composition.

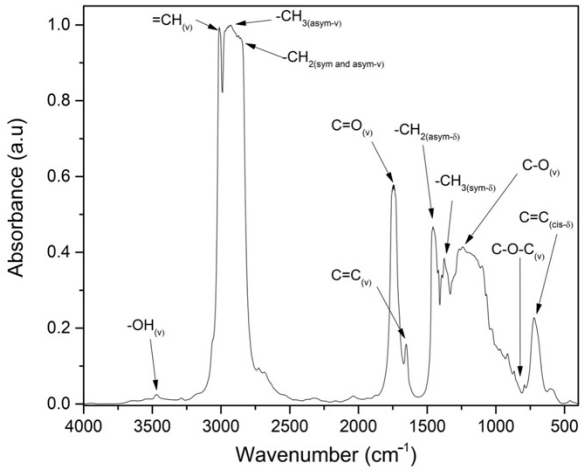

Figure IV.1.6. FTIR spectrum of CSO.

The monitoring of the epoxidation reaction by FTIR spectroscopy at different MR and temperatures has been focused on the characteristic peaks corresponding to double bonds (Figure IV.1.7.) and the plot evolution of the oxirane oxygen content (O_o) (Figure IV.1.8.). All spectra are obtained after 8 h of epoxidation reaction time. Figure IV.1.7a represents the plot evolution of the peak at 3010 cm^{-1} ($=CH_{(v)}$). It is possible to observe that the peak decreases drastically using MR 1.50 at 75 °C, which is in concordance with the analysis done by titration. This indicates the low quantity of available doubles bonds after the epoxidation reaction. Figure IV.1.7b,c show the graphical evolution of the peaks at 1652 ($C=C_{(v)}$) and 723 cm^{-1} ($C=C_{(cis-\delta)}$), respectively, with the same trend mentioned previously. In general, the characteristic peaks of double bonds decrease when MR increase from 0.75 to 1.50 and the temperature reaches 75 °C, obtaining fewer available double bonds.

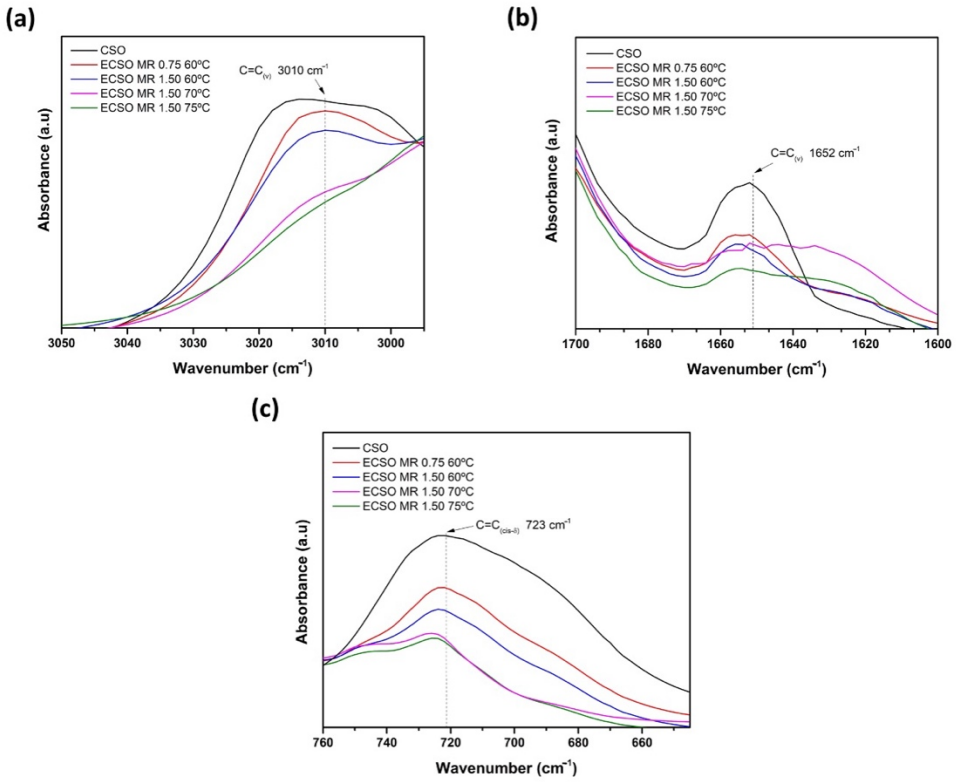

Figure IV.1.7 .FTIR spectra of ECSO obtained with different epoxidation conditions by the analysis of characteristic peaks of the double bonds (a) 3010 cm^{-1} (=$CH_{(v)}$), (b) 1652 cm^{-1} (C=$C_{(v)}$) and (c) 723 cm^{-1} (C=$C_{(cis\text{-}\delta)}$).

On the other hand, the increase of MR from 0.75 to 1.50, leads to a higher intensity of the oxirane oxygen group peak, (C-O-$C_{(v)}$), located at 821 cm^{-1}, following the same trend as the titration method as it is observed in Figure IV.1.8a. This new molecular group, not detectable in CSO, increases due to the insertion of oxygen into the double bonds through peracetic acid formed by the epoxidation reaction process. In parallel form, in Figure IV.1.8b, the same trend for the hydroxyl group (-$OH_{(v)}$) can be observed at 3470 cm^{-1}. In this case, greater MR accelerates the presence of hydroxyl groups by oxirane ring decomposition in the ECSO structure, as has been reported by Goud *et al.*[65]. The main reason is that the great amount of hydrogen peroxide employed contributes to the epoxy group formation, whereas another quantity is led to opening the oxirane ring obtaining hydroxyl groups [45].

With regard to the temperature effect, the temperature at 75 °C increases the intensity of the peaks corresponding to the hydroxyl group, compared with the MR

effect. It indicates that the opening of the oxirane ring is more pronounced at higher temperatures than the MR ranges studied. This behavior has also been reported by Dinda *et al.* [44] during cottonseed epoxidation, where the highest content of hydroxyl groups was obtained at 75 °C. In addition, this effect is increased with VOs with higher initial IV, which contributes to obtaining a greater epoxy conversion as well as hydroxyl groups formation in a simultaneous process [66].

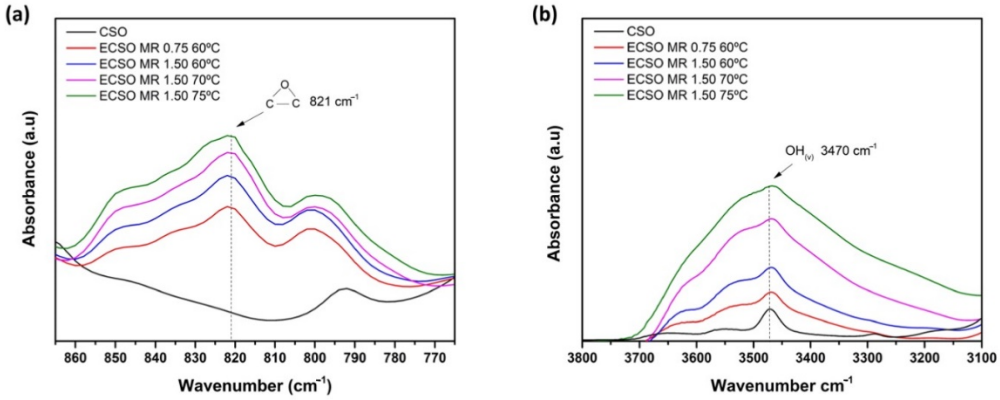

Figure IV.1.8. FTIR spectra of ECSO obtained with different epoxidation conditions by the analysis of characteristics peaks of (a) oxirane oxygen, and (b) hydroxyl groups.

H NMR Analysis

^{1}H NMR spectra were obtained to confirm the change of functional groups in ECSO synthesized with the best conditions in the epoxidation process, i.e., MR 1.50 at 75 °C. In Figure IV.1.9. the ^{1}H NMR spectra of CSO and ECSO are plotted, showing a signal intensity (A) at 5.3–5.5 ppm for CSO. This characteristic peak corresponds to vinyl hydrogens from double bonds, which almost disappeared for the ECSO sample due to the conversion of *IV*. This peak was split into two signals: on the one hand, a small signal of vinyl hydrogen from double bonds located at 5.6 ppm, indicating that few double bonds remain after epoxidation reaction as was corroborated by *IV* and FTIR; on the other hand, a signal at 5.3 ppm for the central hydrogen of the glyceride moiety [67]. In addition, two more signals were observed at 2.02 ppm (C), associated with hydrogen adjacent to double bonds, and at 2.8 ppm (B), corresponding to allyl hydrogen between double bonds. After the epoxidation process, the peak at 2.8 ppm

disappeared completely to show a displacement to 1.5 ppm (F) assigned to methylene hydrogens adjacent to oxirane groups in ECSO. The newly formed group was also registered in two new peaks between 2.85–3.00 I and 3.00–3.25 ppm (D) in ECSO. The first one corresponds to methylene hydrogens between two oxirane oxygen groups, whereas the second is related to hydrogens of the carbons of the new oxirane oxygen group. The evidence of hydroxyl groups formed by the opening of the oxirane ring was observed in the 4–3.4 ppm region as was described by M. Farias *et al.*[68], who evaluated the epoxidation of soybean oil using a homogeneous catalyst such as molybdenum (IV) complex. In that study a lower conversion to oxirane oxygen and selectivity at 80 °C was reported compared to this paper. The ^{1}H NMR spectra obtained were consistent with the previous analysis, confirming the formation of oxirane oxygen in double bonds of the ECSO sample as well as hydroxyl groups as a result of side-reactions.

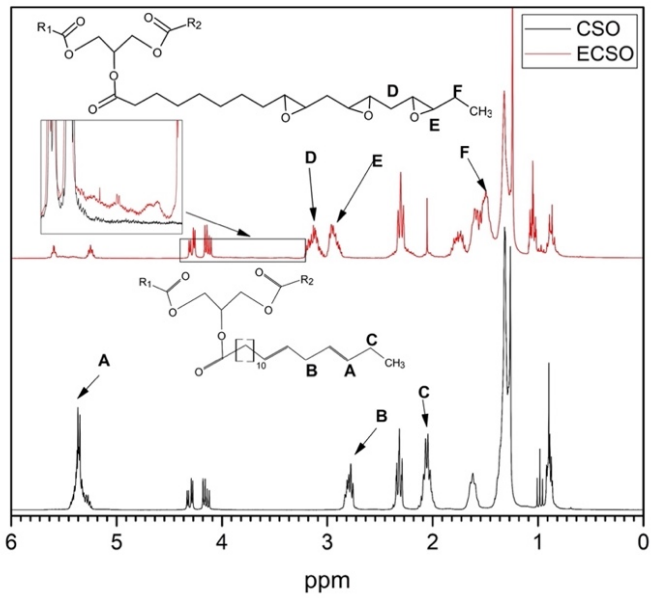

Figure IV.1.9. Comparison of CSO and ECSO by ^{1}H NMR spectra.

Physico-Chemical Properties

Physico-chemical properties such as specific gravity, dynamic viscosity, and colorimetric coordinates have been measured before and after the epoxidation reaction process of the CSO at different MR and temperatures. These parameters can be taken as a quick and easy methodology to monitor the epoxidation process. Results

obtained after 8 h of reaction time are gathered in Table IV.1.4. With respect to specific gravity, low values in VO could be associated with the presence of cis double bonds present in FA structure, which difficult the packaging of the molecular chains [69]. The specific gravity value obtained in CSO, 0.9285, is in concordance with previous studies performed by Uzunova *et al.* [70] with values reported of 0.9288. As the epoxidation reaction advances and greater MR and temperatures are employed to improve the reaction yield, the insertion of oxirane oxygen in the FA structural chain increases the specific gravity of ECSO. Values reach up to 1.026, which is 10.5% higher than untreated CSO. The epoxy groups contribute to increase molecular mass without significant change in its volume due to the variation from sp^2 hybridization of double bond (C=C) to sp^3 hybridization of a single bond. This change improved chain packing, even though the stress on the chains was increased by the insertion of epoxy groups [69].

Regarding the dynamic viscosity of untreated CSO, it depends on the presence of unsaturations in the FA molecular chains. The presence of carbon-carbon double bonds kinks the fatty acid chains, increasing the average distance between them [71]. Therefore, an oil such as untreated CSO with high proportions of linolenic acid, i.e., a high amount of double bonds, results in lower dynamic viscosity compared to more saturated vegetable oils with an average value of 32 mPa·s. In epoxidized samples, dynamic viscosity is substantially higher as the performance of the epoxidation reaction progresses, reaching values of 558 mPa·s. These higher dynamic viscosities are ascribed to the increase of molecular weight and polarity in the structure compared to CSO, thus becoming stronger the interaction between molecules [72]. In addition, this property could also be increased, especially at high temperatures, due to the opening of the oxirane ring to form hydroxyl, ketone, and carboxylic groups that increase the intermolecular bonding and, consequently, increase the viscosity [73].

Table IV.1.4. Comparative of physico-chemical properties of chia seed oil (CSO) and epoxidized chia seed oil (ECSO).

Sample	Specific Gravity (ρ_r)	Dynamic Viscosity (mPa·s)	Colourimetric Coordinates			Colour Variation (ΔE)
			L*	a*	b*	
CSO	$0.9285 \pm 2.2 \cdot 10^{-3}$	32 ± 0.45	75.4 ± 0.21	-6.27 ± 0.30	31.5 ± 0.35	0
ECSO MR 0.75 60 °C	$0.9745 \pm 1.2 \cdot 10^{-3}$	109 ± 0.78	77.1 ± 0.28	6.73 ± 0.21	18.6 ± 0.21	18.4 ± 0.25
ECSO MR 1.50 60 °C	$0.9901 \pm 2.3 \cdot 10^{-3}$	163 ± 0.73	76.5 ± 0.23	2.91 ± 0.17	13.8 ± 0.49	19.9 ± 0.19
ECSO MR 1.50 70 °C	$1.0175 \pm 1.7 \cdot 10^{-3}$	420 ± 0.87	76.4 ± 0.28	-3.69 ± 0.35	4.47 ± 0.16	27.1 ± 0.44
ECSO MR 1.50 75 °C	$1.0260 \pm 2.9 \cdot 10^{-3}$	558 ± 1.02	79.6 ± 0.42	-2.85 ± 0.36	4.50 ± 0.21	27.5 ± 0.42

Finally, the variation of the color as a consequence of the epoxidation process can be observed in Figure IV.1.10. The untreated CSO is characterized by a yellow color, attributed to the high value of b* and L* (31.5 and 75.4 respectively), which are in concordance with values reported by Timilsena *et al.* [57]. As the yield of the reaction progresses by increasing the MR and the temperature, the greater presence of epoxy groups and lower *IV* in ECSO leads to decrease the yellow color, as it is possible to quantify by analyzing the b* parameter (decrease from 31.5 in CSO to 4.50 in ECSO). Regarding a*, a slightly reddish color (a* > 0) was observed in epoxidized samples with lesser epoxy groups (<6.3 wt.%) and higher *IV* (>80 g I_2/100 g of oil) such as MR 0.75 and 1.50 at 60 °C. As the epoxidation yield increases, a* decreases from 6.73 for ECSO MR 0.75 at 60 °C up to negative values such as −3.69 and −2.85 for MR 1.50 at 70 °C and 75 °C, respectively, characterized by a lightly green color. Alarcon *et al.* [74] reported pale-yellow color in both epoxidized Baru and Macaw vegetable oils with epoxy content of 5.98 wt.% and 5.39 wt.%, respectively, but with low *IV* content (<15 g I_2/100 g of oil) regardless the initial color of virgin oil. Therefore, the change of color observed from yellow (CSO) to reddish or to pale-yellow of different epoxidized samples can be attributed to the final *IV* change, regardless of the epoxy content of the epoxidized sample. Besides, the brightness (L*) of ECSO slightly increases after each epoxidation process, where the highest value was obtained for

MR 1.50 at 75 °C. The noticeable color change can be quantified by analysing the color change (ΔE). Aguero *et al.* [75] reported that a value greater than 5 implies a change visible to the naked eye. In this case, an increase of noticeable color change has been observed for all epoxidation conditions ($\Delta E > 5$) compared to CSO, where no significant changes were observed between 70 °C and 75 °C.

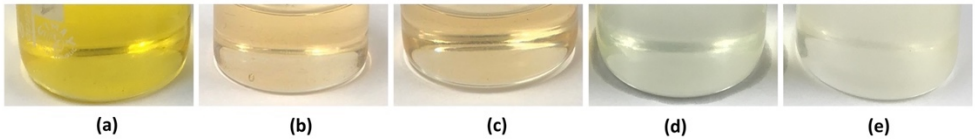

Figure IV.1.10. Influence of the MR and temperature on the color during the epoxidation process of the chia seed oil (CSO). (a) Untreated chia seed oil (CSO), (b) ECSO MR 0.75 at 60 °C, (c) ECSO MR 1.50 at 60 °C, (d) ECSO MR 1.50:1 at 70 °C and I ECSO MR 1.50 at 75 °C.

Conclusions

This research work assesses the development of a novel EVO obtained from chia seed oil (CSO). Previously to the epoxidation process, the fatty acid profile of CSO analyzed by GC showed polyunsaturated fatty acids (PUFAs) up to 84.9%, highlighting a proportion of α-Linolenic acid higher than 68.6%. These results make CSO an excellent candidate to be an alternative to the current commercial epoxidized oils. Variables such as MR and temperature have been studied in the epoxidation process. Results obtained with a MR 1.50 provide more O_o caused by more peracetic acid formed that contributes to epoxy group formation. In a second step, the effect of the temperature was evaluated at 60, 70, and 75 °C. Epoxidation reaction at 75 °C provided the highest O_o (8.26 wt.%) and lowest *EEW* (193 g·eq^{-1}) with conversion to oxirane of 74.8%, and the reduction of the iodine value from 197 g I_2/100 g oil up to 13.1 g I_2/100 g oil, with a conversion for double bonds of 93.4%. Although the conversion to oxirane is less than 90%, O_o obtained is similar to or even higher than available commercial epoxidized vegetable oils. The use of higher ratios of reactants and temperatures has not been carried out due to the problems provided by side-reactions as the oxirane ring cleavage, which reduces the efficiency of the process. The main functional groups formed by the epoxidation process have been confirmed by FTIR and ^{1}H NMR spectroscopy, where both were in concordance with tendencies

observed in the titration method. The influence of the epoxidation process in physico-chemical parameters such as specific gravity, dynamic viscosity, and color measurement has been reported, demonstrating that these parameters, as well as FTIR studies, can be used for rapid monitoring of the reaction. Results indicate that the epoxidation process implied a substantial increase in specific gravity and dynamic viscosity. All epoxidized samples showed an evident color variation ($\Delta E > 5$) from yellow (CSO) to light reddish for samples with higher *IV* (>80 g I_2/100 g of oil) or to pale-yellow for samples with lower *IV* (<35 g I_2/100 g of oil), that can be ascribed to the final *IV* change of epoxidized samples. Therefore, it is possible to conclude that ECSO is a highly potential EVO considered an alternative to the current epoxidized oils on the market, from an environmental point of view, and with high interest to be used in the manufacture of polymers and biopolymers.

Acknowledgments

This research work was funded by the Ministry of Science and Innovation-"Retos de la Sociedad". Project reference: PID2020-119142RA-I00. I. Dominguez-Candela wants to thank Universitat Politècnica de València for his FPI grant (PAID-2019- SP20190013) and Generalitat Valenciana (GVA) for his FPI grant (ACIF/2020/233).

References

[1] Biermann, U.; Bornscheuer, U.; Meier, M.A.R.; Metzger, J.O.; Schäfer, H.J. Oils and Fats as Renewable Raw Materials in Chemistry. Angew. Chem. Int. Ed. 2011, 50, 3854–3871. https://doi.org/10.1002/anie.201002767.

[2] Corma, A.; Iborra, S.; Velty, A. Chemical Routes for the Transformation of Biomass into Chemicals. Chem. Rev. 2007, 107, 2411–2502. https://doi.org/10.1021/cr050989d.

[3] Bioplastics, E. Bioplastics Market Data. Available online: https://www.european-bioplastics.org/. 2021. (accessed on 19 April 2022).

[4] Danov, S.M.; Kazantsev, O.A.; Esipovich, A.L.; Belousov, A.S.; Rogozhin, A.E.; Kanakov, E.A. Recent advances in the field of selective epoxidation of vegetable oils and their derivatives: A review and perspective. Catal. Sci. Technol. 2017, 7, 3659–3675. https://doi.org/10.1039/c7cy00988g.

[5] Mungroo, R.; Pradhan, N.C.; Goud, V.V.; Dalai, A.K. Epoxidation of Canola Oil with Hydrogen Peroxide Catalyzed by Acidic Ion Exchange Resin. J. Am. Oil Chem. Soc. 2008, 85, 887–896. https://doi.org/10.1007/s11746–008–1277-z.

[6] Chieng, B.; Ibrahim, N.; Then, Y.; Loo, Y. Epoxidized Vegetable Oils Plasticized Poly (lactic acid) Biocomposites: Mechanical, Thermal and Morphology Properties. Molecules 2014, 19, 16024–16038. https://doi.org/10.3390/molecules191016024.

[7] Sahoo, S.K.; Khandelwal, V.; Manik, G. Development of toughened bio-based epoxy with epoxidized linseed oil as reactive diluent and cured with bio-renewable crosslinker. Polym. Adv. Technol. 2018, 29, 565–574. https://doi.org/10.1002/pat.4166.

[8] Tee, Y.B.; Talib, R.A.; Abdan, K.; Chin, N.L.; Kadir Basha, R.; Md Yunos, K.F. Comparative Study of Chemical, Mechanical, Thermal, and Barrier Properties of Poly (Lactic Acid) Plasticized with Epoxidized Soybean Oil and Epoxidized Palm Oil. Bioresources 2015, 11, 1518–1540. https://doi.org/10.15376/biores.11.1.1518–1540.

[9] Xiong, Z.; Yang, Y.; Feng, J.; Zhang, X.; Zhang, C.; Tang, Z.; Zhu, J. Preparation and characterization of poly (lactic acid)/starch composites toughened with epoxidized soybean oil. Carbohydr. Polym. 2013, 92, 810–816. https://doi.org/10.1016/j.carbpol.2012.09.007.

[10] Janković, M.R.; Govedarica, O.M.; Sinadinović-Fišer, S.V. The epoxidation of linseed oil with in situ formed peracetic acid: A model with included influence of the oil fatty acid composition. Ind. Crops Prod. 2020, 143, 111881.

[11] Carbonell-Verdu, A.; Bernardi, L.; Garcia-Garcia, D.; Sanchez-Nacher, L.; Balart, R. Development of environmentally friendly composite matrices from epoxidized cottonseed oil. Eur. Polym. J. 2015, 63, 1–10. https://doi.org/10.1016/j.eurpolymj.2014.11.043.

[12] Derawi, D.; Salimon, J. Optimization on Epoxidation of Palm Olein by Using Performic Acid. Eur. J. Chem. 2010, 7, 1440–1448. https://doi.org/10.1155/2010/384948.

[13] Garcia-Garcia, D.; Carbonell-Verdu, A.; Arrieta, M.P.; Loppez-Martinez, J.; Samper, M.D. Improvement of PLA film ductility by plasticization with epoxidized karanja oil. Polym. Degrad. Stab. 2020, 179, 109259. https://doi.org/10.1016/j.polymdegradstab.2020.109259.

[14] Sahoo, S.K.; Khandelwal, V.; Manik, G. Development of completely bio-based epoxy networks derived from epoxidized linseed and castor oil cured with citric acid. Polym. Adv. Technol. 2018, 29, 2080–2090. https://doi.org/10.1002/pat.4316.

[15] Vianello, C.; Piccolo, D.; Lorenzetti, A.; Salzano, E.; Maschio, G. Study of Soybean Oil Epoxidation: Effects of Sulfuric Acid and the Mixing Program. Ind. Eng. Chem. Res. 2018, 57, 11517–11525. https://doi.org/10.1021/acs.iecr.8b01109.

[16] Zheng, J.L.; Wärnå, J.; Salmi, T.; Burel, F.; Taouk, B.; Leveneur, S. Kinetic modeling strategy for an exothermic multiphase reactor system: Application to vegetable oils epoxidation using P rileschajew method. AIChE J. 2016, 62, 726–741.

[17] Cai, X.; Ait Aissa, K.; Estel, L.; Leveneur, S. Investigation of the physicochemical properties for vegetable oils and their epoxidized and carbonated derivatives. J. Chem. Eng. Data 2018, 63, 1524–1533.

[18] Shuttleworth, P.S.; Díez-Pascual, A.M.; Marco, C.; Ellis, G. Flexible bionanocomposites from epoxidized hemp seed oil thermosetting resin reinforced with halloysite nanotubes. J. Phys. Chem. B 2017, 121, 2454–2467.

[19] Chia Seeds Market Size Worth $4.7 Billion by 2025. Available online: https://www.grandviewresearch.com/press-release/global-chia-seeds-market (accessed on 15 April 2022).

[20] Shen, Y.; Zheng, L.; Jin, J.; Li, X.; Fu, J.; Wang, M.; Guan, Y.; Song, X. Phytochemical and biological characteristics of mexican chia seed oil. Molecules 2018, 23, 3219.

[21] Ullah, R.; Nadeem, M.; Imran, M.; Taj Khan, I.; Shahbaz, M.; Mahmud, A.; Tayyab, M. Omega fatty acids, phenolic compounds, and lipolysis of cheddar cheese supplemented with chia (*Salvia hispanica L.*) oil. J. Food Process. Preserv. 2018, 42, e13566.

[22] Nadeem, M.; Imran, M.; Taj, I.; Ajmal, M.; Junaid, M. Omega-3 fatty acids, phenolic compounds and antioxidant characteristics of chia oil supplemented margarine. Lipids Health Dis. 2017, 16, 1–12.

[23] Dominguez-Candela, I.; Ferri, J.M.; Cardona, S.C.; Lora, J.; Fombuena, V. Dual plasticizer/thermal stabilizer effect of epoxidized chia seed oil (*Salvia hispanica L.*) to improve ductility and thermal properties of poly (lactic acid). Polymers 2021, 13, 1283.

[24] Warwel, S. Complete and partial epoxidation of plant oils by lipase-catalyzed perhydrolysis. Ind. Crops Prod. 1999, 9, 125–132.

[25] Biermann, U.; Friedt, W.; Lang, S.; Lühs, W.; Machmüller, G.; Metzger, J.O.; Rüsch gen. Klaas, M.; Schäfer, H.J.; Schneider, M.P. New syntheses with oils and fats as renewable raw materials for the chemical industry. Angew. Chem. Int. Ed. 2000, 39, 2206–2224.

[26] Wallace, J.C. Encyclopedia of Chemical Technology, 3rd ed.; John Wiley and Sons: New York, NY, USA, 1978; Volume 9.

[27] de Quadros, J.V.; Giudici, R. Epoxidation of soybean oil at maximum heat removal and single addition of all reactants. Chem. Eng. Process. Process Intensif. 2016, 100, 87–93.

[28] Okieimen, F.E.; Bakare, O.I.; Okieimen, C.O. Studies on the epoxidation of rubber seed oil. Ind. Crops Prod. 2002, 15, 139–144. https://doi.org/10.1016/s0926–6690(01)00104–2.

[29] Otabor, G.O.; Ifijen, I.H.; Mohammed, F.U.; Aigbodion, A.I.; Ikhuoria, E.U. Alkyd resin from rubber seed oil/linseed oil blend: A comparative study of the physiochemical properties. Heliyon 2019, 5, e01621.

[30] Benaniba, M.; Belhaneche-Bensemra, N.; Gelbard, G. Epoxidation of sunflower oil with peroxoacetic acid in presence of ion exchange resin by various processes. Energ. Educ. Sci. Technol. 2008, 21, 71.

[31] Huang, Y.B.; Yao, M.Y.; Xin, P.P.; Zhou, M.C.; Yang, T.; Pan, H. Influence of alkenyl structures on the epoxidation of unsaturated fatty acid methyl esters and vegetable oils. RSC Adv. 2015, 5, 74783–74789. (restar uno a todo a partir de aquí)

[32] Sun, S.; Yang, G.; Bi, Y.; Liang, H. Enzymatic epoxidation of corn oil by perstearic acid. J. Am. Oil Chem. Soc. 2011, 88, 1567–1571.

[33] Sienel, G.; Rieth, R.; Rowbottom, K.T. Epoxides. In Ullmann's Encyclopedia of Industrial Chemistry, 6th ed.; Wiley & Sons: Hoboken, NJ, USA, 2003; Volume 12, pp. 269–284.

[34] Yadav, G.; Satoskar, D. Kinetics of epoxidation of alkyl esters of undecylenic acid: Comparison of traditional routes vs. Ishii-Venturello chemistry. J. Am. Oil Chem. Soc. 1997, 74, 397–407.

[35] Leveneur, S. Thermal safety assessment through the concept of structure–reactivity: Application to vegetable oil valorization. Org. Process Res. Dev. 2017, 21, 543–550.

[36] Moreno, V.C.; Russo, V.; Tesser, R.; Di Serio, M.; Salzano, E. Thermal risk in semi-batch reactors: The epoxidation of soybean oil. Process Saf. Environ. Prot. 2017, 109, 529–537.

[37] Tan, S.; Chow, W. Biobased epoxidized vegetable oils and its greener epoxy blends: A review. Polym.-Plast. Technol. Eng. 2010, 49, 1581–1590.

[38] Cai, X.; Zheng, J.L.; Aguilera, A.F.; Vernières–Hassimi, L.; Tolvanen, P.; Salmi, T.; Leveneur, S. Influence of ring-opening reactions on the kinetics of cottonseed oil epoxidation. Int. J. Chem. Kinet. 2018, 50, 726–741.

[39] Jadhav, P.D.; Patwardhan, A.V.; Kulkarni, R.D. Kinetic study of in situ epoxidation of mustard oil. Mol. Catal. 2021, 511, 111748.

[40] Sienkiewicz, A.M.; Czub, P. The unique activity of catalyst in the epoxidation of soybean oil and following reaction of epoxidized product with bisphenol A. Ind. Crops Prod. 2016, 83, 755–773.

[41] Di Serio, M.; Russo, V.; Santacesaria, E.; Tesser, R.; Turco, R.; Vitiello, R. Liquid–liquid–solid model for the epoxidation of soybean oil catalyzed by Amberlyst-16. Ind. Eng. Chem. Res. 2017, 56, 12963–12971.

[42] Wai, P.T.; Jiang, P.; Shen, Y.; Zhang, P.; Gu, Q.; Leng, Y. Catalytic developments in the epoxidation of vegetable oils and the analysis methods of epoxidized products. RSC Adv. 2019, 9, 38119–38136.

[43] Goud, V.V.; Patwardhan, A.V.; Pradhan, N.C. Studies on the epoxidation of mahua oil (Madhumica indica) by hydrogen peroxide. Bioresour. Technol. 2006, 97, 1365–1371. https://doi.org/10.1016/j.biortech.2005.07.004.

[44] Dinda, S.; Patwardhan, A.V.; Goud, V.V.; Pradhan, N.C. Epoxidation of cottonseed oil by aqueous hydrogen peroxide catalysed by liquid inorganic acids. Bioresour. Technol. 2008, 99, 3737–3744. https://doi.org/10.1016/j.biortech.2007.07.015.

[45] Omonov, T.S.; Kharraz, E.; Curtis, J.M. The epoxidation of canola oil and its derivatives. RSC Adv. 2016, 6, 92874–92886. https://doi.org/10.1039/C6RA17732H.

[46] Cai, C.; Dai, H.; Chen, R.; Su, C.; Xu, X.; Zhang, S.; Yang, L. Studies on the kinetics of in situ epoxidation of vegetable oils. Eur. J. Lipid Sci. Technol. 2008, 110, 341–346. https://doi.org/10.1002/ejlt.200700104.

[47] Pérez, J.E.; Haagenson, D.; Pryor, S.; Ulven, C.; Wiesenborn, D. Production and characterization of epoxidized canola oil. Trans. ASABE 2009, 52, 1289–1297.

[48] Garea, S.-A.; Corbu, A.-C.; Deleanu, C.; Iovu, H. Determination of the epoxide equivalent weight (EEW) of epoxy resins with different chemical structure and functionality using GPC and 1H-NMR. Polym. Test. 2006, 25, 107–113.

[49] Durbetaki, A.J. Direct Titration of Oxirane Oxygen with Hydrogen Bromide in Acetic Acid. Anal. Chem. 1956, 28, 2000–2001. https://doi.org/10.1021/ac60120a055.

[50] Kasote, D.M.; Badhe, Y.S.; Hegde, M.V. Effect of mechanical press oil extraction processing on quality of linseed oil. Ind. Crops Prod. 2013, 42, 10–13. https://doi.org/10.1016/j.indcrop.2012.05.015.

[51] Ixtaina, V.Y.; Martinez, M.L.; Spotorno, V.; Mateo, C.M.; Maestri, D.n.M.; Diehl, B.W.K.; Nolasco, S.M.; Tomas, M.C. Characterization of chia seed oils obtained by pressing and solvent extraction. J. Food Compos. Anal. 2011, 24, 166–174. https://doi.org/10.1016/j.jfca.2010.08.006.

[52] La Scala, J.; Wool, R.P. Effect of FA composition on epoxidation kinetics of TAG. J. Am. Oil Chem. Soc. 2002, 79, 373–378.

[53] Demin, M.; Rabrenovic, B.; Pezo, L.; Lalicic-Petronijevic, J. Influence of chia seeds (*Salvia hispanica L.*) and extra virgin olive oil addition on nutritional properties of salty crackers. J. Food Meas. Charact. 2020, 14, 378–387. https://doi.org/10.1007/s11694–019–00300–7.

[54] Ayerza, R. Oil content and fatty acid composition of chia (*Salvia hispanica L.*) from five northwestern locations in Argentina. J. Am. Oil Chem. Soc. 1995, 72, 1079–1081. https://doi.org/10.1007/BF02660727.

[55] Kulczyński, B.; Kobus-Cisowska, J.; Taczanowski, M.; Kmiecik, D.; Gramza-Michalowska, A. The Chemical Composition and Nutritional Value of Chia Seeds-Current State of Knowledge. Nutrients 2019, 11, 1242. https://doi.org/10.3390/nu11061242.

[56] Imran, M.; Nadeem, M.; Manzoor, M.F.; Javed, A.; Ali, Z.; Akhtar, M.N.; Ali, M.; Hussain, Y. Fatty acids characterization, oxidative perspectives and consumer acceptability of oil extracted from pre-treated chia (*Salvia hispanica L.*) seeds. Lipids Health Dis. 2016, 15, 162. https://doi.org/10.1186/s12944-016-0329-x.

[57] Timilsena, Y.P.; Vongsvivut, J.; Adhikari, R.; Adhikari, B. Physicochemical and thermal characteristics of Australian chia seed oil. Food Chem. 2017, 228, 394–402. https://doi.org/.

[58] Campanella, A.; Baltanás, M.A.; Capel-Sanchez, M.; Campos-Martin, J.; Fierro, J. Soybean oil epoxidation with hydrogen peroxide using an amorphous Ti/SiO2 catalyst. Green Chem. 2004, 6, 330–334.

[59] Santacesaria, E.; Russo, V.; Tesser, R.; Turco, R.; Di Serio, M. Kinetics of performic acid synthesis and decomposition. Ind. Eng. Chem. Res. 2017, 56, 12940–12952. (restar uno a partir de aquí)

[60] Campanella, A.; Baltanás, M.A. Degradation of the oxirane ring of epoxidized vegetable oils in liquid–liquid heterogeneous reaction systems. Chem. Eng. J. 2006, 118, 141–152. https://doi.org/.

[61] Gan, L.; Goh, S.; Ooi, K. Kinetic studies of epoxidation and oxirane cleavage of palm olein methyl esters. J. Am. Oil Chem. Soc. 1992, 69, 347–351.

[62] Samper, M.D.; Petrucci, R.; Sanchez-Nacher, L.; Balart, R.; Kenny, J.M. Properties of composite laminates based on basalt fibers with epoxidized

vegetable oils. Mater. Eng. 2015, 72, 9–15. https://doi.org/10.1016/j.matdes.2015.02.002.

[63] Fombuena, V.; Petrucci, R.; Dominici, F.; Jordá-Vilaplana, A.; Montanes, N.; Torre, L. Maleinized Linseed Oil as Epoxy Resin Hardener for Composites with High Bio Content Obtained from Linen Byproducts. Polymers 2019, 11, 301.

[64] Timilsena, Y.P.; Vongsvivut, J.; Tobin, M.J.; Adhikari, R.; Barrow, C.; Adhikari, B. Investigation of oil distribution in spray-dried chia seed oil microcapsules using synchrotron-FTIR microspectroscopy. Food Chem. 2019, 275, 457–466.

[65] Goud, V.V.; Dinda, S.; Patwardhan, A.V.; Pradhan, N.C. Epoxidation of Jatropha (Jatropha curcas) oil by peroxyacids. Asia Pac. J. Chem. Eng. 2010, 5, 346–354.

[66] Kim, J.R.; Sharma, S. The development and comparison of bio-thermoset plastics from epoxidized plant oils. Ind. Crops Prod. 2012, 36, 485–499.

[67] DeHonor-Marquez, E.; Nieto Alarcón, J.F.; Vigueras Santiago, E.; Hernández López, S. Effective and Fast Epoxidation Reaction of Linseed Oil Using 50 wt% Hydrogen Peroxyde. Am. J. Chem. 2018, 8, 99–106.

[68] Farias, M.; Martinelli, M.; Bottega, D.P. Epoxidation of soybean oil using a homogeneous catalytic system based on a molybdenum (VI) complex. Appl. Catal. A Gen. 2010, 384, 213–219.

[69] Harry-O'kuru, R.E.; Biresaw, G.; Tisserat, B.; Evangelista, R. Synthesis of Polyformate Esters of Vegetable Oils: Milkweed, Pennycress, and Soy. J. Lipids 2016, 2016, 3128604. https://doi.org/10.1155/2016/3128604.

[70] Uzunova, G.; Nikolova, K.; Perifanova, M.; Gentscheva, G.; Marudova, M.; Antova, G. Physicochemical characterization of chia (*Salvia hispanica L.*) seed oil from Argentina. Bulg. Chem. Commun. 2016, 48, 131–135.

[71] Wool, R.; Sun, X.S. Bio-Based Polymers and Composites; Elsevier: Amsterdam, The Netherlands, 2011.

[72] Wu, X.; Zhang, X.; Yang, S.; Chen, H.; Wang, D. The study of epoxidized rapeseed oil used as a potential biodegradable lubricant. J. Am. Oil Chem. Soc. 2000, 77, 561–563.

[73] Monono, E.M.; Haagenson, D.M.; Wiesenborn, D.P. Characterizing the epoxidation process conditions of canola oil for reactor scale-up. Ind. Crops Prod. 2015, 67, 364–372.

[74] Alarcon, R.T.; Gaglieri, C.; Lamb, K.J.; North, M.; Bannach, G. Spectroscopic characterization and thermal behavior of baru nut and macaw palm vegetable oils and their epoxidized derivatives. Ind. Crops Prod. 2020, 154, 112585.

[75] Agüero, A.; Morcillo, M.d.C.; Quiles-Carrillo, L.; Balart, R.; Boronat, T.; Lascano, D.; Torres-Giner, S.; Fenollar, O. Study of the Influence of the Reprocessing Cycles on the Final Properties of Polylactide Pieces Obtained by Injection Molding. Polymers 2019, 11, 1908. https://doi.org/10.3390/polym11121908.

materials

MDPI

Article

Physicochemical Characterization of Novel Epoxidized Vegetable Oil from Chia Seed Oil

Ivan Dominguez-Candela [1], Alejandro Lerma-Canto [2], Salvador Cayetano Cardona [1], Jaime Lora [1] and Vicent Fombuena [2,*]

[1] Instituto de Seguridad Industrial, Radiofísica y Medioambiental (ISIRYM), Universitat Politècnica de València (UPV), Plaza Ferrándiz y Carbonell, s/n, 03801 Alcoy, Spain; ivdocan@doctor.upv.es (I.D.-C.); scardona@iqn.upv.es (S.C.C.); jlora@iqn.upv.es (J.L.)

[2] Technological Institute of Materials (ITM), Universitat Politècnica de València (UPV), Plaza Ferrándiz y Carbonell 1, 03801 Alcoy, Spain; allercan@epsa.upv.es

* Correspondence: vifombor@upv.es

Abstract: In this study, a novel epoxidized vegetable oil (EVO) from chia seed oil (CSO) has been obtained, with the aim to be employed in a great variety of green products related to the polymeric industry, as plasticizers and compatibilizers. Previous to the epoxidation process characterization, the fatty acid (FA) composition of CSO was analyzed using gas chromatography (GC). Epoxidation of CSO has been performed using peracetic acid formed in situ with hydrogen peroxide and acetic acid, applying sulfuric acid as catalyst. The effects of key parameters as temperature (60, 70, and 75 °C), the molar ratio of hydrogen peroxide:double bond (H_2O_2:DB) (0.75:1.0 and 1.50:1.0), and reaction time (0–8 h) were evaluated to obtain the highest relative oxirane oxygen yield (Y_{oo}). The evaluation of the epoxidation process was carried out through iodine value (*IV*), oxirane oxygen content (O_o), epoxy equivalent weight (*EEW*), and selectivity (*S*). The main functional groups were identified by means of FTIR and ^{1}H NMR spectroscopy. Physical properties were compared in the different assays. The study of different parameters showed that the best epoxidation conditions were carried out at 75 °C and H_2O_2:DB (1.50:1), obtaining an O_o value of 8.26% and an *EEW* of 193 (g·eq^{-1}). These high values, even higher than those obtained for commercial epoxidized oils such as soybean or linseed oil, show the potential of the chemical modification of chia seed oil to be used in the development of biopolymers.

Keywords: chia seed oil; fatty acids composition; epoxidized vegetable oil; epoxy equivalent weight

check for updates

Citation: Dominguez-Candela, I.; Lerma-Canto, A.; Cardona, S.C.; Lora, J.; Fombuena, V. Physicochemical Characterization of Novel Epoxidized Vegetable Oil from Chia Seed Oil. *Materials* **2022**, *15*, 3250. https://doi.org/10.3390/ma15093250

Academic Editor: Andrei Victor Sandu

Received: 31 March 2022
Accepted: 28 April 2022
Published: 30 April 2022

Publisher's Note: MDPI stays neutral with regard to jurisdictional claims in published maps and institutional affiliations.

1. Introduction

Nowadays, fossil-based materials use is increasing greenhouse gas emissions, wastes in landfills, and the exhaustion of non-renewable resources [1]. This situation leads to the need to find new alternatives in order to decrease the elevated production of fossil-based materials. One of the most promising renewables resources is vegetable oils (VO) because of their availability, relatively low cost, and non-toxicity [2]. According to the latest data of European Bioplastics Association, the land used to produce the renewable feedstock is approximately 0.0013% in 2021 and is estimated to increase up to 0.058% in 2026 [3]. This increase continues to be a very low value compared with food and feed land used (25% in 2021), indicating that there is not competition between the renewable feedstock for feed, food, and the production of bioplastics. In case of VO production, it increases each year where approximately 20% is used for industrial applications due to the concern of environmental problems [4]. VO is mainly formed by triglycerides, which are composed of three fatty acids (FAs) connected to glycerol molecules. In their structure, carbon-carbon double bonds enable VO to be easily transformed, increasing their reactivity. One of the several ways to take advantage of these double bonds in VO is through the epoxidation reaction, which introduces oxirane oxygen in double bonds [5].

Bloque II: plastificación

IV.2 "Dual Plasticizer/Thermal Stabilizer Effect of Epoxidized Chia Seed Oil (*Salvia hispanica L.*) to Improve Ductility and Thermal Properties of Poly(Lactic Acid)"

Ivan Dominguez-Candela[1], Jose Miguel Ferri[2], Salvador Cayetano Cardona[1], Jaime Lora[1], Vicent Fombuena[2]

[1] Instituto de Seguridad Industrial, Radiofísica y Medioambiental (ISIRYM), Universitat Politècnica de València (UPV), Plaza Ferrándiz y Carbonell, s/n, 03801 Alcoy, Spain

[2] Technological Institute of Materiales (ITM), Universitat Politècnica de València (UPV), Plaza Ferrándiz y Carbonell 1, 03801 Alcoy, Spain

Polymers

2021, 13(8), p.1283-1299.

"Dual Plasticizer/Thermal Stabilizer Effect of Epoxidized Chia Seed Oil (*Salvia hispanica L.*) to Improve Ductility and Thermal Properties of Poly(Lactic Acid)"

Abstract

The use of a new bio-based plasticizer derived from epoxidized chia seed oil (ECO) was applied in a poly(lactic acid) (PLA) matrix. ECO was used due to its high epoxy content (6.7%), which led to an improved chemical interaction with PLA. Melt extrusion was used to plasticize PLA with different ECO content in the 0–10 wt.% range. Mechanical, morphological, and thermal characterization was carried out to evaluate the effect of ECO percentage. Besides, disintegration and migration tests were studied to assess the future application in packaging industry. Ductile properties improve by 700% in elongation at break with 10 wt.% ECO content. Field emission scanning electron microscopy (FESEM) showed a phase separation with ECO content equal or higher than 7.5 wt.%. Thermal stabilization was improved 14 °C as ECO content increased. All plasticized PLA was disintegrated under composting conditions, not observing a delay up to 5 wt.% ECO. Migration tests pointed out a very low migration, less than 0.11 wt.%, which is to interest to the packaging industry.

Keywords

PLA; epoxidized chia seed oil (ECO); plasticizers; migration; disintegration.

Introduction

Currently, a global plastics production of 368 million tons was recorded in 2019, an increment of 2.5% from 2018. Conventional polymers such a polyethylene (PE), polypropylene (PP), polyvinyl chloride (PVC), poly(ethylene terephthalate) (PET), polystyrene (PS), and polyamide (PA), represent approximately 70% of plastic demand in Europe. With regard to the packing industry, which represents around 40% of total demand, these polymers are leading the plastic demand [1]. The majority are non-biodegradables as well as manufactured by petrochemical industries (non-renewable resources) [2]. The food packaging industry generates a large volume of waste due to it short-lifespan and its recycling is often limited to those not contaminated with food products. According to Plastics Europe 2020, about 39.5% of post-consumer waste was recycled, while 18.5% (3.2 million tons) ended up in landfills [1]. These non-recycled plastics need to be managed to avoid the presence in seas, lakes, and rivers which threatens the environment [3,4].

Concerning biodegradable polymers, their presence is increasing in the food packing industry. Several biodegradable polymers such as poly(lactic acid) (PLA), thermoplastic polyurethane (TPU), and polyhydroxyalkanoates (PHAs) have been applied as new alternatives [5–8]. The most employed polymer is PLA (about 10.9%), which is obtained by fermentation of polysaccharides or sugar extracted from potato, sugarcane, corn, etc., thus obtained by renewable resources [9]. PLA is currently manufactured for common applications such as salad cups, lamination films, drinking cups, containers, etc. [10]. Biodegradation of PLA is produced by hydrolysis, resulting in harmless and non-toxic substances [11,12]. Nowadays, PLA is considered economically competitive and its properties such as good processability, high transparency, water solubility resistance, biodegradability, recyclability, etc., make it suitable for good packaging [13,14]. Besides, the energy saved in production is around 22–55% with regard to petroleum-based polymers, thus contributing to a decrease in environmental impact [15]. PLA is characterized by its high tensile modulus, although some drawbacks such as brittle nature with elongation at break of less than 9%, a narrow processing window, poor thermal stability, etc., are detected [16,17]. Several

methodologies to improve ductile properties have been carried out successfully using copolymers, blends, or plasticizers in a PLA matrix [18–20].

The plasticizer market is increasing its annual demand in the polymeric industries. Phthalates (PTs) are a common plasticizer and additive to provide transparency, flexibility, and durability properties to a polymer matrix, commonly found in food packaging, medical equipment, building materials, toys, etc. [21,22]. The annual world production of PTs as plasticizer is approximately 80% [21]. However, studies show a migration phenomenon from polymer matrix to element in contact causing health and environment impact. It is well known that exposure of PTs to human lives produces endocrine damage, and reproduction and carcinogenic effects [23]. According to the European Union and other organizations, specific PTs such as diisobutyl phthalate (DIBP) or diethylhexyl phthalate (DEHP) among others, are banned for contents above 0.1 wt.% [24]. Among other alternatives, poly(ethylene glycol) (PEG), polyethylene oxide (PEO), and adipates are widely studied in a PLA matrix, obtaining an excellent improvement of ductile properties [25–27]. However, petrochemical-based plasticizers are questioned for toxicity and therefore there is a continuous attempt to obtain bio-based plasticizers [28].

Vegetable oils (VOs) are an interesting route to achieve renewable plasticizers for three main reasons: they are widely available, have a low toxicity, and are biodegradable. Two reactive sites are identified in fatty acids of vegetable oils to bring compatibility with a polymer matrix: double bonds and ester groups [29]. To increase this compatibility, vegetable oil can be epoxidized, which consists of introducing epoxy groups (oxirane ring) in double bonds. Several studies reported the use of epoxidized vegetable oils in PLA matrix, thus obtaining a bio-based polymer with high performance as a plasticizer. Some epoxidized oils such as epoxidized linseed oil (ELO) and epoxidized soybean oil (ESBO) are available commercially at competitive prices. Several studies using epoxidized oil with a non-elevated number of oxirane groups have been reported. The study performed by Qiong Xu *et al*. [30] reported an improvement of elongation at break from 3.98 to 6.5% using 9 wt.% of ESBO. Further percentage led to a decrease in ductile properties due to plasticizer saturation. Garcia-Garcia *et al*. [31] found an increment of elongation at break from 7.8 to 15% with 5

wt.% of epoxidized Karanja oil. In respect to impact energy, an evident improvement of 32% was obtained, confirming an effective plasticization. More interesting results were found by Balart *et al.* [32], who reported an increment of 450% of elongation at break with respect to neat PLA employing ELO with 8% of epoxy groups.

Chia seed oil (CO) is a promising VO characterized by its high iodine value (above 190 g I_2/100 g oil) [33], becoming suitable to be epoxidized. Epoxidized chia seed oil has not been previously applied in a polymer matrix and could present an elevated epoxy content, improving the compatibility between PLA.

As different authors have reported that the interaction between PLA and epoxidized chia seed oil (ECO) could occur between the carbonyl group, from ester linkage, present in the PLA main chain and the epoxy group of ECO. This reaction mechanism was proposed by Al-Mulla *et al*. [34]. Although the interaction mechanism is not very strong, the terminal location of the hydroxyl groups in PLA gives them a high availability to react with the epoxy groups [30]. Thus, based on these previous studies, Figure IV.2.1 shows the chemical interaction between PLA and ECO. This new bio-based plasticizer could be an alternative to ELO and ESBO plasticizers. For this reason, the aim of this work is studying the potential of epoxidized chia seed oil as a new bio-based plasticizer for PLA to be used in the packaging sector. Mechanical and thermal properties were tested to evaluate the effect of different percentage of ECO in a PLA matrix. A migration test was evaluated as an important property in the packaging sector. Finally, a disintegration test was carried out to evaluate the effect of ECO in polymer degradation.

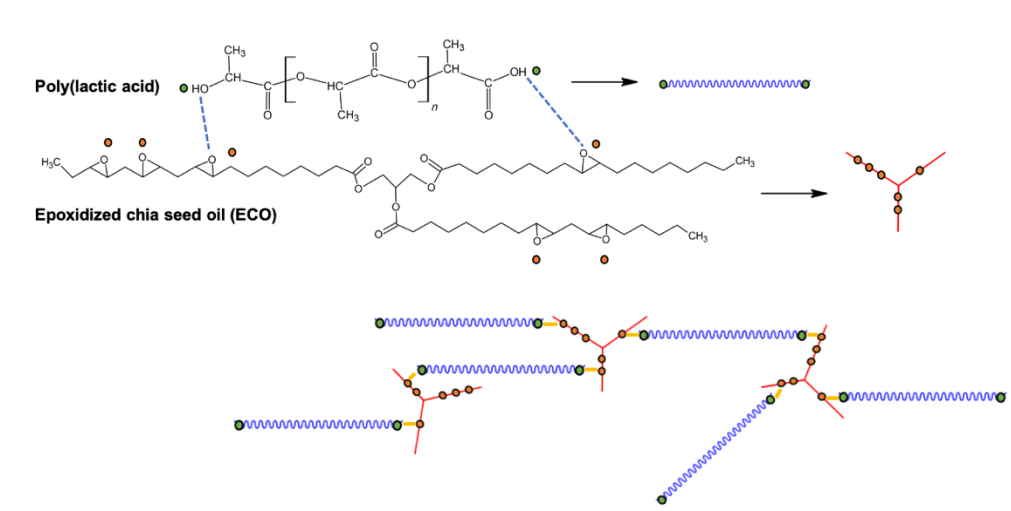

Figure IV.2.1. Schematic representation of chemical interactions between PLA and ECO.

Experimental

Materials

Poly(lactic acid) (PLA) with a commercial grade 2003D was supplied by NatureWorks LLC (Minnetonka, MN, USA). Its density was 1.24 g cm^{-3}, with an approximate molecular weight of 120,000 g mol^{-1}. The base of the plasticizer was chia oil extracted through cold pressing extraction using a CZR-309 press machine (Changyouxin Trading Co., Zhucheng, China) from edible chia seed (*Salvia hispanica, L.*) supplied by Frutoseco (Bigastro, Alicante, Spain). The oil was characterized by a density of 0.928 g cm^{-3} at 25 °C and iodine value of 197. Epoxidation process was carried out in situ with hydrogen peroxide (30% *v/v*), acetic acid (99.7%), and sulfuric acid (97%) supplied by Sigma Aldrich (Sigma Aldrich, Madrid, Spain). Epoxidized chia seed oil (ECO) presented an epoxy content of 6.71%, equivalent to 238 EEW (Equivalent Epoxy Weight). This value was obtained following the guidelines of the ASTM D1652–97. ECO presented an iodine value of 25 and density of 1.026 g cm^{-3} at 25 °C, which made it suitable to be used as plasticizer.

In the first stage, PLA pellets were dried at 60 °C for 24 h to remove moisture. After this, PLA pellets and ECO were weighed according to the compositions indicated in Table IV.2.1. Percentages of ECO were selected, taking into account published articles that consider that more than 10% of oil shows signs of plasticizer

saturation [35–37]. All the five compositions selected were extruded at constant speed (40 rpm) using a twin-screw co-rotating extruder from DUPRA S.L (Castalla, Alicante, Spain) with the following temperature profiles: 162.5 (feeding zone), 165, 170, and 175 °C (die). After extrusion, samples were air-cooled to room temperature, pelletized, and dried again at 60 °C for 24 h for further processing by injection. Each composition was shaped by injected molding using a Meteor 270/75 from Mateu & Solé (Barcelona, Spain) at temperature profiles of 170, 180, 190, and 200 °C from feed section to injection nozzle. Cavity filling time was 1 s and the cooling time was set to 10 s.

Table IV.2.1. Composition of ECO plasticized PLA materials and labelling.

Reference	Parts by weight (wt.%)	
	PLA	**ECO**
PLA	100	0
PLA_2.5%ECO	97.5	2.5
PLA_5%ECO	95	5
PLA_7.5%ECO	92.5	7.5
PLA_10%ECO	90	10

Mechanical and Thermal Characterization

The effect of ECO on mechanical properties was studied using standard tensile, impact test, and hardness. Tensile properties were obtained in a universal test machine ELIB 30 from S.A.E Ibertest (Madrid, Spain). Five different samples were tested using 5 kN load cell and a crosshead speed of 10 mm min^{-1} according to ISO 527. Furthermore, an axial extensometer from S.A.E Ibertest (Madrid, Spain) was used to obtain tensile modulus with high accuracy. The impact strength was tested in a 1 J Charpy pendulum from Metrotec S.A. (San Sebastián, Gipuzkoa, Spain), as is indicated in ISO 179. Shore D hardness was carried out following the guidelines of the ISO 868 using a durometer 673-D from J. Bot S.A (Barcelona, Spain). In both tests, a minimum of 5 samples were used and the results shown are the obtained average.

Thermomechanical properties were assessed by using standard Vicat softening temperature (VST) by using a load of 5 kg and a heating rate of 50 °C $\cdot h^{-1}$ according to ISO 306. Moreover, heat deflection temperature (HDT) was obtained following the

guidelines of ISO 75 with a load of 296 g and a heating rate of 120 °C·h^{-1}. Both values were obtained in a Vicat-HDT station mod. DEFLEX 687-A2 from Metrotec S.A. (San Sebastián, Gipuzkoa, Spain). At least five different specimens for each composition were tested and average values were calculated.

Additionally, storage modulus (G') and damping factor (tan δ) were evaluated in torsion mode by dynamic mechanical thermal analysis (DMTA) in an oscillatory rheometer AR-G2 from TA instrument (New Castle, Delaware, USA). Shaped samples (4 × 10 × 40 mm^3) were evaluated with a dynamic program from 30 to 110 °C using a heating rate of 2 °C·min^{-1}. The maximum deformation was set to 0.1% with a constant frequency of 1 Hz.

Thermal transitions of PLA plasticized with different contents of ECO were obtained by differential scanning calorimetry (DSC) in a DSC mod. 821 from Mettler-Toledo Inc. (Schwerzenbach, Switzerland). Samples with an average weight of 6–8 mg were subjected to the following temperature program: 1st heating program from 25 to 300 °C at 10 °C·min^{-1} to remove thermal history, 2nd cooling program from 300 to 25 °C at 10 °C·min^{-1}, and 3rd heating program from 25 to 300 °C at 10 °C·min^{-1}. All thermal cycles were performed in a nitrogen atmosphere with a flow rate of 66 mL·min^{-1}. The percentage of crystallinity of different PLA formulations with ECO was determined by Equation IV.2.1:

$$X_c\ (\%) = \left[\frac{\Delta H_m - \Delta H_{cc}}{\Delta H_{m(100\%)}}\right] \cdot \frac{1}{w_{sample}} \times 100 \qquad \textbf{Equation IV.2.1}$$

where ΔH_{cc} and ΔH_m represent cold crystallization and melting enthalpies (J·g^{-1}), respectively. The weight amount of PLA is represented by w_{sample} (g). Theoretical melting of PLA 100% crystalline ($\Delta H_{m(100\%)}$) was 93 J·g^{-1}, as is reported [10].

Thermogravimetric analysis was carried out in a TGA/SDTA 851 thermobalance from Mettler-Toledo Inc (Schwerzenbach, Switzerland). A heating ramp from 30 to 700 °C at constant heating rate of 10 °C·min^{-1} and constant flow rate of nitrogen (66 mL·min^{-1}) were set to evaluate samples with average weight of 10 mg.

The temperature when a 5% weight loss has been reached and the maximum degradation were obtained in order to evaluate thermal stability of the different samples of PLA plasticized with ECO.

Morphology Characterization

Fractured surface from impact test was observed by field emission scanning electron microscopy (FESEM) model ZEISS ULTRA 55 from Oxford Instruments (Oxfordshire, UK). Previously fractured surfaces were coated with a thin metallic layer (Au-Pd alloy) employing a sputter coater EM MED020 from Leica Microsystems (Wetzlar, Germany) to avoid electrical charging. All samples were observed using an acceleration voltage of 2 kV.

Disintegration Under Composting Conditions

Disintegration test was conducted in aerobic conditions according to ISO 20200 at temperature of 58 °C and a relative humidity of 55% using a synthetic compost reactor (300 × 200 × 100 mm^3). Sample sizing of 25 × 25 × 1 mm^3 were placed in a carrier bag and buried in controlled soil. Previously, all films manufactured with neat and plasticized PLA with ECO were dried at 40 °C over 24 h. Seven different samples of each formulation were employed for the disintegration process under composting conditions. Each control day (3, 7, 14, 17, 21, 24, and 28 days), a different sample of each formulation was unburied while the rest remained in the process. The removed samples were washed with distilled water and dried 24 h before to be weighed in an analytical balance. All tests were carried out in triplicate to ensure reliability. Average disintegration percentage of extracted samples was calculated using Equation IV.2.2.

$$W_l\ (\%) = \frac{w_0 - w}{w_0} \cdot 100 \qquad \textbf{Equation IV.2.2}$$

where w_0 is referred to initial dry weight of the sample and w is the weight of the sample extracted from compost soil on different days after drying. Furthermore, optical images were taken to record the progression of disintegration along time.

Migration of Plasticizer by Solvent Extraction Test

Migration test was studied by solvent extraction using n-hexane solvent as is indicated by several reports [36,38,39]. Samples of PLA and PLA plasticized with ECO were immersed in n-hexane solvent at different temperatures (30, 40, 50, and 60 °C) over 8 h in an air circulating oven mod. Selecta 2001245 by JP Selecta S.A. (Barcelona, Spain). Before and after experiments, all samples were dried at 40 °C for 24 h to ensure the absence of solvent. The weight loss of plasticizer (WL_p) obtained by migration test was calculated using Equation IV.2.3.

$$WL_p\ (\%) = \frac{w_b - w_a}{w_b} \cdot 100 \qquad \textbf{Equation IV.2.3}$$

where w_b is the weight of samples before experiment and w_a is the weight after migration test.

Results and discussion

Effect of ECO in PLA on the Mechanical Properties

One of the main disadvantages of PLA is its low ductile property, which gives it a characteristic brittleness. As is shown in Figure IV.2.2., neat PLA used in the present study reaches an elongation at break of 8% and a tensile strength higher than 45 Mpa. The resulting tensile modulus was higher than 3100 Mpa, as plotted in Figure IV.2.3. The plasticization effect was clearly observed in the different formulations of PLA with ECO. For example, the addition of 2.5 wt.% of ECO (PLA_2.5%ECO) provided higher ductile properties, with an elongation at break around 18%. Consequently, mechanical properties like tensile strength and tensile modulus slightly decreased (40.9 and 3040 Mpa, respectively), which was attributed to the elastomeric and toughening effect of ECO plasticizer. In Figure IV.2.2, it was possible to observe how the slope of the stress–strain curve became lower as the ECO content in the samples increased. This decrease resulted in a lower tensile modulus. At the same time, the elongation at break increased notably, reaching values of 64.5% for

samples with 10 wt. % of ECO. As a consequence of this variation in mechanical and ductile properties, the toughness of the samples was clearly improved. This increase represents a 700% rise compared to neat PLA. Therefore, the presence of epoxy groups in ECO interacts with hydroxyl groups present in PLA, decreasing intermolecular forces and, consequently, increasing its ductile properties [30]. These results are in accordance with previous studies on the use of epoxidized vegetable oils like PLA plasticizer. Yu-Qiong *et al.* [30] reported an increase of 123% employing epoxidized palm oil. This lower increase in elongation values was due to the lower content of epoxy groups in palm oil (3.23%) with respect to chia oil (6.71%), which is one of the main parameters to be taken into account. For example, other authors have reported similar increases of 700% or even higher using epoxidized vegetable oils with content of epoxy groups around 5.8% [36,40,41]. Thus, stronger interactions occurred as epoxy content increased due to the increased presence of reactive groups Therefore, in view of the results obtained, it seems that once epoxy group values of 5.8% or higher were reached, a saturation effect was shown, not reaching further increases in the elongation at break. Where the use of ECO with PLA appeared to have a direct effect was on the attenuating effect of the sharp drop in mechanical properties. For example, Chieng *et al.* [35] reported that using palm oil in 10 wt.% proportion reduces the tensile strength of the neat PLA by almost 50%. However, this decrease was only 21% when ECO was employed. Therefore, the higher oxirane oxygen content in ECO than, for example in palm oil, can interact more strongly with PLA chains leading to intense polymer-plasticizer interactions allowing to maintain mechanical and ductile balanced properties. As a consequence of these interactions between PLA and ECO, it was remarkable that samples with 7.5 and 10 wt.% ECO content provided constant values in tensile mechanical properties. On the other hand, this attenuation of decrease in mechanical properties also suggested, as other cited authors have pointed out, that a percentage higher than 10 wt.% produces a negative effect on ductile properties due to the excess of plasticizer and a possible phase separation. Some authors like Sanyang *et al.* [42] and Rizzuto *et al.* [43] remarked that once all free volume is full of plasticizer, a decrease of elongation at break occurs due to free volume reduction. Similar results were reported by Emad *et al.* [44], who observed a decrease of elongation at break above of 9 wt.% of epoxidized palm oil. Therefore,

PLA_10%ECO obtained the highest elongation at break (64.3%), together with a reduction of 6.7% in tensile modulus (2893 Mpa) and 21% in tensile strength (33.4 Mpa) in respect to initial value (PLA neat).

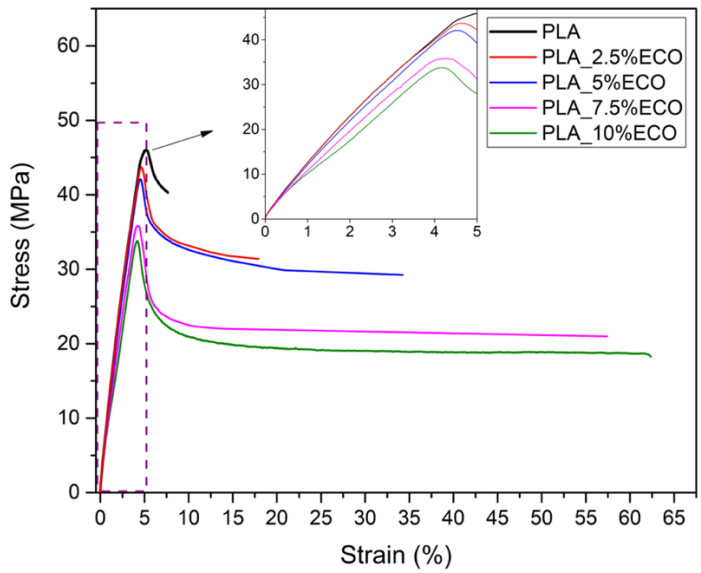

Figure IV.2.2. Plot evolution of characteristic stress-strain curves of PLA with different epoxidized chia seed oil (ECO) contents.

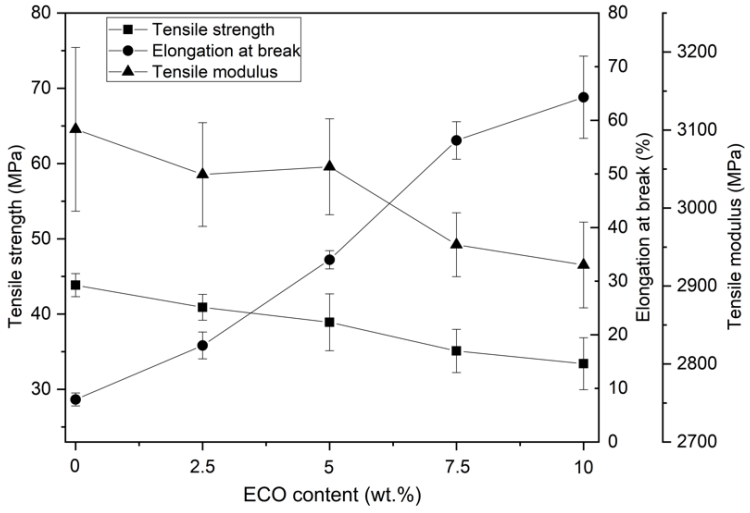

Figure IV.2.3. Plot evolution of tensile mechanical properties of PLA with different epoxidized chia seed oil (ECO) contents.

Other techniques that provide substantial information about the plasticizing effect of ECO on PLA are the Charpy impact test and Shore D hardness. As shown previously, the addition of ECO provides a plasticizing effect. As a result, tensile

strength and tensile modulus decrease slightly with increment of ECO, contrary to the elongation at break. Impact absorbed energy is a parameter related to the ductile properties and toughness. Therefore, as expected initially, PLA is a brittle polymer, which has a low impact absorption capacity (37.1 J·m^{-2}), but adding ECO improves absorbed impact energy due to elastomeric and toughing effect (Figure IV.2.4.). It is possible to observe how an increase from 2.5 to 10 wt.% of ECO provides a gradual gain in impact absorption capacity. Sample ECO_10%ECO obtained the highest value (68.3 J·m^{-2}), which represented an increase of 85% with respect to non-plasticized PLA. These results were in concordance with Carbonell-Verdu *et al.* [45], who evaluated the plasticization effect on PLA using a 7.5 wt.% of epoxidized cottonseed oil, obtaining an increase on the impact of absorbed energy of 18%. Again, the greater content of epoxy groups in ECO (6.7%) compared to cottonseed oil (5.8%), provided higher ductile properties. On the other hand, the plasticizing effect of ECO inversely affected the hardness of the samples. As the ECO content increased, the hardness decreased. However, in the same way that the tensile strength analysis showed a stabilization in the decrease of the properties of ECO_7.5%ECO and ECO_10%ECO samples, the difference between the hardness of neat PLA and ECO_10%ECO sample was only less than 6%.

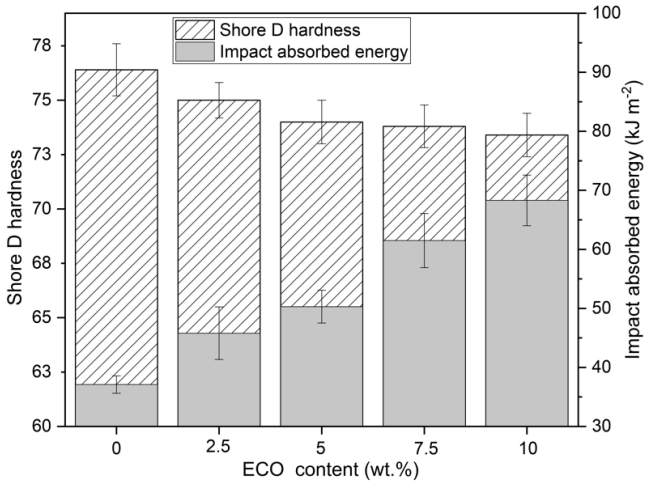

Figure IV.2.4. Plot evolution of Shore D hardness and impact absorbed energy of PLA with different epoxidized chia seed oil (ECO) content.

Regarding the morphological changes produced by the incorporation of ECO to PLA, Figure IV.2.5a showed a brittle morphology with smooth surface and very

low plastic deformation characteristic of neat PLA. With increasing ECO content, remarkable changes can be observed. Figure IV.2.5b, which represents PLA_2.5%ECO, showed a slight change in surface roughness. PLA_5%ECO, Figure IV.2.5c, shows a rougher surface as well as presence of filaments thus indicating an increase in ductility as a consequence of plasticization. So, an increase in roughness and a higher filament density was observed with increasing ECO. However, a higher presence of plasticizer (equal or more than 7.5 wt.%) began to display some spherical voids due to the plasticizer saturation, Figure IV.2.5d,e. A similar finding was reported by Ferri et al [46]., who observed spherical voids above 5 wt.% of maleinized linseed oil as a plasticizer for PLA. Phase separation was produced, and a worse miscibility occurred [31]. Finally, in Figure IV.2.5f, the presence of high density of filaments and voids in sample PLA_10%ECO, indicating a plasticizer saturation, can be observed better (2500×).

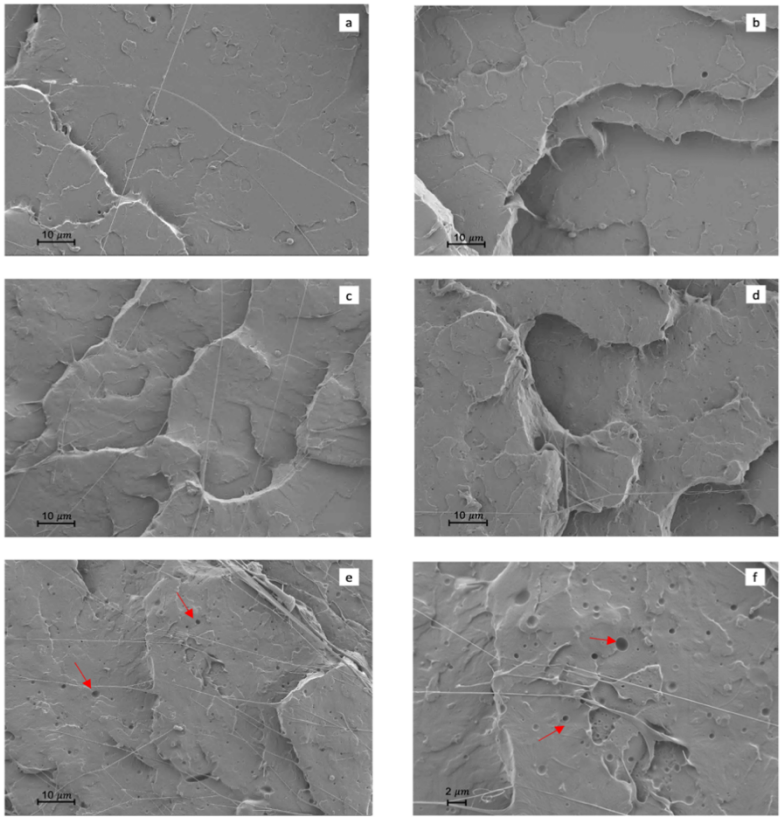

Figure IV.2.5. Fracture surface morphology of Charpy test at 1000x by field emission scanning electron microscopy (FESEM): (a) neat PLA; (b) PLA_2.5%ECO; (c) PLA_5%ECO; (d) PLA_7.5%ECO; I PLA_10%ECO; and (f) PLA_10%ECO at 2500×.

Effect of ECO in PLA on the Thermomechanical Properties of PLA

Storage modulus (G') and damping factor (tan δ) were assessed by dynamic mechanical response. In Figure IV.2.6, the viscoelastic behavior of PLA_ECO formulations were exposed. Two characteristic changes in the storage modulus could be distinguished. The first change, between 50 and 70 °C, was the drop of storage modulus, which was related to glass transition temperature (T_g) at around 60 °C, as reported by Yong *et al.* [47]. The second change, between 80 and 100 °C, was recognized as the beginning of cold crystallization process. The addition of ECO to PLA resulted in a loss of storage modulus at lower temperatures. This was due to the plasticizing effect that ECO exerts on the PLA matrix, which increases the free volume between PLA chains before a saturation effect, decreasing the interaction between them [48]. In addition, at room temperature, neat PLA showed a storage modulus value of 1300 Mpa, while the plasticized PLA formulations showed a decrease of this modulus up to 1000 Mpa as a consequence of the plasticization effect. On the other hand, the beginning of cold crystallization decreased as ECO content increased, obtaining a shift from 87 up to 84 °C for plasticized PLA. This effect was due to plasticizer enabling the rearrangement in packed structure under lower energetic conditions.

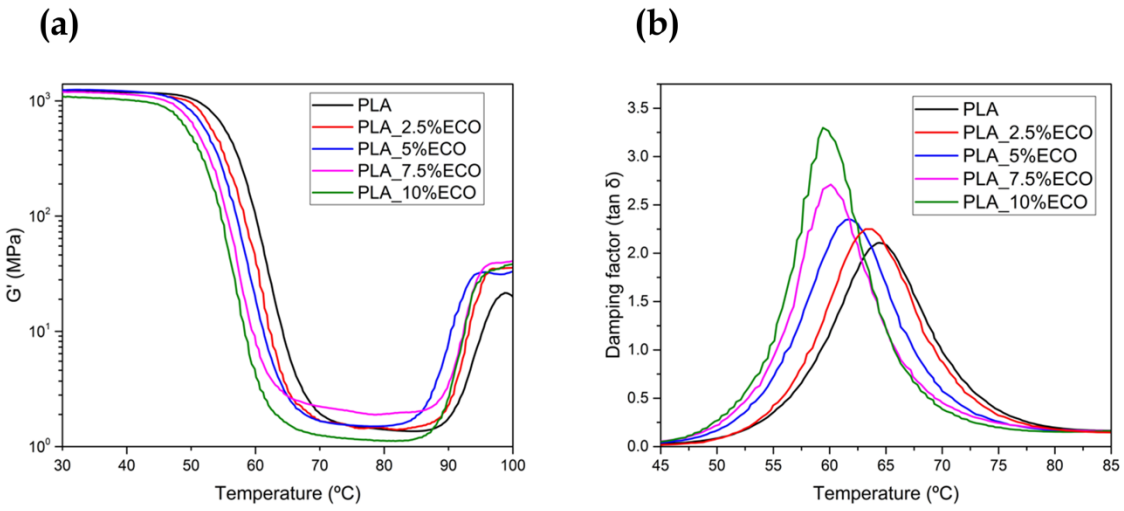

Figure IV.2.6. Plot evolution of dynamic mechanical thermal analysis (DMTA) of PLA with different ECO contents: (a) storage modulus (G'); (b) damping factor (tan δ).

The temperature of the tan δ peak was a great manner to obtain an accurate value of T_g which was moved to lower temperatures as ECO content increased. Specifically, the T_g values were reduced from 64.2 (PLA neat) up to 61.9 and 59.5 °C for PLA_5%ECO and PLA_10%ECO, respectively. Regarding tan delta peak magnitude, it is related to their molecular mobility. As Chieng *et al.* [35] reported, the addition of plasticizer content led to increase the intensity of tan delta due to higher molecular mobility caused by the plasticizing effect. Then, a significant increase in respect to neat PLA in the magnitude of the damping factor was observed with higher ECO content. On the other hand, Silverajah *et al.* [49] observed that increasing the content of epoxidized palm oil plasticizer in PLA led to decrease the temperature of tan δ peak.

Table IV.2.2 shows a summary of values obtained for Vicat softening temperature (VST) and heat deflection temperature (HDT) of neat PLA and PLA plasticized with ECO. These thermomechanical parameters are directly related to mechanical resistant properties. For this reason, the decreasing trend was the same that had been observed previously in tensile strength and modulus. Regarding VST, a remarkable decrease was detected when ECO content increased. Neat PLA had a VST of 56.6 °C, while samples with 7.5 and 10 wt.% ECO, respectively, reduced this value 4.4 °C. A similar trend was observed in HDT values, obtaining a difference of 2.6 °C between neat PLA and PLA_10%ECO sample. The addition of ECO to PLA samples in different percentages facilitated the sliding of the polymeric chains, being also favored by the slight increase in temperature that takes place in the VST and HDT tests. The ECO molecules decreased the intermolecular attraction forces between the PLA and the macromolecules, obtaining the plasticization of the materials [50].

Table IV.2.2. Vicat softening temperature (VST) and heat deflection temperature (HDT) of PLA with different epoxidized chia seed oil (ECO) content.

Reference	VST (°C)	HDT (°C)
PLA	56.6 ± 1.5	52.8 ± 0.5
PLA_2.5%ECO	55 ± 1.2	51.8 ± 0.6
PLA_5%ECO	53.2 ± 1.3	50.4 ± 0.4
PLA_7.5%ECO	52.2 ± 1.1	50.4 ± 0.6
PLA_10%ECO	52.2 ± 1.4	50.2 ± 0.4

Effect of ECO in PLA on the Thermal Properties of PLA.

The addition of ECO led to a change in the main thermal transitions of neat PLA. Neat PLA presented a T_g at 62 °C, cold crystallization temperature (T_{cc}) at 119.4 °C, and melt temperature T_m at 150 °C, as can be seen in Table IV.2.3. As percentage of ECO increased in PLA matrix, a remarkable decrease of T_g values (62 °C from neat PLA up to 56.8 °C for PLA_10%ECO) was observed. It was seen that PLA_7.5%ECO and PLA_10%ECO showed similar T_g values (56.3 and 56.8 °C, respectively), demonstrating the plasticizer saturation effect. Additionally, the T_{cc} values presented a slight decrease with respect to neat PLA, obtaining in all plasticizer formulations lower values than neat PLA. Melt temperature I presented also a slight decrease with the incorporation of ECO, concluding that the presence of plasticizer also affected the melt temperature due to the increase of chain mobility. The same evolution was reported by Garcia-Garcia *et al.* [31], who employed epoxidized Karanja oil in PLA. Addition of ECO allowed to increase the free volume of polymer chains and thus provide better movement at lower temperatures [48]. The changes in the degree of crystallinity (X_c) also indicated the chain motions of PLA. It was clearly observed that X_c of PLA increased with the rise of ECO content, confirming that plasticizer enables the mobility of chains to form stable crystallites at lower energy conditions. Specifically, above 5 wt.% ECO, more evident changes were observed, where the highest crystallinity was found at PLA_10%ECO with 11.5%. This value was almost 67% higher than neat PLA, indicating the enhancement of chain mobility.

Table IV.2.3. Main thermal parameters of PLA plasticized with different ECO contents obtained using DSC.

Reference	T_g (°C)[1]	T_{cc} (°C)[2]	ΔH_{cc} (J g^{-1})[3]	T_m (°C)[4]	ΔH_m (J g^{-1})[5]	X_c (%)[6]
PLA	62.0	119.4	8.00	150.0	15.0	7.5
PLA_2.5%ECO	60.0	117.3	12.5	149.7	19.6	7.9
PLA_5%ECO	59.2	117.7	10.9	149.0	18.4	8.5
PLA_7.5%ECO	56.3	118.0	11.6	148.2	20.3	10.1
PLA_10%ECO	56.8	118.5	8.4	148.4	18.0	11.5

[1] Glass transition temperature; [2] Cold crystallization temperature; [3] Cold crystallization enthalpy; [4] Melt temperature; [5] Melt enthalpy; [6] Degree of crystallization.

Thermogravimetric analysis (TGA) was assessed for PLA formulations with different contents of ECO. Temperature at 5% weight loss ($T_{5\%}$) and temperature at maximum degradation (T_{max}) showed an important increase in thermal stabilization. CO presented higher thermal stability at elevated temperatures than neat PLA, obtaining in $T_{5\%}$ around of 320 °C and T_{max} around of 425 °C, as was reported by Timilsena *et al.* [33]. On the other hand, in order to study the influence of the epoxidation process in thermal stability of the vegetable oil, the authors compared an epoxidized linseed oil [51] and virgin linseed oil [52], obtaining very similar results. Linseed oil is characterized by an epoxy content very similar to ECO. For this reason, thermal stability of CO could be considered the same as ECO. Thus, as can be seen in Figure IV.2.7a, higher contents of ECO provided an improvement of thermal stabilization with respect to neat PLA. Regarding weight loss derivate (Figure IV.2.7b), it was observed that samples up to 5 wt. % ECO showed an increase of $T_{5\%}$, while higher contents caused a decrease, possibly due to the first evidence of plasticizer saturation [31]. On the other hand, T_{max} of neat PLA was 390.4 °C and increased up to 404.9 °C for PLA formulations with a 2.5–5% ECO, showing a slight decrease when the saturation effect was beginning. Typical plasticizers employed in PLA as citrate esters or ATBC reduce thermal stability of PLA when their content increases [53,54]. However, in this report, different trends were observed in $T_{5\%}$ and T_{max}. Addition of ECO produced an evident delay of degradation temperature, as was reported by Garcia-Garcia *et al*. [20], who used epoxidized oils as plasticizers. The reason for this behavior was due to the presence of epoxy groups of ECO that allowed the scavenging of acid groups, obtaining a better thermal stabilization [55].

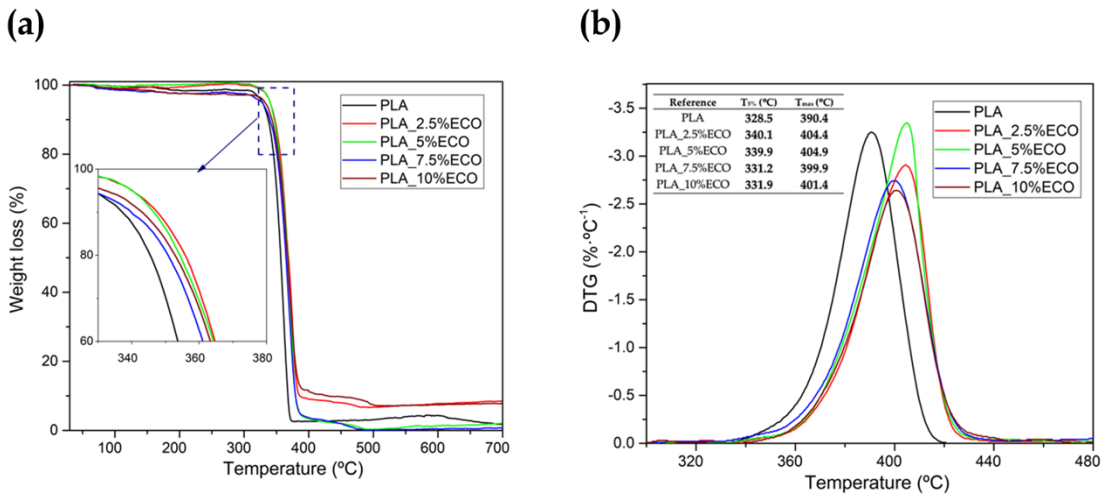

Figure IV.2.7. Thermal parameters of degradation of PLA with different epoxidized chia seed oil (ECO) contents. (a) Weight loss; (b) derivative thermogravimetry. T_5% is temperature at 5% weight loss; T_{max} is temperature at maximum degradation.

Disintegration Under Composting Conditions

Disintegration process under compost soil of neat and plasticized PLA is shown in both Figure IV.2.8 and Figure IV.2.9, in which the visual appearance and the weight loss in respect to the initial mass, respectively, are plotted. After 3 days of incubation, film samples changed their visual appearance from translucid to opaque due to increased crystallinity and possible water absorption. It is important to remark that this experiment was conducted at thermophile conditions, with constant temperature of 58 °C and 50% relative humidity. The proximity to the T_g, as was studied by DSC, can induce an increment of chain mobility and thus the crystallization that causes the increasing opacity [31]. After 7 days buried in controlled compost soil, neat PLA and the sample with less amount of ECO, started the embrittlement process and slight weight loss, as plotted in Figure IV.2.9. However, samples with higher amounts of ECO did not show any signs of disintegration. After 14 days buried, visual changes and weight loss were evident in all samples. Neat PLA disintegrates faster than plasticized PLA with ECO. Neat PLA obtained the highest weight loss with 60.2%, while PLA_10%ECO lost 35% of its initial weight. Above 21 days buried in controlled conditions, samples showed a physical inconsistency and disintegration. According to ISO 20200, a disintegrable material was considered when the degree of disintegration achieved 90%. Neat PLA and samples with 2.5 and 5 wt.% of ECO

achieved more than 90% of weight loss in respect to their initial value. However, samples with 7.5 and 10 wt. % needed 3 more days to reach this value, indicating a delay of the disintegration process provided by an increasing amount of ECO. These results are in concordance with Balart *et al.* [56], who observed a reduction of disintegration capacity by increasing the epoxidized linseed oil content in PLA matrix. This delay was directly related with the fact that samples plasticized with ECO possess a higher degree of crystallinity as reported in Table IV.2.3. Biodegradability is usually done by lipases, proteases, and esterase secreted from microorganism in the soil compost [57] and this microorganism acts faster in amorphous domains [58,59]. Thus, addition of ECO leads to a delay in the disintegrations process but, in general terms, PLA films developed with ECO can be considered as biodegradable according to ISO 20200.

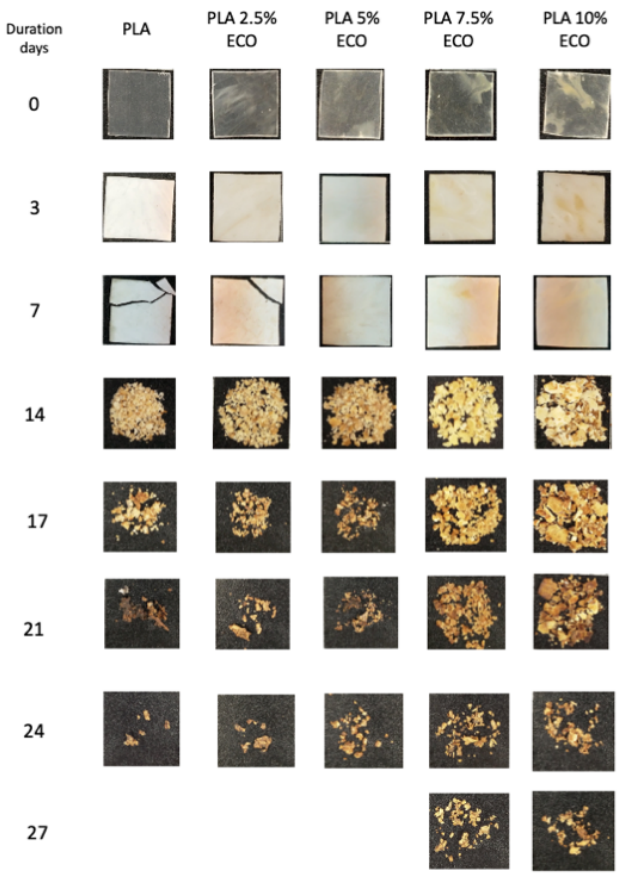

Figure IV.2.8. Visual appearance of disintegration under composting conditions.

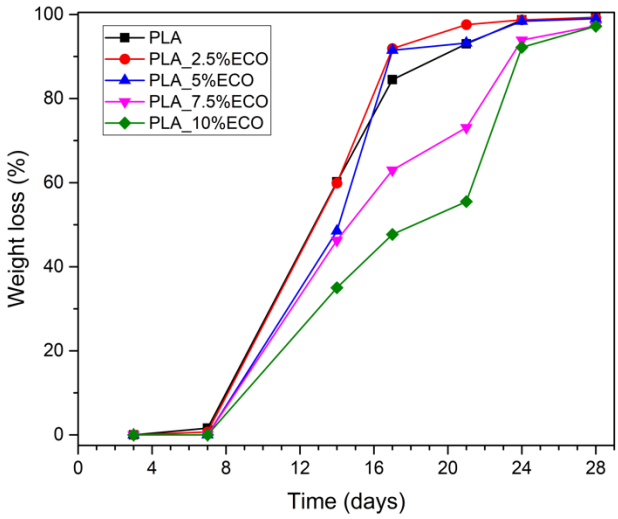

Figure IV.2.9. Weight loss recorded during disintegration test.

Migration of ECO by Solvent Extraction Test

PLA is considered a safe polymer for food contact applications [60]. For this reason, the development of a new plasticizer, as ECO, needs to be studied due to plasticizer migration being an important drawback [61,62]. Plasticizer migration is defined as the capacity of transferring plasticizer molecules from the surface of the matrix to the contact medium [63] and the assay developed by solvent extraction is a quite aggressive test to provide information about the potential use at industrial scale. In Figure IV.2.10, the percentage of migration of plasticizer from PLA matrix using *n*-hexane as dissolvent at different temperatures is plotted. Neat PLA, taken as control sample, presented a similar value below 0.02% between 30 and 60 °C due to absence of plasticizer. Regarding plasticized PLA with ECO, an increment of percentage of migration is appreciated as temperature increases achieving a highest migration of 0.108% with PLA_7.5%ECO and PLA_10%ECO at 60 °C. These results were lower than those reported by Carbonell-Verdu *et al.* [45], who employed epoxidized cottonseed oil, obtaining values up to 0.12%. A higher content of epoxy groups in ECO provided stronger interactions with the hydroxyl groups of PLA matrix and, as a consequence, lower migration levels in respect to other plasticizers with less reactive groups, indicating a correct functionality to be employed at an industrial scale. On the other hand, the high molecular weight characterizing the vegetable oils (around 900 g mol^{-1}) could be another positive effect to minimize the migration level, compared

with industrial plasticizers with lower molecular weight, as for example tributyl citrate plasticizers (350–400 g·mol^{-1}) [48].

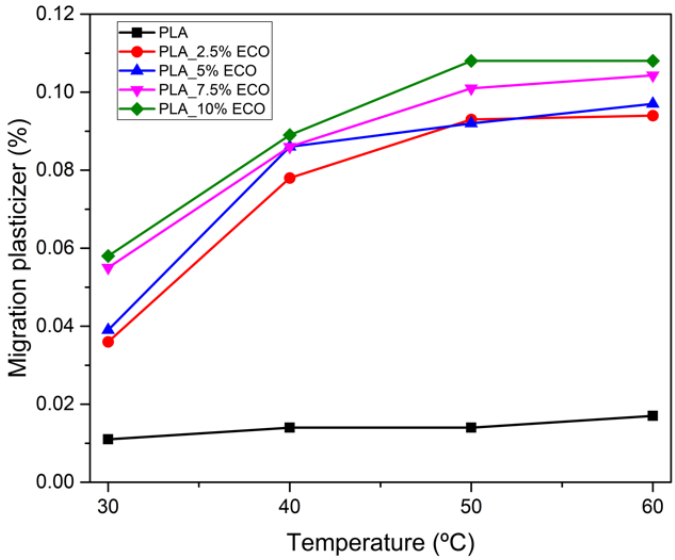

Figure IV.2.10. Migration of epoxidized chia seed oil (ECO) plasticizer in PLA matrix by n-hexane solvent extraction.

Conclusions

Epoxidized chia seed oil (ECO) was applied in a PLA matrix to evaluate its effect as a new bio-based plasticizer. The low elongation at break of neat PLA (8%) was improved up to values of 64.5% using 10 wt.% ECO, obtaining an improvement of 700%. Morphological images showed spherical voids at equal or higher percentage of 7.5 wt.% ECO in PLA matrix, indicating the beginning of plasticizer saturation. With regard to absorbed impact energy, an almost twice as high value was obtained with 10 wt.% ECO in respect to neat PLA, and, as a consequence, a decrease of hardness. Then, ECO led to enhanced chain mobility of PLA, which induced an increase in free volume and a reduction in intermolecular forces. This lubrication of chains also led to reduce the glass temperature around 4.7 °C with 7.5–10 wt.% ECO and slightly the cold crystallization temperature. Thermal stability was highly improved up to 14.0 °C in respect to neat PLA. The disintegration ability of PLA up to 5 wt.% ECO content was not affected, meanwhile at 7.5–10 wt.%, it was slightly delayed, being considered, in general terms, biodegradable formulations. Finally, very low migration of plasticizer was detected in migration test by using *n*-hexane. The

maximum migration recorded was 0.108% with 10 wt.% ECO at 60 °C, while lower migration was obtained (<0.06%) at 30 °C. Therefore, ECO is a promising bio-based plasticizer with potential to be applied in the packaging industry.

Acknowledgements

D-C wants to thank Universitat Politècnica de València for his FPI grant (PAID-2019-SP20190013) and Generalitat Valenciana (GVA) for his FPI grant (ACIF/2020/233). J.M. F. thanks the postdoc contract (APOSTD/2019/122) Generalitat Valenciana (2019-2021).

References

[1] Europe, P. Plastics—The Facts An analysis of European plastics production, demand and waste. Plastics Europe, Brussels https://www.plasticseurope.org/download_file/force/4261/181. Accessed, 2021.

[2] Muthuraj, R.; Misra, M.; Mohanty, A.K. Biodegradable compatibilized polymer blends for packaging applications: A litera-ture review. J. Appl. Polym. Sci. 2018, 135, 45726, doi:10.1002/app.45726.

[3] Yonkos, L.T.; Friedel, E.A.; Perez-Reyes, A.C.; Ghosal, S.; Arthur, C.D. Microplastics in Four Estuarine Rivers in the Chesa-peake Bay, U.S.A. Environ. Sci. Technol. 2014, 48, 14195–14202, doi:10.1021/es5036317.

[4] Song, Y.K.; Hong, S.H.; Jang, M.; Han, G.M.; Rani, M.; Lee, J.; Shim, W.J. A comparison of microscopic and spectroscopic iden-tification methods for analysis of microplastics in environmental samples. Mar. Pollut. Bull. 2015, 93, 202–209, doi:10.1016/j.marpolbul.2015.01.015.

[5] Râpă, M.; Miteluț, A.C.; Tănase, E.E.; Grosu, E.; Popescu, P.; Popa, M.E.; Rosnes, J.T.; Sivertsvik, M.; Darie-Niță, R.N.; Vasile, C. Influence of chitosan on mechanical, thermal, barrier and antimicrobial properties of PLA-biocomposites for food packaging. Compos. Part. B Eng. 2016, 102, 112–121, doi:10.1016/j.compositesb.2016.07.016.

[6] Muller, J.; González-Martínez, C.; Chiralt, A. Combination of poly (lactic) acid and starch for biodegradable food packaging. Materials 2017, 10, 952.

[7] Ivonkovic, A.; Zeljko, K.; Talic, S.; Lasic, M. Biodegradable packaging in the food industry. J. Food Saf. Food Qual. 2017, 68, 26–38.

[8] Musioł, M.; Sikorska, W.; Adamus, G.; Janeczek, H.; Kowalczuk, M.; Rydz, J. (Bio)degradable polymers as a potential mate-rial for food packaging: Studies on the (bio)degradation process of PLA/(R,S)-PHB rigid foils under industrial composting conditions. Eur. Food Res. Technol. 2016, 242, 815–823, doi:10.1007/s00217-015-2611-y.

[9] Murariu, M.; Dubois, P. PLA composites: From production to properties. Adv. Drug Deliv. Rev. 2016, 107, 17–46, doi:10.1016/j.addr.2016.04.003.

[10] Vink, E.T.; Rábago, K.R.; Glassner, D.A.; Gruber, P.R. Applications of life cycle assessment to NatureWorks™ polylactide (PLA) production. Polym. Degrad. Stab. 2003, 80, 403–419, doi:10.1016/s0141-3910(02)00372-5.

[11] Gross, R.A.; Kalra, B. Biodegradable polymers for the environment. Science 2002, 297, 803–807.

[12] Castro-Aguirre, E.; Iñiguez-Franco, F.; Samsudin, H.; Fang, X.; Auras, R. Poly(lactic acid)—Mass production, processing, industrial applications, and end of life. Adv. Drug Deliv. Rev. 2016, 107, 333–366, doi:10.1016/j.addr.2016.03.010.

[13] Leja, K.; Lewandowicz, G. Polymer biodegradation and biodegradable polymers-A review. Pol. J. Environ. Stud. 2010, 19, 255–266.

[14] Malathi, A.; Santhosh, K.; Nidoni, U. Recent trends of biodegradable polymer: Biodegradable films for food packaging and application of nanotechnology in biodegradable food packaging. Curr. Trends Technol. Sci. 2014, 3, 73–79.

[15] Rasal, R.M.; Janorkar, A.V.; Hirt, D.E. Poly (lactic acid) modifications. Prog. Polym. Sci. 2010, 35, 338–356.

[16] Farah, S.; Anderson, D.G.; Langer, R. Physical and mechanical properties of PLA, and their functions in widespread applica-tions—A comprehensive review. Adv. Drug Deliv. Rev. 2016, 107, 367–392, doi:10.1016/j.addr.2016.06.012.

[17] Shayan, M.; Azizi, H.; Ghasemi, I.; Karrabi, M. Influence of modified starch and nanoclay particles on crystallization and thermal degradation prop-erties of cross-linked poly (lactic acid). J. Polym. Res. 2019, 26, 1–12.

[18] Lemmouchi, Y.; Murariu, M.; Dos Santos, A.M.; Amass, A.J.; Schacht, E.; Dubois, P. Plasticization of poly(lactide) with blends of tributyl citrate and low molecular weight poly(d,l-lactide)-b-poly(ethylene glycol) copolymers. Eur. Polym. J. 2009, 45, 2839–2848, doi:10.1016/j.eurpolymj.2009.07.006.

[19] Kowalczyk, M.; Pluta, M.; Piorkowska, E.; Krasnikova, N. Plasticization of polylactide with block copolymers of ethylene glycol and propylene glycol. J. Appl. Polym. Sci. 2012, 125, 4292–4301, doi:10.1002/app.36563.

[20] Garcia-Garcia, D.; Fenollar, O.; Fombuena, V.; Lopez-Martinez, J.; Balart, R. Improvement of Mechanical Ductile Properties of Poly(3-hydroxybutyrate) by Using Vegetable Oil Derivatives. Macromol. Mater. Eng. 2017, 302, 1600330, doi:10.1002/mame.201600330.

[21] Yang, J.; Li, Y.; Wang, Y.; Ruan, J.; Zhang, J.; Sun, C. Recent advances in analysis of phthalate esters in foods. Trac Trends Anal. Chem. 2015, 72, 10–26, doi:10.1016/j.trac.2015.03.018.

[22] Khosravi, K.; Price, G.W. Determination of phthalates in soils and biosolids using accelerated solvent extraction coupled with SPE cleanup and GC–MS quantification. Microchem. J. 2015, 121, 205–212, doi:10.1016/j.microc.2015.03.013.

[23] Liu, X.; Sun, Z.; Chen, G.; Zhang, W.; Cai, Y.; Kong, R.; Wang, X.; Suo, Y.; You, J. Determination of phthalate esters in environ-mental water by magnetic Zeolitic Imidazolate Framework-8 solid-phase extraction coupled with high-performance liquid chromatography. J. Chromatogr. A 2015, 1409, 46–52, doi:10.1016/j.chroma.2015.07.068.

[24] Stevens, M. Polymer Chemistry: An Introduction; Oxford University Press: New York, NY, USA, 1999.

[25] Chieng, B.W.; Ibrahim, N.A.; Yunus, W.M.Z.W.; Hussein, M.Z. Plasticized poly(lactic acid) with low molecular weight poly(ethylene glycol): Mechanical, thermal, and morphology properties. J. Appl. Polym. Sci. 2013, 130, 4576–4580, doi:10.1002/app.39742.

[26] Tsou, C.-H.; Gao, C.; De Guzman, M.; Wu, D.-Y.; Hung, W.-S.; Yuan, L.; Suen, M.-C.; Yeh, J.-T. Preparation and characterization of poly(lactic acid) with adipate ester added as a plasticizer. Polym. Polym. Compos. 2018, 26, 446–453, doi:10.1177/0967391118809210.

[27] Shirai, M.; Grossmann, M.; Mali, S.; Yamashita, F.; Garcia, P.; Müller, C. Development of biodegradable flexible films of starch and poly(lactic acid) plasticized with adipate or citrate esters. Carbohydr. Polym. 2013, 92, 19–22, doi:10.1016/j.carbpol.2012.09.038.

[28] Bocqué, M.; Voirin, C.; Lapinte, V.; Caillol, S.; Robin, J.-J. Petro-based and bio-based plasticizers: Chemical structures to plas-ticizing properties. J. Polym. Sci. Part. A: Polym. Chem. 2016, 54, 11–33, doi:10.1002/pola.27917.

[29] Vieira, M.G.A.; da Silva, M.A.; dos Santos, L.O.; Beppu, M.M. Natural-based plasticizers and biopolymer films: A review. Eur. Polym. J. 2011, 47, 254–263, doi:10.1016/j.eurpolymj.2010.12.011.

[30] Xu, Y.-Q.; Qu, J.-P. Mechanical and rheological properties of epoxidized soybean oil plasticized poly(lactic acid). J. Appl. Polym. Sci. 2009, 112, 3185–3191, doi:10.1002/app.29797.

[31] Garcia-Garcia, D.; Carbonell-Verdu, A.; Arrieta, M.; López-Martínez, J.; Samper, M. Improvement of PLA film ductility by plasticization with epoxidized karanja oil. Polym. Degrad. Stab. 2020, 179, 109259, doi:10.1016/j.polymdegradstab.2020.109259.

[32] Balart, J.; Fombuena, V.; Fenollar, O.; Boronat, T.; Sánchez-Nacher, L. Processing and characterization of high environmental efficiency composites based on PLA and hazelnut shell flour (HSF) with biobased plasticizers derived from epoxidized lin-seed oil (ELO). Compos. Part. B: Eng. 2016, 86, 168–177, doi:10.1016/j.compositesb.2015.09.063.

[33] Timilsena, Y.P.; Vongsvivut, J.; Adhikari, R.; Adhikari, B. Physicochemical and thermal characteristics of Australian chia seed oil. Food Chem. 2017, 228, 394–402, doi:10.1016/j.foodchem.2017.02.021.

[34] Al-Mulla, E.A.J.; Yunus, W.M.Z.W.; Ibrahim, N.A.B.; Rahman, M.Z. A. Properties of epoxidized palm oil plasticized polytlac-tic acid. J. Mater. Sci. 2010, 45, 1942–1946.

[35] Chieng, B.W.; Ibrahim, N.A.; Then, Y.Y.; Loo, Y.Y. Epoxidized Vegetable Oils Plasticized Poly(lactic acid) Biocomposites: Mechanical, Thermal and Morphology Properties. Molecules 2014, 19, 16024–16038, doi:10.3390/molecules191016024.

[36] Carbonell-Verdu, A.; Samper, M.D.; Garcia-Garcia, D.; Sanchez-Nacher, L.; Balart, R. Plasticization effect of epoxidized cottonseed oil (ECSO) on poly(lactic acid). Ind. Crop. Prod. 2017, 104, 278–286, doi:10.1016/j.indcrop.2017.04.050.

[37] Garcia-Garcia, D.; Ferri, J.M.; Montanes, N.; Lopez-Martinez, J.; Balart, R. Plasticization effects of epoxidized vegetable oils on mechanical properties of poly(3-hydroxybutyrate). Polym. Int. 2016, 65, 1157–1164, doi:10.1002/pi.5164.

[38] Fenollar, O.; Sanchez-Nacher, L.; Garcia-Sanoguera, D.; López, J.; Balart, R. The effect of the curing time and temperature on final properties of flexible PVC with an epoxidized fatty acid ester as natural-based plasticizer. J. Mater. Sci. 2009, 44, 3702–3711, doi:10.1007/s10853-009-3495-7.

[39] Carbonell-Verdu, A.; Garcia-Sanoguera, D.; Jordá-Vilaplana, A.; Sanchez-Nacher, L.; Balart, R. A new biobased plasticizer for poly(vinyl chloride) based on epoxidized cottonseed oil. J. Appl. Polym. Sci. 2016, 133; 43642/1–43642/10, doi:10.1002/app.43642.

[40] Thuy, N.T.; Nam, B.X.; Duc, V.M. Study to improve the properties of polylactic acid by epoxidized crude rubber seed oil. Vietnam. J. Chem. 2019, 57, 735–740, doi:10.1002/vjch.2019000111.

[41] Thakur, S.; Cisneros-Lopez, E.O.; Pin, J.-M.; Misra, M.; Mohanty, A.K. Green Toughness Modifier from Downstream Corn Oil in Improving Poly(lactic acid) Performance. Acs Appl. Polym. Mater. 2019, 1, 3396–3406, doi:10.1021/acsapm.9b00832.

[42] Rizzuto, M.; Mugica, A.; Zubitur, M.; Caretti, D.; Müller, A.J. Plasticization and anti-plasticization effects caused by poly(lactide-ran-caprolactone) addition to double crystalline poly(l-lactide)/poly(ε-caprolactone) blends. CrystEngComm 2016, 18, 2014–2023, doi:10.1039/c5ce02559a.

[43] Sanyang, M.L.; Sapuan, S.M.; Jawaid, M.; Ishak, M.R.; Sahari, J. Effect of sugar Palm-derived cellulose reinforcement on the mechanical and water barrier

properties of sugar palm starch biocomposite films. Polymers, 2015, 7; 1106-1124.

[44] Al-Mulla, E.A.J.; Ibrahim, N.A.B.; Shameli, K.; Ahmad, M.B.; Yunus, W.M.Z.W. Effect of epoxidized palm oil on the mechani-cal and morphological properties of a PLA–PCL blend. Res. Chem. Intermed. 2014, 40, 689–698.

[45] Carbonell-Verdu, A.; Boronat, T.; Quiles-Carrillo, L.; Fenollar, O.; Dominici, F.; Torre, L. Valorization of Cotton Industry Byproducts in Green Composites with Polylactide. J. Polym. Environ. 2020, 28, 2039–2053, doi:10.1007/s10924-020-01751-6.

[46] Ferri, J.M.; Garcia-Garcia, D.; Montanes, N.; Fenollar, O.; Balart, R. The effect of maleinized linseed oil as biobased plasticizer in poly(lactic acid)-based formulations. Polym. Int. 2017, 66, 882–891, doi:10.1002/pi.5329.

[47] Yong, A.X.; Sims, G.D.; Gnaniah, S.J.; Ogin, S.L.; Smith, P.A. Heating rate effects on thermal analysis measurement of T g in composite materials. Advanced Manufacturing. Polym. Compos. Sci. 2017, 3, 43–51.

[48] Dobircau, L.; Delpouve, N.; Herbinet, R.; Domenek, S.; Le Pluart, L.; Delbreilh, L.; Ducruet, V.; Dargent, E. Molecular mobility and physical ageing of plasticized poly(lactide). Polym. Eng. Sci. 2015, 55, 858–865, doi:10.1002/pen.23952.

[49] Silverajah, V.S.G.; Ibrahim, N.A.; Yunus, W.M.Z.W.; Abu Hassan, H.; Woei, C.B. A Comparative Study on the Mechanical, Thermal and Morphological Characterization of Poly(lactic acid)/Epoxidized Palm Oil Blend. Int. J. Mol. Sci. 2012, 13, 5878–5898, doi:10.3390/ijms13055878.

[50] Alam, J.; Alam, M.; Raja, M.; Abduljaleel, Z.; Dass, L.A. MWCNTs-Reinforced Epoxidized Linseed Oil Plasticized Polylactic Acid Nanocomposite and Its Electroactive Shape Memory Behaviour. Int. J. Mol. Sci. 2014, 15, 19924–19937, doi:10.3390/ijms151119924.

[51] Jebrane, M.; Cai, S.; Panov, D.; Yang, X.; Terziev, N. Synthesis and characterization of new vinyl acetate grafting onto epox-idized linseed oil in aqueous media. J. Appl. Polym. Sci. 2015, 132, doi:10.1002/app.42089.

[52] Suryanarayana, C.; Rao, K.C.; Kumar, D. Preparation and characterization of microcapsules containing linseed oil and its use in self-healing coatings. Prog. Org. Coat. 2008, 63, 72–78, doi:10.1016/j.porgcoat.2008.04.008.

[53] Arrieta, M.P.; Samper, M.D.; López, J.; Jiménez, A. Combined Effect of Poly(hydroxybutyrate) and Plasticizers on Polylactic acid Properties for Film Intended for Food Packaging. J. Polym. Environ. 2014, 22, 460–470, doi:10.1007/s10924-014-0654-y.

[54] Arrieta, M.; de Dicastillo, C.L.; Garrido, L.; Roa, K.; Galotto, M. Electrospun PVA fibers loaded with antioxidant fillers extracted from Durvillaea antarctica algae and their effect on plasticized PLA bionanocomposites. Eur. Polym. J. 2018, 103, 145–157, doi:10.1016/j.eurpolymj.2018.04.012.

[55] Torres-Giner, S.; Montanes, N.; Fenollar, O.; García-Sanoguera, D.; Balart, R. Development and optimization of renewable vinyl plastisol/wood flour composites exposed to ultraviolet radiation. Mater. Des. 2016, 108, 648–658, doi:10.1016/j.matdes.2016.07.037.

[56] Balart, J.F.; Montanes, N.; Fombuena, V.; Boronat, T.; Sánchez-Nacher, L. Disintegration in Compost Conditions and Water Uptake of Green Composites from Poly(Lactic Acid) and Hazelnut Shell Flour. J. Polym. Environ. 2017, 26, 701–715, doi:10.1007/s10924-017-0988-3.

[57] Tokiwa, Y.; Calabia, B.P. Biodegradability and biodegradation of poly(lactide). Appl. Microbiol. Biotechnol. 2006, 72, 244–251, doi:10.1007/s00253-006-0488-1.

[58] Gil-Castell, O.; Badia, J.; Kittikorn, T.; Strömberg, E.; Martínez-Felipe, A.; Ek, M.; Karlsson, S.; Ribes-Greus, A. Hydrothermal ageing of polylactide/sisal biocomposites. Studies of water absorption behaviour and Physico-Chemical performance. Polym. Degrad. Stab. 2014, 108, 212–222, doi:10.1016/j.polymdegradstab.2014.06.010.

[59] Ray, S.S.; Yamada, K.; Ogami, A.; Okamoto, M.; Ueda, K. New Polylactide/Layered Silicate Nanocomposite: Nanoscale Control Over Multiple Properties. Macromol. Rapid Commun. 2002, 23, 943–947, doi:10.1002/1521-3927(200211)23:163.0.co;2-f.

[60] Conn, R.; Kolstad, J.; Borzelleca, J.; Dixler, D.; Filer, L.; Ladu, B.; Pariza, M. Safety assessment of polylactide (PLA) for use as a food-contact polymer. Food Chem. Toxicol. 1995, 33, 273–283, doi:10.1016/0278-6915(94)00145-e.

[61] Till, D.; Reid, R.; Schwartz, P.; Sidman, K.; Valentine, J.; Whelan, R. Plasticizer migration from polyvinyl chloride film to solvents and foods. Food Chem. Toxicol. 1982, 20, 95–104, doi:10.1016/s0278-6915(82)80016-1.

[62] Wang, X.; Song, M.; Liu, S.; Wu, S.; Thu, A.M. Analysis of phthalate plasticizer migration from PVDC packaging materials to food simulants using molecular dynamics simulations and artificial neural network. Food Chem. 2020, 317, 126465, doi:10.1016/j.foodchem.2020.126465.

[63] Hakkarainen, M. Migration of Monomeric and Polymeric PVC Plasticizers. Chromatogr. Sustain. Polym. Mater. 2008, 211, 159–185, doi:10.1007/12_2008_140.

polymers

MDPI

Article

Dual Plasticizer/Thermal Stabilizer Effect of Epoxidized Chia Seed Oil (*Salvia hispanica* L.) to Improve Ductility and Thermal Properties of Poly(Lactic Acid)

Ivan Dominguez-Candela [1], Jose Miguel Ferri [2], Salvador Cayetano Cardona [1], Jaime Lora [1] and Vicent Fombuena [2,*]

[1] Instituto de Seguridad Industrial, Radiofísica y Medioambiental (ISIRYM) Universitat Politècnica de València (UPV), Plaza Ferrándiz y Carbonell s/n, 03801 Alcoy, Spain; ivdocan@doctor.upv.es (I.D.-C.); scardona@iqn.upv.es (S.C.C.); jlora@iqn.upv.es (J.L.)

[2] Technological Institute of Materials (ITM), Universitat Politècnica de València (UPV), Plaza Ferrándiz y Carbonell 1, 03801 Alcoy, Spain; joferaz@upvnet.upv.es

* Correspondence: vifombor@upv.es

Abstract: The use of a new bio-based plasticizer derived from epoxidized chia seed oil (ECO) was applied in a poly(lactic acid) (PLA) matrix. ECO was used due to its high epoxy content (6.7%), which led to an improved chemical interaction with PLA. Melt extrusion was used to plasticize PLA with different ECO content in the 0–10 wt.% range. Mechanical, morphological, and thermal characterization was carried out to evaluate the effect of ECO percentage. Besides, disintegration and migration tests were studied to assess the future application in packaging industry. Ductile properties improve by 700% in elongation at break with 10 wt.% ECO content. Field emission scanning electron microscopy (FESEM) showed a phase separation with ECO content equal or higher than 7.5 wt.%. Thermal stabilization was improved 14 °C as ECO content increased. All plasticized PLA was disintegrated under composting conditions, not observing a delay up to 5 wt.% ECO. Migration tests pointed out a very low migration, less than 0.11 wt.%, which is to interest to the packaging industry.

Keywords: PLA; epoxidized chia seed oil (ECO); plasticizers; migration; disintegration

Citation: Dominguez-Candela, I.; Ferri, J.M.; Cardona, S.C.; Lora, J.; Fombuena, V. Dual Plasticizer/Thermal Stabilizer Effect of Epoxidized Chia Seed Oil (*Salvia hispanica* L.) to Improve Ductility and Thermal Properties of Poly(Lactic Acid). *Polymers* **2021**, *13*, 1283. https://doi.org/10.3390/polym13081283

Academic Editor: Beom Soo Kim

Received: 20 March 2021
Accepted: 12 April 2021
Published: 14 April 2021

1. Introduction

Currently, a global plastics production of 368 million tons was recorded in 2019, an increment of 2.5% from 2018. Conventional polymers such a polyethylene (PE), polypropylene (PP), polyvinyl chloride (PVC), poly(ethylene terephthalate) (PET), polystyrene (PS), and polyamide (PA), represent approximately 70% of plastic demand in Europe. With regard to the packing industry, which represents around 40% of total demand, these polymers are leading the plastic demand [1]. The majority are non-biodegradables as well as manufactured by petrochemical industries (non-renewable resources) [2]. The food packaging industry generates a large volume of waste due to it short-lifespan and its recycling is often limited to those not contaminated with food products. According to Plastics Europe 2020, about 39.5% of post-consumer waste was recycled, while 18.5% (3.2 million tons) ended up in landfills [1]. These non-recycled plastics need to be managed to avoid the presence in seas, lakes, and rivers which threatens the environment [3,4].

Concerning biodegradable polymers, their presence is increasing in the food packing industry. Several biodegradable polymers such as poly(lactic acid) (PLA), thermoplastic polyurethane (TPU), and polyhydroxyalkanoates (PHAs) have been applied as new alternatives [5–8]. The most employed polymer is PLA (about 10.9%), which is obtained by fermentation of polysaccharides or sugar extracted from potato, sugarcane, corn, etc., thus obtained by renewable resources [9]. PLA is currently manufactured for common applications such as salad cups, lamination films, drinking cups, containers, etc. [10].

Bloque III: incorporación de cargas lignocelulósicas

IV.3 "Contribution to a Circular Economy Model: From Lignocellulosic Wastes from the Extraction of Vegetable Oils to the Development of a New Composite"

Ivan Dominguez-Candela[1], Daniel Garcia-Garcia[2], Aina Perez-Nakai[2], Alejandro Lerma-Canto[2], Jaime Lora[1], Vicent Fombuena[2]

[1] Instituto de Seguridad Industrial, Radiofísica y Medioambiental (ISIRYM), Universitat Politècnica de València (UPV), Plaza Ferrándiz y Carbonell, s/n, 03801 Alcoy, Spain

[2] Technological Institute of Materiales (ITM), Universitat Politècnica de València (UPV), Plaza Ferrándiz y Carbonell 1, 03801 Alcoy, Spain

Polymers

2021, 13(14), p.2269-3269.

"Contribution to a Circular Economy Model: From Lignocellulosic Wastes from the Extraction of Vegetable Oils to the Development of a New Composite"

Abstract

The present works focuses on the development of a novel fully bio-based composite using a bio-based high-density polyethylene (Bio-HDPE) obtained from sugar cane as matrix and a by-product of extraction of chia seed oil (CO) as filler, with the objective of achieving a circular economy model. The research aims to revalorize an ever-increasing waste stream produced by the growing interest in vegetable oils. From the technical point of view, the chia seed flour (CSF) was chemically modified using a silane treatment. This treatment provides a better interfacial adhesion as was evidenced by the mechanical and thermal properties as well as field emission scanning electron microscopy (FESEM). The effect of silane treatment on water uptake and disintegration rate was also studied. On the other hand, in a second stage, an optimization of the percentage of treated CSF used as filler was carried out by a complete series of mechanical, thermal, morphological, colour, water absorption and disintegration tests with the aim to evaluate the new composite developed using chia by-products. It is noteworthy as the disintegration rate increased with the addition of CSF filler, which leads to obtain a partially biodegradable wood plastic composite (WPC) and therefore, becoming more environmentally friendly.

Keywords

Chia seed flour; wood plastic composite; silane treatment; bio-polyethylene; circular economy

Introduction

A global polymer production of 368 million tons was recorded in 2019. In Europe 58 million tons were produced and almost 25% of plastic post-consumer wastes is directly deposited in landfills [1]. The majority of conventional polymers are manufactured from fossil resources and are non-biodegradable. The most used polymers are polypropylene (PP), high- and low-density polyethylene (HDPE and LDPE) and polyvinylchloride (PVC), which represent some 60% of the plastics used [1,2]. Due to the mismanagement of these plastic products, most of which are single-use products, they can end up in landfills, oceans or other terrestrial ecosystems where they can affect wildlife and probably human health [3]. The use of biopolymers could be an excellent proposal for the plastics industry in order to overcome these drawbacks.

In recent years, biopolymers are gaining importance as a sustainable alternative to conventional polymers. They provide a 65% energy savings as well as between 30% and 80% less greenhouses gases emissions during their production compared to conventional polymers [4]. A biopolymer material is defined as a polymer that either is biodegradable, bio-based or has both properties [5]. This definition provides for three different types of biopolymers: (1) from renewable resources and biodegradable such as poly(lactic acid) (PLA) or polyhydroxyalkanoates (PHA); (2) from renewable resources and non-biodegradable, such as biopolyethylene (bio-PE) or biopolypropylene (bio-PP); (3) from fossil fuels and biodegradable such as polybutylene succinate (PBS) or poly(ε-caprolactone) (PCL) [6]. However, despite the great progress in biopolymers, these are still expensive, and, in some cases, present lower mechanical properties compared to conventional polymers. A growing alternative is the use of vegetable oils (VOs) that can be used as a raw material to obtain new products due to their ready availability and relative low cost. VOs present biodegradability and low toxicity, thus making them an attractive proposal for the plastic industry [7]. In addition, VOs and fatty acids from VOs, are considered one of the most important feedstocks to produce polymers materials and bio-based functional polymers [8,9]. The production of vegetable oils reached 210 million tons in 2020, which represents an increase of 25% in the last 8 years [10]. This production

is mainly targeted to two sectors: human consumption and the chemical industry. Regarding human consumption, palm oil and soybean oil are the most consumed VOs, representing a 64% of worldwide production [10]. Moreover, VOs, which are mainly formed by triglycerides, can be chemically modified for the polymer industry due to the reactivity of the double bonds present in their structure. Commercially, there are non-modified VOs such as linseed oil or rapeseed oil used to protect the surface of woods [11], and modified VOs such as soybean and linseed oil used as a plasticizer in thermoplastics [7,12–15]. This increment of VO production is generating a large volume of residual cake as a by-product of oil extraction from whole seeds. Approximately more than 60% of entire seed is residual cake [16–18], a large volume of 524 million tons was produced in 2020. This residual cake, which is a lignocellulosic residue, is usually used as dietary supplement for livestock feed [19]. Another possible propose is reuse of the by-product as a lignocellulosic filler in the polymer industry contributing to the circular economy.

Wood plastic composites (WPCs), which consist of the addition of natural fillers in a polymeric matrix, are gaining more importance in order to reuse wastes from different industries. Some compounds from vegetable oil industry wastes such as linseed [20], palm [21], sunflower [22] or rapeseed [23] have been reported as lignocellulosic fillers in WPCs. This movement contributes to the circular economy, where residual cake rises in value as a filler to manufacture a sustainable composite. WPCs present attractive advantages such as low prices, excellent balance between mechanical properties, lightness, etc., [24]. Besides, they are eco-friendly, renewable, partially or completely biodegradable and they also lead to a decrease of the greenhouse effects [25]. The final properties of WPCs depend on the matrix, filler species and content, and the coupling agent used, among other aspects [25,26]. Another advantage of WPCs is that they can be applied as possible substitutes for natural wood due to their similar appearance. Several types can be used in furniture, fences, garden objects and so on [27]. However, although WPC have been widely studied, no evidence has been found previously or at least it is not available in the literature on the introduction of chia wastes from the vegetable oil industry as a lignocellulosic filler in polymer matrices.

Chia seed is commonly known for representing the highest food source of α-linolenic acid (omega-3) as well as a high nutritional content [28]. The current interest has led to a worldwide sales volume of some 90,000 metric tons for whole chia seed in 2017 [29] which represents the largest chia seed product market share at 45% [30]. Regarding chia seed oil (CO), it is becoming more widely used as a cooking oil, to manufacture health food supplements and in cosmetic products [31]. In addition, the high antioxidant capacity of CO has been employed to provide long shelf life in food products [32]. In 2018, CO accounted with market share of 20%, and is projected to present an annual growth rate of 23.4% from 2019 to 2025 [30]. Furthermore, modified CO could be suitable to use in the polymer industry due to its elevated unsaturated fatty acid levels, indicated by an iodine value of 190 [33]. In a previous work, epoxidized chia seed oil was obtained and applied successfully as a bio-plasticizer in a polymer matrix [34]. With the constant increment of CO production for the mentioned applications and taking into account that the CO extraction yield is around 25–30%, a percentage of residual cake around 70% of whole chia seed is produced after oil extraction. Therefore, the introduction of these lignocellulosic fillers in a polymer matrix to obtain a WPC could be an attractive proposal to reuse the by-products from CO extraction.

Traditionally, WPCs have been widely studied with conventional polymer matrices of petrochemical origin such as HDPE [24], LDPE [35], PP [22], PVC [36] and PS [37]. The growing tendency to manufacture green composites has increased the use of biopolymers to reduce greenhouse gas emissions. As an alternative, bio-based high-density polyethylene (Bio-HDPE) could be an interesting green substitute to the polymers of petrochemical origin. Bio-HDPE is obtained by conventional polymerization of ethylene obtained from catalytic dehydration of bioethanol which comes from natural resources [38]. One of the main advantages is that it presents the same physical properties, especially high ductility, and resistance, compared to polyethylene from petrochemical resources [39]. Besides, it presents easy processability to obtain injected pieces, which makes it suitable to industrial scale [40]. However, one of the main disadvantages is its non-biodegradability, although this can

be partially resolved by adding lignocellulosic fillers which are biodegradable, thus manufacturing a WPC.

Given the current situation in which the use of vegetable oils in the polymer and food industry is attracting great interest, it is necessary to provide technical solutions to the possible waste generated in order to find a solution that is based on the circular economy. Therefore, the main objective of the present work was the reuse of the lignocellulosic waste obtained after the extraction of chia seed oil (*Salvia hispanica. L*) in a polymeric matrix based on Bio-HDPE. The study of compatibilization as well as the optimization of the lignocellulosic filler percentage is the polymeric matrix were carried out. A complete characterization of the composites has been carried out by means of mechanical (tensile, flexural, Charpy Impact Test or Shore D Hardness), thermal (DSC, TGA), thermo-mechanical (DTMA) and morphological techniques (Field Emission Scanning Electron Microscopy or FESEM) as well as water uptake, colourimetry and disintegration tests.

Experimental

Materials and Methods

This paper has been divided in two parts. In the first part, the influence of a silane coupling agent has been determined, through the comparison of treated and untreated Bio-HDPE with 20 wt.% chia seed flour (CSF). In the second stage, an optimization of percentage of filler has been carried out in samples with 10, 20, 30 and 40 wt.% of treated CSF with silane coupling agent.

Materials

Commercial bio-based high-density polyethylene (Bio-HDPE) HA7260 grade has been employed as polymer matrix and was supplied by Braskem (Sao Paulo, Brazil). This polymer presents a minimum bio-based content of 94%, being obtained from bioethanol derived from sugarcane. Bio-HDPE present a density of 0.955 g·cm^{-3} and melt flow index 20 g·10 min^{-1} at 20 °C. As a lignocellulosic filler a residual cake

obtained after cold pressed extraction of chia seed oil from entire chia seed (CS) supplied by Frutoseco (Bigastro, Alicante, Spain). Was used. The residual cake was milled using an ultra-centrifugal mill from Retsch GmbH (Düsseldorf, Germany) at 8000 rpm and equipped with 0.25 mm sieve. After milling, CSF was obtained for use as a lignocellulosic filler. As silane coupling agent 3-(2-aminoethylamine) propyl]trimethoxysilane (APS) provided by Sigma Aldrich (Madrid, Spain) was employed.

Silane Treatment

Firstly, the selection of the coupling agent must be detailed. It is known that due to the highly nonpolar nature of the Bio-HDPE and the polar nature of the lignocellulosic filler, CSF, the use of compatiblizers is needed. Different options are reported in the previous literature: alkaline or esterification treatment of the lignocellulosic filler, use of titanate, zirconate or silane coupling agents or copolymerization with active molecules like maleic anhydride or acrylic acid, for example [41–44]. Silanization is one of the most employed methods to improve the adhesion/interaction between a polymer matrix and a lignocellulosic fiber. In previous works, APS has been compared with other silanes (glycidyl silane) and maleic anhydride, obtaining the best resistant mechanical and thermal properties [45]. In other studies, APS was compared with titanate and zirconate coupling agents in biocomposites developed with Bio-HDPE and eggshells. APS gave very similar results compared to titanate and better ones than zirconate treatment, despite the fact that the load introduced was calcium carbonate and not lignocellulosic. In addition, in previous studies, APS was used as a coupling agent in WPCs developed with Bio-HDPE, demonstrating an improvement of the interaction between fiber and polymeric matrix. Jordá-Vilaplana *et al.* [46] used APS to improve the interaction between Bio-HDPE thermoplastic matrix and short fibers of *Cortaderia selloana* (Pampa grass). On the other hand, Carbonell *et al.* [47] compared the use of APS and a polyethylene graft-maleic anhydride copolymer in biocomposites developed with slate fiber and Bio-HDPE. The results showed as APS leads to higher fiber-matrix interactions with positive effects on overall mechanical properties.

In the present study the silane treatment was carried out following the method reported by Fombuena *et al.* [48]. Briefly, 1 wt.% of APS with respect to filler weight was dissolved in water/acetone (50/50 v/v) to hydrolyze the silane to a silanol. The use of different solvents such as methanol or acetone has been broadly studied, but Pickering *et al.* [49] reported that acetone improves the roughness of the lignocellulosic fillers, resulting in a large specific area. Immediately, the pH of the solution was adjusted to 3.5 using acetic acid and the mixture was stirred for 15 min to ensure homogenization. The acid conditions improve the silane to silanol hydrolysis as well as slow down the self-condensation, which consists of the reaction between silanols forming polysiloxane structures [50]. The formation of polysiloxanes may hinder the diffusion of silanols into the lignocellulosic filler during the adsorption step [51]. In the following step, CSF were immersed in the previously obtained solution and mechanically stirred for 15 min. Finally, the CSF treated with amine silane was dried in an oven at 40 °C for 24 h to remove all residual solvents. In this step silanol molecules are adsorbed onto the lignocellulosic filler, acting as a chemical bridge in the interface after drying which allows to form chemical Si-O-C bonds between silanol groups and the hydroxyl groups presents in cellulose [52].

Sample Preparation

Prior to manufacture, untreated (UTCSF) and treated chia seed flour (TCSF) with APS were dried in an air oven at 50 °C during 24 h to remove the residual moisture. In the first stage, Bio-HDPE with 20 wt.% of UTCSF and TCSF were processed. In the second stage, five samples with compositions (by weight) of 0, 10, 20, 30 and 40% of TCSF were manufactured. All samples were weighed following the proportions of the Table IV.3.1. Compounds were hand mixed using a zip bag to homogenize them. The mixtures were introduced into a twin-screw extruder from DUPRA S.L. (Castalla, Alicante, Spain) at constant rate of 40 rpm. The temperature profile was set to 160 °C (feeding zone), 160 °C, 165 °C and 170 °C (die). Afterwards, the composites were pelletized to be injected using an injected molding machine Meteor 270/75 from Mateu & Solé (Barcelona, Spain) with the following temperature profile: 160 °C (feeding zone), 160 °C, 165 °C and 170 °C (die). Cavity filling time and cooling time were set to 1 s and 10 s, respectively.

Table IV.3.1. Weight composition of Bio-HDPE with chia seed flour (CSF) materials and labelling.

Reference	Parts by Weight (wt.%)		
	Bio-HDPE[1]	UTCSF[2]	TCSF[3]
Bio-HDPE	100	0	0
10T	90	0	10
20UT	80	20	0
20T	80	0	20
30T	70	0	30
40T	60	0	40

[1] Bio-based high-density polyethylene; [2] Untreated chia seed

Mechanical and Thermal Characterization

Tensile, flexural, hardness and impact testz were carried out in order to analyze the mechanical properties. Tensile and flexural testz were carried out with an Ibertest ELIB 30 universal testing machine from S.A.E. Ibertest (Madrid, Spain) at room temperature. A load cell of 5 kN and crosshead speed of 10 mm·min^{-1} were used. Sample sizes were 150 mm length, 4 mm thickness and 10 mm wide for tensile test as was indicated by ISO 527. Moreover, an axial extensometer from S.A.E Ibertest was employed to measure the tensile modulus with high accuracy. Regarding the flexural and impact tests, the samples sizes were 80 × 10 × 4 mm^3. The impact tests were performed using a 1 J Charpy pendulum from Metrotec S.A (San Sebastián, Spain) according to ISO 179. Samples were notched with a "V" at 45° and radius of 0.25 mm. Shore D hardness mesurments were carried out with a model 673-D durometer from Instrumentos J. Bot S.A. (Barcelona, Spain) according to ISO 868. At least five samples were tested to calculate the average values and deviations.

Regarding thermo-mechanical properties, evolution in storage modulus (G') were assessed by dynamic mechanical thermal analysis (DMTA) in an oscillatory rheometer AR G2 from TA Instruments (New Castle, DE, USA) equipped with a torsion clamp for solid samples. Rectangular sample sizing 40 × 10 × 4 mm^3 were tested to a ramp temperature from −50 °C to 100 °C at a constant heating rate of 2 °C·min^{-1}. Frequency tested was 1 Hz and maximum percentage of deformation 0.1%.

Thermal properties of samples were evaluated using Differential Scanning Calorimetry (DSC) and Thermogravimetric Analysis (TGA). DSC tests were performed in a mod. 821 DSC from Mettler Toledo Inc. (Schwerzenbach, Switzerland). Samples with a weight of 5–10 mg were evaluated using a heating program from 30 °C to 300 °C at heating rate of 10 °C·min^{-1} with a constant flow rate of 66 mL·min^{-1} in nitrogen atmosphere. The percentage crystallinity of Bio-HDPE compositions with CSF was determined by Equation IV.3.1:

$$X_c\ (\%) = \left[\frac{\Delta H_m - \Delta H_{cc}}{\Delta H_{m(100\%)} \cdot w_s}\right] \times 100 \qquad \textbf{Equation IV.3.1}$$

where ΔH_{cc} and ΔH_m represent the crystallization and cold enthalpies, respectively. $\Delta H_{m(100\%)}$ was the melt enthalpy of theoretically 100% crystalline of Bio-HDPE structure, which value reported in bibliography was 293 J·g^{-1} [53] and w_s was the weight proportion of green composites.

Thermal decomposition studies were carried out in a TGA/SDTA 851 from Mettler Toledo Inc. with a heating program from 30 °C up to 700 °C at 20 °C·min^{-1} as heating rate in a nitrogen atmosphere with a constant flow rate of 66 mL·min^{-1}. Samples with an average of 10 mg were employed in the TGA evaluations. Both 5% weight loss and maximum degradation temperatures were measured in order to assess the thermal stability of Bio-HDPE with different lignocellulosic filler compositions.

Morphology Chatacterization

The surface morphology of fractured samples in the Charpy Impact test of Bio-HDPE with CSF treated and untreated were analyzed with a Zeiss Ultra 55 Field Emission Scanning Electron Microscope (FESEM) supplied by Oxford Instruments (Oxfordshire, UK). All fractured surfaces were coated for 120 s with a thin layer of Au-Pd alloy. This process was carried out under vacuum conditions using an EM MED020 sputter coater from Leica Microsystems (Wetzlar, Germany) following the methodology employed by Quiles-Carillo *et al.* [54]. All samples were observed with an accelerating voltage of 2 kV.

Water Uptake

Water absorption was determined with samples of 80 × 10 × 4 mm² size which were immersed in distilled water at 23 ± 1 °C. Previous to water immersion, samples were dried in air oven at 40 °C over 24 h to remove any residual moisture. Different samples were taken from the water, dried with a dry cloth to eliminate surface moisture and weighed for each control day (from 1 to 18 weeks). Total water absorption (W_{abs}) in the studied period was calculated by Equation IV.3.2:

$$W_{abs}\ (\%) = \frac{w - w_0}{w_0} \cdot 100 \qquad \textbf{Equation IV.3.2}$$

where w refers to the sample weight after taking it out of the water immersion bath and w_0 is the initial dry weight before immersion.

Colour Characterization

Colour coordinates of samples were determined in a Konica CM-3600d Colorflex-DIFF2, from Hunter Associates Laboratory, Inc (Reston, VA, USA). The colorimeter was calibrated using a white standard tile and the ASTM E313 method was used with standard illuminant D65 and observer angle of 10°. System employed was CIE Lab colour space according to the following criteria: L* represents luminance, where L* = 0 indicantes dark and L* = 100 lightness; a* represents from red (a* > 0) to green (a* < 0) and b* represents from yellow (b* > 0) to blue (b* < 0). At least five different samples were measured and the average and desviation standard values were reported. Moreover, colour difference compared to neat sample (Bio-HDPE) was calculated by Equation IV.3.3:

$$\Delta E^*_{ab} = \sqrt{(\Delta L^*)^2 + (\Delta a^*)^2 + (\Delta b^*)^2} \qquad \textbf{Equation IV.3.3}$$

where ΔE^*_{ab}, Δa^* and Δb^* are the variations in colour coordinates L*, a* and b*, respectively, between neat Bio-HDPE and Bio-HDPE with CSF filler. The colour changes of samples were evaluated according to the following assessment: ΔE^*_{ab} < 1) means unnoticiable colour change, (ΔE^*_{ab}) between 1 and 2 means a slight difference

that was only noticeable by an experienced observer, (ΔE^*_{ab}) between 2 and 3.5 indicate that an unexperienced observer can notice the difference, (ΔE^*_{ab}) values in the 3.5–5 range means a clear noticeable difference in colour and values higher than 5 leads to the observer noticing a different colour [55].

Degradation under Composting Conditions

Degadation tests were conducted under aerobic conditions following the recommendations of the ISO 20200 norm. A 300 × 200 × 100 mm^3 synthethic compost reactor was used where the conditions of temperature and relative humidity were 58 °C and 55%, respectively. Previously to burying, all samples were dried in an air oven at 40 °C during 24 h. Six different samples of each composition were employed for each control day under composting conditions. The selected control days were: 8, 14, 21, 28, 47 and 90. Different samples of each composition were unburied while the rest remained in the process. The unburied samples were washed and dried during 24 h to remove humidity and weighed on an analytical balance. To ensure reliability, all tests were carried out in triplicate. The percetage of degradation of extracted samples was measured by Equation IV.3.4:

$$\mathrm{W}\ (\%) = \frac{w_0 - w_s}{w_0} \cdot 100 \qquad \textbf{Equation IV.3.4}$$

where w_0 referred to the initial dry weight of the sample and w_s was the weight of the sample extracted from compost soil on different days after drying.

Results and discussion

CSF Extraction Yield

Whole chia seeds were crushed in a cold press machine to extract the oil and subsequently determine the extraction yield. The extraction method was performed at room temperature for two reasons: firstly, to avoid any chemical changes in the extracted oil that can be induced by high temperatures and to use less energy in the extraction, thus reducing operation costs. Moreover, mechanical extraction is preferable to a chemical extraction because it avoids the use of petrochemical solvents.

After a second extraction process a yield of 67.7 wt.% was obtained. No more extraction trials were carried out due to very low yield obtained, considered non-economically feasible as Ixtaina *et al.* [56] reported. Therefore, this elevated amount of residual cake (67.7%) produced after extraction of CO, was considered a potential candidate to apply in green composites as renewable fillers contributing to the circular economy.

First Stage. Effect of Silane Treatment

The effect of untreated and treated CSF filler in a Bio-HDPE matrix was investigated by evaluating the tensile, ductile, hardness and impact properties. Table IV.3.2 gathers the properties obtained. Firstly, the tensile strength of Bio-HDPE was around 373 Mpa and decreased with the addition of CSF filler (untreated and treated). This behavior was expected due to the addition of filler, which causes a decrease in interfacial adhesion because the filler tends to form agglomerates increasing the stress concentrations and, as a result, lower tensile strength [57]. Regarding the effect of silane treatment, which was evaluated with 20 wt.% of CSF, it was observed that the 20UT sample presented 10.8% less tensile strength than the 20T sample. This reduction of tensile strength was attributed to weak interfacial adhesion between UTCSF and the Bio-HDPE matrix. It is known that organosilanes consist of two different reactive molecules: the silanol groups react with the hydroxyl groups presents in CSF, whereas the functional groups of the APS react with the polymeric matrix by covalent bonding [58]. In addition, it has been reported that treatment of lignocellulosic flour with APS coupling agent improved the interfacial adhesion with Bio-HDPE [59]. This better adhesion/interaction allowed a uniform stress distribution from polymer to filler, achieving a higher tensile strength than untreated samples. Similar findings have been reported by Ihamounchen *et al.* [60], who evaluated the addition of olive husk flour (OHF) treated with vinyltriacetoxysilane (OHFTA) in HDPE. In this study an increment from 13% to 3% in tensile strength with 10 and 30 wt.% of OHF was reached compared to untreated samples, respectively. Regarding tensile modulus, the untreated sample (20UT) presented a value of 374 Mpa whereas a treated sample (20T) showed an increment of 5.9% compared to the 20UT sample. Finally, elongation at break was dramatically decreased after filler addition. Bio-HDPE presented a high

elongation at break of 520%, showing high ductility properties as has been reported previously [44]. When 20 wt.% of untreated CSF was added, this parameter dropped drastically to a value below 36%, which is 93% lower than Bio-HDPE. On the other hand, if this amount of filler is treated with APS the decrease is pronounced, but lower than 90% with respect to the Bio-HDPE. Therefore, it has been observed that CSF treated with APS presented higher elongation at break than a 20UT sample with an improvement of 41%. Comparing these results with the use of a polypropylene-graft-maleic copolymer (PP-g-ma) as compatibilizer between peanut shell and polyethylene, lower enhancement in elongation at break were obtained [61]. In this study the introduction of PP-g-ma does not improve this feature compared to sample without compatibilizer, which highlights the efficiency of the APS.

With regard to flexural properties, no significant changes were recorded in flexural strength with the addition of CSF filler. In addition, the silane treatment with APS does not show significant differences. Regarding flexural modulus of the 20UT sample, a decrease from 804 Mpa for neat Bio-HDPE to 784 Mpa was observed. Regarding samples with CSF treated with APS, an evident improvement was observed compared to 20UT samples. The same behavior was obtained by Boronat *et al.* [44] who evaluated Bio-HDPE with eggshells with silane treatment. In another study, a maleic anhydride grafted polystyrene (Xibond™ 160) was employed as a compatibilizer in a cellulose/ABS composite [62]. The addition of this copolymer led to a 1.75% improvement of the flexural modulus compared to a sample without compatibilizer. This value was lower than that obtained with APS in the current study that achieved an improvement of 7% regarding the untreated sample. In general, these tendencies were in concordance with values previously recorded for tensile properties, where samples treated with silane present higher mechanical resistances properties than untreated samples.

Regarding Shore D hardness, it increased with addition of CSF due to the intrinsic hardness of lignocellulosic filler which leads to an increase of the hardness of the composite [63]. In relation to untreated and treated CSF, there was a slight improvement with the 20T sample. This fact was attributed to the strong adhesion between CSF and the matrix produced after silane treatment [64]. On the other hand,

the impact energy, that is related to the deformation capacity, is highly sensitive of stress concentrators [65]. The addition of 20 wt.% of CSF led to a decrease in impact absorbed energy compared to Bio-HDPE. In this instance, it has not been possible to transfer the impact load from the matrix to the filler thus reducing the impact absorbed energy with CSF addition. Comparing 20UT and 20T samples, an improvement of 13% in impact energy was observed when filler was treated with APS. This behavior was due to the silane coupling agent acting as a bridge between CSF and Bio-HDPE matrix through chemical bonding, which reduces any crack propagation by means of a good dispersal of the impact energy [66].

Table IV.3.2. Mechanical properties for Bio-HDPE with untreated and treated chia seed flour.

Reference	Tensile Strength (Mpa)	Tensile Modulus (Mpa)	Elongation at Break (%)	Flexural Strength (Mpa)	Flexural Modulus (Mpa)	Shore D Hardness	Impact Absorbed Energy (kJ·m^{-2})
Bio-HDPE[1]	19.0 ± 1.2	373.0 ± 16.0	520.0 ± 18.5	23.9 ± 1.21	804.0 ± 38.0	56.6 ± 0.5	2.75 ± 0.2
20UT[2]	10.7 ± 0.5	374.0 ± 14.7	35.9 ± 5.7	23.13 ± 0.76	784.9 ± 34.5	61.0 ± 0.7	1.67 ± 0.08
20T[3]	12.0 ± 0.4	396.5 ± 14.5	50.8 ± 5.4	24.1 ± 0.5	839.8 ± 21.6	62.2 ± 1.0	1.88 ± 0.1

[1] Bio-based high-density polyethylene; [2] 20 wt.% untreated chia seed flour; [3] 20 wt.% treated chia seed flour.

In Figure IV.3.1, the morphology of fractured surfaces from Charpy tests are shown with the aim of evaluating the effect of silane treatment on the interfacial adhesion between CSF and the matrix. As can be observed in Figure IV.3.1a, Bio-HDPE showed the typical rough and irregular surface of a ductile polymer as also reported by Rojas *et al.* [67]. As it has been described previously, the treatment of CSF with APS has a positive effect on mechanical resistance properties such as strength, modulus, or hardness whereas a decrease of mechanical ductile properties such as elongation at break was detected. The effect of silane treatment can be compared in Figures IV.3.1b,c at 1000× where CSF particles are highlighted with a yellow arrow. In the case of an untreated sample (20UT) a clear gap can be distinguished in the perimeter between the polymer matrix and a CSF particle highlighted by the red arrow in Figure IV.3.1b. This gap indicated the lack of particle-matrix interaction that does not allow it to transfer stress, and this justifies the decrease in elongation at break and impact energy [60]. Moreover, Toro *et al.* [68] indicated that when cracks are produced by an impact, these are propagated towards the poor interfacial regions,

leading a break in the composites with low stresses. Regarding the treated sample (20T), the gap between the CSF particle and polymer matrix has been broadly reduced when CSF was treated with silane coupling, as has been highlighted with a red arrow in Figure IV.3.1c. This indicated that a better interfacial adhesion was achieved between the two phases. This confirms the enhancement of mechanical properties and elongation at break compared to untreated samples. Bijaisoradat *et al*. [69] also observed that voids between filler and matrix was reduced when evaluating wood flour treated by trimethoxy (propyl)silane (MPS) in HDPE.

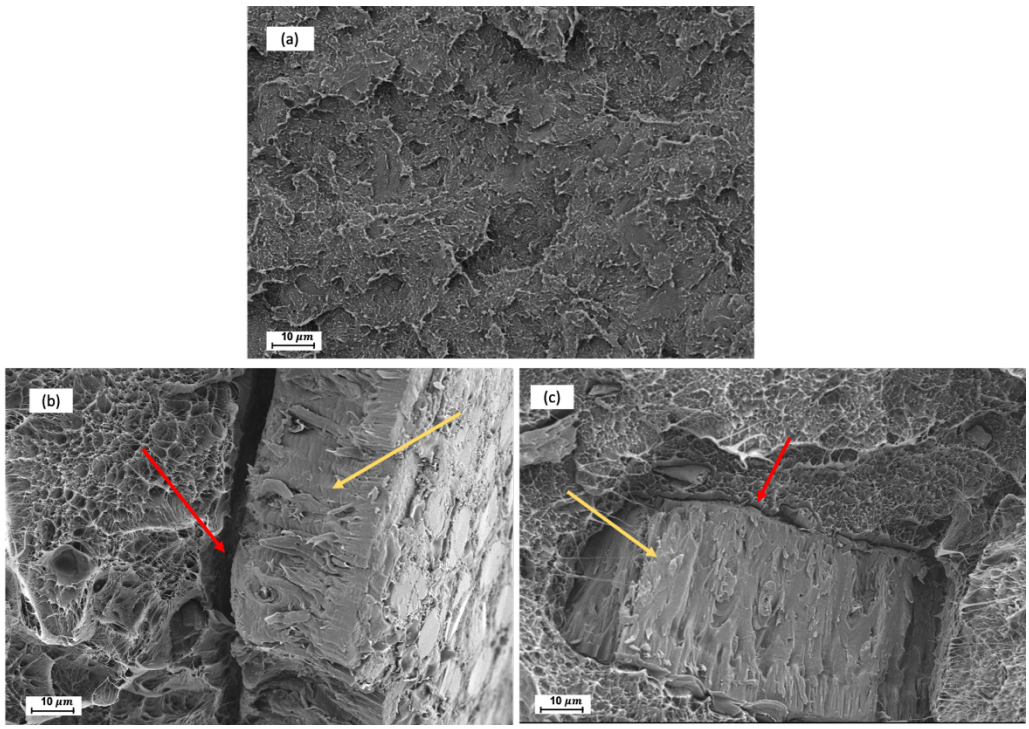

Figure IV.3.1. Fracture surface morphology of Charpy test by FESEM at 1000x: (a) Bio-based high-density polyethylene; (b) 20 wt.% untreated chia seed flour; (c) 20 wt.% treated chia seed flour.

The effect of untreated and treated CSF filler in the Bio-HDPE matrix was studied by DMTA in torsion mode. Figure IV.3.2 shows the storage modulus (G') of samples with respect to the temperature. Firstly, Bio-HDPE presented the lowest G' as was expected. As has been mentioned previously, the tensile and flexural modulus presented a clear increase with 20UT and 20T samples compared to Bio-HDPE. In this case, the same trend was observed because of the restriction of polymer chain mobility through addition of CSF filler, hence increasing the stiffness of the composite [70]. Regarding the effect of silane treatment, it was observed that 20T sample presented a

higher G' than the 20UT sample over all temperatures, which means an increase of 2.5% at room temperature. This fact can be explained by the better compatibility between CSF and matrix as was observed in FESEM. These values were in concordance with the mechanical properties discussed above.

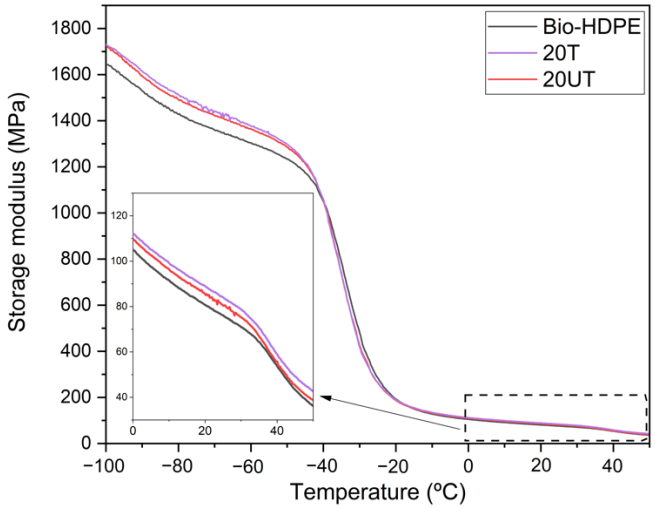

Figure IV.3.2. Evolution of storage modulus (G') of bio-based high-density polyethylene (Bio-HDPE) with 20 wt.% of untreated (20UT) and treated (20T) chia seed flour.

The influence of silane coupling treatment on the thermal properties has been investigated by DSC. Table IV.3.3 gathers the main thermal properties. Bio-HDPE showed a melt temperature of 131 °C, a value in concordance with the result of Quiles-Carillo *et al.* [71]. In addition, it was observed that the melting temperature of 20UT and 20T samples are not affected significantly compared to Bio-HDPE. It has been widely reported that silane coupling agent does not directly affect the melting temperature [59,72,73]. With respect to the melting enthalpy, it was decreased with addition of CSF filler due to both the effect of filler content and the matrix reduction (Bio-HDPE). Finally, the effect of silane treatment on crystallinity is shown in Table IV.3.3. The addition of treated CSF (20T) allowed an increase in the crystallinity compared to untreated CSF (20UT). This behavior was due to a better interaction between phases that may improve the nucleation activity with the presence of CSF treated with APS [74]. Therefore, the lack of interaction of untreated CSF led to difficult the arrangement of molecular chains, decreasing the crystallinity.

Table IV.3.3. Main thermal parameters of Bio-HDPE with untreated and treated chia seed flour obtained using DSC.

Reference	Tm (°C)[1]	ΔHm (J g^{-1})[2]	Xc (%)[3]
Bio-HDPE[4]	131.0	154.2	55.8
20UT[5]	131.8	105.8	49.5
20T[6]	131.5	126.1	57.8

[1] Melt temperature; [2] Melt enthalpy; [3] Degree of crystallization; [4] Bio-based high-density polyethylene; [5] 20 wt.% untreated chia seed flour; [6] 20 wt.% treated chia seed flour.

Thermogravimetric analysis (TGA) was performed to assesses the thermal stability of neat Bio-HDPE, CSF particles and the effect of silane treatment with 20 wt.% of CSF in the Bio-HDPE matrix. Figure IV.3.3 shows the TGA curves and the first derivative (DTG). As observed in Figure IV.3.3a, a weight loss of Bio-HDPE was associated with a single-phase degradation. At a temperature of 100 °C no weight loss due to evaporation of residual moisture was measured in the samples, due to their characteristic hydrophobic nature. Bio-HDPE degradation proceeded in one step that began about 350 °C up to 520 °C where a weight loss of 99% was measured. This one step degradation was produced by random scission of the C-C and C-H bonds present in Bio-PE [75]. A similar temperature profile trend was observed by Montanes *et al.* [76]. Regarding the weight loss of CSF, it was associated with the four stages characteristic of lignocellulosic particles. The initial weight loss recorded was 7.5% in the 30–220 °C range, which was attributed to evaporation of residual moisture contained in the particles [77]. The second step was produced between 220 °C and 350 °C approximately, with a weight loss of 40%. This loss was due to the decomposition of low molecular weight products such as hemicellulose. The third stage corresponds to around 60% of weight loss in the 350–410 °C range due to decomposition of cellulose. The last step, characterized by a weight loss of 75%, was related to lignin degradation at temperatures above than 410 °C [78]. Two different stages were identified in the evaluation of the effect of CSF particles in the Bio-HDPE matrix. The first stage, at temperatures in the 280–430 °C range, was related to the lignocellulosic filler decomposition mentioned above. It was observed that addition of CSF filler led to decrease in the thermal stability. The second stage was measured above 430 °C and is characterized by Bio-HDPE degradation. Regarding the effect of silane treatment, a

treated sample (20T) displayed higher thermal stability than an untreated (20UT) one. This could be attributed to the improvement of matrix filler interactions after silane coupling agent addition, which led to enhanced thermal stability [64]. In Figure IV.3.3(b) two maximum degradation stages can be observed for all samples. The first stage was related to CSF degradation at temperatures around 350 °C, thus not displaying any evidence of weight loss for Bio-HDPE as expected. In addition, the maximum temperature for the first stage was not shifted depending on the CSF filler surface treatment. Finally, the second stage was related to Bio-HDPE degradation. In this case, the second maximum degradation temperature was 498 °C and no signs of changes were recorded, maintaining the thermal stability. However, the results reported by Fonsenca *et al.* [62] showed a shift to lower temperatures of the peak maximum peak degradation of ABS with a cellulose fiber composite using a maleic anhydride grafted polystyrene as compatibilizer, reducing the thermal stability.

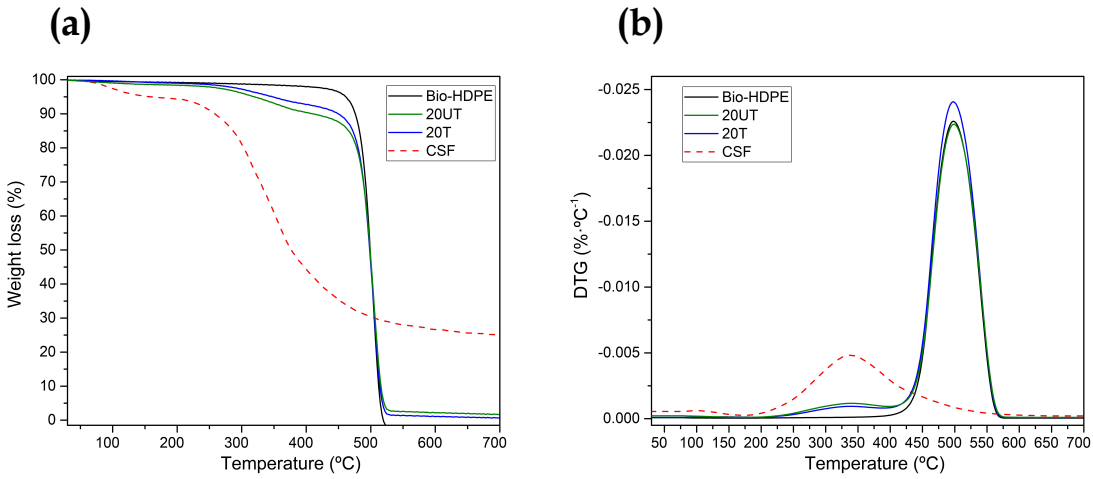

Figure IV.3.3. Thermal parameters of degradation of bio-based high-density polyethylene (Bio-HDPE) with 20 wt.% of untreated (20UT) and treated (20T) chia seed flour (CSF). (a) Weight loss; (b) Derivative thermogravimetry.

With the objective of measuring the effect of silane treatment on the water uptake of the developed composites, the absorption of water was evaluated by means of immersion in distiller water for 18 weeks. In Figure IV.3.4 it can be observed that Bio-HDPE presented less than 0.05 wt.% water absorption. It is known that polyethylene is a hydrophobic polymer as has been reported by Perthue *et al.* [79], who reported the same absorption value. In addition, CSF presents the hydrophilic nature characteristic

of lignocellulosic fillers. Thus, the addition of filler leads to an increase in the water absorption of composites. The free hydroxyl groups present in CSF may react with hydrogen bonds of water allowing water to diffuse inside the composite [80]. The effect of silane treatment on CSF was clearly observed by comparing 20UT and 20T samples. A decrease of 17% in water absorption was recorded for the 20T sample compared to the 20UT sample. After silane treatment there is less availability of hydroxyl groups in CSF filler to create hydrogen bonding with water, thus rendering lignocellulosic filler more hydrophobic [81]. In addition, we should remark that from 14 to 18 days, a constant water uptake was measured for all samples studied, indicating no further absorption.

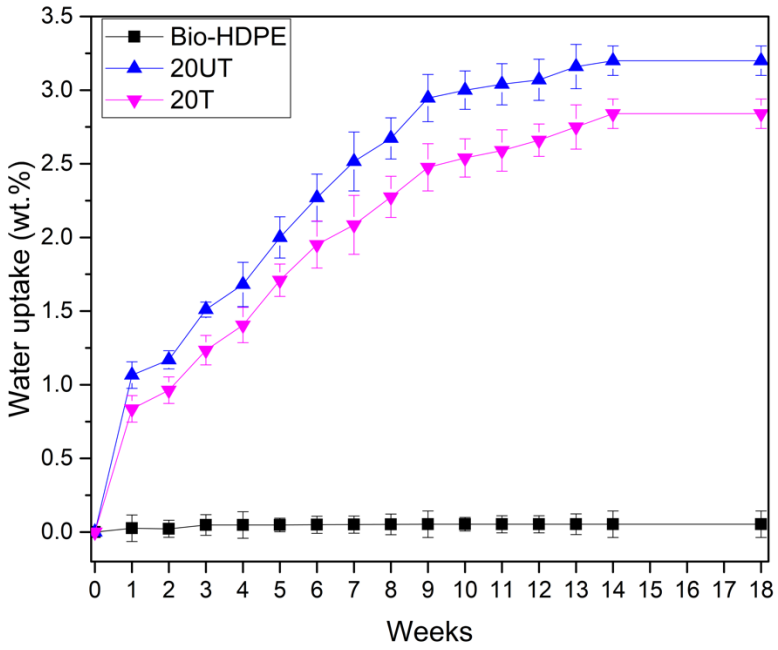

Figure IV.3.4. Water uptake of bio-based high-density polyethylene (Bio-HDPE) with 20 wt.% of untreated (20UT) and treated (20T) chia seed flour.

Degradation of Bio-HDPE with untreated and treated CSF filler is shown in Figure IV.3.5. Bio-HDPE presents several features such as high molecular weight, hydrophobicity and the lack of functional groups that are recognizable by microbial systems, which make it essentially a non-biodegradable polymer [82,83]. After 8 days, Bio-HDPE does not show any weight loss whereas 20UT and 20T samples presented a slight weight loss. On the 21st day a weight loss higher than 2.5% was recorded for both untreated and treated samples with 20 wt.% of CSF. According to Peng *et al.* [77],

lignocellulosic filler is biodegradable at a reasonable rate and can be fully degraded after longer periods ranging from 1 to 3 months using the soil burial method. The recorded degradation was related to the lignocellulosic filler which biodegrades due to the deterioration of lignin, hemicellulose and cellulose caused by microorganisms [84]. It should be mentioned that the Bio-HDPE matrix was not affected after 90 days, displaying a weight loss of less than 0.05% as plotted in Figure IV.3.5. Regarding to effect of silane treatment, the 20UT sample achieved a higher disintegration rate than 20T sample, reaching 8.5% and 4.21% after 18 weeks, respectively. It is known that hydrophilic nature of lignocellulosic filler facilitates the transfer of water and microorganisms or enzymes into the composite, thus speeding up the disintegration process [74]. The improvement of interfacial adhesion due to silane treatment hinders the introduction of water and microorganism action in composites, reducing the degradation [74]. This behavior was in concordance with the water uptake results obtained, where the 20UT sample present a higher water absorption than a 20T sample, thus leading to a sped-up disintegration rate.

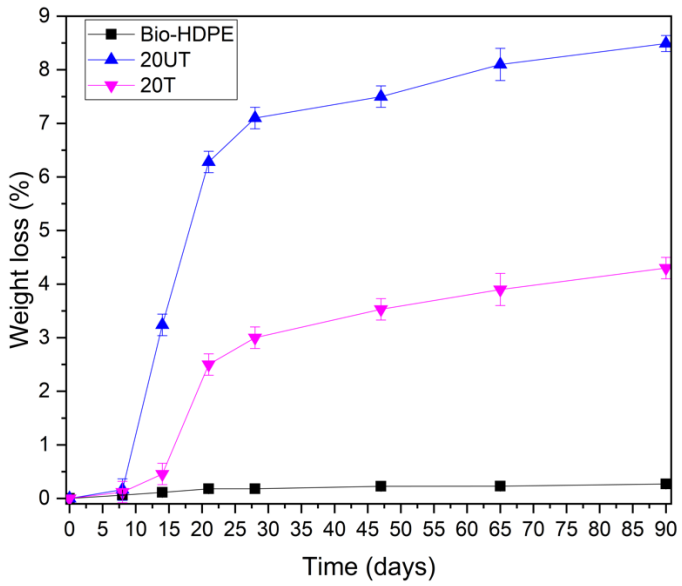

Figure IV.3.5. Weight loss of bio-based high-density polyethylene (Bio-HDPE) with 20 wt.% of untreated (20UT) and treated (20T) chia seed flour.

After studying the effect of silane coupling agent in Bio-HDPE with CSF filler, it has been determined that in general, silane treatment improves the mechanical resistance properties and main aspects such as the water uptake capacity and

minimizes the disintegration rate under composting conditions. By FESEM it has been observed how the gap between filler and matrix was reduced with silane treatment, which justifies the mechanical property improvement. Moreover, silane agent provided a nucleation effect, a decrease of the water absorption due to decrease of available hydroxyl groups and thus slightly decreased the rate of degradation.

Second Stage. Evaluation of CSF Filler Percentage

Once the effect of APS as a coupling agent had been studied, the aim was to study how CSF filler content modified with APS affects the mechanical, thermal, and morphological properties of the Bio-HDPE. The same order of characterization as in the first stage was followed.

Tensile properties of Bio-HDPE with different content of CSF are shown in Figure IV.3.6. As can be seen in Figure IV.3.6a, the tensile strength decreased with increasing filler content. The lowest tensile strength recorded was 8 Mpa for the 40T sample, which was a decrease of 58% compared with Bio-HDPE. This behaviour was directly related to the interfacial adhesion between CSF and matrix, which is crucial in reinforced composites to allow the tranfer of a small stress to filler particles during deformation [45]. Therefore, a higher content of filler implies less interaction between the matrix and particles, and thus more stress concentration appeared that induces the strength to decrease [85]. Regarding the tensile modulus, Figure IV.3.6b showed an increase with addition of CSF content in the matrix. In this case, the highest elastic modulus was obtained for the 40T sample, which represents an increment of 22% compared to neat Bio-HDPE. No significant difference was observed when comparing the 30T and 40T samples, indicating that a higher addition of CSF filler does not necessarily lead to an increase of elastic modulus. In addition, the increment of elastic modulus could confirm that CSF presents the rigid nature typical of lignocellulosic fillers. This trend indicated an increment of stiffness of composite due to restriction of chain mobility caused by the presence of filler particles [63]. Finally, as was shown in Figure IV.3.6c, the elongation at break of Bio-HDPE decreased dramatically as the filler content increased, going from 520% for Bio-HDPE to 23.5% for the 40T sample, respectively. This behaviour was attributed to the presence of stress caused by the

dispersed rigid filler that increased the higher the filler content is [61]. This trend has also been found by Chun *et al.* [72] when studying the effect of coconut shell powder (CSP) with 3-aminopropyl-triethoxysilane (3-APE) silane coupling in a PLA matrix. In this study, despite the enhancement of interfacial adhesion obtained using aminosilane, a reduction of elongation at break occurred.

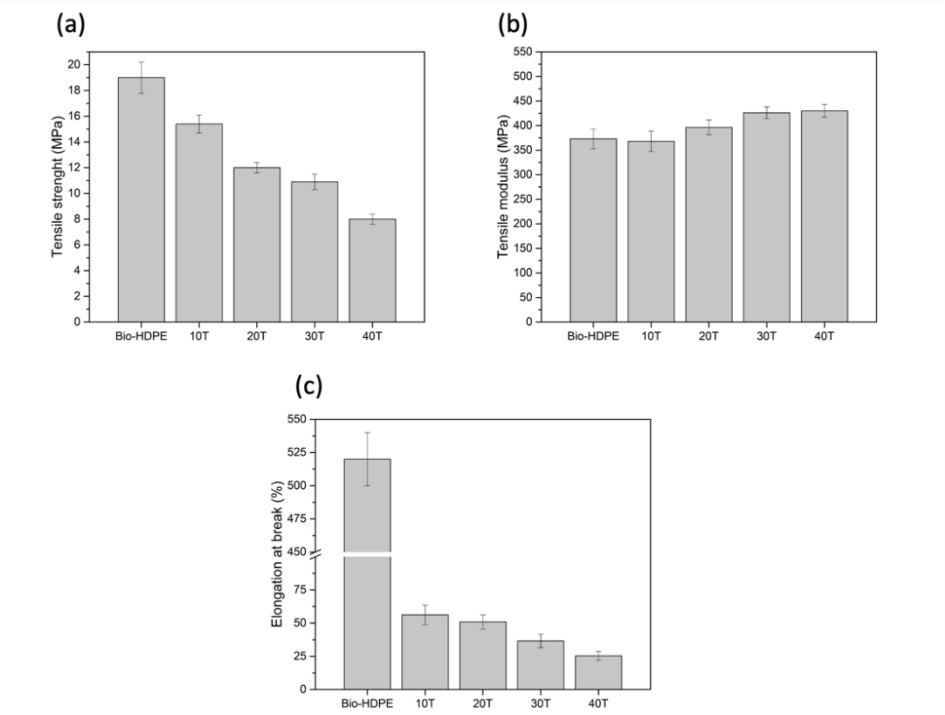

Figure IV.3.6. Effect of weight percentage of treated chia seed flour with APS on tensile properties in bio-based high-density polyethylene (Bio-HDPE): (a) Tensile strength; (b) Tensile modulus; (c) Elongation at break.

A similar behaviour was observed in flexural properties (Figure IV.3.7). As shown in Figure IV.3.7, the flexural strength decreased slightly with the addition of CSF to the matrix. Although the changes recorded are not very significant, a clear tendency was observed. The lowest flexural strength measured was 21.7 Mpa for 40 wt.% of CSF, representing a decrease of 9.6% compared to Bio-HDPE with 24 Mpa. With respect to flexural modulus, it was highly improved with the addition of filler. Addition up to 20 wt.% of CSF showed an increase of 4% compared to unfilled material, achieving an average value of 845 Mpa approximately. However, a very similar addition of 30 wt.% showed a significant increment of 10% and 18% in flexural modulus regarding Bio-HDPE for 30 and 40 wt.%, respectively. As mentioned above,

for the lowest filler content (10 and 20 wt.%) a slight increase was measured. This fact is due to better filler dispersion in the matrix as well as the substantial distance between filler particles. Nevertheless, the flexural modulus for high filler content was increased noticeably because the distance was decreased by the addition of filler and the effect of each CSF particle was superposed providing an evident enhancement [86]. In general, these tendencies were in concordance with the previously recorded tensile properties, where the tensile modulus increased, and tensile strength decreased as filler content was added.

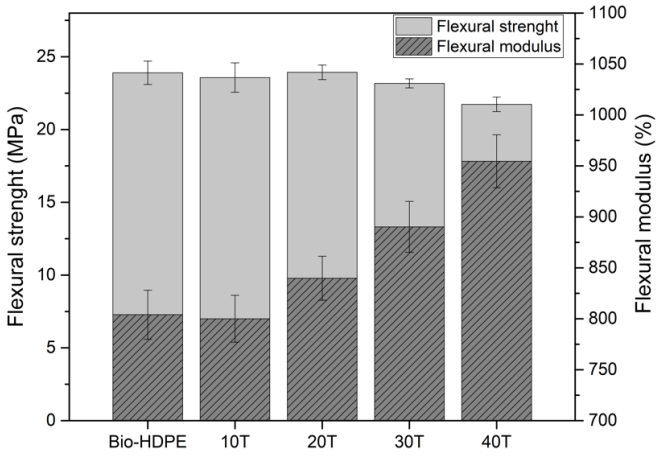

Figure IV.3.7. Effect of weight percentage of treated chia seed flour with APS on flexural properties in bio-based high-density polyethylene (Bio-HDPE).

Shore D hardness and impact absorbed energy results are gathered in Table IV.3.4. Firstly, hardness is related to the mechanical resistance properties and a gradual increase was observed as the addition of CSF filler increased. In this case, the 40T sample showed a Shore D hardness of 63, which represents an increment of 11% compared to Bio-HDPE. This fact was expected because lignocellulosic filler presents higher hardness than the soft polymer matrix, which leads to an increase in the hardness of composites [87]. It should be noted that the evolution of hardness was in concordance with the tensile and flexural modulus results. In contrast, the toughness of composites, which is the ability to absorb energy during deformation, was decreased as the addition of CSF to the matrix increased. The lowest impact absorbed energy recorded was 1.6 kJ·m^{-2} for 40 wt.% of CSF, which represents a decrease of 38% compared to Bio-HDPE (2.6 kJ·m^{-2}). As expected, filler addition generated higher

stress concentration as well as restricted the deformation, which leads to decreased absorbed energy [88]. Furthermore, this tendency was in concordance with the evolution of elongation at break and the typical mechanical ductile properties mentioned above.

Table IV.3.4. Effect of weight percentage of treated chia seed flour with APS on Shore D Hardness and impact absorbed energy.

Reference	Shore D Hardness	Impact Absorbed Energy (kJ·m^{-2})
Bio-HDPE[1]	56.6 ± 0.7	2.75 ± 0.20
10T2	59.4 ± 0.9	1.92 ± 0.10
20T2	61.0 ± 0.7	1.88 ± 0.08
30T2	62.2 ± 1.1	1.65 ± 0.12
40T2	63.0 ± 0.8	1.62 ± 0.10

[1] Bio-based high-density polyethylene; [2] wt.% of treated chia seed flour.

In Figure IV.3.8 the fractured surface morphology after impact tests of Bio-HDPE with different percentages of treated CSF with APS are shown in order to evaluate filler-matrix interactions. In Figure IV.3.8a the typical irregular and rough surface of a ductile polymer like Bio-HDPE is shown, where an absence of CSF particles is observed. In general, after addition of CSF particles, highlighted in yellow arrows (Figures IV.3.8b-e), good bonding by Bio-HDPE matrix was observed. As mentioned previously, CSF particles treated with APS showed improved compatibility with matrix reducing the gap between phases. Nevertheless, as higher CSF particle addition levels, more presence of small gaps in the perimeter between CSF and the surrounding Bio-HDPE matrix was observed as marked by orange arrows. It is known that a higher presence of particles in the matrix, despite using compatibilizers, generates more voids between particles and the matrix [89]. This fact causes an increment of stress concentrators and therefore a loss of mechanical properties as was shown previously [85]. Similar findings were obtained by Garcia-Garcia *et al.* [61] who evaluated different percentages of peanut shell powder (PSN) in a Bio-HDPE matrix, where despite the use of compatibilizers, some voids between particles and the matrix causing a decrease in elongation at break and tensile strength are still observed.

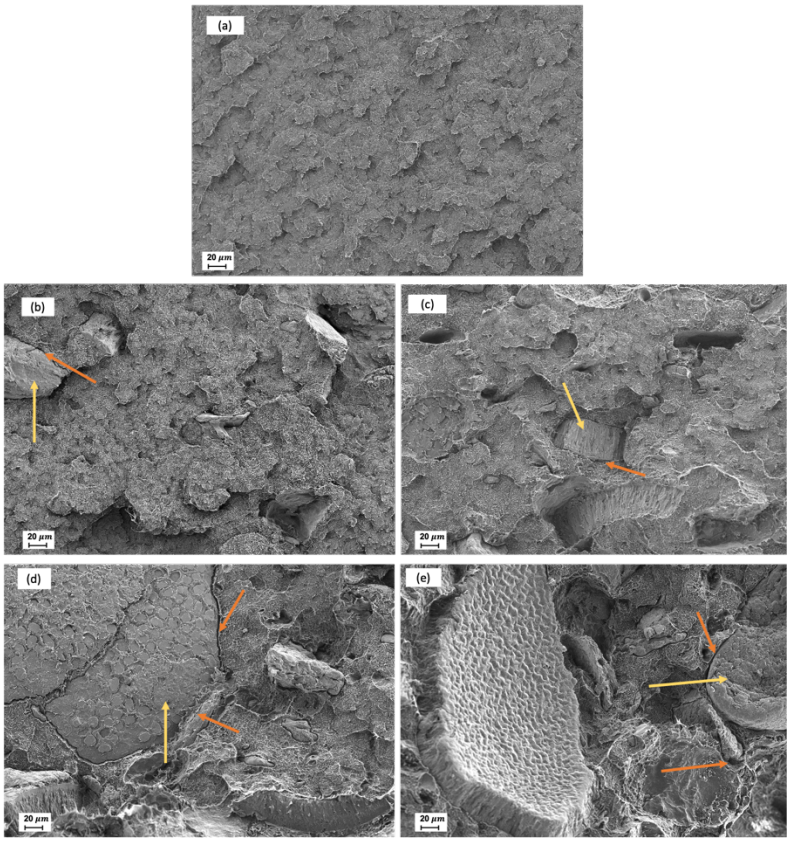

Figure IV.3.8. Fracture surface morphology of Charpy test by FESEM at 250 × with different percentage of treated chia seed flour: (a) Bio-based high-density polyethylene; (b) 10 wt.%; (c) 20 wt.% (d) 30 wt.%; I 40 wt.%.

DMTA in torsion mode, plotted in Figure IV.3.9, represents the evolution of storage modulus (G') with respect to temperature for Bio-HDPE and different composites developed with Bio-HDPE and CSF. Storage modulus, which is related to the stiffness of a material, decreased as the temperature increased for all analyzed samples. However, the addition of filler increased the storage modulus values regarding neat Bio-HDPE, with higher values as the CSF content increases. This was more clearly observed at low temperatures (−100 to −80 °C). With respect to room temperature, it was observed that the 40T sample presents a G' of 105 Mpa, which represents an increment of 20% compared to neat Bio-HDPE. This fact confirmed the reinforcing effect that CSF filler provides, which acts as an interlock point in Bio-HDPE matrix that leads to restricted chain mobility, thus increasing the stiffening behaviour of composites [63]. This trend was also measured previously in tensile and flexural modulus. In addition, a similar behavior has been reported by Barczewski *et al.* [20] who evaluated different linseed cake (LC) percentages in HDPE composites. In

this study, an increase of G' with addition of LC was also observed, being more noticeable at low temperatures.

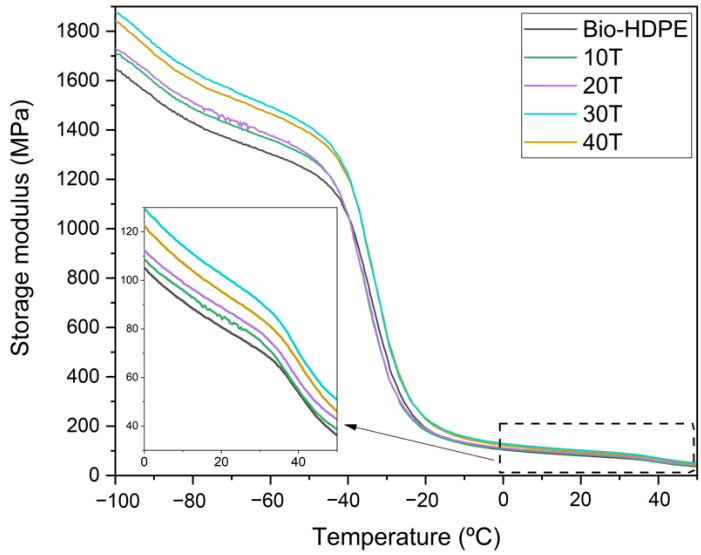

Figure IV.3.9. Evolution of storage modulus (G') in bio-based high-density polyethylene (Bio-HDPE) with different weight percentage of treated chia seed flour with APS.

Thermal analysis was performed in order to assess the main thermal transitions and thermal stability for Bio-HDPE and different composites developed with Bio-HDPE and CSF. Thermal parameters obtained by DSC are gathered in Table IV.3.5. It was observed that the addition of CSF to the Bio-HDPE matrix barely affects the melting temperature. Regarding crystallinity, which is directly related to melting enthalpy (ΔH_m), it was increased with the presence of a low amount of filler (10 and 20 wt.%). This increment in the crystallinity was due to the nucleating effect provided by the CSF filler [90]. However, a CSF content higher than 20 wt.% led to a decrease of the crystallinity with the lowest value being 49.1% for 40 wt.% of CSF. In general, the crystallinity of composites reinforced with particles depends on two factors: the first is the nucleation effect of fillers and the second is the hindering effect produced by fillers that difficult the movement of molecular chains. However, although filler presented a nucleation effect, high amounts of filler such as 30 and 40 wt.% lead to difficulties in the arrangement of molecular chains, thus decreasing the crystallinity [91]. This tendency was also reported by Xiong *et al.* [59] who evaluated HDPE with wood flour with different coupling agents.

Table IV.3.5. Main thermal parameters of Bio-HDPE with different weight percentage of treated chia seed flour with APS obtained using DSC.

Reference	Tm (°C)[-1]	ΔHm (J g^{-1})[2]	Xc (%)[3]
Bio-HDPE[4]	131.0	154.2	55.8
10T [5]	131.8	151.4	59.2
20T [5]	131.5	126.1	57.8
30T [5]	130.8	105.7	51.5
40T [5]	131.0	86.3	49.1

[1] Melt temperature; [2] Melt enthalpy; [3] Degree of crystallization; [4] Bio-based high-density polyethylene; [5] wt.% of treated chia seed flour.

In Figure IV.3.10 both TGA curves and their first derivative (DTG) of different composites developed with Bio-HDPE and CSF are plotted. Bio-HDPE presented a temperature for a weight loss of 5 wt.% ($T_{5\%}$) of around 460.3 °C. The addition of CSF particles in the Bio-HDPE matrix led to a decrease of $T_{5\%}$ as CSF filler was added. As shown in Figure IV.3.10a, $T_{5\%}$ was reduced from 460.3 °C (Bio-HDPE) to 262.3 °C for the 40T sample, which means a decrease of 43%; hence, reduced thermal stability compared to neat Bio-HDPE. This decrease of $T_{5\%}$ is due to the decomposition of the lignocellulosic filler produced in the 220–410 °C range, as exposed previously. In addition, a higher temperature of 410 °C was related to Bio-HDPE degradation, not showing significant changes. Finally, the residual weight recorded from 520 °C to 700 °C, was higher as CSF filler was added, probably due to the presence of more ash content [92]. In Figure IV.3.10b the first derivative is shown, where two maximum degradation stages in composite reinforced with CSF are clearly observed. The first stage (T_{max1}) was related to CSF filler degradation which occurred at about 338 °C, and the second stage (T_{max2}) with Bio-HDPE degradation at 498 °C. As can be observed, the addition of CSF to the matrix does not affect the T_{max1} and T_{max2}. Similar findings have been reported by Yong *et al.* [93] for wood plastic composites using polyethylene and wood fiber with different formulations.

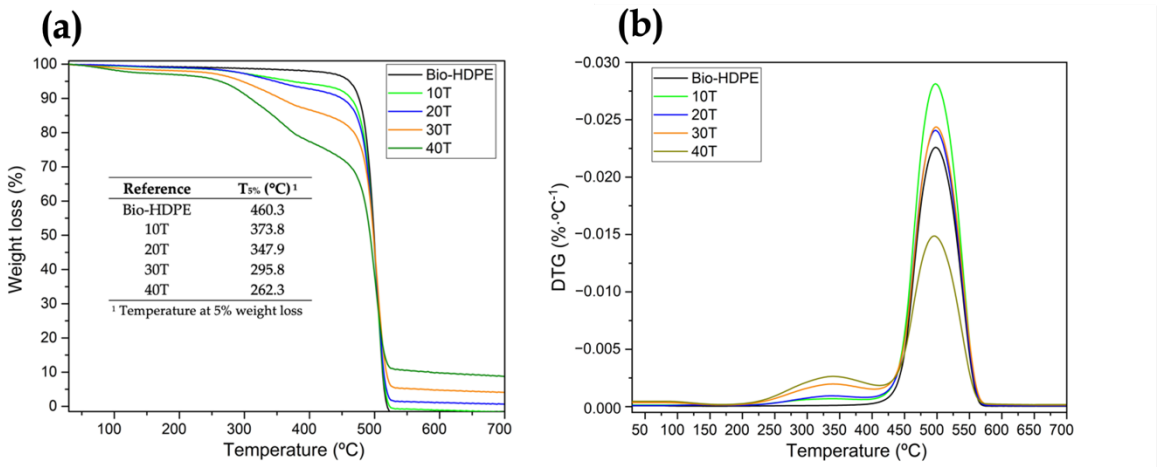

Figure IV.3.10. Thermal parameters of degradation of bio-based high-density polyethylene (Bio-HDPE) with different weight percentage of treated chia seed flour with APS. (a) Weight loss; (b) Derivative thermogravimetry. $T_{5\%}$ is temperature at 5% weight loss; T_{max1} and T_{max2} is maximum degradation temperature for first and second stage.

Water absorption of Bio-HDPE with different percentages of CSF filler have been measured. The results obtained after 18 weeks are shown in Figure IV.3.11. This phenomenon depends on the capabilities of matrix and filler to absorb water. Firstly, Bio-HDPE presented less than 0.05% of water absorption which confirms its hydrophobic nature. The addition of CSF filler provided an increment of water absorption due to the hydrophilic nature of CSF, as was described previously. In agreement with the literature, initially a higher water absorption was observed that gradually slows down until saturation was achieved, being in this case at 18 weeks [94]. The addition up to 20 wt.% presented a slight increase in water absorption reaching almost 3%. However, a notable increase was observed for 30 and 40 wt.% of CSF, where values of 8.25% and 11% were obtained, respectively. This increment of water absorption could be attributed to the presence of mucilage in CSF, which is a polysaccharide gum that represents about 6% of the weight and provides higher water-holding capacity [80]. Chen *et al.* [95] studied the water uptake of rice husk (RH) in a HDPE matrix, reaching values of about 7% with 40 wt.%. Furthermore, Liu *et al.* [96] has also reported a water absorption of less than 11% with 50 wt.% of wood flour in a PP matrix, observing a lower value compared to a 40T sample. Nevertheless, general values of water absorption in WPCs are around 14–16% [95,97,98]. Therefore,

although Bio-HDPE with CSF particles presented higher values than some WPCs, probably due to the presence of mucilage, it remained below that of general WPCs.

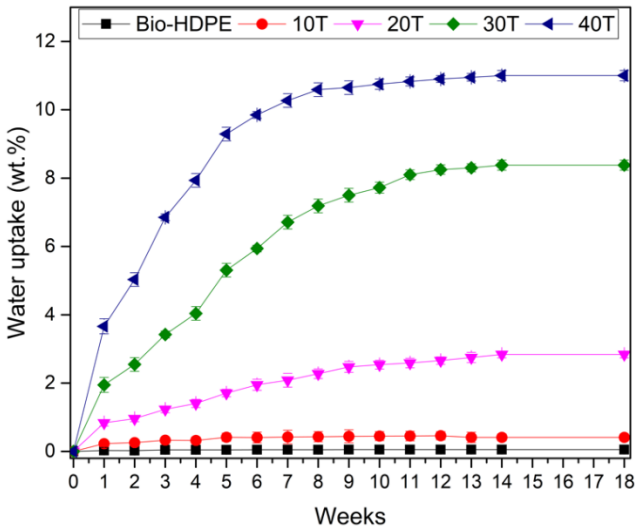

Figure IV.3.11.. Water uptake of bio-based high-density polyethylene (Bio-HDPE) with different weight percentage of treated chia seed flour with APS.

The appearence of materials with fillers are crucial to imitate wood as closely as possible. Parameters such as colour or luminance are important in this approach. Colour coordinates of different Bio-HDPE/CSF composites are gathered in Table IV.3.6 by the values of L*(luminance), a* (green to red), b* (blue to yellow) and colour change (ΔE_{ab}^{*}). Moreover, the visual appearance of samples is shown in Figure IV.3.12. Firstly, the sample with highest luminance was Bio-HDPE, caused by its white colour with a value of 71.3. With the addition of lignocellulosic filler, luminance was reduced in the range of 36.6–42.5 compared to neat Bio-HDPE. Regarding a*, Bio-HDPE presented a negative value of −2.6 which was close to 0 that indicates the closeness to white colour. On the contrary, the rest of samples had positive values due to the characteristic brown colour of chia seed flour [99]. Higher values of a* coordinate have been reported by Jorda-Reolid *et al.* [100] who employed Bio-HDPE with argan shell wastes. In this study a higher a* value above 5 was reported, thus a reddish brown colour was obtained [100]. Referring to colour coordinate b*, it is an indicative of blue to yellow colours. Bio-HDPE presented a negative value of –2.68 which is in concordance with Rojas *et al.* [67]. The rest of samples had values between 5.72 and 8 which indicate a tonality approaching yellow. Regarding the colour change variation,

it should be noted that a difference of colour change between Bio-HDPE and CSF composites exists. This change was more noticeable as the addition of CSF fillers was increased.

Table IV.3.6. Colour coordinates (L*, a*, b*) for different weight percentage of treated chia seed flour with APS.

Reference	L*[1]	a*[2]	b*[3]	Δ_{Eab}*[4]
Bio-HDPE	71.3 ± 0.3	−2.6 ± 0.1	−2.68 ± 0.02	
10T[5]	42.5 ± 0.1	4.15 ± 0.08	6.92 ± 0.1	31.1
20T[5]	42.1 ± 0.2	4.89 ± 0.2	7.96 ± 0.1	32.0
30T[5]	36.6 ± 0.1	4.24 ± 0.07	5.72 ± 0.09	36.3
40T[5]	37.2 ± 0.1	4.65 ± 0.1	6.73 ± 0.08	36.1

[1] Luminance; [2] Green to red; [3] Blue to yellow; [4] Colour change regarding neat bio-based high-density polyethylene (Bio-HDPE); [5] wt.% of treated chia seed flour.

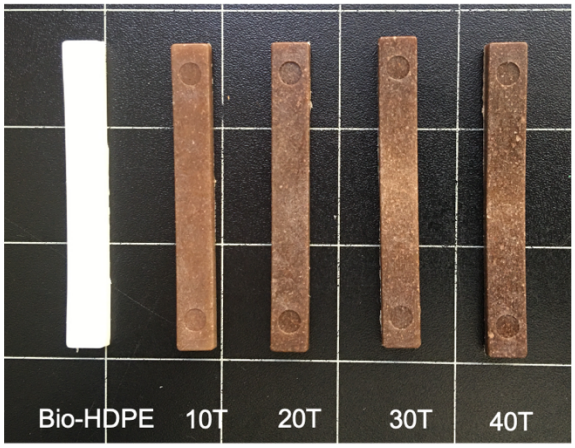

Figure IV.3.12. Visual appearance of bio-based high-density polyethylene (Bio-HDPE) with different weight percentage of treated chia seed flour with APS.

The disintegration process of Bio-HDPE with different percentages of CSF is plotted in Figure IV.3.13. As it was mentioned previously, Bio-HDPE is a non-biodegradable polymer and no sign of weight loss was recorded after 90 days. The absence of hydrolysable zones in its structure that can be attacked by microorganisms means that after 90 days of testing, the disintegrated mass is almost nil. However, the addition of CSF filler, as expected, increased the disintegration rate up to 6% weight loss after only 8 days for a 40T sample. It is known that lignocellulosic filler, which is

composed of lignin, hemicellulose and cellulose, is biodegraded by microorganisms [84]. Disintegration weight loss was greatly increased up to 21 days with addition of filler, where 16.5% of weight loss was measured in the 40T sample. However, from 21 to 90 days only a slight increase from 16.5% up to 20% was shown by the 40T sample. The applied standard, ISO 20200, establishes that any substance from developed composites that is able to pass through a 2 mm sieve is considered as a degraded material. These disintegrated materials are composed mostly of lignocellulosic fillers and possibly microplastics. The eventual microplastic formed may be further degraded by other additional mechanism such as thermo-oxidative or photo-oxidative degradation, leading to formation of a more hydrophilic layer then suitable for microorganism degradation [101]. This last mechanism will take a longer time as well as will depend on abiotic factor before microorganisms can assimilate it. Therefore, following the definition of biodegradable polymer established by the UNE EN 13432 standard, which establishes that the disintegration rate after 90 days of testing must be greater than 90% by weight, the composite developed cannot be considered as totally biodegradable, but it can be considered partially biodegradable. Another crucial aspect was the visual appearance of composites after 12 weeks, which is shown in Figure IV.3.14. With the addition of CSF, the appearance change was more noticeable due to the disintegration rate compared to the initial day (Figure IV.3.10), and 30T and 40T samples displayed a more brittle aspect. Therefore, it could be concluded that, although is not considerable a fully biodegradable WPC, it is partially biodegradable.

Therefore, although a fully biodegradable WPC is not obtained, the addition of a residue from the extraction of chia oil allows the development of a composite with the balanced properties provided by the bio-HDPE and with a biodegradability of around 20% by weight of the composite after 12 weeks of testing. Among interesting areas of applications, the packaging sector could be highlighted due to its partially biodegradability in order to reduce the environmental impact.

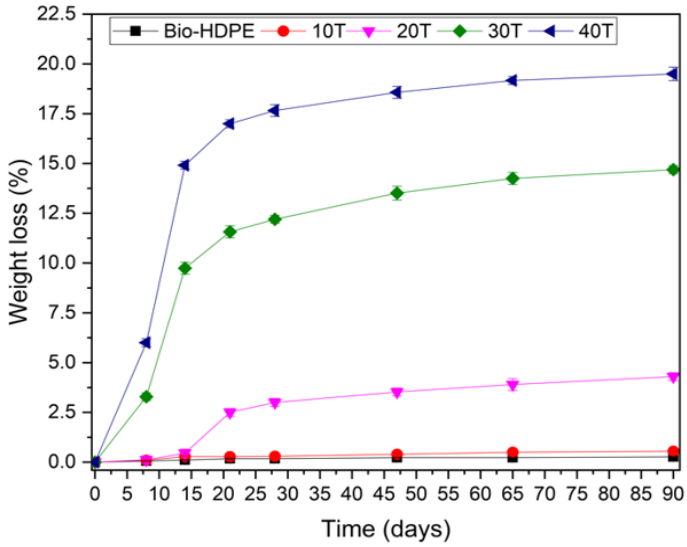

Figure IV.3.13. Weight loss of bio-based high-density polyethylene (Bio-HDPE) with different weight percentage of treated chia seed flour with APS.

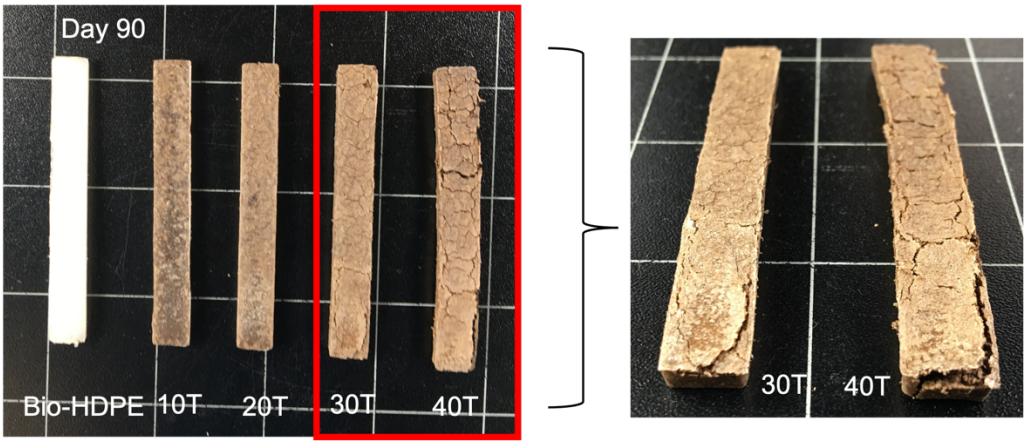

Figure IV.3.14. Visual appearance of disintegration of bio-based high-density polyethylene (Bio-HDPE) with different weight percentage of treated chia seed flour with APS under compost conditions.

Conclusions

In this work, a new composite was obtained from the residual waste remaining after chia seed oil extraction. In the first stage, the effect of a silane coupling agent [3-(2-aminoethylamine) propyl]-trimethoxysilane (APS) treatment were examined by comparing untreated and treated samples with 20 wt. %. The improvement of interfacial adhesion between treated CSF with APS and Bio-HDPE matrix was observed by FESEM. As a result of this better interaction, an enhancement in general

mechanical properties was obtained compared to untreated CSF, with an improvement of 41% in elongation at break. Regarding water uptake, the sample with APS recorded a decrease of 17% compared to untreated sample, caused by the reduction of available hydroxyl groups in the lignocellulosic filler. Consequently, in the test of disintegration under composting conditions, a sample treated with APS recorded a reduction of the weight loss of 50% due to its more hydrophobic nature resulting from the silane treatment which hinders the penetration of water and microorganisms.

In the second stage, an optimization of the amount of CSF filler has been carried out. The addition of 40 wt.% of CSF resulted in improvements of 22% and 18% in tensile and flexural modulus compared to neat Bio-HDPE, respectively. The addition of CSF caused a slight decrease of thermal stability due to the presence of lignocellulosic filler, but aesthetically, the characteristic brown colour of the composites developed made them suitable to for manufacturing furniture or food packaging. The degree of water uptake was similar to that of other wood plastic composites on the market, while the study of disintegration by composting shows a weight loss ratio 20% higher than that of Bio-HDPE, a positive aspect to be taken into account in the development of new composites for sectors with products with short life cycles.

Acknowledgements

I. D-C wants to thank Universitat Politècnica de València for his FPI grant (PAID-2019-SP20190013) and Generalitat Valenciana (GVA) for his FPI grant (ACIF/2020/233).

References

[1] Europe, P. Plastics—The facts 2020: An analysis of European Plastics Production, Demand and Waste. Available online: https://www.plasticseurope.org/download_file/force/4829/181 (accessed on 29 April 2021)

[2] Luzi, F.; Torre, L.; Kenny, J.M.; Puglia, D. Bio- and Fossil-Based Polymeric Blends and Nanocomposites for Packaging: Structure-Property Relationship. Materials 2019, 12, doi:10.3390/ma12030471.

[3] Lithner, D.; Larsson, A.; Dave, G. Environmental and health hazard ranking and assessment of plastic polymers based on chemical composition. Sci. Total Environ. 2011, 409, 3309–3324, doi:10.1016/j.scitotenv.2011.04.038.

[4] Ahvenainen, R. Novel Food Packaging Techniques; Elsevier: Amsterdam, The Netherlands, 2003.

[5] Mangaraj, S.; Yadav, A.; Bal, L.M.; Dash, S.; Mahanti, N.K. Application of biodegradable polymers in food packaging industry: A comprehensive review. J. Packag. Technol. Res. 2019, 3, 77–96.

[6] Niaounakis, M. Biopolymers: Processing and Products; William Andrew: Amsterdam, The Netherlands, 2014.

[7] Varganici, C.-D.; Rosu, L.; Rosu, D.; Mustata, F.; Rusu, T. Sustainable wood coatings made of epoxidized vegetable oils for ultraviolet protection. Environ. Chem. Lett. 2021, 19, 307–328, doi:10.1007/s10311-020-01067-w.

[8] Carlos Ronda, J.; Lligadas, G.; Galia, M.; Cadiz, V. Vegetable oils as platform chemicals for polymer synthesis. Eur. J. Lipid Sci. Technol. 2011, 113, 46–58, doi:10.1002/ejlt.201000103.

[9] de Espinosa, L.M.; Meier, M.A.R. Plant oils: The perfect renewable resource for polymer science?! Eur. Polym. J. 2011, 47, 837–852, doi:10.1016/j.eurpolymj.2010.11.020.

[10] Production of vegetable oils worldwirde since 2000. Available online: https://www.statista.com/statistics/263933/production-of-vegetable-oils-worldwide-since-2000/ (accessed on 1 April 2021).

[11] Lee, S.H.; Ashaari, Z.; Lum, W.C.; Halip, J.A.; Ang, A.F.; Tan, L.P.; Chin, K.L.; Tahir, P.M. Thermal treatment of wood using vegetable oils: A review. Constr. Build. Mater. 2018, 181, 408–419, doi:10.1016/j.conbuildmat.2018.06.058.

[12] Jin, F.L.; Park, S.J. Thermomechanical behavior of epoxy resins modified with epoxidized vegetable oils. Polym. Int. 2008, 57, 577–583, doi:10.1002/pi.2280.

[13] Xu, Y.Q.; Qu, J.P. Mechanical and Rheological Properties of Epoxidized Soybean Oil Plasticized Poly(lactic acid). J. Appl. Polym. Sci. 2009, 112, 3185–3191, doi:10.1002/app.29797.

[14] Fenollar, O.; Garcia-Sanoguera, D.; Sanchez-Nacher, L.; Lopez, J.; Balart, R. Effect of the epoxidized linseed oil concentration as natural plasticizer in vinyl plastisols. J. Mater. Sci. 2010, 45, 4406–4413.

[15] Arrieta, M.P.; Samper, M.; Jiménez-López, M.; Aldas, M.; López, J. Combined effect of linseed oil and gum rosin as natural additives for PVC. Ind. Crops Prod. 2017, 99, 196–204.

[16] Baryeh, E.A. Effects of palm oil processing parameters on yield. J. Food Eng. 2001, 48, 1–6, doi:10.1016/s0260-8774(00)00137-0.

[17] Jokic, S.; Nagy, B.; Zekovic, Z.; Vidovic, S.; Bilic, M.; Velic, D.; Simandi, B. Effects of supercritical CO2 extraction parameters on soybean oil yield. Food Bioprod. Process. 2012, 90, 693–699, doi:10.1016/j.fbp.2012.03.003.

[18] Kasote, D.M.; Badhe, Y.S.; Hegde, M.V. Effect of mechanical press oil extraction processing on quality of linseed oil. Ind. Crop. Prod. 2013, 42, 10–13, doi:10.1016/j.indcrop.2012.05.015.

[19] Ajila, C.M.; Brar, S.K.; Verma, M.; Tyagi, R.D.; Godbout, S.; Valero, J.R. Bio-processing of agro-byproducts to animal feed. Crit. Rev. Biotechnol. 2012, 32, 382–400, doi:10.3109/07388551.2012.659172.

[20] Barczewski, M.; Mysiukiewicz, O.; Klozinski, A. Complex modification effect of linseed cake as an agricultural waste filler used in high density polyethylene composites. Iran. Polym. J. 2018, 27, 677–688, doi:10.1007/s13726-018-0644-3.

[21] Zuhri, M.Y.M.; Sapuan, S.M.; Ismail, N. Oil Palm Fibre Reinforced Polymer Composites: A Review. Prog. Rubber Plast. Recycl. Technol. 2009, 25, 233–246, doi:10.1177/147776060902500403.

[22] Fuqua, M.A.; Chevali, V.S.; Ulven, C.A. Lignocellulosic byproducts as filler in polypropylene: Comprehensive study on the effects of compatibilization and loading. J. Appl. Polym. Sci. 2013, 127, 862–868, doi:10.1002/app.37820.

[23] Paciorek-Sadowska, J.; Borowicz, M.; Isbrandt, M.; Czuprynski, B.; Apiecionek, L. The Use of Waste from the Production of Rapeseed Oil for Obtaining of New Polyurethane Composites. Polymers 2019, 11, doi:10.3390/polym11091431.

[24] Huang, L.; Mu, B.S.; Yi, X.; Li, S.J.; Wang, Q.W. Sustainable Use of Coffee Husks for Reinforcing Polyethylene Composites. J. Polym. Environ. 2018, 26, 48–58, doi:10.1007/s10924-016-0917-x.

[25] Sanjay, M.R.; Madhu, P.; Jawaid, M.; Senthamaraikannan, P.; Senthil, S.; Pradeep, S. Characterization and properties of natural fiber polymer composites: A comprehensive review. J. Clean. Prod. 2018, 172, 566–581, doi:10.1016/j.jclepro.2017.10.101.

[26] Li, X.; Lei, B.; Lin, Z.; Huang, L.; Tan, S.; Cai, X. The utilization of bamboo charcoal enhances wood plastic composites with excellent mechanical and thermal properties. Mater. Des. 2014, 53, 419–424, doi:10.1016/j.matdes.2013.07.028.

[27] Ivorra-Martinez, J.; Manuel-Manogil, J.; Boronat, T.; Sanchez-Nacher, L.; Balart, R.; Quiles-Carrillo, L. Development and Characterization of Sustainable Composites from Bacterial Polyester Poly(3-Hydroxybutyrate-co-3-hydroxyhexanoate) and Almond Shell Flour by Reactive Extrusion with Oligomers of Lactic Acid. Polymers 2020, 12, doi:10.3390/polym12051097.

[28] Ali, N.M.; Yeap, S.K.; Ho, W.Y.; Beh, B.K.; Tan, S.W.; Tan, S.G. The Promising Future of Chia, *Salvia hispanica L.* J. Biomed. Biotechnol. 2012, doi:10.1155/2012/171956.

[29] Sales volume of chia seeds worldwide in 2017, by type. Available online: https://www.statista.com/statistics/860314/global-chia-seed-sales-volume-by-type/ (accessed on 15 April 2021).

[30] Chia Seeds Market Size Worth $4.7 Billion By 2025. Available online: https://www.grandviewresearch.com/press-release/global-chia-seeds-market (accessed on 17 April 2021).

[31] Shen, Y.B.; Zheng, L.Y.; Jin, J.; Li, X.J.; Fu, J.N.; Wang, M.Z.; Guan, Y.F.; Song, X. Phytochemical and Biological Characteristics of Mexican Chia Seed Oil. Molecules 2018, 23, doi:10.3390/molecules23123219.

[32] Cofrades, S.; Santos-López, J.; Freire, M.; Benedí, J.; Sánchez-Muniz, F.; Jiménez-Colmenero, F. Oxidative stability of meat systems made with W1/O/W2 emulsions prepared with hydroxytyrosol and chia oil as lipid phase. LWT Food Sci. Technol. 2014, 59, 941–947.

[33] Timilsena, Y.P.; Vongsvivut, J.; Adhikari, R.; Adhikari, B. Physicochemical and thermal characteristics of Australian chia seed oil. Food Chem. 2017, 228, 394–402, doi:10.1016/j.foodchem.2017.02.021.

[34] Dominguez-Candela, I.; Ferri, J.M.; Cardona, S.C.; Lora, J.; Fombuena, V. Dual Plasticizer/Thermal Stabilizer Effect of Epoxidized Chia Seed Oil (*Salvia hispanica L.*) to Improve Ductility and Thermal Properties of Poly (Lactic Acid). Polymers 2021, 13, 1283.

[35] Darie, R.N.; Bercea, M.; Kozlowski, M.; Spiridon, I. Evaluation of properties of LDPE/oak wood composites exposed to artificial ageing. Cellul. Chem. Technol. 2011, 45, 127–135.

[36] Shah, H.L.; Matuana, L.M. Novel coupling agents for PVC/wood-flour composites. J. Vinyl Addit. Technol. 2005, 11, 160–165, doi:10.1002/vnl.20056.

[37] Kaseem, M.; Hamad, K.; Deri, F.; Ko, Y.G. Effect of Wood Fibers on the Rheological and Mechanical Properties of Polystyrene/Wood Composites. J. Wood Chem. Technol. 2017, 37, 251–260, doi:10.1080/02773813.2016.1272127.

[38] Goldemberg, J.; Coelho, S.T.; Guardabassi, P. The sustainability of ethanol production from sugarcane. Energy Policy 2008, 36, 2086–2097, doi:10.1016/j.enpol.2008.02.028.

[39] Babu, R.P.; O'connor, K.; Seeram, R. Current progress on bio-based polymers and their future trends. Progress Biomater. 2013, 2, 1–16.

[40] Siracusa, V.; Blanco, I. Bio-Polyethylene (Bio-PE), Bio-Polypropylene (Bio-PP) and Bio-Poly(ethylene terephthalate) (Bio-PET): Recent Developments in Bio-Based Polymers Analogous to Petroleum-Derived Ones for Packaging and Engineering Applications. Polymers 2020, 12, doi:10.3390/polym12081641.

[41] Taşdemır, M.; Biltekin, H.; Caneba, G.T. Preparation and characterization of LDPE and PP—Wood fiber composites. J. Appl. Polym. Sci. 2009, 112, 3095–3102.

[42] Zahedi, M.; Tabarsa, T.; Ashori, A.; Madhoushi, M.; Shakeri, A. A comparative study on some properties of wood plastic composites using canola stalk, Paulownia, and nanoclay. J. Appl. Polym. Sci. 2013, 129, 1491–1498.

[43] Petchwattana, N.; Covavisaruch, S.; Chanakul, S. Mechanical properties, thermal degradation and natural weathering of high density polyethylene/rice hull composites compatibilized with maleic anhydride grafted polyethylene. J. Polym. Res. 2012, 19, 1–9.

[44] Boronat, T.; Fombuena, V.; Garcia-Sanoguera, D.; Sanchez-Nacher, L.; Balart, R. Development of a biocomposite based on green polyethylene biopolymer and eggshell. Mater. Des. 2015, 68, 177–185, doi:10.1016/j.matdes.2014.12.027.

[45] Fombuena, V.; Petrucci, R.; Dominici, F.; Jorda-Vilaplana, A.; Montanes, N.; Torre, L. Maleinized Linseed Oil as Epoxy Resin Hardener for Composites with

High Bio Content Obtained from Linen Byproducts. Polymers 2019, 11, doi:10.3390/polym11020301.

[46] Jordá-Vilaplana, A.; Carbonell-Verdú, A.; Samper, M.-D.; Pop, A.; Garcia-Sanoguera, D. Development and characterization of a new natural fiber reinforced thermoplastic (NFRP) with Cortaderia selloana (Pampa grass) short fibers. Compos. Sci. Technol. 2017, 145, 1–9.

[47] Carbonell-Verdú, A.; García-García, D.; Jordá, A.; Samper, M.; Balart, R. Development of slate fiber reinforced high density polyethylene composites for injection molding. Compos. Part. B Eng. 2015, 69, 460–466.

[48] Fombuena, V.; Bernardi, L.; Fenollar, O.; Boronat, T.; Balart, R. Characterization of green composites from biobased epoxy matrices and bio-fillers derived from seashell wastes. Mater. Design 2014, 57, 168–174, doi:10.1016/j.matdes.2013.12.032.

[49] Pickering, K.L.; Abdalla, A.; Ji, C.; McDonald, A.; Franich, R.A. The effect of silane coupling agents on radiata pine fibre for use in thermoplastic matrix composites. Compos. Part. A Appl. Sci. Manuf. 2003, 34, 915–926.

[50] Salon, M.C.B.; Gerbaud, G.; Abdelmouleh, M.; Bruzzese, C.; Boufi, S.; Belgacem, M.N. Studies of interactions between silane coupling agents and cellulose fibers with liquid and solid-state NMR. Magn. Reson. Chem. 2007, 45, 473–483.

[51] Xie, Y.; Hill, C.A.; Xiao, Z.; Militz, H.; Mai, C. Silane coupling agents used for natural fiber/polymer composites: A review. Compos. Part. A Appl. Sci. Manuf. 2010, 41, 806–819.

[52] Zhu, J.; Zhu, H.; Njuguna, J.; Abhyankar, H. Recent development of flax fibres and their reinforced composites based on different polymeric matrices. Materials 2013, 6, 5171–5198.

[53] Wunderlich, B. Thermal Analysis; Elsevier: New York, NY, USA, 1990.

[54] Quiles-Carrillo, L.; Blanes-Martínez, M.; Montanes, N.; Fenollar, O.; Torres-Giner, S.; Balart, R. Reactive toughening of injection-molded polylactide pieces using maleinized hemp seed oil. Eur. Polym. J. 2018, 98, 402–410.

[55] Aguero, A.; del Carmen Morcillo, M.; Quiles-Carrillo, L.; Balart, R.; Boronat, T.; Lascano, D.; Torres-Giner, S.; Fenollar, O. Study of the Influence of the Reprocessing Cycles on the Final Properties of Polylactide Pieces Obtained by Injection Molding. Polymers 2019, 11, doi:10.3390/polym11121908.

[56] Ixtaina, V.Y.; Martinez, M.L.; Spotorno, V.; Mateo, C.M.; Maestri, D.M.; Diehl, B.W.K.; Nolasco, S.M.; Tomas, M.C. Characterization of chia seed oils obtained by pressing and solvent extraction. J. Food Compos. Anal. 2011, 24, 166–174, doi:10.1016/j.jfca.2010.08.006.

[57] Ge, X.; Li, X.; Meng, Y. Tensile properties, morphology, and thermal behavior of PVC composites containing pine flour and bamboo flour. J. Appl. Polym. Sci. 2004, 93, 1804–1811.

[58] Abdelmouleh, M.; Boufi, S.; Belgacem, M.N.; Dufresne, A. Short natural-fibre reinforced polyethylene and natural rubber composites: Effect of silane coupling agents and fibres loading. Compos. Sci. Technol. 2007, 67, 1627–1639, doi:10.1016/j.compscitech.2006.07.003.

[59] Xiong, C.; Qi, R.; Wang, Y. Wood-Thermoplastic Composites from Wood Flour and High-Density Polyethylene. J. Appl. Polym. Sci. 2009, 114, 1160–1168, doi:10.1002/app.30707.

[60] Ihamouchen, C.; Djidjelli, H.; Boukerrou, A.; Krim, S.; Kaci, M.; Martinez, J.J. Effect of Surface Treatment on the Physicomechanical and Thermal Properties of High-Density Polyethylene/Olive Husk Flour Composites. J. Appl. Polym. Sci. 2012, 123, 1310–1319, doi:10.1002/app.34172.

[61] Garcia-Garcia, D.; Carbonell-Verdu, A.; Jorda-Vilaplana, A.; Balart, R.; Garcia-Sanoguera, D. Development and characterization of green composites from

bio-based polyethylene and peanut shell. J. Appl. Polymer. Sci. 2016, 133, doi:10.1002/app.43940.

[62] Fonseca, L.P.; Waldman, W.R.; De Paoli, M.A. ABS composites with cellulose fibers: Towards fiber-matrix adhesion without surface modification. Compos. Part. C Open Access 2021, 5, 100142.

[63] Balart, J.F.; Garcia-Sanoguera, D.; Balart, R.; Boronat, T.; Sanchez-Nacher, L. Manufacturing and properties of biobased thermoplastic composites from poly(lactid acid) and hazelnut shell wastes. Polymer. Compos. 2018, 39, 848–857, doi:10.1002/pc.24007.

[64] Maziad, N.A.; El-Nashar, D.E.; Sadek, E.M. The effects of a silane coupling agent on properties of rice husk-filled maleic acid anhydride compatibilized natural rubber/low-density polyethylene blend. J. Mater. Sci. 2009, 44, 2665–2673, doi:10.1007/s10853-009-3349-3.

[65] Gharbi, A.; Hassen, R.B.; Boufi, S. Composite materials from unsaturated polyester resin and olive nuts residue: The effect of silane treatment. Ind. Crops Prod. 2014, 62, 491–498, doi:10.1016/j.indcrop.2014.09.012.

[66] Liu, Y.; Lv, X.; Bao, J.; Xie, J.; Tang, X.; Che, J.; Ma, Y.; Tong, J. Characterization of silane treated and untreated natural cellulosic fibre from corn stalk waste as potential reinforcement in polymer composites. Carbohydr. Polym. 2019, 218, 179–187.

[67] Rojas-Lema, S.; Torres-Giner, S.; Quiles-Carrillo, L.; Gomez-Caturla, J.; Garcia-Garcia, D.; Balart, R. On the Use of Phenolic Compounds Present in Citrus Fruits and Grapes as Natural Antioxidants for Thermo-Compressed Bio-Based High-Density Polyethylene Films. Antioxidants 2021, 10, doi:10.3390/antiox10010014.

[68] Toro, P.; Quijada, R.; Arias, J.L.; Yazdani-Pedram, M. Mechanical and morphological studies of poly(propylene)-filled eggshell composites. Macromol. Mater. Eng. 2007, 292, 1027–1034, doi:10.1002/mame.200700147.

[69] Bijaisoradat, O.; Yue, L.; Manas-Zloczower, I.; Manuspiya, H. Wood flour-high density polyethylene composites: Influence of silanization and esterification on mechanical properties. J. Appl. Polym. Sci. 2021, 138, doi:10.1002/app.50197.

[70] Petinakis, E.; Yu, L.; Edward, G.; Dean, K.; Liu, H.; Scully, A.D. Effect of matrix–particle interfacial adhesion on the mechanical properties of poly (lactic acid)/wood-flour micro-composites. J. Polym. Environ. 2009, 17, 83–94.

[71] Quiles-Carrillo, L.; Montava-Jorda, S.; Boronat, T.; Sammon, C.; Balart, R.; Torres-Giner, S. On the Use of Gallic Acid as a Potential Natural Antioxidant and Ultraviolet Light Stabilizer in Cast-Extruded Bio-Based High-Density Polyethylene Films. Polymers 2020, 12, doi:10.3390/polym12010031.

[72] Chun, K.S.; Husseinsyah, S.; Osman, H. Mechanical and thermal properties of coconut shell powder filled polylactic acid biocomposites: Effects of the filler content and silane coupling agent. J. Polym. Res. 2012, 19, 1–18.

[73] Srubar, W.V., III.; Pilla, S.; Wright, Z.C.; Ryan, C.A.; Greene, J.P.; Frank, C.W.; Billington, S.L. Mechanisms and impact of fiber-matrix compatibilization techniques on the material characterization of PHBV/oak wood flour engineered biobased composites. Compos. Sci. Technol. 2012, 72, 708–715, doi:10.1016/j.compscitech.2012.01.021.

[74] Calabia, B.P.; Ninomiya, F.; Yagi, H.; Oishi, A.; Taguchi, K.; Kunioka, M.; Funabashi, M. Biodegradable Poly(butylene succinate) Composites Reinforced by Cotton Fiber with Silane Coupling Agent. Polymers 2013, 5, 128–141, doi:10.3390/polym5010128.

[75] Ueno, T.; Nakashima, E.; Takeda, K. Quantitative analysis of random scission and chain-end scission in the thermal degradation of polyethylene. Polym. Degrad. Stab. 2010, 95, 1862–1869.

[76] Montanes, N.; Garcia-Sanoguera, D.; Segui, V.J.; Fenollar, O.; Boronat, T. Processing and Characterization of Environmentally Friendly Composites from

Biobased Polyethylene and Natural Fillers from Thyme Herbs. J. Polym. Environ. 2018, 26, 1218–1230, doi:10.1007/s10924-017-1025-2.

[77] Peng, M.C.; Sethu, V.; Selvarajoo, A. Performance study of chia seeds, chia flour and Mimosa pudica hydrogel as polysaccharide-based superabsorbent polymers for sanitary napkins. Mater. Today Commun. 2021, 26, doi:10.1016/j.mtcomm.2020.101712.

[78] Lee, S.H.; Wang, S.Q. Biodegradable polymers/bamboo fiber biocomposite with bio-based coupling agent. Compos. Part. A Appl. Sci. Manuf. 2006, 37, 80–91, doi:10.1016/j.compositesa.2005.04.015.

[79] Perthue, A.; Bussiere, P.-O.; Baba, M.; Larche, J.-F.; Therias, S.; Karasu, F.; Croutxe-Barghorn, C. Impact of particle size in PE/ATH composites: The relationship between the interphase and water uptake. Prog. Org. Coat. 2018, 114, 145–153, doi:10.1016/j.porgcoat.2017.10.001.

[80] Verdu, S.; Vasquez, F.; Ivorra, E.; Sanchez, A.J.; Barat, J.M.; Grau, R. Physicochemical effects of chia (*Salvia hispanica L.*) seed flour on each wheat bread-making process phase and product storage. J. Cereal Sci. 2015, 65, 67–73, doi:10.1016/j.jcs.2015.05.011.

[81] Girones, J.; Mendez, J.A.; Boufi, S.; Vilaseca, F.; Mutje, P. Effect of silane coupling agents on the properties of pine fibers/polypropylene composites. J. Appl. Polym. Sci. 2007, 103, 3706–3717, doi:10.1002/app.25104.

[82] Harshvardhan, K.; Jha, B. Biodegradation of low-density polyethylene by marine bacteria from pelagic waters, Arabian Sea, India. Mar. Pollut. Bull. 2013, 77, 100–106, doi:10.1016/j.marpolbul.2013.10.025.

[83] Tokiwa, Y.; Calabia, B.P.; Ugwu, C.U.; Aiba, S. Biodegradability of plastics. Int. J. Mol. Sci. 2009, 10, 3722–3742.

[84] da Silva, A.M.B.; Martins, A.B.; Santana, R.M.C. Biodegradability studies of lignocellulosic fiber reinforced composites. In Fiber Reinforced Composites; Elsevier: Amsterdam, The Netherlands, 2021; pp. 241–271.

[85] García-García, D.; Carbonell, A.; Samper, M.; García-Sanoguera, D.; Balart, R. Green composites based on polypropylene matrix and hydrophobized spend coffee ground (SCG) powder. Compos. Part B Eng. 2015, 78, 256–265.

[86] Zhang, J.; Koubaa, A.; Xing, D.; Liu, W.; Wang, Q.; Wang, X.; Wang, H. Improving lignocellulose thermal stability by chemical modification with boric acid for incorporating into polyamide. Mater. Design 2020, 191, 108589.

[87] Georgopoulos, S.T.; Tarantili, P.; Avgerinos, E.; Andreopoulos, A.; Koukios, E. Thermoplastic polymers reinforced with fibrous agricultural residues. Polym. Degrad. Stab. 2005, 90, 303–312.

[88] Ndiaye, D.; Matuana, L.M.; Morlat-Therias, S.; Vidal, L.; Tidjani, A.; Gardette, J.L. Thermal and mechanical properties of polypropylene/wood-flour composites. J. Appl. Polym. Sci. 2011, 119, 3321–3328.

[89] Ramos, M.; Dominici, F.; Luzi, F.; Jiménez, A.; Garrigós, M.C.; Torre, L.; Puglia, D. Effect of almond shell waste on physicochemical properties of polyester-based biocomposites. Polymers 2020, 12, 835.

[90] Hejna, A.; Barczewski, M.; Kosmela, P.; Mysiukiewicz, O.; Kuzmin, A. Coffee silverskin as a multifunctional waste filler for high-density polyethylene green composites. J. Compos. Sci. 2021, 5, 44.

[91] Liang, Z.; Pan, P.; Zhu, B.; Dong, T.; Inoue, Y. Mechanical and Thermal Properties of Poly(butylene succinate)/Plant Fiber Biodegradable Composite. J. Appl. Polym. Sci. 2010, 115, 3559–3567, doi:10.1002/app.29848.

[92] Hejna, A.; Sulyman, M.; Przybysz, M.; Saeb, M.R.; Klein, M.; Formela, K. On the correlation of lignocellulosic filler composition with the performance properties of poly (ε-caprolactone) based biocomposites. Waste Biomass Valorization 2020, 11, 1467–1479.

[93] Guo, Y.; Zhu, S.; Chen, Y.; Li, D. Thermal Properties of Wood-Plastic Composites with Different Compositions. Materials 2019, 12, doi:10.3390/ma12060881.

[94] Hosseinihashemi, S.K.; Arwinfar, F.; Najafi, A.; Nemli, G.; Ayrilmis, N. Long-term water absorption behavior of thermoplastic composites produced with thermally treated wood. Measurement 2016, 86, 202–208.

[95] Chen, R.S.; Ab Ghani, M.H.; Ahmad, S.; Salleh, M.N.; Tarawneh, M.a.A. Rice husk flour biocomposites based on recycled high-density polyethylene/polyethylene terephthalate blend: Effect of high filler loading on physical, mechanical and thermal properties. J. Compos. Mater. 2015, 49, 1241–1253.

[96] Liu, R.; Peng, Y.; Cao, J.; Chen, Y. Comparison on properties of lignocellulosic flour/polymer composites by using wood, cellulose, and lignin flours as fillers. Compos. Sci. Technol. 2014, 103, 1–7.

[97] Tajvidi, M.; Najafi, S.K.; Moteei, N. Long-term water uptake behavior of natural fiber/polypropylene composites. J. Appl. Polym. Sci. 2006, 99, 2199–2203.

[98] Tamrakar, S.; Lopez-Anido, R.A. Water absorption of wood polypropylene composite sheet piles and its influence on mechanical properties. Constr. Build. Mater. 2011, 25, 3977–3988.

[99] Hatamian, M.; Noshad, M.; Abdanan-Mehdizadeh, S.; Barzegar, H. Effect of roasting treatment on functional and antioxidant properties of chia seed flours. NFS J. 2020, 21, 1–8.

[100] Jorda-Reolid, M.; Gomez-Caturla, J.; Ivorra-Martinez, J.; Stefani, P.M.; Rojas-Lema, S.; Quiles-Carrillo, L. Upgrading Argan Shell Wastes in Wood Plastic Composites with Biobased Polyethylene Matrix and Different Compatibilizers. Polymers 2021, 13, doi:10.3390/polym13060922.

[101] Restrepo-Flórez, J.-M.; Bassi, A.; Thompson, M.R. Microbial degradation and deterioration of polyethylene—A review. Int. Biodeterior. Biodegrad. 2014, 88, 83–90.

polymers

MDPI

Article

Contribution to a Circular Economy Model: From Lignocellulosic Wastes from the Extraction of Vegetable Oils to the Development of a New Composite

Ivan Dominguez-Candela [1], Daniel Garcia-Garcia [2], Aina Perez-Nakai [2], Alejandro Lerma-Canto [2], Jaime Lora [1] and Vicent Fombuena [2,*]

[1] Instituto de Seguridad Industrial, Radiofísica y Medioambiental (ISIRYM), Universitat Politècnica de València (UPV), Plaza Ferrándiz y Carbonell 1, 03801 Alcoy, Spain; ivdocan@doctor.upv.es (I.D.-C.); jlora@iqn.upv.es (J.L.)

[2] Technological Institute of Materials (ITM), Universitat Politècnica de València (UPV), Plaza Ferrándiz y Carbonell 1, 03801 Alcoy, Spain; dagarga4@epsa.upv.es (D.G.-G.); aipena@epsa.upv.es (A.P.-N.); allercan@epsa.upv.es (A.L.-C.)

* Correspondence: vifombor@upv.es

Abstract: The present works focuses on the development of a novel fully bio-based composite using a bio-based high-density polyethylene (Bio-HDPE) obtained from sugar cane as matrix and a by-product of extraction of chia seed oil (CO) as filler, with the objective of achieving a circular economy model. The research aims to revalorize an ever-increasing waste stream produced by the growing interest in vegetable oils. From the technical point of view, the chia seed flour (CSF) was chemically modified using a silane treatment. This treatment provides a better interfacial adhesion as was evidenced by the mechanical and thermal properties as well as field emission scanning electron microscopy (FESEM). The effect of silane treatment on water uptake and disintegration rate was also studied. On the other hand, in a second stage, an optimization of the percentage of treated CSF used as filler was carried out by a complete series of mechanical, thermal, morphological, colour, water absorption and disintegration tests with the aim to evaluate the new composite developed using chia by-products. It is noteworthy as the disintegration rate increased with the addition of CSF filler, which leads to obtain a partially biodegradable wood plastic composite (WPC) and therefore, becoming more environmentally friendly.

Keywords: chia seed flour; wood plastic composite; silane treatment; bio-polyethylene; circular economy

Citation: Dominguez-Candela, I.; Garcia-Garcia, D.; Perez-Nakai, A.; Lerma-Canto, A.; Lora, J.; Fombuena, V. Contribution to a Circular Economy Model: From Lignocellulosic Wastes from the Extraction of Vegetable Oils to the Development of a New Composite. *Polymers* **2021**, *13*, 2269. https://doi.org/10.3390/polym13142269

Academic Editor: Le Quan Ngoc Tran

Received: 4 June 2021
Accepted: 6 July 2021
Published: 10 July 2021

1. Introduction

A global polymer production of 368 million tons was recorded in 2019. In Europe 58 million tons were produced and almost 25% of plastic post-consumer wastes is directly deposited in landfills [1]. The majority of conventional polymers are manufactured from fossil resources and are non-biodegradable. The most used polymers are polypropylene (PP), high- and low-density polyethylene (HDPE and LDPE) and polyvinylchloride (PVC), which represent some 60% of the plastics used [1,2]. Due to the mismanagement of these plastic products, most of which are single-use products, they can end up in landfills, oceans or other terrestrial ecosystems where they can affect wildlife and probably human health [3]. The use of biopolymers could be an excellent proposal for the plastics industry in order to overcome these drawbacks.

In recent years, biopolymers are gaining importance as a sustainable alternative to conventional polymers. They provide a 65% energy savings as well as between 30% and 80% less greenhouses gases emissions during their production compared to conventional polymers [4]. A biopolymer material is defined as a polymer that either is biodegradable, bio-based or has both properties [5]. This definition provides for three different

IV.4 "Novel compatibilizers and plasticizers developed from epoxidized and maleinized chia oil in composites based on PLA and chia seed flour"

Ivan Dominguez-Candela[1], Jaume Gomez-Caturla[2], Salvador Cayetano Cardona[1], Jaime Lora[1], Vicent Fombuena[2]

[1] Instituto de Seguridad Industrial, Radiofísica y Medioambiental (ISIRYM), Universitat Politècnica de València (UPV), Plaza Ferrándiz y Carbonell, s/n, 03801 Alcoy, Spain

[2] Technological Institute of Materiales (ITM), Universitat Politècnica de València (UPV), Plaza Ferrándiz y Carbonell 1, 03801 Alcoy, Spain

European Polymer Journal

2022, 173, 111289.

"Novel compatibilizers and plasticizers developed from epoxidized and maleinized chia oil in composites based on PLA and chia seed flour"

Abstract

Novel compatibilizers and plasticizers derived from epoxidized chia seed oil (ECO) and maleinized chia seed oil (MCO) have been applied in composites based on poly(lactic acid) (PLA) and 15 wt.% chia seed flour (CSF). Results obtained have been compared to conventional silane coupling agent, (3-glycidyloxypropyl) trimethoxysilane (GPS), and a petroleum-based compatibilizer, poly(styrene-co-glycidyl methacrylate) copolymer (Xibond, ®). The compatibilization effect of green composites were assessed by FTIR. The addition of all four compatibilizers improved the ductile mechanical and thermal properties of the composites. The morphology analysis revealed an improvement of interfacial adhesion of the CSF particles into the PLA matrix. In particular, ECO and MCO composites showed a roughness with long filaments in their morphology which plays a crucial role in improving the ductile properties highly. The elongation at break was 10 and 8 times higher using ECO and MCO, respectively, compared to uncompatibilized composite. Moreover, the composites manufactured showed low values (<9%) in the water uptake assay and a negligible compostability delay. The use of novel compatibilizers based on modified vegetable oils could mean an interesting proposal to obtain an entirely environmentally friendly composite with a remarkable ductile property.

Keywords

Epoxidized chia seed oil, maleinized chia seed oil, poly(lactic acid) (PLA), chia seed flour, compatibilizer.

Introduction

At present, one of the leading environmental concerns is the continuous generation of plastic wastes after human consumption. In Europe, plastics production reached 62 million tonnes in 2018, of which 29 million tonnes were collected to be treated [1]. Despite this target, 7.25 million tonnes were still sent to landfills. Therefore, an interesting proposal to overcome this environmental problem is to substitute the most commonly used petrochemical and non-biodegradable plastics, known as *commodities* (LDPE, HDPE, PVC, PP, PS, etc.), by bioplastics, i.e., polymers that are biodegradable, bio-based or both features.

Regarding bioplastics, the most remarkable are the biodegradable and fully or partially bio-based polymers, because they allow reducing the dependency of fossil resources and, therefore, greenhouse gas emissions. Poly(lactic acid) – (PLA) is one of the most used biodegradable polymers due to its competitive price, the suitable thermal stability to be industrially processed, good mechanical properties that can be compared to several non-biodegradable polymers, high transparency, etc. [2]. For these reasons, PLA involves 24% of the global market production of biodegradable polymers, followed by poly(butylene succinate) (PBS) and poly(butylene adipate-co-terephthalate) (PBAT) with a value of 23% [3]. Nevertheless, the major drawback is its inherent brittleness and poor compatibility with organic fillers, as those that can be used to develop green composites, making some commercial applications difficult.

Thus, improving the ductile properties and enhancing the interfacial adhesion between organic fillers and polymeric matrix are two of the most critical challenges for the biopolymers and composites PLA-based sector. In previous literature, several strategies have been performed based on the physical and chemical processes of lignocellulosic filler. Some physical methods based on plasma treatment and ultraviolet radiation with interesting results were obtained using lignocellulosic filler [4,5]. Besides, conventional chemical surface treatments on fillers such as acetylation [6], esterification [7], or alkaline procedure [8] were also studied. In addition, one of the most used chemical surface treatments is silanization, which employs a silane coupling agent to improve the matrix-particle interaction. Numerous reports have

demonstrated the effectiveness of treating the lignocellulosic filler with a silane coupling agent [9-11]. However, currently, the straightforward strategy is regarding the use of reactive compatibilizers. In this case, the compatibilizers used are based on polymers with reactive groups that form new chemical bonds between matrix and lignocellulosic particles during melt processing [12]. Recent researches are focusing on the functionalization of vegetable oils due to their several reactive groups present in their chemical structure. So far, the most employed and available commercially vegetable oils are based on epoxidized and maleinized linseed and soybean oils [13-16]. However, there is practically no literature on the use of chia seed oil (CO) from *Salvia hispanica. L.*, one of the vegetable oils with the greatest potential due to its high unsaturated fatty acid content.

CO is a promising vegetable oil due to the high availability of double bonds, even higher than linseed oil, making it suitable to be chemically modified by diverse reactions. In a previous study, CO was subjected to an epoxidation process to obtain a bio-based plasticizer to be applied in the PLA matrix, giving rise to a successful behaviour [17]. On the other hand, the maleinization process of the CO has never been reported in previous literature, as far as we know. For this reason, the main objective of the present work is to compare the employment of epoxidized chia seed oil (ECO) and maleinized chia seed oil (MCO) with a conventional silane coupling agent, i.e., (3-glycidyloxypropyl) trimethoxysilane (GPS), and a petroleum-based compatibilizer, i.e., poly(styrene-co-glycidyl methacrylate) random copolymer (Xibond), as plasticizers and compatibilizers in composites based on PLA and organic fillers.

As organic filler, the lignocellulosic waste from chia seed after oil extraction has been employed in flour form. This organic filler, which is chia seed flour (CSF), should be taken into account because the annual growth rate of CO from 2019 to 2025 is expected to be around 23% [18]. Moreover, considering the high CO production trend corresponding to 20% of the market share of chia seed and that the lignocellulosic waste is approximately 70% of whole chia seeds, a large amount of wastes is being generated. In order to contribute to circular economy and add value to this high amount of by-product in CO production, CSF is considered an interesting candidate to be employed in polymer industry to obtain high environmentally friendly

composites. The addition of this filler was also reported previously in bio-based high-density polyethylene, becoming a composite partially biodegraded [19].

Therefore, to develop a more circular economy model in polymeric products applicable to sectors such as packaging, automotive, or even interior design, a novel fully biodegradable composite has been developed using PLA and lignocellulosic wastes from CO production. Mechanical, thermal, morphological, water uptake, and disintegration by composting tests have been used for comparing plasticizers and compatibilizers based on epoxidized and maleinized chia oil with coupling agents based on silanes and poly(styrene-co-glycidyl methacrylate) for the first time.

Experimental

Materials

The aliphatic polyester PLA used in this work was a commercial-grade 6201D supplied in pellet form by NatureWorks LLC (Minnetonka, Minnesota, USA). This PLA has a density of 1.24 g·cm^{-3} and an approximate molecular weight of 120,000 g·mol^{-1}. The melt flow index (MFI) is 15-30 g·(10 min)$^{-1}$ measured at 210 ^{o}C and using a nominal load of 2.16 kg, which is suitable for injection molding.

Edible chia seed (*Salvia hispanica, L.*) was supplied by Frutoseco (Bigastro, Alicante, Spain). CO was obtained from edible chia seed by a cold mechanical extraction method using a CRZ-309 press machine (Changyouxin Trading Co., Zhucheng, China). The residual cake obtained was subjected to mill process using an ultra-centrifugal mill from Retsch GmbH (Düsseldorf, Germany) working at a rotating speed of 8000 rpm with 0.25 mm sieve. As a result of this process, chia seed flour (CSF) was obtained as a lignocellulosic filler.

Concerning compatibilizers, a silane coupling agent (3-glycidyloxypropyl) trimethoxysilane (GPS) was obtained from Sigma Aldrich (Madrid, Spain). The GPS density is 1.07 g·cm^{-3} with a molecular weight of 236.34 g·mol^{-1}. As a petrochemical compatibilizer, Xibond ™ 920 was used, which is a poly(styrene-co-glycidyl methacrylate) random copolymer supplied by Polyscope (Geleem, The Netherlands).

It presents a molecular weight value of 50,000 g·mol^{-1}, a glass transition temperature of 95 ^{o}C, and a glycidyl methacrylate content of 20% mole fraction. Finally, as a bio-based compatibilizer, CO was employed with two different chemical modifications: epoxidation and maleinization. The epoxidation process of CO was carried out as indicated in a previous report [17]. ECO presents an epoxy content of 6.71% with an iodine value of 25 g I_2 · (100 g)$^{-1}$ and density of 1.026 g·cm^{-3}, following the guidelines of ASTM D1652, ISO 3961, and ISO 1675, respectively. The maleinization process was performed by adding maleic anhydride (MA) with purity >98% supplied by Sigma Aldrich (Madrid, Spain). A total of 9 g of MA per 100 g of CO was used following the method reported by Lerma-Canto *et al.* [20]. MCO presents an acid value of 120 mg KOH · g^{-1} according to ISO 660, a density of 1.040 g·cm^{-3}, and an iodine value of 104 g I_2 · (100 g)$^{-1}$. The chemical structure of each compatibilizer is shown in Figure IV.4.1.

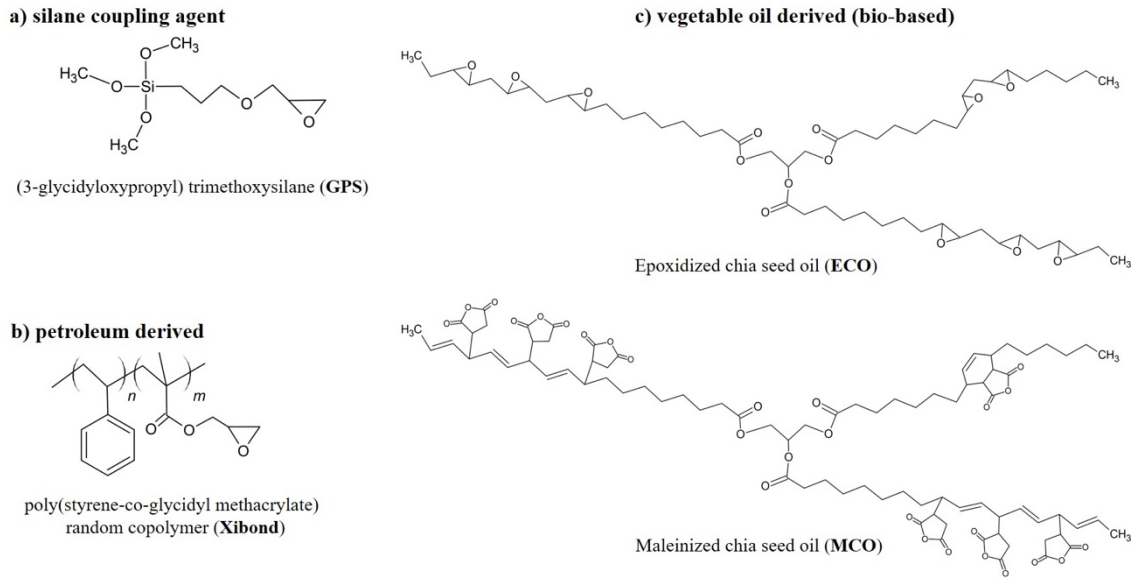

Figure IV.4.1. Scheme of the chemical structure of different compatibilizers used.

Preparation of PLA/CSF composites with compatibilizers

Previously to the preparation of composites, PLA, CSF, and Xibond were dried at 40 ^{o}C over 36 h using an air oven to remove the residual moisture. All samples were weighed according to the proportions gathered in Table IV.4.1 and following the recommendations of the previous related literature. All mixed compositions were processed in a twin-screw co-rotating extruder from Dupra S.L. (Castalla, Alicante,

Spain) at a constant rate of 40 rpm. The temperature profile was set from the hopper to the die as follows: 162.5 ºC, 165 ºC, 170 ºC, and 175 ºC. After this, samples obtained were air-cooled at room temperature and pelletized. Before injection, all samples were dried again at 60 ºC for 24 h. Afterwards, each formulation was shaped into pieces by injected molding from Mateu & Solé (Barcelona, Spain) and PLA/CSF composites with different compatibilizers were obtained. The temperature profile was set as follows: 190 ºC (hopper), 195 ºC, 197 ºC, and 200 ºC (injection nozzle). Regarding cavity filling and cooling time, they were set to 1 s and 10 s, respectively.

Table IV.3.1. Summary of compositions and codes of samples manufactured.

Nº sample	PLA content (wt. %)	CSF content (wt. %)	Compatibilizer Employed	Compatibilizer content (wt. %)	Reference	Code
1	100	-	-	-		PLA
2	85	15	-	-	[21]	PLA/CSF
3	85	15	GPS	1[1]	[22-24]	PLA/CSF_S
4	84	15	Xibond	1[2]	[25]	PLA/CSF_X
5	77.5	15	ECO	7.5[2]	[17]	PLA/CSF_ECO
6	77.5	15	MCO	7.5[2]	[20]	PLA/CSF_MCO

[1] Respect to filler; [2] Respect to composite

Infrared spectroscopy

Fourier-transformed infrared spectroscopy (FTIR) was performed using a Bruker S.A. Vector 22 (Madrid, Spain). FTIR instrument was coupled to single reflection attenuated total reflectance (ATR) accessory with a diamond ATR crystal (Madison,Wisconsin, USA). Each scan was collected using a wavelength between 400-4000 cm^{-1} from 12 scans at 4 cm^{-1} of spectral resolution. All spectra were normalized using the Perkin-Elmer software Spectrum.

Mechanical characterization

Mechanical assays such as tensile, impact, and hardness tests were carried out to evaluate the influence of the compatibilization effect in PLA/CSF composites. The tensile characterization was carried out in a universal test machine Ibertest ELIB 30

from S.A.E. Ibertest (Madrid, Spain), using a 5 kN load cell and a crosshead rate of 10 mm·min^{-1}. Samples of size 150 x 10 x 4 mm^3 were used following the recommendation of the ISO 527. In addition, the tensile modulus was obtained accurately using an axial extensometer from S.A.E. Ibertest (Madrid, Spain). The impact strength was measured in a 1 J Charpy's pendulum from Metrotec S.A. (Madrid, Spain) with a sample size of 80 x 10 x 4 mm^3 according to the guidelines of the ISO 179. Regarding hardness, a Shore D durometer model 676-D from J. Bot S.A. (Barcelona, Spain) was used as suggested by the ISO 868 standard. All mechanical tests were carried out at room temperature and at least five different specimens per sample were tested to obtain the average and deviation values.

Morphology characterization

The morphologies of fractured surfaces from the impact test of PLA/CSF with different compatibilizers were observed by field emission scanning electron microscopy (FESEM). This measurement was carried out in a ZEISS ULTRA 55 from Oxford Instruments (Oxfordshire, UK) using an acceleration voltage of 2 kV. Previously to observation, all fractured surfaces were coated with an Au-Pd alloy thin layer over 120 s under vacuum in a sputter coater EM MED020 from Leica Microsystems (Wetzlar, Germany). CSF sizes were measured by means of Image J Launcher v 1.52k and the data presented was an average from 50 SEM micrographs.

Thermal characterization

The thermal behaviour of PLA/CSF with different compatibilizers was analysed by differential scanning calorimetry (DSC) and thermogravimetric analysis (TGA). The main thermal transitions of PLA/CSF composites were obtained by DSC in a Mettler-Toledo calorimeter 821e from Mettler Toledo Inc. (Schwerzenbach, Switzerland). The dynamic temperature program was set as follows: an initial heating from 30 to 300 ºC to remove the thermal history, a cooling cycle from 300 to 30 ºC, and finally a heating program from 30 to 300 ºC. All samples with an average of 5-10 mg were subjected to a cooling and heating rate of 10 ºC·min^{-1} according to ASTM D3418. All thermal cycles were carried out in nitrogen atmosphere with a constant flow rate

of 66 mL·min^{-1}. The degree of crystallinity (X_c) of composites was determined using Equation IV.4.1:

$$X_c\ (\%) = 100 \times \frac{\Delta H_m - \Delta H_{cc}}{\Delta H^0_{m(100\%)} \cdot w_{PLA}} \qquad \textbf{Equation IV.4.1}$$

where ΔH_m and ΔH_{cc} stand for the melt and cold crystallization enthalpies (J.g^{-1}), respectively, w_{PLA} is the PLA weight proportion and $\Delta H^0_{m(100\%)}$ corresponds to the melt enthalpy of a theoretical fully crystalline PLA structure which is 93 J·g^{-1} [26].

The thermal stability of composites was evaluated by TGA analysis in a TGA/SDTA 851 thermobalance from Mettler-Toledo Inc. (Schwerzenbach, Switzerland). Samples with an average weight of 10 mg were subjected to a dynamic heating ramp from 30 to 700 ºC at a constant heating rate of 10 ºC·min^{-1}. All tests were carried out under a constant nitrogen flow (66 mL·min^{-1}). In addition, the first derivative thermogravimetric curves (DTG) were also obtained to evaluate the maximum degradation temperature of PLA/CSF composites.

Thermomechanical characterization

The dynamic mechanical thermal analysis (DMTA) of PLA/CSF with different compatibilizers was evaluated in an oscillatory rheometer AR-G2 (TA Instruments, New Castle, USA). The changes in storage modulus (G') and damping factor (tan δ) were recorded in a torsion-shear mode with rectangular samples of size 40 x 10 x 4 mm^3. Samples were subjected to a thermal program from 25 to 140 ºC at a heating rate of 2 ºC·min^{-1}, a maximum shear deformation (γ) of 0.1%, and a frequency of 1 Hz.

Water uptake

Samples of size 80 x 10 x 4 mm^3 were immersed in distilled water at 23 ± 1 ºC to evaluate the water absorption of PLA/CSF with different compatibilizers. The water uptake was carried out following the guidelines of the ISO 62. Previously to start the test, all samples were dried using an air oven at 50 ºC for 24 h to remove the residual moisture. Three different samples of each composition were immersed to

calculate the average and deviations values. Every week samples were taken out, dried using a dry cloth to remove the surface moisture, weighed in an analytical balance, and then immersed again to follow the water uptake evolution. The weight changes were measured for a period of 12 weeks. The water absorption (W) was calculated by the weight gain regarding the dried sample weight using Equation IV.4.2:

$$W\ (\%) = 100 \cdot \frac{w_f - w_0}{w_0} \qquad \textbf{Equation IV.4.2}$$

where w_f is the final weight of the sample after taking it out each week and w_0 is the dry weight of the sample.

Disintegration under compost conditions

A disintegration test was carried out under anaerobic conditions at a temperature of 58 ºC and relative humidity of 55%, as indicated by the ISO 20200. Seven different samples of each composition were shaped (25 x 25 x 1 mm^3) corresponding to each control day: 4, 8, 11, 15, 18, 23, and 31. Samples of each composition were dried in an air oven at 40 ºC for 24 h. The dried samples were placed in a carrier bag and buried in a synthetic compost reactor (300 x 200 x 100 mm^3). At previously selected days, samples of each composition were unburied, washed, dried over 24 h, and subsequently weighed in an analytical balance while the remaining samples remained in the compost reactor. All tests were carried out in triplicate to ensure the reliability of the process. The percentage of weight loss (W_L) was determined by Equation IV.4.3:

$$W_L\ (\%) = 100 \cdot \frac{w_0 - w}{w_0} \qquad \textbf{Equation IV.4.3}$$

where w is the final weight of the unburied samples for each control day after washing and drying and w_0 is the initial dry weight of the sample.

Results and discussion

FTIR analysis

To investigate the interaction of green composites, FTIR spectra of neat PLA and PLA/CSF composites were obtained as is shown in Figure IV.4.2. Neat PLA presented two weak peaks attributed to antisymmetric and symmetric stretching vibration (-CH_2) at 2996 and 2962 cm^{-1}, respectively [27]. The three bands between 1500-1300 cm^{-1} are assigned to symmetric and antisymmetric deformational vibrations (C-H) in the methyl groups (CH_3) [28]. The strong peak located at 1748 cm^{-1} is ascribed to C=O stretching vibration of the carbonyl group [29]. Others strong peaks are observed between 1250 and 1000 cm^{-1} which are assigned to C-O and C-O-C stretching vibrations [30]. The addition of CSF in PLA matrix showed the same main peaks compared to PLA neat, although different intensity and/or shifts were observed, remarking at 1748, 1184 and 1078 cm^{-1}. This effect was also reported by Lima *et al.* [31] when the effect of 10-20 wt.% of mango's kernel in PLA matrix was studied. These changes suggest that CSF addition interferes physically with PLA molecules hindering the movement [32]. Moreover, the new peaks are related to lignocellulosic filler, which might be not interacting completely with PLA. This peaks at 3500-3700 cm^{-1} are assigned to hydroxyl groups (-OH) stretching vibration present in the lignocellulosic filler of CSF [33].

Regarding the use of compatibilizers, the effect was observed compared to uncompatibilized PLA/CSF composite. In case of PLA/CSF_S composite, GPS coupling agent has two functional group: the first functional group is an alkoxy group that can be hydrolyzed to form active silanols, thus interacting with hydroxyl groups of lignocellulosic filler [34]; the second is an epoxy group that can link with hydroxyl end groups of PLA matrix leading the silane coupling agent to act as a chemical bridge [35]. In this regard, according to Garcia-Garcia *et al.* [36], this chemical interaction is associated to the contribution of bonds Si-O-Si and Si-O-C, which emphasize the peaks presents at 1108 cm^{-1} and 1220 cm^{-1}, respectively. This increase of intensity can be observed in PLA/CSF_S composite compared to uncompatibilized PLA/CSF composite, suggesting that new chemical bonds have been formed, which improve

the interaction between filler and matrix. The addition of Xibond as compatibilizer showed an increase of intensity and shift at 1746, 1178 and 1078 cm^{-1}, suggesting interaction between CSF, PLA and compatibilizer. The glycidyl methacrylate functional group is highly reactive with condensation polymers such as PLA and lignocellulosic fillers by means of hydroxyl groups of both PLA and CSF filler [37]. In the case of functionalized vegetable oils in PLA/CSF composites, the chemical groups such as oxirane and maleic anhydride present in ECO and MCO, respectively, can react with the terminal hydroxyl groups of lignocellulosic filler, whereas the remaining groups are also available to react with hydroxyl groups of PLA chains [38, 39]. Both showed a broader and shifted peaks at 1748, 1180 and 1080 cm^{-1} which suggests the intermolecular interaction between PLA, filler and bio-based compatibilizers as was reported in literature [40, 41]. The presence of both modified vegetable oils showed a small peak at 2854 cm^{-1} that is attributed to the stretching vibration of $-CH_2-CH_3$ for incorporation of aliphatic chains [42]. In general, FTIR results suggest chemical interaction using all compatibilized composites compared to uncompatibilized PLA/CSF composite. In addition, a reduction of intensity between 3500-3700 cm^{-1} associated to hydroxyl groups in CSF filler structure was observed. This fact could also support the reaction between PLA and CSF filler by means of compatibilizers [43].

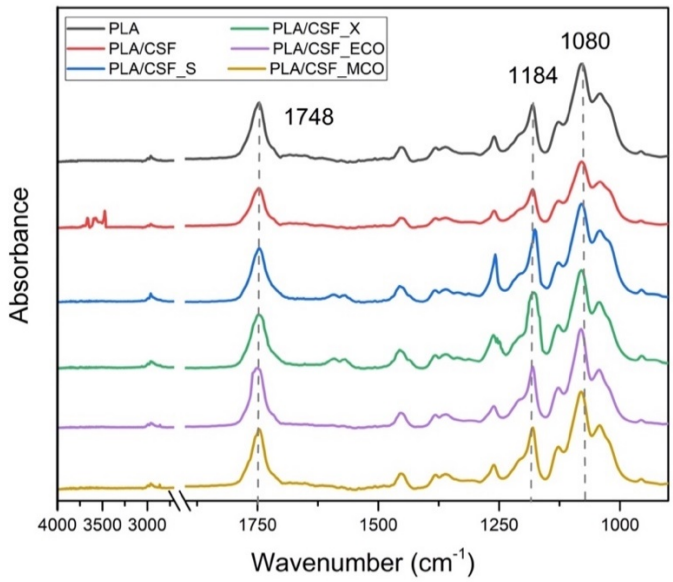

Figure IV.4.2. FTIR spectra of poly(lactic acid) (PLA) and 15 wt.% chia seed flour (CSF) composites with different compatibilizers.

Mechanical properties of PLA/CSF composites with compatibilizers

Tensile properties of PLA/CSF composites with different compatibilizers are shown in Figure IV.4.3a. The tensile strength of neat PLA presented a value of 42 Mpa that decreased up to 15 Mpa with the addition of 15 wt.% of untreated CSF, as plotted in Figure IV.4.3a. It is worthy to note that CFS particles present a hydrophilic nature as common lignocellulosic fillers and, on the other hand, the PLA matrix is a hydrophobic polyester [44]. This results in a low interaction between CSF filler and PLA matrix, leading to a stress concentrator effect and subsequently decreasing the tensile strength [45]. With the surface treatment of CSF particles with GPS, an improvement of 19.2% compared to PLA/CSF composite was observed, probably due to the new bonds formed between CSF and PLA matrix by means of silane molecule. The addition of petrochemical copolymer Xibond recorded the highest tensile strength (21 Mpa), i.e., an increase of 35.4% with respect to PLA/CSF composite. In the case of bio-based functionalized vegetable oils, i.e., ECO and MCO, both presented the lowest tensile strength with a decrease of 63% compared to uncompatibilized PLA/CSF composite. This remarkable decrease is directly related to the plasticizing effect provided by modified vegetable oils, which causes a reduction of the tensile strength [46].

Regarding tensile modulus, the addition of 15 wt.% of untreated CSF particles to the PLA matrix provided an increase from 3100 Mpa (neat PLA) up to 3500 Mpa. It is worthy to note that tensile modulus is related to the ratio of tensile strength to elongation at break, where both properties decrease because of the addition of CSF. In this case, the decrease of elongation at break was much more pronounced, leading to an increase in the tensile modulus, as observed in Figure IV.4.3a. The most remarkable values were obtained using PLA/CSF composites compatibilized with GPS and copolymer Xibond. Both presented similar values with an enhancement of 17.7 % compared to uncompatibilized PLA/CSF composite. This behaviour is typical of conventional compatibilizers that contribute to improving the stress transfer between matrix and particle, thus increasing the tensile modulus [12]. However, the addition of both modified vegetable oils led to obtaining the lowest values, 3050 Mpa approximately, which is a reduction of 15% compared to uncompatibilized PLA/CSF

composite. This decrease agrees with values reported by Kamarudin *et al.* [47], who evaluated the addition of epoxidized Jatropha oil in PLA matrix with kenaf fiber as a filler. According to this study, the reduction of tensile modulus is related to the intrinsic flexibility that modified vegetable oils provide.

Concerning elongation at break, PLA is a hard but brittle polymer with a value of 8%, as shown in Figure IV.4.3b. As expected, the addition of 15 wt.% of untreated CSF reduced the elongation at break up to 1.6% because of the loss of cohesion between filler and matrix. This property was slightly improved in PLA/CSF composites compatibilized with GPS and copolymer Xibond, enhancing the interfacial adhesion as mentioned above. In this case, CSF treated with GPS provided higher values than Xibond, obtaining a more ductile composite in both cases. Finally, the highest values were observed with the addition of functionalized vegetable oils in PLA/CSF composites. The elongation at break increased to 16% and 13% with ECO and MCO, respectively, which is 10 and 8 times higher than the PLA/CSF composite. It is known that some compatibilizers, particularly modified vegetable oils, act as plasticizers as well. On the one hand, the compatibilization effect with lignocellulosic filler has been reported. It is important to take into account that both oxirane and maleic anhydride present in ECO and MCO, respectively, can react with the terminal hydroxyl groups of lignocellulosic filler and PLA chains, leading to some potential reactions such as linear chain-extension, branching, and even cross linker structures, acting as a bridge [38, 39]. On the other hand, they also present a plasticization effect that increases the free volume of PLA chains, thus increasing the chain mobility and consequently improving the ductile properties [48]. Therefore, modified vegetable oils can provide a dual function: a compatibilization effect due to an increase of polymer-filler interaction and plasticization effect. Similar behaviour was reported by Mahmud *et al.* [49] when evaluating the addition of epoxidized soybean oil (ESO) as a compatibilizer in PLA with cellulose powder.

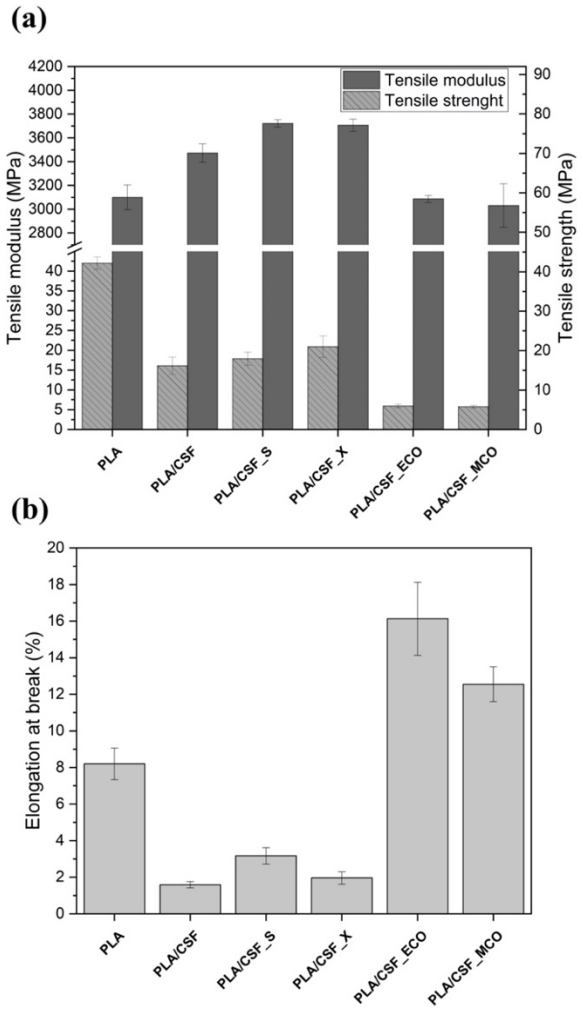

Figure IV.4.3. Mechanical properties of poly(lactic acid) (PLA) and 15 wt.% chia seed flour (CSF) composites with different compatibilizers; (a) tensile strength and modulus, (b) elongation at break.

Regarding impact-absorbed energy and Shore D hardness, results are summarized in Table IV.4.2. The brittleness of PLA was reflected in impact-absorbed energy with a value of 37.1 kJ/m^2. The incorporation of 15 wt.% of untreated CSF induced a reduction up to 13.6 kJ/m^2, observing a decrease of 61% compared to neat PLA. This embrittlement of the composite is related to the weak interaction between CSF filler and PLA matrix, which causes a negative effect on the impact toughness. This result is in complete agreement with the tensile results obtained. For all tested PLA/CSF composites with compatibilizers, the toughness was improved, obtaining higher values than uncompatibilized PLA/CSF composite. The impact-absorbed energy is directly related to the chemical structure of compatibilizers and their ability to react with different components.

In all compatibilization attained, the functional groups react with PLA and cellulose present in the CSF. As per results, both GPS and Xibond seem to give a similar enhancement of the toughness, being an improvement of 15.5% compared to uncompatibilized PLA/CSF. On the one hand, GPS compatibilizer presents a silanol group in one end that can react with hydroxyl groups of CSF, whereas the other functional group is an epoxy group that is linked to hydroxyl groups of PLA. On the other hand, Xibond compatibilizer, which contains a functional glycidyl methacrylate (GMA) group, is ready to react with both hydroxyl groups of CSF and PLA matrix, acting as a chemical bridge during the reactive extrusion process. The trend of impact-absorbed energy for the composites modified with vegetable oils was identical to the elongation at break, corroborating that polymer-matrix interaction has been improved and did not show significant differences. Therefore, the use of bio-based functionalized vegetable oils showed the highest impact-absorbed energy, as expected. The functional groups present in ECO and MCO, i.e., epoxy and maleic anhydride, respectively, can react with both hydroxyl groups contained in CSF and PLA matrix. As a result of this interaction, i.e., a compatibilization and plasticizing effect, the impact-absorbed energy has been improved. According to the previous elongation at break results, PLA/CSF_ECO composite also presented the highest toughness, suggesting higher reactivity than the MCO compatibilizer.

About Shore D hardness, neat PLA presented a value of 74.0 that increased up to 76.8 with the addition of 15 wt.% untreated CSF, which is related to the intrinsic hardness of CSF. The addition of compatibilizers slightly improved the hardness compared to uncompatibilized PLA/CSF composite but, nevertheless, did not show significant differences considering the standard deviation. Similar behaviour was reported by Liminana *et al.* [50], who applied different compatibilizers in poly(butylene succinate) (PBS) composites with almond shell flour. However, considering the average value, the hardness achieved by modified vegetable oils was slightly lower than that of other compatibilizers due to the plasticization effect that ECO and MCO can provide.

Table IV.4.2. Impact-absorbed energy and Shore D hardness of poly(lactic acid) (PLA) and 15 wt.% chia seed flour (CSF) composites with different compatibilizers.

Sample	Impact-absorbed energy (kJ/m^2)	Shore D hardness
PLA	37.1 ± 1.8	74.0 ± 2.3
PLA/CSF	13.6 ± 0.4	76.8 ± 3.2
PLA/CSF_S	15.7 ± 0.3	79.0 ± 2.6
PLA/CSF_X	15.6 ± 0.2	79.1 ± 2.0
PLA/CSF_ECO	16.5 ± 0.3	77.1 ± 2.4
PLA/CSF_MCO	16.2 ± 0.3	77.9 ± 1.6

Morphology of CSF and PLA/CSF composites with compatibilizers

The morphology of CSF particles observed by SEM at 500x as well as particle size distribution are shown in Figure IV.4.4. As can be observed in Figure IV.4.4a, the shape of CSF had an irregular morphology with tendency to form aggregates because of their elevated hydrophilicity. This morphology was also observed by Lascano *et al*. [51] who studied the shape of flax flour particles as filler in bio-based epoxy resin. Moreover, CSF particles showed rough surfaces that can be ascribed to the crushing process due to high hardness of this type of lignocellulosic filler. The distribution size of CSF particles, which was obtained with an average of 50 SEM images, was approximately 137 μm as shown in Figure IV.4.4b. The particle size plays an important role in the mechanical properties of green composites. Crespo *et al.* [52] reported that almond shell particle sizes higher than 150 μm could lead to mechanical impairment caused by greater heterogeneity of fillers within polymer matrix.

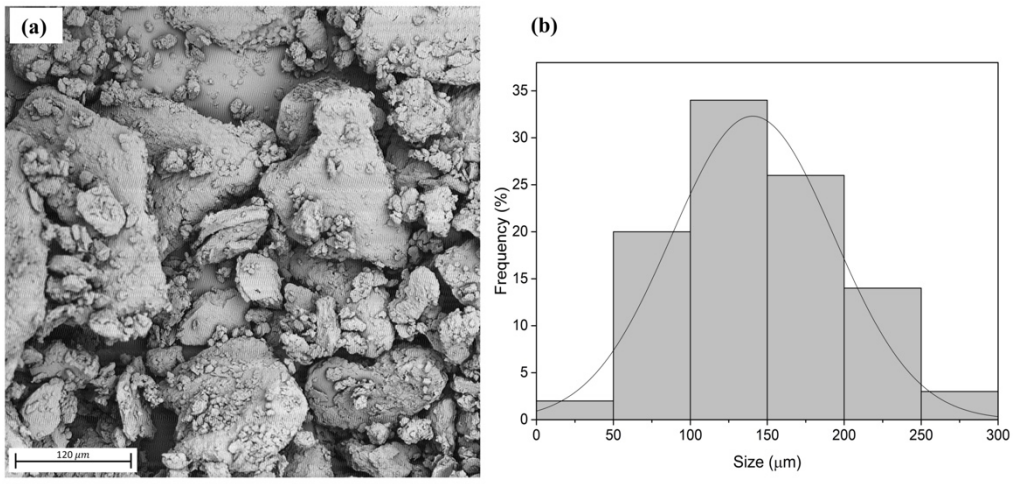

Figure IV.4.4. (a) Surface morphology of chia seed flour (CSF) by field emission electron microscopy (FESEM) at 500x; (b) Histogram of CSF particles.

In the case of the surface morphology of fractured samples after Charpy´s Impact test. Is gathered in Figure IV.4.5. The first SEM image, Figure IV.4.5a, corresponds to a neat PLA sample which showed a smooth and flat surface typical of brittle polymers with no evidence of plastic deformation. In contrast, the addition of CSF particles, highlighted in yellow arrow in Figure IV.4.5b, increased the micro-crack formation. The lack of interaction between CSF particle and PLA matrix, highlighted in red arrow where an evident gap was observed, led to the loss of the continuity of composite. Consequently, CSF particles acted as a stress concentrator, which is in concordance with the previous brittle behaviour exposed in the mechanical test. In Figure IV.4.5c, the effect of silane treatment in CSF particles can be observed. In this case, CSF particles were better embedded in the PLA matrix with previous treatment with GPS, thus reducing the particle-matrix distance and obtaining an almost undetectable gap. The interfacial enhancement of particle-matrix interaction with silane coupling agent was also reported by several authors [53, 54]. Similar morphology was observed with the addition of copolymer Xibond in PLA/CSF composite, indicating the enhancement of interaction as plotted in Figure IV.4.5d. This supports the above-reported mechanical results, where better compatibilization corresponds to an improvement of mechanical properties compared to untreated CSF/PLA composite. Regarding ECO and MCO compatibilizers, Figures IV.4.5e and IV.4.5f, both presented a good enough interaction due to the tiny gap between CSF

and PLA matrix, as with previously commented compatibilizers occur. This fact could be ascribed to the compatibilization effect that increase the interfacial adhesion due to chemical interaction. The reactive points of both modified vegetable oils, oxirane and anhydride maleic groups, can interact with hydroxyl groups of CSF and PLA matrix, leading to improvement of interfacial adhesion. Nevertheless, the matrix morphology showed a significant difference compared to PLA/CSF_S and PLA/CSF_X composites. The plasticization effect was observed due to the presence of characteristic long filaments from plastic deformation and a rougher surface [55] both in PLA/CSF_ECO and in PLA/CSF_MCO. Similar morphologies have been reported using different modified vegetable oils such as acrylated epoxidized soybean oil [56] or maleinized linseed oil [57] with fillers in PLA matrix. Comparing the morphology samples with the addition of ECO and MCO, no significant difference was observed, as shown in Figure IV.4.5e and IV.4.5f. Besides, it is known that modified vegetable oils are not completely miscible in the PLA matrix; thus, relatively high amounts can induce to form spherical voids that worsen the miscibility, with a negative effect on PLA ductile properties [13]. In a previous report [17], the ECO content was optimized in 7.5 wt.%, obtaining a high improvement of ductile properties, i.e., 612% and 66% in elongation at break and impact-absorbed energy, respectively. Although the gap between PLA and CSF was reduced and consequently a better mechanical interaction was obtained, the high results representative of a plasticizing effect (elongation at break and impact-absorbed energy) showed how the latter effect is more pronounced than the compatibilizer effect.

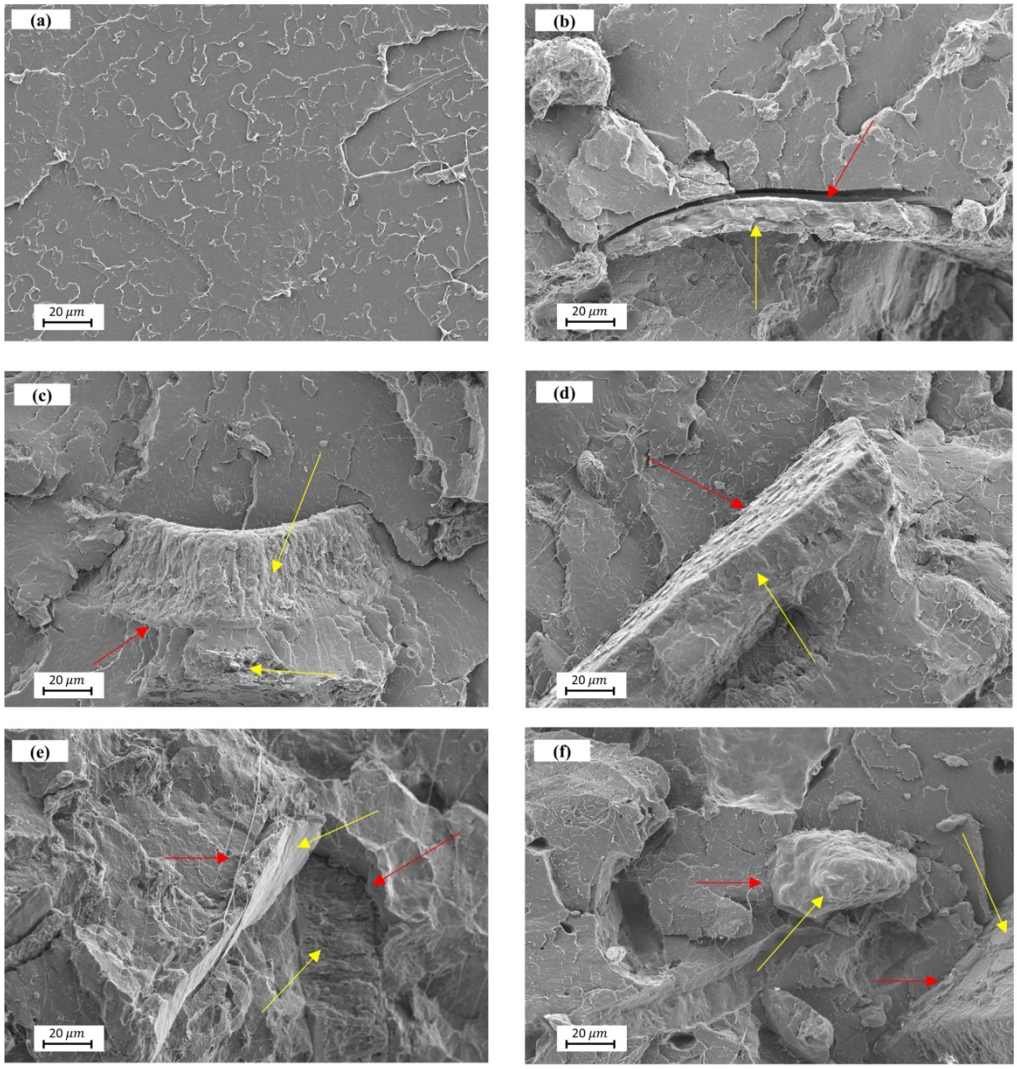

Figure IV.4.5. Surface morphology of fractured samples by field emission electron microscopy (FESEM) of poly(lactic acid) (PLA) and 15 wt.% chia seed flour (CSF) composites at 500x: (a) PLA; (b) PLA/CSF; (c) PLA/CSF_S; (d) PLA/CSI; I PLA/CSF_ECO; (f) PLA/CSF_MCO.

Thermal properties of PLA/CSF composites with compatibilizers

The thermal behaviour of neat PLA and PLA/CSF composites with different compatibilizers has been evaluated using DSC and TGA with a heating rate of 10 $^{o}C \cdot min^{-1}$. Table IV.4.3. gathered the main thermal parameters obtained from DSC. The first thermal transition, located at around 60 ^{o}C, corresponds to glass transition temperature (T_g). Firstly, neat PLA presented a T_g value of 62 ^{o}C that was reduced up to 60.4 ^{o}C with the addition of untreated CSF particles. This behaviour is related to the increment of free volume as well as chain mobility by loose packing of filler in the matrix due to a lack of interaction between them [58]. The same evolution was also

reported by Ortiz-Barajas *et al.* [59] when introduced coffee husk flour in PLA. Regarding PLA/CSF_S and PLA/CSF_X composites, they presented a similar value in the 60.8-61.3 ºC range, obtaining slightly higher values than PLA/CSF composite probably by the increase of the interfacial adhesion between CSF particles and PLA matrix [60]. Nevertheless, T_g values of functionalized vegetable oils presented an evident decrease of 59.6 ºC and 57.0 ºC for PLA/CSF_MCO and PLA/CSF_ECO composites, respectively. This effect supports the plasticizing effect that can be ascribed to the reduction of intermolecular forces, so inducing to increase its mobility [61]. Furthermore, these results are in concordance with the ductile properties where PLA/CSF_ECO composite presented the best ductility as well as the lowest T_g value, mainly due to the increase of the chain mobility. The second thermal transition is related to cold crystallization temperature (T_{cc}), being around 119.4 ºC in the case of neat PLA. This value did not vary significantly with the addition of CSF particles. However, the lowest value was obtained for PLA/CSF_S composite, which is 115.9 ºC, suggesting that previous silane treatment of CSF filler favours the crystal nucleation, thus shifting the T_{cc} at lower temperatures [62]. The use of Xibond, ECO, and MCO compatibilizers recorded a similar value in the 128.1-129.5 ºC range, being almost 10 ºC higher than PLA/CSF composite. This delayed of T_{cc} for the latter compatibilizers could be related to the formation of chain extended, branched, or even cross-linked structures of PLA with a higher impediment to crystallize [63]. In fact, this phenomenon also supports the low value of cold crystallization enthalpy recorded during heating scan as plotted in Figure IV.4.6. The last thermal transition is related to the melting tempIure I. Neat PLA showed a T_m value of 150.2 ºC, whereas the addition of CSF particles only decreased about 0.8 ºC. It is worthy to note that a double melting peak was formed by adding CSF particles. The explanation could be related to the formation of less perfect crystals that over the melting process can be melted, recrystallize into spherulites with thicker lamellar thicknesses and, therefore, re-melt at higher temperatures [64]. Kong *et al.* [65] also reported the double melting peak for the addition of eggshell in a PLA matrix. Nevertheless, the surface treatment of CSF particles with GPS led to decrease the T_m up to 148.6 ºC as well as slightly suppress the double melting peak. This fact is probably caused by the enhancement of interfacial adhesion that promotes the formation of crystalline structures with more

perfect crystals than PLA/CSF composite. A similar result was reported by Luo *et al.* [66] with the addition of corn fibers treated with a combination of alkali and silane agent in a PLA matrix. In the case of composite with Xibond, ECO, and MCO compatibilizers, a single melting peak with similar T_m values was obtained. This indicates a homogenous crystalline structure with similar lamellar thicknesses. Related to enthalpies, the degree of crystallinity (X_c) of composites has been evaluated. Firstly, neat PLA presented an X_c value of 7.7%. According to the literature, the X_c of composites depends on the nucleation ability of each filler and its content [67]. In particular, the addition of CSF particles reduced the crystallinity to 1.2%, confirming that it interrupts the packing process of PLA chains, becoming a matrix almost amorphous. This effect was also in line with our previous studies using a different polymer matrix [19]. All compatibilized composites showed an evident increase of crystallinity compared to PLA/CSF composite, except for PLA/CSF_X that presents a slight increase. In the case of CSF particles treated with silane, the crystallinity was enhanced up to the value of 5.8% caused by the better interaction between phases that may increase the nucleation activity of manufactured composite [68]. Finally, for both ECO and MCO compatibilizers, its addition induced to increase the crystallinity to 5.1% and 7.5%, respectively, that is around 5 and 7 times higher regarding to PLA/CSF composite. The incorporation of functionalized vegetable oils resulted in a plasticization effect that increases the chain mobility and therefore favoring the crystal formation. Similar results were also reported by Quiles-Carillo *et al.* [56] with the addition of epoxidized soybean oil in PLA/orange peel flour composite. In this study, a X_c value of 8.31% was obtained compared to 5% of uncompatibilized composite, being a lower difference than present paper.

Table IV.4.3. Main thermal properties of poly(lactic acid) (PLA) and 15 wt.% chia seed flour (CSF) composites with different compatibilizers in terms of glass transition temperature (T_g), cold crystallization temperature (T_{cc}), cold crystallization enthalpy (ΔH_{cc}), melting Temperature I, melting enthalpy (ΔH_m) and crystallinity (X_c).

Sample	T_g (°C)	T_{cc} (°C)	ΔH_{cc} (J g^{-1})	T_m (°C)	ΔH_m (J g^{-1})	X_c (%)
PLA	62.0 ± 0.7	119.4 ± 1.0	8.4 ± 0.7	150.2 ± 1.2	15.6 ± 1.3	7.7 ± 0.6
PLA/CSF	60.4 ± 0.5	119.1 ± 1.2	24.3 ± 1.3	149.4 ± 0.8	25.2 ± 1.5	1.2 ± 0.3
PLA/CSF_S	60.8 ± 0.9	115.9 ± 1.2	17.3 ± 0.5	148.6 ± 0.7	21.9 ± 0.7	5.8 ± 1.6
PLA/CSF_X	61.3 ± 0.7	129.3 ± 1.3	1.10 ± 0.1	151.4 ± 1.3	2.3 ± 0.2	1.5 ± 0.2
PLA/CSF_ECO	57.0 ± 1.0	129.5 ± 1.2	0.95 ± 0.1	151.2 ± 1.2	4.6 ± 0.5	5.1 ± 0.9
PLA/CSF_MCO	59.6 ± 0.8	128.1 ± 1.1	2.16 ± 0.3	151.7 ± 1.3	7.5 ± 1.1	7.5 ± 0.9

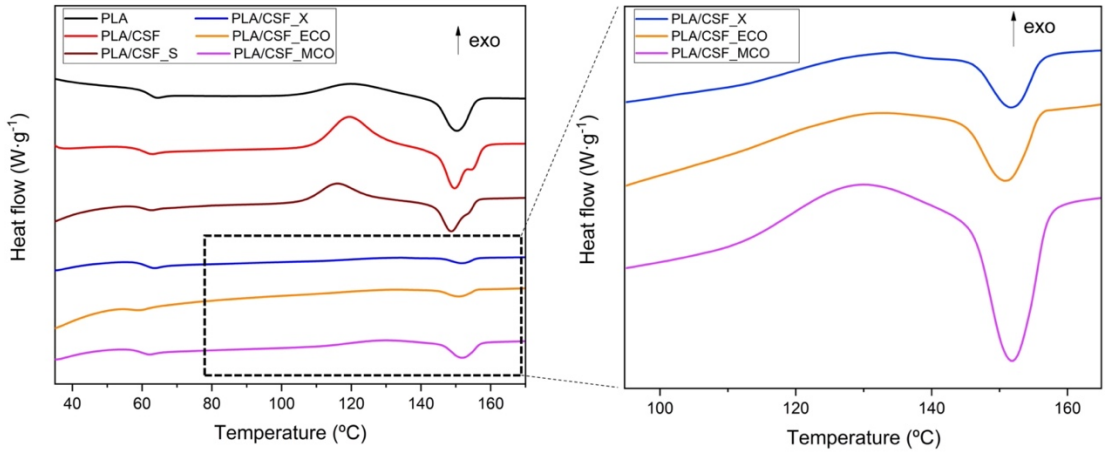

Figure IV.4.6. Differential scanning calorimetry (DSC) of poly(lactic acid) (PLA) and 15 wt.% chia seed flour (CSF) composites with different compatibilizers at 10 °C·min^{-1}.

The thermal degradation of neat PLA, CSF filler, and PLA/CSF composites with different compatibilizers is shown in Figure IV.4.7. Firstly, the thermal degradation of CSF particles is characterized by four main weight losses steps: residual moisture removal, cellulose degradation, hemicellulose degradation, and, finally, lignin degradation. As shown in Figure IV.4.7, the first step occurred in the 30-220 °C range, whereas at higher temperatures, from 220 to 700 °C, it was attributed to the thermal degradation of cellulose, hemicellulose, and lignin [69]. At the end of thermal degradation, the remaining weight loss can be attributed to the mineral

content present in the filler. Similar behaviour was reported by Lee *et al.* [70] using bamboo fiber as a lignocellulosic filler.

Regarding composites manufactured, neat PLA was thermally degraded in a single step, as can be observed in Figure IV.4.7a. This drop was produced by chain-scission of macromolecules of PLA through the breakage of ester groups into smaller fragments [71]. The addition of CSF particles reduced the temperature required for 5 wt.% of weight loss ($T_{5\%}$) from 328.4 ºC for neat PLA up to 264.9 ºC. As plotted in Figure IV.4.7a, PLA/CSF composite showed a reduction of the thermal stability associated with its low degradation temperature, which is characteristic of the presence of CSF fillers. Similar thermal degradation was reported by Qien and Sheng [62] with bamboo cellulose in PLA composites. Nevertheless, incorporating compatibilizers enhanced the thermal stability of manufactured composite, where $T_{5\%}$ is delayed approximately 45-50 ºC for all compatibilizers compared to PLA/CSF composite. The significant difference when composites are compatibilized could be directly associated with the improvement of matrix-polymer interaction, which hinders the removal of volatile products over thermal degradation [37]. In addition, the maximum degradation rate temperature (T_{max}) was also determined by the first derivate of weight loss, as observed in Figure IV.4.7b. As expected, neat PLA presented the highest value of 390.9 ºC, taking into account the absence of CSF fillers. On the contrary, the lowest T_{max} was observed for PLA/CSF composite with a value of 320.5 ºC, being in concordance with the trend of $T_{5\%}$ value. As happened previously, the addition of compatibilizers also delayed the T_{max} values in the 353.8-359.9 ºC range. It should point out that the highest improvement was obtained for PLA/CSF_ECO composite and this can be related to the higher reactivity with CSF filler and matrix compared to other compatibilizers. Furthermore, according to Agüero *et al.* [72], the epoxidized vegetable oils present low solubility in a PLA matrix, thus providing a thermal oxidation effect due to the non-reacted epoxy groups, whereas the remaining oil also could act as a physical barrier to hinder the volatile products.

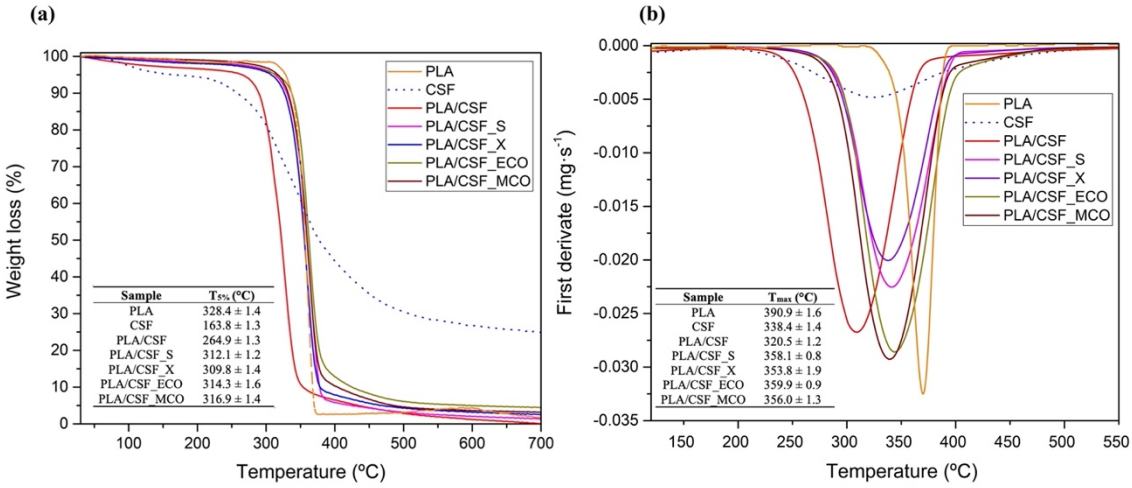

Figure IV.4.7. (a) Thermogravimetric analysis (TGA) and (b) first derivate thermogravimetric (DTG) curves of poly(lactic acid) (PLA) and 15 wt.% chia seed flour (CSF) composites with different compatibilizers.

Thermomechanical properties of PLA/CSF composites with compatibilizers

The evolution of storage modulus (G') and damping factor (tan δ) as a function of temperature for all manufactured composites are plotted in Figure IV.4.8(a-b), respectively. Concerning storage modulus, neat PLA was characterized by a value of 1200 Mpa at room temperature (30 ºC), being the lowest G' value which is in concordance with the previous mechanical results. As expected, the addition of CSF filler increased the stiffness of composite up to 1600 Mpa, which means an increment of 33.3% compared to neat PLA. This remarkable improvement in the mechanical resistance properties by the addition of lignocellulosic filler was also reported by several authors [73, 74], explained by the mobility restriction of polymers chains. Nevertheless, the addition of compatibilizers caused a reduction of G' values regarding uncompatibilized PLA/CSF composite, thus indicating an increase of mechanical ductile properties. Aguero *et al.* [75] suggested that using a compatibilizer improves the compatibility between PLA and fillers and, therefore, increases the ductility. It should be remarked that the functionalized vegetable oils, i.e., ECO and MCO, provided the lowest G' value in the 1371-1400 Mpa range, which corroborates the dual function of compatibilizer and plasticizer. At temperatures between 50-90 ºC, the G' value sharply decreases due to the glass-rubber transition that corresponds to

the T_g [76]. Over 90 ºC, a second thermal transition was observed related to the rearrange of PLA chains into a more packed structure characterized by the cold crystallization process. During this process, both stiffness and density increase because of the highly ordered structure [77]. The incorporation of CSF in PLA matrix led to delay the cold crystallization process compared to neat PLA, indicating that CSF filler interrupts the packaging process of PLA matrix [21]. Regarding compatibilizers, in general, slight differences are shown compared to uncompatibilized composite under shear deformation stress as function of temperature, excepting for PLA/CSF_MCO. This shift to higher temperatures of PLA/CSF_MCO composite can be related to formation of macromolecular structures that delayed the cold crystallization as was described above [78]. After cold crystallization, the G' values obtained for all compatibilized composites were higher compared to neat PLA.

In relation to the damping factor (tan δ), it indicates the degree of molecular mobility and is used to estimate the T_g value. Neat PLA showed the lowest T_g value of 63 ºC and was highly increased with the addition of CSF fillers up to 77 ºC. This shift to higher temperatures suggests that CSF filler decreased the PLA molecular mobility, i.e., the PLA chain was restricted. A similar remarkable increase was observed by other researchers with the addition of different lignocellulosic fillers in the PLA matrix [21]. With the addition of compatibilizers, a reduction of T_g value was observed, suggesting that manufactured composites presented higher chain mobility. In the case of PLA/CSF_S and PLA/CSF_X composites, it should be noted that the reduction of the T_g value was relatively low. Similar values were reported by Aguero *et al.* [25] that observed a slight decrease using Xibond and silane coupling agent as compatibilizers in PLA based on short flaxseed fibers. The addition of functionalized vegetable oils showed a much-pronounced T_g reduction. Both ECO and MCO compatibilizers enhanced the molecular chain mobility due to the flexibility provided by triglyceride molecules that lead to interact with CSF particles and PLA matrix. The PLA/CSF_ECO composite recorded a lower T_g value than using the MCO compatibilizer, indicating higher chain mobility as was above exposed in ductile and thermal properties. Then, the addition of both bio-based compatibilizers decreases the T_g by about 5-6% regarding PLA/CSF composite. This trend was also reported by

Quiles-Carrillo *et al.* [79], who evaluated the effect of different compatibilizers such as aromatic carbodiimide, maleinized linseed oil, and epoxy-based styrene-acrylic monomer in PLA filled with almond shell flour (ASF).

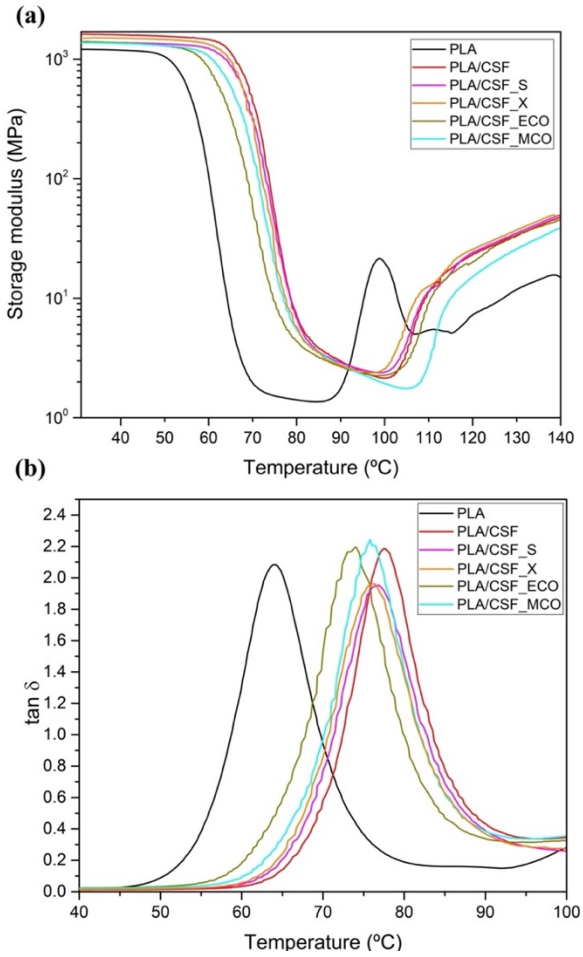

Figure IV.4.8. Dynamic mechanical thermal analysis (DMTA) of poly(lactic acid) (PLA) and 15 wt.% chia seed flour (CSF) composites with different compatibilizers; (a) storage modulus (G') and (b) damping factor (tan δ).

The evolution of water absorption of PLA/CSF composites with different compatibilizers after being submerged for 12 weeks is plotted in Figure IV.4.9. Firstly, neat PLA presented the lowest water absorption with an approximately content of 0.75 wt.%. This value corroborates the expected hydrophobic behaviour of PLA [80]. In agreement with the literature, the addition of lignocellulosic filler provides an increment of water absorption of the manufactured composite. The free hydroxyl groups (-OH) present in hemicellulose and cellulose may react with the hydrogen bonding of water [81]. In fact, the addition of CSF particles that present a hydrophilic

nature led to increasing the water absorption of PLA/CSF composite up to 5.9 wt.% after 12 weeks of immersion. Nevertheless, the addition of CSF with a previous silane treatment reduced the final water content up to 3 wt.%, being a reduction of almost 50% compared to PLA/CSF composite. It is known that surface treatment of fillers with silanes reduced the availability of hydroxyl groups [82], and therefore, it decreased the water diffusion into the composite. The addition of copolymer Xibond also showed a reduction of water absorption compared to PLA/CSF composite. This result suggests that the available hydroxyl groups of CSF were reduced due to interaction with the copolymer, thus hindering the diffusion of water. Furthermore, the highest water absorption value recorded was 9.3 wt.% for the MCO compatibilizer, meaning an increment of 57.6% regarding PLA/CSF composite. This behaviour can be attributed to the plasticization effect that increases the free volume and enhances the water diffusion into composite [13]. This trend is similar to one reported by Burgada *et al.* [83], who obtained the highest water absorption with a value of 7.5 wt.% using maleinized linseed oil (MLO) in polypropylene with short hemp fiber. Comparing the PLA/CSF_MCO composite value with other studies, the water absorption is not considered high. Several studies have evaluated the water uptake by wood-plastic composites (WPCs) with values about 15-16% in HDPE-based WPCs [84] or even around 12% with PLA-based WPCs [85]. It is important to remark that a water uptake in WPCs of 25% is commonly accepted, being the minimum level to begin the decrease of mechanical properties and bacterial growth [86]. Therefore, water uptake of PLA/CSF_MCO composite can guarantee no growth of bacterial and dimensional stability to be used in outdoor applications. However, the addition of ECO recorded a value of 4.51 wt.%, meaning a lower value than PLA/CSF and PLA/CSF_MCO composite. As shown, the addition of ECO and MCO provides different water absorption values despite both presenting the dual function of compatibilizer and plasticizer. This comparison of results suggests that PLA/CSF_ECO composite presents less available hydroxyl groups in CSF particles that can react further with water, thus reducing water absorption. As commented previously, the compatibilizing effect is related to interaction with lignocellulosic filler and PLA chains. Therefore, this phenomenon may be explained by a higher compatibilization effect, i.e., higher reactivity of ECO compared to MCO that reduces the water

absorption of composite. This is in concordance with values obtained in TGA and DTG curves that show the highest thermal stability because of the high reactivity and, therefore, more interaction between CSF and PLA matrix. A similar finding was reported by Shafiq *et al.* [87] when the addition of epoxidized vegetable oil in polypropylene with rubber seed shell showed a decrease in water absorption compared to uncompatibilized composite.

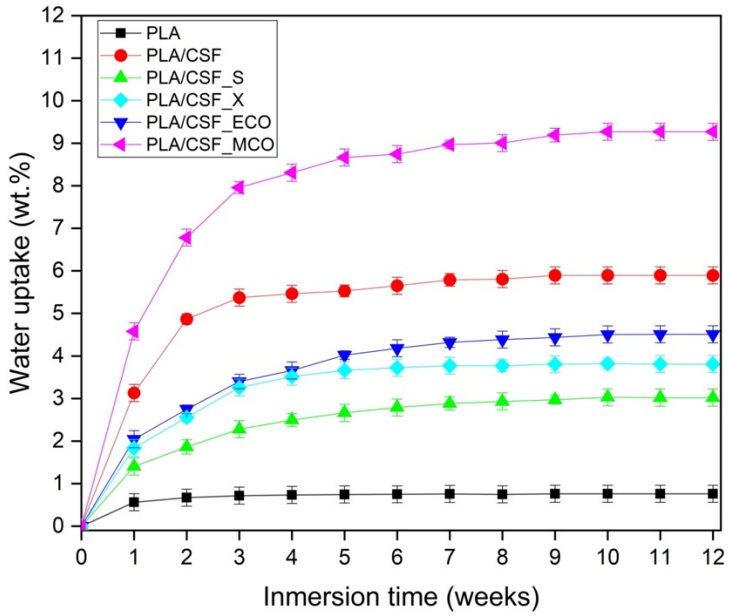

Figure IV.4.9. Water uptake of poly(lactic acid) (PLA) and 15 wt.% chia seed flour (CSF) composites with different compatibilizers.

Disintegration under composting conditions of PLA/CSF composites with compatibilizers

The weight loss of PLA/CSF composites with different compatibilizers was carried out to evaluate their effect on the disintegration process under composting conditions. The weight loss and the visual appearance can be observed in Figure IV.4.10 and Figure IV.4.11, respectively. At the beginning, i.e., zero-time, neat PLA presented its typical translucid appearance that becomes dark brown for the addition of CSF filler. The addition of compatibilizers slightly changed the colour appearance compared to PLA/CSF composite, as plotted in Figure IV.4.10. After 4 days, no sign of weight loss was recorded for all composites, while an evident change in visual appearance was observed. Neat PLA showed a shift from translucid to opaque due to

the increment of chain mobility that induced the crystallization of the PLA matrix. This effect is attributed to the proximity of the test temperature, which is 58 ºC, to the T_g value of the sample [88]. The same behaviour was obtained for all PLA/CSF composites, where it is suggested that the opacity of the PLA matrix induces the samples to become whiter. This phenomenon was also reported by Balart *et al.* [46], who assessed the disintegration compost of PLA with hazelnut shell flour. On the 8th day, neat PLA and PLA/CSF composite recorded a weight loss of 14% and 23%, respectively, noting a visual aspect more brittle for PLA/CSF composite. According to Da silva *et al.* [89], lignocellulosic fillers, which are mainly composed of cellulose, hemicellulose, and lignin, can be degraded by microorganism action. Nevertheless, it has been previously reported in the literature that neat PLA disintegrates faster than composites with lignocellulosic filler [90, 91] due to the biodegradation rate of the lignocellulosic fillers is slower than PLA matrix [92]. In this case, PLA/CSF composites showed a contrary behavior, at least in the early incubation days. It is known that the hydrophilic nature of lignocellulosic fillers leads to transfer water as well as enzymes or microorganism easily into the composite that induces to increase the degradation rate [68]. Moreover, the microorganism action is faster in amorphous domains [80, 93], and therefore, PLA/CSF composite presented a higher weight loss than neat PLA due to its low crystallinity. For all PLA/CSF composites with compatibilizers, the disintegration rate was delayed, recording values lower than 2%. This reduction can be ascribed to better compatibility between CSF filler and PLA matrix as well as the effect of crystallinity and water uptake. On the 11th day, all compatibilized PLA/CSF composites, that presented a disintegration rate lower than PLA/CSF composite and neat PLA, started to lose a significantly higher value than 10% except for PLA/CSF_ECO composite. On the 15th day, a remarkable increase in weight loss was recorded, particularly for the PLA/CSF composite with a value of 80%. On the contrary, both epoxidized and maleinized vegetable oils showed the lowest weight loss, being 10% and 30%, respectively. It should be pointed out that although PLA/CSF_ECO composite presented less crystallinity than PLA/CSF_MCO composite, the water uptake was highly reduced which hinders the disintegration rate. This difference was also corroborated with no breakage in visual appearance. After 18th day, neat PLA showed the highest degradation rate, about 88%, which was

above of PLA/CSF composite. After 31 days, neat PLA was totally disintegrated as expected due to its biodegradability, while all PLA/CSF composites presented a similar weight loss in the 94-90% range although the initial degradation rate was different. These results suggest that, irrespective of the compatibilizer used, after 31 days of testing, the rate of disintegration by composting is the same. Therefore, it can be concluded that all bio-based novel manufactured composites are considered disintegrable regardless the compatibilizer employed.

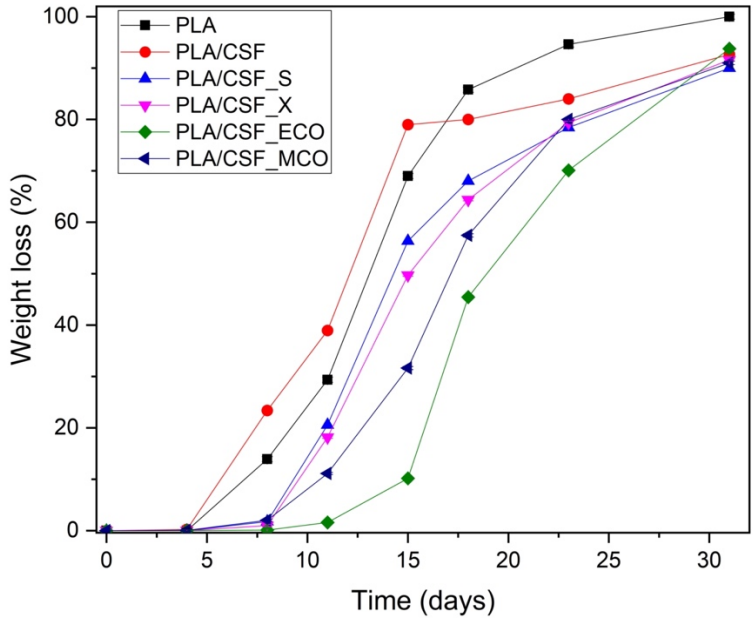

Figure IV.4.10. Weight loss during the disintegration process in controlled compost oil of poly(lactic acid) (PLA) and 15 wt.% chia seed flour (CSF) composites with different compatibilizers.

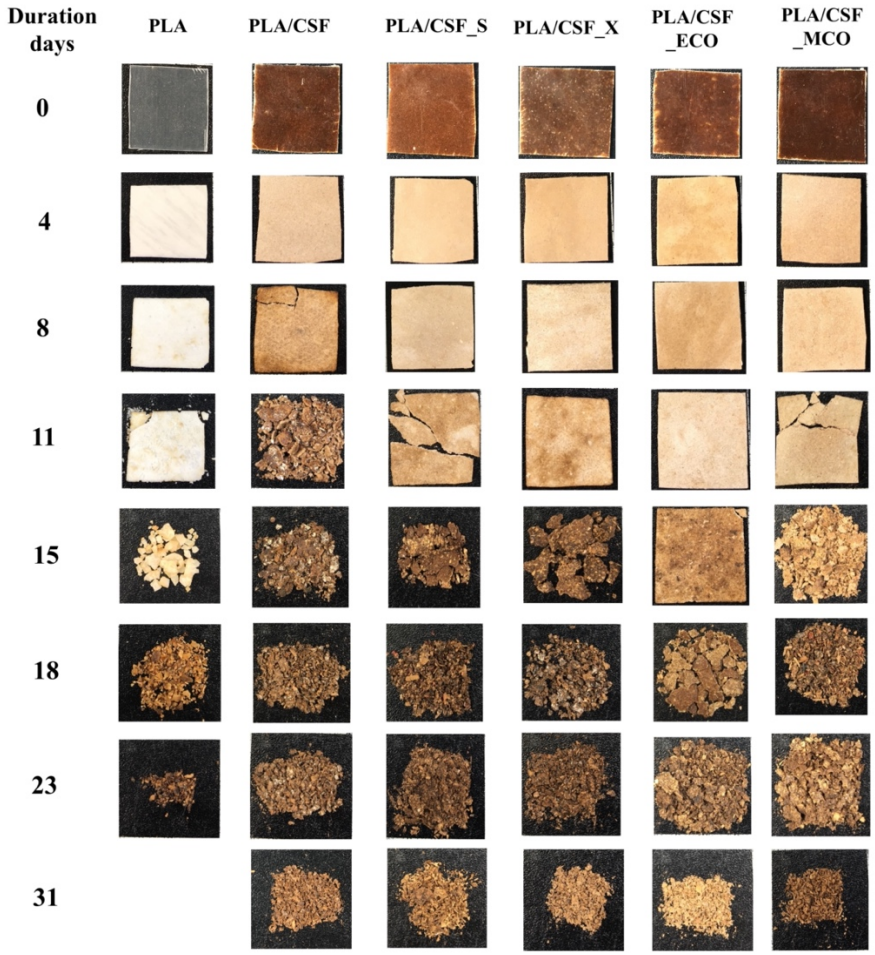

Figure IV.4.11. Visual appearance of the disintegration process in controlled compost oil of poly(lactic acid) (PLA) and 15 wt.% chia seed flour (CSF) composites with different compatibilizers.

Conclusions

Novel green composites based on PLA and CSF filler at 15 wt.% have been developed. The poor interfacial adhesion between CSF filler and PLA was improved by testing four different compatibilizers. FTIR results suggested chemical interaction in all compatibilized composites. The mechanical properties showed different results depending on the compatibilizer employed. Both PLA/CSF_S and PLA/CSF_X composite obtained an increment of mechanical resistance, toughness, and hardness. In the case of modified chia seed oil by epoxidation and maleinization, the ductile properties were remarkably improved, attaining the highest elongation at break, which means 10 and 8 times higher regarding the PLA/CSF composite, respectively.

The enhancement of interfacial adhesion between CSF fillers and PLA matrix was also corroborated by the surface morphology of the fractured surfaces, where this enhancement was observed. Thermal properties of all compatibilized composites pointed to a higher crystallinity than PLA/CSF composite, suggesting an improvement of chain mobility. Furthermore, the addition of compatibilizers caused a delay of 33-39 ºC in the maximum degradation rate confirming the higher polymer-matrix interaction, highlighting PLA/CSF_ECO composite with a value of 360 ºC. Concerning DMTA analysis, Tg values were reduced compared to PLA/CSF composite indicating higher chain mobility provided by the addition of compatibilizers, particularly for PLA/CSF_ECO composite. In general, the water uptake was reduced using compatibilizers due to the decrease of available hydroxyl groups that can react with water further. In particular, PLA/CSF_MCO presented the highest value, which is 100% higher than PLA/CSF_ECO, because of its lower reactivity that induces water diffusion into the composite. Finally, the disintegration test concluded that the use of different compatibilizers did not affect the compostability of composites, being an advantage considering all properties provided. Therefore, as a general conclusion, it has been developed composites based on PLA and by-products coming from CO extraction industry. The addition of CSF in PLA matrix gives high added value to the waste contributing to the circular economy. Besides, the novel bio-based compatibilizers and plasticizers derived from chia seed oil such as ECO and MCO, were employed for the first time with the aim of improving the polymer-matrix interaction. The results shows that PLA with CSF by using the novel compatibilizers from the same seed, are an interesting proposal from both economic and environmental point of view to be applied at industrial level to manufacture fully renewable composites.

Acknowledgements

This research work was funded by the Ministry of Science and Innovation-"Retos de la Sociedad". Project references: PID2020-119142RA-I00. I. Dominguez-Candela wants to thank Universitat Politècnica de València for his FPI grant (PAID-2019-SP20190013) and Generalitat Valenciana-GVA (ACIF/2020/233). J. Gomez-Caturla wants to thank Generalitat Valenciana-GVA, for his FPI grant

(ACIF/2021/185) and grant FPU20/01732 funded by MCIN/AEI/10.13039/501100011033.

References

[1] Europe P. Plastics–the facts 2020: An Analysis of European Plastics Production, Demand and Waste. Plastics Europe, Brussels. Available online: https://plasticseurope.org/wp-content/uploads/2021/09/Plastics_the_facts-WEB-2020_versionJun21_final.pdf (accessed on 21 September 2021).

[2] Leja K, Lewandowicz G. Polymer biodegradation and biodegradable polymers-a review. Polish Journal of Environmental Studies. 2010;19.

[3] Data BM. European Bioplastics. Available online: wwweuropean-bioplasticsorg/market (accessed on 20 October 2021). 2017.

[4] Kocaman S, Karaman M, Gursoy M, Ahmetli G. Chemical and plasma surface modification of lignocellulose coconut waste for the preparation of advanced biobased composite materials. Carbohydrate polymers. 2017;159:48-57.

[5] Torres-Giner S, Montanes N, Fenollar O, García-Sanoguera D, Balart R. Development and optimization of renewable vinyl plastisol/wood flour composites exposed to ultraviolet radiation. Materials & Design. 2016;108:648-58.

[6] Zhang W, Zhang X, Liang M, Lu C. Mechanochemical preparation of surface-acetylated cellulose powder to enhance mechanical properties of cellulose-filler-reinforced NR vulcanizates. Composites Science and Technology. 2008;68:2479-84.

[7] Yan X, Diao M, Yu Y, Gao F, Wang E, Wang Z. Influence of esterification and ultrasound treatment on formation and properties of starch nanoparticles and their impact as a filler on chitosan based films characteristics. International Journal of Biological Macromolecules. 2021;179:154-60.

[8] Ikhlef S, Nekkaa S, Guessoum M, Haddaoui N. Effects of alkaline treatment on the mechanical and rheological properties of low-density polyethylene/spartium junceum flour composites. International Scholarly Research Notices. 2012;2012.

[9] Maziad N, El-Nashar D, Sadek E. The effects of a silane coupling agent on properties of rice husk-filled maleic acid anhydride compatibilized natural rubber/low-density polyethylene blend. Journal of materials science. 2009;44:2665-73.

[10] Pothan LA, Thomas S. Polarity parameters and dynamic mechanical behaviour of chemically modified banana fiber reinforced polyester composites. Composites Science and Technology. 2003;63:1231-40.

[11] Xie Y, Hill CA, Xiao Z, Militz H, Mai C. Silane coupling agents used for natural fiber/polymer composites: A review. Composites Part A: Applied Science and Manufacturing. 2010;41:806-19.

[12] Nyambo C, Mohanty AK, Misra M. Effect of maleated compatibilizer on performance of PLA/wheat Straw-Based green composites. Macromolecular Materials and Engineering. 2011;296:710-8.

[13] Ferri J, Garcia-Garcia D, Sánchez-Nacher L, Fenollar O, Balart R. The effect of maleinized linseed oil (MLO) on mechanical performance of poly (lactic acid)-thermoplastic starch (PLA-TPS) blends. Carbohydrate polymers. 2016;147:60-8.

[14] Garcia-Campo MJ, Quiles-Carrillo L, Masia J, Reig-Pérez MJ, Montanes N, Balart R. Environmentally friendly compatibilizers from soybean oil for ternary blends of poly (lactic acid)-PLA, poly (ε-caprolactone)-PCL and poly (3-hydroxybutyrate)-PHB. Materials. 2017;10:1339.

[15] Retegi A, Algar I, Martin L, Altuna F, Stefani P, Zuluaga R. Sustainable optically transparent composites based on epoxidized soy-bean oil (ESO) matrix and high contents of bacterial cellulose (BC). Cellulose. 2012;19:103-9.

[16] Samper M, Petrucci R, Sánchez-Nacher L, Balart R, Kenny J. New environmentally friendly composite laminates with epoxidized linseed oil (ELO) and slate fiber fabrics. Composites Part B: Engineering. 2015;71:203-9.

[17] Dominguez-Candela I, Ferri JM, Cardona SC, Lora J, Fombuena V. Dual Plasticizer/Thermal Stabilizer Effect of Epoxidized Chia Seed Oil (*Salvia hispanica L.*) to Improve Ductility and Thermal Properties of Poly (Lactic Acid). Polymers. 2021;13:1283.

[18] Chia Seeds Market Size Worth $4.7 Billion By 2025. Grand View Research. 2019. Available online: https://www.grandviewresearch.com/press-release/global-chia-seeds-market (accessed on 14 October 2021).

[19] Dominguez-Candela I, Garcia-Garcia D, Perez-Nakai A, Lerma-Canto A, Lora J, Fombuena V. Contribution to a Circular Economy Model: From Lignocellulosic Wastes from the Extraction of Vegetable Oils to the Development of a New Composite. Polymers. 2021;13:2269.

[20] Lerma-Canto A, Gomez-Caturla J, Herrero-Herrero M, Garcia-Garcia D, Fombuena V. Development of Polylactic Acid Thermoplastic Starch Formulations Using Maleinized Hemp Oil as Biobased Plasticizer. Polymers. 2021;13:1392.

[21] Carbonell-Verdu A, Boronat T, Quiles-Carrillo L, Fenollar O, Dominici F, Torre L. Valorization of Cotton Industry Byproducts in Green Composites with Polylactide. Journal of Polymers and the Environment. 2020;28:2039-53.

[22] Tran TPT, Bénézet J-C, Bergeret A. Rice and Einkorn wheat husks reinforced poly (lactic acid)(PLA) biocomposites: Effects of alkaline and silane surface treatments of husks. Industrial Crops and Products. 2014;58:111-24.

[23] Quiles-Carrillo L, Boronat T, Montanes N, Balart R, Torres-Giner S. Injection-molded parts of fully bio-based polyamide 1010 strengthened with waste derived slate fibers pretreated with glycidyl-and amino-silane coupling agents. Polymer Testing. 2019;77:105875.

[24] Samper M, Petrucci R, Sánchez-Nacher L, Balart R, Kenny J. Effect of silane coupling agents on basalt fiber–epoxidized vegetable oil matrix composite materials analyzed by the single fiber fragmentation technique. Polymer Composites. 2015;36:1205-12.

[25] Agüero Á, Garcia-Sanoguera D, Lascano D, Rojas-Lema S, Ivorra-Martinez J, Fenollar O. Evaluation of different compatibilization strategies to improve the performance of injection-molded green composite pieces made of polylactide reinforced with short flaxseed fibers. Polymers. 2020;12:821.

[26] Arrieta MP, Samper MD, López J, Jiménez A. Combined effect of poly (hydroxybutyrate) and plasticizers on polylactic acid properties for film intended for food packaging. Journal of Polymers and the Environment. 2014;22:460-70.

[27] San Román MS, Holgado MJ, Salinas B, Rives V. Drug release from layered double hydroxides and from their polylactic acid (PLA) nanocomposites. Applied clay science. 2013;71:1-7.

[28] Braun B, Dorgan JR, Dec SF. Infrared spectroscopic determination of lactide concentration in polylactide: an improved methodology. Macromolecules. 2006;39:9302-10.

[29] Kemala T, Budianto E, Soegiyono B. Preparation and characterization of microspheres based on blend of poly (lactic acid) and poly (ε-caprolactone) with poly (vinyl alcohol) as emulsifier. Arabian Journal of Chemistry. 2012;5:103-8.

[30] Torres-Giner S, Gimeno-Alcañiz JV, Ocio MJ, Lagaron JM. Optimization of electrospun polylactide-based ultrathin fibers for osteoconductive bone scaffolds. Journal of Applied Polymer Science. 2011;122:914-25.

[31] Lima EMB, Middea A, Neumann R, Thiré RMdSM, Pereira JF, de Freitas SC. Biocomposites of PLA and Mango Seed Waste: Potential Material for Food

Packaging and a Technological Alternative to Reduce Environmental Impact. Starch-Stärke. 2021;73:2000118.

[32] Lima EMB, Lima AM, Minguita APS, Rojas dos Santos NR, Pereira ICS, Neves TTM. Poly (lactic acid) biocomposites with mango waste and organo-montmorillonite for packaging. Journal of Applied Polymer Science. 2019;136:47512.

[33] Wan L, Zhang Y. Jointly modified mechanical properties and accelerated hydrolytic degradation of PLA by interface reinforcement of PLA-WF. Journal of the Mechanical Behavior of Biomedical Materials. 2018;88:223-30.

[34] Sepe R, Bollino F, Boccarusso L, Caputo F. Influence of chemical treatments on mechanical properties of hemp fiber reinforced composites. Composites Part B: Engineering. 2018;133:210-7.

[35] Yu T, Ren J, Li S, Yuan H, Li Y. Effect of fiber surface-treatments on the properties of poly (lactic acid)/ramie composites. Composites Part A: Applied Science and Manufacturing. 2010;41:499-505.

[36] García-García D, Carbonell A, Samper M, García-Sanoguera D, Balart R. Green composites based on polypropylene matrix and hydrophobized spend coffee ground (SCG) powder. Composites Part B: Engineering. 2015;78:256-65.

[37] Quiles-Carrillo L, Balart R, Boronat T, Torres-Giner S, Puglia D, Dominici F. Development of Compatibilized Polyamide 1010/Coconut Fibers Composites by Reactive Extrusion with Modified Linseed Oil and Multi-functional Petroleum Derived Compatibilizers. Fibers and Polymers. 2021;22:728-44.

[38] Masek A, Cichosz S, Piotrowska M. Biocomposites of Epoxidized Natural Rubber/Poly (lactic acid) Modified with Natural Fillers (Part I). International Journal of Molecular Sciences. 2021;22:3150.

[39] Pawlak F, Aldas M, López-Martínez J, Samper MD. Effect of different compatibilizers on injection-molded green fiber-reinforced polymers based on

poly (lactic acid)-maleinized linseed oil system and sheep wool. Polymers. 2019;11:1514.

[40] Chen T, Wu Y, Qiu J, Fei M, Qiu R, Liu W. Interfacial compatibilization via in-situ polymerization of epoxidized soybean oil for bamboo fibers reinforced poly (lactic acid) biocomposites. Composites Part A: Applied Science and Manufacturing. 2020;138:106066.

[41] Kamarudin SH, Abdullah LC, Aung MM, Ratnam CT, Jusoh ER. A study of mechanical and morphological properties of PLA based biocomposites prepared with EJO vegetable oil based plasticiser and kenaf fibres. Materials Research Express. 2018;5:085314.

[42] Mahmud S, Long Y, Wang J, Dai J, Zhang R, Zhu J. Waste cellulose fibers reinforced polylactide toughened by direct blending of epoxidized soybean oil. Fibers and Polymers. 2020;21:2949-61.

[43] Frone A, Berlioz S, Chailan JF, Panaitescu D, Donescu D. Cellulose fiber-reinforced polylactic acid. Polymer Composites. 2011;32:976-85.

[44] Nampoothiri KM, Nair NR, John RP. An overview of the recent developments in polylactide (PLA) research. Bioresource technology. 2010;101:8493-501.

[45] Angelini S, Cerruti P, Immirzi B, Santagata G, Scarinzi G, Malinconico M. From biowaste to bioresource: Effect of a lignocellulosic filler on the properties of poly (3-hydroxybutyrate). International Journal of Biological Macromolecules. 2014;71:163-73.

[46] Balart J, Fombuena V, Fenollar O, Boronat T, Sánchez-Nacher L. Processing and characterization of high environmental efficiency composites based on PLA and hazelnut shell flour (HSF) with biobased plasticizers derived from epoxidized linseed oil (ELO). Composites Part B: Engineering. 2016;86:168-77.

[47] Kamarudin SH, Abdullah LC, Aung MM, Ratnam CT. Mechanical and physical properties of Kenaf-reinforced Poly (lactic acid) plasticized with epoxidized Jatropha Oil. BioResources. 2019;14:9001-20.

[48] Chieng BW, Ibrahim NA, Then YY, Loo YY. Epoxidized vegetable oils plasticized poly (lactic acid) biocomposites: mechanical, thermal and morphology properties. Molecules. 2014;19:16024-38.

[49] Mahmud S, Long Y, Abu Taher M, Xiong Z, Zhang R, Zhu J. Toughening polylactide by direct blending of cellulose nanocrystals and epoxidized soybean oil. Journal of Applied Polymer Science. 2019;136:48221.

[50] Liminana P, Garcia-Sanoguera D, Quiles-Carrillo L, Balart R, Montanes N. Development and characterization of environmentally friendly composites from poly (butylene succinate)(PBS) and almond shell flour with different compatibilizers. Composites Part B: Engineering. 2018;144:153-62.

[51] Lascano D, Garcia-Garcia D, Rojas-Lema S, Quiles-Carrillo L, Balart R, Boronat T. Manufacturing and characterization of green composites with partially biobased epoxy resin and flaxseed flour wastes. Applied Sciences. 2020;10:3688.

[52] Crespo J, Balart R, Sanchez L, Lopez J. Mechanical behaviour of vinyl plastisols with cellulosic fillers. Analysis of the interface between particles and matrices. International journal of adhesion and adhesives. 2007;27:422-8.

[53] Chun KS, Husseinsyah S, Osman H. Mechanical and thermal properties of coconut shell powder filled polylactic acid biocomposites: effects of the filler content and silane coupling agent. Journal of Polymer Research. 2012;19:1-8.

[54] Moazeni N, Mohamad Z, Dehbari N. Study of silane treatment on poly-lactic acid (PLA)/sepiolite nanocomposite thin films. Journal of Applied Polymer Science. 2015;132.

[55] Carbonell-Verdu A, Samper MD, Garcia-Garcia D, Sanchez-Nacher L, Balart R. Plasticization effect of epoxidized cottonseed oil (ECSO) on poly (lactic acid). Industrial Crops and Products. 2017;104:278-86.

[56] Quiles-Carrillo L, Montanes N, Lagaron JM, Balart R, Torres-Giner S. On the use of acrylated epoxidized soybean oil as a reactive compatibilizer in injection-

molded compostable pieces consisting of polylactide filled with orange peel flour. Polymer International. 2018;67:1341-51.

[57] Gonzalez L, Agüero A, Quiles-Carrillo L, Lascano D, Montanes N. Optimization of the loading of an environmentally friendly compatibilizer derived from linseed oil in poly (lactic acid)/diatomaceous earth composites. Materials. 2019;12:1627.

[58] Jandas P, Mohanty S, Nayak S. Thermal properties and cold crystallization kinetics of surface-treated banana fiber (BF)-reinforced poly (lactic acid)(PLA) nanocomposites. Journal of thermal analysis and calorimetry. 2013;114:1265-78.

[59] Ortiz-Barajas DL, Arévalo-Prada JA, Fenollar O, Rueda-Ordóñez YJ, Torres-Giner S. Torrefaction of Coffee Husk Flour for the Development of Injection-Molded Green Composite Pieces of Polylactide with High Sustainability. Applied Sciences. 2020;10:6468.

[60] Gregorova A, Hrabalova M, Kovalcik R, Wimmer R. Surface modification of spruce wood flour and effects on the dynamic fragility of PLA/wood composites. Polymer Engineering & Science. 2011;51:143-50.

[61] Sanyang ML, Sapuan SM, Jawaid M, Ishak MR, Sahari J. Effect of plasticizer type and concentration on tensile, thermal and barrier properties of biodegradable films based on sugar palm (Arenga pinnata) starch. Polymers. 2015;7:1106-24.

[62] Qian S, Sheng K. PLA toughened by bamboo cellulose nanowhiskers: Role of silane compatibilization on the PLA bionanocomposite properties. Composites Science and Technology. 2017;148:59-69.

[63] Corre Y-M, Duchet J, Reignier J, Maazouz A. Melt strengthening of poly (lactic acid) through reactive extrusion with epoxy-functionalized chains. Rheologica Acta. 2011;50:613-29.

[64] Orue A, Eceiza A, Arbelaiz A. Preparation and characterization of poly (lactic acid) plasticized with vegetable oils and reinforced with sisal fibers. Industrial Crops and Products. 2018;112:170-80.

[65] Kong J, Han C, Yu Y, Dong L. Production and characterization of sustainable poly (lactic acid)/functionalized-eggshell composites plasticized by epoxidized soybean oil. Journal of materials science. 2018;53:14386-97.

[66] Luo H, Zhang C, Xiong G, Wan Y. Effects of alkali and alkali/silane treatments of corn fibers on mechanical and thermal properties of its composites with polylactic acid. Polymer Composites. 2016;37:3499-507.

[67] Ludueña L, Vázquez A, Alvarez V. Effect of lignocellulosic filler type and content on the behavior of polycaprolactone based eco-composites for packaging applications. Carbohydrate polymers. 2012;87:411-21.

[68] Calabia BP, Ninomiya F, Yagi H, Oishi A, Taguchi K, Kunioka M. Biodegradable poly (butylene succinate) composites reinforced by cotton fiber with silane coupling agent. Polymers. 2013;5:128-41.

[69] Tserki V, Matzinos P, Kokkou S, Panayiotou C. Novel biodegradable composites based on treated lignocellulosic waste flour as filler. Part I. Surface chemical modification and characterization of waste flour. Composites Part A: Applied Science and Manufacturing. 2005;36:965-74.

[70] Lee S-H, Wang S. Biodegradable polymers/bamboo fiber biocomposite with bio-based coupling agent. Composites Part A: Applied Science and Manufacturing. 2006;37:80-91.

[71] Sánchez-Jiménez PE, Pérez-Maqueda LA, Perejón A, Criado JM. Generalized kinetic master plots for the thermal degradation of polymers following a random scission mechanism. The Journal of Physical Chemistry A. 2010;114:7868-76.

[72] Agüero Á, Lascano D, Garcia-Sanoguera D, Fenollar O, Torres-Giner S. Valorization of linen processing by-products for the development of injection-

molded green composite pieces of polylactide with improved performance. Sustainability. 2020;12:652.

[73] Părpăriță E, Darie RN, Popescu C-M, Uddin MA, Vasile C. Structure–morphology–mechanical properties relationship of some polypropylene/lignocellulosic composites. Materials & Design. 2014;56:763-72.

[74] Agustin-Salazar S, Cerruti P, Medina-Juárez LÁ, Scarinzi G, Malinconico M, Soto-Valdez H. Lignin and holocellulose from pecan nutshell as reinforcing fillers in poly (lactic acid) biocomposites. International Journal of Biological Macromolecules. 2018;115:727-36.

[75] Aguero A, Quiles-Carrillo L, Jorda-Vilaplana A, Fenollar O, Montanes N. Effect of different compatibilizers on environmentally friendly composites from poly (lactic acid) and diatomaceous earth. Polymer International. 2019;68:893-903.

[76] Al-Itry R, Lamnawar K, Maazouz A, Billon N, Combeaud C. Effect of the simultaneous biaxial stretching on the structural and mechanical properties of PLA, PBAT and their blends at rubbery state. European Polymer Journal. 2015;68:288-301.

[77] Yu Y, Cheng Y, Ren J, Cao E, Fu X, Guo W. Plasticizing effect of poly (ethylene glycol) s with different molecular weights in poly (lactic acid)/starch blends. Journal of Applied Polymer Science. 2015;132.

[78] Ojijo V, Ray SS. Super toughened biodegradable polylactide blends with non-linear copolymer interfacial architecture obtained via facile in-situ reactive compatibilization. Polymer. 2015;80:1-17.

[79] Quiles-Carrillo L, Montanes N, Garcia-Garcia D, Carbonell-Verdu A, Balart R, Torres-Giner S. Effect of different compatibilizers on injection-molded green composite pieces based on polylactide filled with almond shell flour. Composites Part B: Engineering. 2018;147:76-85.

[80] Deroiné M, Le Duigou A, Corre Y-M, Le Gac P-Y, Davies P, César G. Accelerated ageing of polylactide in aqueous environments: Comparative

study between distilled water and seawater. Polymer degradation and stability. 2014;108:319-29.

[81] Kuciel S, Jakubowska P, Kuźniar P. A study on the mechanical properties and the influence of water uptake and temperature on biocomposites based on polyethylene from renewable sources. Composites Part B: Engineering. 2014;64:72-7.

[82] Girones J, Méndez JA, Boufi S, Vilaseca F, Mutjé P. Effect of silane coupling agents on the properties of pine fibers/polypropylene composites. Journal of Applied Polymer Science. 2007;103:3706-17.

[83] Burgada F, Fages E, Quiles-Carrillo L, Lascano D, Ivorra-Martinez J, Arrieta MP. Upgrading Recycled Polypropylene from Textile Wastes in Wood Plastic Composites with Short Hemp Fiber. Polymers. 2021;13:1248.

[84] Ab Ghani MH, Ahmad S. The comparison of water absorption analysis between counterrotating and corotating twin-screw extruders with different antioxidants content in wood plastic composites. Advances in Materials Science and Engineering. 2011;2011.

[85] Liu R, Peng Y, Cao J, Chen Y. Comparison on properties of lignocellulosic flour/polymer composites by using wood, cellulose, and lignin flours as fillers. Composites Science and Technology. 2014;103:1-7.

[86] Zabel RA, Morrell JJ. Wood microbiology: decay and its prevention: Academic press; 2012.

[87] Shafiq MD, Ismail H. The effect of epoxidized vegetable oil and phthalic anhydride as compatibilizers on properties of rubber seed shell/polypropylene composites. Iranian Polymer Journal. 2021;30:547-57.

[88] Garcia-Garcia D, Carbonell-Verdu A, Arrieta M, López-Martínez J, Samper M. Improvement of PLA film ductility by plasticization with epoxidized karanja oil. Polymer degradation and stability. 2020;179:109259.

[89] da Silva AMB, Martins AB, Santana RMC. Biodegradability studies of lignocellulosic fiber reinforced composites. Fiber Reinforced Composites: Elsevier; 2021. P. 241-71.

[90] Mathew AP, Oksman K, Sain M. Mechanical properties of biodegradable composites from poly lactic acid (PLA) and microcrystalline cellulose (MCC). Journal of Applied Polymer Science. 2005;97:2014-25.

[91] Kumar R, Yakubu M, Anandjiwala R. Biodegradation of flax fiber reinforced poly lactic acid. eXPRESS Polymer Letters. 2010;4:423-30.

[92] Zandi Aa, Zanganeh A, Hemmati F, Mohammadi-Roshandeh J. Thermal and biodegradation properties of poly (lactic acid)/rice straw composites: effects of modified pulping products. Iranian Polymer Journal. 2019;28:403-15.

[93] Luo Y-B, Wang X-L, Wang Y-Z. Effect of TiO_2 nanoparticles on the long-term hydrolytic degradation behavior of PLA. Polymer degradation and stability. 2012;97:721-8.

European Polymer Journal 173 (2022) 111289

Contents lists available at ScienceDirect

European Polymer Journal

journal homepage: www.elsevier.com/locate/europolj

Novel compatibilizers and plasticizers developed from epoxidized and maleinized chia oil in composites based on PLA and chia seed flour

Ivan Dominguez-Candela [a,*], Jaume Gomez-Caturla [b], S.C. Cardona [a], Jaime Lora-García [a], Vicent Fombuena [b]

[a] Instituto de Seguridad Industrial, Radiofísica y Medioambiental (ISIRYM) Universitat Politècnica de València (UPV), Plaza Ferrándiz y Carbonell, s/n 03801, Alcoy, Spain
[b] Technological Institute of Materials (ITM), Universitat Politècnica de València (UPV), Plaza Ferrándiz y Carbonell 1, 03801 Alcoy, Spain

ARTICLE INFO

Keywords:
Epoxidized chia seed oil
Maleinized chia seed oil
poly(lactic acid) (PLA)
Chia seed flour
Compatibilizer

ABSTRACT

Novel compatibilizers and plasticizers derived from epoxidized chia seed oil (ECO) and maleinized chia seed oil (MCO) have been applied in composites based on poly(lactic acid) (PLA) and 15 wt% chia seed flour (CSF). Results obtained have been compared to conventional silane coupling agent, (3-glycidyloxypropyl) trimethoxysilane (GPS), and a petroleum-based compatibilizer, poly(styrene-co-glycidyl methacrylate) copolymer (Xibond, ®). The compatibilization effect of green composites were assessed by FTIR. The addition of all four compatibilizers improved the ductile mechanical and thermal properties of the composites. The morphology analysis revealed an improvement of interfacial adhesion of the CSF particles into the PLA matrix. In particular, ECO and MCO composites showed a roughness with long filaments in their morphology which plays a crucial role in improving the ductile properties highly. The elongation at break was 10 and 8 times higher using ECO and MCO, respectively, compared to uncompatibilized composite. Moreover, the composites manufactured showed low values (<9%) in the water uptake assay and a negligible compostability delay. The use of novel compatibilizers based on modified vegetable oils could mean an interesting proposal to obtain an entirely environmentally friendly composite with a remarkable ductile property.

1. Introduction

At present, one of the leading environmental concerns is the continuous generation of plastic wastes after human consumption. In Europe, plastics production reached 62 million tonnes in 2018, of which 29 million tonnes were collected to be treated [1]. Despite this target, 7.25 million tonnes were still sent to landfills. Therefore, an interesting proposal to overcome this environmental problem is to substitute the most commonly used petrochemical and non-biodegradable plastics, known as *commodities* (LDPE, HDPE, PVC, PP, PS, etc.), by bioplastics, i.e., polymers that are biodegradable, bio-based or both features.

Regarding bioplastics, the most remarkable are the biodegradable and fully or partially bio-based polymers, because they allow reducing the dependency of fossil resources and, therefore, greenhouse gas emissions. Poly(lactic acid) – (PLA) is one of the most used biodegradable polymers due to its competitive price, the suitable thermal stability to be industrially processed, good mechanical properties that can be compared to several non-biodegradable polymers, high transparency, etc. [2]. For these reasons, PLA involves 24% of the global market production of biodegradable polymers, followed by poly(butylene succinate) (PBS) and poly(butylene adipate-co-terephthalate) (PBAT) with a value of 23% [3]. Nevertheless, the major drawback is its inherent brittleness and poor compatibility with organic fillers, as those that can be used to develop green composites, making some commercial applications difficult.

Thus, improving the ductile properties and enhancing the interfacial adhesion between organic fillers and polymeric matrix are two of the most critical challenges for the biopolymers and composites PLA-based sector. In previous literature, several strategies have been performed based on the physical and chemical processes of lignocellulosic filler. Some physical methods based on plasma treatment and ultraviolet radiation with interesting results were obtained using lignocellulosic filler [4,5]. Besides, conventional chemical surface treatments on fillers such as acetylation [6], esterification [7], or alkaline procedure [8] were also studied. In addition, one of the most used chemical surface treatments is silanization, which employs a silane coupling agent to improve the

* Corresponding author.
E-mail address: ivdocan@doctor.upv.es (I. Dominguez-Candela).

https://doi.org/10.1016/j.eurpolymj.2022.111289
Received 4 February 2022; Received in revised form 25 April 2022; Accepted 17 May 2022
Available online 21 May 2022

Bloque IV: termoestables

IV.5 "Development of a novel epoxy resin based on epoxidized chia oil as matrix and maleinized chia oil as bio-renewable crosslinker"

Ivan Dominguez-Candela[1], Aina Perez-Nakai[2], Elena Torres-Roca[3], Jaime Lora[1], Vicent Fombuena[2]

[1] Instituto de Seguridad Industrial, Radiofísica y Medioambiental (ISIRYM), Universitat Politècnica de València (UPV), Plaza Ferrándiz y Carbonell, s/n, 03801 Alcoy, Spain

[2] Technological Institute of Materiales (ITM), Universitat Politècnica de València (UPV), Plaza Ferrándiz y Carbonell 1, 03801 Alcoy, Spain

[3] Textile Industry Research Association (AITEX), Plaza Emilio Sala 1, Alcoy 03801, Spain.

Journal of Applied Polymer Science

2023, 140(10), e53574.

"Development of a novel epoxy resin based on epoxidized chia oil as matrix and maleinized chia oil as bio-renewable crosslinker"

Abstract

In this work novel thermosetting resins with high bio-based content have been developed derived from chia seed oil (CO). Epoxidized chia seed oil (ECO) was used as bio-based epoxy matrix with different mixtures of crosslinker agents, i.e., methyl nadic anhydride (MNA) as petroleum-derived and maleinized chia seed oil (MCO) as bio-based crosslinker. The chemically modified oils from CO, i.e., ECO and MCO, and MNA were analyzed by titration and FT-IR. Additional ^{1}H NMR analysis was performed to characterize MCO structure. Two different behaviors were observed using the mixtures of crosslinkers. On one hand, MNA increases the rigidity with bio-based content of 54.2 %. On the other hand, the addition of MCO provides higher ductility with bio-based content up to 98 %. The same trend was observed by DMTA analysis. The novel cured resins were successfully crosslinked as demonstrated by the mechanical properties, FT-IR analyses, and gel content. Based on the results, it is concluded that MCO presents higher reactivity than MNA, decreasing curing time with possible energy saving at industrial level. In general, the results showed that adding the appropriate amount of MCO, green thermosetting resins with the desired thermal and mechanical properties can be manufactured with high bio-based content.

Keywords

chia seed oil; bio-based epoxy resin; epoxidized chia seed oil, maleinized chia seed oil; ductility; curing time

Introduction

Currently, there is an urgent need to develop innovative technologies and materials from renewable resources in order to reduce dependence on fossil resources. The current inflation that has led to a sharp increase in the prices of goods and services, together with the current energy crisis, exacerbated by the war in Ukraine, has further highlighted the need for a change in the production model [1,2]. For years, the scientific community has been focusing on the need to develop polymeric materials from biomass or plant derivatives, such as starch [3], cellulose [4], lignin [5], marine resources [6], lipids [7] and vegetable oils (VO) [8], in as much as the utilization of renewable raw materials is one of the *12 Principles of Green Chemistry* [9]. This is evidenced by the large number of publications related to materials developed from these precursors.

Of all these renewable precursors, the use of VO is worth highlighting. These have a series of advantages and physicochemical properties that make them particularly interesting in the development of new eco-efficient materials [10, 11]. First, they can act as precursors for the development of an infinite number of new products for engineering use, such as cosmetic products and shampoos [12], lubricants [13], plasticizers [14], emulsifiers [15], or even new thermoset polymers [16] as will be detailed in the current study. Moreover, current data on the production of vegetable oils show their increased production, abundant availability, and relatively low price compared to other precursors obtained from biomass [17].

The main constituent of the VO are triglycerides, which are the product of the esterification of three fatty acids and glycerol. These fatty acids can be classified according to the number of unsaturations (C=C double bonds), giving rise to saturated fatty acids (SFAs), for example, palmitic acid, monounsaturated fatty acids (MUFAs), such as oleic acid, or polyunsaturated fatty acids (PUFAs), such as linolenic acid. The average value of unsaturations can be expressed in terms of the iodine value (*IV*) (g $I_2 \cdot 100\ g^{-1}$). Therefore, according to this parameter, those oils with *IV* higher than 100-150, known as drying oils, will be those of greatest industrial interest [18]. This justifies that oils from linseed [19], soybean [20], hemp [21], or tung [22] are the most

commonly used in industrial applications. However, it is worth noting that one of the VO with the highest *IV*, chia seed oil (CO) (*Salvia hispanica L.*), with a value of over 190 g I_2 ·100 g^{-1} [23], and a market with a growth rate of over 23 % between 2019 and 2025 [24], has hardly any bibliography related to its possible industrial applications.

For the aforementioned industrial applications, especially in the preparation of polymeric materials, it is necessary to take advantage of the double bonds (C=C) as reactive sites, to cause a functionalization of the triglycerides. In the specific case of thermosetting polymers, these reactive sites act as crosslinking points of the tridimensional chain. Some of these chemical modifications are epoxidation and maleinization. During epoxidation, the double bonds present in the triglycerides are oxidized generating oxirane groups [25]. Current literature shows a wide market for its use as a plasticizer and stabilizer of Poly(vinyl chloride) (PVC)[26-29] and a new opportunity for the development of bio-based thermosetting epoxy resins [30].

Besides, to convert VO into a curable thermosetting matrix, the addition of a hardener acting as a curing agent is necessary. The most employed hardeners in epoxy-type resins are anhydrides, and amines [31]. Many works have been developed using different epoxidized VOs such as linseed [32], soybean [33], or hemp seed oil [34] crosslinked with petrochemical-based hardeners. Nevertheless, different studies show the toxicity of aliphatic-, cycloaliphatic- and aromatic-amines, as well as the relationship between sensitization and asthma problems related to anhydrides (methyl tetrahydrophthalic anhydride (MTHPA), or tetrahydrophthalic anhydride (THPA) among others) [35,36]. However, fewer works have been reported using epoxy resin and bio-based hardeners from VOs. For instance, Stemmelen *et al.* [37] studied the curing process of epoxidized linseed oil (ELO) as epoxy resin and aminated grapeseed oil (AGSO) as an alternative bio-crosslinker. Other study carried out by the same author was the ELO crosslinked with fatty amides from VOs [38]. Another proposal of bio-based crosslinker is the maleinization of VOs, which consists of the reaction of maleic anhydride (MA) with a double bond, that allows the development of thermosetting resins derived almost entirely from VOs [39]. Takahashi *et al.* [40] characterized commercial epoxidized soybean oil (ESO) crosslinked with maleinized linseed oil (MLO), obtaining by DTMA a value of glass

transition temperature (T_g) of -41 ºC. Samper *et al.* [41] and Fombuena *et al.* [32] developed thermoset resins based on ESO and composites based on ELO and flax fabrics as reinforcement respectively using mixtures of MNA and MLO as crosslinker agents. Therefore, the use of MLO has been studied previously but, to the best of our knowledge, there is no bibliography related to the oil with the highest unsaturation, CO.

Thus, the overall objective of this study is to develop and optimize novel thermosetting resins obtained from the use of epoxidized chia oil (ECO) as matrix and maleinized chia oil (MCO) as hardener to reach high bio-based content. Different amounts of crosslinker in combination with an anhydride of petrochemical origin, methyl nadic anhydride (MNA), have been systematically varied to test a wide range of thermo-mechanical properties of the new thermoset resin.

Experimental

Materials

In order to obtain thermosetting resins with high bio-based content, two modifications of CO were carried out. First, CO was extracted from chia seed provided by Frutoseco (Bigastro, Alicante, Spain). This extraction was performed by cold mechanical extrusion using a CRZ-309 press machine (Changyouxin Trading Co., Zhucheng, China). Afterward, CO was chemically modified by epoxidation and maleinization processes to introduce reactive points in fatty acid chains. The epoxidation of CO was carried out using a molar ratio of hydrogen peroxide:acetic acid:double bond (H_2O_2:CH_3COOH:DB) of 2:0.5:1 following the procedure described in previous report [42]. ECO was used as epoxy matrix with an epoxy equivalent weight (EEW) of 219 g·equiv^{-1} and an iodine value (*IV*) of 19.8 g I_2·100 g^{-1}. Two different crosslinkers were added to ECO epoxy matrix.

On one hand, MCO was performed by the maleinization process adding MA with purity >98% (Sigma Aldrich, Madrid, Spain) to CO. The process was carried out following the methodology described by Lerma-Canto *et al.* [43] as follows: 300 g of CO was introduced in a three-neck round flask heated up to 180 ºC with a constant

stirring rate of 200 rpm. First, 9 g of MA per 100 g of CO was added to the round flask for 1 h at constant stirring rate. The same procedure was carried out at 200 and 220 ºC each hour, with a total reaction time of 3 h. Finally, MCO was cooled down to room temperature and centrifuged at 4000 rpm for 10 min in order to allow the separation of possible unreacted MA. As result, MCO presented an acid value content of 120 g·equiv^{-1} and *IV* of 104 g I_2·100 g^{-1}. This product was used as bio-based crosslinker to substitute by a petrochemical derived, hence increasing the bio-based content.

On the other hand, MNA supplied by Sigma Aldrich (Madrid, Spain) was used as petrochemical crosslinker. MNA has an anhydride equivalent weight (AEW) of 178.2 g · equiv^{-1}. Additionally, the initiator of crosslinking reaction was 1-methyl imidazole (99 %), supplied by Sigma Aldrich (Madrid, Spain). This initiator is widely used for anhydride epoxy resins in order to promote the reaction [44]. In this case, 2 wt.% respect to a mixture of both ECO and crosslinker was added as is recommended in the literature [44]. All chemical structures are gathered in Figure IV.5.1.

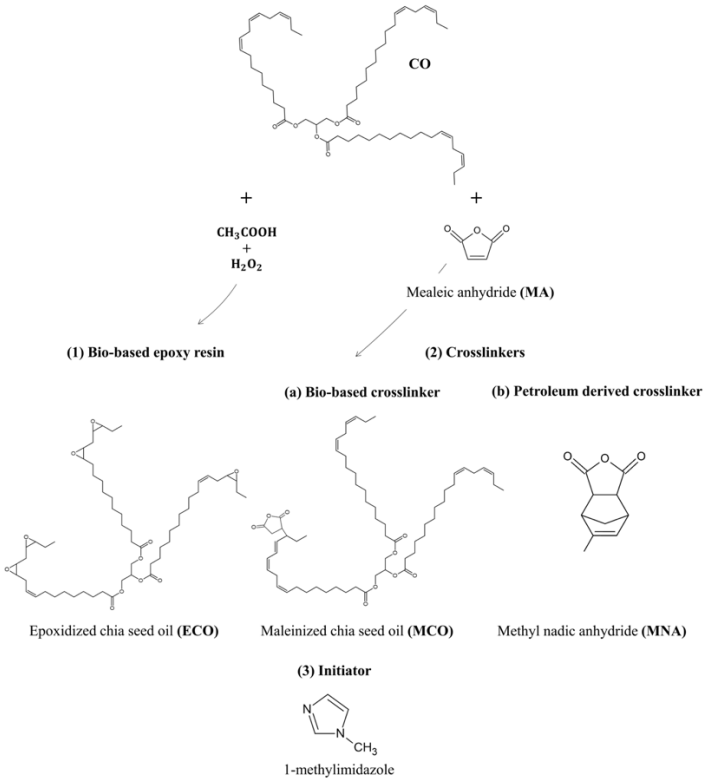

Figure IV.5.1. Monomer preparation and chemical structure of bio-based epoxy resin, crosslinkers and initiator. Note that only generic addition of maleic anhydride in MCO is shown, but various modes can take place.

Characterization of raw materials

The main functional groups of raw materials were identified by Fourier Transform Infrared (FT-IR) spectrophotometer. Samples were spread on the KBr windows and analyzed in a Bruker Vector 22 (Bruker Española S.A, Madrid, Spain). FT-IR spectra was recorded using a range of 4000-400 cm^{-1}, averaging 20 scans with 4 cm^{-1} resolution.

^{1}H NMR was employed to confirm the chemical structure of novel bio-based crosslinker. ^{1}H NMR spectra of MCO was recorded on a Bruker AMX 500 unit (Bruker BioSpin GmbH, Rheinstetten, Germany) at 25 °C. The sample was dissolved in 0.6 mL using deuterated chloroform as solvent and mixed for 10 s. Subsequently, dissolution was transferred to 5 mm NMR tubes for data acquisition.

The iodine value (IV) is an index that indicates the amount of double bonds available in fatty acid chains. The IV was determined by titration process using sodium thiosulfate solution following the guidelines of ISO 3961.

The oxirane oxygen content and epoxy equivalent weight (EEW) measured in % and grams of resin containing 1 g equivalent of epoxy groups, respectively, indicates the conversion of double bonds to epoxy groups within fatty acid chains of vegetable oil. Both values were obtained for ECO by means of CH_3COOH-HBr titration process using ASTM D1652

The acid value is used to evaluate the maleinization process of MCO and the measurement was carried out by KOH standard solution as is indicated in ISO 660:2009.

Preparation of samples

The samples were prepared using a formulation ratio EEW:AEW of 1:1 due to this relationship shows a stoichiometric equilibrium between reactive points and balanced properties in a similar system based on ESO and anhydride crosslinkers [46]. ECO was mixed with different proportions of crosslinkers (MNA and MCO) according to percentage of molar ratio as gathered the Table IV.5.1. The mixture was

mechanically mixed at room temperature with an intensive mixer (Brabender Instruments Co. Germany) at 100 rpm for 10 min to ensure good mixing. Afterward, 1-methyl imidazole was added to the mixture and mixed until a homogeneous mixture of all components were obtained. The mixtures were placed in silicone molds with dimensions of 80 × 10 × 4 mm^3 and the curing cycle was carried out at 90 ^oC for 3 h followed by post-curing at 130 ^oC for 1 extra hour in an air oven model Conterm 80L from J.P Selecta (Barcelona, Spain).

Table IV.5.1. Mixture percentages of ECO crosslinked with different proportions of MNA and MCO.

Sample	MNA (%)	MCO (%)	Bio-based content (%)
MNA100	100	0	54.2
MNA70:MCO30	70	30	69.4
MNA50:MCO50	50	50	78.5
MNA30:MCO70	30	70	86.8
MCO100	0	100	98.0

Characterization of the curing process

Dynamic differential scanning calorimetry (DSC) was used in order to study the curing process of the different combinations of resin-hardeners developed. The calorimetric analysis was performed using Mettler-Toledo DSC 821 (Mettler-Toledo, Schwerzenbach, Switzerland). The samples used were in the range of 4-6 mg and were underwent to dynamic program from 30 to 300 ^oC at heating rate of 10 $^oC\ min^{-1}$. All experiments were carried out in a nitrogen atmosphere with a constant flow at 66 mL min^{-1}.

In addition, isothermal curing of samples was also tested by plate-plate oscillatory rheometer using AR-G2 (TA Instrument, New Castle) equipped with two parallel plates (D=25 mm). The analysis was conducted using isothermal temperature of 90 ^oC until sample was fully cured. The maximum deformation (γ) and frequency were set to 0.1 % and 1 Hz, respectively, in order to assess the evolution of the phase angle (δ).

Gel content

The cured samples were soaked in acetone as solvent according to literature [47]. Samples were initially weighed (w_0), around 1.5 g by sample, and were subjected to Soxhlet extraction to examine any unreacted resin. All extractions were conducted for 24 h and subsequently dried overnight at 60ºC. Each sample was performed by triplicate. The dried sample (w_f) was weighted, and gel content was calculated using the next equation:

$$\text{Gel content (\%)} = \frac{w_f}{w_0} \cdot 100 \qquad \textbf{Equation IV.5.1}$$

FTIR

Fourier-transformed infrared spectroscopy (FT-IR) equipped with a single reflection attenuated total reflectance (ATR) accessory with a diamond ATR crystal (Madison, Wisconsin) was performed for cured samples. The wavelength range was 4000-600 cm^{-1} with a spectral resolution of 4 cm^{-1} and 12 scans. All FT-IR spectra were normalized by using the Perkin-Elmer software Spectrum.

Mechanical characterization

Mechanical characterization of the different resins developed were studied through flexural, hardness and Charpy impact tests. The flexural tests were conducted on a universal testing machine model ELIB 30 from S.A.E. Ibertest (Madrid, Spain) according to standard ISO 178. A fixed crosshead rate of 5 mm min^{-1} and load cell of 5 kN were set.

Regarding the impact tests, these were carried out using a 6 J Charpy pendulum (Metrotec S.A., San Sebastián, Spain) according to the guidelines of the ISO 179. Sample sizes of 80 × 10 × 4 mm^3 were used in both flexural and Charpy impact tests. The hardness tests were performed using a Shore D Durometer model 673-D from J. Bolt Instruments (Barcelona, Spain) as indicated by ISO 868. At least five samples were

tested at room temperature for each characterization test and the average values were calculated.

Dynamic mechanical thermal analysis (DMTA) was carried out in an oscillatory rheometer AR-G2 (TA Instruments, New Castle). Samples with a sample size of $36 \times 0.6 \times 0.25$ mm^3 were subjected to torsion-shear mode with a thermal program from -20 to 100 ºC at a heating rate of 10ºC/ min. The maximum shear deformation (γ) and frequency were set at 0.1% and 1 Hz, respectively.

Field emission scanning electron microscopy (FESEM)

The morphologies of fractured samples from impact tests were evaluated for each formulation. A field emission scanning electron microscopy (FESEM) with a Zeiss Ultra 55 from Oxford Instruments (Abingdon, UK) was used. Previously to place in FESEM vacuum chamber, sample surfaces were coated with gold-palladium alloy under vacuum conditions using a sputter coater EM MED020 (Leica Microsystems, Wetzlar, Germany). The acceleration voltage applied to electron beam was 2 kV.

Results and discussion

Functional group analysis of raw materials

The novel epoxy resin and crosslinker from modified CO, ECO and MCO, as well as MNA were subjected to qualitative characterization by means of FT-IR and quantitative by titration method. In the case of the novel MCO as bio-based crosslinker, H-NMR analysis was performed to corroborate the maleated groups formation. The FTIR spectrums of raw materials are depicted in Figure IV.5.2 to identify the main reactive points. First, the Figure IV.5.2a shows the unmodified CO taking as a basis for subsequent chemical modifications. In the CO spectra, the characteristics peaks of double bonds are located at 3010 cm^{-1} caused by stretching of cis-olefinic bonds (=$CH_{(v)}$), 1652 cm^{-1} due to stretching of disubstituted cis-olefins (C=$C_{(v)}$) and 723 cm^{-1} for the combination of rocking vibration and out of plane deformation in cis-disubstituted olefins (C=$C_{(cis\text{-}\delta)}$). In the ECO spectrum (Figure IV.5.2b), the almost disappearance of double bonds peaks particularly at 3010 (=$CH_{(v)}$)

and 723 cm^{-1} ($C=C_{(cis-\delta)}$) compared to CO, confirming that the epoxidation process took place. As result, the characteristic ($C-O-C_{(v)}$) stretching peak at 821 cm^{-1} appeared and was associated to oxirane oxygen group [48], providing evidence that double bonds were replaced by oxirane oxygen group.

Regarding MCO, the FTIR spectra is plotted in Figure IV.5.2c. The maleinization process can follow several paths: the most common is -ene reaction for the addition of MA where unsaturation remains, even though Diels-Alder condensation can be also proceeded in some cases when conjugated carbon-carbon double bonds are present in fatty acid chains [49]. As can be observed in Figure IV.5.2c, the peaks of double bonds decreased, probably due to Diels-Alder condensation when conjugated double bonds are formed through -ene reaction. It should point out that CO presents high availability of double bonds in triglyceride (average of 2.24 per each fatty acid from ^1H NMR) [23] with IV of 196 g $I_2 \cdot 100\ g^{-1}$, thus there is probability that Diels-Alder condensation reaction takes place. The characteristic peaks associated to the addition of anhydride groups are observed at 1859 and 1781 cm^{-1} corresponding to symmetric and asymmetric vibrations of carbonyl ($C=O_{(v)}$), respectively. Furthermore, it should be mentioned that band at 1859 cm^{-1} was an overtone of 918 cm^{-1}, which are related to the structure of five carbon of succinic anhydride [50]. In addition, the wider band between 1800-1700 cm^{-1} regarding unmodified CO also corresponds to MA moiety that is attached to fatty acid chains.

The petroleum derived crosslinker MNA (Figure IV.5.2d), showed a shift of the peak from 3010 to 3050 cm^{-1} ($=CH_{(v)}$), whereas peaks at 1652 ($C=C_{(v)}$) and 723 cm^{-1} ($C=C_{(cis-\delta)}$) remained in the same position. The three peaks were observed due to double bond within structure, as was observed in the previous raw materials. Besides, symmetric and asymmetric vibration of ($C=O_{(v)}$) was also detected at 1859 and 1781 cm^{-1}, respectively, as well as the presence of peak at 918 cm^{-1} similar to anhydride group in MCO, being the reactive points that are readily to react with both ECO and MCO.

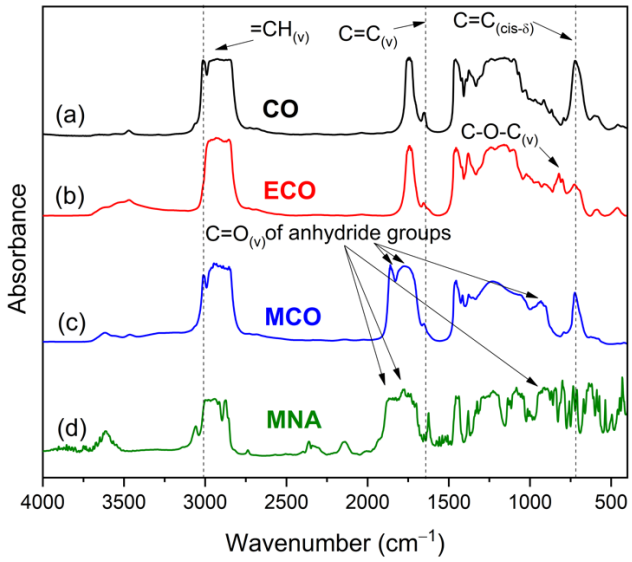

Figure IV.5.2. Fourier transform infrared (FT-IR) spectrum of raw materials: (a) CO, (b) ECO, (c) MCO and (d) MNA.

As a further characterization of MCO as novel bio-based crosslinker, ^{1}H NMR spectroscopy was carried out to confirm the formation of maleated groups onto triglyceride structure. As can be seen in Figure IV.5.3, the signal intensity observed at 2.8-3.2 ppm is attributed to methine and methylene protons of succinic groups on MCO structure, confirming the formation of maleated groups. As aforementioned, -ene reaction and Diels-Alder condensation can take place, appearing peaks between 5.5-6.5 ppm that correspond to conjugated double bonds formed during -ene reaction and double bonds of Diels-Alder condensation as a consequence of -ene reaction [51]. Therefore, the possible incorporation types of MA on MCO structure are shown in Figure IV.5.3. In addition, the residual MA can be also followed with ^{1}H NMR spectroscopy at 7.03 ppm, where any peak was observed.

Regarding MA grafting, an estimation can be obtained by considering the reactions supposed. Taking into account that the conversion of the double bonds is 45.9% and the average of double bonds present in the CO structure is 6.72, a value approximated of 3.15 maleated groups per triglyceride are obtained. However, the analysis done by the ^{1}H NMR spectra showed an average content of maleated groups of 1.1 in the MCO (Figure IV.5.3). This value of 1.1 maleated groups per triglyceride is in agreement with the values obtained in previous studies [52] and very close to the

1.35 present in commercial MLO [53]. According to the study carried out by Amos *et al.* [54], it was concluded that during maleinized reaction exists a competition between the degradation of the MA functionalities and the addition of MA to double bonds, which could be the reason for this lower yield reaction. With this approximation of 1.1 maleate groups per triglyceride and with an average molecular weight of 936 g·mol^{-1}, the resulting AEW is around 841 g·equi^{-1}.

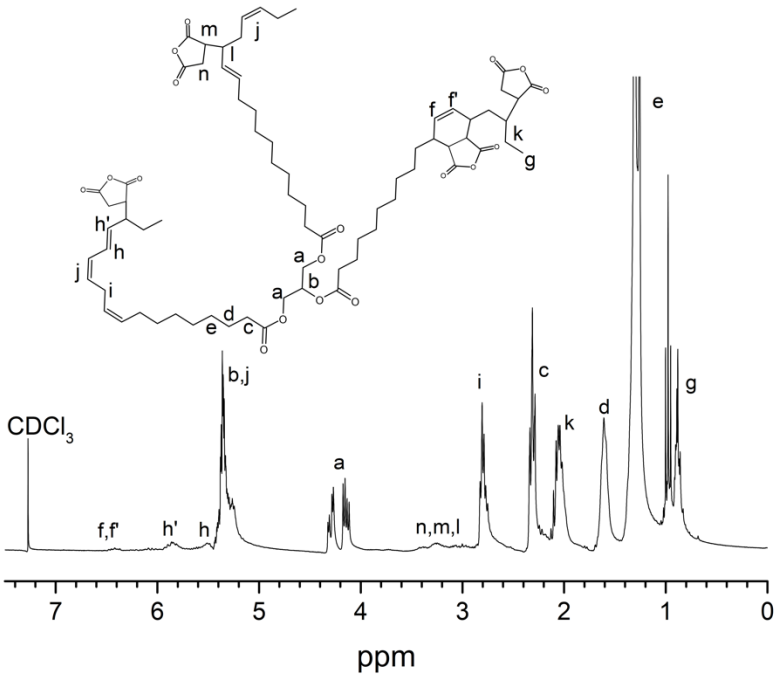

Figure IV.5.3. ^{1}H NMR spectra of novel bio-based crosslinker (MCO) with possible types of MA incorporation.

Regarding the values obtained by titration methods, the IV of the unmodified CO was found to be 196 g I_2·100 g^{-1}. These elevated value of unsaturations are related to fatty acid composition of CO, which were reported in previous study [23]. Briefly, the most representative fatty acids are: monounsaturated integrated by oleic acid (4.32%) and polyunsaturated such as Linoleic (15.8%) and Linolenic (68.6%) which provide the most double bonds with 2 and 3 double bonds per each fatty acid, respectively. These results show the high availability of the double bonds to react further in epoxidation and maleinization reactions. In the ECO sample, the IV obtained decreased to 19.8 g I_2·100 g^{-1}, confirming that the epoxidation process took place during the chemical modification of the oil. On the other hand, to corroborate if

this decrease in the availability of the double bonds is due to the additions of epoxy groups, the EEW and the oxirane oxygen content were determined. Values of 219 g·equiv^{-1} for the EEW and 7.27 % for the oxirane oxygen content confirmed that the introduction of epoxy groups in the CO has been carried out successfully. In the case of MCO, the maleinization reaction also decreased the availability of the double bonds, giving a result of 104 g I_2·100 g^{-1}.

Characterization of the curing process

In a first stage, the curing process of novel epoxy resins based on ECO was evaluated by dynamic scanning calorimetry (DSC). The characteristic exothermic peak (Figure IV.5.4) provides information regarding the crosslinking reaction between epoxy resin and crosslinker employed, where the main calorimetric values, that is, the temperature of the exothermic curing peak (T_p) (ºC), representative of the maximum crosslinking rate of the molecules, and normalized enthalpy (J·g^{-1}), are also gathered. As it can be observed, the crosslinking process of ECO with MNA (MNA100 sample) starts around 80 ºC and ends in the range of 230-240 ºC, where the T_p was observed at 188.2 ºC. This exothermic peak is attributed to ring opening reaction between both epoxy groups of ECO and anhydride groups of crosslinkers. Furthermore, this peak is related to reactivity of the compounds in curing process as has been reported by Chen *et al.* [55] The addition of MCO shifted the peak to lower temperatures, for instance, a decrease from 188.2 to 179.4 ºC was observed for MNA100 and MNA50:MCO50 samples, respectively. Besides, MNA30:MCO70 and MCO samples shows a decrease in the T_p of 18.1 % and 23.1 % respectively. Thus, it is possible to confirm that higher proportion of MCO than MNA provides a significant drop in crosslinking temperature. These results suggest that anhydride group present in MCO has higher reactivity than MNA, indicating faster cure reaction and consequently a possible energy saving in industrial processes. In this regard, Xin *et al.* [56] studied the curing behavior of epoxy resin with different curing agents such as hexahydrophthalic anhydride (HHPA) and MNA. Despite in this study is not working with long chains of crosslinker such as vegetable oils, it is shown that HHPA, which chemical structure is very similar to anhydride group attach in the MCO molecule, presented higher reactivity than MNA with the corresponding decrease of the peak temperature.

Additionally to this effect, the high flexibility provided by aliphatic chains of triglycerides could enable to react easily [57], thus giving higher reactivity to the anhydride group of bio-based crosslinker.

With regard to enthalpy of crosslinking reaction, it provides the energy released as consequence of curing reaction. In general, the curing reaction in presence of strong Lewis bases such as imidazole involves two steps: the initiation of reaction by means of nucleophilic attack of the nitrogen of 1-methyl imidazole to either anhydride or the epoxy group. This generates an active oxyanion in one end whereas the other functional group is quaternary nitrogen cation [58]. The second step is the propagation, where the active oxyanion could react with the epoxy or anhydride group, being in this case from ECO and MNA and/or MCO, respectively. As a result, an alkoxide or carboxylate anion is formed [59], respectively, starting the polymerization of ECO and crosslinkers. In this sense, the maximum enthalpy reaction was found to be 160.9 J g^{-1} for MNA100 sample, value that is even higher than commercial epoxy resin-amine reaction (140 J g^{-1}) [60]. Following the same trend as in T_p, a reduction of area under the curve was observed as MCO content increased. Regarding MCO 100 sample, was possible to observe a sharp decrease of 55.3 % of enthalpy compared to MNA100. This reduction is indicating that MCO presents fewer reactive points, that is, less maleated groups per gram taking into account that the molecular weight of MCO is around 936 g mol^{-1} compared to 178.18 g mol^{-1} of MNA. Similar explanation and finding was reported in the study of ELO with a maximum mixture of MNA and MLO (50:50 wt.%) [41].

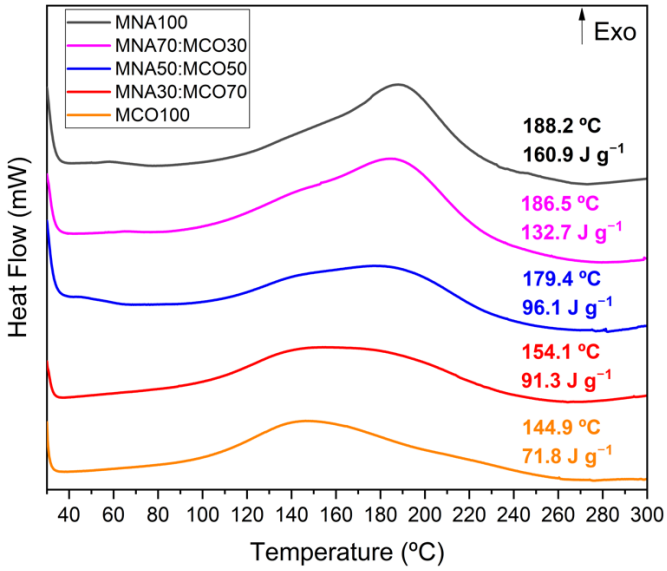

Figure IV.5.4. Differential scanning calorimetry (DSC) of ECO crosslinked with different MNA:MCO mixtures at 10 °C min^{-1}.

Three parameters related to the curing time of all mixtures were measured through plate-plate oscillatory rheometry: (I) the maximum time when the resin stay in liquid state, determined while the δ is around 90 ° due to that when sinusoidal stress is applied to the sample, the elongation/deformation response is delayed 90 °, (II) the maximum time for handling the resin, known as gel time (T_g) and determined when δ is 45 ° and finally, (III) the time where the crosslinking has been completed and resin behaves as elastic solid, value of δ around 0 °. Values obtained are summarized in Table IV.5.2. The isothermal temperature chosen to develop the assay (90 °C), was selected by considering the data obtained by previous assay of DSC. In this assay it is possible to determinate as a minimum of 90 °C is needed to start the crosslinking process. As it is possible to observe, MCO content has notable effect in the crosslinking time. The MNA100 sample needed more than 80 min (4854 s) to start the crosslinking process, while the T_g was around 103 min (6225 s). MNA 100 sample can be fully crosslinked after 143 min (8639 s). It is worthy to note that with the lowest content of MNA, that is, 70MNA:30MCO sample, these parameters are reduced between a 90-96 % respect to sample without the presence of MCO. In the case of sample cured fully with MCO, the descent is more pronounced, giving that is, a T_g of

only 155 s. These values are very close in comparison with the study developed by Fombuena *et al.* [61] which studied the curing time of commercial epoxy resin with a minimum biobased content of 55 % obtaining a T_g close to 150 s. These dates are in concordance with values obtained in DSC and corroborate the higher reactivity of MCO compared with the petrochemical anhydride, MNA. Thus, it can conclude that using an isothermal process of 90 ºC for 3 h is enough time to crosslink the novel epoxy resins in industrial applications. Moreover, according to literature, post-curing process is recommended in order to ensure that all samples are fully cured as well as improve the mechanical properties. For that reason, the temperature of post curing was 130 ºC for 1 extra hour [62].

Table IV.5.2. Phase angle (δ) as a function of curing time of ECO crosslinked with different MNA:MCO mixtures obtained by plate-plate oscillatory rheometry.

Sample	Crosslinking onset ($\delta \approx 90$ º) [s]	Gel time (Tg) ($\delta = 45$ º) [s]	Crosslinking endset ($\delta \approx 0$ º) [s]
MNA100	4854	6225	8639
MNA70:MCO30	1268	1736	3897
MNA50:MCO50	654	865	2195
MNA30:MCO70	221	350	794
MCO100	54	155	663

Gel content

The gel content of the different samples has been assessed to study the crosslinking density. All thermosetting samples showed relatively high gel content in the range of 96-97.9 % as summarized the Table IV.5.3. The lowest gel content value was obtained by MNA100 sample (96.0%), even though the difference is very low compared to other samples (<2%). Therefore, no significant difference is observed between samples that contain MCO as bio-crosslinker and petrochemical crosslinker. Then, it is possible to conclude that MCO addition can increase slightly the crosslinking density, giving well-crosslinked structures. In addition, these high values also indicate that all samples were fully crosslinked with the curing cycle employed for the manufactured thermosetting. It should mention that although gel content is similar between samples (1.94% of the difference between them), the physical

consistency of the sample after Soxhlet extraction is improved as MCO is added (Figure IV.5.5). This fact could be attributed to high crosslinking ability of modified VO during the curing cycle, being in concordance with the high reactivity reported in DSC values.

Table IV.5.3. Gel content of ECO crosslinked with different MNA:MCO mixtures.

Sample	Gel content (%)
MNA100	96.0 ± 0.09
MNA70:MCO30	97.5 ± 0.02
MNA50:MCO50	97.5 ± 0.1
MNA30:MCO70	97.6 ± 0.02
MCO100	97.9 ± 0.05

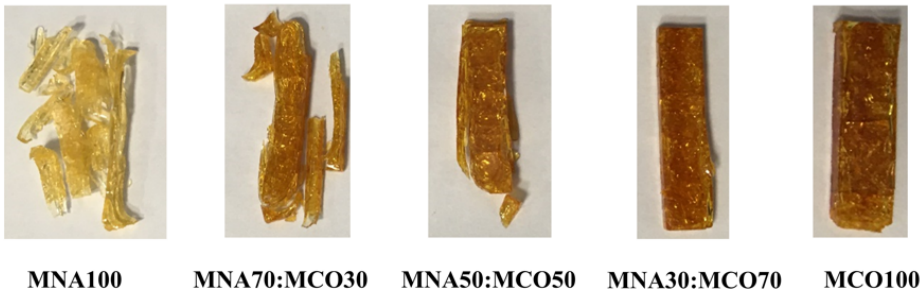

Figure IV.5.5. Visual appearance of ECO crosslinked with different MNA:MCO mixtures after Soxhlet extraction.

Fourier-transformed infrared

The crosslinking reaction was corroborated using FT-IR spectroscopy to confirm the formation of the chemical bonds between epoxy resin (ECO) and crosslinkers (MNA and/or MCO) in cured samples. Figure IV.5.6 shows the FT-IR spectra of all samples highlighting the main characteristic peaks. As was commented above in FT-IR of raw materials, the characteristics peaks of functional groups are located at 1859 and 1781 cm^{-1} for anhydride groups on MNA or MCO structure, and 821 cm^{-1} for epoxy group on ECO structure. These peaks, highlighted in vertical black dashes, disappeared for all samples due to opening of epoxy ring and anhydride groups. Nevertheless, MNA100 sample showed a low intensity peak related to epoxy group (821 cm^{-1}), suggesting that not all epoxy groups were opening to interact with

the crosslinker. Regarding the main groups that evidence the chemical bonds formed, carbonyl C=O stretching at 1735 cm^{-1} and C-O-C stretching in the range 1210-1160 cm^{-1}, have been highlighted with vertical red dots in FT-IR spectra [63]. Therefore, the presence of these peaks confirms the chemical interaction between epoxy resin (ECO) and compatibilizer (MNA and/or MCO).

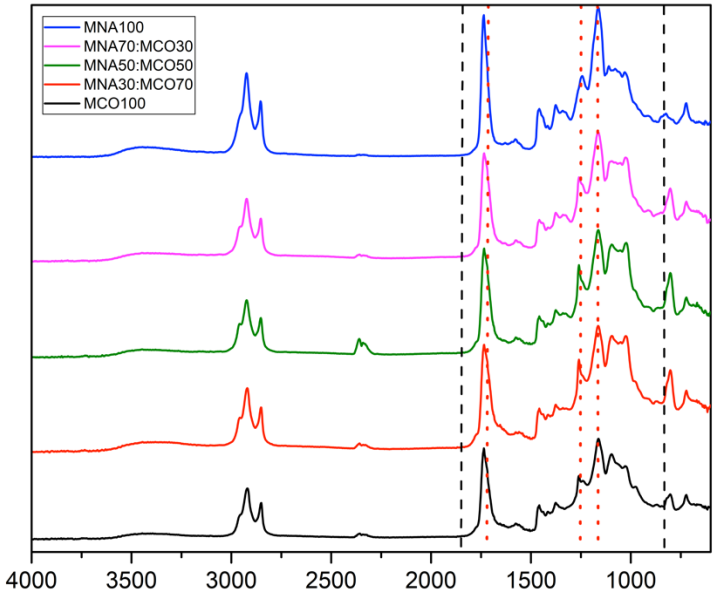

Figure IV.5.6. Fourier transform infrared **(**FT-IR) spectra of cured samples of ECO crosslinked with different MNA:MCO mixtures.

Mechanical properties

The effect of bio-based crosslinker (MCO) on the flexural test is shown in Figure IV.5.7. First, MNA100 sample showed the highest flexural strength and modulus with values of 57 and 765 Mpa, respectively. This sample, with bio-based content of 54.2 %, can be compared to other epoxidized VO in literature, taking into account that curing cycle can also affect the final mechanical behavior. Espana *et al.* [46] obtained values for flexural strength and modulus of 20.7 and 432 Mpa, respectively, using ESO with MNA. On the other side, Samper *et al.* [41] showed values of 60.8 and 1772.0 Mpa for flexural strength and modulus, respectively, using ELO with MNA. These differences with this study can be ascribed to different amount of linkage points of epoxy resins used. In this regard, ECO with EEW (219 g·$equiv^{-1}$) is located between both ESBO and ELO with EEW of 238 and 178 g·$equiv^{-1}$, respectively. Although flexural modulus of

ELO was much higher than ECO (1.4 times higher), almost similar values were obtained in terms of tensile strength. In case of the addition of MCO, as greater is the content, the flexural strength and modulus decreases as can be observed, obtaining a more ductile resin. The MNA70:MCO30 sample showed a sharp reduction in both flexural strength and flexural modulus with values of 4.85 and 1.2 Mpa, respectively. This behavior is suggesting that MCO presents a high impact in flexural properties in the cured samples. It seems that once MCO is in higher proportion than MNA (from MNA50:MCO50 sample), the properties are kept invariable playing MCO a big role in mechanical properties of the cured samples. It is worthy to note that mechanical properties of samples are strictly related to chemical structure of crosslinker as was observed. Whereas MNA provides a very compact and rigid crosslinking unit [64], the functionalized long chains of fatty acids lead to increase the free volume and therefore, the chain mobility increase which contributes to improve the flexibility of thermosetting resins [65]. A schematic proposal of polymerization can be seen in Figure IV.5.8, where the maleated group through -ene reaction is shown even though different modes are also present.

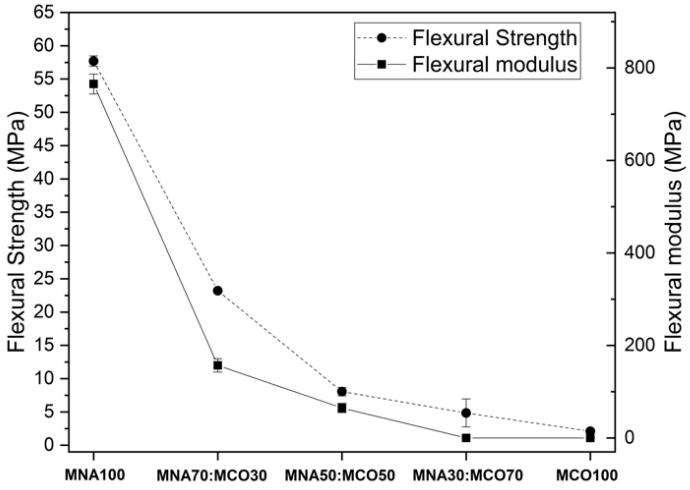

Figure IV.5.7. Flexural properties of ECO crosslinked with different MNA:MCO mixtures.

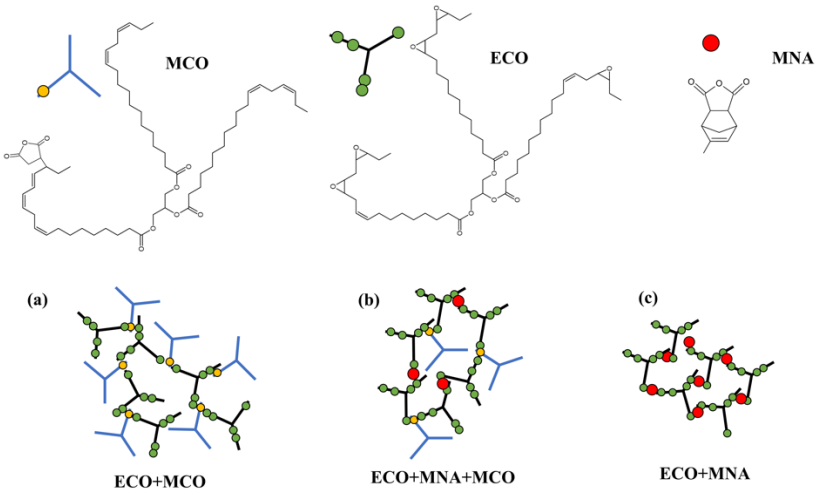

Figure IV.5.8. Schematic proposal of polymerization effect of different MNA:MCO mixtures on crosslinked ECO structures.

Regarding impact-absorbed energy and Shore D hardness, values are gathered in Table IV.5.4. Impact-absorbed energy is related to capacity to absorb energy during an impact. In this regard, MNA 100 sample showed the lowest impact absorption capacity due to its fragile behavior provided by rigid molecule of MNA employed as crosslinker. In the case of bio-based crosslinker, as MCO content increase, higher energy absorbed was obtained due to these samples were more flexible. For instance, an improvement of 181 % was achieved with MNA30:MCO70 regarding to MNA100, then obtaining higher ductile properties. The increment of impact-absorbed energy as greater is MCO content can be explained by the presence of long flexible aliphatic chain in both ECO and MCO. Similar explanation and finding were reported for epoxy blends with ELO and petroleum epoxy resin with cardanol-derived phenalkamine (PKA) [66]. Regarding to MCO100 sample, the deformation took place but not break was obtained during this test, meaning that whole energy of impact was absorbed by the sample. This behavior was also observed by Espana *et al.* [46] who studied ESBO with MNA in ratio of 1:0.7 (EEW:AEW). On contrary, Shore D hardness values decreased from 60.9 to 32.2 for MNA100 and MCO100 sample, respectively, in consequence of more ductile behavior. The addition of MCO as bio-based crosslinker led to obtain less compact structure for the increment of free volume provided by the long chains of MCO, thus reducing the hardness of cured sample. Moreover, these values are in concordance with flexural tests, which corroborates that addition of

MCO contributes to increase the flexibility. As one can observe, depending on formulation, it is possible to manufacture thermosetting samples with wide range of mechanical properties from high rigidity to high ductility with bio-based content up to 98 %.

Table IV.5.4. Influence of cured samples based on ECO crosslinked with different MNA:MCO mixtures in terms of impact-absorbed energy and shore D hardness.

Sample	Impact-absorbed energy (kJ m^{-2})	Shore D hardness
MNA100	5.2 ± 0.4	60.9 ± 2.9
MNA70:MCO30	8.4 ± 1.1	50.4 ± 3.9
MNA50:MCO50	12.1 ± 1.1	43.9 ± 3.8
MNA30:MCO70	14.5 ± 2.0	35.7 ± 2.8
MCO100	Didn't break	32.2 ± 2.8

The thermomechanical performance of the samples was analyzed by DMTA. In Figure IV.5.9 is shown the storage modulus (E') and damping factor (tan δ) curves as a function of temperature. Concerning E', MNA100 sample reported a value of 820 Mpa at room temperature (20 ºC), which value is close to the obtained with ELO crosslinked with MNA [41]. In general, with increasing MCO content, E' decreases gradually from 820 to 100 Mpa at room temperature for MNA 100 and MCO 100 sample, respectively, indicating a change of behavior from rigid to flexible materials. These values are in concordance with the mechanical properties obtained above, where long chains of MCO provide more flexibility to cured samples and then, it results in lower E'. In relation to the damping factor, this value provides information to estimate the T_g of the samples. It was observed that as increased the MCO content, T_g values decreased even though with a different peak shape. This trend was also expected as a result of flexibility provided by MCO as bio-based crosslinker. For example, MNA100 sample exhibit a narrow peak curve with T_g value of 55.4 ºC, whereas it becomes broader and less intense gradually as increase the MCO content up to values of 28.6 ºC for MCO100 sample. It is known that the dynamic mechanical properties of thermosetting depend on the composition and chemical structure [68]. In this regard, the rigid structure of MNA presents a small free volume that hinders the movement of molecular chains at lower temperature, only increasing the free

volume as temperature arises in order to procedure the glass transition (narrow peak). On contrary, MCO contains a flexible structure with high free volume that ease the movement of molecular chains at lower temperature, which results in a wider peak with less intensity as MCO content increases.

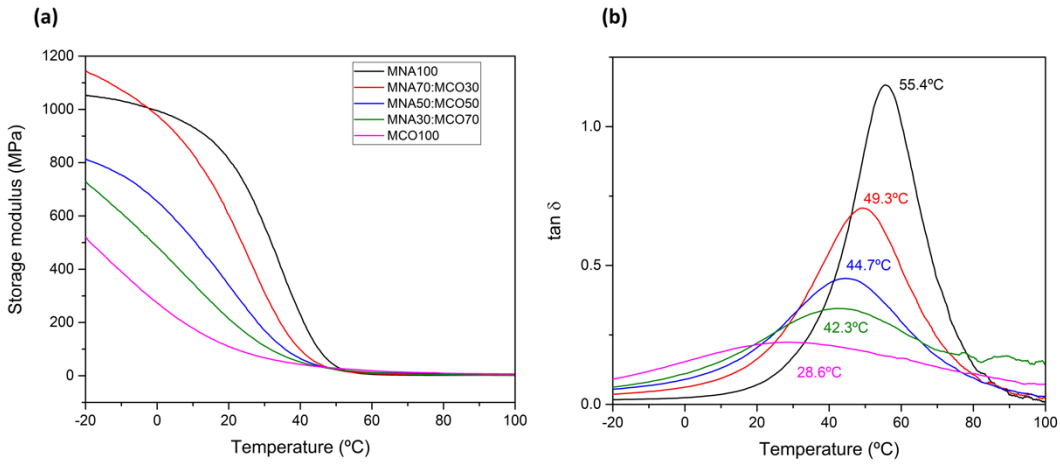

Figure IV.5.9. Dynamic mechanical thermal analysis (DMTA) of ECO crosslinked with different MNA:MCO mixtures; (a) storage modulus (E') and (b) damping factor.

Morphology of cured samples

To reveal the effect of the incorporation of MCO as crosslinker and consequently the relationship between the mechanical behavior of the resins developed with the morphology of the fractured surface, an analysis by SEM were carried out as shown in Figure IV.5.10. The sample fractured of ECO crosslinked with 100 MNA showed a typical morphology for rigid and fragile materials characterized by homogenous and smooth surface, Figure IV.5.10a. In this regard, the typical waves were not observed due to high fragility of sample. Similar fragile surface has been reported in thermosetting resins of ELO and MNA [68]. As was expected, the addition of MCO gave rougher surface with an evident multiple microcracks advancing in direction of the break. With regard to MNA70:MCO30 sample, it becomes to display a small and low presence of crests as well as a remaining smooth surface, Figure IV.5.10b. This fractured surface indicates an improvement of toughness properties [69]. As increase MCO content (MNA50:50MCO sample), an increment of both size and number of waves were observed. It is remarkable that from this formulation

onwards, the mechanical properties such as flexural and absorbed energy, become to reach a plateau what can be ascribed to the presence of this specific fractured surface. In case of the highest MCO content fracture surface (MNA30:MCO70), a continuous advancing front of cracks with rippled edges were observed in Figure IV.5.10d that confirms the highest toughening behavior after cracking. In addition, no obvious phase separation was observed in all samples neither with MNA nor mixtures with MNA and MCO, which indicates a good compatibility with homogenous crosslinking network. This is an advantage compared to some authors where observed a phase separation in mixtures with ESO and glycerol or pentaerythritol based aliphatic epoxy resin from renewable sources [45].

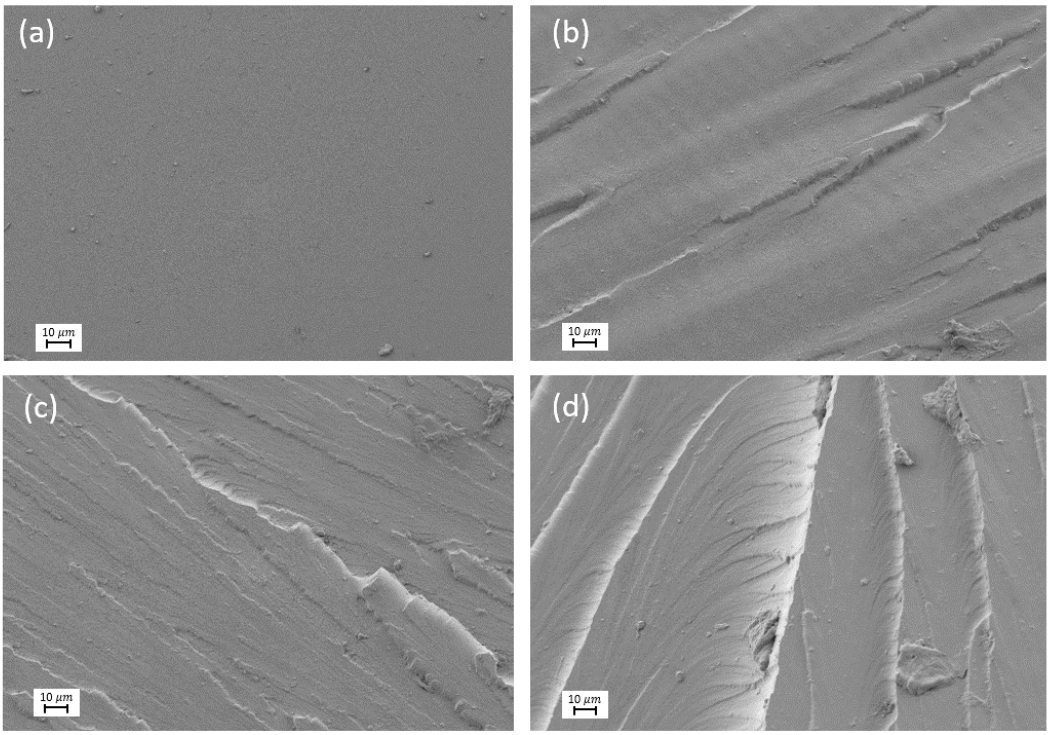

Figure IV.5.10. SEM images of fractured samples of crosslinked ECO with different MNA:MCO mixtures at 500×: (a) MNA100, (b) MNA70:MCO30, (c) MNA50:MCO50 and (d) MNA70:MCO30.

Conclusions

Novel epoxy resins based on ECO as bio-based epoxy matrix has been assessed with different crosslinkers mixtures (MNA and/or MCO). The main functional groups of raw materials were identified by means of titration method and FT-IR, especially for ECO and MCO that were obtained through chemical modification from

CO with the aim to be employed for the first time in thermosetting resins. Besides, the success of the reaction of MCO was characterized for the first time using ^{1}H NMR spectroscopy with AEW of 841 g·equiv^{-1}. According to our DSC results, all samples start to cure around 80 ^{o}C and finish in the range of 230-240 ^{o}C. Furthermore, the addition of MCO leads to shift the temperature of exothermic curing peak to lower temperatures from 188.2 ^{o}C for 100MNA sample to 144.9 ^{o}C for 100MCO sample, indicating higher reactivity of MCO compared to MNA. The isothermal curing at 90 ^{o}C in plate-plate oscillatory rheometer also corroborated the higher reactivity of MCO achieving a gel time of 150 s for sample fully cured with MCO (100MCO sample) with a high bio-based content of 98 %. These values are found to be very close to cured samples with commercial epoxy resin with low-medium bio-based content of 55 %. This faster curing compared to MNA could mean a possible energy saving from industrial point of view. All cured samples had high gel contents of about 96-97.9%, which indicates well-crosslinked structures. In addition, FT-IR of cured samples demonstrates the chemical interaction of ECO and MNA/MCO. In terms of mechanical properties, the addition of MCO provides more flexibility, thus increasing the impact-absorbed energy and decreasing the flexural properties and shore D values. A similar trend was observed in DMTA analysis with a decrease of E' from 820 to 100 Mpa at room temperature and T_g from 55.4 to 28.6 ^{o}C as greater is the addition of MCO. The T_g of 100MCO (28.6 ^{o}C) was much higher than reported in literature for commercial ECO and MCO cured sample with T_g value of -41 ^{o}C. The mechanical behavior was corroborated by SEM images of fractured samples, which showed a rough surface as MCO content increased, giving more ductility to the thermosetting resins. Therefore, by adding the adequate amount of MCO as bio-based crosslinker, it is possible to tailor the desired thermal and mechanical properties of thermosetting resins based on ECO, improving the ductility, and curing time. In addition to this wide range of properties, from environmental point of view, the bio-based content of cured resins is in the range of 54.2%-98 %, thus giving a noticeable feature to these green epoxy resins even reaching almost fully bio-based content (98 %) using only MCO as bio-renewable crosslinker.

Acknowledgements

This research work was funded by the Ministry of Science and Innovation-"Retos de la Sociedad". Project references: PID2020-119142RA-I00. I. Dominguez-Candela wants to thank Universitat Politècnica de València for his FPI grant (PAID-2019-SP20190013) and Generalitat Valenciana-GVA (ACIF/2020/233).

References

[1] M. N. Belgacem, Gandini, A. Monomers, Polymers and Composites from Renewable Resources; 2008; pp. 1-553.

[2] C. K. Williams, Hillmyer, M. A. Polymers from renewable resources: A perspective for a special issue of polymer reviews. Polymer Reviews 2008, 48, 1-10, doi:10.1080/15583720701834133.

[3] P. J. Halley, Truss, R. W., Markotsis, M. G., Chaleat, C., Russo, M., Sargent, A. L., Tan, I., Sopade, P. A. A Review of Biodegradable Thermoplastic Starch Polymers. In Proceedings of the Symposium on Polymer Performance and Degradation held at Pacifichem 2005 Conference, Honolulu, HI, Dec, 2005; pp. 287-300.

[4] A. Chakrabarty, Teramoto, Y. Recent Advances in Nanocellulose Composites with Polymers: A Guide for Choosing Partners and How to Incorporate Them. Polymers 2018, 10, doi:10.3390/polym10050517.

[5] M. Parit, Jiang, Z. Towards lignin derived thermoplastic polymers. International Journal of Biological Macromolecules 2020, 165, 3180-3197, doi:10.1016/j.ijbiomac.2020.09.173.

[6] D. Garcia-Garcia, Quiles-Carrillo, L., Montanes, N., Fombuena, V., Balart, R. Manufacturing and Characterization of Composite Fibreboards with Posidonia oceanica Wastes with an Environmentally-Friendly Binder from Epoxy Resin. Materials 2018, 11, doi:10.3390/ma11010035.

[7] A. Qurat ul, Zia, K. M., Zia, F., Ali, M., Rehman, S., Zuber, M. Lipid functionalized biopolymers: A review. International Journal of Biological Macromolecules 2016, 93, 1057-1068, doi:10.1016/j.ijbiomac.2016.09.071.

[8] X. He, Wu, G., Yan, Y. Advances in platform compounds and polymers from vegetable oils. Sheng wu gong cheng xue bao = Chinese journal of biotechnology 2017, 33, 701-719, doi:10.13345/j.cjb.160404.

[9] P. Anastas, Eghbali, N. Green Chemistry: Principles and Practice. Chemical Society Reviews 2010, 39, 301-312, doi:10.1039/b918763b.

[10] J. Carlos Ronda, Lligadas, G., Galia, M., Cadiz, V. Vegetable oils as platform chemicals for polymer synthesis. European Journal of Lipid Science and Technology 2011, 113, 46-58, doi:10.1002/ejlt.201000103.

[11] G. Lligadas, Ronda, J. C., Galia, M., Cadiz, V. Renewable polymeric materials from vegetable oils: a perspective. Materials Today 2013, 16, 337-343, doi:10.1016/j.mattod.2013.08.016.

[12] G. A. Smith. Hemp Oil Ethoxylates for Home and Personal Care Applications. J. Am. Oil Chem. Soc. 2020, 97, 32-32.

[13] N. A. Masripan, Salim, M. A., Omar, G., Mansor, M. R., Saad, A. M., Hamid, N. A., Syakir, M. I., Dai, F. Vegetable Oil as Bio-Lubricant and Natural Additive in Lubrication: A Review. International Journal of Nanoelectronics and Materials 2020, 13, 161-176.

[14] P. Jia, Xia, H., Tang, K., Zhou, Y. Plasticizers Derived from Biomass Resources: A Short Review. Polymers 2018, 10, doi:10.3390/polym10121303.

[15] C. Burgos-Diaz, Wandersleben, T., Marques, A. M., Rubilar, M. Multilayer emulsions stabilized by vegetable proteins and polysaccharides. Current Opinion in Colloid & Interface Science 2016, 25, 51-57, doi:10.1016/j.cocis.2016.06.014.

[16] S. N. H. Mustapha, Rahmat, A. R., Arsad, A. Bio-based thermoset nanocomposite derived from vegetable oil: a short review. Reviews in Chemical Engineering 2014, 30, 167-182, doi:10.1515/revce-2013-0010.

[17] A. H. M. Azam, Sarmidi, T., Nor, A. S. M., Zainuddin, M. CO-MOVEMENT AMONG WORLD VEGETABLE OIL PRICES: A WAVELET-BASED ANALYSIS. International Journal of Business and Society 2020, 21, 1068-1086.

[18] N. Karak, Karak, N. Vegetable oil-based polymer composites; 2012; pp. 247-270.

[19] M. Zuk, Richter, D., Matula, J., Szopa, J. Linseed, the multipurpose plant. Industrial Crops and Products 2015, 75, 165-177, doi:10.1016/j.indcrop.2015.05.005.

[20] H. Barcena, Tuachi, A., Zhang, Y. Z. Teaching Green Chemistry with Epoxidized Soybean Oil. Journal of Chemical Education 2017, 94, 1314-1318, doi:10.1021/acs.jchemed.6b00672.

[21] B. Matthaus, Bruhl, L. Virgin hemp seed oil: An interesting niche product. European Journal of Lipid Science and Technology 2008, 110, 655-661, doi:10.1002/ejlt.200700311.

[22] H. Harish, Rajanna, S., Prakash, G. S., Ahamed, S. M. Extraction of biodiesel from tung seed oil and evaluating the performance and emission studies on 4-stroke CI engine. In Proceedings of the 4th International Conference on Advances in Materials and Manufacturing Applications (IConAMMA), India, Aug 29-31, 2019; pp. 4869-4877.

[23] I. Dominguez-Candela, Lerma-Canto, A., Cardona, S. C., Lora, J., Fombuena, V. Physicochemical Characterization of Novel Epoxidized Vegetable Oil from Chia Seed Oil. Materials 2022, 15, doi:10.3390/ma15093250.

[24] Chia Seeds Market SizeWorth $4.7 Billion by 2025. Available online: (accessed on

[25] Z. S. Petrovic, Zlatanic, A., Lava, C. C., Sinadinovic-Fiser, S. Epoxidation of soybean oil in toluene with peroxoacetic and peroxoformic acids – kinetics and side reactions. European Journal of Lipid Science and Technology 2002, 104, 293-299, doi:10.1002/1438-9312(200205)104:5<293::aid-ejlt293>3.0.co;2-w.

[26] A. Carbonell-Verdu, Garcia-Sanoguera, D., Jorda-Vilaplana, A., Sanchez-Nacher, L., Balart, R. A new biobased plasticizer for poly(vinyl chloride) based on epoxidized cottonseed oil (vol 33, 43642, 2016). Journal of Applied Polymer Science 2016, 133, doi:10.1002/app.43924.

[27] O. Fenollar, Garcia-Sanoguera, D., Sanchez-Nacher, L., Lopez, J., Balart, R. Characterization of the curing process of vinyl plastisols with epoxidized linseed oil as a natural-based plasticizer. Journal of Applied Polymer Science 2012, 124, 2550-2557, doi:10.1002/app.34645.

[28] M. Li, Li, S. H., Xia, J. L., Ding, C. X., Wang, M., Xu, L. N., Yang, X. H., Huang, K. Tung oil based plasticizer and auxiliary stabilizer for poly(vinyl chloride). Materials & Design 2017, 122, 366-375, doi:10.1016/j.matdes.2017.03.025.

[29] M. T. Taghizadeh, Nalbandi, N., Bahadori, A. Stabilizing effect of epoxidized sunflower oil as a secondary stabilizer for Ca/Hg stabilized PVC. Express Polym. Lett. 2008, 2, 65-76, doi:10.3144/expresspolymlett.2008.9.

[30] V. Fombuena, Petrucci, R., Dominici, F., Jorda-Vilaplana, A., Montanes, N., Torre, L. Maleinized Linseed Oil as Epoxy Resin Hardener for Composites with High Bio Content Obtained from Linen Byproducts. Polymers 2019, 11, 18, doi:10.3390/polym11020301.

[31] C. Ding, Matharu, A. S. Recent Developments on Biobased Curing Agents: A Review of Their Preparation and Use. ACS Sustain. Chem. Eng. 2014, 2, 2217-2236, doi:10.1021/sc500478f.

[32] M. D. Samper, Petrucci, R., Sanchez-Nacher, L., Balart, R., Kenny, J. M. New environmentally friendly composite laminates with epoxidized linseed oil

(ELO) and slate fiber fabrics. Composites Part B-Engineering 2015, 71, 203-209, doi:10.1016/j.compositesb.2014.11.034.

[33] C. F. Frias, Serra, A. C., Ramalho, A., Coelho, J. F. J., Fonseca, A. C. Preparation of fully biobased epoxy resins from soybean oil based amine hardeners. Industrial Crops and Products 2017, 109, 434-444, doi:10.1016/j.indcrop.2017.08.041.

[34] S. Zhang, Liu, T., Hao, C., Mikkelsen, A., Zhao, B., Zhang, J. Hempseed Oil-Based Covalent Adaptable Epoxy-Amine Network and Its Potential Use for Room-Temperature Curable Coatings. ACS Sustain. Chem. Eng. 2020, 8, 14964-14974, doi:10.1021/acssuschemeng.0c05223.

[35] Epoxy Resins and Curing Agents: Toxicology, Health, Safety and Environmental Aspects. Plastics Europe Epoxy Resins Committee; Brussels, Belgium, 2006; pp. 1-28.

[36] Cyclic Acid Anhydrides: Health-Based Recommended Occupational Exposure Limit;. 2010.

[37] M. Stemmelen, Pessel, F., Lapinte, V., Caillol, S., Habas, J. P., Robin, J. J. A Fully Biobased Epoxy Resin from Vegetable Oils: From the Synthesis of the Precursors by Thiol-ene Reaction to the Study of the Final Material. Journal of Polymer Science Part a-Polymer Chemistry 2011, 49, 2434-2444, doi:10.1002/pola.24674.

[38] M. Stemmelen, Lapinte, V., Habas, J.-P., Robin, J.-J. Plant oil-based epoxy resins from fatty diamines and epoxidized vegetable oil. European Polymer Journal 2015, 68, 536-545, doi:10.1016/j.eurpolymj.2015.03.062.

[39] H. Warth, Mulhaupt, R., Hoffmann, B., Lawson, S. Polyester networks based upon epoxidized and maleinated natural oils. Angewandte Makromolekulare Chemie 1997, 249, 79-92, doi:10.1002/apmc.1997.052490106.

[40] T. Takahashi, Hirayama, K.-I., Teramoto, N., Shibata, M. Biocomposites composed of epoxidized soybean oil cured with terpene-based acid anhydride

and cellulose fibers. Journal of Applied Polymer Science 2008, 108, 1596-1602, doi:10.1002/app.27866.

[41] M. D. Samper, Ferri, J. M., Carbonell-Verdu, A., Balart, R., Fenollar, O. Properties of biobased epoxy resins from epoxidized linseed oil (ELO) crosslinked with a mixture of cyclic anhydride and maleinized linseed oil. Express Polym. Lett. 2019, 13, 407-418, doi:10.3144/expresspolymlett.2019.34.

[42] I. Dominguez-Candela, Ferri, J. M., Cardona, S. C., Lora, J., Fombuena, V. Dual Plasticizer/Thermal Stabilizer Effect of Epoxidized Chia Seed Oil (*Salvia hispanica L.*) to Improve Ductility and Thermal Properties of Poly(Lactic Acid). Polymers 2021, 13, 16, doi:10.3390/polym13081283.

[43] A. Lerma-Canto, Gomez-Caturla, J., Herrero-Herrero, M., Garcia-Garcia, D., Fombuena, V. Development of Polylactic Acid Thermoplastic Starch Formulations Using Maleinized Hemp Oil as Biobased Plasticizer. Polymers 2021, 13, doi:10.3390/polym13091392.

[44] B. Ellis. Chemistry and technology of epoxy resins; Springer: 1993.

[45] P. Niedermann, Szebenyi, G., Toldy, A. Effect of Epoxidized Soybean Oil on Curing, Rheological, Mechanical and Thermal Properties of Aromatic and Aliphatic Epoxy Resins. J. Polym. Environ. 2014, 22, 525-536, doi:10.1007/s10924-014-0673-8.

[46] J. M. Espana, Sanchez-Nacher, L., Boronat, T., Fombuena, V., Balart, R. Properties of Biobased Epoxy Resins from Epoxidized Soybean Oil (ESBO) Cured with Maleic Anhydride (MA). J. Am. Oil Chem. Soc. 2012, 89, 2067-2075, doi:10.1007/s11746-012-2102-2.

[47] A. Ito, Semba, T., Taki, K., Ohshima, M. Effect of the Molecular Weight between Crosslinks of Thermally Cured Epoxy Resins on the CO2-Bubble Nucleation in a Batch Physical Foaming Process. Journal of Applied Polymer Science 2014, 131, doi:10.1002/app.40407.

[48] J. R. Kim, Sharma, S. The development and comparison of bio-thermoset plastics from epoxidized plant oils. Industrial Crops and Products 2012, 36, 485-499, doi:10.1016/j.indcrop.2011.10.036.

[49] L. Quiles-Carrillo, Blanes-Martinez, M. M., Montanes, N., Fenollar, O., Torres-Giner, S., Balart, R. Reactive toughening of injection-molded polylactide pieces using maleinized hemp seed oil. European Polymer Journal 2018, 98, 402-410, doi:10.1016/j.eurpolymj.2017.11.039.

[50] L. Candy, Vaca-Garcia, C., Borredon, E. Synthesis and characterization of oleic succinic anhydrides: Structure-property relations. J. Am. Oil Chem. Soc. 2005, 82, 271-277, doi:10.1007/s11746-005-1066-5.

[51] C. Gaglieri, Alarcon, R. T., de Moura, A., Magri, R., da Silva-Filho, L. C., Bannach, G. Green and Efficient Modification of Grape Seed Oil to Synthesize Renewable Monomers. Journal of the Brazilian Chemical Society 2021, 32, 2120-2131, doi:10.21577/0103-5053.20210104.

[52] E. Lackinger, Schmid, L., Sartori, J., Isogai, A., Potthast, A., Rosenau, T. Novel paper sizing agents from renewables. Part 1: Preparation of a paper sizing agent derived from natural plant oils. Holzforschung 2011, 65, 3-11, doi:10.1515/hf.2011.007.

[53] R. Vendamme, Olaerts, K., Gomes, M., Degens, M., Shigematsu, T., Eevers, W. Interplay Between Viscoelastic and Chemical Tunings in Fatty-Acid-Based Polyester Adhesives: Engineering Biomass toward Functionalized Step-Growth Polymers and Soft Networks. Biomacromolecules 2012, 13, 1933-1944, doi:10.1021/bm300523e.

[54] R. C. Amos, Kuska, M., Mesnager, J., Gauthier, M. Thermally induced maleation of soybean and linseed oils: From benchtop to pilot plant. Industrial Crops and Products 2021, 166, doi:10.1016/j.indcrop.2021.113504.

[55] W. Chen, Li, P., Yu, Y., Yang, X. Curing kinetics study of an epoxy resin system for T800 carbon fiber filament wound composites by dynamic and isothermal

DSC. Journal of Applied Polymer Science 2008, 107, 1493-1499, doi:10.1002/app.26861.

[56] J. Xin, Zhang, P., Huang, K., Zhang, J. Study of green epoxy resins derived from renewable cinnamic acid and dipentene: synthesis, curing and properties. Rsc Advances 2014, 4, 8525-8532, doi:10.1039/c3ra47927g.

[57] K. Huang, Zhang, P., Zhang, J., Li, S., Li, M., Xia, J., Zhou, Y. Preparation of biobased epoxies using tung oil fatty acid-derived C_{21} diacid and C_{22} triacid and study of epoxy properties. Green Chemistry 2013, 15, 2466-2475, doi:10.1039/c3gc40622a.

[58] S. Kumar, Samal, S. K., Mohanty, S., Nayak, S. K. Study of curing kinetics of anhydride cured petroleum-based (DGEBA) epoxy resin and renewable resource based epoxidized soybean oil (ESO) systems catalyzed by 2-methylimidazole. Thermochimica Acta 2017, 654, 112-120, doi:10.1016/j.tca.2017.05.016.

[59] A. Paramarta, Webster, D. C. Bio-based high performance epoxy-anhydride thermosets for structural composites: The effect of composition variables. Reactive & Functional Polymers 2016, 105, 140-149, doi:10.1016/j.reactfunctpolym.2016.06.008.

[60] H. A. Shnawa. Curing and thermal properties of tannin-based epoxy and its blends with commercial epoxy resin. Polymer Bulletin 2021, 78, 1925-1940, doi:10.1007/s00289-020-03192-6.

[61] V. Fombuena, Bernardi, L., Fenollar, O., Boronat, T., Balart, R. Characterization of green composites from biobased epoxy matrices and bio-fillers derived from seashell wastes. Materials & Design 2014, 57, 168-174, doi:10.1016/j.matdes.2013.12.032.

[62] C. H. Lin, Wu, C. Y., Wang, C. S. Synthesis and properties of phosphorus-containing advanced epoxy resins. II. Journal of Applied Polymer Science 2000, 78, 228-235, doi:10.1002/1097-4628(20001003)78:1<228::Aid-app270>3.3.Co;2-q.

[63] A. Marotta, Faggio, N., Ambrogi, V., Cerruti, P., Gentile, G., Mija, A. Curing Behavior and Properties of Sustainable Furan-Based Epoxy/Anhydride Resins. Biomacromolecules 2019, 20, 3831-3841, doi:10.1021/acs.biomac.9b00919.

[64] G. Ragosta, Musto, P., Scarinzi, G., Mascia, L. Effects of perfluoroether concentration and curing protocol on morphology and mechanical properties of toughened TGDD/MNA resin systems. Polymer 2003, 44, 2081-2090, doi:10.1016/s0032-3861(03)00060-0.

[65] B. De, Gupta, K., Mandal, M., Karak, N. Biodegradable Hyperbranched Epoxy from Castor Oil-Based Hyperbranched Polyester Polyol. ACS Sustain. Chem. Eng. 2014, 2, 445-453, doi:10.1021/sc400358b.

[66] S. K. Sahoo, Khandelwal, V., Manik, G. Development of toughened bio-based epoxy with epoxidized linseed oil as reactive diluent and cured with bio-renewable crosslinker. Polymers for Advanced Technologies 2018, 29, 565-574, doi:10.1002/pat.4166.

[68] S. Wang, Wang, J. L., Ji, Q., Shultz, A. R., Ward, T. C., McGrath, J. E. Miscibility and morphologies of poly(arylene ether phenyl phosphine oxide/sulfone) copolymer/vinyl ester resin mixtures and their cured networks. Journal of Polymer Science Part B-Polymer Physics 2000, 38, 2409-2421, doi:10.1002/1099-0488(20000915)38:18<2409::Aid-polb80>3.0.Co;2-g.

[69] M. D. Samper, Fombuena, V., Boronat, T., Garcia-Sanoguera, D., Balart, R. Thermal and Mechanical Characterization of Epoxy Resins (ELO and ESO) Cured with Anhydrides. J. Am. Oil Chem. Soc. 2012, 89, 1521-1528, doi:10.1007/s11746-012-2041-y.

[69] H. Miyagawa, Mohanty, A. K., Misra, M., Drzal, L. T. Thermo-physical and impact properties of epoxy containing epoxidized linseed oil, 1 – Anhydride-cured epoxy. Macromol. Mater. Eng. 2004, 289, 629-635, doi:10.1002/mame.200400004.

Received: 5 September 2022 | Revised: 2 December 2022 | Accepted: 16 December 2022

DOI: 10.1002/app.53574

RESEARCH ARTICLE

Applied Polymer SCIENCE WILEY

Development of a novel epoxy resin based on epoxidized chia oil as matrix and maleinized chia oil as bio-renewable crosslinker

Ivan Dominguez-Candela[1] | **Aina Perez-Nakai**[2] | **Elena Torres-Roca**[3] | **Jaime Lora-Garcia**[1] | **Vicent Fombuena**[2]

[1]Instituto de Seguridad Industrial, Radiofisica y Medioambiental (ISIRYM), Universitat Politècnica de València (UPV), Alcoy, Spain

[2]Technological Institute of Materials (ITM), Universitat Politècnica de València (UPV), Alcoy, Spain

[3]Textile Industry Research Association (AITEX), Alcoy, Spain

Correspondence
Ivan Dominguez-Candela, Instituto de Seguridad Industrial, Radiofisica y Medioambiental (ISIRYM), Universitat Politècnica de València (UPV), Plaza Ferrándiz y Carbonell, s/n 03801 Alcoy, Spain.
Email: ivdocan@doctor.upv.es

Funding information
Ministry of Science and Innovation, Grant/Award Number: PID2020-119142RA-I00; Universitat Politècnica de València, Grant/Award Number: PAID-2019-SP20190013; Generalitat Valenciana, Grant/Award Number: ACIF/2020/233

Abstract

In this work novel thermosetting resins with high bio-based content have been developed derived from chia seed oil (CO). Epoxidized chia seed oil (ECO) was used as bio-based epoxy matrix with different mixtures of crosslinker agents, that is, methyl nadic anhydride (MNA) as petroleum-derived and maleinized chia seed oil (MCO) as bio-based crosslinker. The chemically modified oils from CO, that is, ECO and MCO, and MNA were analyzed by titration and FT-IR. Additional ^{1}H NMR analysis was performed to characterize MCO structure. Two different behaviors were observed using the mixtures of crosslinkers. On one hand, MNA increases the rigidity with bio-based content of 54.2%. On the other hand, the addition of MCO provides higher ductility with bio-based content up to 98%. The same trend was observed by DMTA analysis. The novel cured resins were successfully crosslinked as demonstrated by the mechanical properties, FT-IR analyses, and gel content. Based on the results, it is concluded that MCO presents higher reactivity than MNA, decreasing curing time with possible energy saving at industrial level. In general, the results showed that adding the appropriate amount of MCO, green thermosetting resins with the desired thermal and mechanical properties can be manufactured with high bio-based content.

KEYWORDS

bio-based epoxy resin, chia seed oil, curing time, ductility, epoxidized chia seed oil, maleinized chia seed oil

1 | INTRODUCTION

Currently, there is an urgent need to develop innovative technologies and materials from renewable resources in order to reduce dependence on fossil resources. The current inflation that has led to a sharp increase in the prices of goods and services, together with the current energy crisis, exacerbated by the war in Ukraine, has further highlighted the need for a change in the production model.[1,2] For years, the scientific community

Bloque V: cristales líquidos

Previamente a la realización de la investigación de la modificación del aceite de chía para la obtención de cristales líquidos, se llevó a cabo un estudio previo para abordar su futura caracterización.

Los cristales líquidos, denominado en inglés "liquid crystals" (LCs), pueden ser definidos como sustancias que presentan estados de agregación intermedios de la materia. Los LCs se sitúan termodinámicamente entre un sólido ordenado y un liquido isotrópico [1]. Presentan un cierto grado de fluidez similar al de los líquidos, y una orientación parcial de las moléculas cuyo orden posicional es nulo o escaso, dando lugar a propiedades físicas anisotrópicas. Esta mesofase puede darse lugar en respuesta a la temperatura obteniendo LCs termotrópicos, o a la concentración obteniendo LCs lipotrópicos. En el caso de LCs enfocados a la aplicación energética, se emplea los termotrópicos.

Generalmente, uno de los requisitos para que un determinado compuesto muestre un mesomorfismo, es que la geometría molecular sea larga y relativamente estrecha, obteniendo moléculas altamente anisotrópicas [2]. Además, es necesario que la molécula presente una parte rígida como puede ser un bifenilo y una parte flexible, como la cadena de hidrocarburos. El tipo de mesofase que presente el LC dependerá de la estructura química y de la flexibilidad del núcleo, que hará variar la forma geométrica de la molécula y, por tanto, su posición y orientación en el espacio. Las moléculas de los LCs se ordenan al disminuir la temperatura, partiendo de un líquido isotrópico hasta llegar al estado sólido pasando por la mesofase [3].

En el estudio realizado previamente a la modificación del aceite de chía, se emplea cristales líquidos con nucleo curvado (bent-core) para captar y almacenar energía. Los bent-core LC presentan un fuerte orden polar de forma macroscópica que, en ausencia de cargas libres, es un material dieléctrico que puede ser empleado en condensadores para almacenar energía. El orden polar proporciona la capacidad a las moléculas para alinearse en dirección al campo eléctrico, variando la constante dieléctrica del material. En función de la temperatura, frecuencia y voltaje aplicado, se generan cambios en esta capacidad de almacenar energía. Junto a este almacenamiento de energía, en el estudio también se emplean compuestos que

contiene grupos azos permitiendo la interacción con la luz ultravioleta (365 nm). La interacción se lleva a cabo mediante la isomerización de posición *trans* a *cis* de los grupos azos en presencia de luz ultravioleta que, al cesarse la luz, volverá a la posición inicial liberando energía. Por ello, se estudia el efecto de la luz ultravioleta en la capacidad de almacenar energía, empleando grupos azos en la estructura de los bent-core LCs. Los materiales empleados son mezclas de un compuesto mayoritario (NG75) que no presenta grupos azos (95% molar) con 5% molar de un compuesto con 1 grupo azo (IP33) y, por otro lado, con 5% molar de otro compuesto (IP31) que contiene dos grupos azos. De esta forma, se evalúa la capacidad de cada mezcla para el almacenamiento de energía e interacción con la luz ultravioleta.

A partir del estudio realizado, se permite conocer el comportamiento dieléctrico de mezclas con presencia de compuestos con diferentes tipos de mesofases. Esto se emplea como base para la caracterización del aceite de chía modificado para emplearse como cristal líquido en diferentes campos. Además, considerando la problemática medioambiental actual, los autores están continuamente buscando diferentes métodos de obtención de materiales de origen renovable. En el estudio realizado por Martinez-Felipe *et al*. [4], se empleó el aceite de palma para la obtención de cristales líquidos. Los glicolípidos obtenidos presentaban una molécula rígida polar derivada de la manosa, mientras que la parte flexible hidrofóbica se obtuvo empleando el aceite de palma. La finalidad de este trabajo fue la obtención de diferentes tipos de glicolípidos de origen renovable para la obtención de nuevos surfactantes. Por tanto, el estudio futuro será la obtención de un glicolípido derivado del aceite de chía para conocer su potencial como cristal líquido. Se estudiará su comportamiento molecular para poder evaluar las posibles aplicaciones que pueda presentar, siendo una de ellas como surfactante y/o vinculado con el artículo previo como material candidato en el almacenamiento de energía.

REFERENCES

[1] A. M. Felipe. Preparation and characterization of new materials for electrolytes used in Direct Methanol Fuel Cells. Citeseer, 2009.

[2] S. Chandrasekhar, Ranganath, G. Discotic liquid crystals. Reports on Progress in Physics 1990, 53, 57.

[3] D.-K. Yang, Wu, S.-T. Fundamentals of liquid crystal devices; John Wiley & Sons: 2014.

[4] A. Martinez-Felipe, Velayutham, T. S., Aripin, N. F. K., Yusoff, M., Farquharson, E., Hashim, R. Glycolipids from natural sources: dry liquid crystal properties, hydrogen bonding and molecular mobility of Palm Kernel oil mannosides. Liquid Crystals 2020, 47, 1180-1194, doi:10.1080/02678292.2020.1750719.

IV.6 "Light-responsive bent-core liquid crystals as candidates for energy conversion and storage"

Ivan Dominguez-Candela[1-3], Iman Zulkhairi[1], Inmaculada Pintre[4], Nurul Fadhilah Kamalul Aripin[5,6], Jaime Lora[2], Vicent Fombuena[3], M. Blanca Rosa[4], Alfonso Martinez-Felipe[1,7]

[1] Chemical Process and Materials Research Group, School of Engineering, University of Aberdeen, King's College, Aberdeen AB24 3UE, Scotland, UK.

[2] Instituto de Seguridad Industrial, Radiofísica y Medioambiental (ISIRYM) Universitat Politècnica de València (UPV), Plaza Ferrándiz y Carbonell, s/n 03801 Alcoy, Spain.

[3] Technological Institute of Materials (ITM), Universitat Politècnica de València (UPV), Plaza Ferrándiz y Carbonell 1, 03801 Alcoy, Spain.

[4] Instituto de Nanociencia y Materiales de Aragón, Departamento de Química Orgánica, Facultad de Ciencias, Universidad de Zaragoza-CSIC, Campus San Francisco, E-50009 Zaragoza, Spain.

[5] School of Chemical Engineering, College of Engineering, Universiti Teknologi MARA, 40450 Shah Alam, Selangor, Malaysia.

[6] Department of Chemistry, School of Natural and Computing Sciences, University of Aberdeen, King's College, Aberdeen AB24 3UE, Scotland, UK.

[7] Centre for Energy Transition, University of Aberdeen, King's College, Aberdeen AB24 3UE, Scotland, UK.

Journal of Material Chemistry C

2022, 10, 18200.

"Light-responsive bent-core liquid crystals as candidates for energy conversion and storage"

Abstract

We have assessed the potential of light-responsive bent-core liquid crystals as candidate materials for energy conversion and storage applications. Samples comprise two chromophore bent-core compounds containing either one (IP33) or two (IP31) azobenzene groups, and their 5% (molar) mixtures with one non-chromophore bent-core compound (NG75), which was also measured as a reference material. The pristine compounds and their mixtures were introduced in thin transparent Indium Tin Oxide (ITO) cells, and were characterized by polarised optical microscopy, UV-visible spectrophotometry, impedance spectroscopy, and ferroelectric analysis, under different conditions of electrical fields and UV irradiation. All materials display smectic C polar phases (SmCP) except IP31, which forms columnar phases (Col), and IP33, IP31 and their mixtures exhibit light-responsiveness when irradiated at 365 nm due to reversible *trans*-to-*cis* photoisomeration of the azobenzene units. All the bent-core based materials exhibit, at least, two dielectric relaxations, associated to different modes of molecular reorientation under weak alternating electrical fields (1 V_{rms}), as well as ferroelectric response that leads to permanent polarization under the application of strong alternating fields (~ 75 kV·cm^{-1}) at frequencies associated to the Goldstone-mode (1 Hz). Samples show considerable conductivity values and relaxor behaviour for liquid crystals, which can be tuned by application of UV light. In addition, we have induced in IP31 isothermal phase transitions from columnar to smectic phases (*via* the isotropic melt), by a combination of light and electrical stimuli. Our results confirm the potential of these bent-core compounds as light-harvesters for energy applications.

Introduction

The development of innovative electrolytes that can improve the efficiency of renewable energy conversion and storage will play a decisive role to reduce greenhouse emissions and reach net-zero targets globally [1]. Liquid crystals hold promise as advanced materials in different renewable technologies, due to their ability to interact with, and respond to, external sources, resulting in tailor-made nanostructures [2-4]. More specifically, azobenzene-containing compounds can exhibit liquid crystalline phases controllable by light excitation, *via trans*-to-*cis* photoisomeration. In its ground state, the azobenzene *trans* isomer is linear, and hence compatible with liquid crystalline phases, since it tends to promote order and interactions in the mesophase range. When excited with UV light at certain frequencies, the *trans*-isomer bends, normally disrupting the liquid crystal order. Even though azobenzenes have been studied for several decades [5-7], they continue to attract interest due to their potential to promote long-range macroscopic changes induced by short-range molecular modifications [8-12].

Bent-core liquid crystals, BCLCs, exhibit anti-ferroelectric and ferroelectric behaviour with high figures of merit, which can be useful for energy storage applications. BCLCs can form columnar (Col, former B_1), polar smectic C (SmCP, former B_2), twist grain boundary dark conglomerate (DC) or helical nanofilament (HNF, former B_4) phases among others [13-20]. Generally, BCLC molecular designs show several aromatic rings forming an angle through a central meta-substituted ring (which facilitates molecular packing) various linking groups, and flexible terminal chains at one or both end of the molecule (which reduce the melting point). The bent-core mesogenic units lead to biaxial properties, and the relative orientation of polar groups present at the core respect to the molecular axes promotes the appearance of local dipole moments. Upon application of electric fields, the cooperative alignment of these dipoles can result in local (within the liquid crystalline regions or layers) and macroscopic (through the material) polarization, which can be further maintained if the viscous forces are strong enough once the field is removed [21, 22].

In this work, we combine the application of electric fields and light to explore new phenomena in BLCSs that can lead to energy conversion and storage from solar sources [23-27]. We analyse the photo-dielectric and photo-ferroelectric response of bent-core liquid crystals containing azobenzenes as chromophore groups. We also investigate the photoinduction of isothermal phase transitions in the materials, as a mechanism to control the nanostructure of future electrolytes.

Experimental

Materials and cells preparation

Five materials were studied in this work. Three pristine bent-core compounds were used, containing six aromatic rings at the core, which is linked to long flexible chains (-$OC_{14}H_{29}$). The pristine materials already reported by us are designated as: NG75 (non-chromophore), IP31 (containing two azobenzene groups), and IP-33 (containing one azobenzene group), see Figure IV.6.1. Their synthesis and full characterization are described in detail elsewhere, and are summarised as Electronic Supplementary Information, see Table IV.S6.1 [28-30]. In short, NG75 and IP33 display smectic C polar phases (SmCP), and IP31 shows a columnar phase (Col). Additionally, two mixtures, containing NG75 (95%, molar) and either IP33 or IP31 (5% molar, each), were prepared by melting above the clearing temperatures of the respective compounds. The choice of composition was based on some of our previous results obtained for liquid crystal dimers, which showed that 5% molar was the minimum concentration of azobenzene molecules required to promote photoinduced effects in the corresponding mixtures [31].

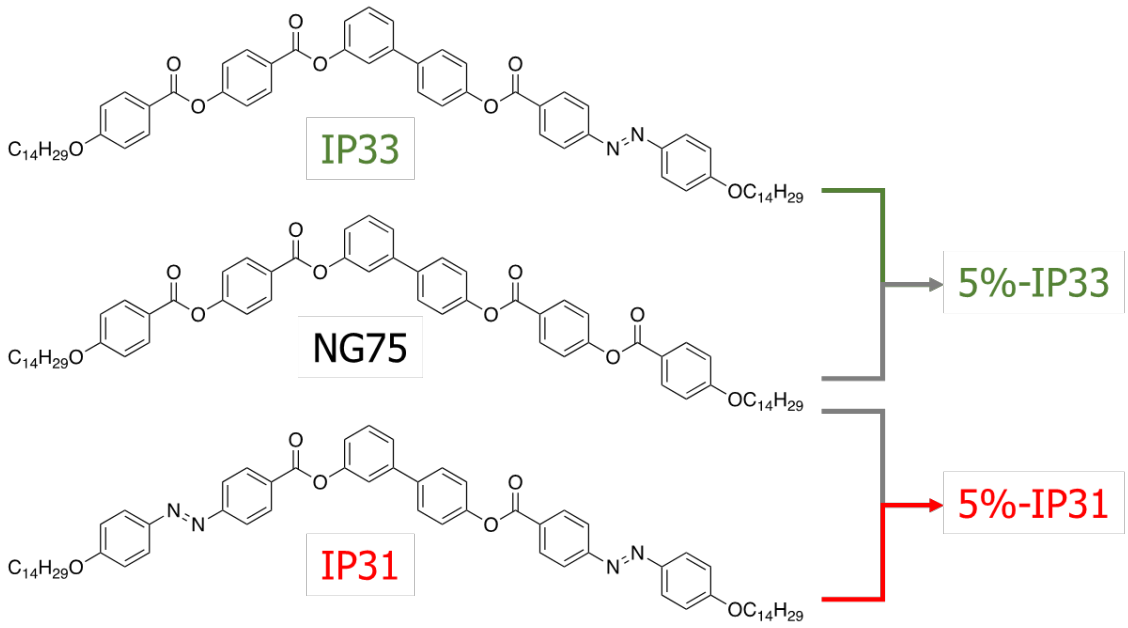

Figure IV.6.1. Chemical structure and notation used to refer to the pristine bent-core compounds (NG75, IP33 and IP33) and mixtures containing 5% molar % of azobenzene molecules (5%-IP33 and 5%-IP31).

The pristine materials and the mixtures were filled from their melt into commercial ITO-coated (Indium Tin Oxide) glass cells (SG100A080uG180, Instec) by capillary action, using a Linkam TM600 hot stage, see Figure IV.S6.1. Cells have an active area of $A = 100\ mm^2$, thickness of $h = 8\ \mu m$, resistance of 100Ω, and their overall capacitance, C_o can be calculated as:

$$C_o = \frac{\varepsilon_o A}{h} = 1.11 \times 10^{-10} F \qquad \textbf{Equation IV.6.1}$$

with $\varepsilon_o = 8.854 \times 10^{-12} F \cdot m^{-1}$ is the permittivity of vacuum. The ITO cells were then connected to the different analysers using two aluminium foils attached to the sides of the glass cells with RS PRO conductive silver paint.

Characterisation techniques

Temperature was controlled by placing the cells on top of a Linkam THMS 600 heating stage coupled to a TMS 91 control unit, with ±0.1 ^{o}C accuracy. For phase observation, the heating stage was placed on an Olympus Bx5m polarised optical microscope, POM, equipped with cross polarisers. Phase behaviour was further

assessed by differential scanning calorimetry, DSC, using a Mettler Toledo QA200 calorimeter. The thermograms were obtained in heating, cooling, and reheating cycles, at ±10 ^{o}C min^{-1} rates, under inert (N_2) atmosphere. Complex impedance spectroscopy was carried out using the Solartron Modulab XM frequency response analyser (FRA). Frequency sweeps ranged from 0.01 to 10^6 Hz, using alternating fields of 1 V_{rms} amplitude; some additional isothermal experiments were taken at a fixed frequency of 1 Hz, in the time domain. The ferroelectric response was analysed by a RT66C Test System (Radiant Inc), by measuring the polarization of the cells, through hysteresis loops of sinusoidal fields in the ±75 kV · cm^{-1} range, and at different frequencies.

The effect of UV irradiation was investigated using a Dymax Bluewave QX4 TM LED pot-curing system, controlled by a Dymax ACCU-CALTM 50-LED instrument. Samples were irradiated at 365 nm, at different light intensities (up to 1200 mW · cm^{-2}) measured with a detector. The UV-vis spectra of the materials were collected for tetrahydrofuran (THF) solutions, or for thin films cast on quartz slides. Selected samples were irradiated with UV light (365 nm, 260 mW·cm^{-2}), and the UV-visible spectra were obtained as a function of exposure and relaxation time, using a VARIAN Cary 50 Scan UV-vis spectrophotometer, between 250 nm and 550 nm. Additional dielectric and ferroelectric measurements were carried under the application of different programs of UV light irradiation, using the Dymax Bluewave QX4 TM LED pot-curing system. Most of these experiments were carried out at a fixed intensity of 200 mW · cm^{-2}, but further details on the experimental conditions are given below at the respective sections.

Results and discussion

Phase behaviour

The thermal properties of the pristine compounds and the 5% mixtures inside the ITO cells are summarised in Table IV.6.1, based on POM observations. NG75 and IP33 display granulated textures, see Figure IV.6.2a and 2b, which are consistent with the formation of liquid crystalline smectic C (SmC) phases. More specifically, both compounds were assigned to form smectic C antiferroelectric polar (anticlinic) phases,

SmC_AP_A [28, 29, 32, 33], which were confirmed by ferroelectric experiments. IP31, on the other hand, shows banana leaf textures, consistent with the formation of oblique columnar phases, Col_{ob}, Figure IV.6.2c [28]. The thermal behaviour of the three pristine compounds is also in good agreement with DSC measurements on their respective powder samples, see Figure IV.S6.2 and Table IV.6.1. We attribute minor temperature value deviations to heat transfer and potential anchoring effects with the ITO cells surfaces. As expected, the 5% mixtures (5%-IP31 and 5%-IP33) exhibit similar microscopic textures as NG75 (95% molar), which confirms the formation of SmC polar (SmCP) phases in comparable temperature ranges, Figure IV.6.2d and 2e.

Table IV.6.1. Thermal parameters obtained for the bent-cores by differential scanning calorimetry (DSC), measured on second heating (10 $^{o}C \cdot min^{-1}$) scans, and by polarized optical microscopy (POM) measured on cooling (1 $^{o}C \cdot min^{-1}$).

Sample	DSC		POM	
	T_{Cr-M}/°C (ΔH_{Cr-M} (kJ·mol^{-1}))	T_{M-I}/°C (ΔH_{M-I} (kJ·mol^{-1}))	T_{I-M}/°C	T_{M-Cr}/°C
NG75	77.2 (13.74)	159.7 (24.76)	161.6	-*[a]
IP33	118.4 (58.05)	163.3 (25.55)	163.6	110.0[a]
IP31	139.9 (31.30)	168.3 (21.08)	170.5	134.9[b]
5%-IP33	75.1 (15.89)[c]	156.2 (20.08)[c]	161.8	-*[a]
5%-IP31	74.0 (15.50)[c]	153.6 (18.77)[c]	161.8	-*[a]

* Not visible under POM. Crystallisation was further confirmed under dielectric measurements; Cr: crystal; M: mesophase SmCP; b) Col; I: isotropic liquid; ΔH: enthalpy; T: transition temperature; c: enthalpy values were calculated using the molecular weight of NG75.

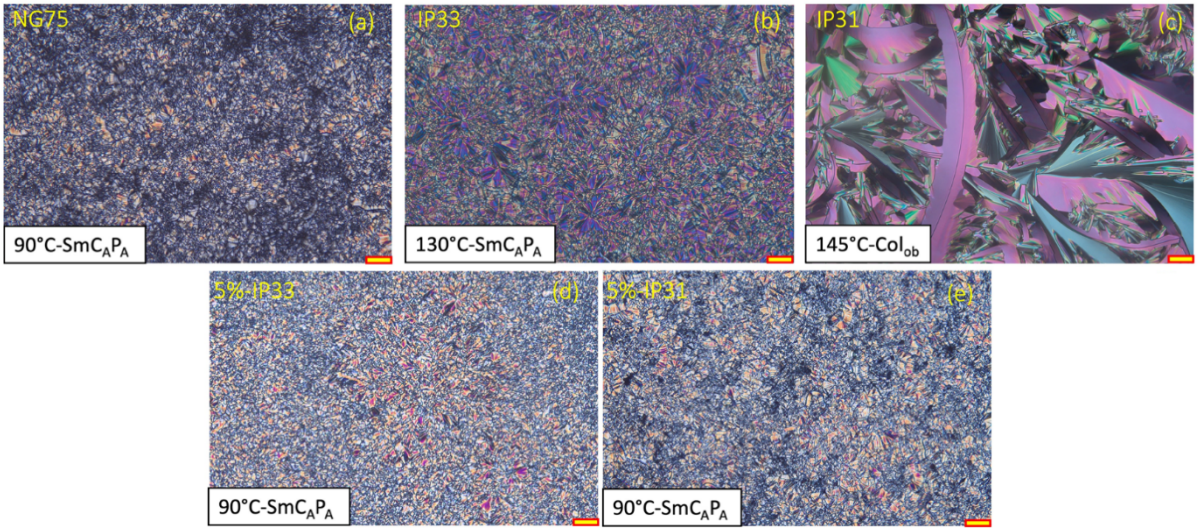

Figure IV.6.2. Selected polarized optical microphotographs showing the mesophases displayed by the pristine bent-core compounds (a, b, c) and the mixtures containing 5% of IP33 (d) and IP31 (e). Scale bar corresponds to 40 μm. SmC$_A$P$_A$: smectic C antiferroelectric polar (anticlinic); Col$_{ob}$: oblique columnar.

Dielectric analysis

The dielectric responses of NG75, IP31, IP33 and their mixtures (5%-IP31 and 5%-IP33) are summarized in Figure IV.6.3, where we show 3D-plots of their dielectric loss factor (ε'', relative to ε_0) as a function of frequency and temperature. Their isothermal 2D curves used to prepare these 3D graphs, as well as the plots for the dielectric elastic constant, ε' (relative to ε_0), and the real component of the complex conductivity, σ', can be found as supplementary information (Figure IV.S6.3 to IV.S6-.5, resp.). NG75 displays several dielectric processes in Figure IV.6.3a, which we have initially labelled as γ, β and α, in increasing temperature order. At sufficiently high temperatures, the rise of ε'' observed at low frequencies is attributed to the existence of strong direct current (dc) conductivity between the electrodes, σ_{dc} [34]. Since the low-temperature process (γ) appears in a very narrow frequency range at very low temperatures, and seems to be associated to the crystal phase, we will focus on the higher temperature processes.

Both α and β are well-defined in the smectic materials, Figure IV.6.3a, b, d and e, and shift towards lower frequencies on cooling, suggesting these are dielectric

relaxations. In order to discriminate their molecular origin, we have superimposed direct current electric fields of different intensities (0.5 to 4 V) to the alternating field (±1 V_{rms}) and measured ε'' in similar frequency sweeps as in Figure IV.6.3. The results for NG75 are illustrated in Figure IV.6.4 and show that the low-frequency relaxation (α) decreases and shifts to lower frequencies at increasing dc fields. This phenomenon is typical of a Goldstone(phason)-mode relaxation, which involves cooperative motions of the molecules within the smectic layers, albeit without varying the tilt angle [35-38]. The application of dc electric fields perturbs the cooperative interactions and then the relaxation is suppressed. The β process of NG75 at higher frequencies, on the other hand, remains unaffected upon dc electric fields, and can be associated to a soft(amplitude)-mode relaxation, when molecules vary their tilt angle, θ, within the same plane. IP33 shows similar dielectric relaxations and comparable dielectric response as NG75, Figure IV.6.3b.

IP31, on the other hand, displays the dielectric regions discussed above, even though the α process is less defined than in the smectic materials, Figure IV.6.3c. This may be due to the existence of strong constrains to reorient molecules within columnar structures. On applying dc electrical fields, the β process of IP31 is enhanced, see Figure IV.S6.6, which is accompanied with a slight displacement of its maxima. Therefore, the molecular origin of the β relaxation must be different in IP31, and this is confirmed by its higher activation energy, E_a, compared to NG75 and IP33, see Figure IV.6.5. A process in a similar frequency/temperature range was identified previously for bent-cores containing sulphur atoms, and was attributed to the rotation of the molecules around their molecular long axis [39]. The α process of IP31, appearing at lower frequencies, can be linked to longer-range phenomena probably involving macro dipole moments within the columns, which consequently shows very small temperature dependence [40]. Interestingly, the α region of IP31 decreases under the application of dc fields, even though it is not inhibited, unlike for NG75. This fact may reflect the stronger constrains for cooperative molecular motions (in response to dc fields) found in columnar nanostructures, compared to smectic phases.

As expected, the two mixtures depict a similar dielectric response as NG75, Figure IV.6.3d and 3e, which is also consistent with their similar phase behaviour [40].

The Arrhenius plots corresponding to the maximum frequency of the ε'' peaks in both the α and β relaxations, f_{max}, deviate to some extent from linearity and follow Vogel-Fulcher-Tamman (VFT) behaviour, see Figure IV.6.5. This indicates that the molecular motions within the smectic layers are controlled by viscous forces. The Goldstone-mode (α process in our notation) has activation energies in the 50 kJ·mol^{-1} range in the mesophase, which is typical of locally activated rotation motions of rod-like molecules, previously observed in smectic liquid crystals [41-44]. Interestingly, the soft-mode (β process), has higher E_a values than the α relaxation, which reflects a stronger energy barrier for the bent-core molecules to modify their tilt angle, θ. These are still in the same range as other processes in smectic materials [35]. The higher activation energies estimated in the crystal phase indicate stronger interactions and mobility constrains due to the increase in order at lower temperatures.

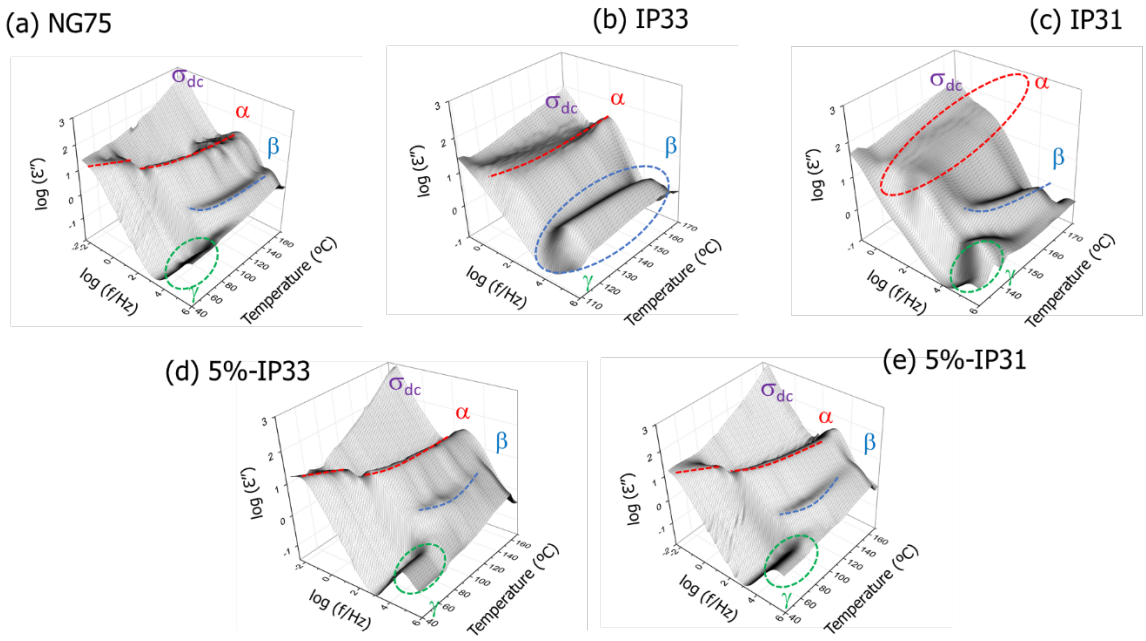

Figure IV.6.3. 3D-plots showing the dielectric loss factor, ε'', as a function of frequency and temperature, corresponding to: (a) NG75; (b) IP33; (c) IP31; (d) 5%-IP33; and I 5%-IP31, obtained in isothermal steps, on cooling from their isotropic phases.

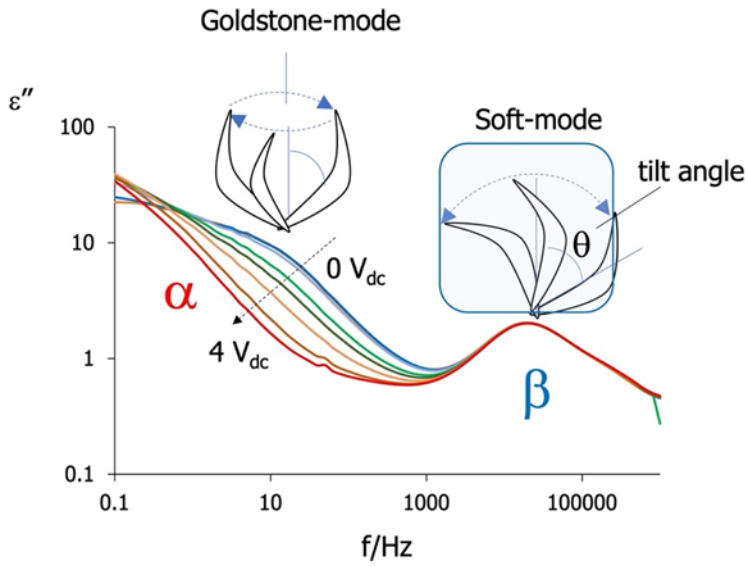

Figure IV.6.4. Effect of direct current electrical fields of various amplitudes on the dielectric loss factor, ε'', measured in the smectic phase of NG75 (T=90 ºC), and assignation of the α and β relaxations to molecular modes.

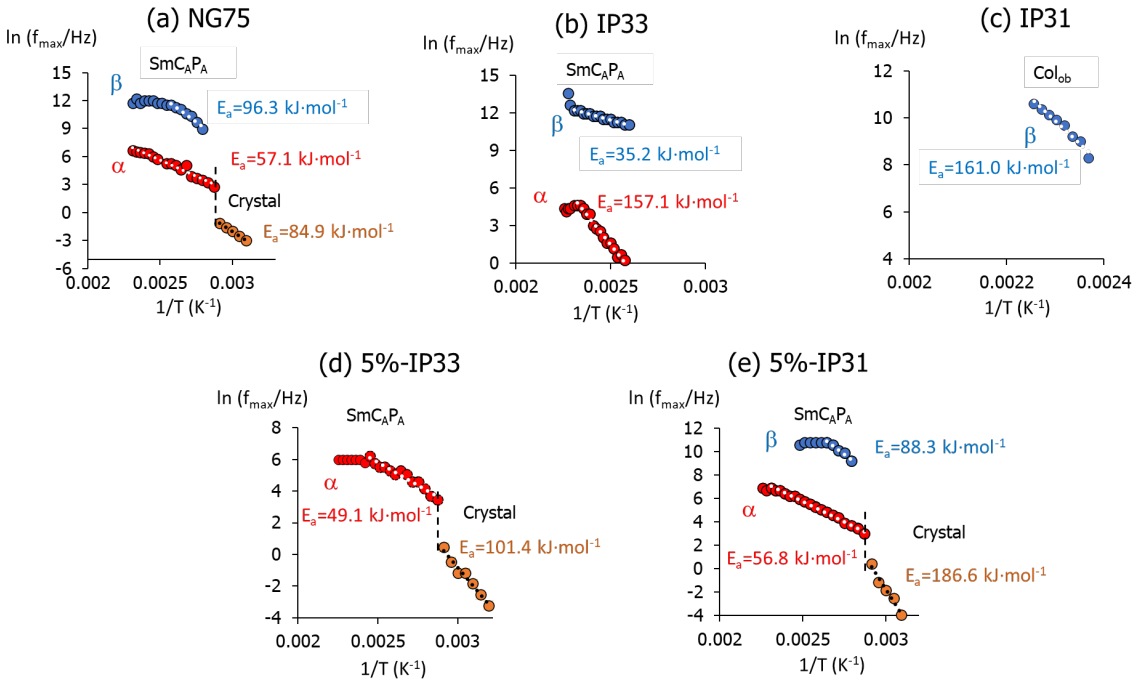

Figure IV.6.5. Arrhenius plots obtained for the maxima (f_{max}) of the dielectric loss factor curves, ε'', and apparent activation energies, E_a, estimated for the α and β relaxations (see white points as selected linear regions).

The appearance of plateaus in the double logarithmic plots of the real component of the complex conductivity, σ', Figure IV.S6.5, denotes direct conductivity in the bent-core molecules, with σ_{dc} values in the 10^{-9} to $10^{-4} \cdot S\ cm^{-1}$ range. Even though these are much lower than those exhibited by benchmark electrolytes for batteries or fuel cells ($\sim 10^{-1} \cdot S\ cm^{-1}$) [45, 46], the occurrence of direct conductivity opens the opportunity to promote ionic mobility activated by molecular motions within liquid crystal structures [43,47-55]. It is also worth noting that, within the electric fields ranges applied (±1 V_{rms}, 4 V), we did not observe noticeable textural changes in our samples under the microscope, and we will return to this observation later.

Ferroelectric response

We have assessed the ferroelectric response of our bent-core materials by applying strong alternating electrical fields (in the ±75 $kV \cdot cm^{-1}$ range) following triangular hysteresis loops, at different temperatures and frequencies. All samples exhibit non-linear polarisation response, and remanent polarisation (at zero voltage, P_r), typical of ferroelectric behaviour, which is illustrated for IP33 in Figure IV.6.6.

The application of electrical fields in NG75 and IP33 (and 5%-IP33 and 5%-IP31) induces textural changes, which may indicate molecular rearrangements and polarisation within the smectic layers, but we could not find evidence of phase transitions. The absence of field-induced phase transitions in our samples is not surprising, since the threshold electrical field required to collapse the mesophase of these bent-core compounds are reported in the 100 $kV \cdot cm^{-1}$ range [29], which we could not reach due to experimental constrains. Dark conglomerate phases (DC) in NG75 were not observed either, which may be due to strong anchoring effects at the surface of our ITO cells. The columnar organisations of IP31 also remain during the hysteresis cycles, but some stripes appear in the banana leaves textures within the liquid crystal domains, particularly visible after several cycles and at low frequencies, Figure IV.S6.7a to IV.S6.7f. Similar features are also observed due to the appearance of lamellar (or pseudo-layered) organisations [56-58] or flexoelectric effects [59, 60] in nematic phases. Even though SmCP structures can develop from columnar phases in bent-core materials (inducing B1 to B2 phase transitions), this normally occurs if the

sample is cooled down from the isotropic liquid, under application of low frequency alternating electrical fields [28, 61].

The values of remanent polarisation (P_r) and saturated polarisation (P_s, at the highest voltage), and the effects on textural changes, are more prominent at low frequencies where Goldstone-modes are prevalent, see Figure IV.S6.7. As expected, the ferroelectric response improves with temperature within the mesophase, see Figure IV.S6.8b, attributed to the higher molecular mobility illustrated by the Arrhenius plots in Figure IV.6.5. These dependences with temperature and frequency are comparable for the five samples under study. Polarisation values are within the range of other SmC materials (~0.5 $\mu C \cdot cm^{-2}$)[62].

Both 5%-IP33 and 5%-IP31 show ferroelectric response, and the introduction of the azobenzene compounds modifies the initial response of NG75 in the mixtures, with similar saturated polarisation values, P_s, but lower remanent polarisations, P_r, Table IV.S6.2. Therefore, whilst the NG75 ferroelectric behaviour seems to be weakened, the mixtures gain in relaxor response and capacity to store energy (E_s, $J \cdot cm^{-3}$), calculated from the integrated area in the polarization-electric field (P-E) hysteresis loops, see Figure IV.S6.8a. It is worth noting how the mixtures response is controlled by the azobenzene compounds, even though these only represent 5% of their overall molar composition. Despite the low energy values (8.79 – 9.28 $mJ \cdot cm^{-3}$ range), compared to inorganic relaxors (180 – 4000 $mJ \cdot cm^{-3}$ range [63, 64]) these results illustrate the capacity of our mixtures (and pristine materials) to harvest energy.

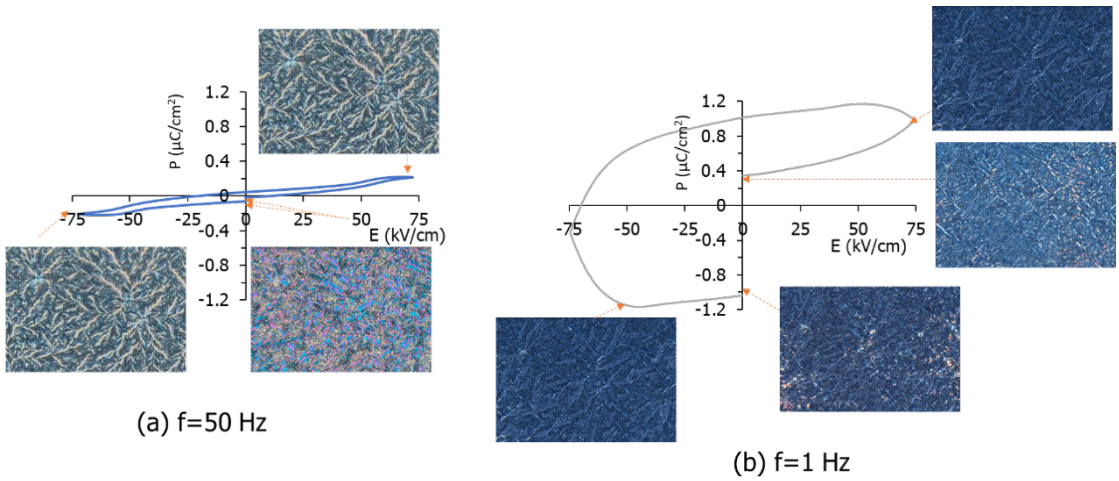

Figure IV.6.6. Hysteresis loops and associated polarised optical micrographs showing the ferroelectric response of IP33 at: (a) 50Hz and (b) 1 Hz (T=130 ºC, SmCP phase).

Light response and light effect on the dielectric and conductivity response

Figure IV.6.7a shows the UV-visible spectra of IP31, IP33, and their 5% mixtures in NG75, obtained in tetrahydrofuran (THF) solutions (~10^{-5} M) at room temperature. All solutions show one strong band centred at around ~365 nm, due to the lowest-energy $\pi^* \leftarrow \pi$ transition in the *trans*-azobenzene isomer, and a much smaller intensity absorption peak in the visible region (~440 nm), assigned to a weak $\pi^* \leftarrow n$ transition in the *cis*-azobenzene [65]. Upon UV irradiation (365 nm; 260 mW·cm^{-2}), the azobenzenes undergo *trans*-to-*cis* photo-induced isomerisation, evidenced by a decrease in the ~365 nm band and a simultaneous (slight) increase of the ~440 nm band, illustrated for IP31 in Figure IV.6.7b. When the solutions are kept in the dark after illumination, the UV-vis spectra recover their initial shape (prior to UV illumination) before 24 hours after exposure, due to thermally induced *cis*-to-*trans* back-relaxation of the azobenzene groups [66], see also **Fig. S10**. There are no significant differences in the range of back (thermal) isomeration kinetics of the four solutions (compounds), which is illustrated by their half-live ($t_{1/2}$) values (between 4 and 6 hours) estimated from the maxima of the time-dependent curves, see Table IV.S6.3 obtained from Figure IV.S6.11.

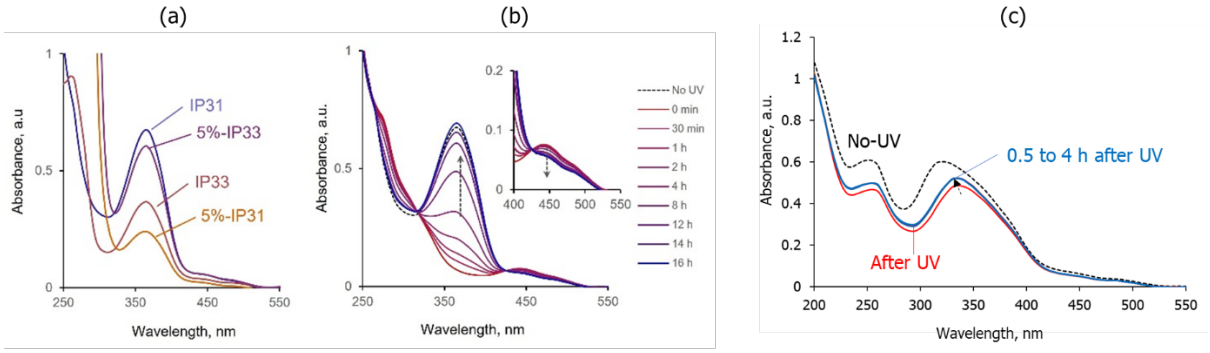

Figure IV.6.7. UV-visible spectra of the light-responsive bent-core based samples: (a) IP33, IP31, 5%-IP33 and 5%-IP31 measured in ~10^{-5} M THF solutions at room temperature (IP31 and IP33: 1.2 x 10^{-5} M; 5%-IP31: 11.3 x 10^{-5} M; 5%-IP33: 37.8 x 10^{-5} M). IP31 spectra measured before and at different times after light irradiation (260 mW · cm^{-2}; 365 nm): (b) in THF solution at room temperature; and (c) on a film cast on quartz at its mesophase (145 °C). Arrows in (b) and (c) indicate signal recovery after UV irradiation (t = 0 min) while samples were kept in the dark.

The UV-vis absorption spectra measured on quartz films (at the mesophase) show lower intensities than their respective THF solutions, probably due to their thicknesses, see Figure IV.S6.7c for IP31. Interestingly, the maxima of the absorbance peaks appear at lower wavenumbers (~ 325 nm), together with multiple shoulders. This response denotes the formation of azobenzene aggregates in the films, and more specifically, such low frequency values are consistent with predominant head-to-head stacking of aromatic rings to form H-aggregates [67]. Illumination of the films with a 365 nm UV source (260 mW · cm^{-2}) promotes less acute changes in the curves than in solution, which could have a two-fold explanation. On the one hand, the high viscosity of the mesophase (consistent with the formation of H-aggregates) may inhibit some of the motions necessary for the *trans*-to-*cis* isomerization [42]. On the other hand, at high temperatures the thermally activated *cis*-to-*trans* back-relaxation is favoured, displacing the equilibrium towards the formation of *trans* azobenzene isomers [31]. It is worth noting that the maxima of the absorption peak in Figure IV.6.7c appears at larger wavelengths after irradiation. We hypothesize that this could be due to a selective photoisomerization of the (predominant) H-aggregates in the films, while azobenzene groups arranged in head-to-tail arrangements (J-aggregates) seem to be less affected by UV-irradiation. We also note that, after 0.5 hours, the UV-vis signal does not change to a great extent during the whole experiment duration (4

hours). This behaviour could be useful for light-energy storage, even though we acknowledge that further time-dependent experiments will be necessary to confirm, and shed more light on, the mechanisms involved.

We have applied UV irradiation (365 nm) to control the dielectric response of the light-responsive bent-core based materials, and we illustrate some of these effects in Figure IV.6.8, where we show the real component of their complex conductivity, σ', measured at their mesophases (T=90 ^{o}C). Light irradiation (200 $mW \cdot cm^{-2}$) enhances σ' at lower frequencies, and such selective increase rules out mere thermal effects on the conductivity response. Interestingly, the rise in conductivity seems more effective in the smectic materials, i.e., the 5% mixtures and IP33, Figure IV.6.8a, 8c and 8d. We believe that the presence of *cis*-isomers may enhance the alignment of the layer(s) adjacent to the cells surfaces, facilitating long-range conductivity [31]. We cannot rule out, however, that continuous *trans*-to-*cis*-to-*trans* photoisomeration, or the occurrence of iso-mesophase micro transitions, may also favour such alignment. As expected, similar irradiation doses have neglectable effects on the conductivity of NG75, see Figure IV.S6.12.

Most of these light-induced effects observed in the bent-core based materials are fully reversible and can be tuned to some extent by changing the experimental conditions. In Figure IV.S6.13 and IV.S6.14 we display a selection of graphs that illustrate the effect of temperature on their dielectric loss factor, ε''. Even though a closer (and quantitative) inspection is out of the scope of this paper, the response seems to be favoured at medium-low temperatures within the mesophase. This observation seems consistent with the promotion of the *cis*-to-*trans* thermal relaxation at high temperatures, resulting in a less acute light-response.

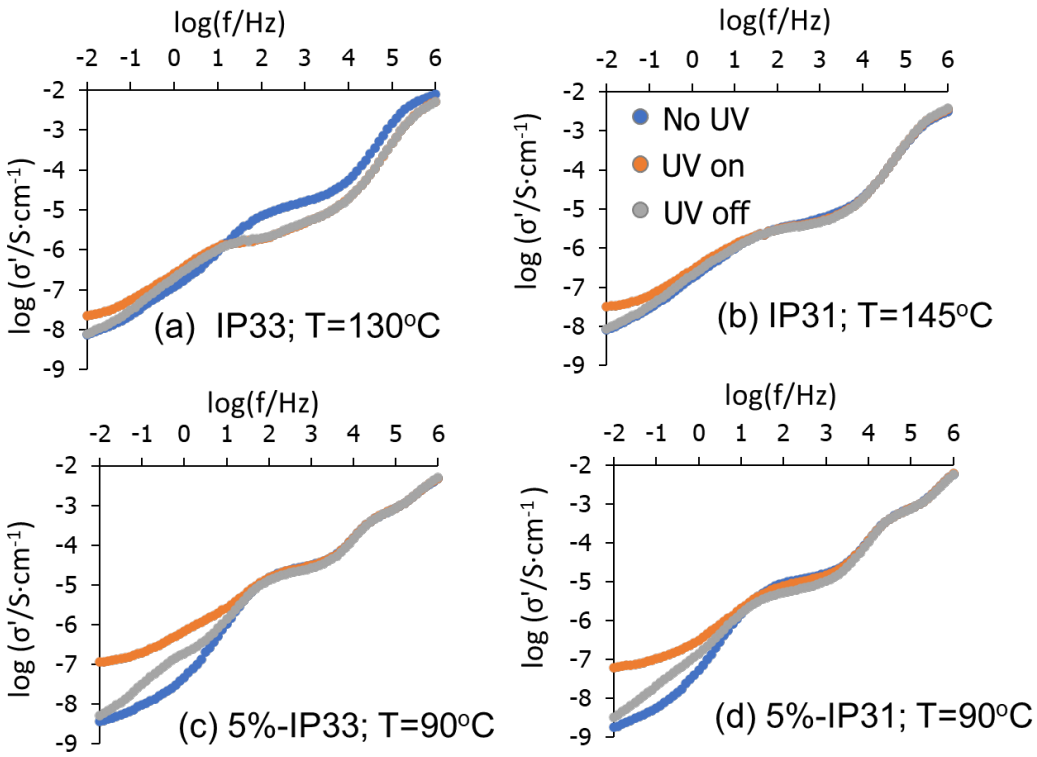

Figure IV.6.8. Frequency dependence of the real component, σ', of the complex conductivity, σ^*, measured at the mesophases of the light-responsive bent-core based materials before (blue), during (orange) and after (grey) UV illumination (200 mW · cm^{-2}; 365 nm).

The curves in Figure IV.6.8 (and Figure IV.S6.13 and IV.S6.14) were taken after two minutes of light irradiation (and then cessation), but they do not capture the dynamics of the photoisomeration process. Hence, we have monitored the time dependence of the dielectric elastic constant of our materials, ε', during irradiation cycles (T=130 ºC, 365 nm, and 200 mW · cm^{-2}), at a fixed frequency of 1 Hz (for consistency with our ferroelectric results). Figure IV.6.9 displays how irradiation promotes an almost immediate and linear rise in the ε' values (first step) followed by a slower Increase to reach a plateau (second step). The first step can be linked to the fast *trans*-to-*cis* photoisomeration of the azobenzene groups, initiated at the surface exposed to UV irradiation, with the bent geometry of the *cis*-azobenzenes further contributing to the local dipole moment of the bent-core molecule. The second step could be related to molecular reorganisations within the bulk of the mesophase, which further increase the dielectric response. These profiles agree with those obtained previously for other light-responsive liquid crystals [68, 69].

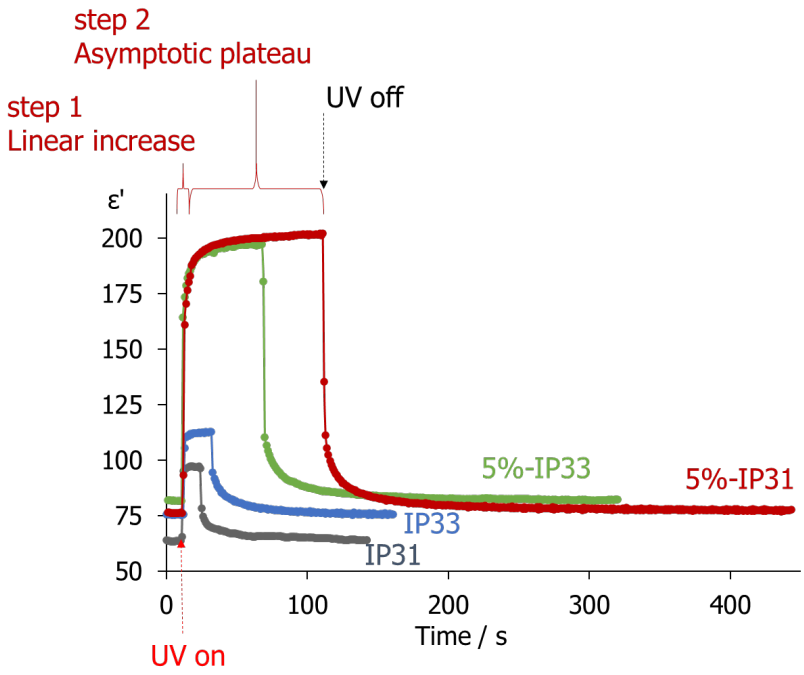

Figure IV.6.9. Time-dependence of the dielectric elastic constant, ε', measured at 1 Hz and 160 ºC (mesophases range) for the four light-responsive bent-cores under study, when submitted to UV off-on-off cycles (200 mW · cm^{-2}; 365 nm). Arrows and steps correspond to 5%-IP31.

After UV light is switched off, the curves in Figure IV.6.9 follow a similar, yet reversed and slower, two-step decrease: a fast drop in values followed by negative exponential decay until the initial ε' values are recovered asymptotically. These results are consistent with the curves in Figure IV.6.8 and confirm that the processes have reached steady states long before 120 s (2 minutes), see Table IV.S6.4. It is worth noting, however, that even though the responses from the four samples are comparable (all samples at 130 ºC yield 95% of the final values under illumination after 28 s and recover 95% of the initial value after 40 s of UV cessation), the second step seems to be slightly slower in the 5% mixtures, compared to the response of the pristine IP33 and IP31. This opens the possibility to control the dielectric properties *via* composition and promote storage effects with small amounts of light-responsive dopants.

Light irradiation under high voltages: isothermal phase transitions

Figure IV.6.10 illustrates the effect of UV light during the application of ferroelectric hysteresis loops (±75 kV · cm^{-1} range) measured at 1 Hz. Table IV.6.2

summaries the values obtained for P_s, P_R, energy stored and efficiency of energy storage (η) in the mesophase, estimated as:

$$\eta = \frac{E_S}{(E_S + E_L)} \qquad \textbf{Equation IV.6.2}$$

corresponding to the fraction of energy stored (E_S) respect to the overall energy involved in the process (including the area within the hysteresis loop, E_L), highlighted in Figure IV.S6.8.

As expected, polarisation (P_s, P_R) increases for the samples during irradiation due to *trans*-to-*cis* photoisomerationm which is consistent with the increase in ε' values in Figure IV.6.9, whereas the curves tend to recover their initial values after UV is switched off. On the other hand, UV irradiation promotes lower E_S and higher E_L values in all samples, see Figure IV.6.10, resulting in lower efficiencies, η. The reduction of E_S during UV irradiation could be attributed to a dissipation of certain amount of energy during reorientation of the azobenzene groups when UV is switched on, which results in higher E_L (broad hysteresis loop). Such energy effects can be particularly strong if the polarisation mechanism involves rotational (non-planar) reconfigurations of the azobenzenes [70].

Once irradiation is ceased, E_S and η increase for the four samples with a value higher than in the initial conditions, which is an interesting strategy to attain better capacity of dipole reorientation in cyclic processes. The η values (in the 0.198-8.49% range) are comparable to those reported by Kumar *et al.* for specific compositions of ceramics doped with zirconate titanate; the low efficiency was then attributed to domain wall movements that affected the main ferroelectric parameters [71]. As mentioned previously, whilst the E_s values in the mixtures are low (0.87 – 4.06 mJ · cm^{-1}), the UV irradiation effect to the dipole reorientation (P_s, P_R) opens the possibility to moderate the hysteresis loop behaviour *via* UV irradiation.

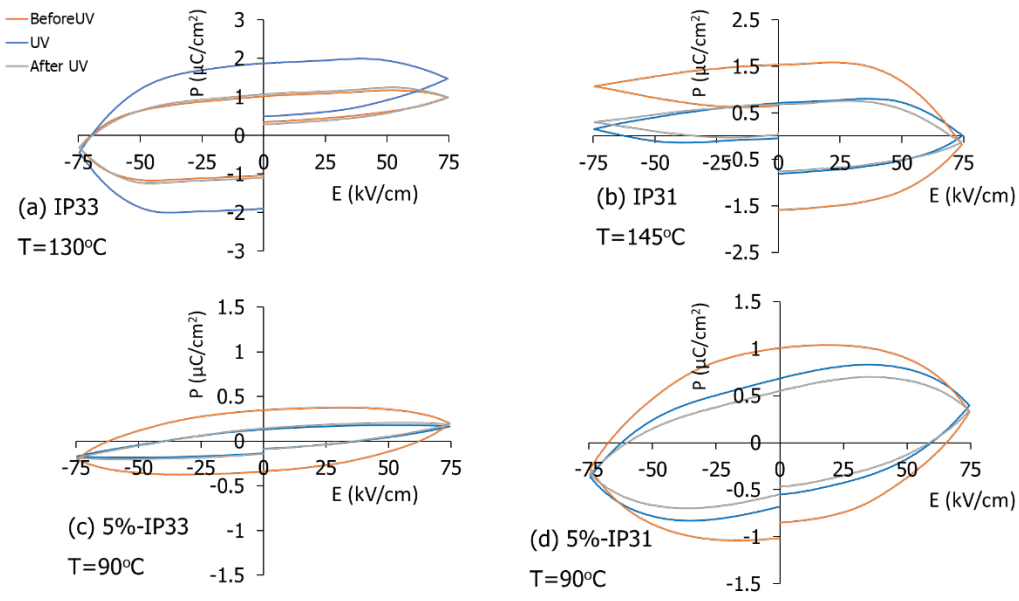

Figure IV.6.10. Hysteresis loops showing the effect of light on the ferroelectric response for the samples containing azo-bent core molecules (values taken at 1 Hz in their mesophases).

Table IV.6.2. Values for saturated polarization values, P_s, remanent polarisation, P_r, energy storage (E_s) and efficiency (η), as a function of UV light irradiation during 1 Hz ferroelectric loops, estimated at their respective mesophases: 130 ºC (a); 145 ºC (b); 90 ºC (c, d).

Sample	Before UV				During UV			
	P_S (μC/cm²)	P_R (μC/cm²)	E_S (mJ/cm³)	η (%)	P_S (μC/cm²)	P_R (μC/cm²)	E_S (mJ/cm³)	η (%)
IP33[a]	0.979	1.012	6.91	6.63	1.479	1.875	4.23	1.37
IP31[b]	0.0149	0.711	3.52	5.26	-0.180	1.510	2.69	1.18
5%-IP33[c]	0.167	0.133	1.85	7.65	0.192	0.345	0.865	1.12
5%-IP31[c]	0.395	0.681	3.91	4.03	0.326	1.00	0.421	0.198

Sample	After UV			
	P_S (μC/cm²)	P_R (μC/cm²)	E_S (mJ/cm³)	η (%)
IP33[a]	0.933	1.018	8.27	4.63
IP31[b]	-0.037	0.662	4.03	3.32
5%-IP33[c]	0.185	0.141	2.45	8.49
5%-IP31[d]	0.339	0.549	4.06	3.17

As discussed above, the application of electrical fields (on its own) did not promote isothermal phase transitions in our bent-core based materials. Alternatively, the application of UV irradiation can destabilise the liquid crystalline order by an increase of curved *cis*-azobenzene isomers that are not compatible with the mesophase, and promote phase transitions [72, 73]. It is then interesting to study the coupled effect of electrical fields and light irradiation on the phase structure of our bent-core based samples. Even though the experiments in Figure IV.6.10. did not result in phase transitions, we have found that isothermal clearing from the mesophases can occur under certain conditions near the clearing point, T_{cl} (up to $T-T_{cl}$=-7K). Due to the high clearing temperatures of these compounds, the *trans*-to-*cis* equilibrium is displaced towards the thermal back photoisomeration and the formation of *trans* isomers, and very high light intensities are required to yield isothermal isotropisation (> 1000 $mW \cdot cm^{-2}$).

Whilst phase transitions from ordered mesophases to disordered melts are common, see for example [74, 75], we now investigate whether a combination of light and electrical fields could promote an isothermal transition between different mesophases. Even though the columnar phase cannot be transformed isothermally into a smectic phase by the mere application of electrical fields, [28, 61] our results in Figure IV.6.6 have already suggested the formation of some layered ordering after the application of several hysteresis cycles. Alternatively, we have found a phase transition route for IP31 consisting of: first promoting isotropisation of its columnar phase by irradiation with strong UV light intensities near the clearing point, $T-T_{cl}$ =-4K, Figure IV.6.11a, followed by the application of a strong electrical field (in the dark), which yields a new granular texture consistent with smectic phases, Figure IV.6.11(b).

To our knowledge, this could be the first example when a smectic phase is formed isothermally from a columnar phase (through an isotropic melt) in a bent-core based material [76]. By restricting the area exposed to electrical fields, we have obtained cells with coexisting (induced) smectic and (original) columnar phases separated by an interface, see Figure IV.6.12. This phenomenon can be very useful to build grating devices with regions having different physical properties, by using photomasks [77]. We note that, either the application of electrical fields when cooling

from the isotropic melt (no UV irradiation), or the removal of the electrical fields when reforming the mesophase after UV irradiation (no electrical field in the dark), on their own, only lead to the reappearance of columnar phases in IP31.

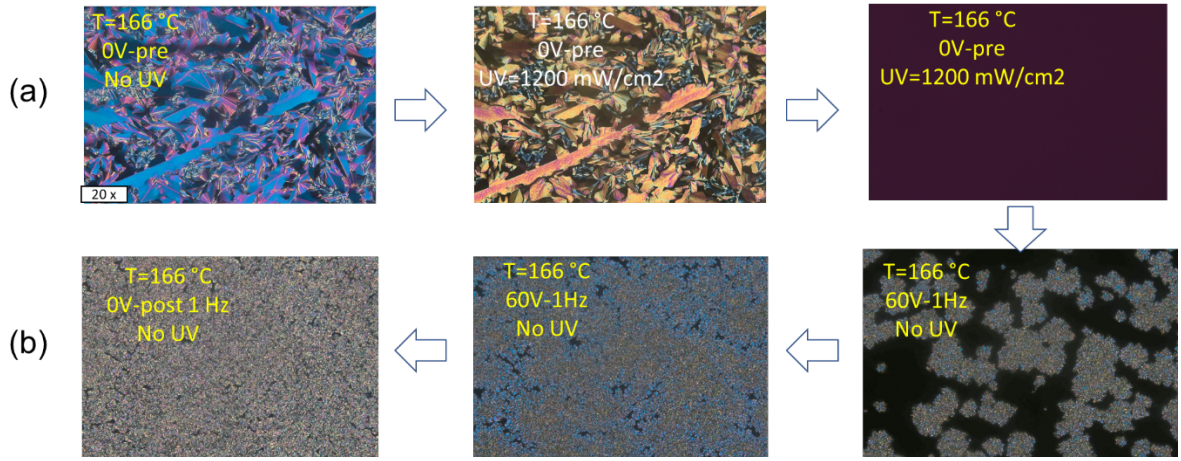

Figure IV.6.11. Polarised optical micrographs obtained for IP31 at T=166 ºC: (a) application of UV irradiation (1200 mW · cm^{-2}; 365 nm), followed by (b) strong electrical fields (75 kV · cm^{-1}), resulting in a granular smectic phase.

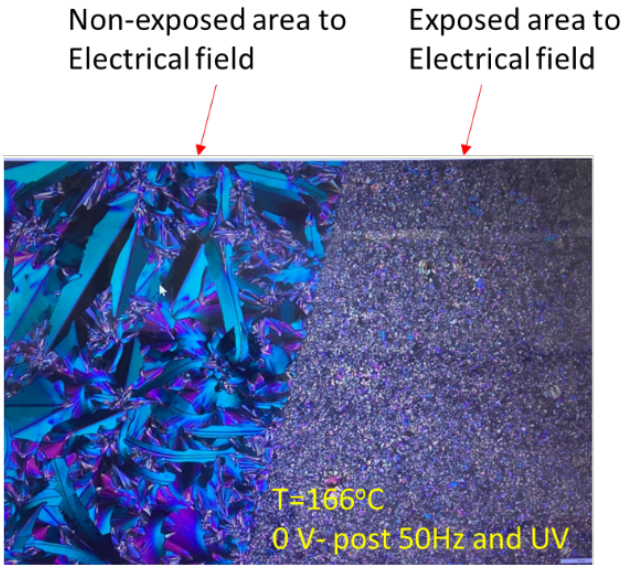

Figure IV.6.12. Polarised optical micrograph obtained for a IP31 sample following the UV and electrical fields cycle described in Figure IV.6.11, resulting in coexisting regions of columnar and smectic phases.

Conclusions

We have demonstrated the potential of the five bent-core based materials under study to transfer or store electrical energy, by a combination of dielectric, ferroelectric, and relaxor behaviour. Their response to electrical stimuli is related to Goldstone-modes of molecular reorientational motions within the smectic or columnar fields, activated at low frequencies (~1 Hz).

In addition, the presence of chromophore groups in pristine materials or in mixtures, has been used as a mechanism to harvest light energy, by triggering *trans*-to-*cis* photoisomeration of azobenzene groups. Light irradiation enhances conductivity and polarisation, even at low concentrations of photochromic groups. The ultimate reason for such improvement is unclear, due to the low yield of *cis*-azobenzene isomers expected at high temperatures, and will be the object of further research. We hypothesise that the disruption of the local liquid crystalline packing by the curved geometry of the *cis*-isomers can promote motions that facilitate the electrical signal in these materials. However, we cannot rule out that the concentration of *cis*-isomers near the glass electrodes enhances the alignment in smectic materials. Our next steps to design functional energy storage materials will involve controlling the size of the polar regions to increase polarisation and promoting steric hindrance That inhibit certain rotational mechanisms necessary for the *cis*-to-*trans* back isomerisation of the azobenzenes. Some of these facts could explain the UV-vis response observed by the films in the mesophase, and could ultimately lead to irreversible structural and excited states.

The induction of an isothermal columnar to smectic phase transition in IP31 (*via* isotropisation) by a combination of light and electrical fields is a promising tool to develop electric response through the formation (and control) of layered nanostructures. Examples in the literature of light-induced ordered phases are rare, normally attributed to nanophase separation [78], hence our results can be applied to other fields of liquid crystals, soft matter, and nanotechnology.

Acknowledgements

IDC would like to thank the Universitat Politècnica de València (UPV), for the FPI grant (PAID-2019-SP20190013), the Generalitat Valenciana (GVA) and the European Social Found (ESF), for the FPI grant (ACIF/2020/233) and the mobility grant (CIBEFP/2021/53). NFKA would like to thank Universiti Teknologi MARA (UiTM) for sponsoring her academic sabbatical leave and allowing her to work on this project. AMF would like to thank the Carnegie Trust for the Universities of Scotland, for the Research Incentive Grant RIG008586, the Royal Society and Specac Ltd., for the Research Grant RGS\R1\201397, the Royal Society of Chemistry for the award of a mobility grant (M19- 0000), and the Scottish Government and the Royal Society of Edinburgh for the award of a SAPHIRE project. The authors from INMA greatly appreciate financial support from projects of the Spanish Government PGC2018-093761-B-C31 [MCIU/AEI/FEDER, UE] and the Gobierno de Aragón/FEDER (research group E47_20R). Thanks are given to the nuclear magnetic resonance, mass spectrometry, and thermal analysis services of the INMA (Univ. Zaragoza-CSIC).

Supplementary information

Figures

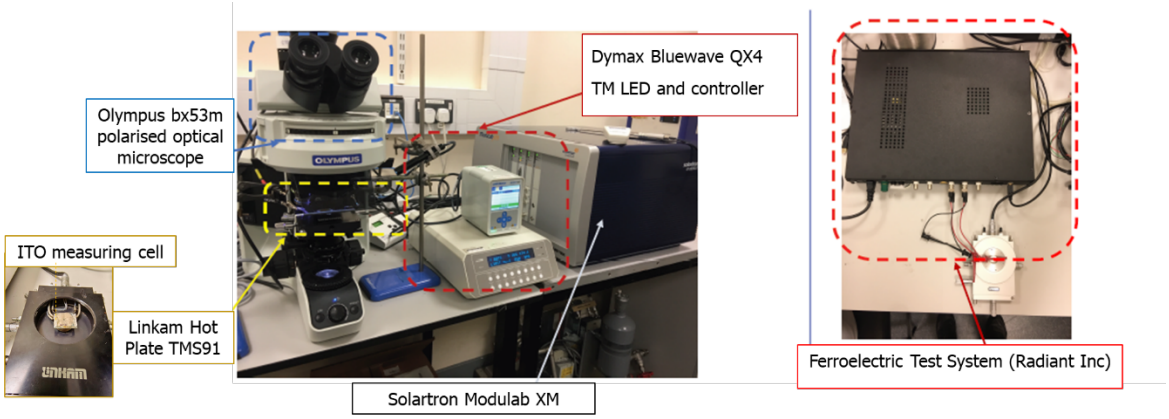

Figure IV.S6.1. Picture of the experimental setting including the polarised optical microscope, the Linkam heating stages holding the ITO measuring cells, the Dymax Bluewave QX4 TM LED probe, and connexions to the dielectric and ferroelectric analysers.

Figure IV.S6.2. Differential scanning calorimetry (DSC) thermograms obtained for the five samples under study, in their cooling (above), and second heating (below) scans at ±10 $^{o}C \cdot min^{-1}$. The small peak appearing at around 100 ^{o}C on the reheating curves of NG75-containing compounds did not correspond to any phase transition reported earlier (see **Table IV.S6.1** below), nor was visible under our current microscope experiments.

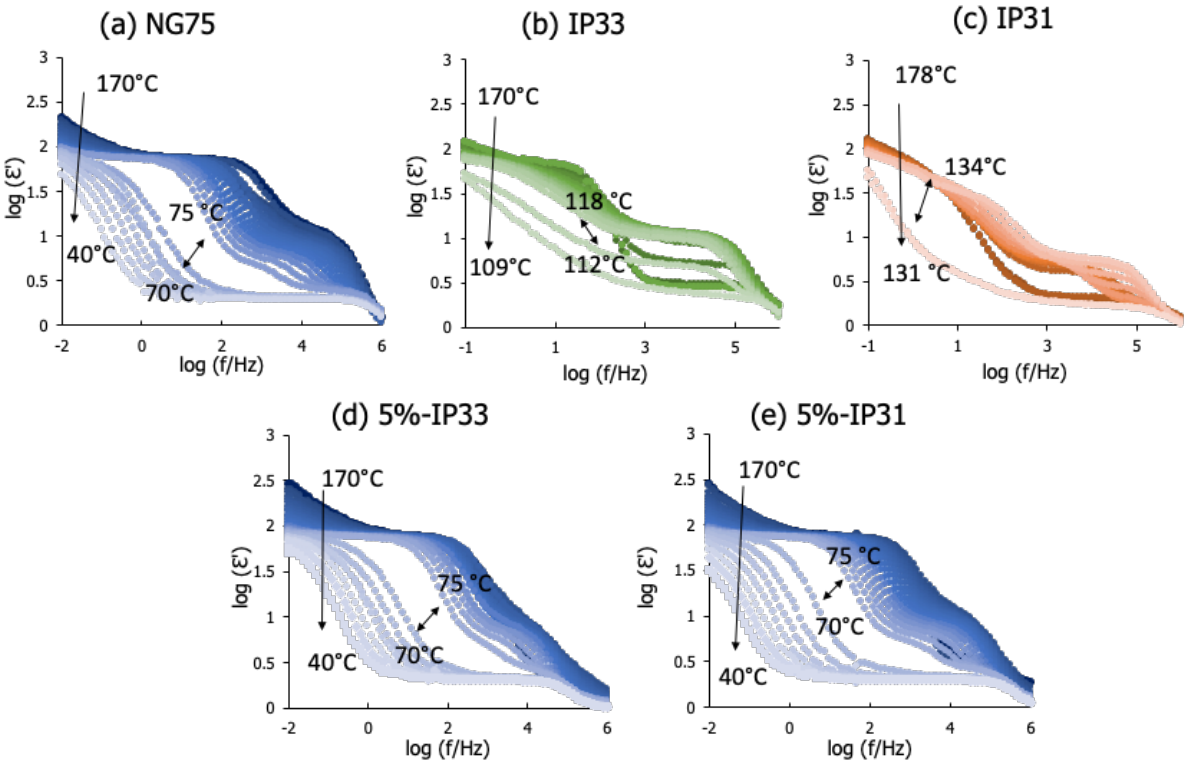

Figure IV.S6.3. Double logarithmic plots of the dielectric elastic constant, ε', as a function of frequency and temperature, corresponding to the five bent-core based materials, obtained in isothermal steps on cooling from their isotropic phases.

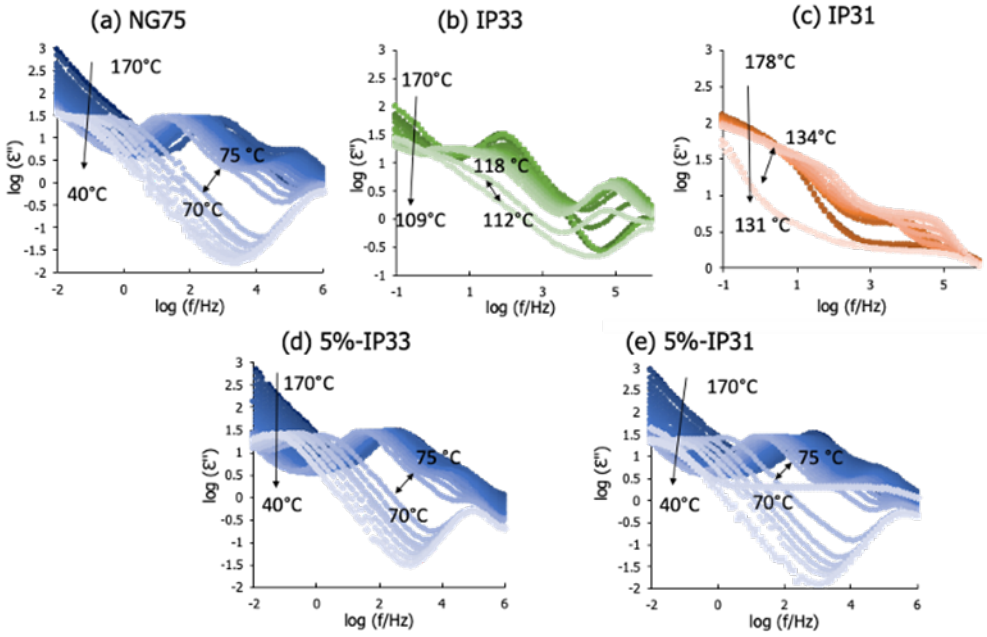

Figure IV.S6.4. Double logarithmic plots of the dielectric loss factor, ε'', as a function of frequency and temperature, corresponding to the five bent-core based materials, obtained in isothermal steps on cooling from their isotropic phases.

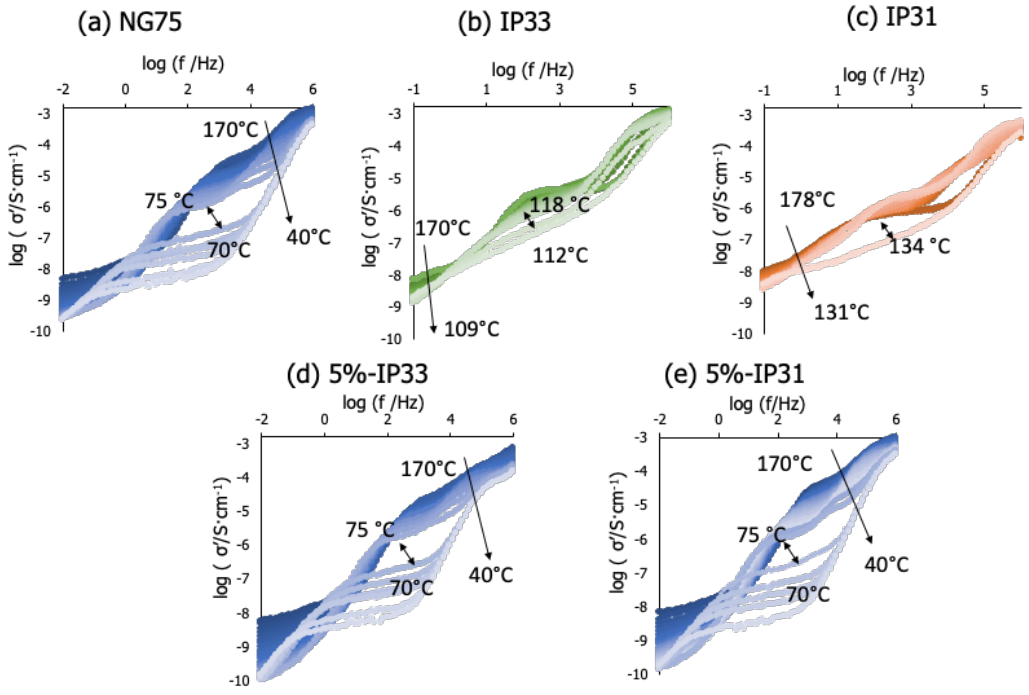

Figure IV.S6.5. Double logarithmic plots of the real component of the complex conductivity, σ', as a function of frequency and temperature, corresponding to the five bent-core based materials, obtained in isothermal steps on cooling from their isotropic phases.

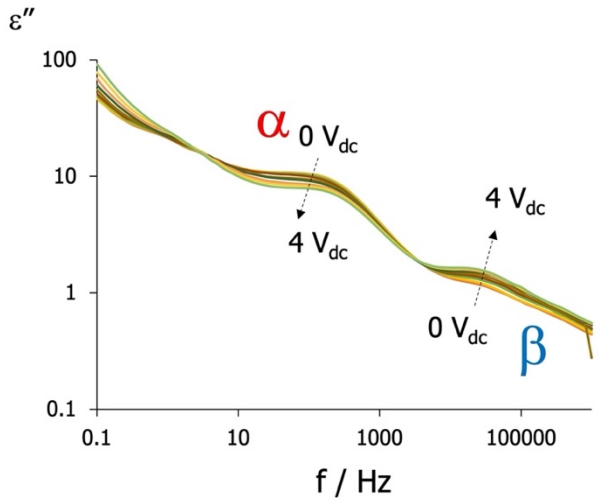

Figure IV.S6.6. Effect of direct current electrical fields of various amplitudes on the dielectric loss factor, ε'', measured in the columnar phase of IP31 (T=145 °C), and assignation of the α and β relaxations.

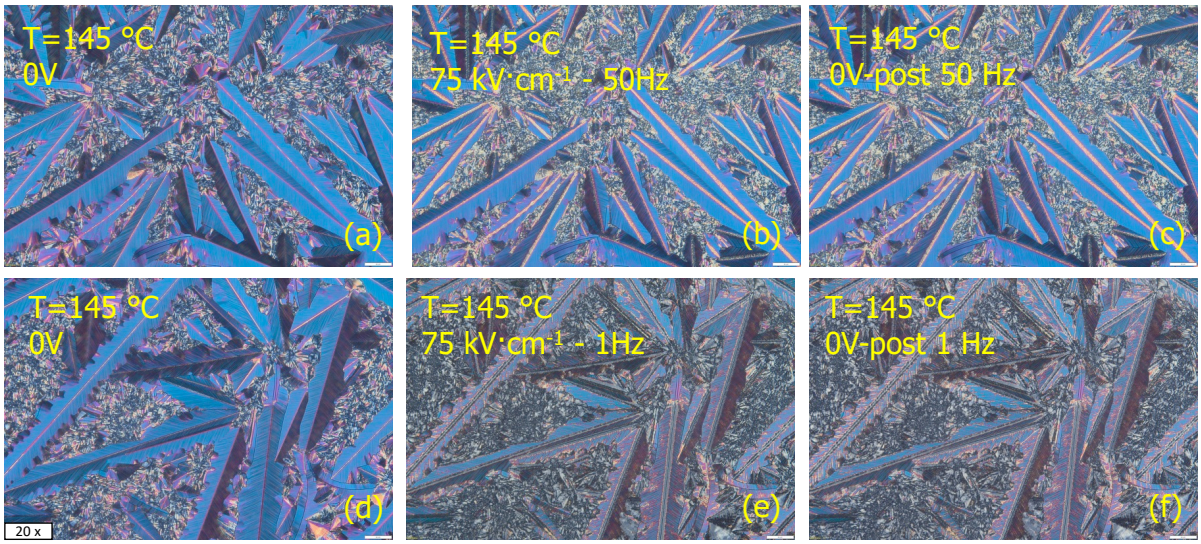

Figure IV.S6.7. Polarised optical micrographs obtained for IP31 at 145 °C, showing the banana leaves textures typical of columnar phases, before (left), during (middle) and after (right) application of electrical fields at 50 Hz (up) and 1 Hz (down).

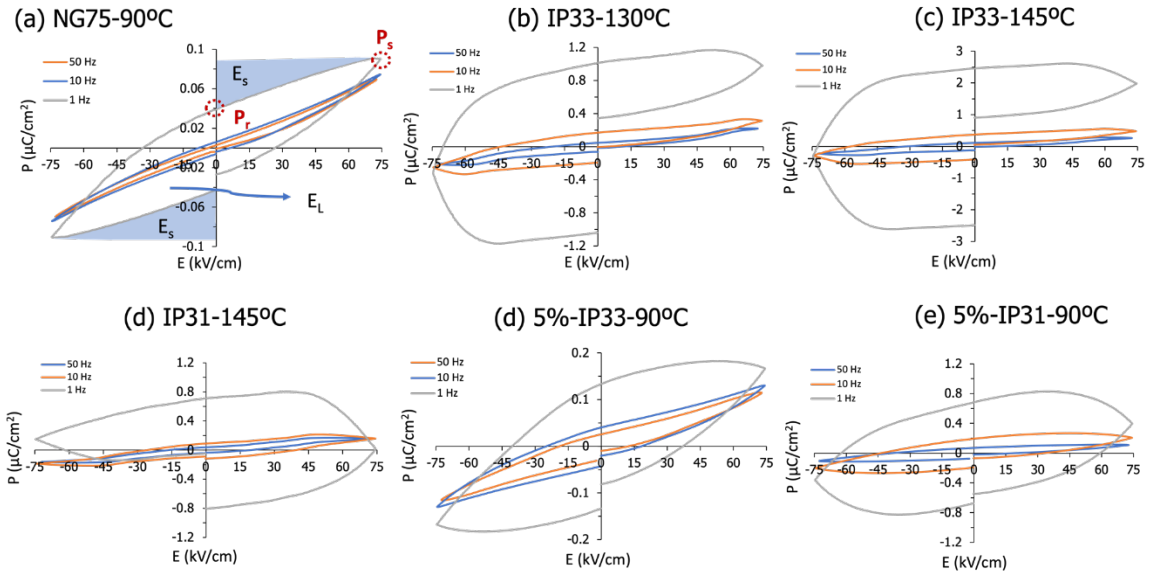

Figure IV.S6.8. Hysteresis loops showing the ferroelectric response of the five samples; frequency dependence.

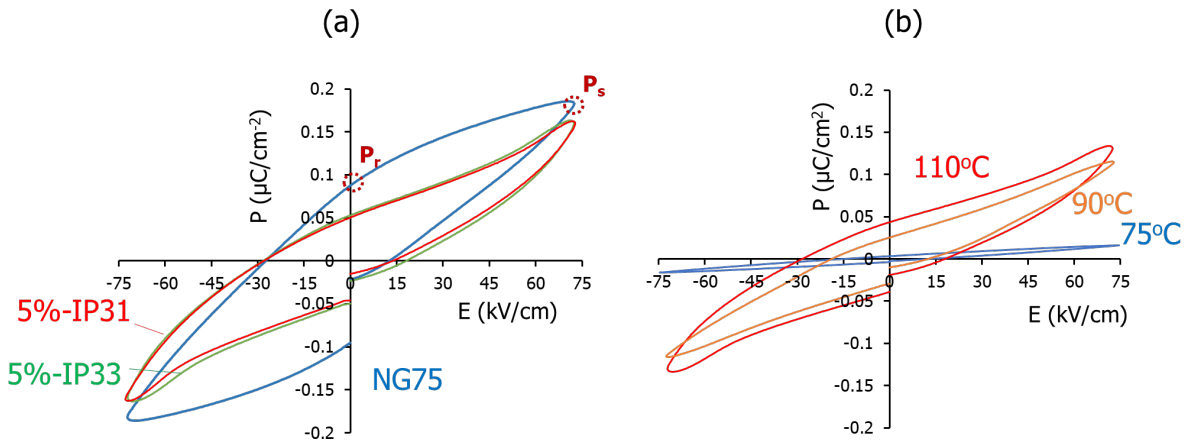

Figure IV.S6.9. Hysteresis loops showing the ferroelectric response of: (a) NG75 and its mixtures with IP33 and IP31 (130 °C, 50 Hz); (b) temperature effect on 5%-IP33 in its smectic phase (50 Hz).

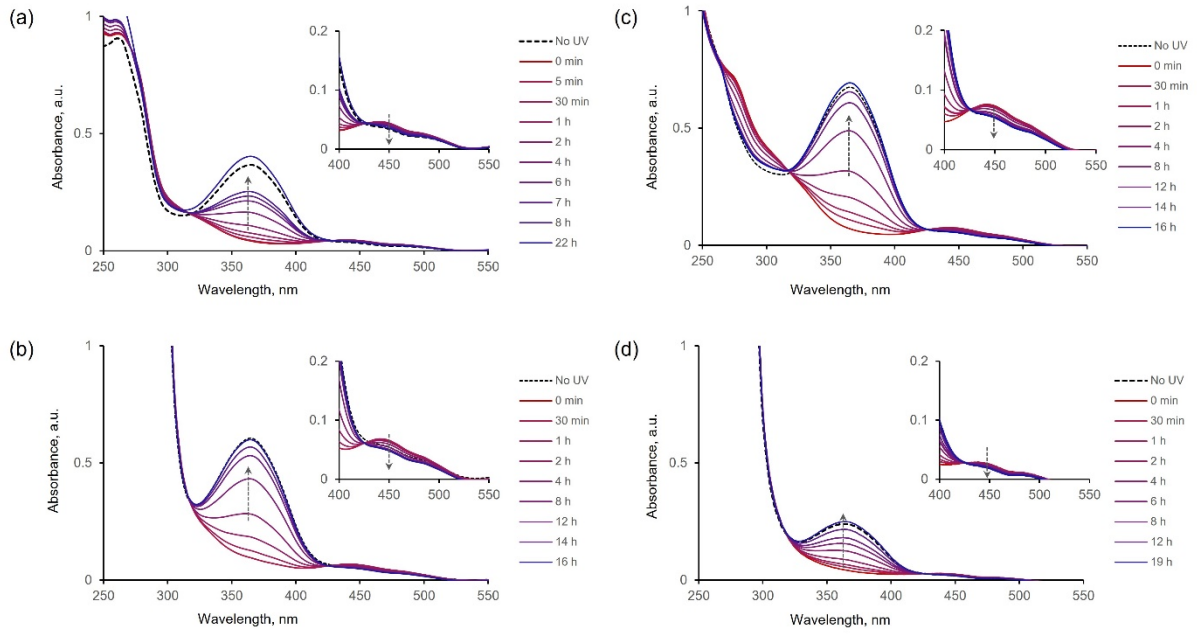

Figure IV.S6.10. UV-visible spectra of the light-responsive bent-core based materials measured before and at different times after light irradiation (260 mW · cm^{-2}; 365 nm): (a) IP33; (b) 5%-IP33; (c) IP31; (d) 5%-IP31. Insets show the π* ← n transition in the *cis*-azobenzene at peak ~440 nm. Measurements were taken for THF solutions at room temperature (IP31 and IP33: 1.2 x 10^{-5} M; 5%-IP31: 11.3 x 10^{-5} M; 5%-IP33: 37.8 x 10^{-5} M).

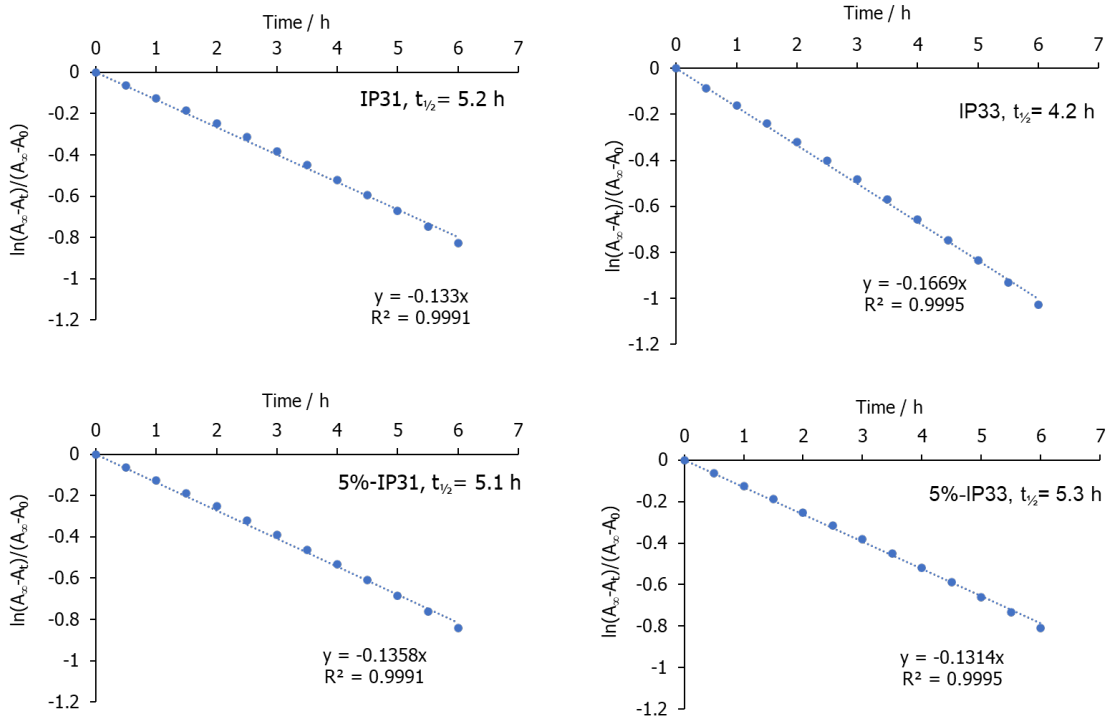

Figure IV.S6.11. Graphs showing the kinetics of *cis*-to-*trans* (thermal) back-isomerisation for the pristine samples in solution, using the maximum absorbance values (~440 nm) of their UV-visible

spectra at different times while kept in the dark (A_t) after light irradiation (A_0) (260 mW · cm^{-2}; 365 nm), until the curves recover their initial values prior to irradiation (A_∞). Estimation of the half-life times, $t_{1/2}$.

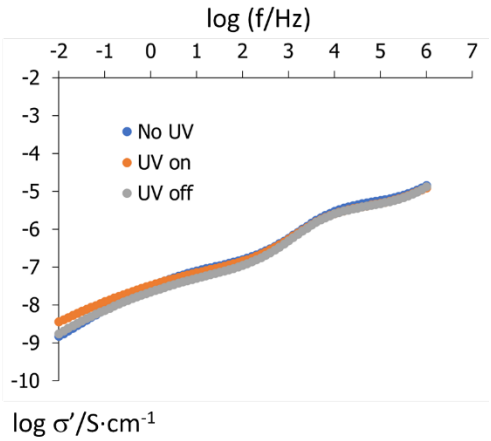

Figure IV.S6.12. Frequency dependence of the real component, σ', of the complex conductivity, σ*, measured at the mesophase of NG75 before (blue), during (orange) and after (grey) UV illumination (200 mW · cm^{-2}; 365 nm).

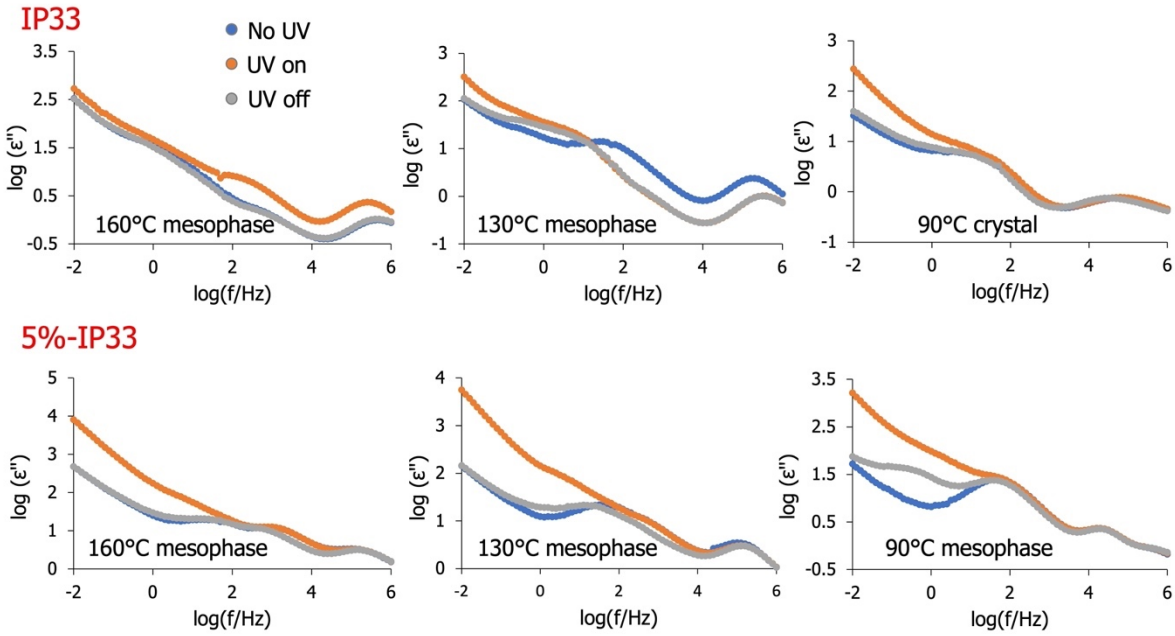

Figure IV.S6.13. Selected double logarithmic plots of the dielectric loss factor, ε'', as a function of frequency and temperature, for IP33 and 5%-IP33, measured before (No UV), during (UV on), and after (UV off), light irradiation (200 mW · cm^{-2}; 365 nm).

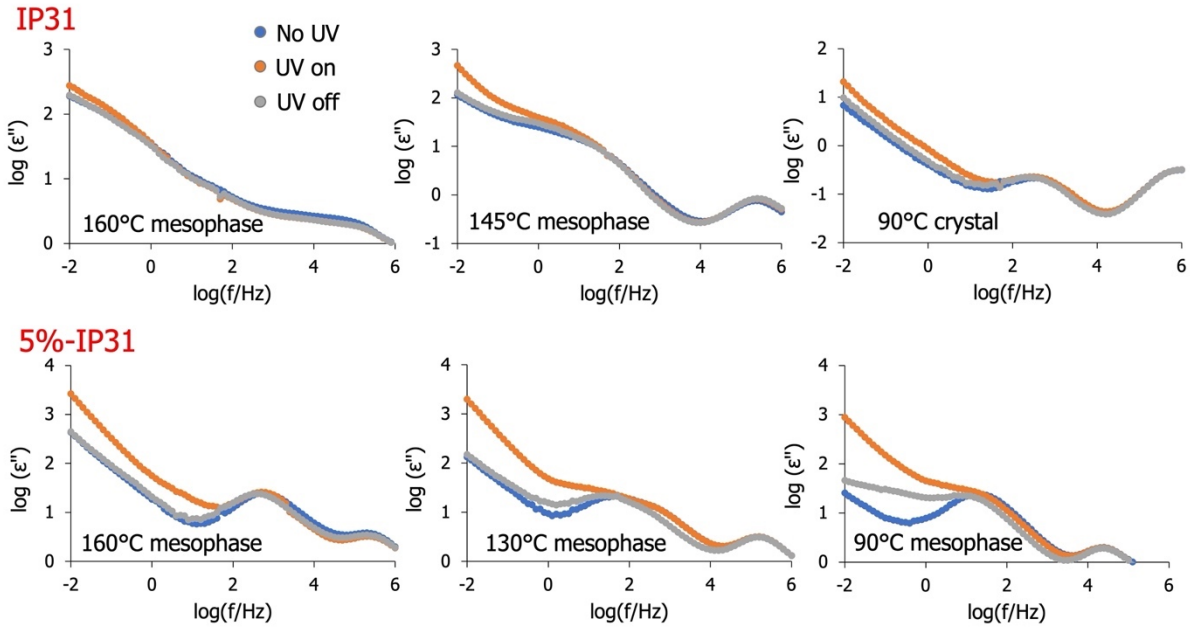

Figure IV.S6.14. Selected double logarithmic plots of the dielectric loss factor, ε", as a function of frequency and temperature, for IP31 and 5%-IP31, measured before (No UV), during (UV on), and after (UV off), light irradiation (200 mW · cm^{-2}; 365 nm).

Tables

Table IV.S6.1. Phase transition temperatures (obtained by polarised optical microscopy, POM, on heating and cooling ranges, 10 $^{o}C \cdot min^{-1}$); and phase structure parameters obtained by Small Angle X-ray diffraction, SAXS, for the three pristine samples.

Sample	Mesophase range / °C (*)	Parameters / Å Measured spacings/Å (Miller index)
NG75	Cr 74.2 SmC_AP_A 156.9 I	c: 42.5
	I 156.5 SmCAPA 67.7 Cr	42.8 (001), 21.2 (002), 14.1 (003)
IP33	Cr 116.4 SmC_AP_A 163.1 I	c: 44.3
	I 159.6 SmC_AP_A 101.4 Cr	44.3 (001), 22.2 (002), 14.8 (003)
IP31	Cr 139.1 Col_{ob} 165.3 I	a: 92.0 c: 48.0 b : 87.5^{o}
	I 160.9 Col_{ob} 127.8 Cr	47.8 (001), 46.1 (200), 43.2 (101)
		41.7 (-101), 33.9 (201), 26.6 (301)

(*) Cr: crystal, SmCAPA, smectic C antiferroelectric polar (anticlinic) mesophase, Colob: columnar oblique mesophase, I: isotropic liquid.

Table IV.S6.2. Values for saturated polarisation values, P_s, remanent polarisation, P_r, and energy storage, estimated for NG75 and its mixtures with IP33 and IP31, at 130 ^{o}C, and 50 Hz.

Sample	P_S ($\mu C \cdot cm^{-1}$)	P_R ($\mu C \cdot cm^{-2}$)	Energy stored ($mJ \cdot cm^{-3}$)
NG75	0.182	0.0878	5.164
5%-IP33	0.159	0.0530	8.791
5%-IP31	0.159	0.0500	9.278

Table IV.S6.3. Half-live ($t_{1/2}$) values estimated for the *cis*-isomers, obtained from the maxima of the UV-vis curves as a function of time, **Figure IV.S6.10**.

Sample	$t_{1/2}$ / h
IP33	4.2
IP31	5.2
5%-IP33	5.3
5%-IP31	5.1

Table IV.S6.4. Times required to yield 95% of the steady state ε′ during isothermal experiments upon irradiation (correlate to **Figure IV.S6.9.**)

Sample	UV on	UV off
	Time / s	
IP33	3	32
IP31	3	32
5%-IP33	12	39
5%-IP31	28	40

References

[1] International Energy Agency, Global Energy Review. 2020

[2] Y. Shen, Dierking, I. Perspectives in Liquid-Crystal-Aided Nanotechnology and Nanoscience. Applied Sciences-Basel 2019, 9, doi:10.3390/app9122512.

[3] A. Martinez-Felipe. Liquid crystal polymers and ionomers for membrane applications. Liquid Crystals 2011, 38, 1607-1626, doi:10.1080/02678292.2011.624201.

[4] P. K. Bhowmik, Noori, O., Chen, S. L., Han, H., Fisch, M. R., Robb, C. M., Variyam, A., Martinez-Felipe, A. Ionic liquid crystals: Synthesis and characterization via NMR, DSC, POM, X-ray diffraction and ionic conductivity of asymmetric viologen bistriflimide salts. Journal of Molecular Liquids 2021, 328, doi:10.1016/j.molliq.2021.115370.

[5] A. Natansohn, Rochon, P. Photoinduced motions in azo-containing polymers. Chemical Reviews 2002, 102, 4139-4175, doi:10.1021/cr970155y.

[6] H. M. D. Bandara, Burdette, S. C. Photoisomerization in different classes of azobenzene. Chemical Society Reviews 2012, 41, 1809-1825, doi:10.1039/c1cs15179g.

[7] G. S. Hartley. The cis-form of azobenzene. Nature 1937, 140, 281-281, doi:10.1038/140281a0.

[8] A.-L. Leistner, Pianowski, Z. L. Smart Photochromic Materials Triggered with Visible Light. European Journal of Organic Chemistry 2022, 2022, doi:10.1002/ejoc.202101271.

[9] G. A. Leith, Martin, C. R., Mathur, A., Kittikhunnatham, P., Park, K. C., Shustova, N. B. Dynamically Controlled Electronic Behavior of Stimuli-Responsive Materials: Exploring Dimensionality and Connectivity. Advanced Energy Materials 2022, 12, doi:10.1002/aenm.202100441.

[10] H. Sugiyama, Sato, S., Nagai, K. Photo-isomerization, photodimerization, and photodegradation polyimides for a liquid crystal alignment layer. Polymers for Advanced Technologies 2022, 33, 2113-2122, doi:10.1002/pat.5683.

[11] B. Zhang, Feng, Y., Feng, W. Azobenzene-Based Solar Thermal Fuels: A Review. Nano-Micro Letters 2022, 14, doi:10.1007/s40820-022-00876-8.

[12] A. R. Ibrahim, Khyasudeen, M. F., Husband, J., Alauddin, S. M., Aripin, N. F. K., Velayutham, T. S., Martinez-Felipe, A., Abou-Zied, O. K. p-Methoxy Azobenzene Terpolymer as a Promising Energy-Storage Liquid Crystal System. Journal of Physical Chemistry C 2021, 125, 22472-22482, doi:10.1021/acs.jpcc.1c07081.

[13] T. Niori, Sekine, T., Watanabe, J., Furukawa, T., Takezoe, H. Distinct ferroelectric smectic liquid crystals consisting of banana shaped achiral molecules. Journal of Materials Chemistry 1996, 6, 1231-1233, doi:10.1039/jm9960601231.

[14] J. Etxebarria, Ros, M. B. Bent-core liquid crystals in the route to functional materials. Journal of Materials Chemistry 2008, 18, 2919-2926, doi:10.1039/b803507e.

[15] H. Takezoe, Takanishi, Y. Bent-core liquid crystals: Their mysterious and attractive world. Japanese Journal of Applied Physics Part 1-Regular Papers

Brief Communications & Review Papers 2006, 45, 597-625, doi:10.1143/jjap.45.597.

[16] C. Tschierske. Development of Structural Complexity by Liquid-Crystal Self-assembly. Angewandte Chemie-International Edition 2013, 52, 8828-8878, doi:10.1002/anie.201300872.

[17] R. A. Reddy, Tschierske, C. Bent-core liquid crystals: polar order, superstructural chirality and spontaneous desymmetrisation in soft matter systems. Journal of Materials Chemistry 2006, 16, 907-961, doi:10.1039/b504400f.

[18] A. Eremin, Jakli, A. Polar bent-shape liquid crystals – from molecular bend to layer splay and chirality. Soft Matter 2013, 9, 615-637, doi:10.1039/c2sm26780b.

[19] H. Takezoe. Polar liquid crystals – ferro, antiferro, banana, and columnar. Molecular Crystals and Liquid Crystals 2017, 646, 46-65, doi:10.1080/15421406.2017.1284377.

[20] K. V. Le, Takezoe, H., Araoka, F. Chiral Superstructure Mesophases of Achiral Bent-Shaped Molecules – Hierarchical Chirality Amplification and Physical Properties. Advanced Materials 2017, 29, doi:10.1002/adma.201602737.

[21] M. Hird. Ferroelectricity in liquid crystals-materials, properties and applications. Liquid Crystals 2011, 38, 1467-1493, doi:10.1080/02678292.2011.625126.

[22] D. R. Link, Natale, G., Shao, R., Maclennan, J. E., Clark, N. A., Korblova, E., Walba, D. M. Spontaneous formation of macroscopic chiral domains in a fluid smectic phase of achiral molecules. Science 1997, 278, 1924-1927, doi:10.1126/science.278.5345.1924.

[23] M. Gong, Song, F., Li, H., Lin, X., Wang, J., Zhang, L., Wang, D. Optimizing energy harvesting performance of silicone elastomers by molecular grafting of azobenzene to the macromolecular network. Rsc Advances 2021, 11, 19088-19094, doi:10.1039/d1ra01433a.

[24] S. M. Alauddin, Aripin, N. F. K., Velayutham, T. S., Chaganava, I., Martinez-Felipe, A. The role of conductivity and molecular mobility on the photoanisotropic response of a new azo-polymer containing sulfonic groups. Journal of Photochemistry and Photobiology a-Chemistry 2020, 389, doi:10.1016/j.jphotochem.2019.112268.

[25] G. G. Nair, Prasad, S. K., Hiremath, U. S., Yelamaggad, C. V. Effect of light on the polarization of a banana-shaped achiral compound doped with a photoactive azobenzene material. Journal of Applied Physics 2001, 90, 48-52, doi:10.1063/1.1376408.

[26] M. Martinez-Abadia, Robles-Hernandez, B., Rosario de la Fuente, M., Gimenez, R., Blanca Ros, M. Photoresponsive Cyanostilbene Bent-Core Liquid Crystals as New Materials with Light-Driven Modulated Polarization. Advanced Materials 2016, 28, 6586-+, doi:10.1002/adma.201600311.

[27] M. Martinez-Abadia, Varghese, S., Gimenez, R., Ros, M. B. Multiresponsive luminescent dicyanodistyrylbenzenes and their photochemistry in solution and in bulk. Journal of Materials Chemistry C 2016, 4, 2886-2893, doi:10.1039/c5tc02852c.

[28] C. L. Folcia, Alonso, I., Ortega, J., Etxebarria, J., Pintre, I., Ros, M. B. Achiral bent-core liquid crystals with azo and azoxy linkages: Structural and nonlinear optical properties and photoisomerization. Chemistry of Materials 2006, 18, 4617-4626, doi:10.1021/cm060256p.

[29] J. Ortega, Folcia, C. L., Etxebarria, J., Martinez-Perdiguero, J., Gallastegui, J. A., Ferrer, P., Gimeno, N., Blanca Ros, M. Electric-field-induced phase transitions in bent-core mesogens determined by x-ray diffraction. Physical Review E 2011, 84, doi:10.1103/PhysRevE.84.021707.

[30] M. Martinez-Abadia, Robles-Hernandez, B., Villacampa, B., de la Fuente, M. R., Gimenez, R., Ros, M. B. Cyanostilbene bent-core molecules: a route to functional materials. Journal of Materials Chemistry C 2015, 3, 3038-3048, doi:10.1039/c5tc00201j.

[31] D. Zaton, Karamoula, A., Strachan, G. J., Storey, J. M. D., Imrie, C. T., Martinez-Felipe, A. Photo-driven effects in twist-bend nematic phases: Dynamic and memory response of liquid crystalline dimers. Journal of Molecular Liquids 2021, 344, doi:10.1016/j.molliq.2021.117680.

[32] I. C. Pintre, Gimeno, N., Serrano, J. L., Ros, M. B., Alonso, I., Folcia, C. L., Ortega, J., Etxebarria, J. Liquid crystalline and nonlinear optical properties of bent-shaped compounds derived from 3,4 '-biphenylene. Journal of Materials Chemistry 2007, 17, 2219-2227, doi:10.1039/b700636e.

[33] D. Shen, Pegenau, A., Diele, S., Wirth, I., Tschierske, C. Molecular design of nonchiral bent-core liquid crystals with antiferroelectric properties. Journal of the American Chemical Society 2000, 122, 1593-1601, doi:10.1021/ja993572w.

[34] A. Martinez-Felipe, Imrie, C. T., Ribes-Greus, A. Study of Structure Formation in Side-Chain Liquid Crystal Copolymers by Variable Temperature Fourier Transform Infrared Spectroscopy. Industrial & Engineering Chemistry Research 2013, 52, 8714-8721, doi:10.1021/ie303130e.

[35] L. Guo, Gomola, K., Gorecka, E., Pociecha, D., Dhara, S., Araoka, F., Ishikawa, K., Takezoe, H. Transition between two orthogonal polar phases in symmetric bent-core liquid crystals. Soft Matter 2011, 7, 2895-2899, doi:10.1039/c0sm01233e.

[36] S. U. Vallerien, Kremer, F., Kapitza, H., Zentel, R., Frank, W. FIELD-DEPENDENT SOFT AND GOLDSTONE MODE IN A FERROELECTRIC LIQUID-CRYSTAL AS STUDIED BY DIELECTRIC-SPECTROSCOPY. Physics Letters A 1989, 138, 219-222, doi:10.1016/0375-9601(89)90032-7.

[37] L. Guo, Gorecka, E., Pociecha, D., Vaupotic, N., Cepic, M., Reddy, R. A., Gornik, K., Araoka, F., Clark, N. A., Walba, D. M., Ishikawa, K., Takezoe, H. Ferroelectric behavior of orthogonal smectic phase made of bent-core molecules. Physical Review E 2011, 84, doi:10.1103/PhysRevE.84.031706.

[38] F. Gouda, Skarp, K., Lagerwall, S. T. DIELECTRIC STUDIES OF THE SOFT MODE AND GOLDSTONE MODE IN FERROELECTRIC LIQUID-CRYSTALS. Ferroelectrics 1991, 113, 165-206, doi:10.1080/00150199108014063.

[39] J. Ortega, de la Fuente, M. R., Etxebarria, J., Folcia, C. L., Diez, S., Gallastegui, J. A., Gimeno, N., Ros, M. B., Perez-Jubindo, M. A. Electric-field-induced B-1-B-2 transition in bent-core mesogens. Physical Review E 2004, 69, doi:10.1103/PhysRevE.69.011703.

[40] A. V. Gorbunov, Putzeys, T., Urbanaviciute, I., Janssen, R. A. J., Wubbenhorst, M., Sijbesma, R. P., Kemerink, M. True ferroelectric switching in thin films of trialkylbenzene-1,3,5-tricarboxamide (BTA). Physical Chemistry Chemical Physics 2016, 18, 23663-23672, doi:10.1039/c6cp03835b.

[41] S. M. Alauddin, Aripin, N. F. K., Velayutham, T. S., Martinez-Felipe, A. Liquid Crystalline Copolymers Containing Sulfonic and Light-Responsive Groups: From Molecular Design to Conductivity. Molecules 2020, 25, doi:10.3390/molecules25112579.

[42] S. M. Alauddin, Ibrahim, A. R., Aripin, N. F. K., Velayutham, T. S., Abou-Zied, O. K., Martinez-Felipe, A. New side-chain liquid crystalline terpolymers with anhydrous conductivity: Effect of azobenzene substitution on light response and charge transfer. European Polymer Journal 2021, 146, doi:10.1016/j.eurpolymj.2020.110246.

[43] L. Vanti, Alauddin, S. M., Zaton, D., Aripin, N. F. K., Giacinti-Baschetti, M., Imrie, C. T., Ribes-Greus, A., Martinez-Felipe, A. Ionically conducting and photoresponsive liquid crystalline terpolymers: Towards multifunctional polymer electrolytes. European Polymer Journal 2018, 109, 124-132, doi:10.1016/j.eurpolymj.2018.08.033.

[44] A. Martinez-Felipe, Santonja-Blasco, L., Badia, J. D., Imrie, C. T., Ribes-Greus, A. Characterization of Functionalized Side-Chain Liquid Crystal Methacrylates Containing Nonmesogenic Units by Dielectric Spectroscopy. Industrial & Engineering Chemistry Research 2013, 52, 8722-8731, doi:10.1021/ie3031339.

[45] K. A. Mauritz, Moore, R. B. State of understanding of Nafion. Chemical Reviews 2004, 104, 4535-4585, doi:10.1021/cr0207123.

[46] A. C. Luntz, McCloskey, B. D. Nonaqueous Li-Air Batteries: A Status Report. Chemical Reviews 2014, 114, 11721-11750, doi:10.1021/cr500054y.

[47] K. Kishimoto, Suzawa, T., Yokota, T., Mukai, T., Ohno, H., Kato, T. Nano-segregated polymeric film exhibiting high ionic conductivities. Journal of the American Chemical Society 2005, 127, 15618-15623, doi:10.1021/ja0549594.

[48] A. Concellon, Hernandez-Ainsa, S., Barbera, J., Romero, P., Luis Serrano, J., Marcos, M. Proton conductive ionic liquid crystalline poly(ethyleneimine) polymers functionalized with oxadiazole. Rsc Advances 2018, 8, 37700-37706, doi:10.1039/c8ra08253g.

[49] A. Concellon, Liang, T., Schenning, A. P. H. J., Luis Serrano, J., Romero, P., Marcos, M. Proton-conductive materials formed by coumarin photocrosslinked ionic liquid crystal dendrimers. Journal of Materials Chemistry C 2018, 6, 1000-1007, doi:10.1039/c7tc05009g.

[50] T. Kobayashi, Ichikawa, T., Kato, T., Ohno, H. Development of Glassy Bicontinuous Cubic Liquid Crystals for Solid Proton-Conductive Materials. Advanced Materials 2017, 29, doi:10.1002/adma.201604429.

[51] T. Liang, van Kuringen, H. P. C., Mulder, D. J., Tan, S., Wu, Y., Borneman, Z., Nijmeijer, K., Schenning, A. P. H. J. Anisotropic Dye Adsorption and Anhydrous Proton Conductivity in Smectic Liquid Crystal Networks: The Role of Cross-Link Density, Order, and Orientation. Acs Applied Materials & Interfaces 2017, 9, 35218-35225, doi:10.1021/acsami.7b09386.

[52] G. S. McHattie, Imrie, C. T., Ingram, M. D. Ionically conducting side chain liquid crystal polymer electrolytes. Electrochimica Acta 1998, 43, 1151-1154, doi:10.1016/s0013-4686(97)10013-5.

[53] J. Yang, Wang, Y., Yang, G., Zhan, S. New anhydrous proton exchange membranes based on fluoropolymers blend imidazolium poly (aromatic ether

ketonejs for high temperature polymer electrolyte fuel cells. International Journal of Hydrogen Energy 2018, 43, 8464-8473, doi:10.1016/j.ijhydene.2018.03.128.

[54] X. Yang, Tan, S., Liang, T., Wei, B., Wu, Y. A unidomain membrane prepared from liquid-crystalline poly(pyridinium 4-styrene sulfonate) for anhydrous proton conduction. Journal of Membrane Science 2017, 523, 355-360, doi:10.1016/j.memsci.2016.10.010.

[55] S. Yuan, Guo, X., Aili, D., Pan, C., Li, Q., Fang, J. Poly(imide benzimidazole)s for high temperature polymer electrolyte membrane fuel cells. Journal of Membrane Science 2014, 454, 351-358, doi:10.1016/j.memsci.2013.12.007.

[56] M. Cestari, Diez-Berart, S., Dunmur, D. A., Ferrarini, A., de la Fuente, M. R., Jackson, D. J. B., Lopez, D. O., Luckhurst, G. R., Perez-Jubindo, M. A., Richardson, R. M., Salud, J., Timimi, B. A., Zimmermann, H. Phase behavior and properties of the liquid-crystal dimer 1 ‘’,7 ‘’-bis(4-cyanobiphenyl-4 ‘- yl) heptane: A twist-bend nematic liquid crystal. Physical Review E 2011, 84, doi:10.1103/PhysRevE.84.031704.

[57] B. Robles-Hernandez, Sebastian, N., Rosario de la Fuente, M., Lopez, D. O., Diez-Berart, S., Salud, J., Ros, M. B., Dunmur, D. A., Luckhurst, G. R., Timimi, B. A. Twist, tilt, and orientational order at the nematic to twist-bend nematic phase transition of 1 ‘’,9 ‘’-bis(4-cyanobiphenyl-4 ‘-yl) nonane: A dielectric, H-2 NMR, and calorimetric study. Physical Review E 2015, 92, doi:10.1103/PhysRevE.92.062505.

[58] R. Walker, Pociecha, D., Storey, J. M. D., Gorecka, E., Imrie, C. T. The Chiral Twist-Bend Nematic Phase (N*(TB)). Chemistry-a European Journal 2019, 25, 13329-13335, doi:10.1002/chem.201903014.

[59] O. Elamain, Hegde, G., Fodor-Csorba, K., Komitov, L. Field-induced optically isotropic state in bent core nematic liquid crystals: unambiguous proof of field-

induced optical biaxiality. Journal of Physics D-Applied Physics 2013, 46, doi:10.1088/0022-3727/46/45/455101.

[60] D. Wiant, Gleeson, J. T., Eber, N., Fodor-Csorba, K., Jakli, A., Toth-Katona, T. Nonstandard electroconvection in a bent-core nematic liquid crystal. Physical Review E 2005, 72, doi:10.1103/PhysRevE.72.041712.

[61] J. Martinez-Perdiguero, Etxebarria, J., Folcia, C. L., Ortega, J., Gimeno, N., Ros, M. B. Pseudolayered structure of the columnar B1 phase of bent-core liquid crystals. Physical Review E 2010, 82, doi:10.1103/PhysRevE.82.041706.

[62] A. Jakli. Liquid crystals of the twenty-first century – nematic phase of bent-core molecules. Liquid Crystals Reviews 2013, 1, 65-82, doi:10.1080/21680396.2013.803701.

[63] M. M. El-Desoky, Wally, N. K., Ali, A. M., Harby, A. E., Hannora, A. E. Relaxor ferroelectric-like behavior in 10PbTiO(3)-10Fe(2)O(3)-30V(2)O(5)-50B(2)O(3) glass for energy storage applications. Journal of Materials Science-Materials in Electronics 2021, 32, 22408-22416, doi:10.1007/s10854-021-06727-3.

[64] W. Shi, Zhang, L., Jing, R., Hu, Q., Zeng, X., Alikin, D. O., Shur, V. Y., Wei, X., Gao, J., Liu, G., Yan, Y., Jin, L. Relaxor antiferroelectric-like characteristic boosting enhanced energy storage performance in eco-friendly (Bi0.5Na0.5)TiO3-based ceramics. Journal of the European Ceramic Society 2022, 42, 4528-4538, doi:10.1016/j.jeurceramsoc.2022.04.057.

[65] G. S. Kumar, Neckers, D. C. PHOTOCHEMISTRY OF AZOBENZENE-CONTAINING POLYMERS. Chemical Reviews 1989, 89, 1915-1925, doi:10.1021/cr00098a012.

[66] I. Chaganava, Kilosanidze, B., Kakauridze, G., Oriol, L., Pinol, M., Martinez-Felipe, A. Induction of the vector polyphotochromism in side-chain azopolymers. Journal of Photochemistry and Photobiology a-Chemistry 2018, 354, 70-77, doi:10.1016/j.jphotochem.2017.09.067.

[67] A. Concellon, Blasco, E., Martinez-Felipe, A., Carlos Martinez, J., Sics, I., Ezquerra, T. A., Nogales, A., Pinol, M., Oriol, L. Light-Responsive Self-Assembled Materials by Supramolecular Post-Functionalization via Hydrogen Bonding of Amphiphilic Block Copolymers. Macromolecules 2016, 49, 7825-7836, doi:10.1021/acs.macromol.6b01112.

[68] S. K. Prasad, Madhuri, P. L., Satapathy, P., Yelamaggad, C. V. A soft-bent dimer composite exhibiting twist-bend nematic phase: Photo-driven effects and an optical memory device. Applied Physics Letters 2018, 112, doi:10.1063/1.5040298.

[69] S. K. Prasad, Nair, G. G., Hegde, G., Sandhya, K. L., Rao, D. S. S., Lobo, C. V., Yelamaggad, C. V. Photoinduced effects in nematic liquid crystals. Phase Transitions 2005, 78, 443-455, doi:10.1080/01411590500185690.

[70] J. Casellas, Bearpark, M. J., Reguero, M. Excited-State Decay in the Photoisomerisation of Azobenzene: A New Balance between Mechanisms. Chemphyschem 2016, 17, 3068-3079, doi:10.1002/cphc.201600502.

[71] A. Kumar, Raju, K. C. J., Ryu, J., James, A. R. Composition dependent ferro-piezo hysteresis loops and energy density properties of mechanically activated (Pb1-xLax)(Zr0.60Ti0.40)O-3 ceramics. Applied Physics a-Materials Science & Processing 2020, 126, doi:10.1007/s00339-020-3356-4.

[72] S. K. Prasad. Photo-Stimulated and Photo-Suppressed Phase Transitions. Molecular Crystals and Liquid Crystals 2009, 509, 1059-1069, doi:10.1080/15421400903065887.

[73] D. A. Paterson, Xiang, J., Singh, G., Walker, R., Agra-Kooijman, D. M., Martinez-Felipe, A., Gan, M., Storey, J. M. D., Kumar, S., Lavrentovich, O. D., Imrie, C. T. Reversible Isothermal Twist-Bend Nematic-Nematic Phase Transition Driven by the Photoisomerization of an Azobenzene-Based Nonsymmetric Liquid Crystal Dinner. Journal of the American Chemical Society 2016, 138, 5283-5289, doi:10.1021/jacs.5b13331.

[74] S. Shruthi, Smahel, M., Kohout, M., Shanker, G., Hegde, G. Influence of linking units on the photo responsive studies of azobenzene liquid Crystals: Application in optical storage devices. Journal of Molecular Liquids 2021, 339, doi:10.1016/j.molliq.2021.116744.

[75] R. S. Hegde, Sunil, B. N., Hegde, G., Prasad, V. Influence of alkyl and alkoxy groups on photoresponsive behaviour of bent-core azo mesogens: Synthesis, mesomorphic and photoswitching properties. Journal of Molecular Liquids 2020, 309, doi:10.1016/j.molliq.2020.113091.

[76] M. Alaasar. Azobenzene-containing bent-core liquid crystals: an overview. Liquid Crystals 2016, 43, 2208-2243, doi:10.1080/02678292.2016.1175676.

[77] N. Begum, Kaur, S., Xiang, Y., Yin, H., Mohiuddin, G., Rao, N. V. S., Pal, S. K. Photoswitchable Bent-Core Nematic Liquid Crystals with Methylated Azobenzene Wing Exhibiting Optic-Field-Enhanced Freedericksz Transition Effect. Journal of Physical Chemistry C 2020, 124, 874-885, doi:10.1021/acs.jpcc.9b09326.

[78] S. K. Prasad, Nair, G. G., Hegde, G. Dynamic self-assembly of the liquid-crystalline smectic A phase. Advanced Materials 2005, 17, 2086, doi:10.1002/adma.200500161.

Journal of Materials Chemistry C

ROYAL SOCIETY OF CHEMISTRY

PAPER

View Article Online
View Journal | View Issue

Check for updates

Cite this: J. Mater. Chem. C, 2022, 10, 18200

Light-responsive bent-core liquid crystals as candidates for energy conversion and storage†

Ivan Dominguez-Candela,[abc] Iman Zulkhairi,[a] Inmaculada Pintre,[d] Nurul Fadhilah Kamalul Aripin,[ef] Jaime Lora-Garcia,[b] Vicent Fombuena,[c] M. Blanca Ros[d] and Alfonso Martinez-Felipe[*ag]

We have assessed the potential of light-responsive bent-core liquid crystals as candidate materials for energy conversion and storage applications. Samples comprise two chromophore bent-core compounds containing either one (IP33) or two (IP31) azobenzene groups, and their 5% (molar) mixtures with one non-chromophore bent-core compound (NG75), which was also measured as a reference material. The pristine compounds and their mixtures were introduced in thin transparent Indium Tin Oxide (ITO) cells, and were characterised by polarised optical microscopy, UV-visible spectrophotometry, impedance spectroscopy, and ferroelectric analysis, under different conditions of electrical fields and UV irradiation. All materials display smectic C polar phases (SmCP) except IP31, which forms columnar phases (Col), and IP33, IP31 and their mixtures exhibit light-responsiveness when irradiated at 365 nm due to reversible *trans*-to-*cis* photoisomerisation of the azobenzene units. All the bent-core based materials exhibit, at least, two dielectric relaxations, associated with different modes of molecular reorientation under weak alternating electrical fields (1 V_{rms}), as well as ferroelectric response that leads to permanent polarisation under the application of strong alternating fields (~75 kV cm^{-1}) at frequencies associated with the Goldstone-mode (1 Hz). Samples show considerable conductivity values and relaxor behaviour for liquid crystals, which can be tuned by application of UV light. In addition, we have induced in IP31 isothermal phase transitions from columnar to smectic phases (*via* the isotropic melt), by a combination of light and electrical stimuli. Our results confirm the potential of these bent-core compounds as light-harvesters for energy applications.

Received 28th September 2022,
Accepted 14th November 2022

DOI: 10.1039/d2tc04106e

rsc.li/materials-c

1. Introduction

The development of innovative electrolytes that can improve the efficiency of renewable energy conversion and storage will play a decisive role to reduce greenhouse emissions and reach net-zero targets globally.[1] Liquid crystals hold promise as advanced materials in different renewable technologies, due to their ability to interact with, and respond to, external sources, resulting in tailor-made nanostructures.[2–4] More specifically, azobenzene-containing compounds can exhibit liquid crystalline phases controllable by light excitation, *via trans*-to-*cis* photoisomerisation. In its ground state, the azobenzene *trans* isomer is linear, and hence compatible with liquid crystalline phases, since it tends to promote order and interactions in the mesophase range. When excited with UV light at certain frequencies, the *trans*-isomer bends, normally disrupting the liquid crystal order. Even though azobenzenes have been studied for several decades,[5–7] they continue to attract interest due to their potential to promote long-range macroscopic changes induced by short-range molecular modifications.[8–12]

Bent-core liquid crystals, BCLCs, exhibit anti-ferroelectric and ferroelectric behaviour with high figures of merit, which can be useful for energy storage applications. BCLCs can form columnar (Col, former B_1), polar smectic C (SmCP, former B_2), twist grain boundary dark conglomerate (DC) or helical

[a] Chemical Process and Materials Research Group, School of Engineering, University of Aberdeen, King's College, Aberdeen AB24 3UE, Scotland, UK. E-mail: a.martinez-felipe@abdn.ac.uk
[b] Instituto de Seguridad Industrial, Radiofísica y Medioambiental (ISIRYM) Universitat Politècnica de València (UPV), Plaza Ferrándiz y Carbonell, s/n 03801 Alcoy, Spain
[c] Technological Institute of Materials (ITM), Universitat Politècnica de València (UPV), Plaza Ferrándiz y Carbonell 1, 03801 Alcoy, Spain
[d] Instituto de Nanociencia y Materiales de Aragón, Departamento de Química Orgánica, Facultad de Ciencias, Universidad de Zaragoza-CSIC, Campus San Francisco, E-50009 Zaragoza, Spain
[e] School of Chemical Engineering, College of Engineering, Universiti Teknologi MARA, 40450 Shah Alam, Selangor, Malaysia
[f] Department of Chemistry, School of Natural and Computing Sciences, University of Aberdeen, King's College, Aberdeen AB24 3UE, Scotland, UK
[g] Centre for Energy Transition, University of Aberdeen, King's College, Aberdeen AB24 3UE, Scotland, UK

† Electronic supplementary information (ESI) available. See DOI: https://doi.org/10.1039/d2tc04106e

V. CONCLUSIONES

V.1. CONCLUSIONES PARCIALES

De acuerdo con los objetivos específicos planteados en la presente tesis, las conclusiones más relevantes de cada uno de los bloques se resumen a continuación:

Bloque I: estudio de los parámetros de la reacción de epoxidación

Los resultados obtenidos del estudio de los parámetros de la reacción de epoxidación del aceite de chía, muestra la capacidad de poder ser empleado como materia prima en diferentes aplicaciones en la industria de polímeros.

El estudio previo de la composición de los AGs del aceite de chía mostró un alto contenido en PUFAs del 84.9%, indicando gran cantidad de dobles enlaces para la incorporación de grupos epoxi. Se estudió el efecto de los ratios molares H_2O_2:DB ((0.75:1) y (1.5:1)) y temperaturas (60, 70 y 75 ^oC) en el grado de epoxidación, observándose que el empleo del ratio molar (1.5:1) H_2O_2:DB y una temperatura de 75 ^oC permitió mejorar el grado de epoxidación hasta un valor de 8.26 % en peso de grupos epoxi o 193 g·eq^{-1} EEW. Esto se pudo corroborar realizando el estudio de FTIR y H NMR. Por último, tanto la densidad y como viscosidad dinámica de los aceites epoxidados aumentaban como consecuencia de la incorporación de grupos epoxi.

Por tanto, los resultados obtenidos demostraron que el ECO se puede considerar como una alternativa a los aceites epoxidados comerciales, como el ELO o ESO. Este alto contenido de grupos epoxi le permite ser empleado para la obtención de bio polímeros con alto rendimiento medioambiental.

Bloque II: plastificación

Los resultados obtenidos permiten concluir que el aceite epoxidado de chía actúa de forma efectiva como plastificante en formulaciones de PLA.

El aceite epoxidado de chía se incorporó en un rango de 2.5-10% en una matriz de PLA. La incorporación mejoró las propiedades dúctiles como el alargamiento a la rotura y la energía absorbida en el impacto, reduciendo la rigidez intrínseca del PLA. Incorporando el 10% de ECO en PLA se observó el mayor alargamiento a la rotura con

una mejora del 700% respecto al PLA sin plastificar. También se observó una disminución en la T_g en torno a 4.7 ºC y una mejora de 14 ºC en la degradación térmica en formulaciones entre 7.5 y 10% de ECO. La morfología de la rotura durante el ensayo de impacto mostró el efecto plastificante, apareciendo la saturación de plastificación a partir de 7.5% de ECO. Respecto a la biodegradación, se observó que la aplicación del nuevo plastificante disminuyó ligeramente la capacidad de compostaje pero obteniéndose formulaciones completamente biodegradables. Por último, la migración del plastificante presentó valores menores del 0.108%.

Por ello, los resultados indicaron que la incorporación de ECO mejora la ductilidad del PLA, la degradación térmica y apenas afecta a la compostabilidad. Por todo ello, y unido a su baja migración del plastificante, la incorporación de ECO es una propuesta interesante para obtener materiales de alto rendimiento medioambiental en la industria de envase y embalaje.

Bloque III: incorporación de cargas lignocelulósicas

Los resultados obtenidos evidencian que el residuo obtenido tras la obtención del aceite de chía puede ser incorporado como carga lignocelulósica aplicando un modelo de economía circular. El aprovechamiento de este residuo permitió la obtención de materiales con alto rendimiento medioambiental.

La carga se incorporó inicialmente en una matriz de Bio-HDPE para la obtención de *Wood Plastic Composites*. Tras el estudio de tratamiento superficial de la carga, se observó que el empleo de silanos, concretamente del APS, mejoraba la adhesión superficial entre carga y la matriz de Bio-HDPE. Esto permitió la mejora del 41% en la elongación a la rotura en formulaciones de 20% de CSF. Por otro lado, la evaluación de la incorporación de CSF entre el 10 y 40% mostró un aumento de la rigidez de las formulaciones a medida que se adiciona más carga. Respecto a la compostabilidad, la incorporación del 40% de CSF permitió una biodegradación del 20% por la presencia de cargas lignocelulósicas. La capacidad de adsorción de agua mostró una relación directa con la degradación, registrando una adsorción aproximada del 11% para formulaciones de 40% de CSF.

Posteriormente, se evaluó la incorporación de un 15% de CSF en formulaciones de PLA utilizando diferentes compatibilizantes. Tras el estudio del efecto de los compatibilizantes, se diferenció dos tipos de comportamiento. Por un lado, el tratamiento superficial de silano empleando el GPS y la incorporación de Xibond, ambos de origen petroquímico, mostraron un aumento en propiedades mecánicas resistentes. Por otro lado, el empleo de 7.5% de ECO y MCO permitió mejorar las propiedades dúctiles hasta 8 y 10 veces más que sin compatibilizar, respectivamente. En todos los casos, se obtuvo una mejora en la interacción entre la partícula y la matriz según los estudios con SEM. Respecto al compostaje, la incorporación de los compatibilizantes en las formulaciones no mostró un retraso en la velocidad de degradación en comparación a la formulación sin compatibilizar.

De forma general, los resultados obtenidos indican que la incorporación de CSF como carga lignocelulósica permite obtener formulaciones con alto rendimiento medioambiental y con menor coste económico, aprovechando los residuos de la industria de extracción del aceite de chía. Además, la incorporación de diferentes tipos de compatibilizantes permite obtener formulaciones con diferentes propiedades, donde los derivados del aceite de chía aumentan la ductilidad debido a su doble efecto compatibilizante y plastificante.

Bloque IV: termoestables

Los resultados obtenidos tras la aplicación del aceite de chía modificado para la obtención de una resina termoestable, evidencia la efectividad de ECO y MCO como matriz y endurecedor, respectivamente.

Tras el estudio de la incorporación de MCO como sustituto del endurecedor petroquímico MNA en matrices de ECO, se observó que el MCO permite aumentar la reactividad de las muestras durante el proceso de curado. Como consecuencia, el tiempo de curado disminuyó considerablemente, registrando tiempos de gel de 155 segundos en la muestra con 100% de MCO. Respecto a las propiedades mecánicas, la ductilidad de las resinas se vio mejorada debido a la presencia de las cadenas flexibles en MCO. En este sentido, la energía absorbida aumentó en un 181% respecto a la formulación con ECO y MNA. Este efecto también se observó en la T_g con diferencias

de hasta 26.8 ºC entre las formulaciones de 100% MNA y 100% MCO. Todas las formulaciones obtenidas fueron curadas correctamente variando el porcentaje de MNA y MCO.

Por tanto, variando las cantidades introducidas de MNA y MCO como endurecedor en matrices de ECO, es posible adaptar las propiedades mecánicas obteniendo tanto resinas rígidas como con cierto grado de ductilidad. Esto da lugar a la obtención de resinas termoestables con alto contenido bio basado, alcanzando hasta un 98% de origen renovable.

Bloque V: cristales líquidos

Los resultados obtenidos indican la capacidad de los LCs como conversores y almacenamientos de energía.

Tras el estudio de LCs con nucleo torcido, se observó que la incorporación de diferentes compuestos al 5% con uno (IP33) y dos (IP31) grupos cromóforos en el compuesto NG75, permitió mejorar el almacenamiento de energía. A pesar de que las propiedades térmicas y las texturas de las mezclas permanecieran similares al compuesto virgen, NG75, las mezclas obtenidas eran capaz de modular su respuesta mediante la aplicación de luz UV.

Por tanto, el empleo de estos LCs en el campo energético permite abrir un nuevo abanico de posibilidades. Si, además, se considera el empleo de LCs obtenidos parcialmente de fuentes renovables, como puede ser a partir de los aceites vegetales, podría permitir el empleo de estos en aplicaciones energéticas o incluso en otros sectores, como el cosmético o farmacéutico.

V.2. CONCLUSIÓN GENERAL

La semilla de chía ha podido ser empleada como un recurso funcional para la obtención de diferentes formulaciones con alto rendimiento medioambiental. Por un lado, los derivados del aceite de chía, siendo el caso del ECO y MCO, se han empleado como aditivos o materias primas en la obtención de polímeros termoplásticos y termoestables. El ECO fue empleado como plastificante, compatibilizante en cargas y matriz en resinas termoestables, mientras que el MCO se aplicó como compatibilizante y endurecedor en resinas. Por otro lado, el empleo de CSF como carga lignocelulósica, permitió obtener formulaciones de Bio-HDPE y PLA con alto contenido bio basado aplicando la economía circular. Por tanto, se puede concluir que las aplicaciones de la semilla de chía realizadas en la presente tesis, permite obtener formulaciones con mayor rendimiento medioambiental, más competitivas a nivel industrial por la disminución del coste de producción, y biodegradables en el caso de las formulaciones enfocadas directamente para la industria del envase y embalaje.

Respecto a los trabajos futuros, la semilla de chía puede emplearse en diferentes aplicaciones debido a que presenta una composición muy variada, dando lugar a nuevas líneas de trabajo. Empleando el aceite como fuente natural, se obtendrá glicolípidos para estudiar su potencial como surfactante para aplicaciones cosméticas o en aplicaciones energéticas para conversión y almacenamiento de energía en presencia de compuestos que interaccionan con la luz solar. Respecto a la harina de chía, su contenido en mucílago y proteínas le permite emplearse como film biodegradable y comestible para la industria alimentaria. Esto permite abrir una línea de investigación para estudiar la influencia del empleo de diferentes plastificantes o la incorporación de nanocargas. Por otro lado, el mucílago también puede emplearse como bio coagulante y/o floculante en el tratamiento de aguas residuales, optimizando la cantidad empleada para cada agua residual específica.